

VOLUME 76 SEPTEMBER 14, 1972 NUMBER 19

JPCHAX

6 67

---

THE JOURNAL OF

PHYSICAL

CHEMISTRY

---

PUBLISHED BIWEEKLY BY THE AMERICAN CHEMICAL SOCIETY

# THE JOURNAL OF PHYSICAL CHEMISTRY

---

**BRYCE CRAWFORD, Jr.,** *Editor*

STEPHEN PRAGER, *Associate Editor*

ROBERT W. CARR, Jr., FREDERIC A. VAN-CATLEDGE, *Assistant Editors*

**EDITORIAL BOARD:** A. O. ALLEN (1970-1974), J. R. BOLTON (1971-1975),  
F. S. DAINTON (1972-1976), M. FIXMAN (1970-1974),  
H. S. FRANK (1970-1974), R. R. HENTZ (1972-1976), J. R. HUIZENGA (1969-1973),  
W. J. KAUZMANN (1969-1973), R. L. KAY (1972-1976), W. R. KRIGBAUM (1969-1973),  
R. A. MARCUS (1968-1972), W. J. MOORE (1969-1973), J. A. POPLER (1971-1975),  
B. S. RABINOVITCH (1971-1975), H. REISS (1970-1974), S. A. RICE (1969-1975),  
F. S. ROWLAND (1968-1972), R. L. SCOTT (1968-1972),  
R. SEIFERT (1968-1972), W. A. ZISMAN (1972-1976)

---

CHARLES R. BERTSCH, *Manager, Editorial Production*

---

AMERICAN CHEMICAL SOCIETY, 1155 Sixteenth St., N.W., Washington, D. C. 20036

## Books and Journals Division

JOHN K. CRUM, *Director*

JOSEPH H. KUNEY, *Head, Business Operations Department*

RUTH REYNARD, *Assistant to the Director*

©Copyright, 1972, by the American Chemical Society. Published biweekly by the American Chemical Society at 20th and Northampton Sts., Easton, Pa. 18042. Second-class postage paid at Washington, D. C., and at additional mailing offices.

All manuscripts should be sent to *The Journal of Physical Chemistry*, Department of Chemistry, University of Minnesota, Minneapolis, Minn. 55455.

*Additions and Corrections* are published once yearly in the final issue. See Volume 75, Number 26 for the proper form.

*Extensive or unusual alterations in an article after it has been set in type are made at the author's expense*, and it is understood that by requesting such alterations the author agrees to defray the cost thereof.

The American Chemical Society and the Editor of *The Journal of Physical Chemistry* assume no responsibility for the statements and opinions advanced by contributors.

Correspondence regarding accepted copy, proofs, and reprints should be directed to Editorial Production Office, American Chemical Society, 20th and Northampton Sts., Easton, Pa. 18042. Manager: CHARLES R. BERTSCH. Assistant Editor: EDWARD A. BORGER. Editorial Assistant: JOSEPH E. YURVATI.

Advertising Office: Centcom, Ltd. (formerly Century Communications Corporation), 142 East Avenue, Norwalk, Conn. 06851.

## Business and Subscription Information

Remittances and orders for subscriptions and for single copies,

notices of changes of address and new professional connections, and claims for missing numbers should be sent to the Subscription Service Department, American Chemical Society, 1155 Sixteenth St., N.W., Washington, D. C. 20036. Allow 4 weeks for changes of address. Please include an old address label with the notification.

Claims for missing numbers will not be allowed (1) if received more than sixty days from date of issue, (2) if loss was due to failure of notice of change of address to be received before the date specified in the preceding paragraph, or (3) if the reason for the claim is "missing from files."

Subscription rates (1972): members of the American Chemical Society, \$20.00 for 1 year; to nonmembers, \$60.00 for 1 year. Those interested in becoming members should write to the Admissions Department, American Chemical Society, 1155 Sixteenth St., N.W., Washington, D. C. 20036. Postage to Canada and countries in the Pan-American Union, \$5.00; all other countries, \$6.00. Single copies for current year: \$3.00. Rates for back issues from Volume 56 to date are available from the Special Issues Sales Department, 1155 Sixteenth St., N.W., Washington, D. C. 20036.

This publication and the other ACS periodical publications are now available on microfilm. For information write to: MICROFILM, Special Issues Sales Department, 1155 Sixteenth St., N.W., Washington, D. C. 20036.

THE JOURNAL OF  
PHYSICAL  
CHEMISTRY

*Volume 76*

SEPTEMBER—DECEMBER 1972

PAGES 2643—4042

INDEXES TO VOLUME 76

BRYCE CRAWFORD, JR., *Editor*

STEPHEN PRAGER, *Associate Editor*

ROBERT W. CARR, JR., FREDERIC A. VAN-CATLEDGE, *Assistant Editors*

EDITORIAL BOARD

A. O. ALLEN  
J. R. BOLTON  
F. S. DAINTON  
M. FIXMAN  
H. S. FRANK  
R. R. HENTZ  
J. R. HUIZENGA

W. J. KAUZMANN  
R. L. KAY  
W. R. KRIGBAUM  
R. A. MARCUS  
W. J. MOORE  
J. A. POPLE  
B. S. RABINOVITCH

H. REISS  
S. A. RICE  
F. S. ROWLAND  
R. L. SCOTT  
R. SEIFERT  
W. A. ZISMAN

CHARLES R. BERTSCH, *Manager, Editorial Production*

---

AMERICAN CHEMICAL SOCIETY

BOOKS AND JOURNALS DIVISION

JOHN K. CRUM  
*Director*

JOSEPH H. KUNEY  
*Head, Business Operations Department*

RUTH REYNARD  
*Assistant to the Director*

---

# THE JOURNAL OF PHYSICAL CHEMISTRY

Volume 76, Number 19 September 14, 1972

JPCHAx 76(19) 2643-2800 (1972)

Mass Spectrometric Study of the Reaction of Dicyanoacetylene with Active Nitrogen Clifford W. Hand* and Ralph H. Obenauf, Jr.	2643
Absolute Rate Constants for the Reaction $O + O_2 + M \rightarrow O_3 + M$ over the Temperature Range 200-364°K Robert E. Huie, John T. Herron, and Douglas D. Davis*	2653
Vapor-Phase Thermal Decomposition of Some Simple Ozonides L. A. Hull, I. C. Hisatsune, and Julian Heicklen*	2659
Quenching of $^3P_1$ Mercury Atoms by Isotopic Aromatic Molecules Gilbert J. Mains and Mendel Trachtman*	2665
Photochemistry of Ethanethiol at 254 and 214 nm Lamar Bridges, Gregory L. Hemphill, and John M. White*	2668
Effect of Ionic Dissociation of Organic Compounds on Their Rate of Reaction with Hydrogen Atoms P. Neta and Robert H. Schuler*	2673
Elementary Processes in the Radiolysis of Aqueous Nitric Acid Solutions: Determination of Both $G_{OH}$ and $G_{NO_2}$ R. W. Matthews, H. A. Mahlman, and T. J. Sworski*	2680
Systematics of $(n, \gamma)$ -Activated Hot $^{128}I$ Reactions in Gaseous Methane and Halomethanes. The Energy Degradation Factor Matthias Yoong, Y. C. Pao, and E. P. Rack*	2685
An Electron Spin Resonance Study of Adsorption Stabilization of Photolytic Trifluoromethyl Radicals on Zeolites P. Svejda	2690
Effect of Hydrogen Adsorption on the Electron Paramagnetic Resonance Spectra of Catalysts Containing Chromium Oxide Lurance M. Webber	2694
Infrared Spectra of Hydrocarbons Adsorbed on Silica-Supported Metals. IV. Butenes on Iridium A. Ravi and N. Sheppard*	2699
Far-Ultraviolet Solvent Spectroscopy M. F. Fox and E. Hayon*	2703
Magnetic Properties of Three Copper(II) Complexes of 2-(2-Aminoethyl)pyridine David Y. Jeter, William E. Hatfield,* and Derek J. Hodgson	2707
Reactions of Recoil Chlorine Atoms with Cis and Trans Olefins W. S. Smith, S. H. Daniel, and Yi-Noo Tang*	2711
Electron Paramagnetic Resonance Spectra of $NH_2$ Radicals Formed by $\gamma$ Irradiation of Ammoniated Zeolites E. F. Vansant and J. H. Lunsford*	2716
Matrix Infrared Spectra and Bonding in the Di- and Triiodomethyl Radicals David W. Smith and Lester Andrews*	2718
Role of Low-Energy Resonances in Some Elementary Processes of Radiation Chemistry K. Funabashi* and T. Kajiwara	2726
Studies on the Formation of Primary Hydrogen Atom Yield ( $G_H$ ) in the $\gamma$ Radiolysis of Water Z. D. Draganić and I. G. Draganić*	2733
The Higher Excited States in Metal-Ammonia Solutions. I. The 2s State J. Logan and N. R. Kestner*	2738
An Examination of the Overspeeding Technique in Relation to Sedimentation Equilibrium G. J. Howlett and L. W. Nichol*	2740

จัดพิมพ์โดย  
16 พ.ย. 2515

Quasi-Elastic Light Scattering from Two-Component Mixtures . . . . .	W. W. Wilson and Charles S. Johnson, Jr.*	2744
Electrocapillary Phenomena at the Stress-Annealed Pyrolytic Graphite Electrode . . . . .	Ikram Morcos	2750
Theory of Hydrophobic Bonding. II. The Correlation of Hydrocarbon Solubility in Water with Solvent Cavity Surface Area . . . . .	Robert B. Hermann	2754
A Solubility Study of Silver Halides in Molten Calcium Nitrate Tetrahydrate . . . . .	Brian Burrows* and Soefjan Noersjamsi	2759
On the Thermodynamics of the Acetic Acid-Triethylamine System . . . . .	Friedrich Kohler,* E. Liebermann, G. Miksch, and Christine Kainz	2764
Adsorption Isotherms and Equations of State of Insoluble Vapors at the Water-Gas Interface as Studied by Gas Chromatography . . . . .	Jerry W. King, Amiya Chatterjee, and Barry L. Karger*	2769
Medium Effects of Urea and Guanidine Hydrochloride on the Volume Changes Produced by Protonation of Carboxylate Groups . . . . .	Sam Katz* and Jane E. Miller	2778
Thermally Stimulated Conductivity of $\gamma$ -Irradiated Triethylamine and 3-Methylpentane Glasses . . . . .	Ashok K. Munjal and Larry Kevan*	2781
Sequence Studies in Liquid-Phase Hydrocarbon Oxidation. I. The Alcohol-Ketone Transition in the Oxidation of Ethylbenzene . . . . .	É. Danóczy, G. Vasvári, and D. Gál*	2785
Extended Hückel Calculations on Polypeptide Chains. IV. The $\phi$ - $\psi$ Energy Surface for a Tetrapeptide of Poly-L-alanine . . . . .	Angelo R. Rossi, Carl W. David, and Robert Schor*	2793
Structural Studies of Stannous Chloride-Potassium Chloride Melts by Raman Spectroscopy . . . . .	Ellen J. Hathaway and Victor A. Maroni*	2796

#### COMMUNICATIONS TO THE EDITOR

Comment on "Studies of Transition Phenomena of Some Organic Solids by Electrical Conductivity Measurement at Low Temperature" . . . . .	A. Dworkin	2798
Reply to the Comment on "Studies of Transition Phenomena of Some Organic Solids by Electrical Conductivity Measurement at Low Temperature" . . . . .	Hajime Kadoi, Yoneho Tabata*, and Keichi Oshima	2799

#### AUTHOR INDEX

Andrews, L., 2718	Gál, D., 2785	Kadoi, H., 2799	Miller, J. E., 2778	Schuler, R. H., 2673
Bridges, L., 2668	Hand, C. W., 2643	Kainz, C., 2764	Morcos, I., 2750	Sheppard, N., 2699
Burrows, B., 2759	Hatfield, W. E., 2707	Kajiwara, T., 2726	Munjal, A. K., 2781	Smith, D. W., 2718
Chatterjee, A., 2769	Hathaway, E. J., 2796	Karger, B. L., 2769	Neta, P., 2673	Smith, W. S., 2711
Daniel, S. H., 2711	Hayon, E., 2703	Katz, S., 2778	Nichol, L. W., 2740	Svejda, P., 2690
Danóczy, É., 2785	Herron, J. T., 2653	Kestner, N. R., 2738	Noersjamsi, S., 2759	Sworski, T. J., 2680
David, C. W., 2793	Hicklen, J., 2659	Kevan, L., 2781	Obenauf, R. H., Jr., 2643	Tabata, Y., 2799
Davis, D. D., 2653	Hemphill, G. L., 2668	King, J. W., 2769	Oshima, K., 2799	Tang, Y.-N., 2711
Draganić, I. G., 2733	Hermann, R. B., 2754	Kohler, F., 2764	Pao, Y. C., 2685	Trachtman, M., 2665
Draganić, Z. D., 2733	Herron, J. T., 2653	Liebermann, E., 2764	Rack, E. P., 2685	Vansant, E. F., 2716
Dworkin, A., 2798	Hisatsune, I. C., 2659	Logan, J., 2738	Ravi, A., 2699	Vasvári, G., 2785
Fox, M. F., 2703	Hodgson, D. J., 2707	Lunsford, J. H., 2716	Rossi, A. R., 2793	Webber, L. M., 2694
Funabashi, K., 2726	Howlett, G. J., 2740	Mahlman, H. A., 2680	Schor, R., 2793	White, J. M., 2668
	Huie, R. E., 2653	Mains, G. J., 2665		Wilson, W. W., 2744
	Hull, L. A., 2659	Maroni, V. A., 2796		Yoong, M., 2685
	Jeter, D. Y., 2707	Matthews, R. W., 2680		
	Johnson, C. S., Jr., 2744	Miksch, G., 2764		

In papers with more than one author the name of the author to whom inquiries about the paper should be addressed is marked with an asterisk in the by-line.

# THE JOURNAL OF PHYSICAL CHEMISTRY

Registered in U. S. Patent Office © Copyright, 1972, by the American Chemical Society

VOLUME 76, NUMBER 19 SEPTEMBER 14, 1972

## Mass Spectrometric Study of the Reaction of Dicyanoacetylene with Active Nitrogen<sup>1</sup>

by Clifford W. Hand\*

University of Alabama, University, Alabama 35486

and Ralph H. Obenauf, Jr.

University of Alabama, University, Alabama 35486 and  
Carnegie-Mellon University, Pittsburgh, Pennsylvania 15213 (Received March 15, 1972)

Publication costs assisted by the University of Alabama

The reaction between active nitrogen and dicyanoacetylene has been studied in a discharge flow reactor over the pressure range 0.7–8 Torr and from room temperature to 200°. The reaction bears great similarity to the equally complex reaction of active nitrogen with acetylene, which supports the hypothesis that the site of initial N atom attack is on an acetylenic rather than a terminal carbon. Three distinct reaction zones are identified, the slow region, the flame region, and the postflame region. The reaction rate is about the same in the slow and postflame regions and at least an order of magnitude faster in the flame region. The flame zone, characterized by intense CN emission, is a chain recombination of N atoms mediated by CN and NCN radicals and initiated by small quantities of C<sub>4</sub>N<sub>2</sub>. In the slow region at low pressure the initial steps are  $N + C_4N_2 \rightleftharpoons NC_4N_2^+ (k_1, k_{-1})$  (1) and  $NC_4N_2^* + N_2 \rightarrow NCN + C_3N + N_2 (k_2)$  (2b). Kinetic data provide the rate constant estimates:  $k_1 = 5.3 \pm 4.3 \times 10^{-15}$  cm<sup>3</sup>/molecule sec,  $k_{-1} \leq 1.4 \pm 1.1 \times 10^8$  sec<sup>-1</sup>, and  $k_2 \leq 7.2 \times 10^{-10}$  cm<sup>3</sup>/molecule sec. At higher pressures the slow region is governed by a more complex chain mechanism, different from that in the flame region. There is a small but significant temperature dependence of the rate constant in the high-pressure region ( $E_a = 700 \pm 450$  cal/mol), but there is no significant temperature dependence in the low-pressure region. Major products observed are C<sub>2</sub>N<sub>2</sub> and C<sub>6</sub>N<sub>2</sub>, and CN and C<sub>2</sub>N are observed as intermediates.

### Introduction

Atom reactions with acetylene and its derivatives have been the subject of numerous investigations over the past 20 years. The reactions of active nitrogen with acetylene, methylacetylene, and dimethylacetylene were first studied by Winkler and coworkers,<sup>2,3</sup> who showed that the major products were HCN and C<sub>2</sub>N<sub>2</sub>. In these early studies there was no attempt to observe any pressure dependence; all experiments were performed at  $1.4 \pm 0.1$  Torr.<sup>4</sup> An extensive study of the reaction of active nitrogen with acetylene was reported in 1969 by Arrington, Bernardini, and Kistiakowsky,<sup>5</sup> who observed a complex system with two

parallel reactions; one was relatively slow and dependent upon pressure, the other was a much faster reaction proposed to be chain branching and initiated by energetic nitrogen molecules rather than nitrogen atoms.

- (1) Submitted to the faculty of Carnegie-Mellon University by R. H. Obenauf, Jr., in partial fulfillment of the requirement for the Ph.D.
- (2) J. Versteeg and C. A. Winkler, *Can. J. Chem.*, **31**, 129 (1953).
- (3) A. Schavo and C. A. Winkler, *ibid.*, **37**, 655 (1959).
- (4) (a) J. Versteeg, Thesis, McGill University, Montreal, 1953; (b) A. Schavo, Thesis, McGill University, Montreal, 1955.
- (5) C. A. Arrington, O. O. Bernardini, and G. B. Kistiakowsky, *Proc. Roy. Soc., Ser. A*, **310**, 161 (1969).

The present work deals with the reaction of active nitrogen with dicyanoacetylene (DCA). Previous



work in this laboratory<sup>6</sup> has shown that the acetylenic carbon atoms are the primary site of attack by ground-state oxygen atoms, and it is of considerable interest to determine if this is also the case with nitrogen atoms.

### Experimental Section

The apparatus, which comprised a discharge-flow reactor with time-of-flight mass spectrometric detection, has been described in detail elsewhere.<sup>6</sup> The flow reactor was constructed of 22-mm Pyrex tubing and wrapped with 24 gauge nichrome heater wire along the entire 50-cm length. Wrappings were at *ca.* 5-mm intervals and spaced further apart near the sampling end to avoid overheating of the portion enclosed by the mass spectrometer chamber. Reactor temperature was measured with a chromel-alumel thermocouple enclosed in a 3-mm (o.d.) Pyrex tube, which entered the reactor through an off-axis sliding seal at the rear of the reactor. The probe was prestressed into a slight upward arc to counteract gravitational sag, and temperature could be measured on the axis of the reactor over its entire 50-cm length. The reactor could be heated to 600°K, and the temperature was constant to about 5%.

Active nitrogen, produced in a microwave discharge in molecular nitrogen, entered the reactor through a side arm located immediately upstream of the heated section.

Dicyanoacetylene (DCA) diluted in nitrogen was introduced to the reactor through a movable, axially mounted probe (6-mm Pyrex tubing). Both the reactant and thermocouple probes entered the reactor through an extension tube which was continuously flushed with undischarged nitrogen, which arrangement limited contact of active nitrogen with fresh unpoisoned surfaces created when the probe position was changed.

A sample of the reacting gas was expanded directly into the TOF ion source, through pinholes of 0.05–0.50-mm diameter depending on the reactor pressure. The pinholes were made from 0.3-mm thick Pyrex plates so that the reacting mixture would contact only Pyrex surfaces prior to sampling. The walls of the reactor were poisoned with 5% HF and rinsed with distilled water, and the same treatment was applied also to the connecting lines upstream to and somewhat beyond the discharge region.

Nitrogen atom concentrations were determined by titration with nitric oxide; the end point was taken to be the nitric oxide flow rate at which *m/e* 14 is reduced to background. This method, as discussed in our previous article,<sup>6</sup> was found to yield more consistent results than the method based on visual estimation of

afterglow extinction. DCA and NO flow rates were measured to an accuracy of 0.5% by monitoring the pressure drop from a known volume with calibrated differential pressure transducers. Molecular nitrogen flow rates were measured within 1% by calibrated capillary flow meters.

Matheson nitrogen (99.997%) was used without further purification as the carrier gas in all experiments. Nitric oxide (Matheson) was purified by passage through 50% aqueous KOH to remove NO<sub>2</sub>, then through anhydrous P<sub>2</sub>O<sub>5</sub> and subsequent trap-to-trap distillation. Dicyanoacetylene was prepared and purified as before,<sup>6</sup> by reaction of acetylenedicarboxamide with P<sub>2</sub>O<sub>5</sub>; the acetylenedicarboxamide was prepared from dimethyl acetylenedicarboxylate (Aldrich) according to the procedure given by Saggiomo.<sup>7</sup> Reagent analysis by mass spectrometry showed no impurities.

The strong chemiluminescence, which appeared under a variety of conditions, was measured with an unfiltered RCA 931A photomultiplier tube positioned 10 cm from the reactor behind two 3 × 8 mm slits. This arrangement permitted observation of emission integrated along a 0.5-cm length of the reactor, typically corresponding to about 3 msec of reaction time. In one experiment a Heath EU-700-51 monochromator was used to obtain a spectrum of the emission.

*General Features of the Reaction.* There are four parameters, namely (1) total pressure (*i.e.*, concentration of molecular nitrogen), (2) N atom concentration, (3) initial reactant ratio, defined by  $R = [\text{DCA}]_0/[\text{N}]_0$ , and (4) temperature, which are, within limits subject to independent manipulation. The visual appearance, rate, and mechanism of the reaction depend markedly on the values of these parameters, and indeed it is appropriate to consider separately three modes, or regions of reaction. At low pressure and moderate reactant ratio, a relatively slow reaction, accompanied by a uniform chemiluminescence, takes place. This we call the "slow region."

As the pressure is increased there is an abrupt increase in the intensity of the chemiluminescence, which becomes concentrated near the inlet probe; in short, a flame is generated. In addition to the changes in distribution, color, and intensity of the chemiluminescence, the "flame region" is marked by a much higher rate of reaction and by the consumption of perhaps 80% of the DCA.

The linear flow velocity may be increased so that the flame fills the entire reactor, or it may be decreased so that the flame is only 5–10 cm long and the slower, "post flame," region may be studied. In all three regions the reaction is chemiluminescent and accom-

(6) C. W. Hand and R. H. Obenauf, Jr., *J. Phys. Chem.*, **76**, 269 (1972).

(7) A. J. Saggiomo, *J. Org. Chem.*, **22**, 1171 (1957).

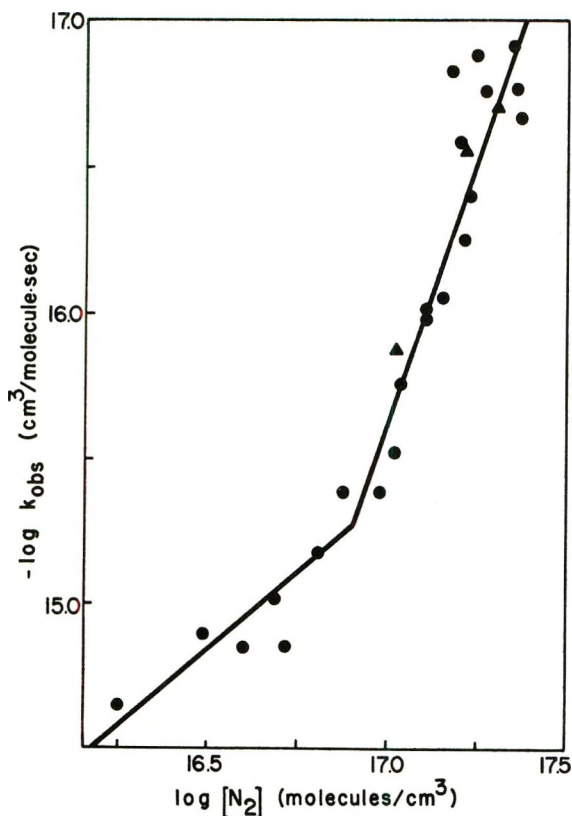


Figure 1. The effect of nitrogen molecule concentration on the observed second-order rate constant at 298–301°K: ● = slow reaction zone; ▲ = post flame zone.

panied by the deposition of brown-black material on the walls of the flow reactor; deposition in the flame region is much more rapid than in the other two, although in no case was sufficient material deposited to permit elemental analysis.

Although the onset of the flame region has been described in terms of total pressure, both the temperature and the reactant ratio,  $R$ , exert a strong influence as well. The flame must be suppressed in order to study the slow region, and the value of  $R$  required for flame suppression varies systematically with total pressure.

For most of our trials the nitrogen atom concentration was about  $2 \times 10^{14}$  atoms/cm<sup>3</sup>, hence the values which follow are relative to this atom concentration. For nitrogen concentrations less than about  $8 \times 10^{16}$  molecules/cm<sup>3</sup> a reactant ratio of 0.2 or less was sufficient to maintain the slow reaction at room temperature. At slightly greater nitrogen concentrations the reaction becomes increasingly sensitive to  $R$ ; for example, at  $[N_2] = 12 \times 10^{16}$  molecules/cm<sup>3</sup>  $R$  must be less than 0.08 and at  $[N_2] = 20 \times 10^{16}$  molecules/cm<sup>3</sup>  $R$  must be less than 0.02 to maintain the slow reaction zone. This trend continues until at  $[N_2] = 25 \times 10^{16}$  molecules/cm<sup>3</sup> a reactant ratio of only 0.005 was sufficient to produce the flame.

**Kinetics of the Slow Reaction Zone.** The rate constant of the reaction responsible for DCA consumption

in the slow region was determined over the pressure range 0.5–8.0 Torr, and the results are collected in Table I<sup>8</sup> and Figure 1. All values for  $k_{\text{obsd}}$  were taken under pseudo-first-order conditions with N atoms in excess, the atom concentration was monitored throughout, and the data were corrected for any change therein. For a given pressure the minimum DCA flow for flame generation was determined and the flow lowered to ensure that the flame would not appear owing to small changes in atom concentration during the run.

Table I: Observed Pseudo-First-Order Rate Constants Obtained under Various Conditions in the Slow Reaction Zone at 298–301°K<sup>a</sup>

$[N_2] \times 10^{-16}$ , molecules/ cm <sup>3</sup>	$[N] \times 10^{-14}$ , atoms/cm <sup>3</sup>	$[C_2N_2]_0/[N]_0$	$k_{\text{obsd}} \times 10^{15}$ , cm <sup>3</sup> /molecule sec
1.78	2.21	0.02	$0.46 \pm 0.09$
3.11	2.24	0.10	$0.79 \pm 0.06$
4.04	1.92	0.06	$0.7 \pm 0.2$
4.89	1.69	0.07	$1.0 \pm 0.2$
5.68	1.34	0.09	$0.65 \pm 0.09$
6.42	2.10	0.07	$1.5 \pm 0.1$
7.30	2.51	0.07	$2.61 \pm 0.07$
8.21	1.89	0.07	$2.1 \pm 0.2$
9.57	2.80	0.06	$2.5 \pm 0.3$
10.5	1.74	0.08	$3.3 \pm 0.5$
10.9	1.91	0.08	$5.6 \pm 0.5$
12.0*	1.67	0.09	$7.7 \pm 1.1$
12.8	2.19	0.08	$9.5 \pm 0.5$
13.0	2.95	0.02	$10.5 \pm 0.3$
14.4	2.24	0.009	$11.3 \pm 1.4$
15.0	2.58	0.02	$15.3 \pm 0.9$
15.8*	1.21	0.10	$38 \pm 5$
15.9	1.81	0.02	$38 \pm 3$
16.7	1.84	0.02	$17 \pm 1$
17.0	1.87	0.01	$24 \pm 3$
17.8	1.72	0.02	$82 \pm 5$
18.7	2.12	0.01	$58 \pm 3$
20.6*	1.74	0.02	$51 \pm 10$
22.0	1.79	0.02	$84 \pm 9$
23.3	2.89	0.01	$59 \pm 9$
24.0	2.42	0.01	$46 \pm 7$

<sup>a</sup> Those results marked by an asterisk were taken in the post-flame zone.

The data of a typical run are plotted in pseudo-first-order form in Figure 2; the value of  $k_{\text{obsd}}$  was obtained from this and similar plots by assuming first-order dependence with respect to N atoms and dividing the slope by the N atom concentration. This assumption is supported by the lack of systematic variation in  $k_{\text{obsd}}$  among measurements made at different N atom concentrations, although it is possible that a higher order dependence on  $[N]$  exists and is concealed by the much stronger dependence on total pressure (*vide infra*).

(8) The errors reported and all subsequent errors are standard errors derived from first-order regression analysis of data.



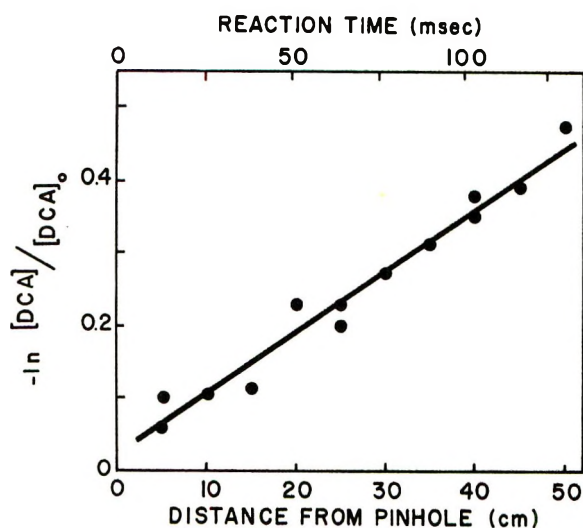


Figure 2. Rate of removal of DCA by N atoms *vs.* time: linear flow velocity = 386 cm/sec; total pressure = 5.20 Torr; 300°K;  $[N] = 1.8 \times 10^{14}$  atom/cm<sup>3</sup>.

Repeated searches of the mass spectra revealed only two stable products of the reaction: cyanogen ( $C_2N_2$ ) was by far the major product, with small quantities of dicyanodiacetylene ( $C_2N_2$ ) being formed at pressures less than about 4 Torr. Peaks at  $m/e$  26 and 38 corresponding to CN and  $C_2N$  were observed at maximum instrument sensitivity. These measurements were made with ionizing energy less than 16.6 V, which is in turn less than the appearance potentials of CN or  $C_2N$  from either  $C_2N_2$  or  $C_4N_2$ . Any other products or intermediates had to be present in concentrations considerably less than  $10^{12}$  particles/cm<sup>3</sup>. The stoichiometric factor could not be measured in the slow region, since in order to prevent the onset of flame a large excess of atoms was required; N atom concentration was sensibly constant throughout the course of the reaction.

The data in Table I are shown graphically in Figure 1, where the logarithmic presentation is a matter of convenience rather than fundamental significance. The two straight lines in Figure 1 are least-square fits to two somewhat arbitrarily chosen groups of rate constants, high and low pressure, and serve primarily to illustrate the most striking feature of this reaction, namely, that the mechanism must be distinctly different in the low- and high-pressure regimes. As indicated by the slopes of the lines, the pressure dependence is approximately first order at low pressures, changing to somewhat greater than third order at high pressures.

In Table II are collected the results of elevated temperature runs at two different total pressures, one from the high-pressure and one from the low-pressure group. The high-pressure rate constants exhibit a significant increase as the temperature is raised and least-squares analysis yields a value of  $700 \pm 450$  cal/mol for the activation energy. The low-pressure data, on the other hand, exhibit no significant temperature depen-

Table II: Observed Pseudo-First-Order Rate Constants for Two Selected Nitrogen Concentrations at Various Temperatures<sup>a</sup>

$[N_2] \times 10^{-16}$ , molecules/ cm <sup>3</sup>	Temp, °K	$[N] \times 10^{-14}$ , atoms/cm <sup>3</sup>	$[C_4N_2]_0/[N]_0$	$k_{obsd} \times 10^{15}$ , cm <sup>3</sup> /molecule sec
4.90	300*			1.05
4.91	380	1.65	0.04	$1.2 \pm 0.2$
4.90	421	1.50	0.03	$1.0 \pm 0.2$
4.90	471	1.69	0.03	$1.0 \pm 0.5$
4.91	479	0.98	0.03	$1.0 \pm 0.6$
14.43	300*			13.0
14.42	335	2.58	0.009	$19 \pm 3$
14.40	336	2.27	0.01	$20 \pm 3$
14.43	378	2.07	0.01	$15 \pm 3$
14.41	419	2.25	0.01	$16 \pm 3$
14.43	446	1.93	0.009	$29 \pm 9$

<sup>a</sup> Trials marked with an asterisk indicate that values were obtained by interpolation of data from Table I.

dence; least-squares treatment gives an activation energy of  $-45 \pm 110$  cal/mol. Trials at temperatures above those reported could not be made due to onset of the flame zone.

*Nitrogen Atom Consumption in the Flame Zone.* In Figure 3 several representative plots of nitrogen atom concentration *vs.* DCA concentration are shown. These data are all obtained at 3.0 Torr under which conditions the flame appears when  $R \geq \sim 0.1$ ; hence the catastrophic decrease in  $[N]$  shown in Figure 3 is associated with the flame zone of the reaction. Although these data all refer to a fixed time (22.5 msec) after mixing, the shape of the plot does not depend strongly on reaction time. Close examination of the initial drop in N atom concentration reveals a slight but significant downward curvature, *i.e.*, the rate of N atom consumption increases in a nonlinear way as more DCA is added. Since a simple rate increase in a second-order reaction as one reactant increases would not show this accelerated behavior, it must be concluded that what is in fact being observed is the transition from the slow region to the much faster flame region.

The shapes of the curves shown in Figure 3 show a striking resemblance to those obtained by Arrington, *et al.*,<sup>5</sup> for the reaction of active nitrogen with acetylene; however, apart from the numerical values of the atom and reactant concentrations, there are two significant differences, as follows.

In Table III are listed the various initial concentrations, that is, concentrations derived from measuring the flow rate into the reactor, of DCA which correspond to the minima in N atom concentration. Also listed are the ratios initial  $[DCA]$ /initial  $[N]$  corresponding to the minima. This ratio has a constant value in the acetylene system,<sup>5</sup> that is, the minimum  $[N]$  was always reached when the acetylene flow rate

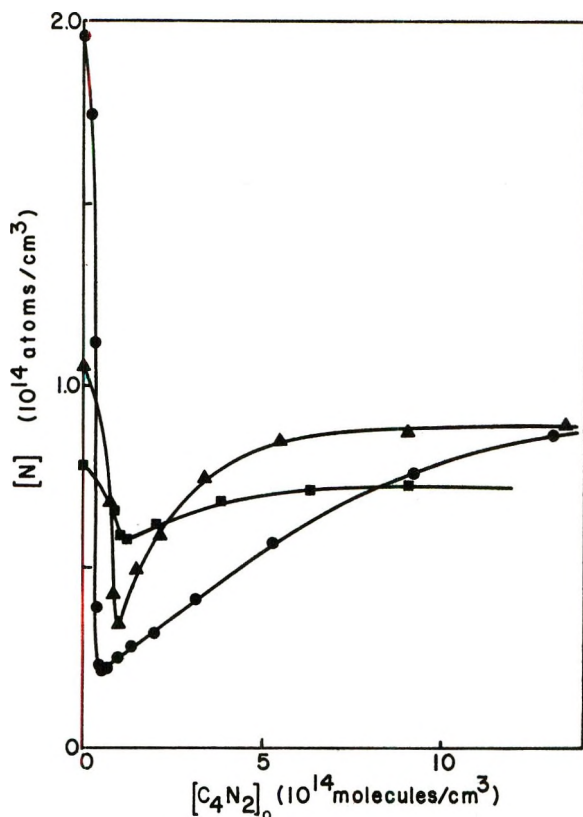


Figure 3. Nitrogen atom concentration 22.5 msec after addition of DCA vs. initial DCA concentration for three initial atom concentrations: linear flow velocity = 888 cm/sec; total pressure = 3.00 Torr; 299°K.

was about 7% of the total reactant flow. Arrington, *et al.*, interpreted this behavior as being due to "a very fast recombination of nitrogen atoms occurring only at low  $([C_2H_2]/[N])_0$  ratios." The mechanism they propose for this fast reaction is a chain recombination with metastable nitrogen molecules ( $A^3\Sigma_u^+$ ) playing the major role as chain carrier. In the DCA reaction, on the other hand, the DCA flow corresponding to the minimum in  $[N]$  depends *inversely* on the initial atom concentration. Secondly, whereas in the acetylene system the minimum  $[N]$  is about  $5 \times 10^{14}$  atoms/cm<sup>3</sup> regardless of the initial atom concentration, with DCA there is again an inverse dependence: minimum  $[N]$  are 2, 3.5, and  $6 \times 10^{13}$  atoms/cm<sup>3</sup> for initial concentrations of 1.95, 1.05, and  $0.8 \times 10^{14}$  atoms/cm<sup>3</sup>, respectively. This behavior is also strongly indicative of a chain mechanism which consumes N atoms in the flame region and which will be discussed (*vide infra*).

Results of mass balance experiments in the flame zone were not reproducible, and values for the stoichiometric factor, that is, the number of N atoms consumed/DCA molecule consumed, ranged from 2 to 12. Such nonreproducibility is also characteristic of chain reactions. The major difficulty in obtaining these data is that the measurements must necessarily be made in the region of Figure 3 where the atom concen-

Table III: Initial Reactant Ratios,  $[C_4N_2]_1/[N]_0$ , Corresponding to the Minima of Figure 3

Pressure, Torr	Reaction time, msec	Initial $[N] \times 10^{-14}$ , atoms/cm <sup>3</sup>	Initial $[C_4N_2] \times 10^{-14}$ , molecules/cm <sup>3</sup>	$\frac{[C_4N_2]_0}{[N]_0}$
2.0	30.0	0.69	1.05	1.52
2.5	19.0	1.15	1.33	1.15
2.5	19.0	1.71	1.21	0.71
3.0	22.5	0.78	1.15	1.48
3.0	22.5	1.05	0.97	0.92
3.0	22.5	1.49	0.75	0.50
3.0	22.5	1.92	0.58	0.30

tration is falling steeply, and hence a minor fluctuation in DCA flow rate will have a disproportionately large effect on the observed mass balance.

As in the slow reaction zone the major product from the reaction was cyanogen,  $C_2N_2$ , with dicyanodiacetylene,  $C_6N_2$ , formed to a much lesser extent and observed only at pressures below 4 Torr; intermediates observed were CN and a small peak at  $m/e$  38 corresponding to  $C_2N$ . Formation of molecular nitrogen could not be observed owing to the large background at  $m/e$  28.

Quantitative measurement of the rate of reaction in the flame zone was not possible, owing to extreme sensitivity to external parameters. Slight changes in reactant concentrations, wall conditioning, or total pressure resulted in a variation in the rate constant over a factor of 20 in some instances. However, all the values which we obtained were at least 10 times greater than those measured in either the slow reaction zone or the postflame region at the same temperature and total pressure.

Bands corresponding to  $CN(B^2\Sigma^+ \rightarrow X^2\Sigma^+)$  and  $CN(A^2\Pi \rightarrow X^2\Sigma^+)$  were identified in the emission spectra of the flame. (Time available for emission measurements was limited by the formation of opaque deposits on the reactor wall, and high resolution spectra could not be obtained.)

*The Postflame Zone.* In the region beyond the flame the reaction rate decreases, and the chemiluminescence, while not entirely extinguished, is greatly reduced in intensity. This behavior is illustrated in Figure 4, where the emission intensity (unfiltered) and the DCA consumption are shown as a function of time. To the eye the chemiluminescence in the postflame region is the same color and about the same intensity as in the preflame, slow reaction zone. The bimolecular rate constant can be calculated from the slope of the line in the postflame zone of Figure 4, and several such determinations yielded postflame rate constants numerically equal to those obtained at the same total pressure, but under conditions in which only the slow reaction took place. These determinations are denoted by asterisks

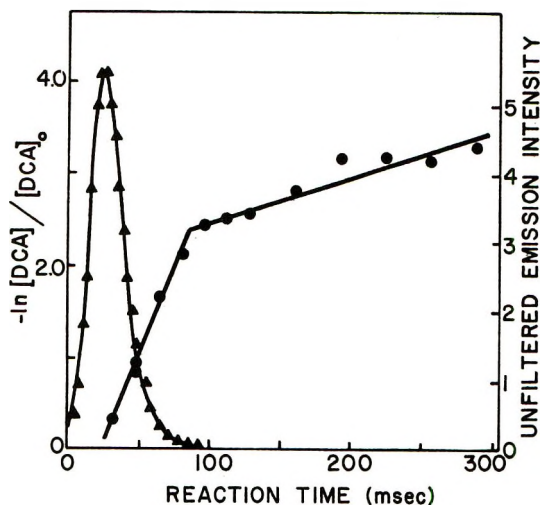


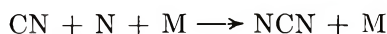
Figure 4. Rate of removal of DCA by N atoms: ●, unfiltered emission (relative units), ▲ vs. time; linear flow velocity = 155 cm/sec; total pressure = 4.88 Torr; 299°K; [N] =  $1.2 \times 10^{14}$  atoms/cm<sup>3</sup>.

in Table I, and by ▲ in Figure 1.<sup>9</sup> These observations lead us to the conclusion that the reaction mechanism is the same in both the preflame and postflame regions.

*Mechanism of the Flame Zone.* Rapid recombination of N atoms has frequently been observed in active nitrogen reaction systems<sup>5,10-12</sup> and is believed to be due to a chain mechanism involving CN and NCN

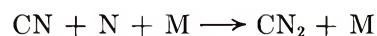


$$\Delta H = -113 \text{ kcal/mol}^{13} \text{ (ground-state products)}$$



$$\Delta H = -113 \text{ kcal/mol}$$

or the analogous possibility with CN<sub>2</sub> rather than NCN



$$\Delta H = -76 \text{ kcal/mol}$$

originally presented by Bayes. A different mechanism involving carbon atoms has been proposed by Safrany and Jaster.<sup>14</sup>



The endothermicity of the second step precludes its importance in a system composed primarily of room temperature nitrogen, and although we did observe some C<sub>2</sub>N, we believe that it originates from subsequent N atom attack on cyanogen, the major product.

Several aspects of the behavior in the flame zone, as illustrated in Figure 3, are sufficient to permit some definite conclusions regarding the mechanism of the reaction. These are the precipitous decrease in atom

Table IV: Selected Heats of Formation

Substance	$\Delta H_f$ , kcal/mol	Ref
N	113	a
N <sub>2</sub> (A <sup>3</sup> Σ <sub>u</sub> <sup>+</sup> )	≤ 142	b
C <sub>2</sub> N <sub>2</sub>	74	a
C <sub>4</sub> N <sub>2</sub>	127	c
C <sub>6</sub> N <sub>2</sub>	183	d
C	171	a
CN	≤ 103	e
C <sub>2</sub> N	184	c
C <sub>3</sub> N	< 99	c
C <sub>4</sub> N	238	f
C <sub>3</sub> N <sub>2</sub>	154	g
CN <sub>2</sub>	140	a
NCN	103	a
C <sub>2</sub>	200	a

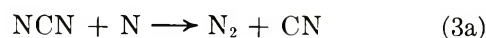
<sup>a</sup> "JANAF Thermochemical Tables," 2nd ed, Dow Chemical Co., Midland, Mich., 1971, p 37. <sup>b</sup> See ref 19. <sup>c</sup> See ref 26. <sup>d</sup> V. H. Dibeler, R. M. Reese, and J. L. Franklin, *J. Amer. Chem. Soc.*, **83**, 1813 (1961). <sup>e</sup> D. W. Setser and D. H. Stedman, *J. Chem. Phys.*, **49**, 467 (1968); V. H. Dibeler and S. K. Liston, *ibid.*, **47**, 4548 (1967). <sup>f</sup>  $\Delta H_f^\circ(\text{C}_4\text{N})$  estimated by taking  $D(\text{NC}_4\equiv\text{N})$  equal to  $D(\text{HC}\equiv\text{N})$ . G. Herzberg, "Molecular Spectra and Molecular Structure, Vol. 3, Van Nostrand, New York, N. Y., 1966. <sup>g</sup> See ref 14.

concentration attendant on the introduction of small quantities of DCA; the fact that the atom concentration reaches a minimum and then increases as more DCA is added; the fact that as the initial atom concentration is increased, less DCA is required to generate the flame; and finally that at higher initial atom concentrations the consumption of atoms is more complete. A chain mechanism is certainly operative, as indicated by the rapidity of atom consumption and the small quantities of DCA required to initiate the consumption. The chain must be initiated by the bimolecular attack of N atoms on DCA, followed by decomposition of the hot adduct to produce chain carriers.



$$\Delta H = -38 \text{ kcal/mol} \quad (2a)$$

The chain can then be propagated by the steps



(9) The data from Figure 4 appear in Table I as the entry at [N<sub>2</sub>] =  $15.8 \times 10^{16}$  molecules/cm<sup>3</sup>.

(10) K. D. Bayes, *Can. J. Chem.*, **39**, 1074 (1961).

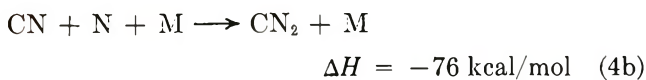
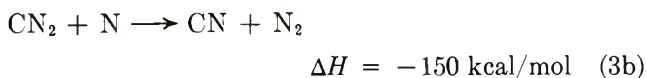
(11) R. L. Brown and H. P. Broida, *J. Chem. Phys.*, **41**, 2053 (1964).

(12) I. M. Campbell and B. A. Thrush, *Proc. Chem. Soc.*, 410 (1964).

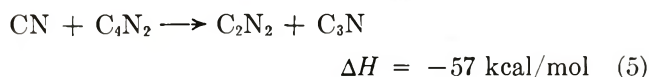
(13) This and all subsequent heats of reaction have been calculated on the basis of the values given in Table IV.

(14) D. R. Safrany and W. Jaster, *J. Phys. Chem.*, **72**, 3305 (1968).

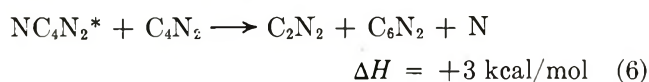
(or by the analogous steps 3b and 4b). The rate of



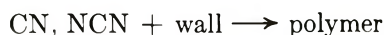
the chain recombination would thus depend on the concentration of NCN, which increases as more DCA is added, hence the precipitous drop in Figure 3. However, on further addition of DCA the N atom concentration increases, indicating a decrease in chain length. This might be due to the removal of chain carriers by



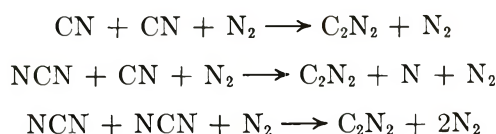
or, equally important, to a decrease in the initiation rate by the competing reaction



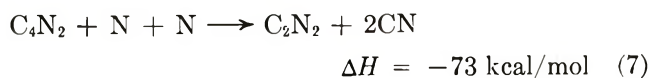
Reactions 5 and 6 account for the observed products, although there are no doubt other reactions which produce  $\text{C}_2\text{N}_2$ . Also, the increasingly important collisional deactivation of  $\text{NC}_4\text{N}_2^*$  would cause the observed decrease in yield of  $\text{C}_6\text{N}_2$  as the pressure is raised. While there is no firm evidence to permit identification of the most important termination step(s), the deposition of polymeric material on the reactor wall is suggestive of heterogeneous termination.



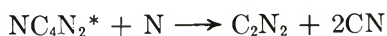
Homogeneous processes may equally well be responsible.



Finally, the fact that at higher initial N atom concentration the recombination is faster and more complete requires that there be an additional initiation step, *second order* in N atoms. The only possibility is



which may be viewed either as a termolecular step or as two bimolecular steps, reaction 1 followed by



The chain recombination of N atoms thus consists of the initiation steps 1, 2a, and 7 in competition with reaction 6, the propagation steps 3a and 4a, and termination by undetermined heterogeneous and homogeneous steps as well as by reaction 5.

*Mechanism in the Slow Reaction Zone.* For a second-order reaction which exhibits pressure dependence the steady-state expression for observed rate constant may be written as the quotient of two polynomials in powers of the third body concentration. If a single mechanism governs the slow reaction throughout the entire pressure range, it should be possible to fit the experimental data to a polynomial of the form

$$k_{\text{obsd}} = \frac{\sum_{i=0} a_i [\text{M}]^i}{\sum_{i=0} b_i [\text{M}]^i} \quad (I)$$

where the coefficients  $a_i$  and  $b_i$  are simple functions (sums and/or products) of the rate constants for the elementary reaction steps. Nonlinear regression analysis of the data from Table I was carried out for polynomials as high as third order, in both numerator and denominator, and although the curves obtained followed the general shape of the observed data, it proved impossible to obtain a good fit unless one or more of the coefficients was allowed to assume a negative value. Since this means one or more negative rate constants, we conclude that a single mechanism, however complicated, cannot explain our data over the entire pressure range. We must therefore separately discuss the high- and low-pressure regions with the dividing line being taken as about 3 Torr, *i.e.*, at the change in slope of the data in Figure 1.

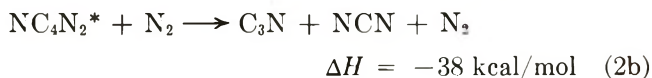
*The Low-Pressure Region.* For nitrogen concentrations less than about  $10^{17}$  molecules/cm<sup>3</sup> the data may be understood in terms of a mechanism similar to that reported by Arrington, *et al.*,<sup>5</sup> for the acetylene reaction. Experimentally we have observed a second-order rate law

$$-d[\text{DCA}]/dt = k_{\text{obsd}}[\text{N}][\text{DCA}]$$

in which the observed rate constant increases with total pressure in an approximately linear fashion. The first step must be the bimolecular combination of the reactants

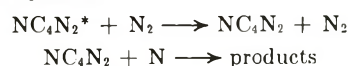


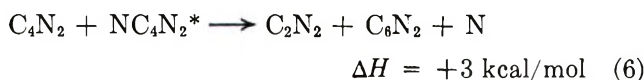
The observed pressure dependence requires that subsequent actions of the hot  $\text{NC}_4\text{N}_2^*$  be bimolecular.<sup>15</sup>



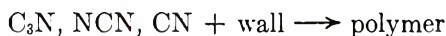
Reaction 3a,  $\text{NCN} + \text{N} \rightarrow \text{CN} + \text{N}_2$ , provides a ready source of the observed CN radical. Reaction of the hot adduct with DCA produces the observed small amounts of dicyanodiacetylene.

(15) Other products are possible in this step, such as  $\text{C}_3\text{N}_2 + \text{CN}$ ,  $\Delta H = 17 \text{ kcal/mol}$ , or  $\text{C}_2\text{N}_2 + \text{C}_2\text{N}$ ,  $\Delta H = 18 \text{ kcal/mol}$ , but these reactions are sufficiently endothermic to be relegated to a minor role. The observed dependence of  $k_{\text{obsd}}$  on pressure can also be accounted for by a scheme comprising reactions 1 and -1 followed by collisional deactivation





Under the low-pressure conditions the radical intermediates diffuse to the wall and are destroyed there in preference to homogeneous termination steps



If the concentration of  $\text{NC}_4\text{N}_2^*$  is assumed to be in steady state, the above reaction sequence leads to

$$-d[\text{DCA}]/dt = k_{\text{obsd}}[\text{N}][\text{DCA}]$$

where

$$k_{\text{obsd}} = \frac{k_1(k_{2b}[\text{N}_2] + 2k_6[\text{DCA}])}{k_{-1} + k_{2b}[\text{N}_2] + k_6[\text{DCA}]} \quad (\text{II})$$

It may further be assumed that  $k_6[\text{DCA}] \ll k_{2b}[\text{N}_2]$ , inasmuch as there is no hint of curvature in any of the data exemplified by Figure 2, and therefore there can be no second-order dependence on DCA in the reaction scheme. Equation II may thus be written in reciprocal form

$$\frac{1}{k_{\text{obsd}}} = \frac{1}{k_1} + \frac{k_{-1}}{k_1 k_{2b}} \frac{1}{[\text{N}_2]} \quad (\text{III})$$

A reciprocal plot of the low-pressure data appears in Figure 5 and the slope and intercept lead to the values

$$k_1 = 5.3 \pm 4.3 \times 10^{-15} \text{ cm}^3/\text{molecule sec}$$

$$k_{-1}/k_1 k_{2b} = 3.76 \pm 0.8 \times 10^{31} \text{ molecule}^2 \text{ sec}/\text{cm}^6$$

An upper limit to  $k_{2b}$  may be set equal to the collision frequency, calculated at 300°K with collision diameters of  $\text{N}_2 = 3.5 \text{ \AA}$  and  $\text{NC}_4\text{N}_2^* = 8.5 \text{ \AA}$ , from which

$$k_{2b} \leq 7.2 \times 10^{-10} \text{ cm}^3/\text{molecule sec}$$

and

$$k_{-1} \leq 1.4 \pm 1.1 \times 10^8 \text{ sec}^{-1}$$

Although the standard errors of the values of  $k_{\text{obsd}}$  quoted in Table I are not excessive for this type of experiment, when the data are plotted in reciprocal form the errors are magnified, leading to large uncertainties in the values of  $k_1$  and  $k_{-1}$ . These should be regarded as order-of-magnitude estimates only.

The magnitude of  $k_1$ , though it is not established with precision, is low enough to merit some discussion. As we have shown there is no appreciable activation energy, hence the steric factor must be on the order of  $10^{-4}$  to  $10^{-5}$ , an unusually low value for reactions of this type. A possible explanation is that the activation entropy is unusually low and that a tightly bound collision complex is formed. This would be expected, for instance, if the N atom addition resulted in a three-membered ring.

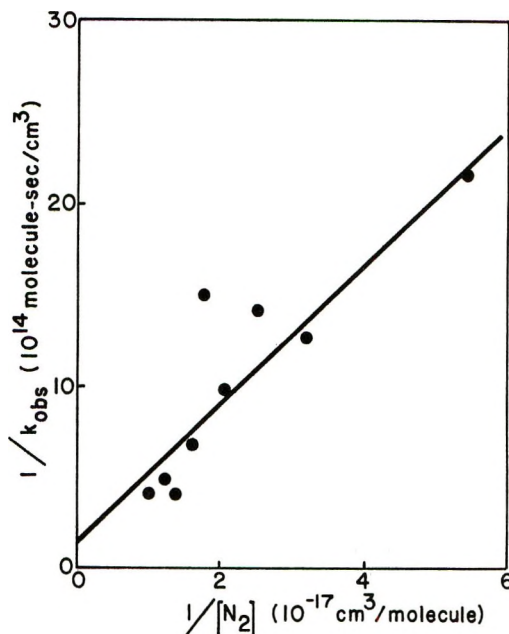
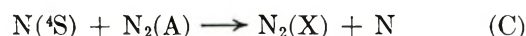
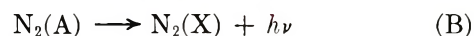


Figure 5. Reciprocal plot of low-pressure data from Table I: slope =  $3.8 \pm 0.8 \times 10^{31} \text{ molecule}^2 \text{ sec}/\text{cm}^6$ ; intercept =  $1.9 \pm 1.8 \times 10^{14} \text{ molecule sec}/\text{cm}^3$ .

*The High-Pressure Region.* Initially we should inquire whether the low-pressure mechanism could be amended or expanded to apply as well to the high-pressure conditions. We have shown in a general way (*vide supra*) that this could not be done, but it is instructive to consider the specific case as well, using real reactions and a plausible (one of several such) mechanism.

One attractive possibility is the participation of excited molecular species, namely  $\text{N}_2(\text{A}^3\Sigma_u^+)$  which is a well-known constituent of active nitrogen.<sup>16</sup> Thrush has demonstrated<sup>17,18</sup> that the A state population in active nitrogen is governed by the decay scheme



from which the steady-state population is

$$[\text{N}_2(\text{A})]_{\text{ss}} = \frac{k_{\text{A}}[\text{N}]^2[\text{N}_2]}{k_{\text{C}}[\text{N}] + k_{\text{B}}}$$

It has recently been shown that the radiative lifetime of  $\text{N}_2(\text{A})$  is about 2 sec,<sup>19-21</sup> using this value and Wray's<sup>22</sup>

(16) A. N. Wright and C. A. Winkler, "Active Nitrogen," Academic Press, New York, N. Y., 1968.

(17) B. A. Thrush, *J. Chem. Phys.*, **47**, 3691 (1967).

(18) J. C. Boden and B. A. Thrush, *Proc. Roy. Soc., Ser. A*, **305**, 93 (1968).

(19) J. A. Meyer, D. H. Klosterboer, and D. W. Setser, *J. Chem. Phys.*, **55**, 2084 (1971).

(20) D. E. Shemansky and N. P. Carleton, *ibid.*, **51**, 682 (1969).

(21) D. E. Shemansky, *ibid.*, **51**, 689 (1969).

(22) K. L. Wray, *ibid.*, **44**, 623 (1966).

value of  $k_C = 5.4 \times 10^{11}$  cm<sup>3</sup>/molecule sec, it is always true in our experiments that  $k_B \ll k_C[N]$ . Hence

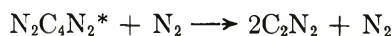
$$[N_2(A)]_{ss} = k_A[N][N_2]/k_C \text{ molecules/cm}^3 \quad (\text{IV})$$

The absolute intensity of emission from  $N_2(A)$ , the Vegard-Kaplan emission, is given by<sup>17</sup>

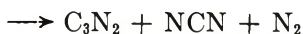
$$k_B[N_2(A)]_{ss} = I_{VK} = 5 \times 10^{-23}[N][N_2] \text{ photons/cm}^3 \text{ sec}$$

and therefore  $[N_2(A)]_{ss} = (I_{VK}/k_B)$  or  $[N_2(A)]_{ss} = 10^{-22}[N][N_2]$ .

From this we calculate, at the highest pressure of our experiments, a value of  $5 \times 10^9$  molecules/cm<sup>3</sup> for the concentration of  $N_2(A)$ . At intermediate and lower pressures the concentration is of course less, but it is continuously repopulated by reaction A and is available for reaction with dicyanoacetylene.



$$\Delta H = -121 \text{ kcal/mol} \quad (9)$$



$$\Delta H = -12 \text{ kcal/mol} \quad (10)$$



$$\Delta H = -67 \text{ kcal/mol} \quad (11)$$

If reactions 8-11 are considered together with reactions A, B, and C, to govern  $N_2(A)$  concentration a steady-state expression may be obtained

$$[N_2(A)]_{ss} = \frac{k_A(k_{-8} - k'[N_2])[N]^2[N_2]}{(k_B + k_C[N])(k_{-8} + k'[N_2]) + k_8k'[C_4N_2][N_2]} \quad (\text{V})$$

where  $k' = k_9 + k_{10} + k_{11}$ . For our system the N atom concentration is large enough so that  $k_B \ll k_C[N]$ , and if also  $k_8[C_4N_2] \ll k_C[N]$ , eq V would become identical with eq IV. The concentration of DCA was always less than 8% of the atom concentration, so we may use the known value of  $k_C$ <sup>22</sup> to obtain the condition  $k_8 \ll 6 \times 10^{-10}$  cm<sup>3</sup>/molecule sec. This is almost certainly true since  $6 \times 10^{-10}$  cm<sup>3</sup>/molecule sec is the gas kinetic collision frequency expressed as a rate constant; thus we conclude that the steady-state concentration of  $N_2(A^3\Sigma_u^+)$  is unaffected by reaction with DCA. We may then apply the steady-state hypothesis to the concentration of  $NC_4N_2^*$ ,  $N_2C_4N_2^*$ , CN, and NCN in the system of reactions 1-11, and, using the same approximation as before,  $k_6[DCA] \ll k_{2b}[N_2]$ , the expression is obtained

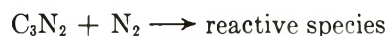
$$k_{\text{obsd}} = 3k_7[N] + \frac{k_1(k_{2a} + k_{2b}[N])}{k_{-1} + k_{2b}[N_2]} \times \frac{(k' + k_{10} + k_{11})k_8 10^{-22}[N_2]^2}{k_{-8} + k'[N_2]} \quad (\text{VI})$$

where  $k_{\text{obsd}}$  is the second-order rate constant for the disappearance of DCA in an excess of N atoms.

This expression could account for a quadratic pressure dependence, which comes about through the two steps



each of which is first order in total pressure. It is simple enough to escalate the pressure dependence to cubic or even quartic by requiring further collisions with  $N_2$ , for instance



but our only justification for doing so would be that the observed pressure dependence cannot be accounted for by any simpler mechanism. Far more serious, however, is that there is no set of numerical values of rate constants which will cause eq VI, or any other steady-state expression derived from a reasonable mechanism, to simultaneously fit the high- and low-pressure data. The conclusion, once again, is that a new and different mechanism becomes operative as the pressure is raised beyond about 3 Torr.

We therefore conclude that at higher pressures DCA is consumed in a chain reaction and that the rapid increase in our reported second-order rate constant is a consequence of increased chain length. In the mechanism which follows, we omit the several reactions involving  $N_2(A^3\Sigma_u^+)$  since there is no evidence for the participation of excited molecular species in the DCA consumption scheme. We also omit the reactions of  $C_2N_2$ , the major product, and although these reactions certainly occur, they do not play a major role in the DCA reaction. The reaction of cyanogen with active nitrogen has been the subject of several studies,<sup>14, 16, 23-25</sup> and the reactive species CN, NCN, and  $C_2N$  are certainly involved. One might argue that the reaction of active nitrogen with DCA is autoaccelerated by the product  $C_2N_2$ , and that therein lies the explanation for the increase in rate constant at higher pressures. The evidence does not, however, support this view: were the reactions autoaccelerated there would be an upward curvature of the plots exemplified by Figure 2 and no such curvature was ever observed. Secondly, in the autoaccelerated case we would expect a correlation between observed rate constant and extent of reaction: no such correlation exists.

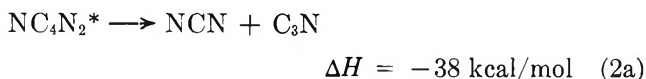
The chain decomposition of DCA is mediated by the chain carrier NCN, produced in the initiation steps



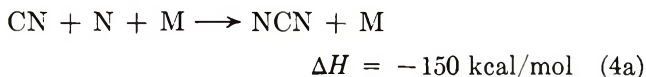
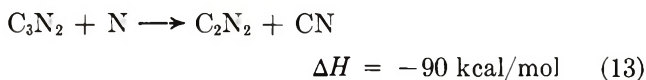
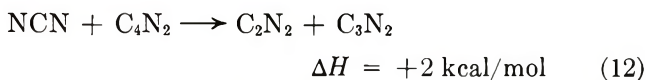
(23) C. Haggart and C. A. Winkler, *Can. J. Chem.*, **38**, 329 (1960).

(24) D. W. Setser and B. A. Thrush, *Proc. Roy. Soc., Ser. A*, **288**, 256 (1965).

(25) D. R. Safrany and W. Jaster, *J. Phys. Chem.*, **72**, 3318 (1968).



which are the same as in the low-pressure mechanism. The propagation steps are



and chain termination occurs by a variety of homogeneous and heterogeneous reactions, just as in the flame zone.

Our observation may be explained in terms of this mechanism as follows. As the pressure rises, the rate of DCA consumption (and hence  $k_{\text{obsd}}$ ) increases owing to the suppression of the diffusion-controlled heterogeneous termination steps. A more important cause for the increase in  $k_{\text{obsd}}$ , however, is the fact that one of the propagation steps, reaction 4a, is termolecular, a feature not usually found in radical-chain mechanisms. It is this feature which explains as well the relative unimportance of the chain in the low-pressure region. In support of the identification of reaction 4a as the major rate-determining step is our observation of the intermediate CN, whereas NCN was below our limit of detectability. The implication is that reactions 12 and 13 proceed much more rapidly than reaction 4a.

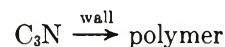
The stable product dicyanodiacetylene,  $\text{C}_6\text{N}_2$ , is

observed only at low pressure as a consequence of reaction 6 since it is not produced by the chain mechanism operative at high pressure.

Some mention should be made, for the sake of completeness, of the subsequent reactions of the radical  $\text{C}_3\text{N}$ . Its heat of formation ( $<99 \text{ kcal/mol}^{26}$ ) is sufficiently low that it cannot be an important source of chain carriers: the reaction



for instance, is endothermic by 75 kcal. The most probable fate of  $\text{C}_3\text{N}$  is to be a contributor to the solid deposit on the reactor wall

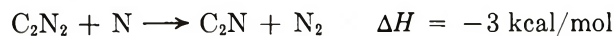


or to recombine *via*



as an additional source of  $\text{C}_6\text{N}_2$ .

Finally, the observation of trace quantities of  $\text{C}_2\text{N}$  is to be expected from subsequent reactions of the major product  $\text{C}_2\text{N}_2$ , for example



which has been postulated as being of primary importance in the reaction of active nitrogen with cyanogen.<sup>14,25</sup>

*Acknowledgments.* We wish to thank the Research Grants Committee of the University of Alabama for a Grant-in-Aid to C. W. H., and Dr. E. S. Hand for helpful comments.

(26) J. A. Meyer and D. W. Setser, *J. Phys. Chem.*, **74**, 3452 (1970)

# Absolute Rate Constants for the Reaction $O + O_2 + M \rightarrow O_3 + M$ over the Temperature Range 200–346°K

by Robert E. Huie,<sup>1,2</sup>

*University of Maryland, College Park, Maryland 20740 and National Bureau of Standards, Washington, D. C. 20234*

John T. Herron,<sup>2</sup>

*National Bureau of Standards, Washington, D. C. 20234*

and Douglas D. Davis\*<sup>3</sup>

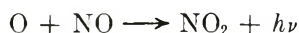
*Chemistry Department, University of Maryland, College Park, Maryland 20740 (Received March 20, 1972)*

*Publication costs assisted by The Petroleum Research Fund*

Using the technique of flash photolysis–resonance fluorescence, absolute rate constants have been measured for the reaction  $O + O_2 + M \rightarrow O_3 + M$ . For the case of  $M = Ar$  the temperature range covered was 200–346°K, and the total pressure was varied from 50 to 500 Torr. Over the indicated temperature range, an Arrhenius plot of the data yielded the expression  $k_{Ar} = (6.57 \pm 0.59) \times 10^{-35} \exp[(1014 \pm 46 \text{ cal mol}^{-1})/RT] \text{ cm}^6 \text{ molecule}^{-2} \text{ sec}^{-1}$ . A comparison of the third-order rate constants for  $M = He, Ar,$  and  $N_2$  gave the relative efficiencies for these three gases as 0.92:1.0:1.6 at 298°K. At 218°K, the efficiencies of Ar to  $N_2$  were in the ratio of 1.0:1.7. The reported rate measurements indicate that the rate of production of stratospheric ozone could be nearly a factor of 2 lower than that estimated from previously reported values of the third-order rate constant.

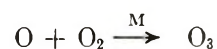
The reaction of atomic oxygen,  $O(^3P)$ , with molecular oxygen is the only important ozone forming reaction in both the troposphere and stratosphere. In order to understand either photochemical air pollution<sup>4</sup> or the ozone balance in the stratosphere,<sup>5–7</sup> the rate constant for this reaction must be known accurately. The need for kinetic information on reactions important in stratospheric chemistry has been emphasized by the recent suggestion that nitrogen oxides emitted by supersonic aircraft might significantly reduce the ozone concentration in the stratosphere.<sup>6,8</sup>

The atomic oxygen–molecular oxygen reaction has been the subject of many studies in recent years,<sup>9–20</sup> the data prior to mid-1967 having been reviewed by Johnston.<sup>20</sup> At room temperature, several techniques have been applied to the study of this reaction and a wide range of experimental parameters covered. The temperature dependence of this reaction, however, has been determined only in experiments using flow systems at low total pressure, with the atomic oxygen decay being followed by the air afterglow reaction<sup>9,10</sup>



In both of these studies, care was taken to prevent the introduction of extraneous active species into the reaction zone which might contribute to the decay of atomic oxygen. As is the case in nearly all flow systems, however, the measured O atom decay might have been influenced by reactions occurring on the walls of the reactor.

Since



is of such importance in stratospheric chemistry and since its rate constant needs to be well established at

(1) This research carried out at the University of Maryland is part of a thesis to be submitted to the Faculty of the University of Maryland in partial fulfillment of the requirements for the degree of Doctor of Philosophy.

(2) Supported in part by the Climatic Impact Assessment Program, Office of the Secretary, Department of Transportation.

(3) Acknowledgment is made by this author to the donors of The Petroleum Research Fund, administered by the American Chemical Society, for support of this research.

(4) P. A. Leighton, "Photochemistry of Air Pollution," Academic Press, New York, N. Y., 1961.

(5) M. Nicolet, *J. Geophys. Res.*, **70**, 679 (1965).

(6) P. J. Crutzen, *Quart. J. Roy. Meteorol. Soc.*, **96**, 320 (1970).

(7) P. J. Crutzen, *J. Geophys. Res.*, **76**, 7311 (1971).

(8) H. Johnston, *Science*, **173**, 517 (1971).

(9) M. A. A. Clyne, D. J. McKenney, and B. A. Thrush, *Trans. Faraday Soc.*, **61**, 2701 (1965).

(10) M. F. R. Mulcahy and D. J. Williams, *ibid.*, **64**, 59 (1968).

(11) G. M. Meaburn, D. Perner, J. LeCalve, and M. Bourene, *J. Phys. Chem.*, **72**, 3920 (1968).

(12) F. Kaufman and J. R. Kelso, *J. Chem. Phys.*, **46**, 4541 (1967).

(13) F. Stuhl and H. Niki, *ibid.*, **55**, 3943 (1971).

(14) R. J. Donovan, D. Husain, and L. J. Kirsch, *Trans. Faraday Soc.*, **66**, 2551 (1970).

(15) H. Hippler and J. Troe, *Ber. Bunsenges. Phys. Chem.*, **75**, 27 (1971).

(16) T. G. Slanger and G. Black, *J. Chem. Phys.*, **53**, 3717 (1970).

(17) P. D. Francis, *Brit. J. Appl. Phys.*, 1717 (1969).

(18) M. C. Sauer, *J. Phys. Chem.*, **71**, 3311 (1967).



temperatures and pressures corresponding to stratospheric conditions, we have undertaken a flash photolysis-resonance fluorescence study of this reaction over a wide temperature and pressure range and under conditions in which neither secondary reactions nor wall reactions were important.

### Experimental Section

The apparatus and technique have been discussed in detail previously.<sup>21,22</sup> In these experiments a mixture of a few Torr of molecular oxygen and a diluent gas (helium, argon, or nitrogen) was flash photolyzed above  $\lambda$  1050 Å, producing on the order of 0.05 to 0.005 mTorr of atomic oxygen. A small portion of the atomic oxygen was continuously excited by an atomic oxygen resonance lamp and the decay of atomic oxygen in the mixture was monitored by following the fluorescence of the atomic oxygen resonance radiation. The fluorescence signal was recorded on a multichannel analyzer, and multiple flashes (>100) were used to generate one kinetic decay curve (see Figure 1). The reaction mixture was changed several times in the course of an experiment to prevent ozone accumulation. The first-order rate constant was determined from a plot of the logarithm of the count rate, corrected for background, against channel number, or time. A good linear fit was found over at least a full decade change in the count rate.

The second-order rate constant at a particular total pressure was calculated from the slope of a plot of this first-order rate constant against the molecular oxygen pressure as shown in Figure 2. In a few cases, when only one or two data points were taken at a given temperature and pressure, a zero intercept was assumed. Finally, the third-order rate constant was derived by dividing the second-order rate constant by the total pressure of the diluent gas. With argon and nitrogen as third bodies, the third-order rate constant at 298°K and around 220°K was also calculated from the slope of a plot of the second-order rate constant against total pressure, as shown in Figure 3. When the inert gas pressure was 100 Torr or less, the contribution to the measured rate from the reaction  $O + O_2 + O_2 \rightarrow O_3 + O_2$  became significant. In those cases, the rate of the reaction with oxygen as the third body was calculated using the rate expression for argon at higher pressures from the present work, and the relative third body efficiencies given by Kaufman and Kelso.<sup>12</sup> This value was then subtracted from the total measured first-order rate. At worst, this correction amounted to about 15% of the total first-order rate constant.

The gases used in this study were Matheson Gold Label<sup>23</sup> helium, argon, and oxygen, and Air Products Ultra-high Purity<sup>23</sup> nitrogen (all better than 99.9% stated purity). All were used without further purification. In the preparation of the gas mixtures, low pressures (1–6 Torr) were measured on a dibutyl

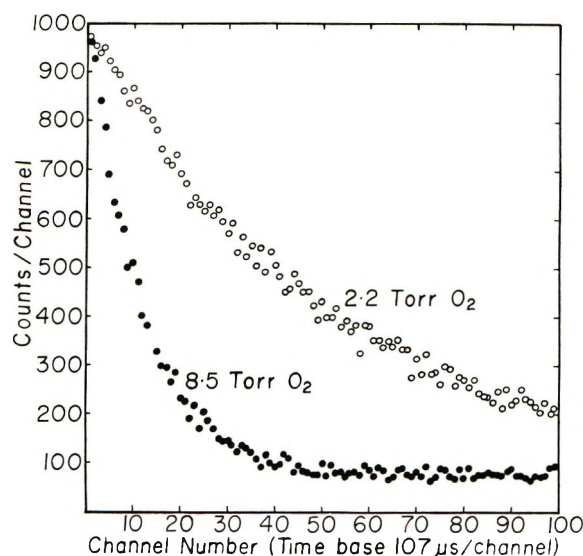


Figure 1. Typical O(<sup>3</sup>P) atom decay curves: flash intensity, 31 J and total pressure, 250 Torr.

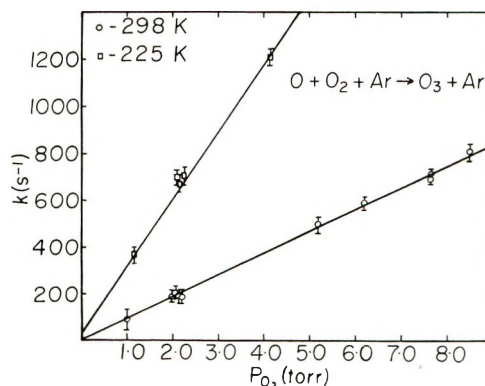


Figure 2. Plot of the experimentally measured first-order rate constant as a function of the O<sub>2</sub> pressure: total pressure, 250 Torr.

phthalate manometer and higher pressures were measured on a two-turn Bourdon gauge. The precision to which various gas mixtures could be made up was determined to be ~3%.

### Results and Discussion

The results of the present study are presented in Tables I–III. The stated error limits were derived

(19) M. C. Sauer and L. M. Dorfman, *J. Amer. Chem. Soc.*, **87**, 3801 (1965).

(20) H. S. Johnston, *Nat. Stand. Ref. Data Ser., Nat. Bur. Stand. (U. S.)*, **20** (1968).

(21) D. D. Davis, A. M. Bass, and W. Braun, *Int. J. Chem. Kinet.*, **2**, 101 (1970).

(22) D. D. Davis, R. E. Huie, J. T. Herron, M. J. Kurylo, and W. Braun, *J. Chem. Phys.*, **56**, 4868 (1972).

(23) Certain commercial instruments and materials are identified in this paper in order to specify adequately the experimental procedure. In no case does such identification imply recommendation or endorsement by the National Bureau of Standards, nor does it imply that the instruments or materials identified are necessarily the best available for the purpose.

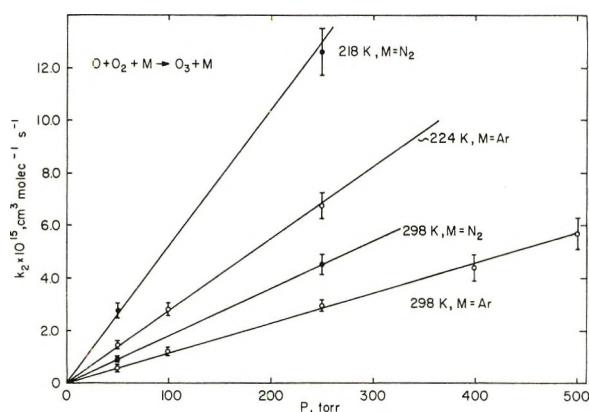


Figure 3. Plot of the second-order rate constants as a function of the total pressure.

Table I: Rate Measurements on the Reaction  $O + O_2 + He \rightarrow O_3 + He$  at 298°K

O <sub>2</sub> , Torr <sup>a</sup>	He, Torr <sup>b</sup>	Flash energy, <sup>c</sup> J	First-order rate constant, sec <sup>-1</sup>	Third-order rate constant × 10 <sup>14</sup> cm <sup>6</sup> molecule <sup>-2</sup> sec <sup>-1</sup>
1.00	250	92	113	
1.00	250	100	113	
1.25	250	39	114	
2.00	250	100	182	
2.53	250	39	258	
5.00	250	92	428	
5.00	250	100	456	
6.20	250	39	578	3.33 ± 0.2

<sup>a</sup> 1 Torr =  $9.65/T \times 10^{18}$  molecules cm<sup>-3</sup>. <sup>b</sup> Pressures greater than 100 Torr are the total pressure M + O<sub>2</sub>, others are pressures of M alone. <sup>c</sup> A flash energy of 80 J corresponds to about  $1.5 \times 10^{-13}$  photons/cm<sup>2</sup> at the reaction cell ( $\lambda < 1800 \text{ \AA}$ ).

Table II: Rate Measurements on the Reaction  $O + O_2 + N_2 \rightarrow O_3 + N_2$

T, °K	O <sub>2</sub> , Torr <sup>b</sup>	N <sub>2</sub> , Torr <sup>b</sup>	Flash energy, <sup>c</sup> J	First-order rate constant, sec <sup>-1</sup>	Third-order rate constant × 10 <sup>14</sup> cm <sup>6</sup> molecule <sup>-1</sup> sec <sup>-1</sup>
218	1.54	50	39	210	
	4.72	50	45	645	12.5 ± 0.9
	7.1	50	37	1037	
	1.31	250	45	667	
	2.38	250	45	1390	11.4 ± 1.2
221	2.88	50	51	334	11.9 ± 0.9
	298	1.03	50	48	40
298	1.42	50	26	59	
	2.79	50	37	117	5.71 ± 0.6
	4.31	50	28	165	
	7.1	50	37	261	
	1.11	250	45	169	
	1.94	250	48	288	5.57 ± 0.6
	2.49	250	39	326	
	4.43	250	39	654	

<sup>a-c</sup> See corresponding footnotes in Table I.

Table III: Rate Measurements on the Reaction  $O + O_2 + Ar \rightarrow O_3 + Ar$

T, °K	O <sub>2</sub> , Torr <sup>a</sup>	Ar, Torr <sup>b</sup>	Flash energy, <sup>c</sup> J	First-order rate constant, sec <sup>-1</sup>	Third-order rate constant × 10 <sup>14</sup> cm <sup>6</sup> molecule <sup>-2</sup> sec <sup>-1</sup>
200	1.17	150	29	333	8.35 ± 0.8
	2.54	150	29	773	
221	1.61	50	31	126	
	2.91	50	31	206	
	3.14	50	34	236	
	4.41	50	34	322	
	4.83	50	31	373	6.62 ± 0.6
225	1.17	250	31	369	
	2.09	250	13	699	
	2.14	250	100	668	
	2.24	250	29	704	
	4.16	250	29	1210	6.30 ± 0.5
227	1.71	100	39	206	
	4.03	100	42	492	6.54 ± 0.7
247	1.01	250	39	206	
	1.98	250	31	362	
265	4.16	250	34	814	5.01 ± 0.4
	0.75	250	54	125	
	1.64	250	54	241	
	4.50	250	58	678	4.44 ± 0.4
	298	1.46	50	39	42
298	2.36	50	31	60	
	2.95	50	34	75	
	4.40	50	31	111	
	4.60	50	29	115	
	6.93	50	31	187	4.09 ± 0.3
	0.71	98	29	35	
	2.08	98	29	96	
	3.67	98	29	159	3.76 ± 0.4
	1.00	250	58	95	
	2.00	250	100	192	
	2.06	250	11	202	
	2.12	250	48	196	
	2.20	250	31	184	
	5.20	250	26	497	
	6.20	250	31	592	
7.66	250	8	714		
7.66	250	93	695		
8.50	250	31	814	3.67 ± 0.2	
3.80	400	29	540	3.40 ± 0.4	
2.07	500	29	375		
3.20	500	26	596	3.51 ± 0.4	
346	2.60	250	29	150	
	4.88	250	29	273	
	7.71	250	29	433	2.82 ± 0.3

<sup>a-c</sup> See corresponding footnotes in Table I.

from a consideration of the maximum and minimum slopes which could be fit through the points plotted in Figure 2 ( $k$  (sec<sup>-1</sup>) vs.  $P_{O_2}$ ). The uncertainty in each of the first-order rate constants plotted in Figure 2 was ~5%. In all cases, the standard deviation derived from a least-squares treatment of the data was less than the error limit derived from a consideration of maximum and minimum slopes. The rate constant for the reaction  $O + O_2 + He \rightarrow O_3 + He$  was determined in this

work only at room temperature and 250 Torr pressure (Table I). Its value under these conditions was  $3.33 \pm 0.2 \times 10^{-34}$  cm<sup>6</sup> molecule<sup>-2</sup> sec<sup>-1</sup>. Since nitrogen is a more efficient quencher of the oxygen resonance fluorescence radiation than helium or argon, rate measurements using this gas were found to be more difficult than those involving He or Ar as the third body. Due to the importance of the reaction  $O + O_2 + N_2 \rightarrow O_3 + N_2$ , however, rate constant measurements were carried out both at 218 and 298°K and at 50 and 250 Torr total pressure (Table II). The respective third-order  $k$  values at these two temperatures, calculated from the slopes in Figure 3, were  $11.7 \pm 1.2 \times 10^{-34}$  and  $5.63 \pm 0.77 \times 10^{-34}$  cm<sup>6</sup> molecule<sup>-2</sup> sec<sup>-1</sup>. For the reaction  $O + O_2 + Ar \rightarrow O_3 + Ar$ , rate measurements were made over the temperature range 200–346°K and over a pressure range 50–500 Torr. These data are presented in Table III and in the form of an Arrhenius plot in Figure 4. The third-order rate constants calculated from the slopes in Figure 3 were  $3.47 \pm 0.3 \times 10^{-34}$  and  $6.36 \pm 0.72 \times 10^{-34}$  cm<sup>6</sup> molecule<sup>-2</sup> sec<sup>-1</sup> at 298°K and about 224°K. A fit of the third-order rate constants from Table III to the Arrhenius equation gave the expression  $k_{Ar} = (6.57 \pm 0.59) \times 10^{-35} \exp[(1014 \pm 46 \text{ cal mol}^{-1})/RT]$  cm<sup>6</sup> molecule<sup>-2</sup> sec<sup>-1</sup>. The stated uncertainties are the standard errors of the least-squares fit to the data. From a consideration of the maximum and minimum slopes which could be fit through the error bars of each point in Figure 4, the indicated uncertainties in A and E were  $\pm 180$  cal/mol and  $\pm 2.15$  cm<sup>6</sup> molecule<sup>-2</sup> sec<sup>-1</sup>, respectively. A comparison of the third-order rate constants for M = He, Ar, and N<sub>2</sub> gave the relative efficiencies of these three gases for deactivation as 0.92:1.0:1.6 at 298°K. At 218°K, the efficiencies of Ar to N<sub>2</sub> were in the ratio 1.0:1.7.

At the lower oxygen pressures used in this work, the absorption of the flash lamp radiation by molecular oxygen in the reaction zone was low, resulting in only a small initial concentration gradient for the oxygen atoms. At higher oxygen pressures, this gradient became larger, thus possibly leading to spurious kinetic results. As illustrated in Figure 2, however, the first-order rate constants were directly proportional to the O<sub>2</sub> pressure over the entire experimental range, demonstrating that no effects on the rate measurements resulted from oxygen atom concentration gradients in the reaction zone.

Another possible source of error in this study, which has been discussed previously,<sup>22</sup> concerns the production of electronically excited oxygen atoms in the flash photolysis of molecular oxygen. In these experiments, a minimum of a 200-μsec delay was employed between the flash photolysis of the reaction mixture and the atom concentration measurements used in determining the rate constants. At the pressures used in this study, the 200-μsec delay would ensure that all atoms

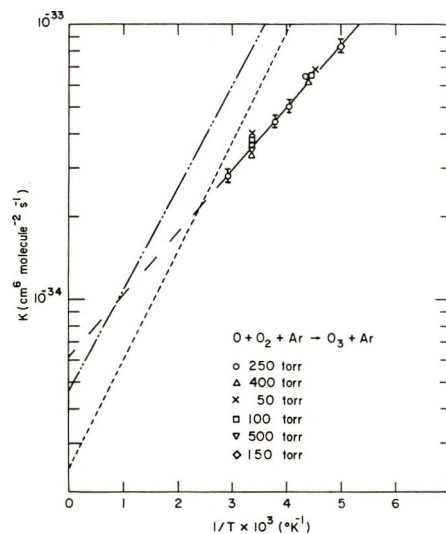


Figure 4. Arrhenius plot of the third-order rate constant for the reaction of atomic oxygen with O<sub>2</sub>: (---) represents values taken from ref 10 and (—) represents values taken from ref 9.

produced by the flash were in the ground electronic state and at thermal equilibrium. In the experiments employing He or Ar as the inert gas, most of the O(<sup>1</sup>D) produced by the flash would be quenched by O<sub>2</sub>, producing O<sub>2</sub>(<sup>1</sup>Σ<sub>g</sub><sup>+</sup>).<sup>24</sup> The excited molecular oxygen could then react with the ozone produced by the O + O<sub>2</sub> + M reaction to regenerate atomic oxygen.<sup>25</sup> Since the concentrations of both O<sub>3</sub> and O<sub>2</sub>(<sup>1</sup>Σ<sub>g</sub><sup>+</sup>) would be proportional to the flash intensity, any contribution from this reaction would be strongly dependent upon the flash intensity. To investigate the possibility that this reaction could have influenced the observed O atom decay, or that any other secondary reactions could have been important, the flash intensity was varied over about a factor of 10 at both 298 and 225°K (see Table III and Figure 2). The observed invariance of the first-order rate constant with flash intensity demonstrates that the rate of atom loss was not being influenced by secondary reactions involving O<sub>2</sub>(<sup>1</sup>Σ<sub>g</sub><sup>+</sup>) and O<sub>3</sub> or any other secondary processes such as O + O<sub>3</sub> → 2O<sub>2</sub> and O + O + M → O<sub>2</sub> + M.

Since the third-order rate constant was obtained from the slopes of the first-order rate against the molecular oxygen partial pressure at a fixed total pressure, the results are independent of any impurities in the inert gas. Additionally, lack of significant dependence of the third-order rate constant on total pressure indicates that no impurity capable of a rapid second-order reaction with atomic oxygen was present in the molecular oxygen. (As indicated earlier, ultrahigh purity gases were used throughout this study.) Other possible systematic errors associated with the use of the

(24) R. J. Donovan and D. Husain, *Chem. Rev.*, **70**, 489 (1970).

(25) T. P. Izod and R. P. Wayne, *Proc. Roy. Soc., Ser. A*, **308**, 81 (1968).

**Table IV:** A Summary of Rate Data on the Reaction  $O + O_2 + M \rightarrow O_3 + M$ 

$T, ^\circ K$	M	$k, \text{cm}^6 \text{molecule}^{-2} \text{sec}^{-1}$	Method	Ref
298	He	$3.33 \times 10^{-34}$	Flash photolysis-resonance fluorescence	This work
298	Ar	$3.63 \times 10^{-34}$		
200-346	Ar	$6.57 \times 10^{-35} \exp(1014 \text{ cal mol}^{-1}/RT)$	Discharge flow	9
218	N <sub>2</sub>	$11.7 \times 10^{-34}$		
298	N <sub>2</sub>	$5.63 \times 10^{-34}$	Thermal decomposition-flow	10
188-373	Ar	$2.44 \times 10^{-35} \exp(1800 \text{ cal mol}^{-1}/RT)$		
213-386	Ar	$4.7 \times 10^{-35} \exp(1680 \text{ cal mol}^{-1}/RT)$	Pulse radiolysis	11
298	CO <sub>2</sub>	$23 \times 10^{-34}$		
298	O <sub>2</sub>	$9.0 \times 10^{-34}$	Thermal decomposition-flow	12
298	He	$6.33 \times 10^{-34}$		
298	CO <sub>2</sub>	$10.2 \times 10^{-34}$	Flash photolysis-chemi- luminescence	13
298	N <sub>2</sub> O	$8.84 \times 10^{-34}$		
298	CO	$4.42 \times 10^{-34}$	Flash photolysis-absorption	14
298	He	$4 \times 10^{-34}$		
298	Ar	$4 \times 10^{-34}$	Photolysis relative to O + NO <sub>2</sub>	15
298	O <sub>2</sub>	$6.5 \times 10^{-34}$		
298	N <sub>2</sub>	$5.6 \times 10^{-34}$	Flash photolysis-resonance fluorescence	16
298	CO <sub>2</sub>	$15 \times 10^{-34}$		
298	N <sub>2</sub> O	$15 \times 10^{-34}$	Discharge flow	17
298	CF <sub>4</sub>	$16 \times 10^{-34}$		
298	SF <sub>6</sub>	$34 \times 10^{-34}$	Pulse radiolysis	18
298	H <sub>2</sub> O	$60 \times 10^{-34}$		
298	O <sub>2</sub>	$6.4 \times 10^{-34}$	Pulse radiolysis	19
298	N <sub>2</sub>	$5.4 \times 10^{-34}$		
298	CO	$6.7 \times 10^{-34}$	K <sub>eq</sub> (review)	20
298	He	$4.6 \times 10^{-34}$		
298	Ar	$5.0 \times 10^{-34}$	K <sub>eq</sub> (review)	28
298	Kr	$4.9 \times 10^{-34}$		
298	N <sub>2</sub>	$8 \times 10^{-34}$		
298	Ar	$4.4 \times 10^{-34}$		
298	N <sub>2</sub>	$7.0 \times 10^{-34}$		
298	O <sub>2</sub>	$1.24 \times 10^{-34}$		
298	Ar	$2.28 \times 10^{-34}$		
298	Ar	$2.48 \times 10^{-34}$		
298	CO <sub>2</sub>	$11.5 \times 10^{-34}$		
298	N <sub>2</sub> O	$9.6 \times 10^{-34}$		
298	He	$1.92 \times 10^{-34}$		
	O <sub>3</sub>	$4.63 \times 10^{-36} \exp(2100 \text{ cal mol}^{-1}/RT)$		
	Ar	$1.16 \times 10^{-36} \exp(2100 \text{ cal mol}^{-1}/RT)$		
	O <sub>2</sub>	$8.14 \times 10^{-36} \exp(890 \text{ cal mol}^{-1}/RT)$		

resonance fluorescence technique have been discussed more fully elsewhere.<sup>22</sup>

In Table IV, the results of the present work are summarized along with rate measurements reported by other workers. Excluded are those discharge flow measurements which were carried out under conditions where the effects of active impurities and metastable molecular oxygen species could have significantly influenced the final results.<sup>26</sup> Most of the earlier kinetic investigations on the system  $O + O_2 + M \rightarrow O_3 + M$  were carried out at a single temperature, 298°K. In three of these studies, oxygen atoms were produced *via* flash photolysis and loss of atomic oxygen was then followed either by  $O + NO$  chemiluminescence (Stuhl and Niki),<sup>13</sup> kinetic absorption spectroscopy (Donovan, Husain, and Kirsch),<sup>14</sup> or resonance fluorescence (Slanger and Black).<sup>16</sup> These results are seen to

agree with the present data to within 30%. In two reported pulse radiolysis studies by Sauer<sup>18</sup> and Sauer and Dorfman,<sup>19</sup> the reaction was followed by monitoring the formation of ozone. The rate constants determined at 298°K were about 50% lower than those measured in this work. In another study, Hippler and Troe<sup>15</sup> used the photolysis of NO<sub>2</sub> at 3660 Å as a means of determining the rate constant for the reaction  $O + O_2 + N_2 \rightarrow O_3 + N_2$  relative to the process  $O + NO_2 \rightarrow NO + O_2$ . In this study the extent of the ozone-producing reaction was determined by measuring the quantum yield for destruction of NO<sub>2</sub> with and without added O<sub>2</sub>. The results from this investigation were about 40% higher than reported here for N<sub>2</sub> as a third body. In both of the latter studies, the experimental

(26) F. Kaufman and J. R. Kelso, *J. Chem. Phys.*, **40**, 1162 (1964).

uncertainties associated with the techniques were sufficiently large as to explain the difference between their results and the present measurements. In an extensive study by Kaufman and Kelso<sup>12</sup> a flow system was employed in which the thermal decomposition of ozone was the atom source and detection of the atoms was by means of chemiluminescence. The agreement between the results of this study and those reported here for the third body gases He, Ar, and N<sub>2</sub> is seen to be within 10%.

As noted in the introduction, the only previous direct data on the temperature dependence of the rate of reaction of atomic oxygen with molecular oxygen are derived from flow system studies. Clyne, McKenney, and Thrush<sup>9</sup> studied the reaction in a plug-flow reactor, using a microwave discharge in oxygen as an atom source. The decay of the oxygen atoms down the reactor was determined by monitoring the chemiluminescence from the reaction  $O + NO \rightarrow NO_2 + h\nu$ . At room temperature, the results of these authors are in reasonable agreement with the present work ( $\pm 15\%$ ). At lower temperatures, however, their data diverge from the present results and are about a factor of 3 higher at 220°K. Mulcahy and Williams<sup>10</sup> also used the  $O + NO$  chemiluminescence to follow the atom concentration, but used the thermal decomposition of ozone as an atom source and carried out the study in a bulb reactor. These authors report a third-order rate constant for Ar which is a factor of 2 higher than the present results at 298°K and a factor of 3 higher at 220°K. In neither study were sufficient data given to allow a detailed discussion of the results. Although specific reasons for the discrepancies between the above studies of the temperature dependence of the  $O + O_2$  reaction and the results of this work cannot be given at present, some possibilities can be considered. In both studies, heterogeneous reactions involving the walls of the reaction vessels are possible sources of error; whereas, in the present work, the reaction time is much shorter than the time for diffusion to the walls. Since wall reactions would be expected to be more important at low temperatures,<sup>27</sup> this could also contribute the stronger temperature dependence observed in these flow studies. Additionally, the results of Mulcahy and Williams<sup>10</sup> depend on the assumption of perfect mixing in their bulb reactor, which if in error could possibly

explain why their results were also higher than those of Clyne, *et al.*<sup>9</sup>

In the review of Johnston<sup>20</sup> on the kinetics of neutral oxygen species, the recommended value for the reaction of atomic oxygen with molecular oxygen was derived from the equilibrium constant and the recommended rate constant for the reverse reaction. The preexponential term obtained by this method is a factor of 5 lower than from the present study, and the exponential term is a factor of 2 higher. At 220°K, this results in a rate constant a factor of 2 higher than reported here. This discrepancy, however, is probably not as unreasonable as it first appears. For example, the ozone bond strength used by Johnston was 24.8 kcal mol<sup>-1</sup>, and the activation energy used for the reverse reaction was 22.7 kcal mol<sup>-1</sup>. An error of 5% in either of these values would be sufficient to account for the observed difference in the exponential factors.

Benson and Axworthy,<sup>28</sup> in an earlier review of ozone decomposition, also derived a value for the recombination rate constant. Their value of the rate constant for the  $O + O_2 + M \rightarrow O_3 + M$  reaction was also based on the rate constant for the reverse reaction and the equilibrium constant. The Arrhenius parameters so derived are not extremely different from those reported here, although at stratospheric temperatures the calculated rate constant is a factor of 1.5 lower than that measured in this work.

In the present work, the rate constant for the reaction of atomic oxygen with molecular oxygen as a function of temperature has been determined in a static system free of the possible uncertainties associated with wall reactions. Rate constants have been measured at temperatures and pressures corresponding to stratospheric conditions. The reported rate measurements indicate that the rate of production of stratospheric ozone could be nearly a factor of 2 lower than that estimated from previously reported values of the third-order rate constant. This could be of considerable importance in estimating the magnitude of possible ozone destruction mechanisms necessary to explain the observed ozone profiles.

(27) J. T. Herron and R. E. Huie, *J. Phys. Chem.*, **73**, 3327 (1969).

(28) S. W. Benson and A. E. Axworthy, *J. Chem. Phys.*, **42**, 2614 (1965).

## Vapor-Phase Thermal Decomposition of Some Simple Ozonides

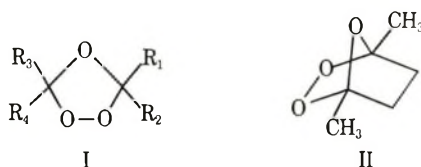
by L. A. Hull, I. C. Hisatsune, and Julian Heicklen\*

Department of Chemistry and Center for Air Environment Studies, The Pennsylvania State University, University Park, Pennsylvania 16802 (Received April 10, 1972)

The thermal decomposition of five secondary ozonides has been studied in the vapor phase. The ozonides and temperature ranges were ethylene ozonide (46–85°), propylene ozonide (59.5–110.5°), isobutene ozonide (70–113°), 2-butene ozonide (80–120°), and 1,2-dimethylcyclopentene ozonide (106–153°). The first four ozonides, which are monocyclic and have  $\alpha$  hydrogen atoms, decompose by a first-order unimolecular process. The mechanism proposed involves a highly ordered transition state in which O–O bond cleavage and H atom transfer occur simultaneously to give molecular products. The bicyclic ozonide does not contain an  $\alpha$  H atom and presumably decomposes solely by O–O bond cleavage. Arrhenius parameters for the decomposition rate coefficients are given.

### Introduction

As part of a general study of ozone-olefin reactions in the gas and condensed phases, we have undertaken a study of the thermal decomposition of some representative secondary ozonides (I and II) in the vapor phase.



- Ia,  $R_1 = R_2 = R_3 = R_4 = H$   
 Ib,  $R_1 = R_2 = R_3 = H; R_4 = CH_3$   
 Ic,  $R_1 = R_2 = H; R_3 = R_4 = CH_3$   
 Id,  $R_1 = R_3 = H; R_2 = R_4 = CH_3$

Previous investigations have been primarily concerned with product studies of liquid-phase thermal decompositions.<sup>1–7</sup> Among those, the studies of Criegee, *et al.*,<sup>2</sup> and of Story, *et al.*,<sup>8</sup> discuss the mechanistic aspects.

Criegee, Kerchow, and Zinke<sup>2</sup> studied the room temperature decomposition of 1-methyl-1-*tert*-butyl ozonide. They found formaldehyde, *tert*-butyl acetate, and methyl *tert*-butyl ketone peroxide as products, on the basis of which the intermediacy of the Criegee zwitterion was proposed.

Bernatek and Hvatum<sup>3</sup> examined the thermal decomposition of three complex multicyclic ozonides in benzene solution, mostly at 100°, but with some runs at 79.15 and 90°. They found the reactions to be first order and believed the rate-controlling step to be the O–O bond cleavage.

Story, *et al.*,<sup>7</sup> reported a careful product study of the thermal decomposition of two ozonides, diisopropyl ozonide and cyclopentene ozonide, in heptane. They found the monocyclic ozonide to decompose primarily to dimethylacetaldehyde and dimethyl acetic acid

with some products arising from further fragmentation. For the bicyclic ozonide they found no decomposition path corresponding to the simple acid-aldehyde cleavage but instead found mostly products that resulted from C–C bond cleavages. The latter result was analogous to that found in the photochemical decompositions of these same two ozonides, namely, extensive  $\beta$  bond cleavages.<sup>8</sup> They concluded that the two thermal decompositions go by way of a biradical intermediate, which in the case of the monocyclic ozonide can intramolecularly transfer a hydrogen atom and decompose into two stable molecules. The bicyclic ozonide also is postulated to yield the biradical intermediate but because of steric constraints it is hindered from intramolecular hydrogen atom transfer and instead decomposes further by  $\beta$  scission. The proposed scheme for the decomposition of the monocyclic ozonide is given in Scheme I.

The above studies include little or no kinetic data. The following results attempt to rectify that deficiency and provide additional information upon which to base a mechanistic proposal.

### Experimental Section

*Ethylene Ozonide (Ia)*. To 50 ml of Matheson Freon 114 (bp 3.6°) condensed in a cold trap at –78°, gaseous ethylene was added at –78° until the solution was

(1) R. Criegee, P. deBruyn, and G. Lohaus, *Justus Liebigs Ann. Chem.*, **583**, 19 (1953).

(2) R. Criegee, A. Kerchow, and H. Zinke, *Chem. Ber.*, **88**, 1878 (1955).

(3) E. Bernatek and M. Hvatum, *Acta Chem. Scand.*, **14**, 836 (1960).

(4) A. Greiner and V. Müller, *J. Prakt. Chem.*, **15**, 313 (1962).

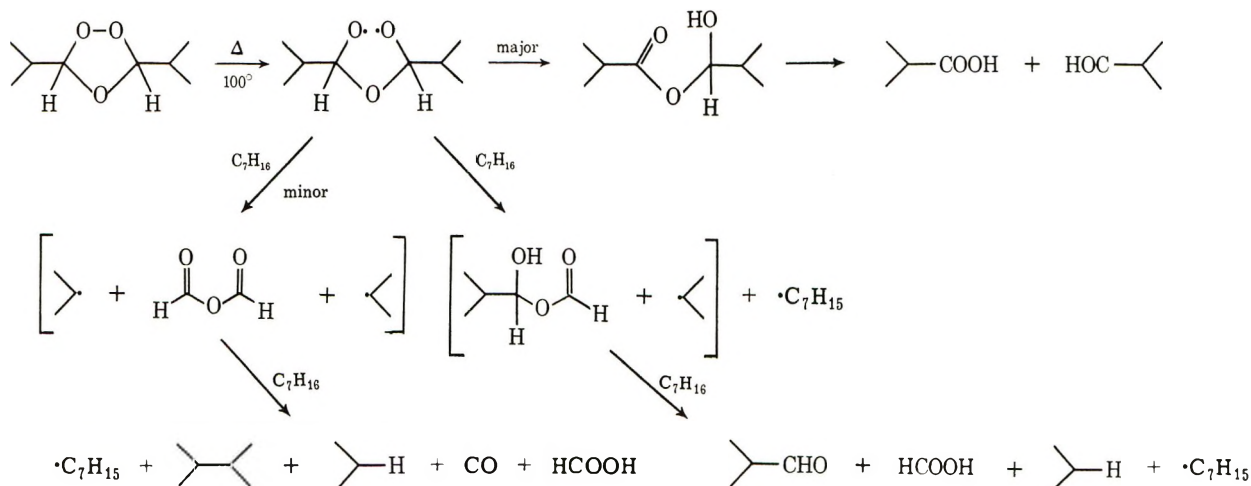
(5) J. Pasero, L. Comeau, and M. Naudet, *Bull. Soc. Chim. Fr.*, 1794 (1963).

(6) E. Briner, G-P. Rossetti, and S. Fliszár, *Helv. Chim. Acta*, **48**, 1076 (1965).

(7) P. R. Story, T. K. Hall, W. H. Morrison, III, and J.-C. Farine, *Tetrahedron Lett.*, 5397 (1968).

(8) P. R. Story, W. H. Morrison, III, T. K. Hall, J.-C. Farine, and C. E. Bishop, *ibid.*, 3291 (1968).

Scheme I



saturated, as evidenced by the bubbling off of the excess ethylene. An  $\text{O}_3\text{-O}_2$  stream was then bubbled through the solution at  $-78^\circ$  at a rate of  $\sim 80$  cc/min and  $5 \times 10^{-5}$  mole of  $\text{O}_3$ /min for about 4 hr (at  $-78^\circ$ ). Ethylene could be detected in the effluent gases, so there was some loss of the olefin. The reaction was stopped upon the appearance of a blue color in the Freon indicating excess  $\text{O}_3$ , which was flushed out by passing  $\text{N}_2$  through the solution. The solvent and any other volatile material were allowed to distil off in a hood overnight by removal of the cooling bath. The product  $\sim 0.25\text{-}0.5$  ml was then fractionated in a vacuum line by bulb-to-bulb distillation to remove nonvolatile polymer, residual solvent, and any other very volatile material. Cooling baths of Dry Ice-isopropyl alcohol and liquid  $\text{N}_2$  were used. Ir spectra of the pure gas taken on a PE Model 225 infrared spectrometer indicated the material to be essentially free of all ketonic-acidic impurities and to be identical with the spectrum of ethylene ozonide obtained by Garvin and Schubert.<sup>9</sup> Less pure samples could be purified by transferring the material to an evacuated 500-ml bulb containing about 0.25 g of  $\text{K}_2\text{CO}_3$  (under vacuum). Agitation of the bulb for a few minutes and subsequent removal of the volatile material revealed it to be free of ketonic-acidic impurities and to be pure ozonide. Little or no loss of ozonide was observed during the above purification. It should be noted that all subsequent steps after the evaporation overnight of the solvent were performed on a vacuum line and the product ozonide was used and stored in the gas phase.

**Propene Ozonide (Ib).** An  $\text{O}_3\text{-O}_2$  stream was bubbled through about 25 ml of Freon 114 and 0.5 ml of propene at  $-78^\circ$  in a cold trap at a rate of  $5 \times 10^{-5}$  mol of  $\text{O}_3$ /min for about 4 hr till the blue color of excess  $\text{O}_3$  was evident. The excess  $\text{O}_3$  was flushed out with nitrogen and the solvent and volatile material were allowed to evaporate overnight. The purification procedure was identical with that of ethylene ozonide, including any

needed treatment with  $\text{K}_2\text{CO}_3$ . The product ir spectrum was again virtually identical with that reported by Garvin and Schubert.<sup>9</sup> It should be noted that the spectrum indicated little if any contamination by cross ozonide products.

**Isobutene Ozonide (Ic).** An  $\text{O}_3\text{-O}_2$  mixture was bubbled through a solution of  $\sim 0.75$  ml of isobutene in 10 ml of Freon 114 at  $-78^\circ$  as described above for about 6 hr. After letting the solvent and volatile material distil off overnight, the residue was purified in the previously described manner. The impurity (acetone) proved more tenacious than previous ketonic impurities but yielded eventually to the Dry Ice-isopropyl alcohol-liquid  $\text{N}_2$  fractionation. The product may have contained a small amount ( $\sim 10\%$ ) of ethylene ozonide as determined by ir. Otherwise the ir spectrum was as reported.<sup>9</sup>

**2-Butene Ozonide (Id).** As above, about 0.75 ml of *trans*-2-butene in about 10 ml of Freon 114 at  $-78^\circ$  was treated with  $\text{O}_3\text{-O}_2$  for about 6 hr. Solvent and volatile material were allowed to evaporate overnight and the material was purified as previously described.

The isolated ozonide used was a mixture of the *cis* and *trans* ozonides; no further purification was attempted. The composition was, on the basis of literature data, about 60% *trans* and 40% *cis* ozonide.<sup>10</sup>

**1,2-Dimethylcyclopentene Ozonide (II).** An  $\text{O}_3\text{-O}_2$  stream was bubbled through a solution of  $\sim 0.6$  ml of 1,2-dimethylcyclopentene in 25 ml of Freon 114 at  $-78^\circ$  for about 4 hr. A white precipitate formed almost immediately upon  $\text{O}_3$  introduction and persisted until the reaction mixture was allowed to warm up during the overnight solvent evaporation. The purification procedure was as previously described. The melting point of the solid was  $-15$  to  $-13^\circ$  and corre-

(9) D. Garvin and C. Schubert, *J. Phys. Chem.*, **60**, 807 (1956).

(10) R. W. Murray, R. D. Youssefeyeh, and P. R. Story, *J. Amer. Chem. Soc.*, **89**, 2429 (1967).

sponded to that of the bicyclic ozonide (lit.<sup>11</sup> mp  $-13.2^\circ$ ).

**Kinetic Apparatus.** The kinetic cell had a path length of 6.3 cm, windows of NaCl fastened to the cell body with Dow Corning Silastic 892 RTV Adhesive/Sealant, and a ground-glass stopcock with an 18/9 ball joint for attachment to a vacuum system. The volume of the cell was about 100 ml with no more than 5% of the cell outside the constant temperature oven.

The oven was a Barnes Eng. Co. (Stamford, Conn.) variable temperature chamber, Model VTC-104 equipped with KBr windows, which proved to be operable up to about  $+120^\circ$ . The temperature within the oven was monitored with an iron-constantan thermocouple attached to a point adjacent to the cell within the oven and read on a Honeywell potentiometer, Model 2732.

Spectra were recorded for kinetic purposes at appropriate time intervals on a Perkin-Elmer Model 21 ir spectrophotometer with an NaCl prism.

**Description of Typical Run.** The oven with the kinetic cell was allowed to equilibrate at the desired temperature overnight while the cell was being evacuated with an oil diffusion pump. A suitable quantity of ozonide was expanded into the vacuum line and then into the kinetic cell. The stopcock on the cell was closed, the oven and cell were transferred to the PE 21 ir spectrometer, and an initial spectrum was taken. The time between the expansion of the ozonide into the cell and the start of the initial spectrum was about 1 min. In most cases the half-life was such that the entire spectrum ( $2.5\text{--}15\ \mu$ ) could be run at appropriate intervals, culminating in a final spectrum after about four-five half-lives. For some temperatures and ozonides the half-lives were short and repeated scans of a limited region ( $5.1\text{--}6.2\ \mu$ ) of the spectrum were made. For some ozonides and temperatures, those with half-lives exceeding 24 hr, points were taken for two-three half-lives and an infinity point was obtained by raising the temperature in the oven for an appropriate amount of time to complete decomposition. The pressure of ozonide in the kinetic cell ranged from 1 to 27 Torr, being generally in the range 2-6 Torr. Rates were obtained from plots of optical density at a particular wavelength *vs.* time for both starting materials and products. The feasible temperature range over which rates could be conveniently studied for a particular ozonide amounted to about  $40^\circ$ .

Where kinetic runs were performed in the presence of an added gas, the sequence of addition to the kinetic cell was that first the ozonide was expanded into the cell, then the desired amount of added gas was expanded into the cell and the run performed as described above.

The one exception to the general procedure was with the 1,2-dimethylcyclopentene ozonide (II). Its rate of decomposition was too slow to measure for any temperature obtainable in the ordinary kinetic cell and

oven. One rate at  $153^\circ$  was obtained, however, using a modified procedure. After taking an initial spectrum of the ozonide in a 10.8-cm long cell with CsI windows, the material in the cell was transferred, using liquid  $N_2$ , to a 500-ml bulb with a Teflon stopcock. The bulb was placed in an oven at  $153^\circ$  for several hours and then the bulb was removed and the material within the bulb was transferred to the 10.8-cm cell at  $25^\circ$  for spectroscopic observation. In this way several data points were obtained. The heat-up and cool-down time of the bulb was negligible in comparison to its reaction half-life of about 30 hr at this temperature.

**Product Identification and Analysis.** For identification purposes the final products from a kinetic run were transferred, using liquid  $N_2$ , to the 10.8-cm long gas-phase cell with CsI windows, and a spectrum taken on a Perkin-Elmer 225 grating infrared spectrometer. The simple molecules, whose spectra were well characterized in the literature, could be readily identified in the product mixtures and accounted for about 90% of these mixtures.

Calibration curves at various pressures and absorbances were made for the various ketonic and acidic products, namely, formic acid, acetic acid, acetaldehyde, and acetone, and were used in conjunction with the final kinetic spectra to obtain quantitative product analyses. For the acids it was also necessary to calibrate the spectra at various temperatures since the spectra varied considerably with temperature. No calibrations were performed for formaldehyde but an approximate concentration was obtained using the pressure and spectrum given by Pierson and coworkers.<sup>12</sup> Also no quantitative product analysis was performed for II since the number of transfers would have made the data somewhat ambiguous.

## Results

Table I lists the various compounds, temperatures, rate coefficients ( $k$ ), and product analyses. For the bicyclic ozonide II, a maximum rate of decomposition was calculated at  $106^\circ$  on the basis of no observed decomposition after about 50 hr at this temperature. Also included in Table I are two experiments in which there were added gases.

The individual kinetic runs all gave linear optical density *vs.* reaction time plots over the time followed, which generally was two-three half-lives, *e.g.*, as shown for ozonide Ic in Figure 1. The rates of decomposition of the ozonides of 2-butene and propene were unaffected by added gases ( $O_2$  and NO, respectively) and, in addition, the product distribution did not change. Also the pressure of starting material had no effect on the rate of decomposition of 2-butene ozonide. Material balance was generally 90% or better, although it was con-

(11) R. Criegee and G. Lohaus, *Chem. Ber.*, **86**, 1 (1953).

(12) R. A. Pierson, A. N. Fletcher, and E. St. Clair Gantz, *Anal. Chem.*, **28**, 1218 (1956).



**Table I:** Products and Rate Coefficients for Ozonide Decomposition

Ozonide	Temp, °C	Amount of ozonide, Torr	Added gas (Torr)	10 <sup>3</sup> k, min <sup>-1</sup>	Products, Torr		
					HCOOH	H <sub>2</sub> CO	
Ethylene ozonide (Ia)	46.0	1.6		0.41 (S, P) <sup>d</sup>	1.5	1.7	
	56.0	2.0		1.46 (S, P)	1.7	1.8	
	71.0	2.1		10.8 (S, P)	1.8	2.0	
	85.0	2.0		40.0 (P)	1.8	2.0	
Propene ozonide (Ib)	59.5	3.7		0.30 (S, P)	HCOOH	CH <sub>3</sub> COOH	CH <sub>3</sub> C(O)H
	74.5	4.1		1.3 (S, P)	3.0	0.4	2.6
	76.0	2.5	NO(17)	2.1 (S, P)	3.3	0.5	2.9
	83.7	5.1		4.2 (S, P)	1.9	0.3	1.9
	99.2	4.6		15.8 (P)	4.1	0.6	4.2
	110.5	4.3		53.4 (P)	3.9	0.6	3.7
Isobutene ozonide (Ic)	70.0	3.0 <sup>a</sup>		0.17 (S, P)	3.5	0.5	3.0
	91.3	1.4		1.07 (P)	CH <sub>3</sub> C(O)CH <sub>3</sub>	HCOOH	
	100.0	2.9		1.8 (S, P)	1.8	1.8	
	109.5	0.94		4.1 (P)	1.3	1.3	
	113.0	2.1		6.5 (S, P)	2.5	2.5	
2-Butene ozonide (Id)	80.0	2.5 <sup>b</sup>		0.112 (S)	CH <sub>3</sub> COOH	CH <sub>3</sub> C(O)H	
	100.0	3.5 <sup>c</sup>		0.66 (S)	1.3	1.3	
	120.0	2.9		3.5 (S)	2.4	3.6	
	120.0	24.0		3.6 (S, P)	2.4	2.9	
	120.0	1.0	O <sub>2</sub> (~100)	3.0 (S)	20.5	27.0	
1,2-Dimethylcyclopentene ozonide (II)	106.0	~2		≤0.002	Cyclopropane	CH <sub>3</sub> C(O)-OC(O)CH <sub>3</sub>	CH <sub>3</sub> COOH
	153	~1		0.38 (P)			

<sup>a</sup> After 2.5 days 0.9 Torr of starting material had decomposed to form 0.9 Torr of HCOOH and 1.2 Torr of (CH<sub>3</sub>)<sub>2</sub>CO. <sup>b</sup> Reaction was followed for a little more than one half-life (125 hr) and there still remained in addition to the amount of product listed 1.1 Torr of starting ozonide. <sup>c</sup> At 27.5 hr 2.1 Torr of ozonide had decomposed to form 2.0 Torr CH<sub>3</sub>CHO and 1.8 Torr CH<sub>3</sub>COOH. <sup>d</sup> S refers to *k* based on decay rate of starting material; P refers to *k* based on production rate of products.

sistently on the low side, implying that other products could have been produced to the extent of about 10%. In the decomposition of II at 153° some of the products identified were cyclopropane, acetic anhydride, and acetic acid. The last product, acetic acid, may have resulted from hydrolysis of the anhydride by adventitious moisture since it seemed to build up at the expense of the anhydride.

Figures 2-5 are plots of the listed rate constants *vs.* 1/*T* from which were calculated activation energies and preexponential factors for each compound as well as rate coefficients at 100°, all of which are listed in Table II. For ozonide II a minimum activation energy, minimum *A* factor, and maximum rate at 100° were calculated using the maximum rate at 106° and the measured rate at 153°. The maximum rate coefficient at 100° is also presented.

### Discussion

It seems clear that the decompositions are unimolecular and first order. The linearity of the kinetic plots and the lack of sensitivity of the rate constants to ozon-

**Table II:** Rate Coefficient Parameters

Compd	<i>k</i> , min <sup>-1</sup> at 100°	<i>k</i> , rel at 100°	<i>E</i> <sub>a</sub> , kcal/mol <sup>a</sup>	Log <i>A</i> , sec <sup>-1</sup> <sup>b</sup>
Ia	2.2 × 10 <sup>-1</sup>	310	27.5	13.60
Ib	1.9 × 10 <sup>-2</sup>	27	25.7	11.55
Ic	2.2 × 10 <sup>-3</sup>	3.1	23.8	9.55
Id	7.0 × 10 <sup>-4</sup>	1	23.4	8.9
II	≤ 1 × 10 <sup>-6</sup>	≤ 0.0014	≥ 36	> 13.3

<sup>a</sup> Uncertainty in *E*<sub>a</sub> is ± 1.5 kcal/mol. <sup>b</sup> Uncertainty in log *A* is ± 1.0.

ide concentration or added gases all imply a simple unimolecular decomposition. The product insensitivity to added NO and O<sub>2</sub> would indicate either noninterceptable radical intermediates or a decomposition which yields the stable molecule products directly.

The mechanism proposed by Story and coworkers,<sup>7,8</sup> and reviewed by Criegee,<sup>13</sup> as depicted in Scheme I is

(13) R. Criegee, *Chimia*, **22**, 392 (1968).

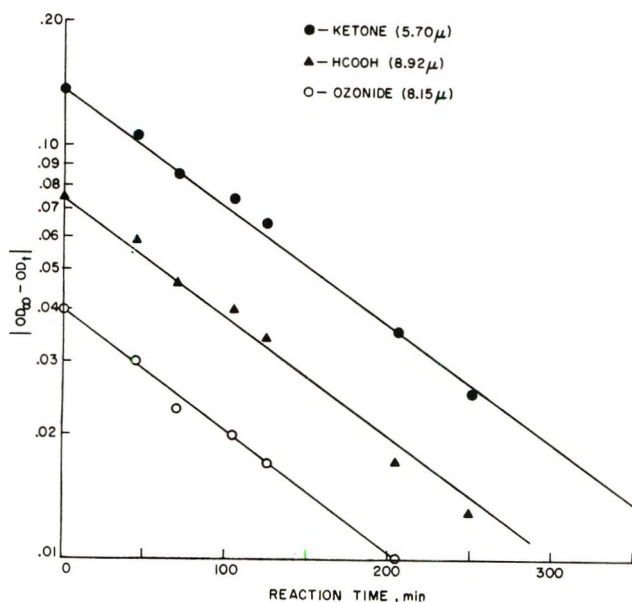


Figure 1. First-order kinetic plot for the decomposition of isobutene ozonide (Ic) at 113° based on reactant decay and product formation.

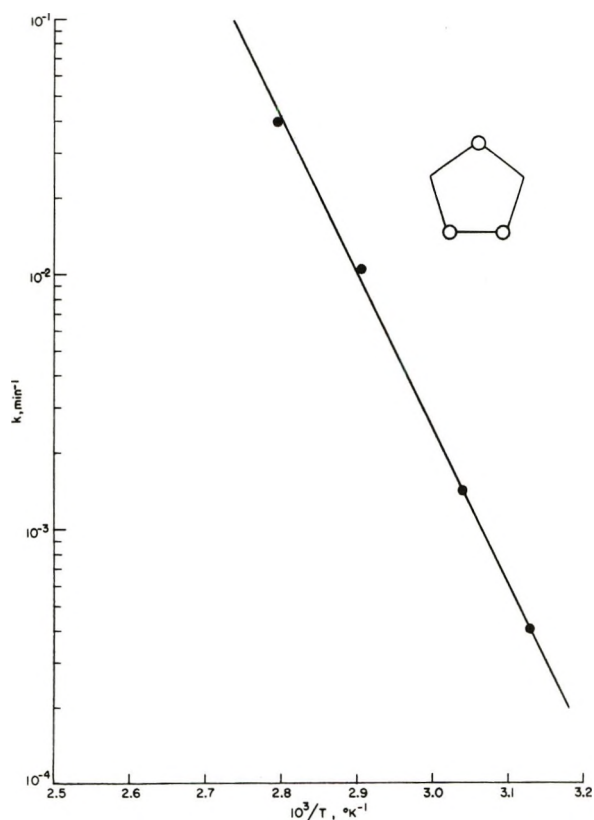


Figure 2. Arrhenius plot for the decomposition of ethylene ozonide.

nearly consistent with the above results. An estimate of a reasonable activation energy for the first step in which a peroxide O-O bond is broken might range somewhere from 32 to 38 kcal/mol. This is estimated either from the activation energies found for simple linear peroxide decompositions which range from about 32 kcal/

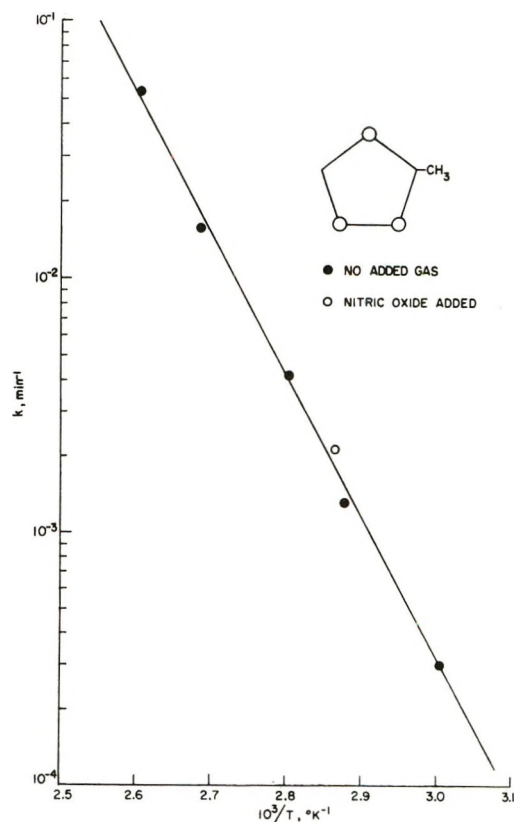


Figure 3. Arrhenius plot for the decomposition of propylene ozonide.

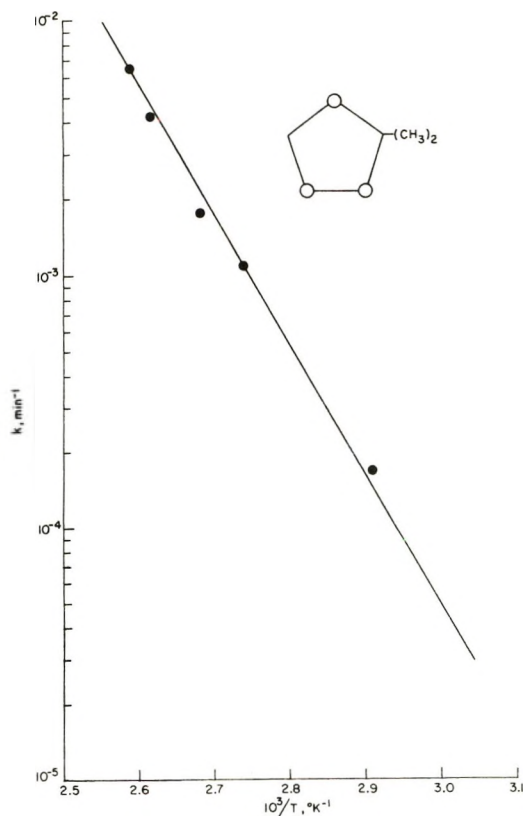


Figure 4. Arrhenius plot for the decomposition of isobutene ozonide.

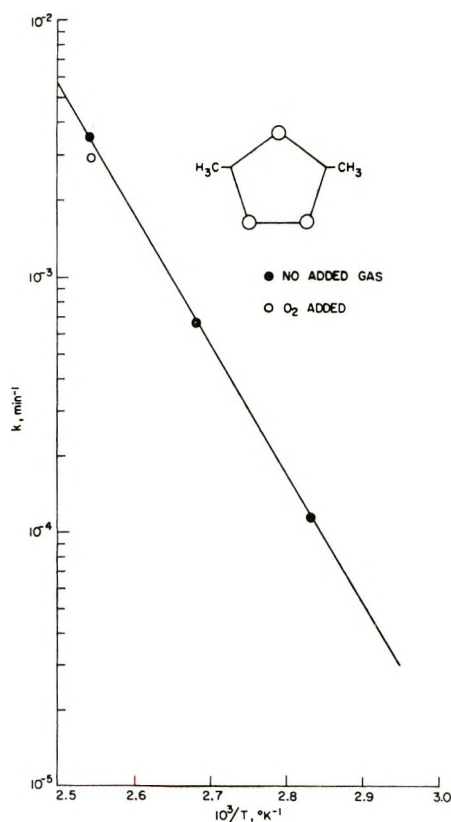


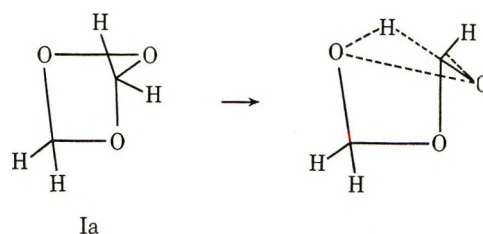
Figure 5. Arrhenius plot for the decomposition of 2-butene ozonide.

mol for diethyl peroxide<sup>14</sup> to about 38 kcal/mol for di-*tert*-butyl peroxide,<sup>15</sup> or from the activation energies found for simple one-bond cleavages for *tert*-butyl peresters which range from about 33 to 38 kcal/mol.<sup>16</sup> It should be noted that, as pointed out by Bartlett and Hiatt<sup>16</sup> in the decomposition of the peresters of the type *tert*-Bu-O-O-CO-R, as the R group is made better able to stabilize a radical and the initial cleavage occurs with a simultaneous two-bond cleavage, the activation energies for decomposition decrease to as low as 23 kcal/mol for R = C<sub>6</sub>H<sub>5</sub>(CH<sub>2</sub>=CH)CH<sub>2</sub>.

The activation energies found for ozonides Ia–Id of 24–27 kcal/mol appear to be significantly inconsistent with an estimate of 32–39 kcal/mol. A possible explanation involving ring strain or an oxygen orbital interaction destabilization of the cyclic peroxide as opposed to the linear peroxides on which the estimates were based is refuted by the observation that the bicyclic ozonide II has a minimum activation energy almost 10 kcal/mol higher than the monocyclic ozonides. At best the trimethylene bridge in II would hold the five-membered trioxalane ring in its most stable least-interacting configuration and at worst the ring could be more strained and held so the oxygens would interact unfavorably. Therefore, at best the bicyclic ozonide would be as stable as the monocyclic ozonides. Its activation energy should therefore be either equal to or

less than that of the monocyclic ozonide. The fact that II has so much higher an  $E_a$  than Ia–Id would indicate the lowering of the activation energy for O–O bond cleavage in Ia–Id is not caused by destabilization of the peroxide bond because of the cyclic nature of the ozonide.

It seems possible instead that the lowered activation energy has its origins in a stabilization of the transition state to decomposition. This lowering could be achieved by making the hydrogen atom transfer synchronous with O–O bond cleavage, as indicated in the figure below for Ia.



The noninterceptability of radical intermediates by O<sub>2</sub> or NO and the very low preexponential factors provide additional support for this proposal. For a cyclic compound to decompose solely by ring bond cleavage, the preexponential factor should be about 10<sup>15</sup> sec<sup>-1</sup>. All of the  $A$  factors for the type-I ozonides are considerably lower than this, and they decrease as substitution increases. Thus, the transition state must be very highly ordered, and H atom transfer must be important in the decomposition process. The varying effects of substitution in ozonides Ia–Id on their respective kinetic parameters can be accounted for on the basis of varying degrees of destabilization of the starting ozonide by steric interference and conflicting requirements in the transition state between compression of the methylene–oxygen distance and stretching of the oxygen–oxygen bond.

The only pathway for decomposition of the bicyclic ozonide II, however, involves exclusive O–O bond breakage to a discrete biradical which is then presented with the possibility of a  $\beta$ -cleavage step yielding cyclopropane and acetic anhydride. Its activation energy of  $\geq 36$  kcal/mol and preexponential factor of  $\geq 2 \times 10^{13}$  sec<sup>-1</sup> is entirely consistent with an initial O–O bond cleavage to a biradical intermediate.

We conclude that in monocyclic ozonides with a substitution pattern such that there is a hydrogen  $\alpha$  to an oxygen, decomposition takes place with some degree of simultaneity between O–O bond cleavage and hydrogen transfer with a consequent lowering of activation

(14) R. E. Rebert and K. J. Laidler, *J. Chem. Phys.*, **20**, 574 (1952).

(15) F. P. Lossing and A. W. Tickner, *ibid.*, **20**, 907 (1952).

(16) P. D. Bartlett and R. R. Hiatt, *J. Amer. Chem. Soc.*, **80**, 1398 (1958).

energy for O-O bond cleavage based on simple peroxide models. In bicyclic and tetrasubstituted ozonides synchronous hydrogen transfer is inhibited or impossible and decomposition takes place *via* a discrete biradical intermediate.

*Acknowledgment.* The authors appreciate a useful conversation with Dr. R. Murray. This work was supported by the Environmental Protection Agency through the Office of Air Programs under Grants No. AP00018 and AP01044, for which we are grateful.

## Quenching of $^3P_1$ Mercury Atoms by Isotopic Aromatic Molecules

by Gilbert J. Mains and Mendel Trachtman\*

Departments of Chemistry, Philadelphia College of Textiles and Science, Philadelphia, Pennsylvania 19144, and Oklahoma State University Stillwater, Oklahoma 74074 (Received October 22, 1971)

Publication costs assisted by Philadelphia College of Textiles and Science

Quenching data are reported for benzene, nine deuterium-substituted benzenes, and three deuterium-substituted toluenes. Attempts to correlate the observed square of collision diameter for the quenching process,  $\sigma^2$ , in terms of simple C-H and C-D bonds and in terms of CH-CH, CH-CD, and CD-CD pairs were unsuccessful. The data were shown to be consistent with a previously proposed mechanism involving exciplex formation and intersystem crossing. An interpretation involving  $^3P_0$  Hg atoms could not be ruled out but was considered unlikely.

### Introduction

Intermolecular transfer of electronic energy is a powerful tool in photochemistry, spectroscopy, and chemical kinetics. More specifically, the technique of mercury photosensitization has proven an invaluable means of generating and studying free radicals near room temperature. Indeed, much of our early knowledge of rate constants for free-radical reactions was obtained this way, and the late E. W. R. Steacie's book, "Atomic and Free Radical Reactions," was a tribute to the power of the method. While much effort has been directed toward the accumulation of data in the subsequent two decades, little progress has been made toward a theoretical understanding of the energy-transfer process. Because of the size of the mercury atom and, hence, the number of assumptions which must be made, there seems little hope of an *ab initio* approach through quantum mechanics even with the high speed computation facilities currently available.

Yang<sup>1</sup> attempted a rationalization of the differences between the energy-transfer (quenching) rates of hydrogen and paraffins in terms of symmetry correlations, treating the (R-H-Hg\*) complex as a nonlinear triatomic system. Vikis and Moser<sup>2</sup> have approached the theoretical problem from the viewpoint of unimolecular rate theory, treating the (R-H-Hg\*) complex as long lived, and assumed applicability of the RRKM theory. Strausz<sup>3</sup> considers the quenching reactions of

excited mercury with paraffins in terms of a simple hydrogen-transfer reaction and has computed potential energies of activation by a modified bond energy-bond order method.

Whereas there is an abundance of quenching data for the excited mercury-paraffin systems, such is far from the circumstance in excited mercury-aromatic hydrocarbon systems. Except for one measurement for benzene, the only broad study of quenching of the  $^3P_1$  Hg\* atoms by aromatic molecules was an earlier report from this laboratory.<sup>4</sup> In this earlier work the reported squares of the collision diameters,  $\sigma^2$ , for the quenching process were shown to be more than 50% greater than those estimated from van der Waals radii. The mechanism which was tentatively advanced to explain these observations, especially the unexpectedly larger quenching rate of C<sub>6</sub>D<sub>6</sub> as compared with C<sub>6</sub>H<sub>6</sub>, involved the formation of a long-lived excited mercury-aromatic exciplex, Hg\*-Ar. It was noted then that the role of  $^3P_0$  Hg atoms in the system was unknown and, until more data were obtained, there was no point in speculating further. The purpose of the present paper is to provide additional Hg\* quenching data for

- (1) K. Yang, *J. Amer. Chem. Soc.*, **89**, 5344 (1967).
- (2) A. C. Vikis and H. C. Moser, *J. Chem. Phys.*, **53**, 2333 (1970).
- (3) O. P. Strausz, private communication, 1972.
- (4) G. J. Mains and M. Trachtman, *J. Phys. Chem.*, **74**, 1647 (1970).

partially deuterated benzenes which, admittedly, will not resolve the question of the role of  $^3P_0$  Hg atoms in these systems, but will contribute information about the effects of deuteration on the quenching process and lend support to the proposed mechanism. (An apparatus to determine the role of  $^3P_0$  Hg atoms in these Hg\*-aromatic hydrocarbon systems is under construction and results from that study will be reported in the future.) The present research is intended as a further contribution to the data on quenching of  $^3P_1$  Hg\* atoms by aromatic hydrocarbon molecules.

### Experimental Section

The apparatus was described previously.<sup>4</sup> Fluorescence measurements, *i.e.*, the determination of the fluorescent photocurrent,  $Q$ , were made randomly at high and low pressures of quenching gas,  $M$ , to avoid systematic errors. The data so obtained were found to be consistent with the modified Stern-Volmer formula developed by Yang.<sup>5</sup> The data were plotted and fitted by the method of least squares to the eq 1, where  $Q$  and  $Q_0$  are the fluorescent photocurrents in the pres-

$$[1 - Q/Q_0]^{-1} = \alpha - \beta[M]^{-1} \quad (1)$$

ence and absence of the quenching gas;  $[M]$  is expressed in moles/liter; and  $\alpha$  and  $\beta$  are constants related to the quenching rate constant,  $k_q$ , and the mean lifetime of  $^3P_1$  Hg\* atoms in the cell,  $\tau$ , by the equation  $\beta = \alpha\tau k_q$ . The ratio of the slope to the intercept,  $\alpha/\beta$ , is a direct measure of the product,  $\tau k_q$ . Since the mean lifetime of the excited mercury atoms can be calculated from the formula derived by Yang<sup>5</sup> for a cell of similar geometry, *i.e.*,  $\tau = \tau_0[1 + 0.25 \times 10^4 pr]$ , where  $\tau_0$  is the mean radiative lifetime of an isolated mercury atom, 0.108  $\mu\text{sec}$ ,  $p$  is the pressure of mercury vapor,  $1.85 \times 10^{-4}$  Torr, and  $r$  is the distance between the irradiated slab of Hg vapor and the window of emerging fluorescence, 3.55 cm in this research,  $k_q$  may be calculated from the observations. Values for the quenching diameter squared,  $\sigma^2$ , can be readily calculated from  $k_q$  from elementary collision theory<sup>6</sup> and are simply related to the quenching cross section,  $\pi\sigma^2/4$ .

The isotopic purity of the benzenes was determined by mass spectrometry using a Consolidated Electrodynamics Corp. Model 21-490 mass spectrometer; isomeric purity was measured by gas chromatography. The isotopic benzenes were found to be 99.5% isotopically pure as certified. No impurities were detected by gas chromatography, and the compounds were therefore used as received.

### Results and Discussion

The results, tabulated as  $\sigma^2$  at 23°, are presented in Table I for benzene and nine deuterated benzenes. Also included are data for three isotopically substituted toluenes. It need be noted that the collision diameters for  $C_6H_6$  and  $C_6D_6$  reported in Table I are larger than

those reported previously.<sup>4</sup> We now report  $\sigma^2$  values of  $49 \pm 3 \text{ \AA}^2$  (compared with  $39 \text{ \AA}^2$ ) and  $74 \pm 2 \text{ \AA}^2$  (compared with  $65 \text{ \AA}^2$ ). The discrepancy is attributed to a lack of statistical precision in the earlier measurements. To avoid such fluctuations in the present work, the data reported in Table I represent no fewer than ten independent experiments for each compound, and the uncertainty limits reflect a 95% confidence level based upon the least-squares fit of the data to eq 1.

Table I: Quenching Data for ( $^3P_1$ ) Hg at 23°

Quencher	$\sigma^2, \text{ \AA}^2$	Quencher	$\sigma^2, \text{ \AA}^2$
$C_6H_6$	$48 \pm 3$	1,3,4,5- $C_6H_2D_4$	$60 \pm 1$
$C_6H_5D_1$	$57 \pm 3$	$C_6HD_5$	$71 \pm 2$
1,2- $C_6H_4D_2$	$65 \pm 2$	$C_6D_6$	$74 \pm 2$
1,3- $C_6H_4D_2$	$56 \pm 5$	$C_6D_5CH_3$	$74 \pm 2$
1,4- $C_6H_4D_2$	$51 \pm 3$	$C_6H_5CD_3$	$46 \pm 2$
1,3,5- $C_6H_3D_3$	$54 \pm 2$	$C_6D_5CD_3$	$58 \pm 3$
1,2,4,5- $C_6H_2D_4$	$72 \pm 2$		

Certain observations need be made regarding the data of Table I. First, while there seems to be a general increase in  $\sigma^2$  as deuterium is added to benzene, the variation is not a linear function of the composition. Thus, any attempt to correlate collision diameters with the numbers of C-H and C-D bonds, successfully applied to aliphatic hydrocarbons<sup>7</sup> is doomed to failure *ab initio*. The difference in  $\sigma^2$  for the ortho, meta, and para isomers of  $C_6H_4D_2$  are quite outside experimental uncertainties and a clear indication of structural effects. Similarly, the differences between the quenching diameter squared for the two structural isomers of  $C_6H_2D_4$  reinforces the existence of structural effects.

The remarkable enhancement of quenching efficiencies whenever two deuterium atoms were substituted in adjacent positions on the benzene ring, *e.g.*, 1,2- $C_6H_4D_2$ , 1,2,4,5- $C_6H_2D_4$ , 1,3,4,5- $C_6H_2D_4$ , and higher deuterated benzenes, suggested that the energy-transfer process might be linked to *pairs* of deuterium atoms located on the aromatic ring. Accordingly, an attempt was made to correlate the observed  $\sigma^2$  data in terms of contributions from the ring structure plus contributions from adjacent CH-CH, CH-CD, and CD-CD sites on the quenching molecule. For example, the square of the quenching diameter for *o*- $C_6H_4D_2$  would be written as the sum  $\sigma_{ring}^2 + 2\sigma_{HD}^2 + 3\sigma_{HH}^2 + \sigma_{DD}^2$ . In this system one would expect identical quenching cross sections for *m*- and *p*- $C_6H_4D_2$  and, indeed, this is observed within the statistical precision of the data. Unfortunately, one would also predict identical values of

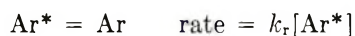
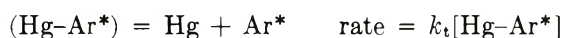
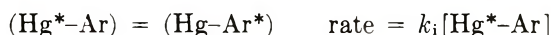
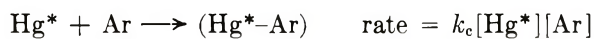
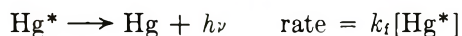
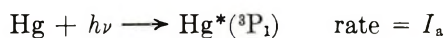
(5) K. Yang, *J. Amer. Chem. Soc.*, **87**, 5294 (1965).

(6) C. K. Yang, *ibid.*, **88**, 4575 (1966).

(7) H. E. Gunning and O. P. Strausz, *Advan. Photochem.*, **1**, 253 (1963).

$\sigma^2$  for the two isomers of  $C_6H_2D_4$ , and this is far from the observation. The para isomer (for H's) has a significantly larger quenching diameter squared than the meta isomer, 72 vs. 60  $\text{\AA}^2$ ! The extension of the correlation to larger structural features, for example to CH-CH-CH type sites, was distasteful and hardly warranted by the data currently available.

While not simply correlatable, the data are understandable in terms of the mechanism advanced earlier, viz.



where it was suggested that variation in  $k_Q$ , i.e., in  $\sigma^2$ , could be rationalized in terms of the fraction of exciplex complexes,  $\text{Hg}^*-\text{Ar}$ , which undergo a type of intersystem crossing to the exciplex,  $\text{Hg}-\text{Ar}^*$ , before decomposing back to  $\text{Hg}^*$  and unexcited aromatic molecule, Ar.

Since the energy levels of aromatic molecules, especially benzene, are well understood, it is possible to identify  $\text{Ar}^*$  as the  $^3B_{1u}$  state which, like the  $^1B_{2u}$ , can only be coupled to the ground state with an  $e_{2g}$  vibration. If we assume the vibration is the  $\nu_{18}$  vibration, as suggested in Herzberg's book<sup>8</sup> and diagrammed earlier by Herzberg,<sup>9</sup> one might expect  $k_i$  to be extremely sensitive to substitution in the 1, 2, 4, and 5 positions. Indeed, the data of Table I confirm this expectation. With the exception of perdeuteriotoluene, which may be ruled out on other bases, all molecules which have at least the 1, 2, 4, and 5 sites deuterated exhibit  $\sigma^2$  values near 70  $\text{\AA}^2$ . Furthermore, all molecules which have at least the 1, 2, 4, and 5 positions protiated exhibit  $\sigma^2$  near 50  $\text{\AA}^2$ . Intermediate cases with fewer than four deuterium atoms at the 1, 2, 4, and 5 sites are intermediate in  $\sigma^2$  and often overlap, so that the order of increasing  $\sigma^2$  is uncertain. Thus, the data of Table I are at least consistent with the mechanism proposed earlier.

It would be satisfying if the  $\sigma^2$  data correlated with the values of  $k_i$  deduced from phosphorescence lifetime measurements and which formed the basis for predictions by Martin and Kalantar<sup>10</sup> for partially deuterated benzenes. Unfortunately, the predicted orders for the *o*-, *p*-, and *m*- $C_6H_4D_2$ , 1,3,5- $C_6H_3D_3$ , and the  $C_6D_4H_2$  compounds are not consistent in Table I. The reasons for this are possibly attributable to phase effects in the phosphorescence measurements. In spite of this, the data in Table I do strongly suggest that the quenching efficiency is related to the probability of intersystem crossing in the aromatic molecule and, in the case of benzenes, involves the vibronic transition  $^1A_{1g} \rightarrow ^3B_{2u}$ . Presumably, the intersystem crossing takes place in the loose collision complex ( $\text{Hg}^*-\text{Ar}$ ).

The authors are cognizant that a mechanistic antagonist would argue that the data of Table I are also explainable in terms of a mechanism involving the metastable  $^3P_0$  state of Hg. However, it would be necessary to postulate that molecules with deuterium atoms in the 1, 2, 4, and 5 ring sites are more efficient in producing  $^3P_0$  atoms than those with hydrogen atoms in these positions. While the authors deem this possibility highly unlikely, they concede the possibility and are undertaking direct measurement of  $^3P_0$  atoms in these systems. Final resolution of this question must be left to a future publication. Based upon the data presented in Table I, the authors favor the exciplex intersystem crossing mechanism suggested originally.  $\text{Hg}_2^*$  excimers are well known<sup>3</sup> in irradiated mercury vapor systems, and recently<sup>11</sup>  $\text{HgO}_2^*$  has been suggested as a long-lived complex in the photooxidation of isotopically excited mercury. These recent observations add credibility to the exciplex mechanism.

*Acknowledgments.* The assistance of R. Gill and G. Reisz in some of the measurements reported here is greatly appreciated. The authors wish to thank the Research Corporation for financial support of this research.

(8) G. Herzberg, "Electronic Spectra and Electronic Structure of Polyatomic Molecules," Van Nostrand, Princeton, N. J., 1966, p 398.

(9) G. Herzberg, "Infrared and Raman Spectra of Polyatomic Molecules," Van Nostrand Co., Princeton, N. J., 1945, p 113.

(10) Cited in J. B. Birks, "Photophysics of Aromatic Molecules," Wiley-Interscience, New York, N. Y., 1970, p 249.

(11) J.-Pierre Morand, Ph.D. Thesis, University of Paris, Orsay, France, 1971.

# Photochemistry of Ethanethiol at 254 and 214 nm<sup>1</sup>

by Lamar Bridges, Gregory L. Hemphill, and John M. White\*

Department of Chemistry, The University of Texas at Austin, Austin, Texas 78712 (Received January 26, 1972)

Publication costs assisted by Robert A. Welch Foundation

Quantum yields of products produced by the photolysis of ethanethiol at 254 and 214 nm have been measured. The major products include hydrogen, ethane, and hydrogen sulfide with ethylene as a minor product. Adding either *n*-butane or helium reduces the yields of ethane, ethylene, and hydrogen sulfide while the yield of hydrogen increases. When photolyzing pure ethanethiol, no pressure dependence is observed. There is, however, a wavelength dependence; the hydrogen quantum yield drops from 0.82 at 254 nm to 0.75 at 214 nm while the quantum yields of ethane, ethylene, and hydrogen sulfide increase. The results are interpreted in terms of a mechanism involving excited hydrogen and ethyl radicals.

## Introduction

In conjunction with investigations of energy partition in the photodissociation of ethanethiol<sup>2</sup> we have studied in detail the primary photochemical processes involved at 254 and 214 nm. These wavelengths were selected because (1) they were used in the energy partition experiments, (2) previous quantum yield studies were available at 254 nm,<sup>3</sup> (3) the absorption spectrum of C<sub>2</sub>H<sub>5</sub>SH suggests that different electronic states may be involved at these two wavelengths, and (4) no data were available at 214 nm.

Steer and Knight<sup>3</sup> have reported a detailed investigation of the photolysis of C<sub>2</sub>H<sub>5</sub>SH at 254 nm. They conclude that the only important primary process is scission of the S-H bond to furnish H and C<sub>2</sub>H<sub>5</sub>S radicals. Dzantiev, *et al.*,<sup>4</sup> in a similar study suggest that scission of the C-S bond is also important and occurs with a quantum yield on the order of 0.1.

We report here the results of our quantum yield and mechanistic studies and suggest a single mechanism with wavelength dependent quantum yields of S-H and C-S bond rupture.

## Experimental Section

All experiments were performed at room temperature (298 ± 3°K) using gas-phase ethanethiol. The reaction vessel for the 254-nm experiments (5 cm diameter and 15 cm long) was constructed of fused quartz with Suprasil windows. At 214 nm a cell of the same dimensions was used except a chemical filter section 5 cm in length was added. The vessels were filled on a standard mercury-free vacuum line pumped by an oil diffusion pump to base pressures near 1 × 10<sup>-6</sup> Torr. This vacuum line was separated from a mercury manometer by means of a magnetic reluctance pressure transducer. Reagent pressures were measured with the manometer by nulling the transducer.

The light sources were a low-pressure Hg resonance lamp (254 nm) and a low-pressure Zn resonance lamp

(214 nm). A Corning 7910 Vycor filter was used with the Hg lamp to remove the 185-nm line. The 203- and 206-nm lines were filtered from the Zn lamp spectrum with 150 Torr of *cis*-2-butene.

Ethanethiol was purified by degassing and distilling under vacuum from -84 (ethyl acetate slush) to -117° (ethanol slush). The middle third was retained and stored in a U-tube at -196°. Reagent grade hydrogen iodide, hydrogen bromide, and butane were thoroughly degassed before use. Reagent grade helium was used directly from the cylinder.

After photolysis the reaction vessel was immersed in liquid nitrogen, connected to a Toepler pump, and the noncondensable gases were pumped into a calibrated volume ( $V = 5.14 \pm 0.06$  cm<sup>3</sup>). The pressure was measured on a mercury manometer with a cathetometer (uncertainty ±0.04 Torr). This sample was then analyzed on a calibrated CEC 21-614 residual gas analyzer. Then the liquid nitrogen bath was replaced with an ethanol slush bath and the vapor phase was pumped off and analyzed as above. Mercury transfer from the Toepler pump to the reaction vessel was eliminated by placing a trap at -78° between the two. In a test photolysis no products were observed when *n*-butane was exposed to 254-nm light (a result confirming that Hg-sensitized reactions were not occurring).

In one set of experiments diethyl disulfide (C<sub>2</sub>H<sub>5</sub>-SSC<sub>2</sub>H<sub>5</sub>) was photolyzed and a search for C<sub>2</sub>H<sub>5</sub>SH was made using gas chromatography. Use was made of a 20% tricresyl phosphate on Chromosorb W column and a thermal conductivity detector. Helium was used as a carrier gas.

(1) Supported in part by the Robert A. Welch Foundation.

(2) (a) J. M. White, R. L. Johnson, Jr., and D. Bacon, *J. Chem. Phys.*, **52**, 5212 (1970); (b) J. M. White and R. L. Johnson, Jr., *ibid.*, **56**, 3787 (1972).

(3) R. P. Steer and A. R. Knight, *Can. J. Chem.*, **47**, 1335 (1969).

(4) B. G. Dzantiev, A. V. Shiskov, and M. S. Unukovich, *Khim. Vys. Energ.*, **3**, 111 (1969).

## Actinometry

Quantum yields were based on chemical actinometry using either HBr or HI photolysis for which the quantum yield of H<sub>2</sub> formation is taken as unity throughout the wavelength range we used.<sup>5-8</sup> The following mathematical relationship was utilized

$$\Phi_i = \frac{[C_i]t_a(1 - 10^{-\alpha_a p_a l})}{[C_a]t_i(1 - 10^{-\alpha_x p_x l})} \Phi_a \quad (1)$$

where *i* refers to one of the products of C<sub>2</sub>H<sub>5</sub>SH photolysis, *a* refers to the actinometer photolysis, and *x* refers to ethanethiol. Φ<sub>*i*</sub> is the quantum yield, C<sub>*j*</sub> the photolysis product concentration, *t<sub>j</sub>* the photolysis time, α<sub>*j*</sub> the extinction coefficient, *p<sub>j</sub>* the reaction vessel pressure, and *l* the length of the reaction vessel.

Photolysis times were selected to minimize errors in the quantum yield measurements due to the absorption of the 214 and 254 nm light by diethyl disulfide, a major product. In the photolysis of pure ethanethiol, less than 1% of the thiol was decomposed except at the lowest pressures (less than 100% absorption by the thiol) where decomposition approached 3%. The percent decomposition of the ethanethiol in the experiments with added *n*-butane was about 2.5% at 254 nm and less than 1% at 214 nm. The HI and HBr decompositions ranged from less than 1% to about 3%.

It is not possible to adequately collimate the light sources used in these experiments without a large sacrifice of intensity since they are low-pressure discharge sources which do not closely approximate point sources. Therefore, we chose to make no collimation; rather we carried out actinometer and ethanethiol photolyses sequentially choosing the actinometer and ethanethiol pressures to make α<sub>*a*</sub>*p<sub>a</sub>* = α<sub>*x*</sub>*p<sub>x</sub>* for each pair of experiments. In this way the absorption of the diverging radiation is identical in both the actinometer experiment and the ethanethiol experiment for *any* path through the reaction vessel. In particular, absorption along paths passing through the side of the reaction vessel are equivalent. In this way we avoided the problem of numerically evaluating the contribution of these nonaxial paths for either the actinometer or the ethanethiol. In order to keep α<sub>*a*</sub>*p<sub>a</sub>* = α<sub>*x*</sub>*p<sub>x</sub>* constant at convenient pressures HI was used as the actinometer at 254 nm while HBr was used at 214 nm.

As a test of the above procedure the quantum yield for H<sub>2</sub> production in the photolysis of H<sub>2</sub>S was determined at 254 nm using HBr as the actinometer. The resulting value Φ<sub>H<sub>2</sub></sub> = 1.03 ± 0.03 is in excellent agreement with the literature value.<sup>9</sup> A further experimental test of this method using a collimated source is described in the following section of this paper.

Extinction coefficients for C<sub>2</sub>H<sub>5</sub>SH, H<sub>2</sub>S, HI, and HBr were determined using a Cary 14 spectrometer and are given in Table I. The values reported for H<sub>2</sub>S, HBr, and HI are in good agreement with litera-

Table I: Extinction Coefficients (Torr<sup>-1</sup> cm<sup>-1</sup>)

Molecule	254 nm	214 nm
C <sub>2</sub> H <sub>5</sub> SH	(3.32 ± 0.04) × 10 <sup>-3</sup>	(1.35 ± 0.03) × 10 <sup>-2</sup>
H <sub>2</sub> S	(1.01 ± 0.04) × 10 <sup>-5</sup>	
HI	(5.82 ± 0.02) × 10 <sup>-3</sup>	
HBr	(5.87 ± 0.02) × 10 <sup>-5</sup>	(6.57 ± 0.04) × 10 <sup>-3</sup>

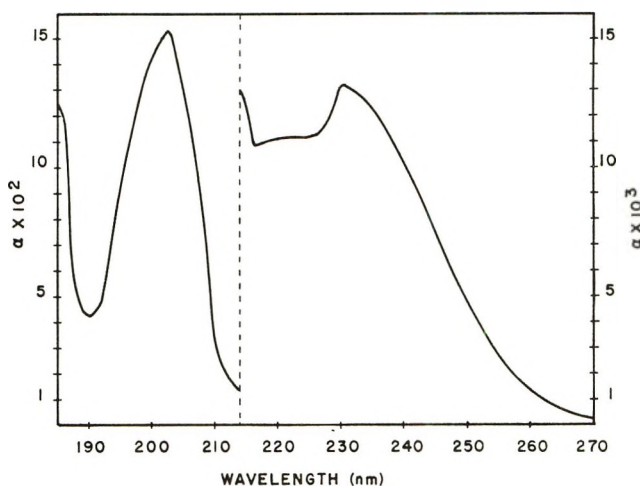


Figure 1. The absorption spectrum of ethanethiol with the extinction coefficient defined as α = log(I<sub>0</sub>/I)/*p*(Torr)*l*(cm).

ture values.<sup>10,11</sup> Figure 1 shows the wavelength dependence of the ethanethiol extinction coefficient.

## Results

*Photolysis of Pure Ethanethiol.* Mass spectrometry was used to measure H<sub>2</sub>, C<sub>2</sub>H<sub>6</sub>, H<sub>2</sub>S, and C<sub>2</sub>H<sub>4</sub> at both wavelengths. The only other product observed, diethyl disulfide, was not measured quantitatively. It is possible that thioacetaldehyde is formed but it would not have been detected under our conditions. Other data<sup>3</sup> may be interpreted as indicating that it is at most a very minor product. All the measured products except hydrogen are condensable at -196°, thus only H<sub>2</sub> was observed in the first pump-off described above. The other products were quantitatively recovered from the cell at ethanol slush temperatures (-117°). This was demonstrated using prepared mixtures whose composition approximated that produced by photolysis. Figures 2 and 3 summarize the quantum yields of these

(5) J. G. Calvert and J. N. Pitts, Jr., "Photochemistry," Wiley, New York, N. Y., 1966, p 782.

(6) R. M. Martin and J. E. Willard, *J. Chem. Phys.*, **40**, 2999 (1964).

(7) G. S. Forbes, J. E. Cline, and B. C. Bradshaw, *J. Amer. Chem. Soc.*, **60**, 1431 (1938).

(8) W. A. Noyes, Jr., and P. A. Leighton, "The Photochemistry of Gases," Dover, New York, N. Y., 1966, p 83.

(9) Reference 5, p 202.

(10) C. F. Goodeve and N. O. Stein, *Trans. Faraday Soc.*, **27**, 393 (1931).

(11) B. J. Hebert and R. M. Martin, *J. Phys. Chem.*, **72**, 3046 (1968).



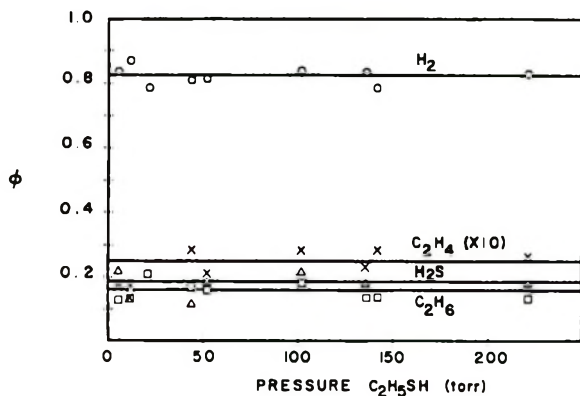


Figure 2. Quantum yields,  $\phi$ , of products from the photolysis of pure ethanethiol at 254 nm vs. pressure of ethanethiol: hydrogen,  $\circ$ ; ethane,  $\square$ ; hydrogen sulfide,  $\Delta$ ; and ethylene (multiplied by 10),  $\times$ .

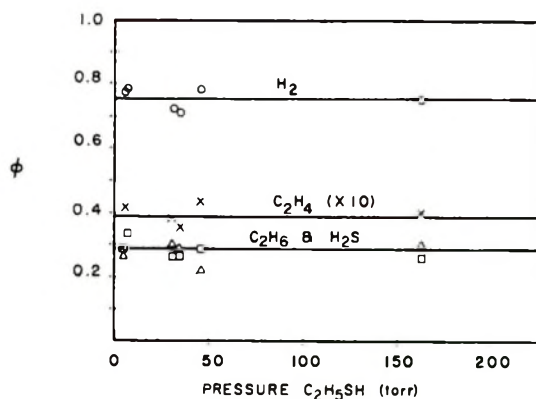


Figure 3. Quantum yields,  $\phi$ , of products from the photolysis of pure ethanethiol at 214 nm vs. pressure of ethanethiol: hydrogen,  $\circ$ ; ethane,  $\square$ ; hydrogen sulfide,  $\Delta$ ; and ethylene (multiplied by 10),  $\times$ .

four products at the two wavelengths employed. We note no detectable variation with pressure of the quantum yield of any product. Table II summarizes the average values of the measured quantum yields with no regard for reactant pressure. The data at 254 nm are in disagreement with those of Steer and Knight<sup>3</sup> who report  $\Phi_{H_2} = 0.97 \pm 0.03$  and give quantum yields of the other products based on this value and relative yields with respect to hydrogen.

In view of this discrepancy and as a further test of our experimental procedures described above, we made a separate determination of the hydrogen quantum

Table II: Average Quantum Yields

Wave-length, nm	$\Phi_{H_2}$	$\Phi_{C_2H_6}$	$\Phi_{H_2S}$	$\Phi_{C_2H_4}$
254	$0.82 \pm 0.02$	$0.16 \pm 0.02$	$0.19 \pm 0.03$	$0.025 \pm 0.006$
214	$0.75 \pm 0.03$	$0.28 \pm 0.03$	$0.28 \pm 0.02$	$0.038 \pm 0.004$

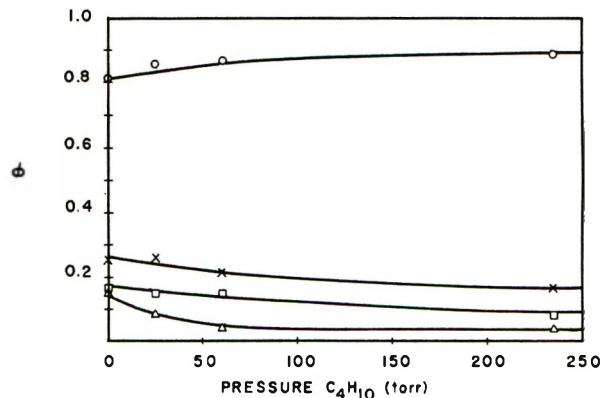


Figure 4. Quantum yields,  $\phi$ , of products as a function of the pressure added *n*-butane for the photolysis of ethanethiol at 254 nm: hydrogen,  $\circ$ ; ethane,  $\square$ ; hydrogen sulfide,  $\Delta$ ; and ethylene (multiplied by 10),  $\times$ .

yield at 254 nm using a collimated light source comprised of a high-pressure mercury arc-monochromator combination. The monochromator furnished a 6.4-nm band pass centered at 254 nm. Using HBr actinometry and eq 1 with  $\alpha_x p_x \neq \alpha_a p_a$  the quantum yield of  $H_2$  was determined as 0.85 in good agreement with the value given in Table II. In the calculation leading to the quantum yield, account was taken of the intensity distribution in the transmitted band and the wavelength variation of extinction coefficients of  $C_2H_5SH$  and HBr.

In one group of experiments at 214 nm the intensity of the light source was varied by a factor of 2 with no change in the quantum yields of the four measured products listed above. In view of this the mechanism proposed below contains no reactions leading to intensity dependent quantum yields.

*Photolysis of Ethanethiol-Thermalizer Mixtures.* In order to evaluate the role played by excited atoms and polyatomic free radicals, we carried out a series of photolyses in which either *n*-butane or helium was added as an energy transfer agent. A blank run at 254 nm using 200 Torr of *n*-butane gave no products and ruled out the possibility of any extra hydrogen being produced by the photolysis of the butane. Also, since the quantum yield of  $H_2$  produced in the photolysis of a 5:1 mixture of *n*-butane and HI was not different from  $\Phi_{H_2}$  for pure HI, no extra hydrogen is produced by reactions of hot H atoms with the butane. Figure 4 and Table III summarize the results obtained with *n*-butane at 254 nm. Table IV lists data collected at 214 nm. The addition of *n*-butane results in a slight increase in the quantum yield of  $H_2$  with accompanying decreases in  $C_2H_6$ ,  $H_2S$ , and  $C_2H_4$  production. Because of interference due to *n*-butane, the recovery of  $H_2S$  was not quantitative, so a short study was made using He as a thermalizing agent at 214 nm. The results listed in Table V show that helium has the same qualitative effect as *n*-butane, namely, its addition lowers the yields of  $C_2H_6$ ,  $H_2S$ , and  $C_2H_4$ . The yield

**Table III:** Photolysis of Ethanethiol and *n*-Butane at 254 nm

PETSH	$\rho_{C_4H_{10}}$	$\Phi_{H_2}$	$\Phi_{C_2H_6}$	$\Phi_{H_2S}$	$\Phi_{C_2H_4}$
42.98	234.7	0.89	0.088	0.038	0.017
43.70	59.42	0.87	0.15	0.048	0.022
43.70	25.09	0.86	0.15	0.09	0.026
43.45	0	0.81	0.17	0.12	0.029

**Table IV:** Photolysis of Ethanethiol and *n*-Butane at 214 nm

PETSH	$\rho_{C_4H_{10}}$	$\Phi_{H_2}$	$\Phi_{C_2H_6}$	$\Phi_{H_2S}$	$\Phi_{C_2H_4}$
46.00	238.76	0.79			
33.80	209.75	0.78	0.19	0.12	0.012
46.19	133.26	0.80	0.14	0.099	0.024
33.29	83.87	0.75	0.22	0.14	0.026
33.32	75.09	0.72	0.21	0.16	0.014
36.24	68.48	0.77	0.21	0.15	0.012
33.68	40.92	0.75	0.22	0.14	0.022
32.50	0	0.72	0.26	0.30	0.039
33.69	0	0.71	0.25	0.29	0.044

**Table V:** Photolysis of Ethanethiol and Helium at 214 nm

PETSH	$\rho_{He}$	$\Phi_{C_2H_6}$	$\Phi_{H_2S}$	$\Phi_{C_2H_4}$
33.70	205.8	0.23	0.23	0.018
31.10	93.55	0.22	0.24	0.017
Arbitrary <sup>a</sup>	0	0.28	0.28	0.039

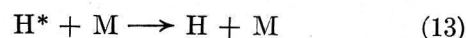
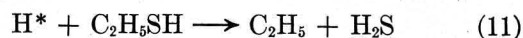
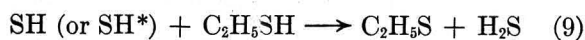
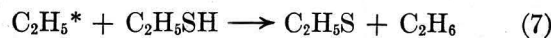
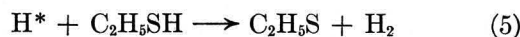
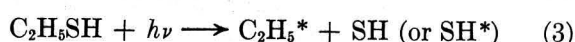
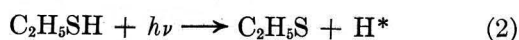
<sup>a</sup> From Table II.

of  $H_2S$  is the same as or slightly larger than the yield of  $C_2H_6$ . Hydrogen yields were not measured in these experiments with added helium.

*Photolysis of  $C_2H_5SSC_2H_5$  in the Presence of  $C_2H_5SH$ .* In a separate kind of experiment we photolyzed  $C_2H_5SSC_2H_5$  in the presence of  $C_2H_5SH$  at 300 nm using the high-pressure Hg arc-monochromator arrangement described above. At this wavelength the disulfide absorbs while the mercaptan is transparent. Using a reactant ratio  $[C_2H_5SSC_2H_5]/[C_2H_5SH] = 0.12$  the photolysis products were analyzed in the same manner as in the photolysis of pure  $C_2H_5SH$ . No  $H_2$ ,  $C_2H_6$ ,  $C_2H_4$ , or  $H_2S$  was detected. In a separate photolysis of pure  $C_2H_5SSC_2H_5$ , gas chromatographic analysis of the products showed small amounts of  $C_2H_5SH$  as the only measurable product.

## Discussion

Considering the above results, we propose the following mechanism as being consistent with all of our observations.



In this mechanism M is taken to include  $C_2H_5SH$ ,  $C_4H_{10}$ , and He. The species bearing asterisks represent energetic non-Boltzmann species. A steady-state treatment of the above mechanism furnishes the following relations.

$$\Phi_{H_2} = \frac{k_4[C_2H_5SH] + k_{12}[M]}{(k_4 + k_{10})[C_2H_5SH] + k_{12}[M]} \Phi_1 \quad (15)$$

$$\Phi_{C_2H_6} = \Phi_2 + \frac{k_{10}[C_2H_5SH]\Phi_1}{(k_4 + k_{10})[C_2H_5SH] + k_{12}[M]} \quad (16)$$

$$\Phi_{C_2H_4} = \Phi_3 + \frac{k_{11}[C_2H_5SH]\Phi_2}{(k_6 + k_{11})[C_2H_5SH] + k_{13}[M]} \quad (17)$$

$$\Phi_{H_2S} = \Phi_2 + \Phi_3 + \frac{k_{11}[C_2H_5SH]\Phi_2}{(k_6 + k_{11})[C_2H_5SH] + k_{13}[M]} + \frac{k_{10}[C_2H_5SH]\Phi_1}{(k_4 + k_{10})[C_2H_5SH] + k_{12}[M]} \quad (18)$$

$$\Phi_{H_2} + \Phi_{C_2H_6} = \Phi_1 + \Phi_2 = 1 - \Phi_3 \quad (19)$$

$$\Phi_{C_2H_6} + \Phi_{C_2H_4} = \Phi_{H_2S} \quad (20)$$

In these expressions  $\Phi_1$ ,  $\Phi_2$ , and  $\Phi_3$  are the quantum efficiencies of processes 2, 3, and 4 of the mechanism. Our results listed in Table II are in agreement with eq 19 and 20. Equation 19 predicts, as observed, that the sum of the hydrogen and ethane quantum yields will be very close to unity when ethylene production is very small. Equation 20 predicts that the quantum yields for hydrogen sulfide and ethane production will be very nearly equal under the same circumstances. Equations 15–18 predict, as shown in the figures, that the addition of thermalizing gases will increase the yield of  $H_2$  and decrease the yields of  $C_2H_6$ ,  $H_2S$ , and  $C_2H_4$ . Further, eq 19 predicts that the sum of the hydrogen and ethane yields should be independent of the butane or helium pressure. The data are consistent with this.

Our results at 254 nm compare quite favorably in a qualitative fashion with those of Steer and Knight.<sup>3</sup> Even quantitatively, the product ratios agree quite well and the major point of disagreement is in the quan-

tum yield for hydrogen formation which we determine as 0.82 while they find 0.97. This difference is of crucial importance in mechanistic considerations because a hydrogen quantum yield of unity independent of substrate pressure would rule out reactions 3 and 4 of our mechanism. To account for their observed ethane, ethylene, and hydrogen sulfide, Steer and Knight<sup>3</sup> propose a sequence of reactions involving excited disulfide molecules formed by the recombination of  $C_2H_5S$  radicals.



These excited molecules then either react with  $C_2H_5SH$  to form various products including  $C_2H_5$ , SH,  $C_2H_4$ , and  $H_2S$  or are thermalized in a series of nonreactive collisions. Our quantum yield data, on the other hand, readily admit reactions 3 and 4 as primary processes at both 254 and 214 nm. Furthermore, our observation of no  $H_2S$ ,  $C_2H_4$ , and  $C_2H_6$  when we photolyze  $C_2H_5SSC_2H_5$  in the presence of  $C_2H_5SH$  rules out the importance of reactions with ethanethiol of excited disulfide molecules. We conclude this on the basis that photolysis of  $C_2H_5SSC_2H_5$  leads to excited disulfide molecules *via* recombination of  $C_2H_5S$  radicals.<sup>12,13</sup> We have, therefore, eliminated reactions of excited disulfide molecules from our mechanism, but have included several reactions of excited atoms and radicals. Hot hydrogen atoms have been shown earlier<sup>2</sup> to be important in the photochemistry of ethanethiol. Reaction 11 is proposed to account for the increase in hydrogen yield and decrease in ethane yield as the system is thermalized. The counterpart of 11 involving thermal hydrogen atoms is expected to play a minor role in comparison to reaction 6.

It is not unreasonable to assume that a significant portion of the available excess energy appears as internal excitation of the ethyl radical when reaction 3 occurs.<sup>14,15</sup> This reaction may also produce excited SH radicals; however, our observations do not require it and the mechanism assumes that excited and thermal HS radicals have the same fate. The competition between reactions 12 and 14 is postulated as an explanation of the observed decrease in ethylene yield with thermalizing agent. They do not influence the net yield of ethane. Being about 9 kcal/mol endothermic 12 is postulated to involve only excited ethyl radicals.

The only sulfur containing product observed other than  $H_2S$  was diethyl disulfide; therefore, the proposed mechanism includes hydrogen atom abstraction reactions involving only the sulfhydryl hydrogen of the substrate. If hydrogens other than sulfhydryl are abstracted from the thiol, our results indicate that the resulting radicals regenerate ethanethiol and an ethylthiyl radical in subsequent encounters; *i.e.*, the net result is the abstraction of a sulfhydryl hydrogen.

It is well known<sup>16,17</sup> that hot hydrogen atoms can abstract H from *n*-butane to form  $H_2$ . This reaction, for our experiments, is equivalent to thermalization because it leads to  $H_2$  formation and is therefore indistinguishable from the combination of reactions 13 and 6. Further, any butyl radicals thus formed will most likely abstract H from  $C_2H_5SH$  to re-form *n*-butane and furnish a  $C_2H_5S$  radical just as the sequence of reactions 13 and 6. Thus in spite of the fact that some hot hydrogens will react with *n*-butane the overall effect is indistinguishable from nonreactive thermalization.

It is possible to estimate  $\Phi_1$ ,  $\Phi_2$ , and  $\Phi_3$  using the experimental data and the postulated mechanism. Equation 15 predicts that the hydrogen quantum yield approaches  $\Phi_1$  when M is large (M other than  $C_2H_5SH$  in this case). Tables III and IV suggest that  $\Phi_1$  is about 0.9 at 254 nm and about 0.8 at 214 nm. Using these values and applying eq 16 at large moderator pressure we estimate  $\Phi_2 \simeq 0.09$  at 254 nm and 0.19 at 214 nm. By difference  $\Phi_3$  is estimated as 0.01 at both wavelengths.

The fraction X of hot H atoms that undergo reaction 11 can be estimated in two ways. First using the above estimates for  $\Phi_1$  and  $\Phi_2$  and the measured  $\Phi_{C_2H_6}$  for pure ethanethiol photolysis, *i.e.*, eq 16

$$X = \frac{k_{10}}{k_4 + k_{10} + k_{12}} = \frac{\Phi_{C_2H_6} - \Phi_2}{\Phi_1} \quad (21)$$

This relation furnishes  $X = 0.091$  and  $0.088$  at 254 and 214 nm, respectively. Alternately eq 15 can be used for the case of pure ethanethiol photolysis together with the above estimates of  $\Phi_1$  to give

$$X = 1 - \Phi_{H_2}/\Phi_1 \quad (22)$$

Our data furnish  $X = 0.09$  and  $0.10$  at 254 and 214 nm, respectively, in good agreement with estimates based on eq 21. The average initial translational energy,  $E_0$ , of hydrogen atoms produced in reaction 2 is wavelength dependent. At 254 and 214 nm the values of  $E_0$  are  $1.00 \pm 0.04^{2a}$  and  $1.48 \pm 0.04^3$  eV, respectively. If the above estimates of X are assumed correct then by implication the ratio  $k_{10}/k_4$  is a slowly varying function of hydrogen atom energy in the range  $E_0 = 1.0$ – $1.5$  eV.

Similarly the fraction Y of  $C_2H_6$  molecules produced by reaction 11 may be estimated in two ways.

$$Y = (\Phi_1 - \Phi_{H_2})/\Phi_{C_2H_6} \quad (23)$$

(12) P. M. Rao, J. A. Copeck, and A. R. Knight, *Can. J. Chem.*, **45**, 1369 (1967).

(13) K. Sayamol and A. R. Knight, *ibid.*, **46**, 999 (1968).

(14) R. E. Rebert and P. Ausloos, *J. Chem. Phys.*, **47**, 2849 (1967).

(15) P. C. Kobrinsky and R. M. Martin, *ibid.*, **48**, 5728 (1968).

(16) R. G. Gann and J. Dubrin, *ibid.*, **47**, 1867 (1967).

(17) L. E. Compton, J. L. Gole, and R. M. Martin, *J. Phys. Chem.*, **73**, 1158 (1969).

$$Y = (\Phi_{C_2H_6} - \Phi_2)/\Phi_{C_2H_6} \quad (24)$$

Equation 3 leads to  $Y = 0.47$  and  $0.31$  at 258 and 214 nm while eq 24 gives  $Y = 0.48$  and  $0.27$ . The fraction of  $C_2H_6$  molecules produced by reaction 12 is estimated from  $(1 - \Phi_2/\Phi_{C_2H_6})$  as 0.047 at 254 nm and 0.104 at 214 nm. These data lead us to the conclusion that the photochemistry of ethanethiol involves three primary processes and a set of hot reactions.

Examining Figure 1 we find that at 214 nm two electronic states appear to be involved in absorption. These states have been discussed by Clark and Simpson<sup>18</sup> and characterized as non-Rydberg transitions with the low-energy transition considered to involve promotion of a nonbonding sulfur electron to an antibonding molecular orbital. The higher energy band is described as promotion from a bonding C-S local

orbital to an antibonding H-S orbital. The implications of the differences in these excitations for the dissociation of ethanethiol are not clear particularly since they relate directly to the excitation process and only indirectly to the dissociation process. From our data the primary processes do vary somewhat in passing from the weak band centered near 230 nm into the wing of the band centered at 200 nm. The effect is not strong, however. It will be of considerable interest to investigate the primary processes at 185 nm since Clark and Simpson<sup>18</sup> describe this band as a local C-S excitation. Assuming this to be the case we might expect C-S bond cleavage to predominate at this wavelength.

(18) L. B. Clark and W. T. Simpson, *J. Chem. Phys.*, **43**, 3666 (1965).

## Effect of Ionic Dissociation of Organic Compounds

### on Their Rate of Reaction with Hydrogen Atoms<sup>1</sup>

by P. Neta and Robert H. Schuler\*

*Radiation Research Laboratories, Center for Special Studies and Department of Chemistry, Mellon Institute of Science, Carnegie-Mellon University, Pittsburgh, Pennsylvania 15213 (Received March 13, 1972)*

*Publication costs assisted by Carnegie-Mellon University and the U. S. Atomic Energy Commission*

Further development of the steady-state *in situ* radiolysis-esr method for the determination of H atom reaction rate constants has enabled measurements to be made in neutral solutions. It is possible, in many cases, to use  $H_2PO_4^-$  to convert  $e_{aq}^-$  into H atoms at pH 7. With certain organic solutes, however, scavenging of  $e_{aq}^-$  by the solute interferes with this conversion and it is necessary to use only the low-residual H atom yield with a corresponding reduction in sensitivity of the measurements. Representative organic solutes have been examined and it is found that only in the cases where acid-base equilibria are involved does the rate constant depend on pH. Typically increases of a factor of  $\sim 2-3$  are observed for the simple organic acids and amino acids upon conversion of COOH to  $COO^-$ . Only in the case of oxalic acid was the rate constant found to decrease in going from pH 1 to 7. Deprotonation of the  $NH_3^+$  group results in an increase in the rate of abstraction from the  $\alpha$  position by a factor of  $\sim 10$  and the rate of addition to aromatic rings by a factor of  $\sim 5$ . Effects in aromatic and heterocyclic systems are, for the most part, relatively small (a factor of 1-3). Formic and barbituric acids are exceptional in that their rate constants for reaction with H atoms increase by two orders of magnitude with an increase in pH over the range of 1-7. The rate constant for reaction of H with  $OH^-$  has been measured to be  $1.5 \times 10^7 M^{-1} sec^{-1}$ .

### Introduction

A steady-state electron spin resonance method for the determination of rate constants for reaction of H atoms in acidic solutions has recently been developed.<sup>2</sup> This method is based on the measurement of the decrease caused by the addition of solutes on the esr signals of H atoms observed during continuous irradiation

of aqueous solutions. Rate constants in acidic solutions (mostly at pH 1) have been measured for many

(1) Supported in part by the U. S. Atomic Energy Commission. Presented at the 20th Radiation Research Society Meeting, Portland, Ore., May 1972.

(2) P. Neta, R. W. Fessenden, and R. H. Schuler, *J. Phys. Chem.*, **75**, 1654 (1971).

organic compounds<sup>2-4</sup> including a considerable number of compounds of biochemical interest.<sup>4</sup> In the latter case, however, it is important to know the rate constants in neutral solution should a biological system be under consideration. Possible changes in rate constants in going from acidic to neutral solutions have been estimated<sup>4</sup> by analogy with the pH effects on the reaction of OH radicals but an experimental verification is still lacking. Only compounds which undergo acid-base equilibria are expected to have pH-dependent rate constants. It is the purpose of the present study to investigate the effect of ionic dissociation on the rate constants for reaction of H atoms.

### Experimental Section

The details of the measurement of the H atom signal by the steady-state *in situ* radiolysis-esr technique have been described previously.<sup>2</sup> In general the intensity of the low-field (inverted) hydrogen line was examined at a continuous dose rate in the range  $10^{19}$ – $10^{20}$  eV g<sup>-1</sup> sec<sup>-1</sup> and the reduction in this intensity at appropriate solute concentrations was observed. The kinetic experiments and treatment of the data are generally similar to the previous ones<sup>2-4</sup> except for adjustment of the pH. All the organic chemicals used were of the same grade as those used previously.<sup>2-4</sup>

In most of the studies at pH 7 phosphate has been used both to buffer the solution and to convert  $e_{aq}^-$  to H atoms *via* the reaction



which has a rate constant of  $7.7 \times 10^6$  M<sup>-1</sup> sec<sup>-1</sup>.<sup>5</sup> The second pK of phosphoric acid is 7.2 so that slightly more than 50% of the phosphate is in the form of  $H_2PO_4^-$  at pH 7. Buffer solutions made from available samples of  $K_2HPO_4$  and  $Na_2HPO_4$  showed relatively small H atom signals, apparently because of impurities in these samples. The maximum signals in the presence of phosphate were obtained by using Baker Analyzed  $KH_2PO_4$  and adjusting the pH to the desired value by adding either Baker Analyzed KOH or HClO<sub>4</sub>. Experiments at pH 1 showed that addition of 0.1 M of this phosphate had only a small effect on the H atom signals (*vide infra*) so that complicating effects of impurities are presumably at a minimum.

### Results and Discussion

In acidic solutions the signal-to-noise ratio of the H atom esr lines is  $\sim 50$ :1.<sup>2</sup> In neutral solutions, where the yield of residual H atoms is only  $\sim 15\%$  as great, a proportionately smaller signal is observed<sup>6</sup> and direct measurement of H atom rate constants by the steady-state esr methods is limited to relatively unreactive compounds. One desires, therefore, to include in the irradiation system a reagent that is capable of converting  $e_{aq}^-$  into H atoms in near neutral solutions. We have explored the use of  $H_2PO_4^-$  as an H atom

source in the esr experiment and found it to be adequate for this purpose for cases where the rate constant of reaction of the solute with  $e_{aq}^-$  is not more than 10 times its rate constant for reaction with H atoms. Where the rate constant for reaction with  $e_{aq}^-$  is greater, either very large corrections have to be made or measurements have to be carried out utilizing only the low yield of residual H atoms. A number of studies have been carried out to examine the properties of the esr experiment at pH values above 1. The rate constants for reaction of a number of representative carboxylic acids, amino acids, amines, and heterocyclic compounds with H atoms have been measured at pH 7 for comparison with the values previously determined at pH 1.

In most of these studies the low-field (inverted) H atom line has been examined but in cases where the high-field line was also examined it was found to have comparable intensity. In principle this experiment is based on a competition between chemical reaction of H atoms and decay with time of the nonequilibrium population of the H atom electron-nuclear spin levels which gives rise to abnormally intense esr signals. Previously the kinetics was treated on the assumption that this decay involved only a relaxation process and was exponential. At this writing it now appears that spin polarization is produced upon partial reaction of the H atoms.<sup>7</sup> Decay of the esr signals will therefore not be purely exponential and the mathematical treatment of the competition kinetics is necessarily somewhat more complex than that given previously. With scavenger present the concentration of H atoms is controlled, to a large extent at least, by reaction with the scavenger and it would appear that the expressions previously used to intercompare the relative rate constants for different compounds do describe the competitive situation quite well.<sup>2</sup>

*Dependence of H Atom Signal on pH and  $[H_2PO_4^-]$ .* Initially it was necessary to investigate the effect of pH and of phosphate concentration on the esr signals of the H atoms in the absence of scavengers. In neutral, as in acidic solutions,<sup>2</sup> the signals observed under steady-state conditions are found to be proportional to the production rate of H atoms. The effect of phosphate concentration on the intensity of the H atom signal is shown in Figure 1 for both solutions. The relative values in the absence of phosphate are given by the limiting dashed lines in the figure. At pH 1 the observed signal corresponds to an H atom yield of 3.65.<sup>8</sup> In neutral solutions the relative signal

(3) P. Neta and R. H. Schuler, *J. Amer. Chem. Soc.*, **94**, 1056 (1972).

(4) P. Neta and R. H. Schuler, *Radiat. Res.*, **47**, 612 (1971).

(5) M. Anbar and E. J. Hart, *Advan. Chem. Ser.*, No. **81**, 79 (1968).

(6) P. Neta, R. W. Fessenden, and R. H. Schuler, *Nature (London), Phys. Sci.*, **237**, 46 (1972).

(7) R. W. Fessenden, private communication.

(8) See, e.g., M. Anbar in "Fundamental Processes in Radiation Chemistry," P. Ausloos, Ed., Interscience, New York, N. Y., 1968, p 651.

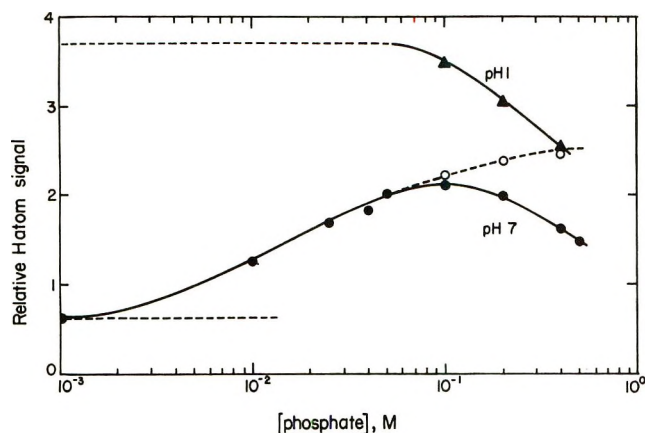


Figure 1. Effect of phosphate concentration on the relative intensity of the low-field (inverted) H atom signal: ●, measurements at pH 7; ▲, measurements at pH 1. The limiting values in the absence of phosphate are given by the dashed lines on the left. At pH 7 this latter value was determined with the use of 2 mM N<sub>2</sub>O to remove e<sub>aq</sub><sup>-</sup>. The open circles represent the data at pH 7 corrected for the decrease in signal observed at pH 1 upon the addition of phosphate.

which corresponds to the residual H atom yield cannot be determined directly because, in the absence of a buffer, H<sup>+</sup> ion produced by the radiolysis builds up and acts as an e<sub>aq</sub><sup>-</sup> scavenger, artificially increasing the observed H atom signal. One can proceed either by adding a buffer which cannot act as an H atom source or by removing e<sub>aq</sub><sup>-</sup>. As described below nitrous oxide was used as a competing electron scavenger and a signal intensity corresponding to the generally accepted value of  $G_H = 0.6^8$  was observed.

Addition of phosphate to deoxygenated water increases the H atom signal gradually. With a  $1 \times 10^{-3}$  M solution the period for reaction of e<sub>aq</sub><sup>-</sup> with H<sub>2</sub>PO<sub>4</sub> is  $\sim 100$  μsec and at the dose rates of these experiments the majority of the electrons disappear by mutual recombination or by reaction with radiolytically produced H<sub>2</sub>O<sub>2</sub>. In general, at low concentrations of electron scavenger the distribution of the electrons among the various possible reaction paths is complex and depends critically upon beam current and other experimental details. Increase in the phosphate concentration above  $10^{-3}$  M results in an increased signal. One, however, never reaches the plateau expected from the signal observed in acidic solutions in the absence of phosphate. A maximum signal of about 60% of this expected value is found in the region of  $10^{-1}$  M phosphate. At higher concentrations a drop in signal is observed and this drop is, to some extent, similar to the decrease observed upon the addition of phosphate at pH 1. It is not clear at this point whether this latter effect is the result of scavenging of the H atom by the phosphate itself or by chemical or magnetic impurities in the phosphate. The curve at pH 1 indicates that the rate constant for reactions of H atoms with phos-

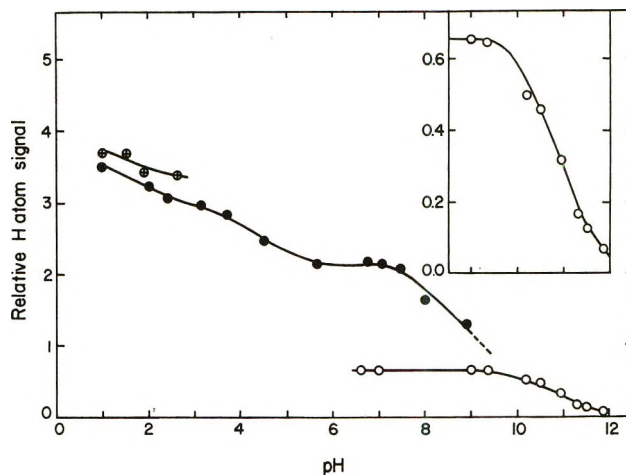


Figure 2. Effect of pH on the relative intensity of the H atom signal: ●, in the presence of 0.1 M phosphate; ⊖, in the absence of phosphate; ○, in the absence of phosphate but in the presence of 2 mM N<sub>2</sub>O to remove e<sub>aq</sub><sup>-</sup>. The insert shows the latter data on an expanded scale along with a curve calculated on the assumption that reduction results simply from scavenging of H· by OH<sup>-</sup> with a rate constant of  $1.5 \times 10^7$  M<sup>-1</sup> sec<sup>-1</sup>.

phoric acid is  $\leq 10^4$  M<sup>-1</sup> sec<sup>-1</sup>. For practical purposes a phosphate concentration near the maximum at 0.1 M was chosen for further study of the neutral system.

The effect of pH on the H atom signal from 0.1 M phosphate solutions is shown by the solid circles in Figure 2. The three ionization equilibria in phosphoric acid have p*K* values of 2.12, 7.21, and 12.67. In the pH region 1–4 a decrease in signal results from a decrease in the rate of scavenging by H<sup>+</sup> so that, as mentioned above, other terminating reactions become more important. Above pH 4 reaction 1 dominates over direct reaction of e<sub>aq</sub><sup>-</sup> with H<sup>+</sup> and a modest plateau results. The pronounced drop in the region of pH 8 is the result of the conversion of H<sub>2</sub>PO<sub>4</sub><sup>-</sup> into HPO<sub>4</sub><sup>2-</sup> which reacts much more slowly with e<sub>aq</sub><sup>-</sup> and is ineffective in converting e<sub>aq</sub><sup>-</sup> into H atoms.

The decrease in signal observed at pH >10 (Figure 2) is caused by the reaction of H with OH<sup>-</sup> and is used to calculate the rate constant for this reaction (see below). The occurrence of this latter reaction, however, effectively limits the range in which the esr experiment is applicable to pH values below 10.

*Kinetic Experiments in the Presence of Phosphate.* The relative rate constants for the reaction of H with different solutes can be obtained from plots of  $(H_0/H - 1)$  vs. concentration where  $H$  and  $H_0$  are the relative H atom signals per unit current of electron beam observed in the presence and absence of added solute (see ref 2). Ethanol served as a reference and was measured with each set of experiments. The concentration of ethanol at which there was a 50% decrease in signal, *i.e.*,  $(H_0/H - 1) = 1$ , was found to be  $4.4 \times 10^{-4}$  M within  $\pm 10\%$  in all experiments in acid and neutral solutions

Table I: Rate Constants for the Reaction of Hydrogen Atoms in Aqueous Solutions

Compound	pK <sub>a</sub> values	k <sub>H</sub> at pH 1 <sup>a</sup>	k <sub>H</sub> at pH 7	k <sub>H</sub> at pH 7/ k <sub>H</sub> at pH 1
Ethanol	15.5	2.6 × 10 <sup>7</sup>	(2.6 × 10 <sup>7</sup> ) <sup>b</sup>	(1.00)
Methanol	15.5	1.6 × 10 <sup>6</sup>	1.6 × 10 <sup>6</sup>	1.00
Hexanol	~15	1.04 × 10 <sup>8</sup>	1.0 × 10 <sup>8</sup>	1.0
Hexylamine	10.6	3.5 × 10 <sup>7</sup>	3.5 × 10 <sup>7</sup>	1.0
Formic acid	3.75	7.5 × 10 <sup>6</sup> <sup>c</sup>	1.3 × 10 <sup>8</sup>	176 <sup>d</sup>
Acetic acid	4.75	8.4 × 10 <sup>4</sup>	4.2 × 10 <sup>5</sup>	6.0
Propionic acid	4.87	6.4 × 10 <sup>6</sup>	1.8 × 10 <sup>7</sup>	2.8
Isobutyric acid	4.86	2.6 × 10 <sup>7</sup>	5.9 × 10 <sup>7</sup>	2.3
Hexanoic acid	4.83	4.6 × 10 <sup>7</sup>	5.3 × 10 <sup>7</sup>	1.15
Glycolic acid	3.83	1.8 × 10 <sup>7</sup>	4.0 × 10 <sup>7</sup>	2.2
Succinic acid	4.21, 5.64	3.5 × 10 <sup>6</sup>	1.1 × 10 <sup>7</sup>	3.2
Oxalic acid	1.27, 4.27	4.1 × 10 <sup>5</sup>	≤ 4 × 10 <sup>4</sup> <sup>e</sup>	≤ 0.1
Glycine	2.3, 9.6	8 × 10 <sup>4</sup>	9 × 10 <sup>4</sup> <sup>e</sup>	1.1
Valine	2.3, 9.7	9 × 10 <sup>6</sup>	1.3 × 10 <sup>7</sup>	1.4
Aspartic acid	1.9, 3.9, 9.7	8 × 10 <sup>5</sup>	2.9 × 10 <sup>6</sup>	3.6
Glutamic acid	2.1, 4.2, 9.6	1.7 × 10 <sup>6</sup>	5.6 × 10 <sup>6</sup>	3.3
Histidine	1.8, 6.0, 9.2	4.8 × 10 <sup>7</sup> <sup>f</sup>	2.5 × 10 <sup>8</sup>	5.2
Aminoacetonitrile	5.34	6.6 × 10 <sup>8</sup>	5.6 × 10 <sup>7</sup>	8.5 <sup>g</sup>
Ascorbic acid	4.1, 11.8	1.1 × 10 <sup>8</sup>	3-6 × 10 <sup>8</sup> <sup>h</sup>	3-6
Benzoic acid	4.17	8.5 × 10 <sup>8</sup>	9.2 × 10 <sup>8</sup>	1.1
Aniline	4.6	4.9 × 10 <sup>8</sup>	2.6 × 10 <sup>9</sup>	5.3
Pyridine	5.2	2.2 × 10 <sup>8</sup>	6.5 × 10 <sup>8</sup>	3.0
Uracil	9.4, ~12	2.8 × 10 <sup>8</sup>	2-3 × 10 <sup>8</sup> <sup>i,j</sup>	~1
Cytosine	4.45, 12.2	9 × 10 <sup>7</sup>	1.0-1.5 × 10 <sup>8</sup> <sup>i</sup>	1.1-1.7
Adenine	4.2, 9.8	8.3 × 10 <sup>7</sup>	0.9-1.5 × 10 <sup>8</sup> <sup>i</sup>	1.1-1.8
Adenosine	3.4, 13	1.1 × 10 <sup>8</sup>	1.4-2 × 10 <sup>8</sup> <sup>i</sup>	1.3-1.8
Barbituric acid	4.03	2.0 × 10 <sup>7</sup>	2.0 × 10 <sup>9</sup>	100
OH <sup>-</sup>			1.5 × 10 <sup>7</sup> <sup>k</sup>	

<sup>a</sup> Previously reported in ref 2-4 (except for aminoacetonitrile). <sup>b</sup> Used as a reference for calculating the other rate constants. <sup>c</sup> The rate constant for formic acid is  $4.5 \times 10^6 M^{-1} \text{sec}^{-1}$ . The value measured at pH 1 contains 40% contribution from the formate ion (see Figure 3). <sup>d</sup> A ratio  $k_{\text{HCOO}^-}/k_{\text{H}^+\text{HCOOH}} = 270$  is calculated from the limiting values derived in Figure 3. <sup>e</sup> Measured using the residual hydrogen atom signal only. All other measurements in phosphate buffered solutions. <sup>f</sup> Rate constant of  $5.1 \times 10^7 M^{-1} \text{sec}^{-1}$  was measured at pH 3. <sup>g</sup> A ratio of 11 can be estimated for the hydrogen abstraction from position  $\alpha$  to the amino as compared to the ammonium group if a correction for the H addition to the cyano group is made (see text). <sup>h</sup> The uncertainty is due to lack of data on the rate constant for  $e_{\text{aq}}^- + \text{ascorbic}$  and correction for this reaction was made using estimated limits. <sup>i</sup> Error is large because of a major correction for  $e_{\text{aq}}^-$  reaction. <sup>j</sup> A value of  $2.4 \times 10^8 M^{-1} \text{sec}^{-1}$  in neutral solution has recently been measured by a competitive technique (L. K. Patterson and K. M. Bansal, *J. Phys. Chem.*, submitted for publication). <sup>k</sup> Measured at pH 10.5-11.5 without phosphate (see text).

and in the presence or absence of phosphate. This fact shows that the ratio of the rate constant for the reaction of H atoms with ethanol to the constant which describes the relaxation of the H atom signal (see ref 2) is independent of pH. It is reasonable to assume, particularly since the rate constant for reaction of H atoms with ethanol is not expected to be dependent on pH, that in fact both constants are invariant. It is noted, for example, that the rate constant for reaction of OH with ethanol is pH independent.<sup>9</sup> We have assumed here that the rate constants are inversely proportional to the concentration ( $[S]_{1/2}$ ) at which the H atom signal is reduced by 50% with the value of  $4.4 \times 10^{-4} M$  observed for ethanol being taken as representative of a rate constant of  $2.6 \times 10^7 M^{-1} \text{sec}^{-1}$ , i.e.,  $k = 1.14 \times 10^4 ([S]_{1/2})^{-1}$ .

In order to examine the validity of the relative rates obtained with the phosphate system at pH 7 it seemed

desirable to study several additional compounds which are expected to have the same rate constants in neutral and in acidic solutions. Methanol and hexanol (both with a  $pK > 15$ ) and hexylamine (as  $C_6H_{13}NH_3^+$  with  $pK = 10.6$ ) served this purpose. In fact the two alcohols and the hexylamine all gave the same competition curves in neutral as in acidic solution (as did ethanol). The rate constants calculated from the data at pH 7 are given in Table I and are seen to be identical with those measured at pH 1. It is seen that where no ionization equilibria are involved there is no apparent dependence of the rate constant on pH. These studies indicate that no difficulty is introduced by using phosphate to convert  $e_{\text{aq}}^-$  to H atoms and thus it becomes possible to make measurements in neutral solution over

(9) M. Anbar and P. Neta, *Int. J. Appl. Radiat. Isotopes*, **18**, 493 (1967).

a wide range of solutes with approximately the same ease as was possible in the more acidic solutions. Measurements on some 20 additional compounds at pH 7 are reported in Table I.

In the above it must be noted, however, that the test solutes do not react rapidly with  $e_{aq}^-$ . In certain cases where  $e_{aq}^-$  reacts with the solute much more rapidly than does H, reduction in the H atom signal will result from scavenging of  $e_{aq}^-$  by the solute in competition with  $H_2PO_4^-$  rather than by H atom scavenging. At 0.1 M phosphate and pH 7 the pseudo-first-order rate constant for reaction 1 is  $(7.7 \times 10^6)(0.05) = 3.9 \times 10^5 \text{ sec}^{-1}$ . For compounds such as oxalate, glycine, and the pyrimidines appreciable scavenging of H atoms occurs only at concentrations where the pseudo-first-order rate constant for reaction of  $e_{aq}^-$  with these compounds is  $>10^5 \text{ sec}^{-1}$  so that it is necessary to make a very significant correction for this latter reaction. Unless indicated otherwise in Table I the corrections for this effect were less than 10%.

*Kinetic Experiments in the Absence of Phosphate.* Because of the above complication it was decided to attempt measurements in neutral solutions containing no phosphate and to use the small residual yield of H atoms in the competition. In these experiments it was necessary to scavenge the electrons and remove them as a source of H atoms and as a complication in the terminating reactions.  $N_2O$  was used for this purpose. The initial experiments with  $N_2O$ -saturated solutions (0.02 M  $N_2O$ ) gave an H atom signal which corresponded to a yield of 0.5. Since the reported rate constants for reaction of H atoms with  $N_2O$  are  $10^4$ – $10^5 M^{-1} \text{ sec}^{-1}$  a drop in signal as high as ~20% might occur as the result of H atom scavenging by the  $N_2O$ . To examine this possibility a solution saturated with 10%  $N_2O$  in  $N_2$  (*i.e.*, 2 mM in  $N_2O$ ) was irradiated and the signal found to increase to a value corresponding to a yield of 0.64. This value is, within experimental error, in agreement with the generally accepted residual H atom yield of 0.6.<sup>8</sup> At pH 1 addition of 2 mM of  $N_2O$  caused no significant decrease in the H atom signal while saturation with  $N_2O$  resulted in ~30% decrease. The  $N_2O$  had been shown mass spectrometrically to contain <0.01%  $O_2$  so that this latter decrease is the result both of H atom and  $e_{aq}^-$  scavenging by the  $N_2O$ . Results in neutral solution with 25, 50, and 100%  $N_2O$  in  $N_2$  indicate that the decrease in signal is proportional to the  $N_2O$  concentration and that the rate constant for H atom scavenging by  $N_2O$  is  $\sim 1 \times 10^5 M^{-1} \text{ sec}^{-1}$ . The effect of this scavenging at 2 mM  $N_2O$  is negligibly small in the competitive experiments.

The effect of ethanol on the signal of the residual H atoms again showed a fractional reduction similar to that in the other experiments. By reference to this result the rate constant for reaction of H atoms with glycine was determined to be  $9 \times 10^4 M^{-1} \text{ sec}^{-1}$ , a value which is essentially identical with that found at

pH 1. Similar experiments were carried out with potassium oxalate but in this case no  $N_2O$  was necessary because the oxalate itself acted to scavenge the electrons without producing H atoms. A rate constant of  $\leq 4 \times 10^4 M^{-1} \text{ sec}^{-1}$  was found. This example is the only one in which the rate constant decreased in going to neutral solution.

The use of the signal of the residual H atoms is limited to solutes which react with rate constants  $< 2 \times 10^8 M^{-1} \text{ sec}^{-1}$ . For more reactive solutes, because the initial signals are small, the signals remaining at the lowest concentrations at which practical studies can be carried out ( $\sim 10^{-4} M$ ) are insufficient for accurate measurement (*i.e.*, less than twice the noise). This is unfortunate since meaningful measurements cannot be made easily in neutral solution on many of the interesting aromatic and heterocyclic compounds which react rapidly with H atoms but which also react rapidly with  $e_{aq}^-$ .

*Reaction of H with  $OH^-$ .* The rate constant for the H +  $OH^-$  reaction was determined in 2 mM  $N_2O$  solutions in the absence of phosphate by comparing the H atom signal over the pH range 9–12 with that at pH 7. The data obtained are presented by the open circles in Figure 2. As is seen in the insert a good competition plot was obtained and from this a rate constant of  $1.5 \pm 0.5 \times 10^7 M^{-1} \text{ sec}^{-1}$  is determined. This value is in reasonable agreement with previous determinations ( $\sim 2 \times 10^7 M^{-1} \text{ sec}^{-1}$ ).<sup>10</sup>

*Effect of pH on the Rate Constant for Reaction of H with Formic Acid.* The rate constant for the reaction of H with formic acid was previously measured<sup>2</sup> at pH 1 and found to be  $7.4 \times 10^5 M^{-1} \text{ sec}^{-1}$ . The rate constant at pH 7 measured in the present study is  $1.3 \times 10^8 M^{-1} \text{ sec}^{-1}$ , *i.e.*, more than two orders of magnitude higher. This latter value is in reasonable agreement with other values previously determined in neutral solution.<sup>11,12</sup> In order to demonstrate that the change in the rate constant depends solely on the acid-base dissociation of formic acid, the pH dependence was studied between pH 0.5 and 7. The results are summarized in Figure 3. Experimentally one measures an apparent rate constant  $k$  which is the weighted average of the rate constants for reaction with the acidic and basic forms of the solute. This apparent rate constant should be given by the expression

$$k = \frac{k_{HCOOH} + k_{HCOO^-}K/[H^+]}{1 + K/[H^+]} \quad (2)$$

where the limiting rate constants  $k_{HCOOH}$  and  $k_{HCOO^-}$  can be determined quite well from the measurements in acidic and neutral solutions. The equilibrium con-

(10) J. Rabani, *Advan. Chem. Ser.*, No. 50, 242 (1962), and references within.

(11) G. Scholes and M. Simic, *J. Phys. Chem.*, 68, 1738 (1964).

(12) J. Rabani and G. Stein, *J. Chem. Phys.*, 37, 1865 (1962).



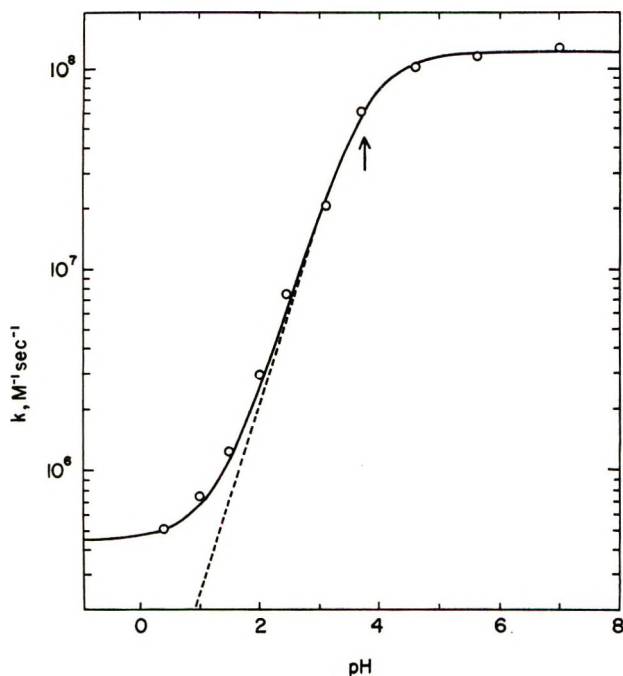


Figure 3. The pH dependence of the rate constant for reaction of H atoms with formic acid. The position of the curve on the horizontal scale is determined by the  $pK$  of formic acid which is indicated by the vertical arrow ( $pK = 3.75$ ). The curve is calculated from eq 2 with  $k_{\text{HCOOH}} = 4.5 \times 10^5 \text{ M}^{-1} \text{ sec}^{-1}$  and  $k_{\text{HCOO}^-} = 1.24 \times 10^8 \text{ M}^{-1} \text{ sec}^{-1}$ .

stant  $K$  is, of course, available from other measurements and has the value of  $1.77 \times 10^{-4} \text{ M}$ . The curve calculated with this equilibrium constant,  $k_{\text{HCOOH}} = 4.5 \times 10^5 \text{ M}^{-1} \text{ sec}^{-1}$  and  $k_{\text{HCOO}^-} = 1.24 \times 10^8 \text{ M}^{-1} \text{ sec}^{-1}$  is the solid curve in Figure 3. The horizontal position of this sigmoidal curve is, in fact, controlled almost entirely by the  $pK$  value of the equilibrium which is indicated by the arrow in the figure. It is also seen in the figure that above a  $\text{pH} \sim 2$  the observed rate is determined almost entirely by the amount of formate ion present. Even at  $\text{pH}$  of 1 almost 50% of the observed rate results from the 0.2% of the formate ion present. The agreement between the points and the solid curve demonstrates that the effect of  $\text{pH}$  on the rate constant is completely accounted for by the equilibrium between formic acid and formate ion.

*Effect of Ionic Dissociation on the Rate Constants.* The rate constants in neutral solutions measured in the present study are summarized in Table I. Rate constants previously determined at  $\text{pH}$  1 are included for comparison. Most of the carboxylic acids examined have  $pK$  values in the range 3–5. While the observed rate constants should obey eq 2 the rate constants measured at  $\text{pH}$  1 and 7 differ so little that they can be taken as accurately representing the rate constants of the acidic and basic forms. With the majority of the compounds the rate constants in neutral solutions are higher than those in acidic solutions but by less than a factor of 10. Exceptions, in addition to formic acid,

include oxalic acid, where the rate constant decreases in going to neutral solution, and barbituric acid, where the rate constant increases by two orders of magnitude. As mentioned above, the alcohols and *n*-hexylamine have the same rate constants at  $\text{pH}$  1 and 7.

It can be seen from the results for the carboxylic acids that dissociation of a carboxyl group increases the rate constant for hydrogen abstraction from the  $\alpha$  position by a factor of 2–3 for both  $\text{CH}_2$  (e.g., propionic acid) and  $\text{CH}$  (e.g., isobutyric acid) groups. The result for acetic acid shows a somewhat larger effect on the  $\text{CH}_3$  group but in this case the rate constant at  $\text{pH}$  1 is so low that even a small increase appears to be quite pronounced. With a long-chain acid, such as hexanoic acid, abstraction takes place to a major extent from more distant positions and the effect on the overall rate is small, as expected. Formic acid is unique in that the hydrogen atom to be abstracted is attached directly to the carboxyl group and its reactivity is greatly influenced by dissociation of this group. Abstraction is known to be the dominant reaction of the formate ion from measurements of HD production from  $\text{DCOO}^-$ .<sup>11</sup> The increase in rate constant by a factor of 270 over the acid form suggests that the C–H bond in formate ion is considerably weaker than that in formic acid.

The reaction of H with oxalic acid is also unique in that it can take place only by addition to the carboxyl groups. Dissociation of both carboxyl groups eliminates most of the carbonyl character and addition becomes more difficult. The rate constant for oxalate is at least 10 times less than that for oxalic acid.

Amino acids are slightly more reactive in neutral than in acid solutions. The zwitterion forms of glycine and valine present at  $\text{pH}$  7 are, respectively, 1.1 and 1.4 times more reactive than the corresponding acid forms. When two carboxyl groups are present their dissociation results in an increase by a factor of  $\sim 3.5$  as in the case of aspartic and glutamic acids. In the case of histidine, dissociation of the carboxyl group above  $\text{pH}$  2 results in a small increase but dissociation of the imidazole moiety above  $\text{pH}$  6 results in further increase by a factor of 5 indicating that this ring is the main site of reaction of H with histidine. The same conclusion has been previously derived from a comparison of the rate constants for histidine and for imidazole.<sup>4</sup>

All the amino acids have an addition  $pK$  for deprotonation of the ammonium group into  $\text{NH}_2$  in the region 9–10. It has already been argued<sup>4</sup> that this dissociation should result in a much greater increase in reactivity than that observed between  $\text{pH}$  1 and 7 but rate constants in strongly basic solutions have not as yet been measured by other methods and, as indicated above, cannot be measured by this esr technique. In order to estimate the change in the rate constant for H abstraction, which results from deprotonation of an amino group, the rate constant for reaction with amino-

acetonitrile (which has the very low  $pK$  value of 5.34) has been measured during the course of this study both at pH 1 and 7. The neutral form was found to be 8.5 times more reactive than the protonated form (Table I). If, as in the case of acetonitrile,<sup>2</sup> addition to the CN group contributes  $1.6 \times 10^6 M^{-1} \text{sec}^{-1}$  to the overall rate, abstraction from the  $\text{CH}_2$  group increases by a factor of 11 in going from  $^+\text{H}_3\text{NCH}_2\text{CN}$  to  $\text{H}_2\text{NCH}_2\text{CN}$ . Similar effects on the  $\alpha$  protons can be expected for the amino acids. For most work of biological interest one is, of course, principally interested in the reactivity of the zwitterion form of the amino acid and this increase in basic solution is of little importance.

In the case of aromatic systems addition to the ring dominates and effects of acid-base equilibria are expected to be small except insofar as they influence the spin density distribution in the ring system. The higher rate constants observed for benzoate and aniline, compared with those for benzoic acid and anilinium ion, are in line with the expected substituent effects.<sup>3</sup> No examples of unsaturated carboxylic acids have been examined but the effects are expected to be small because of the very high rate of addition of H to the double bond.

Rate constants for the pyrimidines and purines cannot be determined very accurately in neutral solutions

because a large correction has to be made for their reaction with  $e_{\text{aq}}^-$ . It can only be estimated that for cytosine, adenine, and adenosine dissociation of the amino group results in only a small increase in reactivity. Uracil appears to react at a very similar rate at pH 1 and 7. A unique pyrimidine molecule is barbituric acid which shows an increase in reactivity by a factor of 100. This effect is clearly the result of a major change in the structure of this molecule. The acidic form is mostly a diketo structure and abstraction from the  $\text{CH}_2$  at position 5 takes place with a relatively low rate constant of  $2 \times 10^7 M^{-1} \text{sec}^{-1}$ . The anion has double bond character at the 5 position and addition can take place very much more rapidly. It has recently been shown that conversion of the acidic to the basic form is accompanied by a very large decrease in the reactivity of barbituric acid toward  $e_{\text{aq}}^-$  which results from the same change in structure.<sup>13</sup> The fact that addition of H atoms to the anion is an order of magnitude more rapid than to uracil suggests the existence of an additional activating effect by the  $\text{O}^-$  group at position 6, somewhat similar to the effect of  $\text{O}^-$  in the aromatic system.<sup>3</sup>

(13) F. A. Peter and P. Neta, *J. Phys. Chem.*, **76**, 630 (1972).

## Elementary Processes in the Radiolysis of Aqueous Nitric Acid

### Solutions: Determination of Both $G_{\text{OH}}$ and $G_{\text{NO}_3}$ <sup>1,2</sup>

by R. W. Matthews,<sup>3</sup> H. A. Mahlman, and T. J. Sworski\*

Chemistry Division, Oak Ridge National Laboratory, Oak Ridge, Tennessee 37830 (Received March 27, 1972)

Publication costs assisted by the U. S. Atomic Energy Commission

Kinetic evidence is presented for concurrent production of two oxidizing radicals in the radiolysis of aqueous 4.0 *M* nitric acid solutions: OH and NO<sub>3</sub> radicals that are presumed to result from the direct interaction of ionizing radiation with water and nitric acid species (NO<sub>3</sub><sup>-</sup> and HNO<sub>3</sub>), respectively. The evidence was obtained from the dependence of  $G(\text{Ce}^{\text{III}})$  on cerium(III) and formic acid concentrations in the radiolysis of cerium(IV)-cerium(III)-formic acid mixtures in air-saturated 4.0 *M* nitric acid solutions with <sup>60</sup>Co  $\gamma$  radiation.  $G_{\text{OH}} = 2.04 \pm 0.09$  and  $G_{\text{NO}_3} = 1.56 \pm 0.12$  were determined with the use of a computer to fit experimental data by the method of least squares to a kinetic equation containing 13 dependent variables. We assume that energy is partitioned between water and nitric acid species in proportion to their electron fraction. If this be true, then there is no evidence for oxidation of nitric acid species by precursors of OH radical such as H<sub>2</sub>O<sup>+</sup> since  $G_{\text{OH}}$  was found to be proportional to electron fraction water.

### Introduction

The importance of the NO<sub>3</sub> radical as an intermediate in the radiolysis of aqueous nitric acid solutions has been the subject of numerous investigations. Four different processes have been proposed for the production of NO<sub>3</sub> radical: reaction of OH radical with nitrate ion in nitric acid solutions;<sup>4</sup> direct interaction of ionizing radiation with nitrate ion;<sup>5</sup> reaction of NO<sub>2</sub> with O atom;<sup>6,7</sup> and reaction of nitrate ion with H<sub>2</sub>O<sup>+</sup>.<sup>8</sup>

The proposal that OH radical is a precursor of NO<sub>3</sub> radical in nitric acid solutions has been substantiated by pulse radiolysis techniques.<sup>9</sup> The effects of pH on NO<sub>3</sub> radical production indicate that the rate of reaction of OH radical with nitrate ion is very small, if it occurs at all, and that NO<sub>3</sub> radical arises from the reaction of OH radical with undissociated nitric acid. These effects of pH have been confirmed by flash photolysis techniques.<sup>10</sup>

The proposal that NO<sub>3</sub> radical is produced by interaction of ionizing radiation with nitrate ion has been substantiated by pulse radiolysis techniques.<sup>11</sup> The dependence of NO<sub>3</sub> radical yields on dose and scavenger concentrations, however, was interpreted as evidence that NO<sub>3</sub> radical is not entirely produced by an elementary process such as ionization. It was suggested that dissociative ionization yields NO<sub>2</sub>, O, and e<sup>-</sup> in a "cage."<sup>6,7</sup> NO<sub>3</sub> radical production was assumed to occur by reaction of NO<sub>2</sub> with O atom in either the cage, the spur, or the bulk of the solution. The evidence for dissociative ionization is questionable since the conclusions from scavenger studies were conflicting: essentially none of the O atoms escape from the spur for <sup>60</sup>Co  $\gamma$  radiolyses,<sup>7</sup> but at least half of the O atoms escape from the spur for pulse radiolyses.<sup>6</sup>

The proposal that NO<sub>3</sub> radical is produced by reaction of nitrate ion with H<sub>2</sub>O<sup>+</sup> has been refuted by pulse radiolysis techniques, at least for neutral solutions.<sup>6,11</sup> The NO<sub>3</sub> radical yield in neutral solutions was found to be a linear function of the energy absorbed by nitrate ion with no contribution from energy absorbed by water. In acid solutions, however, the NO<sub>3</sub> radical yield was found to increase nonlinearly with increase in nitrate ion concentration and appeared to be reaching a limit.<sup>6</sup> This dependence of NO<sub>3</sub> radical yield on nitrate ion concentration in acid solutions has been attributed<sup>12</sup> to reaction of nitrate ion with H<sub>2</sub>O<sup>+</sup>, an example of hole trapping by anions that was postulated in a model for the radiolysis of water based on primordial, isolated single H<sub>2</sub>O<sup>+-e-</sup> pairs.<sup>13</sup>

This paper reports the results from a kinetic analysis of the dependence of  $G(\text{Ce}^{\text{III}})$  on cerium(III) and formic acid concentrations in the radiolysis of cerium(IV)-

(1) Research sponsored by the U. S. Atomic Energy Commission under contract with Union Carbide Corp.

(2) This paper was presented in part at the XXII International Congress of Pure and Applied Chemistry, Sydney, Australia, August 20-27, 1969.

(3) Guest Scientist from the Australian Atomic Energy Commission, Research Establishment, Lucas Heights, New South Wales.

(4) H. Taube and W. C. Bray, *J. Amer. Chem. Soc.*, **62**, 3357 (1940).

(5) J. Bednar and S. Lukac, *Collect. Czech. Chem. Commun.*, **29**, 341 (1964).

(6) M. Daniels, *J. Phys. Chem.*, **73**, 3710 (1969).

(7) M. Daniels and E. E. Wigg, *ibid.*, **73**, 3703 (1969).

(8) J. Bednar, *Collect. Czech. Chem. Commun.*, **27**, 2204 (1962).

(9) R. K. Broszkiewicz, *Int. J. Appl. Radiat. Isotop.*, **18**, 25 (1967).

(10) L. Dogliotti and E. Hayon, *J. Phys. Chem.*, **71**, 3802 (1967).

(11) M. Daniels, *ibid.*, **70**, 3022 (1966).

(12) T. Sawai and W. H. Hamill, *J. Chem. Phys.*, **52**, 3843 (1970).

(13) W. H. Hamill, *J. Phys. Chem.*, **73**, 1341 (1969).

cerium(III)-formic acid mixtures in air-saturated 4.0 M nitric acid solutions with  $^{60}\text{Co}$   $\gamma$  radiation. As reported in our preliminary communication,<sup>14</sup> evidence is presented for the concurrent production of two oxidizing radicals that are presumed to be OH and  $\text{NO}_3$ . Our results confirm the proposal<sup>4</sup> that OH radical reacts in nitric acid solutions to produce the  $\text{NO}_3$  radical. They refute the suggestion<sup>12</sup> that nitrate ion reacts with  $\text{H}_2\text{O}^+$  in acidic solutions since  $G_{OH}$  is proportional to electron fraction water.

### Experimental Section

**Materials.** G. Frederick Smith Chemical Co. cerous nitrate hydrated and Baker Analyzed ceric ammonium nitrate, formic acid, and nitric acid were used without further purification. All solutions were prepared with water from a Barnstead still that was further purified by successive distillations from an acid dichromate solution, from an alkaline permanganate solution, and finally from an all-silica system into silica storage vessels. All solutions were allowed to stand overnight before being irradiated.

**Irradiations.** Solutions in 2-cm cylindrical absorption cells were irradiated in  $^{60}\text{Co}$  sources of the Ghormley-Hochanadel design.<sup>15</sup> Dose rates in solution were determined with the ferrous sulfate dosimeter using  $G(\text{Fe}^{II}) = 15.6$ <sup>16</sup> and a molar extinction coefficient of 2210 for iron(III) at 305 nm and 25° in 0.4 M sulfuric acid solutions.<sup>17</sup> The energy absorbed in 4.0 M nitric acid solutions relative to the ferrous sulfate dosimeter was assumed to be in the ratio of electron densities.

**Analyses.** Changes in cerium(IV) concentration with increase in absorbed dose were determined spectrophotometrically in the irradiation cells using five or six dose increments. The irradiation cells (Pyrocell Manufacturing Co.) had S18-260 silica windows that did not become colored enough during irradiation to interfere with the analyses. A molar extinction coefficient for cerium(IV) in 4.0 M nitric acid solutions of 3670 at 345 nm was determined relative to 5580 at 320 nm in 0.4 M sulfuric acid solutions.<sup>16</sup>

### Results

$G(\text{Ce}^{III})$  is markedly dependent on both cerium(III) and formic acid concentrations in the radiolysis of cerium(IV)-cerium(III)-formic acid mixtures in air-saturated 4.0 M nitric acid solutions as shown in Figure 1. At any particular cerium(III) concentration,  $G(\text{Ce}^{III})$  increases with increase in formic acid concentration. At any particular formic acid concentration,  $G(\text{Ce}^{III})$  decreases with increase in cerium(III) concentration.  $G(\text{Ce}^{III})$  is not simply a function of  $[\text{HCOOH}]/[\text{Ce}^{III}]$ , however, since  $G(\text{Ce}^{III})$  decreases with increase in the total concentration of formic acid and cerium(III) for any particular  $[\text{HCOOH}]/[\text{Ce}^{III}]$ .

All values for  $G(\text{Ce}^{III})$  are initial yields. The

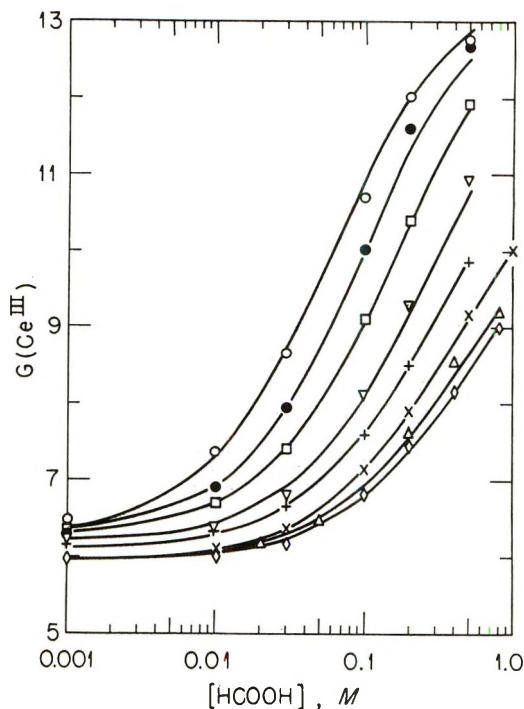


Figure 1. Dependence of  $G(\text{Ce}^{III})$  on  $[\text{Ce}^{III}]$  and  $[\text{HCOOH}]$  in the radiolysis of cerium(IV)-cerium(III)-formic acid mixtures in air-saturated 4.0 M nitric acid solutions with  $^{60}\text{Co}$   $\gamma$  radiation: initial  $[\text{Ce}^{III}] = \text{O}$ ,  $5.0 \times 10^{-4} \text{ M}$ ;  $\bullet$ ,  $1.0 \times 10^{-3} \text{ M}$ ;  $\square$ ,  $2.0 \times 10^{-3} \text{ M}$ ;  $\nabla$ ,  $5.0 \times 10^{-3} \text{ M}$ ;  $+$ ,  $1.0 \times 10^{-2} \text{ M}$ ;  $\times$ ,  $2.0 \times 10^{-2} \text{ M}$ ;  $\triangle$ ,  $4.0 \times 10^{-2} \text{ M}$ ;  $\diamond$ ,  $5.0 \times 10^{-2} \text{ M}$ . Curves are theoretical and represent least-squares fit of the data to eq I.

changes in cerium(IV) concentration were approximately a linear function of dose, except for the solutions with the lowest cerium(III) concentrations of  $1.0 \times 10^{-3}$  and  $5.0 \times 10^{-4} \text{ M}$ . For these dilute cerium(III) solutions, in which the rate of cerium(IV) reduction decreased only slightly with increase in dose, the initial values for  $G(\text{Ce}^{III})$  were estimated from plots of the changes in cerium(IV) concentration for each dose increment as a function of dose.

### Discussion

The effect of formic acid on the radiolysis of aqueous inorganic solutions has been well established. The OH radical, which can oxidize both iron(II)<sup>18</sup> and cerium(III)<sup>19</sup> ions, reacts with formic acid to yield the COOH (or HCOO) radical,<sup>20</sup> which can reduce both

(14) R. W. Matthews, H. A. Mahlman, and T. J. Sworski, *J. Phys. Chem.*, **74**, 3835 (1970).

(15) J. A. Ghormley and C. J. Hochanadel, *Rev. Sci. Instrum.*, **22**, 473 (1951).

(16) C. J. Hochanadel and J. A. Ghormley, *J. Chem. Phys.*, **21**, 880 (1953).

(17) T. J. Sworski, *Radiat. Res.*, **4**, 483 (1956).

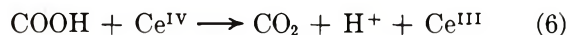
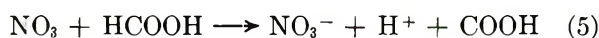
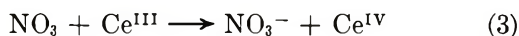
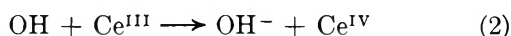
(18) F. Haber and J. Weiss, *Naturwissenschaften*, **20**, 948 (1932).

(19) J. Weiss and D. Porret, *Nature (London)*, **139**, 1019 (1937).

(20) H. Taube, *J. Amer. Chem. Soc.*, **63**, 2453 (1941).

iron(III)<sup>21</sup> and cerium(IV)<sup>22,23</sup> ions. In sulfuric acid solutions, the OH radical also reacts with sulfuric acid anions to yield the SO<sub>4</sub><sup>-</sup> radical,<sup>4</sup> which can either oxidize cerium(III) ion<sup>24</sup> or react with formic acid to yield the COOH (or HCOO) radical.<sup>25</sup> The dependence of  $G(\text{Ce}^{\text{III}})^0$  on cerium(III) and formic acid concentrations in the radiolysis of cerium(IV)-cerium(III)-formic acid mixtures in 4.0 M sulfuric acid solutions yielded kinetic evidence for concurrent production of OH and SO<sub>4</sub><sup>-</sup> radicals in the radiolysis of aqueous sulfuric acid solutions.<sup>26</sup>

*Determinations of Both  $G_{\text{OH}}$  and  $G_{\text{NO}_3}$ .* To explain the dependence of  $G(\text{Ce}^{\text{III}})$  on cerium(III) and formic acid concentrations in the radiolysis of cerium(IV)-cerium(III)-formic acid mixtures in 4.0 M nitric acid solutions, we have considered the following reactions of OH and NO<sub>3</sub> radicals.



We assume that there are primary yields of both OH and NO<sub>3</sub> radicals, that  $G_{\text{OH}}$  and  $G_{\text{NO}_3}$  are independent of both cerium(III) and formic acid concentrations, and that reaction 1 is sensibly irreversible. These assumptions together with the stationary-state hypothesis for OH and NO<sub>3</sub> radical concentrations yield eq I.

$$G(\text{Ce}^{\text{III}}) = G(\text{Ce}^{\text{III}})^0 + \frac{2G_{\text{OH}} \left( 1 + \frac{k_1[\text{H}^+][\text{NO}_3^-]}{k_4[\text{HCOOH}]} \right) / \left( 1 + \frac{k_3[\text{Ce}^{\text{III}}]}{k_5[\text{HCOOH}]} \right)}{1 + \frac{k_2[\text{Ce}^{\text{III}}] + k_1[\text{H}^+][\text{NO}_3^-]}{k_4[\text{HCOOH}]}} + \frac{2G_{\text{NO}_3}}{1 + \frac{k_3[\text{Ce}^{\text{III}}]}{k_5[\text{HCOOH}]}} \quad (\text{I})$$

$G(\text{Ce}^{\text{III}})^0$ , a function of cerium(III) concentration, denotes the value of  $G(\text{Ce}^{\text{III}})$  at any particular cerium(III) concentration in the absence of formic acid.

The experimental data were fit to eq I by the method of least squares using the computer program of Lietzke.<sup>27</sup> Thirteen dependent variables were determined: the values for  $G_{\text{OH}}$ ,  $G_{\text{NO}_3}$ , three rate constant ratios listed in Table I, and eight values for  $G(\text{Ce}^{\text{III}})^0$  shown in Figure 2. The experimental data adhere well to eq I as indicated by the theoretical curves in Figure 1 that illustrate the least-squares fit of the data to eq I. No better fit of theory to the data could be obtained for any positive value of  $k_{-1}[\text{H}_2\text{O}]/(k_3[\text{Ce}^{\text{III}}])$ .

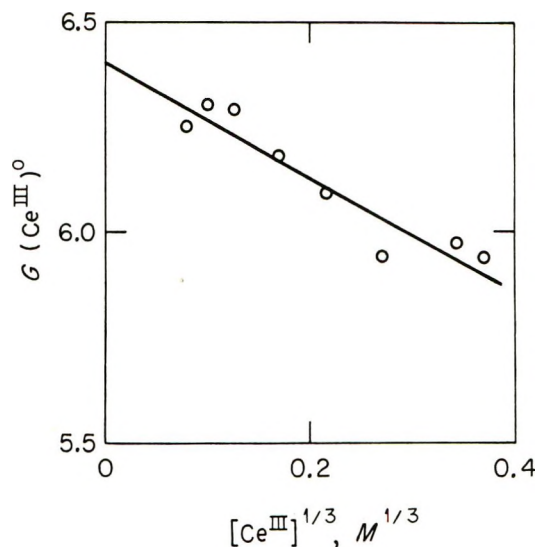


Figure 2. Dependence of  $G(\text{Ce}^{\text{III}})^0$  on  $[\text{Ce}^{\text{III}}]^{1/3}$ . Theoretical values obtained by use of eq I to evaluate 13 dependent variables. Line is theoretical and represents least-squares fit of the data to eq I with the assumption that  $G(\text{Ce}^{\text{III}})^0$  varies linearly with  $[\text{Ce}^{\text{III}}]^{1/3}$ .

Table I: Kinetic Parameters from Least-Squares Fit of Experimental Data to Eq I

$G_{\text{OH}}$	$2.04 \pm 0.09$
$G_{\text{NO}_3}$	$1.56 \pm 0.12$
$k_2/k_4$	$4.1 \pm 0.9$
$k_3/k_5$	$143 \pm 11$
$k_1[\text{H}^+][\text{NO}_3^-]/k_4$	$0.21 \pm 0.03 M$

Figure 2 shows that  $G(\text{Ce}^{\text{III}})^0$  decreases linearly with increase in the cube root of the cerium(III) concentration, to a good approximation, just as previously reported for sulfuric acid solutions.<sup>17,24,26</sup> The experimental data were fit by the method of least squares to eq I with the assumption that  $G(\text{Ce}^{\text{III}})^0$  is a linear function of  $[\text{Ce}^{\text{III}}]^{1/3}$ .  $G(\text{Ce}^{\text{III}})^0$  was found to be equal to  $(6.40 \pm 0.04) - (1.4 \pm 0.2)[\text{Ce}^{\text{III}}]^{1/3}$  with the other kinetic parameters equal within standard errors to those listed in Table I.

We reported in our preliminary communication<sup>14</sup> that  $G_{\text{OH}}$  is proportional to electron fraction water in the radiolysis of aqueous nitric acid solutions. This conclusion is based on three assumptions: energy absorption by water is proportional to electron fraction water; OH radicals result only from energy absorption

(21) E. J. Hart, *J. Amer. Chem. Soc.*, **74**, 4174 (1952).

(22) T. J. Sworski, *ibid.*, **77**, 1074 (1955).

(23) H. E. Spencer and G. K. Rollefson, *ibid.*, **77**, 1938 (1955).

(24) T. J. Sworski, *ibid.*, **78**, 1768 (1956); *Radiat. Res.*, **6**, 645 (1957).

(25) E. J. Hart, *J. Amer. Chem. Soc.*, **83**, 567 (1961).

(26) R. W. Matthews, H. A. Mahlman, and T. J. Sworski, *J. Phys. Chem.*, **76**, 1265 (1972).

(27) M. H. Lietzke, ORNL-3259, Oak Ridge National Laboratory, March 21, 1962.

by water; and the fraction of OH radicals that escape by diffusion from the spur into the bulk of the solution is independent of nitric acid concentration.

Let  $E_W$  denote electron fraction water and  $G_{OH}^0$  denote the  $G$  value for OH radical production based upon energy absorption by water. Then  $G_{OH}^0$  is equal to  $G_{OH}/E_W$ . Our value of  $G_{OH} = 2.04 \pm 0.09$  together with  $E_W = 0.79$  yields  $G_{OH}^0 = 2.58 \pm 0.12$  for 4.0  $M$  nitric acid solutions. This value of  $G_{OH}^0$  is equal within standard errors to  $G_{OH}^0 = 2.59 \pm 0.09$ , the most recent value of  $G_{OH}$  for pure water that has been determined in our laboratory.<sup>28</sup> It is also equal within standard errors to the values for  $G_{OH}^0$  of  $2.51 \pm 0.05$  and  $2.70 \pm 0.04$  that have been determined for 4.0 and 0.4  $M$  sulfuric acid solutions, respectively.<sup>26</sup>

The proportionality between  $G_{OH}$  and  $E_W$  refutes the suggestions<sup>8,12</sup> that nitrate ion at high concentrations reacts with  $H_2O^+$ , a commonly assumed precursor of OH radical, to produce the  $NO_3$  radical with concomitant inhibition of OH radical production. Our determination of  $G_{NO_3}$  confirms the proposals<sup>5,6,11</sup> that direct interaction of radiation with nitrate ion produces the  $NO_3$  and supersedes the previous proposals<sup>29,30</sup> from our laboratory that direct interaction of radiation with nitric acid produces OH and  $NO_2$  radicals.

The total yield of oxidizing radicals in nitric acid solutions has been evaluated previously from the enhancement in  $G(Ce^{III})$  by thallium(I).<sup>29,31</sup> In 4.0  $M$  nitric acid solutions, our determination of  $G_{OH} + G_{NO_3} = 3.6 \pm 0.2$  is in much better agreement with Mahlman's value of 3.9<sup>29</sup> than with an interpolated value of 2.7 from the data of Bugaenko and Roshchektaev.<sup>31</sup>

The generation and reaction kinetics of the  $NO_3$  radical in aqueous solutions were first studied by the flash photolysis of aqueous nitric acid solutions of ceric ammonium nitrate.<sup>32,33</sup> Since further studies<sup>10,34</sup> have led to conflicting viewpoints concerning both the generation and reaction kinetics of the  $NO_3$  radical, there is no firm basis for establishing the validity of our value for  $k_3/k_5$ . Our value of  $143 \pm 11$  for  $k_3/k_5$  in 4.0  $M$  nitric acid solutions is not in agreement with reported values<sup>10</sup> for  $k_3$  of  $(3.7 \pm 0.1) \times 10^5 M^{-1} sec^{-1}$  and  $k_5$  of  $(2.06 \pm 0.1) \times 10^6 M^{-1} sec^{-1}$  in 0.1  $M$   $K_2Ce(NO_3)_6$  solutions.

This disagreement may only reflect the difference in reaction media. There is a marked dependence of  $k_3$  on nitric acid concentration with  $k_3$  increasing from  $(3.55 \pm 0.13) \times 10^5 M^{-1} sec^{-1}$  in dilute nitric acid solutions to about  $1.2 \times 10^6 M^{-1} sec^{-1}$  in 4.0  $M$  nitric acid solutions.<sup>35</sup> The dependence of  $k_5$  on nitric acid concentration has not been determined, but it may decrease with increase in nitric acid concentration since the absolute rate constant for reaction of  $NO_3$  radical with acetic acid decreases from  $(4.6 \pm 0.4) \times 10^4 M^{-1} sec^{-1}$  in 0.1  $M$   $K_2Ce(NO_3)_6$  solutions<sup>10</sup> to  $(2.3 \pm$

$0.2) \times 10^2 M^{-1} sec^{-1}$  for 6.0  $M$  nitric acid solutions with 10  $M$  acetic acid added.<sup>33</sup>

*Reactions of  $NO_3$  Radical in the Spur.* The formation of "molecular" peroxosulfuric acid and peroxodisulfuric acid in the spur was proposed by Boyle<sup>36</sup> as evidence for concurrent production of OH and  $SO_4^-$  radicals in the radiolysis of aqueous sulfuric acid solutions. We substantiated Boyle's proposal by determinations<sup>26</sup> of both  $G_{OH}$  and  $G_{SO_4^-}$ . By analogy with these studies in aqueous sulfuric acid solutions, our determination of both  $G_{OH}$  and  $G_{NO_3}$  in aqueous 4.0  $M$  nitric acid solutions suggests that reactions of  $NO_3$  radical in the spur should be of importance in aqueous nitric acid solutions.

We previously focused attention<sup>37,38</sup> on the marked increase in  $G(Ce^{III})^0$  with increase in nitrate ion concentration in 0.4  $M$  sulfuric acid solutions. The value of  $(6.40 \pm 0.05) - (1.4 \pm 0.2)[Ce^{III}]^{1/2}$  for  $G(Ce^{III})^0$  in air-saturated 4.0  $M$  nitric acid solutions is much larger than the value<sup>26</sup> of  $(2.40 \pm 0.02) - (0.74 \pm 0.06)[Ce^{III}]^{1/2}$  in air-saturated 0.4  $M$  sulfuric acid solutions. We have established<sup>30</sup> that this increase in  $G(Ce^{III})^0$  is due to spur reactions that result in nitrous acid production. There is a concomitant increase in  $G(O_2)$  with this increase in  $G(Ce^{III})^0$  and isotopic studies have indicated<sup>39</sup> two sources for this additional oxygen: (1) joint participation of water and nitrate ion and (2) nitrate ion alone. Reactions of  $NO_3$  radical in the spur may be a source of both nitrous acid and oxygen.

Combination reactions of OH and  $NO_3$  radicals in the spur may yield three peroxy compounds.



Hydrogen peroxide is the source of oxygen in the radiolysis of cerium(IV) solutions in 0.4  $M$  sulfuric acid solutions. In nitric acid solutions, oxygen may also result from oxidation of both  $HNO_4$  and  $N_2O_6$  by cerium(IV).

(28) C. J. Hochanadel and R. Casey, *Radiat. Res.*, **25**, 198 (1965).

(29) H. A. Mahlman, *J. Chem. Phys.*, **35**, 936 (1961).

(30) T. J. Sworski, R. W. Matthews, and H. A. Mahlman, *Advan. Chem. Ser.*, No. 81, 164 (1968).

(31) L. T. Bugaenko and B. M. Roshchektaev, *Khim. Vys. Energ.*, **5**, 472 (1971).

(32) T. W. Martin, A. Henshall, and R. C. Cross, *J. Amer. Chem. Soc.*, **85**, 113 (1963).

(33) T. W. Martin, R. E. Rummel, and R. C. Cross, *ibid.*, **86**, 2595 (1964).

(34) R. W. Glass and T. W. Martin, *ibid.*, **92**, 5084 (1970).

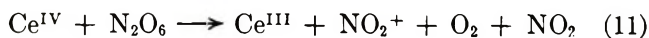
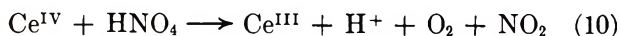
(35) T. W. Martin and R. W. Glass, *ibid.*, **92**, 5075 (1970).

(36) J. W. Boyle, *Radiat. Res.*, **17**, 427 (1962).

(37) T. J. Sworski, *J. Amer. Chem. Soc.*, **77**, 4689 (1955).

(38) H. A. Mahlman, *J. Phys. Chem.*, **64**, 1598 (1960).

(39) H. A. Mahlman, *ibid.*, **67**, 1466 (1963).



Glass and Martin<sup>34</sup> have proposed the sequence of reactions 9 and 11 for the net reduction of cerium(IV) in the photolysis of ceric ammonium nitrate in nitric acid solutions.

We have no evidence that either  $\text{HNO}_4$  or  $\text{N}_2\text{O}_6$  are sufficiently long lived for reactions 10 and 11 to be significant. Both  $\text{HNO}_4$  and  $\text{N}_2\text{O}_6$  may well be unstable intermediates that decompose rapidly to yield nitrous acid and oxygen.



Reaction 12 has been suggested to occur in the photolysis of alkaline nitrate solutions.<sup>40</sup>

The oxygen resulting from intermediate formation of  $\text{N}_2\text{O}_6$  would have nitrate ion alone as the source. The oxygen resulting from intermediate formation of  $\text{HNO}_4$  would have joint participation of nitrate ion and water as the source. Since  $\text{NO}_2$  does not react with either cerium(IV) or cerium(III) ions,<sup>30</sup> nitrous acid would result from production of  $\text{NO}_2$  by reactions 10 and 11.

We cannot determine the importance of  $\text{HNO}_4$  and  $\text{N}_2\text{O}_6$  production in the spur since further contributions to nitrous acid and oxygen production may result from excited states of nitrate ion. Although the

photolysis of aqueous nitric acid solutions does not produce the  $\text{NO}_3$  radical,<sup>34</sup> nitrite ion and molecular oxygen do result from excitation of nitrate ion both in the low-intensity band at 300 nm<sup>40</sup> and in the intense band at 201 nm.<sup>41,42</sup> Excited states of nitrate ion also yield  $\text{NO}_2$  and OH radical pairs, most of which reportedly<sup>40</sup> undergo geminate recombination when produced photochemically. These radical pairs in the spur, however, may result in increased yields of hydrogen peroxide containing oxygen from nitrate ion, originally attributed<sup>43</sup> to reactions of  $\text{NO}_3$  radical with water.

In the radiolysis of concentrated nitrate solutions, excited states of nitrate ion most certainly would result from direct interaction of radiation with nitrate species in solution and may also result from interaction of nitrate ion with excited states of water.<sup>37,44</sup> Although it has long been established that chemical reactions can be induced by photoactivation of water,<sup>45,46</sup> the role of excited states in the radiolysis of aqueous solutions has not yet been established.

(40) M. Daniels, R. V. Meyers, and E. V. Belardo, *J. Phys. Chem.*, **72**, 389 (1968).

(41) U. Shuali, M. Ottolenghi, J. Rabani, and Z. Yelin, *ibid.*, **73**, 3445 (1969).

(42) F. Barat, L. Gilles, B. Hickel, and J. Sutton, *J. Chem. Soc. A*, 1982 (1970).

(43) M. Faraggi, D. Zehavi, and M. Anbar, *Trans. Faraday Soc.*, **67**, 701 (1971).

(44) T. J. Sworski, *Advan. Chem. Ser.*, No. 50, 263 (1965).

(45) H. Fricke and E. J. Hart, *J. Chem. Phys.*, **4**, 418 (1936).

(46) J. Barrett and J. H. Baxendale, *Trans. Faraday Soc.*, **56**, 37 (1960).

# Systematics of (n, $\gamma$ )-Activated Hot $^{128}\text{I}$ Reactions in Gaseous Methane and Halomethanes. The Energy Degradation Factor<sup>1</sup>

by Matthias Yoong, Y. C. Pao,<sup>2</sup> and E. P. Rack\*

Department of Chemistry, University of Nebraska, Lincoln, Nebraska 68508 (Received January 24, 1972)

Publication costs assisted by The U. S. Atomic Energy Commission

It was found in a systematic study of  $^{128}\text{I}$  reactions activated by radiative neutron capture in various gaseous halomethanes that the formation of  $^{128}\text{I}$ -labeled organic products proceeds entirely by hot (requiring excess kinetic energy to occur) reactions. This is unlike the reactions of  $^{128}\text{I}$  with  $\text{CH}_4$  where the organic product  $\text{CH}_3^{128}\text{I}$  was formed not only by hot  $^{128}\text{I}$  atoms but by thermal ion-molecule reactions involving  $\text{I}^+$  in the  $^1\text{D}_2$ ,  $^3\text{P}_0$ ,  $^3\text{P}_1$ , and  $^3\text{P}_2$  states. In the various halomethane systems only two  $^{128}\text{I}$ -labeled organic products were found, those resulting from halogen and hydrogen substitution. The limiting  $^{128}\text{I}$  organic yields in gaseous  $\text{CH}_3\text{F}$ ,  $\text{CH}_3\text{Cl}$ ,  $\text{CH}_3\text{Br}$ , and  $\text{CH}_3\text{I}$  were 11.2, 4.2, 0.67, and 0.20%, respectively. The kinetic energy spectra for (n, $\gamma$ )-activated  $^{128}\text{I}$  atoms or ions were calculated and the results showed that an appreciable fraction of the  $^{128}\text{I}$  species are born with low kinetic energies, in or near the reactive zone. The only physical or chemical parameter that explained the trend in organic yields was the energy degradation factor of the halomethane system, correlating well with the kinetic energy spectrum of  $^{128}\text{I}$ .

## Introduction

In the recent literature, there have been various systematic studies involving gas-phase fluorine and chlorine hot atoms (activated by nuclear reactions) with methane and various halomethanes, suggesting the importance of steric,<sup>3</sup> translational inertial,<sup>4a</sup> and bond energy effects.<sup>4b</sup> Previously there have been no such systematic studies for gas-phase iodine hot atom reactions. Unlike chlorine and fluorine, which are believed to react as atoms, the reactions of iodine<sup>5</sup> are complex, since iodine reacts not only as atoms or ions possessing excess kinetic energy, but also as atoms or ions which are translationally thermalized and electronically excited, especially as  $\text{I}^+$  ( $^1\text{D}_2$ ) and  $\text{I}^+$  ions in  $^3\text{P}_0$ ,  $^3\text{P}_1$ , and  $^3\text{P}_2$  states.

By the use of rare-gas moderators, it is possible to distinguish the organic yields or product yields resulting from "hot atom" processes (requiring excess kinetic energy to occur) from those yields which result from thermal ion-molecule reactions. In this paper we report how various chemical and physical factors influence the progress of (n, $\gamma$ )-activated hot reactions of  $^{128}\text{I}$  with methane and halomethanes in the gas phase. Because  $^{128}\text{I}$  is born with a spectrum of kinetic energies ranging from 0 eV to a maximum of 194 eV, quite low as compared to other nuclear activations, it was of interest to calculate the recoil energy spectrum of the (n, $\gamma$ )-activated  $^{128}\text{I}$  atoms. A substantial number of calculations implementing the idea of a nuclear cascade have been made in the literature,<sup>6-10</sup> all of which have been performed using a Monte Carlo technique for various nuclear activations, but none for the (n, $\gamma$ ) process. In our calculations of  $^{128}\text{I}$  kinetic energy spectra we used the three-dimensional random-walk

equations originally derived by Hsiung and Gordus<sup>11</sup> for the  $^{35}\text{Cl}(n,\gamma)^{36}\text{Cl}$  recoil energy spectra.

## Experimental Section

A description of our sample-making techniques, irradiation procedures, and extraction techniques can be found elsewhere.<sup>5,12</sup> The  $^{128}\text{I}$  organic yields in  $\text{CH}_3\text{Cl}$  and  $\text{CH}_3\text{Br}$  systems were determined from radio assay data employing a RIDL 400 channel pulse height analyzer with two 2 in.  $\times$  2 in.  $\text{NaI}(\text{Tl})$  crystals. Iodine-128-labeled products were separated and identified by a radio-gas chromatograph employing a Wolf window flow radiation detector.

All irradiations were performed at the Omaha VA

(1) This research was supported through an Atomic Energy Commission Contract No. AT(11-1)-1617. This is AEC Document No. (COO-1617-30).

(2) Yen Ching Pao, Department of Engineering Mechanics and Mechanical Engineering, University of Nebraska, Lincoln, Nebr.

(3) L. Spicer and R. Wolfgang, *J. Amer. Chem. Soc.*, **90**, 2426 (1968).

(4) (a) N. Colebourne, J. F. J. Todd, and R. Wolfgang, *J. Phys. Chem.*, **71**, 2875 (1967); (b) T. Smail, R. S. Iyer, and F. S. Rowland, *ibid.*, **75**, 1324 (1971).

(5) (a) E. P. Rack and A. A. Gordus, *J. Chem. Phys.*, **34**, 1855 (1961); (b) E. P. Rack and A. A. Gordus, *J. Phys. Chem.*, **65**, 944 (1961).

(6) M. L. Goldberger, *Phys. Rev.*, **74**, 1268 (1948).

(7) G. Bernardini, E. T. Booth, and S. J. Lindenbaum, *Phys. Res.*, **88**, 1017 (1952).

(8) H. McManus, W. T. Sharp, and H. Gellman, *Phys. Rev.*, **93**, 924 (1954).

(9) J. W. Meadows, *ibid.*, **98**, 744 (1955).

(10) N. Metropolis, R. Bivins, M. Storm, A. Turkevich, J. M. Miller, and G. Frieland, *ibid.*, **110**, 185 (1958).

(11) Chi-Hua Hsiung, Hsien-Chih Hsiung, and A. A. Gordus, *J. Chem. Phys.*, **34**, 535 (1961).

(12) J. B. Nicholas and E. P. Rack, *ibid.*, **48**, 4085 (1968).



Hospital Triga nuclear reactor. The thermal neutron flux was  $1.1 \times 10^{11}$  neutrons  $\text{cm}^{-2} \text{sec}^{-1}$ . The accompanying radiation flux was approximately  $3 \times 10^{17}$   $\text{eV g}^{-1} \text{min}^{-1}$ .

## Results and Discussion

*Nature of Reactive  $^{128}\text{I}$  in Halomethane Systems.* In previous gas-phase studies<sup>5</sup> of  $^{128}\text{I}$  reactions activated by radiative neutron capture in  $\text{CH}_4$ , it was found that  $^{128}\text{I}$  reacts not only by virtue of kinetic energy activation but by thermal processes. Of the 54.4% organic  $^{128}\text{I}$  (as  $\text{CH}_3^{128}\text{I}$ ) about 18.4% forms as a result of hot  $^{128}\text{I}$  reactions, 11% as a result of excited iodine atoms or  $\text{I}^+$  ions in the  $^3\text{P}_2$ ,  $^3\text{P}_1$ , and/or  $^3\text{P}_0$  states, and 25% as a result of reactions of  $\text{I}^+(\text{}^1\text{D}_2)$  ions. From these experiments, no suggestion could be made as to whether the hot reactions were with  $^{128}\text{I}$  atoms or  $^{128}\text{I}^+$  ions.

Three kinds of reactive  $^{128}\text{I}$  species are possible.

(1) A hot neutral atom receiving its kinetic energy by virtue of the radiative neutron capture process.

(2) A hot positive ion receiving its kinetic energy by virtue of the radiative neutron capture process and its positive charge by internal conversion of low nuclear energy states leading to Auger charging (occurring during the "cooling down" of the hot  $^{128}\text{I}$ ).

(3) A hot positive ion receiving its charge by internal conversion and Auger charging after the hot  $^{128}\text{I}$  is chemically stabilized and its kinetic energy by the coulombic repulsion between the  $^{128}\text{I}$  ion and the molecular fragment charged by intramolecular electron transfer.<sup>13</sup>

It was originally suggested by Spicer and Gordus<sup>14</sup> that the IT induced yields are lower than  $(n, \gamma)$ -induced yields because of the lower kinetic energy acquired by the coulombic repulsion in isomeric transition. In a study involving  $^{130}\text{I}$ <sup>15</sup> activated by radiative neutron capture [ $^{129}\text{I}(n, \gamma)^{130}\text{I}^m + ^{130}\text{I}$ ] and isomeric transition [ $^{130}\text{I}^m(\text{IT})^{130}\text{I}$ ], the IT hot organic yield ( $10.0 \pm 1.0\%$ ) was much lower than the  $(n, \gamma)$ -induced organic yield ( $16.6 \pm 2.0\%$ ). These results suggested that the  $(n, \gamma)$ -activated  $^{130}\text{I} + ^{130}\text{I}^m$  hot reactions occur mainly as the result of kinetic energy imparted to the recoil iodine atom or ions following  $\gamma$ -ray cascade while the isomeric transition induced hot reactions occurred by virtue of kinetic energy following coulombic repulsions.

Since the hot  $^{128}\text{I}$  organic yield<sup>5a</sup> (18.4%) is much higher than the  $^{130}\text{I}$  IT-induced yield and we would not expect a mass isotope effect between  $^{128}\text{I}$  and  $^{130}\text{I}$ , it is reasonable to assume that the hot  $^{128}\text{I}$  atoms or ions acquire their kinetic energy mainly by the radiative neutron capture process.

We employed rare-gas moderators to separate the organic yields resulting from hot-atom processes from those resulting from thermal ion-molecule reactions. Figure 1 shows the effect of rare-gas additives on the reactions of  $(n, \gamma)$ -activated  $^{128}\text{I}$  with  $\text{CH}_3\text{F}$ . The

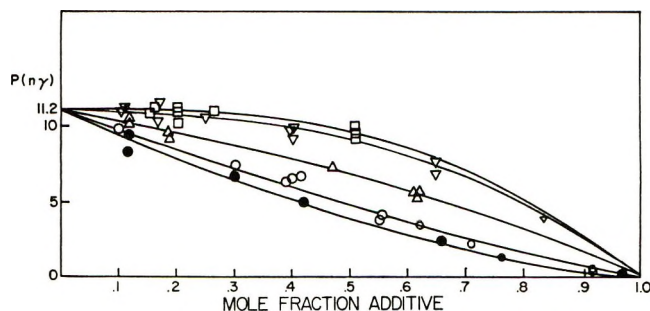


Figure 1. Per cent hot organic yield vs. the mole fraction additives for various rare-gas additives in the reactions of  $(n, \gamma)$ -activated  $^{128}\text{I}$  with  $\text{CH}_3\text{F}$ : (□) helium; (△) argon; (▽) neon; (○) krypton; (●) xenon.

limiting hot organic yield at 0 mole fraction additives is  $11.2 \pm 1.0\%$ . The data when extrapolated to 1 mol % additives appear to give a value of 0% hot organic yield. Unlike the reactions of  $(n, \gamma)$ -activated  $^{128}\text{I}$  with  $\text{CH}_4$ , the reactions of  $(n, \gamma)$ -activated  $^{128}\text{I}$  with  $\text{CH}_3\text{F}$  occurred completely by hot processes. No thermal contributions to the organic yields were observed. In the  $\text{CH}_4$  system,<sup>5a</sup> the reactions of  $\text{I}^+$  in the  $^1\text{D}_2$  state were shown by the consistency of xenon additives being able to reduce the formation of  $\text{CH}_3^{128}\text{I}$  to a greater extent than either Ne, Ar, or Kr additives. In the  $\text{CH}_3\text{F}$  systems the xenon additives like Ne, Ar, and Kr reduced the formation of  $\text{CH}_3^{128}\text{I}$  to 0% indicating the absence of the reactions of translationally thermalized and electronically excited  $\text{I}^+$  ions in  $^1\text{D}_2$  state and  $\text{I}^+$  ions in  $^3\text{P}_0$ ,  $^3\text{P}_1$ , and  $^3\text{P}_2$  states. A similar effect was observed for  $(n, \gamma)$ -activated  $^{128}\text{I}$  with  $\text{CH}_3\text{Cl}$ . The limiting hot organic yield for  $\text{CH}_3\text{Cl}$  system is  $4.2 \pm 0.5\%$ . The limiting hot organic yields for  $\text{CH}_3\text{Br}$  and  $\text{CH}_3\text{I}$  systems are  $0.67 \pm 0.1$  and  $0.2 \pm 0.1\%$ , respectively. Because these yields for  $\text{CH}_3\text{Br}$  and  $\text{CH}_3\text{I}$  systems are quite low, no attempt was made to study the effects of rare-gas moderators on these reactions. Since no thermal reactions were observed for the  $\text{CH}_3\text{F}$  and  $\text{CH}_3\text{Cl}$  systems, we would not expect any for the  $\text{CH}_3\text{Br}$  and  $\text{CH}_3\text{I}$  systems. In the halomethane systems, the  $^{128}\text{I}$  atom or ion reacts completely by virtue of its kinetic activations to form the organic products.

*Calculations of Recoil Energy Spectra.* Unlike other nuclear transformations such as the  $(\gamma, n)$  and  $(n, p)$  processes where all the hot atoms are born with a very high-kinetic energy ( $\sim 10^5$  eV), halogen atoms by virtue of the radiative neutron capture process acquire a spectrum of energies ranging from 0 to  $\sim 10^2$  eV. Since there are no reported calculations of a kinetic energy

(13) A. R. Kazanjian and W. F. Libby, *J. Chem. Phys.*, **42**, 2778 (1965).

(14) L. D. Spicer and A. A. Gordus, "Symposium on Chemical Effects Associated with Nuclear Reactions and Radioactive Transformations," Vol. 1, International Atomic Energy Agency, Vienna, 1965, p 185.

(15) M. Yoong, N. J. Nicholas, and E. P. Rack, *Radiochim. Acta*, in press.

spectrum for  $^{128}\text{I}$ , we calculated the  $^{128}\text{I}$  spectrum because of the importance it may have to the understanding of the systematics of the  $^{128}\text{I}$  hot reactions.

Our calculations of the kinetic energy spectra utilized the previously derived, closed general solutions of the probability distribution function for the three-dimensional random-walk processes reported by Hsiung and Gordus.<sup>11</sup> The general course of the calculations was also very similar to previous computations of this type and will not be discussed except where it differs from them. We employed an IBM-360 Model 651H computer. Our purpose was to improve the statistics that could be obtained by extending our calculations to all possible allowed combinations of  $\gamma$ -ray energies and not limiting our calculations to only a few possible combinations of  $\gamma$ -ray energies as Hsiung and Gordus had done. For each of the two, three, and four random-step processes, we generated 20,000 possible combinations. Of these 20,000 combinations, only those allowed combinations were used in our calculations. The allowed combinations of  $\gamma$ -ray energies are those combinations of energies whose sums are equal to the neutron binding energy associated with the  $^{127}\text{I}(n,\gamma)^{128}\text{I}$  activation. The neutron binding energy for an  $(n,\gamma)$ -activated  $^{128}\text{I}$  atom is equal to 6.805 MeV. It is important to note that the random-walk equations require the use of momentum vectors. In the particular case of  $\gamma$ -ray emission, the energy of a  $\gamma$ -ray differs from the momentum by only a multiplicative constant (the velocity of light).<sup>11</sup> Thus the  $\gamma$ -ray energies were used in our calculations. In order to compute a recoil energy spectrum for  $^{128}\text{I}$  atoms, both the high- and low-energies of the emitted  $\gamma$ -rays of  $(n,\gamma)$ -activated  $^{128}\text{I}$  must be known. The measurements of the  $\gamma$ -rays from  $(n,\gamma)$ -activated  $^{128}\text{I}$  reported by Archer, *et al.*,<sup>16</sup> were used since they reported both the high and low  $\gamma$ -ray energies. However, the details of the low-energy part of the  $\gamma$ -ray spectrum are not well established. They fail to account for the existence of two lines ( $\gamma$ -rays) at 147.01 and 156.18 keV which were resolved by Jones, *et al.*<sup>17,18</sup> These lines are of relatively low intensities ( $3.4 \pm 0.7$  and  $3.6 \pm 0.2$ , respectively) as compared to line 133.31 keV (corresponding to line 132 keV of Archer) whose intensity is 42.0. Although these lines are important in determining the extent of internal conversion leading to Auger charging, ionization, and excitation, the exclusion of these two lines does not significantly affect the computation of the recoil energy spectrum since they are of relatively low intensities. We are only interested in the distribution of the recoil energies imparted to  $(n,\gamma)$ -activated  $^{128}\text{I}$  atoms as a result of  $\gamma$ -ray cascades. The solutions to the probability function for the three-dimensional random-walk processes give the distribution of the recoil energy as a result of  $\gamma$ -ray cascade. They take into account the relative intensities (per 100 captures) of the measured  $\gamma$ -ray energies by weigh-

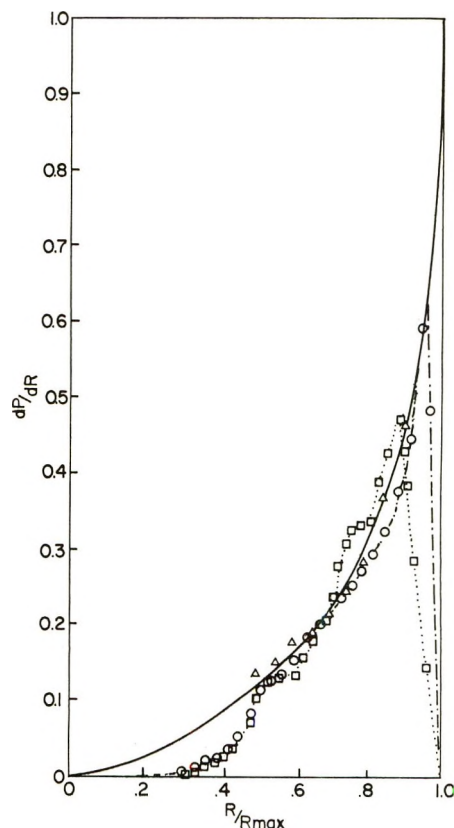


Figure 2. Probability distribution of  $\gamma$ -ray energies (in units of  $\text{MeV}^{-1}$ ) vs. the fraction of the maximum resultant  $\gamma$ -ray energy for two- ( $\Delta$ ), three- ( $\circ$ ), and four- ( $\square$ ) step processes.

ing each  $\gamma$ -ray energy by a degenerate factor equal to its intensity. Thus the random generation of possible allowed combinations of  $\gamma$ -rays would not be affected significantly by the exclusion of the two lines of low intensities.

*(n, $\gamma$ )-Activated  $^{128}\text{I}$  Recoil Spectrum.* Our results in Figure 2 show the probability distribution of  $\gamma$ -ray energies (in units of  $\text{MeV}^{-1}$ ) plotted against  $R/R_{\text{max}}$  (the fraction of the maximum resultant ( $\gamma$ -ray energies) for the two-, three-, and four-unequal-step processes. While Draper<sup>19</sup> reported that the absorption of a neutron by an  $^{127}\text{I}$  nucleus results promptly in a cascade of approximately four  $\gamma$ -rays, the decay scheme of  $^{127}\text{I} + n$  indicates that the recoil energy spectrum involve two  $\gamma$  steps.<sup>20</sup> We have translated both the probability distribution of the two-step process and the sum probability distribution of the two-, three-, and four-step processes in terms of recoil energy in eV. Figure 3 shows the recoil energy spectra for the  $^{128}\text{I}$  atoms ac-

(16) N. P. Archer, L. B. Hughes, T. J. Kenett, and W. V. Prestwich, *Nucl. Phys.*, **83**, 241 (1966).

(17) C. H. W. Jones, *J. Phys. Chem.*, **74**, 3347 (1970).

(18) R. G. Korteling, J. M. D'Auria, and C. H. W. Jones, *Nucl. Phys.*, **A138**, No. 2, 392 (1969).

(19) J. E. Draper, *Phys. Rev.*, **114**, 268 (1959).

(20) C. M. Lederer, J. M. Hollander, and I. Perlman, "Table of Isotopes," Wiley, New York, N. Y., 1967.

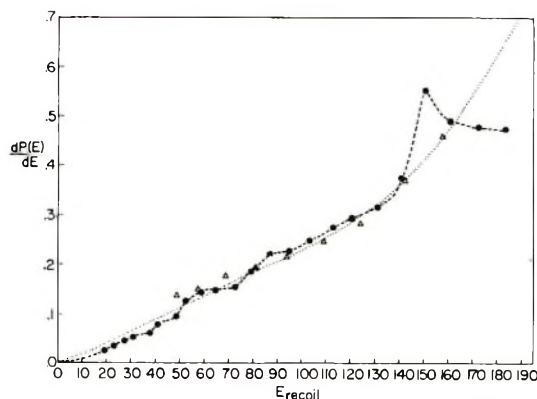


Figure 3. Probability distribution of  $\gamma$ -ray energies (in units of  $\text{MeV}^{-1}$ ) vs. the recoil energies (in units of eV of the  $^{128}\text{I}$  atoms: (.....) indicates spectrum obtained using the two-step process; (—) indicates spectrum calculated summing the two-, three-, and four-step processes.

tivated by radiative neutron capture. The dotted line indicates the recoil energy spectrum obtained using the two-step process and the dash line indicates the recoil energy spectrum calculated as the sum of the two-, three-, and four-step processes. It is of interest to observe the general features of these spectra. In the two-step process, the probability distribution of  $\gamma$ -ray energies increases from zero at low kinetic energies and rises as a logarithmic function. The spectrum obtained as a sum of the two-, three-, and four-step processes behaved in the same manner as that of the two-step process at low-recoil energy range but reached a maximum at 152 eV. Aside from this maximum, both spectra show that a substantial fraction of the  $^{128}\text{I}$  atoms or ions are born in or near the reactive zone  $E_2-E_1$ <sup>21</sup> (roughly estimated to be 80–10 eV for iodine reactions). Those hot atoms born with recoil energies in the range  $E_2-E_1$  can either react on the first collision or on subsequent collisions while possessing kinetic energy in the range  $E_2-E_1$  forming stable organic products, or be reduced in kinetic energy by cooling collisions with the internal moderator. In the  $(n,\gamma)$ -activated system, moderation of the hot  $^{128}\text{I}$  atoms to energies below the reactive zone can be affected in one or two ways: either by rare-gas additives introduced into the system or by the efficiency of the target organic molecules as internal moderators.

The recoil energies imparted to hot  $^{128}\text{I}$  atoms as a result of  $\gamma$ -ray cascade (194 eV) is low compared with  $(n,p)$ -activated tritium atoms (in the order of  $10^5$  eV). In the  $(n,p)$ -activated system it was possible to obtain by successive collisions of hot tritium atoms, a statistically well-defined distribution of energies in the chemically reactive zone  $E_2-E_1$ . However in the  $(n,\gamma)$ -activated  $^{128}\text{I}$  system, we do not obtain a statistically well-defined distribution of energies in the  $E_2-E_1$  zone, violating assumption Ia of the Wolfgang-Estrup kinetic theory.<sup>21,22</sup>

*Kinetic Energy Degradation Factor.* Presented in Table I are the various total hot organic yields for the reactions of  $(n,\gamma)$ -activated  $^{128}\text{I}$  with  $\text{CH}_4$ ,  $\text{CH}_3\text{F}$ ,  $\text{CH}_3\text{Cl}$ ,  $\text{CH}_3\text{Br}$ , and  $\text{CH}_3\text{I}$ .<sup>23</sup> The total hot organic yields are the per cent of the hot  $^{128}\text{I}$  atoms stabilized as hot organic products. In all systems studied, the only hot organic products found by radio-gas chromatography were the halogen and hydrogen substitution products. Because of rapid exchange between  $\text{HI}$  and  $\text{I}_2$  we could not determine the hot yields for the individual abstraction products.

Our results in Table I show a progressive decrease in hot organic yields for  $\text{CH}_3\text{F} > \text{CH}_3\text{Cl} > \text{CH}_3\text{Br} > \text{CH}_3\text{I}$ . By using the method suggested by Spicer and Wolfgang,<sup>3,4</sup> we calculated the areas available for reactions and the resulting expected yields if steric factor were operating for substitution reactions. Our results as seen in Table I indicate that there is no systematic or simple correlation between the hot  $^{128}\text{I}$  organic yields and steric factors, although it has been reported that steric and translational inertial factor influenced hot  $(\gamma,p)$ -activated  $^{39}\text{Cl}$  reactions with  $\text{CH}_4$  molecules.

A bond energy effect was reported by Rowland, *et al.*,<sup>4b</sup> for  $^{18}\text{F}$  substitution for X reaction in halomethanes highly moderated by the major component  $\text{SF}_6$  in the gaseous mixture. The endothermic reactions occur in the near thermal range. In our  $(n,\gamma)$ -activated  $^{128}\text{I}$  reaction with halomethanes, the major component was the halomethanes, allowing the hot  $^{128}\text{I}$  atoms to be moderated internally by collisions mainly with halomethane molecules. We observed no thermal contribution to the organic yields. The organic yields were the result of hot processes. While it is true that the hot  $^{128}\text{I}$  atoms or ions by virtue of their kinetic energy can form organic as well as inorganic products (resulting from substitution or abstraction reactions, respectively), the type of products should depend on the mode of reaction (or collision). If substitution and abstraction occur by the same type of collision, then bond energy may be an important parameter for the formation of inorganic products, which would be in competition with the formation of organic products. However, Wolfgang<sup>24</sup> suggested that the formation of

(21) R. Wolfgang, *J. Chem. Phys.*, **39**, 2983 (1963).

(22) Employing the Wolfgang-Estrup kinetic theory, we calculated the  $I$  (integral probability) and the  $K$  (correction term for  $I$ ) values for the reactions of  $(n,\gamma)$ -activated  $^{128}\text{I}$  with  $\text{CH}_4$  and  $\text{CD}_4$ . If the kinetic theory was applicable to these systems, the  $K$  values should be equal to  $(1/2)I^2$ . The correlations were extremely poor supporting the idea that the  $(n,\gamma)$ -activations does not produce hot atoms of sufficient energies to obey assumption Ia of the Wolfgang-Estrup kinetic theory.

(23) Two different kinds of experiments were performed: (a) those systems containing the halomethanes  $\text{CH}_3\text{X}$  ( $\text{X} = \text{F}, \text{Cl}, \text{and Br}$ ) and  $\text{CH}_3\text{I}$  (the limiting hot organic yields reported in Table I are found by extrapolating the data to zero mole fraction  $\text{CH}_3\text{I}$  additives and were corrected for the 1.1% failure to bond rupture of  $\text{CH}_3\text{I}$  and any radiation induced reactions); and (b) those systems containing  $\text{CH}_3\text{X}$ ,  $\text{CH}_3\text{I}$ ,  $\text{I}_2$ , and rare gas additives. Except for the  $\text{CH}_3\text{I}$  system, all systems contained 700 Torr total pressure and 2 mm of  $\text{CH}_3\text{I}$  and 0.1 mm of  $\text{I}_2$  as scavenger.

(24) R. Wolfgang, *Progr. React. Kinet.*, **3**, 99 (1965).

**Table I:** Observed Hot Organic Yields of (n, $\gamma$ )-Activated  $^{128}\text{I}$  with Halomethanes and the Energy Degradation Factors Calculated for these Halomethane Systems<sup>a</sup>

Target molecule	CH <sub>4</sub>	CH <sub>3</sub> F	CH <sub>2</sub> Cl	CH <sub>2</sub> Br	CH <sub>3</sub> I
% obsd hot organic yields (reactions with (n, $\gamma$ )-activated $^{128}\text{I}$ )	19.00 $\pm$ 2.0	11.20 $\pm$ 1.0	4.12 $\pm$ 0.5	0.67 $\pm$ 0.1	0.20 $\pm$ 0.1
Energy degradation factor	0.40	0.66	0.81	0.98	0.99
C-X bond energy, kcal/mol	104	108	884	70	56
% calcd <sup>b</sup> hot yields	19.00	13.43	13.43	13.43	13.43
IP, eV	12.99	12.8	11.22	10.54	9.54

<sup>a</sup> Bond energy, calculated hot yields, and IP have been added for the purpose of comparison. <sup>b</sup> See ref 2.

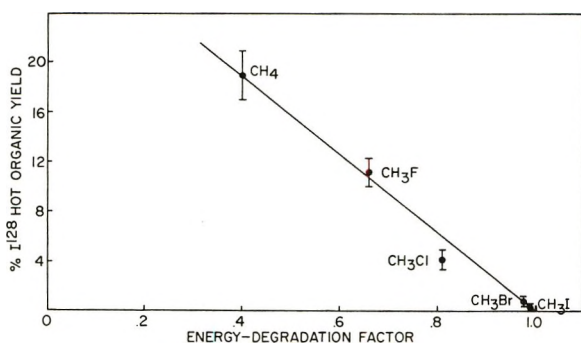


Figure 4. Plot of  $^{128}\text{I}$  hot organic yield vs. the energy degradation factors of the halomethane systems.

organic products has a different mode of reaction from that leading to inorganic products. Undoubtedly, bond energy is important for abstraction process leading to inorganic yield (favored by the weaker bonds of the halomethanes) but should not compete with substitution processes resulting in organic product yields. Therefore the observed decrease in hot organic yields in the halomethanes appears independent of a bond energy effect.

From ionization potential data of the halomethanes, no simple correlation can be made suggesting the reaction of  $^{128}\text{I}$  as an atom or as a positive ion; only  $\text{CH}_3\text{I}$  possesses an ionization potential lower than the iodine atom (10.454 eV). The only systematic trend we were able to find was between the hot  $^{128}\text{I}$  organic yields and the halomethane system's energy degradation factor.<sup>25</sup> The progressive, nearly linear decrease in hot  $^{128}\text{I}$  organic yield with increasing system energy degradation factor can be seen in Figure 4. It is important to note that for atoms born with high kinetic energies such as the (n,p)-activated tritium atoms (10<sup>5</sup> eV) we would not expect the energy degradation factor to be of importance, since the loss of energy upon collision may still result in the atoms having energy in or above the reactive zone. As pointed out in the previous section and from inspection of Figure 3, a significant fraction of the  $^{128}\text{I}$  atoms or ions are born in or near the reactive zone. For atoms or ions born with these low kinetic energies such as (n, $\gamma$ )-activated  $^{128}\text{I}$  atoms, the energy

degradation factor becomes significant because one or two collisions with a halomethane molecule may result in iodine atoms having energies below the reactive zone, removing it from organic combination. While the energy degradation factor depends on the mass of the hot atom and the mass of the moderator molecule (see eq, ref 24), the significance of the energy degradation factor in a reaction system depends upon the recoil energy possessed by the hot atoms (*i.e.*, the kinetic energy spectra of the hot atoms). This is consistent with the kinetic energy isotope effect reported<sup>26</sup> in the reactions of various bromine isotopes activated by radiative neutron capture in gaseous  $\text{CH}_3\text{F}$  and  $\text{CD}_3\text{F}$ . If the energy degradation factor is of "prime importance" for (n, $\gamma$ ) reactions, then the total yields for polyhalomethanes such as  $\text{CH}_2\text{F}_2$ ,  $\text{CHF}_3$ , and  $\text{CF}_4$  should follow the same type of correlation as shown in Figure 4. The energy degradation factors are 0.82, 0.91, and 0.97, respectively, and their corresponding observed hot organic yields are  $1.54 \pm 0.3$ ,  $1.04 \pm 0.2$ , and  $0.57 \pm 0.1\%$ .<sup>27</sup>

Our data on the energy degradation factor suggest that the predominant reason for low hot yields in halomethanes as compared to  $\text{CH}_4$  is the more efficient moderation of the (n, $\gamma$ )-activated  $^{128}\text{I}$  atoms by the halomethane molecules to energies below the reactive zone  $E_2-E_1$ . Since the kinetic energy spectrum for (n, $\gamma$ )-activated  $^{128}\text{I}$  atoms is sufficiently low so that an appreciable fraction is born in or near the reactive zone, we would expect that with increasing energy degradation factors of the halomethane systems, the collisional efficiency in reducing the kinetic energy of the  $^{128}\text{I}$  atoms below the zone increases; hence a decrease in the observed hot organic yield.

This study suggests that one of the prime factors in determining the extent of reaction for (n, $\gamma$ )-activated  $^{128}\text{I}$  atoms or ions is the system's energy degradation factor.

(25) The energy degradation factor is given by the equation  $(E/EN) = 4MaMn/(Ma + Mn)^2$  where  $Ma$  = mass of hot atom and  $Mn$  = mass of target molecule.

(26) R. Helton, M. Yoong, and E. P. Rack, *J. Phys. Chem.*, **75**, 2072 (1971).

(27) N. J. Parks, Ph.D. Thesis, University of Nebraska, 1969.

# An Electron Spin Resonance Study of Adsorption Stabilization of Photolytic Trifluoromethyl Radicals on Zeolites

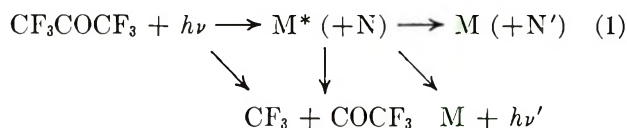
by P. Svejda

*Institute of Physical Chemistry, Technical University Hannover, Hannover, West Germany (Received January 31, 1972)*

The photolytic preparation and the esr spectrum of the  $\text{CF}_3$  radical from hexafluoroacetone (HFA) adsorbed on 13X zeolite at 77°K is reported. The components  $A_{\parallel} = 244$  G and  $B_{\perp} = 102$  G were evaluated assuming a hyperfine coupling tensor with axial symmetry. The radical is regarded as being stabilized in the space available after the lining of the zeolite pores with HFA. It can invert but rotation is completely hindered. The influence of temperature, concentration, time of irradiation, and wavelength of the light on the photolysis of HFA adsorbed on 13X zeolite was investigated. Photolysis of pure HFA and the use of other adsorbents are discussed.

## Introduction

The  $\text{CF}_3$  radical is widely used as a hydrogen abstractor in the study of reaction kinetics in the gas phase<sup>1</sup> and is generally produced by uv photolysis of water-free hexafluoroacetone (HFA) whereby light is



absorbed in the range 330.0–250.0 nm at room temperature.<sup>2</sup>

The photolysis of solid HFA at low temperatures appears to have been neglected in the literature in spite of the potential value as a source of  $\text{CF}_3$ . Recent measurements using this approach on other systems<sup>3,4</sup> have demonstrated the value of the technique where the radicals are stabilized in the solid matrix of the parent compound and then studied by the esr method.

The esr spectrum of the  $\text{CF}_3$  radical has been only rarely observed. The preparation methods used in these cases were electron bombardment of a liquid hexafluoroethane–tetrafluoromethane mixture at 77°K,<sup>5</sup> photolysis of trifluoromethyl iodide in a noble gas matrix at 35°K<sup>6</sup> and at 4.2°K,<sup>7</sup> irradiation of single crystal trifluoroacetamide with electrons at 77°K,<sup>8</sup> and most recently by photolysis of lead(IV) trifluoroacetate in hexafluorobenzene at 77°K.<sup>9</sup>

The spectrum of the freely rotating  $\text{CF}_3$  radical shows basically the four lines of the equivalent F atoms with the nuclear spin quantum number  $I = 1/2$ ,<sup>5,6</sup> and additional second-order splitting due to strong fluorine coupling.<sup>10</sup> The components of the hyperfine tensor were first estimated by Rogers and Kispert.<sup>8</sup>

On the other hand a complicated, many line spectrum is observed for nonrotating statistically oriented  $\text{CF}_3$  radicals in a matrix.<sup>7,9</sup> Maruani, *et al.*,<sup>7</sup> who carried out the most detailed work on the spectrum using

computer simulation techniques could explain most of the lines. The remaining lines were interpreted by the same authors in a subsequent and interesting work by careful consideration of the symmetry of the radical and second-order splitting.<sup>11</sup> Unfortunately, some details of the spectrum are lost in the computer simulations, a point which is undergoing consideration in this laboratory.

On the basis of previous work it is considered that an investigation of other methods for stabilizing the  $\text{CF}_3$  radical could lead to a simple and convenient preparation of samples for esr studies. Preliminary experiments with solid HFA at 77°K were unsuccessful as the radical is not stabilized in the solid matrix at this temperature. It is well known that some free organic radicals adsorbed on surfaces are stable even up to room temperature.<sup>12</sup> The technique has been used almost exclusively for  $\text{CH}_3$  radicals or fragments of alcohols adsorbed on silica gel or alumina.<sup>12,13</sup> The sta-

(1) P. Gray, A. A. Herod, and A. Jones, *Chem. Rev.*, **71**, 247 (1971).

(2) J. G. Calvert and J. N. Pitts, Jr., "Photochemistry," Wiley, New York, N. Y., 1967, p 393.

(3) P. Svejda and D. H. Volman, *J. Phys. Chem.*, **73**, 4417 (1969).

(4) P. Svejda and D. H. Volman, *ibid.*, **74**, 1872 (1970).

(5) R. W. Fessenden and R. Schuler, *J. Chem. Phys.*, **43**, 2704 (1965).

(6) S. W. Charles, P. H. H. Fischer, and C. A. McDowell, *Chem. Phys. Lett.*, **1**, 451 (1967).

(7) J. Maruani, C. A. McDowell, H. Nakajima, and P. Raghunathan, *Mol. Phys.*, **14**, 349 (1968).

(8) M. T. Rogers and L. D. Kispert, *J. Chem. Phys.*, **46**, 3193 (1967).

(9) H. Loeliger, *Helv. Chim. Acta.*, **52**, 153 (1969).

(10) R. W. Fessenden, *J. Chem. Phys.*, **37**, 747 (1962).

(11) J. Maruani, J. A. R. Cope, and M. C. McDowell, *Mol. Phys.*, **18**, 165 (1970).

(12) G. B. Pariiskii, G. M. Shidomirow, and V. B. Kazanskii, *Zh. Strukt. Khim.*, **4**, 364 (1963); J. Turkevich and Y. Fujita, *Science*, **152**, 1619 (1966); M. Fujimoto, M. D. Gesser, B. Garbutt, and A. Cohen, *ibid.*, **154**, 147 (1966).

(13) A. P. Bobrovskii and V. E. Kholmogorov, *Khim. Vys. Energ.*, **2**, 147 (1968).

bility of particular radicals has been considered in terms of active centers, pore size, and specific surface area of the adsorbent. The defined pore size offered by zeolites has unaccountably only been used for inorganic radicals such as  $\text{NO}$ ,<sup>14</sup>  $\text{NO}_2$  and  $\text{ClO}_2$ ,<sup>15</sup>  $\text{NO}_3$ ,<sup>16</sup> and  $\text{O}_2^-$ ,<sup>17</sup> and once to trap radicals after electron bombardment of mesitylene.<sup>18</sup>

The present work describes the investigation of zeolites as adsorbents for the stabilization of  $\text{CF}_3$  radicals after photolysis. ESR spectra from  $\text{CF}_3$  radicals prepared from HFA on 13X zeolite are presented and discussed in terms of the probable stabilization mechanism.

### Experimental Section

Hexafluoroacetone trihydrate (Uvasol Merck) was thoroughly dehydrated over excess  $\text{P}_2\text{O}_5$  in a vacuum apparatus. The gas was condensed at  $77^\circ\text{K}$ , fractionally distilled, purified by repeated pumping and thawing cycles,<sup>3,4</sup> and stored in the dark under grease-free conditions at  $77^\circ\text{K}$ .

The samples were prepared as follows. The powder adsorbents (Table I) were evacuated in a grease-free vacuum line (Teflon taps, mercury diffusion pump) to  $10^{-6}$  Torr in quartz esr tubes and heated to  $400^\circ$  in an electric furnace (controlled by a thermocouple) for 19 hr. They were then exposed to HFA vapor for 15 min at different pressures measured on a Pirani gauge (Thermovac, Leybold). The samples were sealed off and cooled immediately to  $77^\circ\text{K}$ , irradiated in an esr quartz dewar, and mounted in the spectrometer.

**Table I:** Adsorbents Used for the Stabilization of the  $\text{CF}_3$  Radicals

Absorbent	Manu- facturer	Pore size, Å	Average pore size, Å	Specific surface, $\text{m}^2/\text{g}$
Zeolite (binder free)	4A	Brenntag	4	
	10X	Brenntag	7	
	13X	Brenntag	8	
Silica gel	113	Grace	70-150	110
	121	Grace	10-40	21

Two lamps were used for the photolysis. Nearly all of the samples were prepared using lamp 1, a spiral form low-pressure mercury lamp (PCQ X1, UV Products, Calif.) in a Vycor housing which had 90% of its output at 253.7 nm. The other uv source used, lamp 2, was a high-pressure mercury lamp (HBO 200, Osram).

Esr measurements were conducted in a Varian spectrometer (V 4500-10A, X Band, 100-kHz field modulation, V 4560) with a variable low-temperature unit. The exact  $g$  value determination and spectrum measuring was carried out on a second spectrometer (Bruker, BER 402, X Band, 100-kHz field modulation)

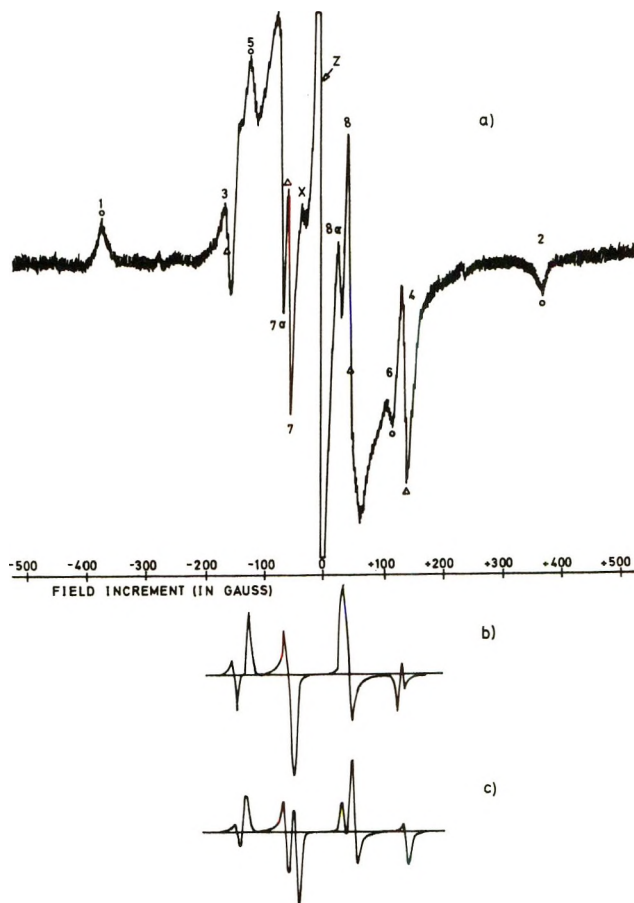


**Figure 1.** ESR spectrum of the  $\text{CF}_3$  radical. (a) Spectrum observed after 3 hr of irradiation of hexafluoroacetone on 13X zeolite with lamp 1 at  $77^\circ\text{K}$ .  $g$  value of the free electron is chosen as reference point. (b) Computer simulated spectrum to scale without second-order splitting (from ref 7). (c) Computer simulation of the spectrum as in (b) but with second-order splitting (from ref 11).

on which the field was linearly variable by means of a H-nmr probe and which enabled the simultaneous recording of field strength and klystron frequency. The error due to the different positions of the sample and the probe was corrected by calibration with DPPH.

The number of radicals was estimated by comparison with a Varian pitch probe at constant spectrometer settings.

### Results

No spectra attributable to radical fractions of HFA produced by the photolysis were observed with the silica gel adsorbents and 4A and 10X zeolites (all con-

(14) B. M. Hoffman and N. J. Nelson, *J. Chem. Phys.*, **50**, 2598 (1969); J. H. Lunsford, *J. Phys. Chem.*, **74**, 1518 (1970); C. L. Gardner and M. A. Weinberger, *Can. J. Chem.*, **48**, 1317 (1970).

(15) T. M. Pietrzak and D. E. Wood, *J. Chem. Phys.*, **53**, 2454 (1970).

(16) T. M. Pietrzak and D. E. Wood, *ibid.*, **46**, 2973 (1967).

(17) K. M. Wang and J. H. Lunsford, *J. Phys. Chem.*, **74**, 1512 (1970).

(18) G. A. Helcké and R. Fantechi, *Mol. Phys.*, **17**, 65 (1969).

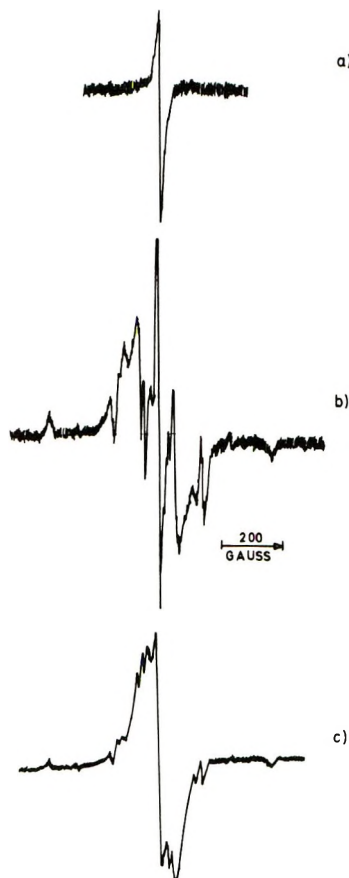


Figure 2. Comparison of the "background" signal of 13X zeolite and the spectrum obtained under different irradiation conditions. (a) ESR spectrum of the 13X zeolite after 3 hr of irradiation with lamp 1 at 77°K. (b) ESR spectrum of  $\text{CF}_3$  radicals after 3 hr of irradiation of HFA on 13X zeolite with lamp 1 at 77°K. (c) ESR spectrum of  $\text{CF}_3$  radicals after 2 hr of irradiation of HFA on 13X zeolite with lamp 2 at 77°K.

tacted with 760-Torr HFA at room temperature before irradiation). The fairly marked background signal (which was also similar on 13X) at  $g = 2.0023$ , with an approximately 60-G line width, was somewhat enlarged after irradiation.

Pure dried HFA,  $\text{HFA} \cdot 1.5\text{H}_2\text{O}$ , and  $\text{HFA} \cdot 3\text{H}_2\text{O}$  gave no esr signal after 3 hr of irradiation with lamp 1 at 77°K (cf. ref 3,4).

Irradiation of a 13X zeolite sample which had been exposed to HFA vapor (760 Torr) with lamp 1 for 3 hr at 77°K yielded the spectrum shown in Figure 1a. The  $g$  value for the free electron was chosen as reference. The signal remained unchanged after 60 hr at 77°K and the relative intensities of the lines were not affected by klystron power up to the maximum level available. The signal corresponds to some  $10^{16}$  spins.

A control sample of 13X not exposed to HFA but otherwise subjected to identical treatment with that above gave a weak background signal before irradiation with a  $g$  value approximately that of the free electron. The amplitude doubled after 3 hr of irradiation at 77°K (lamp 1) and returned to its original size after warming

to room temperature. This "zeolite" background signal (Figure 2a) is completely swamped by the central peak Z and does not influence the spectrum of the radical (Figure 2b).

Spectrum 2c was obtained after 2 hr of irradiation with lamp 2. A similar spectrum was observed when the sample was first irradiated for 3 hr with lamp 1 followed by 9 hr with lamp 2 through a 2-mm Pyrex filter. Spectrum Z + X increases at the expense of the other components. The radiation from lamp 2 through a 2-mm Pyrex filter is ineffective for photolysis.

Slow warming of the sample (15 min equilibration time per 10° step) causes the spectrum to reduce evenly without ever becoming isotropic or without changing its shape, relative line intensities, and line widths. The signal Z + X increases steadily. The spectrum which disappears must therefore belong to a single paramagnetic species and is still visible up to 140–150°K. The spectrum Z + X (Figure 3) remained stable up to 190°K and disappeared at room temperature.

Short periods of irradiation (30 sec up to several minutes) had no effect on the sample; the known spectrum appeared after 15 min of irradiation and reached maximum intensity after 2 hr, remaining constant after further irradiation. Again here the spectrum remained unchanged except in amplitude once it had appeared.

Equal amounts of zeolite were exposed to different pressures of HFA and irradiated. Pressures from  $9 \times 10^{-3}$  Torr upward were investigated. The whole spectrum appeared weakly after 7 hr of irradiation of a sample exposed to  $3 \times 10^{-1}$  Torr HFA, and good spectra were obtained after adsorption at  $8 \times 10^{-1}$ –10 Torr HFA. Again the spectrum varied only in amplitude and no alternation in the shape or line width was observed.

## Discussion

The results of Maruani, *et al.*,<sup>7</sup> and Loeliger<sup>9</sup> enable the spectrum (apart from Z + X) to be attributed to the "power spectrum" of the  $\text{CF}_3$  radical.

The parallel component of the hyperfine coupling tensor, which was assumed to be almost axial sym-

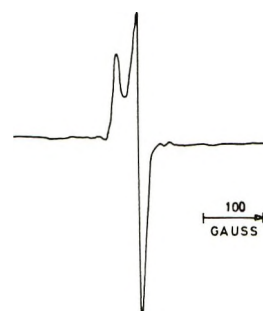


Figure 3. Spectrum of the secondary radical observed after disappearance of the  $\text{CF}_3$  spectrum during warm-up.

metric, was determined following Loeliger<sup>9</sup> from peaks 1 and 2 and 5 and 6 (measured at points marked o, Figure 1a) to be  $A = 244$  G and the normal component  $B = 101.5$  G from peaks 3 and 4 and 7 and 8 (measured at points  $\Delta$ ).

Choosing the exact measurement points with reference to the computer simulated spectrum is somewhat arbitrary at some  $\pm 5$  G. The line width of the outer peaks (1, 2, 3, and 4) averaged 40 G and of the others (5, 6, 7, and 8,) 11 G. The  $g$  value was found to be isotropic within experimental limits at  $2.0036 \pm 0.0003$ .

The lines 7a and 8a are clearly second-order splitting (width *ca.* 10 G, displaced 10 G to smaller field strength) and were found at the positions predicted by Maruani.<sup>11</sup>

As the  $\text{CF}_3$  radical is bent by an angle  $\gamma = 17.8^\circ$  between the axis of symmetry and the plane at right angle to the CF bond, the esr spectrum is very sensitive to a change of that angle showing a variable line in the center of the spectrum. This peak is covered here by Z, but the remainder has the form to be expected for a varying  $\gamma$ .

The computer simulated spectrum<sup>7,11</sup> for an inverting  $\text{CF}_3$  radical without second-order splitting clearly reproduces the outer lines (Figure 1b), and the spectrum with second-order splitting the central lines (Figure 1c).

The spectra are most readily explained assuming stabilization of the  $\text{CF}_3$  radicals in a narrow cage in which rotation is completely hindered, hence the anisotropy, while inversion is possible at 77°K. The space in the cage remains unchanged on warming as seen by the constant line width and hyperfine coupling. The radical disappears by reaction rather than becoming freely rotating or mobile. The cage is most probably a zeolite cavity lined with HFA, in which the HFA shields the radical from the influence of the zeolite walls, and therefore  $\text{CF}_3$  in a HFA pore is observed. The amount of zeolite used in the samples had an estimated total of  $10^{18}$  pores, in which some  $10^{16}$  radicals were observed, which is consistent with this model bearing in mind possible unevenness in irradiation through the sample. The lack of exchange narrowing and independence of the spectrum on concentration indicate that the radicals once produced are not able to leave the cavity.

The isotropic coupling of 149 G and the anisotropic values of  $\alpha = +95$  G,  $\beta_1 = \beta_2 = -47.5$  G calculated from the observed  $A_{\parallel}$  and  $B_{\perp}$  are slightly different from those previously reported, which may be due to the

change in the spin densities in inverting  $\text{CF}_3$  radicals or to changes in the hyperfine coupling by van der Waals forces between the matrix and the radical<sup>19</sup> or both, a problem which is undergoing further consideration in this laboratory.

As the radical reacts and disappears it is replaced by a new compound (about  $5 \times 10^{15}$  spins) whose spectrum (Figure 3), also present weakly as Z + X after the photolysis, suggests a  $\text{CF}_3\text{OO}$  radical with the  $g$  values  $g_{\perp} = 2.0084$  and  $g_{\parallel} = 2.031$  (*cf.* ref 7).

The photolysis of HFA can yield  $\text{CF}_3\text{CO}$  radicals, see eq 1. This species was not observed, however, but it is possible that a signal from  $\text{CF}_3\text{CO}$  or a secondary radical could be concealed in the central peak Z. The  $\text{CF}_3$  spectrum agreed closely with known data; the coupling for  $\beta$  F atoms from  $\text{CF}_3\text{CO}$  could be expected to have an isotropic coupling constant at 20–40 G.<sup>20</sup>

The experiments with the different lamps show that photosensitization by lamp 1 to give stronger  $\text{CF}_3$  formation cannot be ruled out, but without sensitization using lamp 2  $\text{CF}_3$  is also produced. The radicals react even at 77°K under the influence of the long wave uv output of the second lamp which is otherwise only observed on raising the temperature.

The failure to obtain a  $\text{CF}_3$  spectrum using the other adsorbents points to pore size as the decisive factor since the surface area was large and similar in all cases. Radiation damage on the 13X zeolite seemed small; the background signal observed can probably be drastically reduced by thorough purification of the zeolite which would enable reactive photolytic intermediate products to be stabilized on the surface and investigated by esr techniques.

The reason why no radicals were observed after irradiation of solid water-free HFA is considered to be that the HFA matrix is too rigid and cannot accommodate the radicals interstitially.

*Acknowledgment.* The author wishes to thank Professor R. Haul for his interest in the work and for stimulating discussions. Thanks are also due to the directors of the Institute for Organic Chemistry TU Hannover for the use of the Varian spectrometer and in particular to U. Fiederling for his most helpful preparatory investigations. Financial support from the Deutsche Forschungsgemeinschaft is gratefully acknowledged.

(19) F. J. Adrian, *J. Chem. Phys.*, **32**, 972 (1962).

(20) M. Iwasaki, K. Toriyama, and B. Eda, *ibid.*, **42**, 3 (1965).



# Effect of Hydrogen Adsorption on the Electron Paramagnetic Resonance Spectra of Catalysts Containing Chromium Oxide<sup>1</sup>

by Lurance M. Webber

*The Chemistry Department, University of California, Santa Barbara, California (Received January 12, 1972)*

A comparison of the epr spectra of reduced chromia gel,  $\alpha$ -chromia, and 9.5 mol % chromia/alumina impregnated catalysts, measured in a vacuum and in a hydrogen atmosphere, showed that hydrogen adsorption had a strong influence on the Cr(III) ions believed to be responsible for the  $\beta$ -phase signal. Adsorption of hydrogen on chromia/alumina caused an increase in the epr line width, relative intensity, and Weiss constant, thus indicating that the number of Cr(III) ions had increased. Hydrogen adsorption on samples of chromia gel and  $\alpha$ -chromia caused a decrease in the epr line width, relative intensity, and Weiss constant, indicating that the number of Cr(III) ions had decreased. Therefore, it may be suggested that hydrogen adsorption on previously reduced and evacuated chromia/alumina causes surface oxidation of Cr(II) to Cr(III), and that hydrogen adsorption on reduced and evacuated chromia gel and  $\alpha$ -chromia causes the oxidation of Cr(III) possibly to Cr(IV). The presence of an <sup>27</sup>Al superhyperfine structure on the  $\beta$ -phase Cr(III) epr signal indicated that the lower oxidation state shown by chromia/alumina is related to direct interaction between chromium and adjacent aluminum ions.

## Introduction

The epr spectra of catalysts containing chromium oxide have received attention as shown by a review by Poole and MacIver.<sup>2</sup> Most papers on this subject have dealt with chromium oxide supported on aluminum oxide. Most workers agree that there are three major electronic configurations, or phases, that give rise to the epr spectrum of chromia/alumina catalysts prepared by impregnation. These are the  $\delta$  phase, which is thought to arise from Cr(III) ions that are isolated from other chromium ions; the  $\gamma$  phase, attributed to Cr(V) ions; and the  $\beta$  phase, attributed Cr(III) ions which show a degree of antiferromagnetic coupling with adjacent Cr(III) ions. The  $\beta$ -phase signal dominates the spectrum of typical reduced chromia/alumina catalysts. The only signal reported that can be attributed to chromium ions on unsupported chromia catalysts is the  $\beta$  phase.

This paper reports the results of experiments undertaken to determine the influence of hydrogen on the  $\beta$ -phase resonance signal for some reduced chromium oxide catalysts.

## Experimental Section

**Preparation of Samples.** Chromia gel was prepared as described by Ciapetta and Park.<sup>3</sup> Aqueous ammonia was added to a Cr(NO<sub>3</sub>)<sub>3</sub> solution. The resulting gelatinous precipitate was washed, dried, and heated *in vacuo* at 380°. The product had a specific surface (BET, N<sub>2</sub>) of about 200 m<sup>2</sup>, and it gave only a diffuse X-ray diffraction pattern.

The  $\alpha$ -chromia was prepared by heating the gel, prepared as described above, *in vacuo* at 550° for 10 hr. The specific surface was about 30 m<sup>2</sup>, and the diffraction pattern was that of pure  $\alpha$ -chromia.

Supported chromia was prepared by the impregnation of  $\gamma$ -alumina with a Cr(NO<sub>3</sub>)<sub>3</sub> solution. The alumina was obtained by the hydrolysis of triple-distilled aluminum isopropoxide, followed by drying at 625°. The concentration of the Cr(NO<sub>3</sub>)<sub>3</sub> solution was chosen to yield a 9.5 mol % chromia content in the finished catalyst. The resulting emulsion was placed in a rotary evacuator and the moisture was drawn off by an aspirator. The specific surface was about 200 m<sup>2</sup>, and the X-ray diffraction pattern that of  $\gamma$ -alumina.

**Pretreatment.** Further pretreatment of all samples was done *in situ*. The chromia gel was heated in flowing hydrogen for 12 hr at 400°, followed by evacuation for 12 hr at 400°. The  $\alpha$ -chromia was treated in exactly the same way. The chromia-alumina sample was evacuated for 2 hr at 400°, treated in flowing hydrogen for 2 hr at 400°, and finally evacuated again for 2 hr at 400°. More severe pretreatment of one sample is described later. Chromia gel was pretreated for a longer time because it was considerably more difficult to remove water and other adsorbed gases from this preparation. Increasing the time for chromia-alumina resulted in darkening the sample.

**Epr Measurements.** Epr spectra were obtained on evacuated samples after they had been cooled to the desired temperature. For measurements in a hydrogen atmosphere, the samples were exposed to hydrogen at 1 atm, then heated to 300°, and slowly cooled to

(1) Extracted from the dissertation of the author, submitted in partial fulfillment of the requirements for the degree of Doctor of Philosophy in Chemistry at the University of California, Santa Barbara, 1970.

(2) C. P. Poole and D. S. MacIver, *Advan. Catal.*, **17**, 223 (1967).

(3) E. C. Ciapetta and C. J. Park, "Catalysis," Vol. 1, P. H. Emmett, Ed., Reinhold, Baltimore, Md., 1954, p 342.

room temperature before the measurements were made. This procedure was followed to ensure complete surface reaction between the sample and hydrogen.<sup>4</sup>

These measurements were made on a Varian V-4502 x-band epr spectrometer, equipped with a Varian V-4560 100-Hz field modulation and control unit. Spectra at various temperatures were obtained with a Varian V-4540 variable-temperature control unit. The sample holder was modified to permit evacuation and atmosphere control.

The number of electronic spins contributing to the epr signal was determined by comparison with a sample of 1 mol % chromia/alumina, which was treated by heating it *in vacuo* at 500° for 2 hr, followed by hydrogen at 500° for 2 hr. This sample was chosen as a standard because at this low percentage of chromium clusters of chromia are not readily formed,<sup>5</sup> and exchange interaction is low. This is shown by the line width of the epr signal which was 3100 G at 40°. Poole and Itzel<sup>6</sup> estimate that the line width of the  $\beta$ -phase signal resulting from dipole-dipole interaction alone should be about 3000 G.

## Results

The epr spectra of samples of chromia gel,  $\alpha$ -chromia, and 9.5 % chromia/alumina were measured at various temperatures *in vacuo* and in hydrogen. The  $\beta$ -resonance signal present in each case was symmetrical and of a Lorentzian line shape. The value of the  $g$  factor was near 2. There was no variation of the  $g$  factor that could be attributed to either the variation of temperature or to change of atmosphere.

The spectrum of the chromia/alumina sample showed weak  $\delta$ - and  $\gamma$ -phase resonance signals, and the spectra of chromia gel and of  $\alpha$ -chromia contained weak signals which were attributed to color centers. A change of atmosphere had no detectable effect on these signals in the temperature ranges reported here.

The variation of the epr line width with temperature of the  $\beta$ -phase resonance signals is shown by Figure 1. This variation was measured with the sample *in vacuo* or in a hydrogen atmosphere. The line width for the chromia/alumina sample was broadened by the adsorption of hydrogen. The line width was narrowed by hydrogen for chromia gel and for  $\alpha$ -chromia. The narrowing for  $\alpha$ -chromia was quite small owing, probably, to the small specific surface of this sample.

Figure 2 shows the variation with temperature of the relative intensities. For all samples, the relative intensity,  $N$  was calculated from the equation

$$N = KI\Delta H_{pp}^2 \quad (1)$$

where  $I$  is the signal amplitude,  $\Delta H_{pp}$  is the peak to peak line width, and  $K$  is a constant, 1.8, for a curve of Lorentzian distribution.<sup>7</sup> Adsorption of hydrogen decreased the intensity of the  $\beta$ -resonance signals of chromia gel and of  $\alpha$ -chromia, and increased the inten-

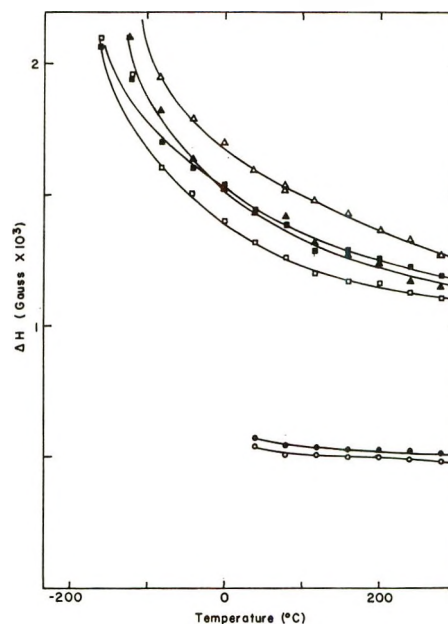


Figure 1. Temperature dependence of the peak to peak (derivative) line width of chromia gel (■ *vac*, □ H<sub>2</sub>),  $\alpha$ -chromia (● *vac*, ○ H<sub>2</sub>), and 9.5 mol % chromia/alumina (▲ *vac*, △ H<sub>2</sub>).

sity for the chromia/alumina sample. The change in relative intensity due to the adsorption of hydrogen on the chromia/alumina sample is shown more readily by the reciprocal of the relative intensity shown in Figure 3.

The epr relative intensity is a measure of the total number of electronic spins in the system and is, therefore, a measure of the magnetic susceptibility. Thus, a plot of the reciprocal of the relative intensity should result in a straight line for a substance which follows the Curie-Weiss law. The reciprocal intensities of the  $\beta$ -resonance signals plotted in Figure 3 were reasonably satisfactory straight lines, and thus, followed the Curie-Weiss law.  $\alpha$ -Chromia showed a deviation from linearity as the temperature of the Néel point (34°) was approached owing to the persistence of anti-ferromagnetic properties.<sup>8</sup> The chromia/alumina sample in hydrogen deviated from linearity below 40°.

When the Curie-Weiss law is followed, the slope and intercept of the lines resulting from reciprocal plots are important constants which can aid in the interpretation of magnetic data. The slope is the Curie constant and the intercept is the Weiss constant. The slopes and intercepts of the linear portion of the reciprocal relative intensity curves are shown in Table I. The Curie constants were essentially unchanged by the adsorption of hydrogen. However, the adsorption of hydrogen

(4) P. W. Selwood, *J. Amer. Chem. Soc.*, **92**, 39 (1970).

(5) R. P. Eischens and P. W. Selwood, *ibid.*, **69**, 2698 (1947).

(6) C. P. Poole and J. F. Itzel, Jr., *J. Chem. Phys.*, **41**, 287 (1964).

(7) Varian Associates Technical Bulletin for the V-4502 epr spectrometer.

(8) Y. Y. Li, *Phys. Rev.*, **84**, 72 (1951).

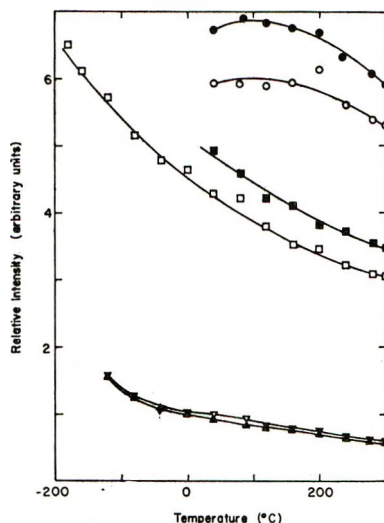


Figure 2. Temperature dependence of the relative intensity of chromia gel (■ vac, □ H<sub>2</sub>),  $\alpha$ -chromia (● vac, ○ H<sub>2</sub>), and 9.5 mol % chromia/alumina (▲ vac, Δ H<sub>2</sub>).

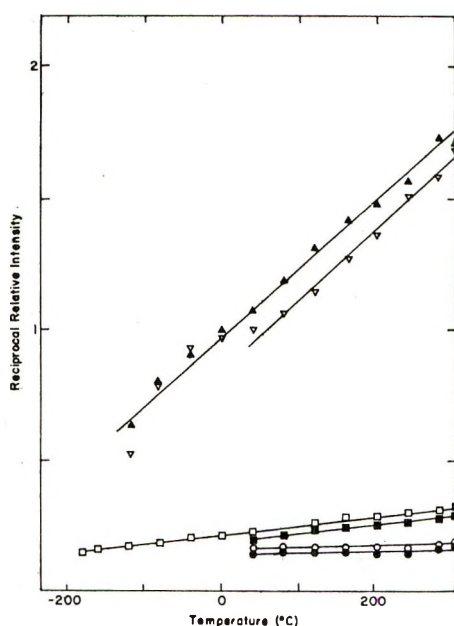


Figure 3. Temperature dependence of the reciprocal of the relative intensity of chromia gel (■ vac, □ H<sub>2</sub>),  $\alpha$ -chromia (● vac, ○ H<sub>2</sub>), and 9.5 mol % chromia/alumina (▲ vac, Δ H<sub>2</sub>).

caused the Weiss constant to become more negative for chromia gel and  $\alpha$ -chromia and more positive for chromia/alumina.

The epr spectrum for the chromia/alumina sample was also measured after the following special pretreatment. The sample was heated in flowing hydrogen at 500°, followed by evacuation at 550° for 24 hr. The relative intensity of the  $\beta$ -phase resonance signal now showed only a slight increase after hydrogen was readmitted. There was no change in the line width and no change in the Curie or Weiss constants. Thus, hydrogen had little influence on the epr spectrum of this sample and

Table I: Slopes and Intercepts of the Reciprocal of the Relative Intensity Curves

Substance	Slope (Curie constant) $\times 10^{-6}$		Intercept (Weiss constant)	
	Vacuum	Hydrogen	Vacuum	Hydrogen
Chromia gel	2.8	2.6	-273	-310
$\alpha$ -Chromia	5.1	4.9	-300	-369
Chromia/alumina	0.38	0.35	-105	-38

hydrogen was probably not adsorbed. A slight flattening of the left lobe of the  $\beta$ -phase resonance signal of this chromia/alumina sample was observed as is shown by the spectrum of Figure 4. Examination of this spectrum under high amplification revealed a new signal which is shown by Figure 5. It was observed to be split into six lines representing the hyperfine splitting by a nuclear spin of 5/2. It is believed that this signal represents the superhyperfine coupling of the Cr(III) unpaired electron spin with the <sup>27</sup>Al nucleus. Interactions between chromium electron spins and aluminum nuclei have been detected by nmr techniques.<sup>9</sup>

## Discussion

A comparison of the epr spectra of the chromium oxide catalysts measured *in vacuo* and in a hydrogen atmosphere shows that hydrogen has an influence on the Cr(III) ions that are responsible for the  $\beta$ -phase resonance signals. However, this influence is altered by the presence of an alumina support.

For the chromia/alumina sample the relative intensity, line width, and Weiss constant all increased with the adsorption of hydrogen. The relative intensity is a measure of the number of spins of Cr(III) ions that contribute to the signal. Thus, its increase indicates that the number of Cr(III) ions was increased.

The line width of the  $\beta$ -phase resonance signal is strongly influenced by the interaction between paramagnetic ions. The widths are broadened by dipole-dipole interaction and narrowed by exchange interaction. The latter process accounts for the differences between chromia/alumina, chromia gel, and  $\alpha$ -chromia. Adsorption of hydrogen on the surface should have little direct influence on this process, but, if the adsorption of hydrogen increases the number of Cr(III) ions contributing to the signal, the signal could be broadened by the increase in the number of ions participating in the dipole-dipole broadening process.

The Weiss constant calculated from the epr relative intensity for the chromia/alumina sample became more positive on hydrogen adsorption. The Weiss constant, like the line width, is strongly dependent on exchange interaction, but the adsorption of hydrogen

(9) D. E. O'Reilly and C. P. Poole, *J. Phys. Chem.*, **67**, 1762 (1963).

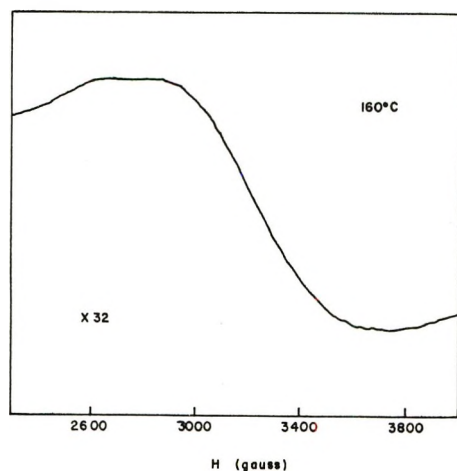


Figure 4. Epr spectrum of 9.5 mol % chromia/alumina showing the flattening of the left lobe of the  $\beta$  phase signal caused by the  $^{27}\text{Al}$  superhyperfine structure.

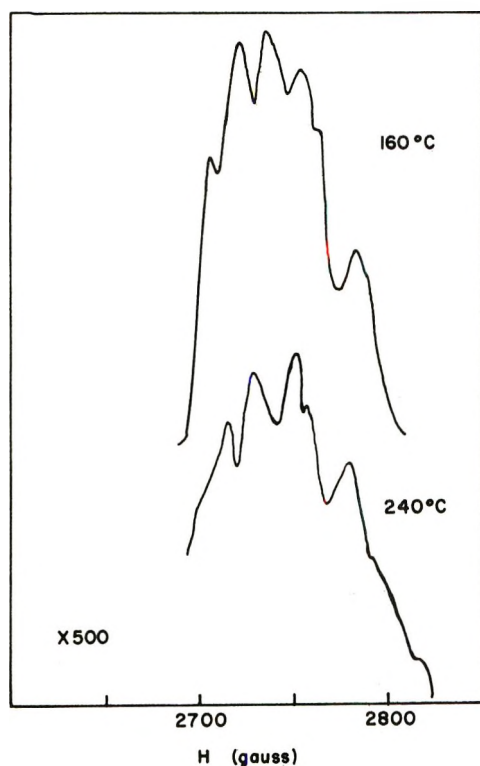


Figure 5. An amplification of the left lobe of the  $\beta$  phase epr signal of 9.5 mol % chromia/alumina showing the  $^{27}\text{Al}$  superhyperfine structure.

should not directly influence the interaction between chromium ions. However, since the Weiss constant is the intercept of the reciprocal intensity, and an increase in the relative intensity results in a decrease in its reciprocal, the intercept must become more positive if the slope or Curie constant does not change. Thus, the increase in the Weiss constant can also be attributed to an increase in the number of Cr(III) ions which contribute to the signal.

The adsorption of hydrogen on chromia gel and

$\alpha$ -chromia influenced their epr spectra in a reverse manner from that on chromia/alumina. The line width, relative intensity, and Weiss constant were all decreased by hydrogen adsorption. If the same arguments as were applied for chromia-alumina are used here, then these decreases resulted from a decrease in the number of Cr(III) ions.

Table II shows a comparison of the number of surface Cr(III) ions per gram as determined from mass and epr. The per cent surface from mass and surface was determined from estimates of the number of surface ions per gram as suggested by Selwood.<sup>10</sup> The total Cr(III) ions from epr was determined from the total calibrated relative intensity of the epr signals measured at 80°, and the surface estimates from epr were based on the change in relative intensity resulting from hydrogen adsorption at 80°. In all cases the number of Cr(III) ions from epr compares favorably with the number of Cr(III) ions from mass and surface. The greatest difference in surface percentage is that shown by the  $\alpha$ -chromia. This difference is probably due to its small surface area and small difference in epr intensity resulting from hydrogen adsorption. The closeness of the per cent surface, as determined by the two methods, shows that it is reasonable to conclude that the change in the epr intensity resulting from hydrogen adsorption is due to a change in the number of Cr(III) ions contributing to the epr signal.

Table II: Comparison of the Number of Cr(III) Ions per Gram as Determined from Mass with Those Determined from the Epr Intensity

	Total Cr(III) $\times 10^{-21}$	Surface Cr(III), %
From mass and surface		
Chromia gel	7.9	8.2
$\alpha$ -Chromia	7.9	1.2
Chromia/alumina	0.37	5
From epr <sup>a</sup> intensity (80°)		
Chromia gel	4.0	8.1
$\alpha$ -Chromia	5.1	13.4
Chromia/alumina	0.22	11.2

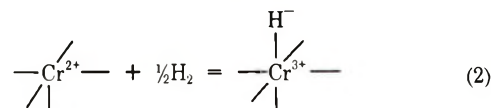
<sup>a</sup> Surface estimates from epr are based on a decrease of intensity on hydrogen adsorption for chromia gel and  $\alpha$ -chromia, an increase for supported.

Van Reijen, *et al.*,<sup>11</sup> using magnetic susceptibility and epr methods, showed that Cr(II) ions were present on the surface of reduced chromia/alumina catalysts. The reduction of the catalyst produced Cr(II) ions after evacuation. Cr(II) with its even number of

(10) P. W. Selwood, *J. Amer. Chem. Soc.*, **88**, 2676 (1966).

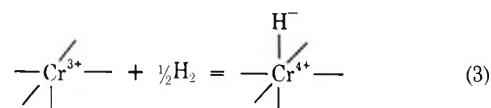
(11) L. L. Van Reijen, W. M. H. Sachtler, P. Cossee, and D. M. Brower, *Proc. Int. Conf. Catal.*, *II*, 3rd, 1963 (1965).

unpaired electrons cannot be detected by epr methods, but, if the evacuated surface chromium ions are in the 2+ oxidation state, then a change in oxidation state would lead to an odd number of electrons which can be detected by epr. The increase in the number of Cr(III) ions indicates that this did happen. Thus, a mechanism for the adsorption on previously reduced and evacuated chromia-alumina surfaces can be proposed. It is suggested that the adsorption of hydrogen leads to the oxidation of Cr(II) to Cr(III) accompanied by the production of a surface hydride ion.



The increase in the number of Cr(III) ions due to this oxidative mechanism would result in the increase of the epr relative intensity, line width, and Weiss constant as described above. Further reduction of the Cr(II) to Cr(I) is not considered since Cr(I), which has an odd number of unpaired electrons, would be detected as a new signal by epr. This would not result in an increase in the  $\beta$ -phase signal.

The adsorption of hydrogen on the reduced and evacuated chromia gel and  $\alpha$ -chromia surfaces caused a decrease in the number of Cr(III) ions instead of an increase as was observed with chromia/alumina. The same oxidative mechanism can account for this decrease, that is, the oxidation of Cr(III) to Cr(IV) if the chromium ions on the evacuated surface are in the 3+ oxidation state instead of 2+.



The oxidation of Cr(III) to Cr(IV) would result in a decrease in the number of Cr(III) ions and a decrease in the epr intensity, line width, and Weiss constant.

The changes in the epr spectra due to hydrogen adsorption described in this paper suggest a gain or loss in the concentration of surface Cr(III) ions. As suggested by Kazanskii and Shvets,<sup>12,13</sup> these changes can also be brought about by changes in symmetry or coordination which would change the crystal field experienced by the Cr(III) ions. The relaxation time would also be changed and the epr spectrum of Cr(III) may not be observable under these circumstances. They believe, through their interpretation of epr and optical spectra, that the reduced and evacuated chromia/alumina surface ions are Cr(III) in a square pyramidal coordination rather than Cr(II) as suggested by Van Reijen, *et al.*, but, as pointed out by Burwell, *et al.*,<sup>14</sup> the square pyramidal Cr(III) should be easier to reduce to Cr(II) which is more stable in a square planar coordination. Furthermore, the theory of Kazanskii does not explain the different effects on the

epr spectra caused by the adsorption of hydrogen on chromia and chromia/alumina as reported in this paper.

Chromia gel and  $\alpha$ -chromia interact with hydrogen in a different way than chromia/alumina. A clue to the reason for this difference can be found by the examination of the epr spectrum of the sample which gave rise to Figure 4. This sample was pretreated at temperatures above 500° compared with 400° for the samples described above. The action of hydrogen on the epr spectrum of this sample, after evacuation, had little or no effect on the line width, relative intensity, or Weiss constant showing that hydrogen was probably not adsorbed. Voltz and Weller,<sup>15</sup> using volumetric methods, found little hydrogen adsorption on a chromia/alumina sample with similar pretreatment. The hydrogen atmosphere had no effect on the epr spectrum of this sample; however, there was an <sup>27</sup>Al hyperfine structure present on the  $\beta$ -phase signal as shown by Figure 5. The presence of a hyperfine structure shows that there is a strong interaction between the chromium and aluminum ions. This hyperfine, though not present on the samples where the epr spectra were influenced by hydrogen, suggests that the alumina support may be responsible for the lower oxidation state experienced by chromia/alumina. That is, the interaction between the aluminum ions and the chromium ions may bring about conditions which favor the formation of Cr(II) ions.

The mechanism of the process which brought about the interaction between chromium and the alumina support and the resulting hyperfine structure is not known; however, it is suggested that free electrons, which should have been present on the oxygen-deficient evacuated chromia/alumina surface forming color centers, may have been transferred to the Cr(III) ions forming Cr(II) ions. This was indicated by the lack of an epr signal which could be attributed to free electrons on the chromia/alumina surface, under conditions where it was found on pure  $\gamma$ -alumina and pure chromia. However, more research is necessary to further characterize the hyperfine signal and determine its influence on the chromia/alumina surface reactions.

## Conclusion

The results reported in this paper show that the  $\beta$ -phase resonance signals of the epr spectra of chromia/alumina and pure chromia are affected by the adsorp-

(12) J. A. Shvets and V. B. Kazanskii, *Kinet. Catal. (USSR)*, **7**, 627 (1966).

(13) V. B. Kazanskii, *ibid.*, **8**, 960 (1967).

(14) R. L. Burwell, Jr., G. L. Haller, K. C. Taylor, and J. S. Read, *Advan. Catal.*, **20**, 1 (1969).

(15) S. E. Voltz and S. W. Weller, *J. Amer. Chem. Soc.*, **76**, 4701 (1954).

tion of hydrogen on the previously reduced and evacuated at 400° surface. This indicated that hydrogen is chemisorbed on the surface chromium ions. However, the changes in the  $\beta$ -phase signal brought about by hydrogen adsorption differ in the direction of the change. The relative intensity of the chromia/alumina was increased in an amount approximately equal to the number of surface chromium ions and the relative intensity of pure chromia was decreased by the same amount. These changes indicate that the chromia/alumina was oxidized from Cr(II) to Cr(III) and chromia was oxidized from Cr(III) to Cr(IV) by the adsorption of hydrogen. This difference in oxidation state is believed to be due to the interaction between the chromium ions and the aluminum support. This interaction was shown by the presence of an  $^{27}\text{Al}$  hyper-

fine structure on the  $\beta$ -phase signal of a chromia/alumina sample which was pretreated at 500°.

Regardless of the mechanism of hydrogen adsorption, the epr spectra of chromia/alumina and pure chromia are influenced differently by that adsorption. This suggests that the surface of chromia/alumina and pure chromia differ from each other in the manner in which they react with hydrogen. Thus, conclusions based on experiments performed on one substance do not necessarily apply to the other.

*Acknowledgment.* The author wishes to express his gratitude for the helpful guidance and advice given him by Professor P. W. Selwood, and to thank him for his help in the preparation of this paper. This research was supported in part by the Army Research Office, Durham.

## Infrared Spectra of Hydrocarbons Adsorbed on Silica-Supported Metals.

### IV. Butenes on Iridium

by A. Ravi and N. Sheppard\*

*School of Chemical Sciences, University of East Anglia, University Plain, Norwich, NOR 88C, England  
(Received April 4, 1972)*

Infrared spectra have been obtained from the surface species resulting from the chemisorption of butene-1, *cis*- and *trans*-butene-2, isobutene, and 2-methylbutene-2 on hydrogen-covered iridium. The first three hydrocarbons give very similar spectra from the adsorbed species. These are interpreted in terms of a mixture of associatively and dissociatively adsorbed species such as  $\text{CH}_3\text{CH}_2\text{CHMCH}_2\text{M}$  and  $\text{CH}_3\text{CH}_2\text{CHM}-\text{CHM}_2$  where **M** denotes a surface metal atom. The alternative, but less probable, species  $\text{CH}_3\text{CHMCH}_2\text{CH}_2\text{M}$  and  $\text{CH}_3\text{CHMCH}_2\text{CHM}_2$  would be consistent with the observed spectra; the spectra are not consistent with the presence of mainly associatively adsorbed species  $\text{CH}_3\text{CHMCHMCH}_3$  derived from butene-2's. The spectrum produced by the chemisorption of isobutene has less strong methyl absorption than would be expected from an associatively adsorbed species; the moderate absorption in the  $2920\text{-cm}^{-1}$  region is such as would be expected from the presence of a greater proportion of  $\text{CH}_2$  groups as in species such as  $\text{CH}_2\text{MCH}(\text{CH}_3)\text{CH}_2\text{M}$ . 2-Methylbutene-2 gave less well-defined spectra from chemisorbed species, but again methyl groups are probably not more numerous than  $\text{CH}_2$  groups. Hydrogenation of the surface species from the linear butenes and from isobutene gave spectra expected from  $\text{CH}_2\text{CH}_2\text{CH}_2\text{CH}_2\text{M}$  and  $(\text{CH}_3)_2\text{CHCH}_2\text{M}$  groups, respectively, when allowance had been made from contributions from physically adsorbed *n*-butane and isobutane, partially released from the surface by the hydrogenation reaction. Dehydrogenation led to reductions in intensity of the spectra of the surface species which were partially restored by rehydrogenation. In several cases heating of the hydrogenated surface species to 150° led to cracking of the hydrocarbon skeleton to give methane. Exchange reactions were observed with deuterium at room temperature leading to weak  $\nu\text{CD}$  and  $\nu\text{OD}$  bands.

#### I. Introduction

Eischens and Pliskin were the first to study the adsorption of butenes on silica-supported metals by infrared spectroscopic methods.<sup>1</sup> On hydrogen-covered nickel supported on Cabosil they observed similar spectra from butene-1 and butene-2 with two absorp-

tion bands near 2959 and 2890  $\text{cm}^{-1}$ . They assigned these bands to  $\text{CH}_3\text{-C}$  groups and  $-\text{CHM}-$  or  $-\text{CH}_2\text{M}-$  groups, respectively, where **M** denotes a surface metal atom. Considering that the methyl absorption was the

(1) R. P. Eischens and W. A. Pliskin, *Advan. Catal.*, **10**, 1 (1958).

weaker of the two, they proposed that in some chemisorbed molecules all four carbon atoms are bonded to the surface implying a considerable degree of dissociative adsorption. Their spectrum obtained after hydrogenation was assigned to *n*-butyl groups, and these latter species were found to undergo dehydrogenation by pumping. On "bare" nickel, butenes were found to adsorb in an even more dissociative fashion to give overall very weak spectra. Clark<sup>2</sup> studied the adsorption of butene-1 and butene-2 on platinum, palladium, and nickel supported on porous glass. Later, Ward investigated<sup>3</sup> the adsorption of butene-1 on Cabosil-supported nickel and platinum. The spectra of surface species obtained after hydrogenation were CH<sub>2</sub>-rich on Ni and methyl-rich on Pt and at that time were interpreted in terms of the presence of *n*-butyl and *sec*-butyl groups, respectively. Morrow and Sheppard's<sup>4</sup> more recent work on butene-1 adsorbed on silica-supported nickel and platinum, studied over a range of temperatures, showed that the methyl-rich spectrum obtained on Pt after hydrogenation<sup>3</sup> was due to contributions from physically adsorbed *n*-butane. They<sup>4</sup> found that initial adsorption of butene-1 gave similar spectra on Pt at all temperatures ( $-78$ ,  $+20$ , and  $+95^\circ$ ) and on Ni at  $-78^\circ$ . This spectrum has an intense band at  $2870\text{ cm}^{-1}$  and medium intensity bands near  $2960$  and  $2930\text{ cm}^{-1}$  and was attributed to an associatively adsorbed species derived from butene-1. At higher temperatures on Ni ( $20$  and  $95^\circ$ ) the  $2870\text{-cm}^{-1}$  band is no longer the most prominent one, and this spectrum was attributed to species with more than two C-M bonds. The following work presents the results obtained from an infrared characterization of surface species formed during the adsorption of butenes on iridium.

## II. Experimental Section

The infrared cell employed for these studies is similar to that employed by Morrow<sup>5</sup> and by Young and Sheppard.<sup>6</sup> Experiments were carried out using a conventional vacuum system giving pressures of *ca.*  $10^{-6}$  Torr. Spectra were taken with a Grubb-Parsons GS 2 diffraction grating double-beam infrared spectrometer.

The preparation of the samples containing 10% iridium is described elsewhere in detail.<sup>7</sup> It should be noted that studies were made only on "hydrogen-covered" metals in the sense described by Eischens and Pliskin.<sup>1</sup> Butenes were obtained from the National Chemical Laboratory, Teddington, U.K., and were stated to be of 99.9% purity.

## III. Results

*A. Butene-1.* The spectra obtained after the adsorption of butene-1 on iridium are shown in Figure 1. In addition to the bands in the  $\nu\text{CH}$  bond-stretching region shown in the figure, weak bands at  $1460$  and  $1385\text{ cm}^{-1}$  in the  $\delta\text{CH}_2$  and  $\delta\text{CH}_3$  angle bending region were also left on the surface after evacuation. Although the

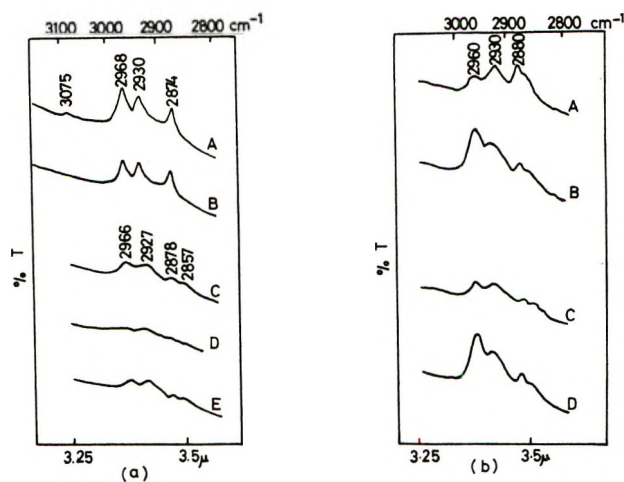


Figure 1. Infrared spectra of butene-1 adsorbed on iridium. (a) A, 10 Torr; B,  $10^{-5}$  Torr; C, addition of H<sub>2</sub>; D, evacuation of H<sub>2</sub>; E, readdition of H<sub>2</sub>. (b) Hydrogenation of butene-1 at low temperatures and variations in the spectra with temperature: A,  $-100^\circ$ ; B,  $-40^\circ$ ; C,  $+25^\circ$ ; D, recooling to  $-40^\circ$ .

spectrum was recorded immediately after admitting the adsorbate and again after overnight standing, no significant differences were found. After evacuation of the cell for an hour at  $10^{-5}$  Torr, the intensity of the main bands dropped by only a small amount but weak bands attributable to  $=\text{CH}$  and  $\text{C}=\text{C}$  groups at  $3075$  and  $1640\text{ cm}^{-1}$  disappeared corresponding to removal of the physically adsorbed hydrocarbons.

The spectrum obtained by adsorption of butene-1 on iridium has prominent absorptions at  $2968$ ,  $2930$ , and  $2874\text{ cm}^{-1}$  which may probably be attributed to  $\text{CH}_3$ ,  $\text{CH}_2$ , and  $\text{CH}_2\text{M}$  groups, respectively.<sup>4</sup> The  $2874\text{-cm}^{-1}$  band probably also contains a contribution from the  $\text{CH}_3(\text{s})$  mode.<sup>8</sup> The ratio of the optical densities of the first two bands is approximately unity and indicates a  $\text{CCH}_2\text{C}/\text{CH}_3$  ratio of between 1 and 2. The general appearance of the spectrum is very similar to that observed by Morrow and Sheppard with butene-1 adsorbed at room temperature on nickel and differs from that from butene-1 on platinum in that the latter spectrum has a considerably stronger low frequency band.

Morrow and Sheppard<sup>4</sup> attributed the spectrum on platinum to the associatively adsorbed species  $\text{CH}_3\text{CH}_2\text{-CHMCH}_2\text{M}$ , the  $\text{CH}_2\text{M}$  group in the four-membered ring being assigned to the strong band near  $2890\text{ cm}^{-1}$ , and

(2) M. Clark, Ph.D. Thesis, Cambridge University, 1960.

(3) J. W. Ward, Ph.D. Thesis, Cambridge University, 1962.

(4) B. A. Morrow and N. Sheppard, *Proc. Roy. Soc., Ser. A*, **311**, 415 (1969).

(5) B. A. Morrow, *J. Sci. Instrum.*, **43**, 487 (1966).

(6) R. P. Young and N. Sheppard, *Trans. Faraday Soc.*, **63**, 2291 (1967).

(7) A. Ravi and N. Sheppard, *J. Catal.*, **22**, 389 (1971).

(8) N. Sheppard and J. W. Ward, *ibid.*, **15**, 50 (1969); however, also see J. C. Lavalley and N. Sheppard, *Spectrochim. Acta, Part A*, **28**, 845 (1972).

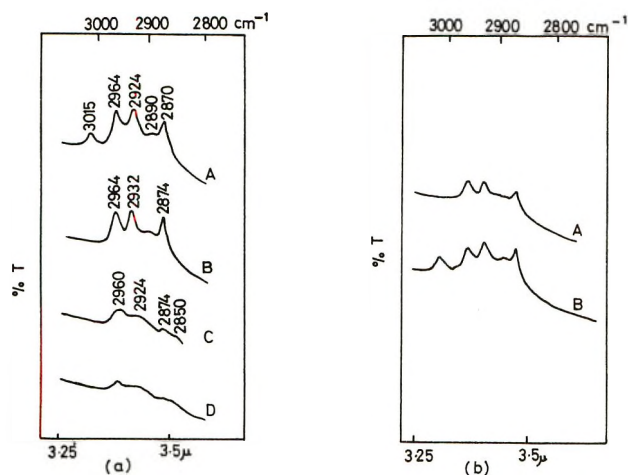


Figure 2. Infrared spectra of butene-2 adsorbed on iridium. (a) *trans*-Butene-2: A, 10 Torr; B,  $10^{-5}$  Torr; C, addition of  $H_2$ ; D, evacuation of  $H_2$ . (b) *cis*-Butene-2: A,  $10^{-5}$  Torr; B, 10 Torr.

that on nickel to analogous surface species containing an overall smaller proportion of  $CH_2M$  groups, *i.e.*, they envisaged species such as  $CH_3CH_2CHMCHM_2$  as also contributing to the spectrum on nickel. We assign our spectra on iridium in an analogous manner, but point out that isomeric associatively adsorbed species such as  $CH_3CHMCH_2CH_2M$  and dissociatively adsorbed species such as  $CH_3CHMCH_2CHM_2$  would provide alternative satisfactory explanations of the observed spectra. Although these alternative species may seem somewhat less probable, we shall see below that the spectra resulting from the adsorption of isobutene on iridium are not easily explicable in terms of simple associatively adsorbed species.

If the assignment of the present spectra is basically correct, this implies that the  $CHM$  and/or  $CHM_2$  groups probably contribute to the background absorption between 2930 and 2874  $cm^{-1}$ , which is slightly more pronounced in the form of submaxima in the otherwise closely analogous spectra from *cis*- and *trans*-butene-2 on iridium as illustrated in Figures 2a and b. Although this spectral interpretation requires some degree of dissociative adsorption, this is not thought to be extensive. On addition of  $H_2$  to the adsorbed butene most of the bands in the spectrum became broader and changed in relative intensity; *n*-butane also appeared in the gas phase. Evacuation weakened the surface spectrum, but on readmission of hydrogen the spectra reappeared with bands of nearly the original intensity. Following the usual assignments,<sup>8</sup> 2966-, 2927-, 2878-, and 2857- $cm^{-1}$  bands in the hydrogenated spectra are attributed to  $\nu CH_3(as)$ ,  $\nu CH_2(as)$ ,  $\nu CH_3(s)$ , and  $\nu CH_2(s)$  vibrations, respectively. The optical density ratio of  $CH_2(as)$  and  $CH_3(as)$  bands in this spectrum was *ca.* 1.2, which indicated that the surface species after hydrogenation probably consists of *n*-butyl groups.<sup>1,8,9</sup> The appearance of *n*-butane is consistent with this conclusion.

From the intensification of the spectra on rehydrogenation it is considered that a fair proportion of the dehydrogenated species are hydrogen deficient compared to *n*-butyl groups and have a number of  $C-M$  bonds to the surface.

When deuterium is added to the adsorbed butene, the  $\nu CH$  bands became weaker, and a  $\nu CD$  band appeared at 2212  $cm^{-1}$  indicating the addition and exchange of deuterium with the surface species.

In a second experiment the hydrogenation reaction was studied at low temperature. The spectra shown in Figure 1b were obtained after adsorption of butene at room temperature, evacuation of the cell, and then introduction of gas-phase hydrogen after cooling the sample to near  $-100^\circ$  for 30 min. The spectra still showed all four  $\nu CH$  bands at the usual frequencies, but the intensity distribution was very abnormal. Specifically the band at 2880  $cm^{-1}$  was the most prominent and that at 2960  $cm^{-1}$  rather weak. As the temperature rose to  $-40^\circ$  in presence of  $H_2$ , the spectrum became more methyl-rich. On warming to room temperature the spectral intensities were restored to the same proportions as in the spectrum obtained by hydrogenation at  $25^\circ$  (Figure 1a). *n*-Butane was again observed in the gas phase at room temperature. The spectrum obtained at  $-100^\circ$  is similar in some respects to that observed by earlier workers on platinum<sup>4</sup> and is attributed to a combination of species of the type  $CH_3-CH_2CHMCH_2M$ , giving the sharp band at 2880  $cm^{-1}$ . Morrow's spectra of model compounds containing  $Pt-CH_2CH_3$  and  $Pt-CH_2CD_3$  groups<sup>9</sup> suggests that unstrained  $CH_2M$  groups give broad bands in the 2900- $cm^{-1}$  region. The present spectrum however has a weak band at 2960  $cm^{-1}$  compared with that at 2930  $cm^{-1}$  suggesting that methyl-deficient surface species such as  $MCH_2CH_2CH_2CH_2M$  or  $M_2CHCH_2CH_2CHM_2$ , etc., might be present. The band near 2860  $cm^{-1}$  should probably also be assigned to  $\nu CH_2(s)$  of  $CCH_2C$  groups.

The spectrum observed at  $-40^\circ$  is attributed to chemisorbed and physisorbed *n*-butane<sup>4</sup> produced in the hydrogenation reaction. At this temperature *n*-butane possibly desorbed from the glass core of the cell and condensed on the adsorbent. This is consistent with the observation that after coming to  $25^\circ$  the extra intensity attributable to condensed *n*-butane was lost, and this hydrocarbon appeared in the gas phase.

These spectral intensity variations due to physical adsorption could be reproduced by alternate cooling and allowing the cell to warm up to room temperature.

*B. trans-Butene-2.* The spectra obtained from the adsorption of *trans*-butene-2 are shown in Figure 2a. The spectrum obtained at 10 Torr represents chemisorbed plus physically adsorbed butene. The band at 3015  $cm^{-1}$  corresponds to  $=CH-$  groups indicating little

(9) B. A. Morrow, *Can. J. Chem.*, **48**, 2192 (1970).



isomerization to butene-1. At  $10^{-5}$  Torr no unsaturated groups were present on the surface. Of the two very weak  $\delta\text{CH}$  bands at 1460 and 1440  $\text{cm}^{-1}$  present in the presence of the olefin, only the 1460- $\text{cm}^{-1}$  band could be detected after evacuation. The overall spectra are very similar to those obtained for chemisorbed butene-1. They are assigned to the species suggested above, but for the latter case possibly with a slightly higher proportion of  $-\text{CHM}$  and/or  $-\text{CH}_2\text{M}$  groups, the latter not in four-membered strained rings, to explain the broad weak band near 2890  $\text{cm}^{-1}$ . It is noteworthy that this spectrum, as that from butene-1, does not have dominant methyl absorption bands and so does not correspond to the associatively adsorbed species  $\text{CH}_3\text{CHMCHMCH}_3$ .

Addition of hydrogen again produced a spectrum with broad bands and *n*-butane was observed in the gas phase. As for butene-1, the spectrum became weaker on evacuation of hydrogen, but the intensity was partly restored on readmission of  $\text{H}_2$ . In a low-temperature study the sample was cooled after the first addition of  $\text{H}_2$ . At *ca.*  $-60^\circ$  a methyl-rich spectrum, similar to that obtained after addition of hydrogen to adsorbed butene-1, is again attributed to the condensation of *n*-butane on the surface. The adsorbed and hydrogenated species was heated at 75 and 150°. No products were observed at 75°, but methane was observed in the gas phase at 150°.

The spectra taken after heating the metal sample to 150° with chemisorbed butene and allowing the cell to come to room temperature were similar to those obtained before heating except that the bands became broader. Such broadness could be attributed to a mixture of surface species with  $\text{C-M}$  bonds probably formed during the decomposition reaction which gave rise to methane.

When deuterium is added to adsorbed butene-2, the drop in intensity of the spectrum in the  $\nu\text{CH}$  region was rapid and considerable. These changes were followed by the appearance of  $\nu\text{CD}$  and  $\nu\text{OD}$  bands at 2220 and 2760  $\text{cm}^{-1}$ , respectively, the latter presumably being formed by metal-catalyzed exchange of surface OH groups.<sup>7</sup>

*C. cis-Butene-2.* The adsorption of the *cis* isomer of butene-2 was investigated briefly to see whether any differences could be found from the adsorption of the *trans* isomer. The spectra at 10 and  $10^{-5}$  Torr of *cis*-butene-2 are similar to those obtained from the *trans*-olefin (Figure 2b). However, complete isomerization had not occurred as the gas phase spectra in the two experiments were not identical. Nevertheless the spectroscopic results show that both molecules adsorb in the same manner. Eischens and Pliskin<sup>1</sup> and Clark<sup>2</sup> also reported similar spectra from the adsorption of *cis*- and *trans*-butene-2 on platinum.

*D. Isobutene.* Infrared investigations of branched chain olefins adsorption are sparse. Ward<sup>3</sup> studied the

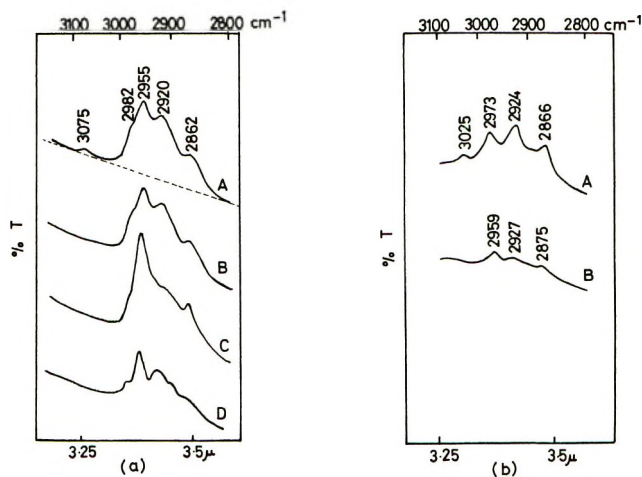


Figure 3. Infrared spectra of branched-chain olefins adsorbed on iridium. (a) Isobutene: A, 10 Torr; B,  $10^{-5}$  Torr; C, addition of  $\text{H}_2$ ; D, evacuation of  $\text{H}_2$ . (b) 2-Methylbutene-2: A, 20 Torr; B,  $10^{-5}$  Torr.

adsorption of isobutene on Ni and Pt and 2-methylbutene-2 on Ni, and Avery studied isobutene adsorbed on palladium.<sup>10</sup>

The spectrum immediately after the addition of isobutene was methyl-rich and interestingly has a high frequency shoulder at 2982  $\text{cm}^{-1}$  (Figure 3a). This may perhaps be attributed to rigidly held methyl groups, *i.e.*, those attached to a surface-bonded carbon atom, *e.g.*,  $(\text{CH}_3)_2\text{CM-}$ . No such band was observed after the adsorption of butene-1 and butene-2. The spectrum after evacuation is similar in contour except for the disappearance of 3075- $\text{cm}^{-1}$  band due to  $=\text{CH}_2$  vibrations from physically adsorbed isobutene. A very weak broad band at *ca.* 1460  $\text{cm}^{-1}$  was also evident at this stage. The optical density ratio of the methylene and methyl bands was about 0.8, indicating approximately two  $\text{CH}_3$  groups per  $\text{CH}_2$  group.

It is not easy to postulate a structure that could unambiguously account for the spectrum observed after initial adsorption. However, the straightforward associatively adsorbed species  $(\text{CH}_3)_2\text{CMCH}_2\text{M}$  does not seem to be present in large quantity as there is no sharp band near 2875  $\text{cm}^{-1}$  for assignment to  $\text{CH}_2\text{M}$  groups in four-membered rings. Also the comparative prominence of the 2920- $\text{cm}^{-1}$  band does suggest the presence of  $\text{CH}_2$  groups, either of the  $\text{C-CH}_2\text{-C}$  type (which is unlikely as this would require skeletal isomerization) or of the  $\text{CH}_2\text{M}$  type in relatively unstrained environments. This suggests that there may be an appreciable proportion of the isomeric associatively adsorbed species  $\text{MCH}_2\text{CH}(\text{CH}_3)\text{CH}_2\text{M}$  present. The present spectra are similar to those obtained by Ward from isobutene on nickel and platinum, but in each case the latter spectra were more methyl-rich. An alternative explanation for some of the intensity of the *ca.* 2920- $\text{cm}^{-1}$  band

(10) N. R. Avery, *J. Catal.*, **19**, 15 (1970).

could be found in terms of the presence of  $\text{CH}_3\text{C}=\text{C}$  groups in surface species such as  $\text{MCH}_2\text{C}(\text{CH}_3)=\text{CHM}$ . Smit<sup>11</sup> has shown that such groupings give the main bands 2970 (m), 2940 (m), and 2920  $\text{cm}^{-1}$  (s) in the  $\nu\text{CH}_3$  region. This is, however, less likely because no appreciable absorption occurred near 3010  $\text{cm}^{-1}$  as would be expected from the accompanying  $\text{C}=\text{CH}$  group.

On addition of  $\text{H}_2$  there is a considerable increase in the intensity of the 2955- $\text{cm}^{-1}$  methyl band and isobutane was observed in the gas phase. A similar result was obtained by Ward<sup>3</sup> for isobutane on platinum, and in considerable measure the spectrum is probably caused by physically adsorbed isobutane. The optical density ratio of  $\text{CH}_2/\text{CH}_3$  bands in presence of  $\text{H}_2$  is 0.5, and on evacuation of  $\text{H}_2$  it is 0.7. The chemisorbed species present after hydrogenation is very probably composed of *sec*-butyl groups,  $(\text{CH}_3)_2\text{CHCH}_2\text{M}$ .

Chemisorbed isobutene when heated to 75 and 150° produced at the latter temperature gaseous methane and isobutane. The spectra retaken after allowing the cell to return to room temperature appeared with reduced intensity, but the relative band intensities re-

mained the same as before heating. When deuterium is added to adsorbed isobutene,  $\nu\text{CH}$  bands become rapidly weak with the appearance of  $\nu\text{CD}$  and  $\text{OD}$  bands.

*E. 2-Methylbutene-2.* The spectra obtained from the adsorption of 2-methylbutene-2 are shown in Figure 3b. Considerable spectral changes on evacuation are again attributable to the removal of physically adsorbed olefin. Addition of hydrogen led to the appearance of isopentane in the gas phase; on evacuation and rehydrogenation similar intensity changes were evident as with other butenes. No specific formulations are suggested for the adsorbed species because all the spectra obtained were rather weak, and there are many possibilities for an adsorbed hydrocarbon of this complexity. However, some methane, in addition to isopentane, was observed in the gas phase after heating the hydrogenated species to 150°.

*Acknowledgment.* One of us (A. R.) is grateful to B. P. (Chemicals) Ltd., for a maintenance grant during the course of the work.

(11) A. Smit, Doctoral Thesis, University of Utrecht, 1972.

## Far-Ultraviolet Solvent Spectroscopy

by M. F. Fox and E. Hayon\*

*Pioneering Research Laboratory, U. S. Army Natick Laboratories, Natick, Massachusetts 01760  
(Received April 19, 1972)*

*Publication costs assisted by the U. S. Army Natick Laboratories*

A systematic study of the far-ultraviolet spectroscopy of some polar liquid solvents has been carried out with the object of extending the range at which the spectroscopy of certain solutes can be determined. The solvents examined include water,  $\text{D}_2\text{O}$ , methyl alcohol,  $\text{CH}_3\text{OD}$ ,  $\text{CD}_3\text{OD}$ , methyl cyanide, ethyl cyanide, *n*-propyl cyanide, trifluoroethyl alcohol, hexafluoro-2-propyl alcohol, dimethoxyethane, and acetone. The effect of temperature on the absorption spectra of these solvents was examined. A considerable blue shift was found for most solvents with decrease in temperature. The most significant temperature effects were found for hydroxylic solvents. Absorption spectra at different temperatures are given, and the transmission limits of the above solvents down to 60,500  $\text{cm}^{-1}$  ( $\sim 165$  nm) have been tabulated.

### Introduction

One of the principal limitations of far-ultraviolet solution spectra is the absorption of the solvent itself. Thus aqueous solution spectra are limited by water absorption, for which<sup>1</sup>  $k = 1.46 \text{ cm}^{-1}$  at 54,090  $\text{cm}^{-1}$  (185 nm) and 298°K. These limitations are also over-emphasized in some cases on inspection of "uv cut-off" charts for spectroscopic solvents. Such charts usually refer to ambient temperatures and 1-10-mm sample

thickness. As part of a program to study the electronic absorption spectra of inorganic and organic molecules into the far-uv region,<sup>2,3</sup> we report the spectra of a number of solvents determined over a wide temperature range and at small sample thickness (optical path).

(1) J. Barrett and A. L. Mansell, *Nature (London)*, **187**, 138 (1960).

(2) M. F. Fox and E. Hayon, *Chem. Phys. Lett.*, **14**, 442 (1972).

(3) M. F. Fox and E. Hayon, to be submitted for publication.

## Experimental Section

**Materials.** Solvents were purified following methods described in the literature.<sup>4</sup> Once the specified physical properties of the solvents were attained, the criterion of purity was taken as "best" when no further decrease in the ultraviolet absorption was obtained on further treatment.

Water was distilled three times, the second and third distillations from permanganate and dichromate, respectively. This water was then irradiated with <sup>60</sup>Co  $\gamma$  rays and subsequently photolyzed with a 2537-Å mercury lamp. D<sub>2</sub>O was distilled from alkaline permanganate under nitrogen.

Methyl alcohol (Eastman Kodak Spectroscopic grade) was allowed to stand in contact with calcium hydride for 24 hr and was then distilled under nitrogen. Isobutyl alcohol, 2,2,2-trifluoroethyl alcohol (both Eastman Kodak), and 1,1,1,3,3,3-hexafluoro-2-propyl alcohol (PCR, Inc., Gainesville, Fla.) were similarly treated.

Spectroscopic grade methyl cyanide and ethyl and *n*-propyl cyanides (isonitrile-free, Eastman Kodak) were distilled from Drierite under nitrogen after allowing to stand for 24 hr. Spectroscopic grade acetone and dimethoxyethane (Eastman and Matheson Coleman and Bell) were similarly treated.

**Spectrophotometry.** A Cary 15 low-uv recording spectrophotometer liberally flushed with very dry gaseous nitrogen (using Linde-Division, Union Carbide liquid nitrogen) was used to obtain the spectra of the absorption cell, and then of the cell with the solvent in the sample beam. Solvent spectra were obtained by subtraction. In the region of interest, cell absorption varied only slightly with wave number. For each determination the reference beam contained a similar, but empty, cell to balance light scattered at the air-silica interface.

Cylindrical cells of 1.0- and 0.1-mm path lengths (Aminco) and 25- or 7  $\times$  10<sup>-3</sup>-mm path length demountable cells (UV-01 Beckman cell) were used. The latter were used as flow-through cells, a low flow rate of solvent being maintained using a syringe backed by a pump. No difficulty was experienced in maintaining, over a wide temperature range, a solvent film in the UV-01 cells using the flow-through technique. In the range 273-328°K, the temperature was controlled by aqueous glycol circulated from a thermostated (and refrigerated) bath, through a Cary cell holder. Thermal contact between cell and holder was maintained using copper plates and wedges. Below 273°K a VLT-2 variable temperature dewar unit with TEM-1C controller (Beckman) was used with solvent samples held in an FH-01 cell (Beckman). The VLT-2 unit was positioned in the sample compartment of the Cary 15 with the outer windows removed. The sample compartment was kept at atmospheric pressure as the

solvent film rapidly disappeared when vacuum was applied.

The molar absorption coefficients given here have been corrected for thermal density variations, using literature values where possible and otherwise by extrapolation. All the solvent spectra were determined in the absence of air by flushing prepurified nitrogen (Matheson) through the solvents.

Millipore filters (Millipore Corp.) were used to remove all particles from the nitrogen used to flush the Cary 15 spectrophotometer. Considerable care was taken to keep continuously all the optical paths within the spectrophotometer clean and in an inert atmosphere.

## Results

The present absorption spectroscopy work for water and D<sub>2</sub>O bridges the gap between the low-energy spectra<sup>1,5</sup> and that obtained from thin film studies using a vacuum spectrograph.<sup>6</sup> Excellent agreement down to 55,000 cm<sup>-1</sup> is found between this work (see Figure 1) and the temperature studies of Halmann, *et al.*,<sup>5</sup> and Barrett, *et al.*,<sup>1</sup> for both water and D<sub>2</sub>O. Decrease in temperature and/or substitution of D<sub>2</sub>O for H<sub>2</sub>O shifts the absorption edge to higher energies (Figure 1). The graphical data of Verrall and Senior<sup>6</sup> have been photographed and enlarged to obtain comparison with our data for H<sub>2</sub>O and D<sub>2</sub>O in the 55,000-61,000-cm<sup>-1</sup> region. Good agreement was obtained as far as the limits of measurement for this work.

One parameter for the percentage of hydrogen bonds "broken" in water has been taken<sup>7</sup> as the ratio between the molar absorption intensities of liquid water and water vapor at the same wave number. Such a comparison is incorrect since the respective absorption maxima are separated by 10,000 cm<sup>-1</sup><sup>6</sup> and perhaps accounts for the result of 0.1% of hydrogen bonds broken at 274°K. When integrated intensities are compared, the opposite result is obtained, the ratio indicating between 50 and 100% hydrogen bonds are broken.

The same shift of the absorption edge to higher energies on deuteration has been found in the spectra of methyl alcohol, methyl alcohol-*d*<sub>1</sub>, and methyl-*d*<sub>3</sub> alcohol-*d*<sub>1</sub> (Figure 2). Decrease in temperature again shifts the absorption edge of methyl alcohol to higher energies. The large liquid range of organic solvents, particularly at low temperatures, is infrequently exploited: *e.g.*, at 195°K methyl alcohol is essentially transparent down to 55,000 cm<sup>-1</sup> and has the same limit as methyl-*d*<sub>3</sub> alcohol-*d*<sub>1</sub> at 273°K. The molar

(4) See, *e.g.*, "Techniques of Organic Chemistry," Vol. VII, A. Weissberger, Ed., Interscience, New York, N. Y., 1955; J. A. Riddick and W. B. Bunger, "Techniques of Chemistry," Vol. II, Interscience, New York, N. Y., 1970.

(5) M. Halmann and I. Platzner, *J. Phys. Chem.*, **70**, 580 (1966).

(6) R. E. Verrall and W. A. Senior, *J. Chem. Phys.*, **50**, 2746 (1969).

(7) D. P. Stevenson, *J. Phys. Chem.*, **69**, 2145 (1965).

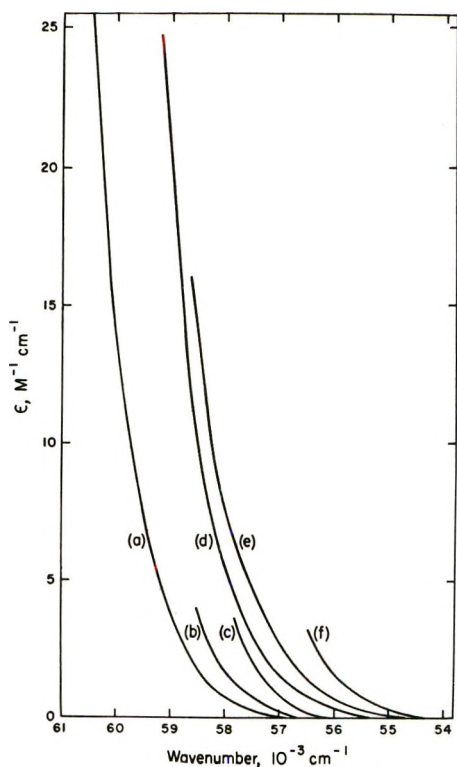


Figure 1. Molar absorption coefficients of liquid  $D_2O$  (curves a, b, and c at 278, 298, and 328°K, respectively) and  $H_2O$  (curves d, e, and f at 274, 298, and 328°K, respectively).

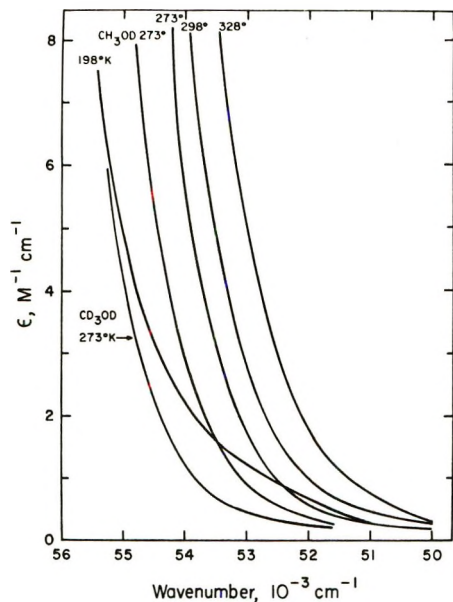


Figure 2. Molar absorption coefficients of  $CH_3OH$  at 328, 298, 273, and 198°K. For comparison, the spectra for  $CH_3OD$  and  $CD_3OD$  both at 273°K are shown.

absorption coefficient of methyl alcohol at  $54,090\text{ cm}^{-1}$  (185 nm) and 298°K obtained in this work,  $8.8\text{ M}^{-1}\text{ cm}^{-1}$ , is close to the value of Weeks, *et al.*,<sup>8</sup>  $8.4\text{ M}^{-1}\text{ cm}^{-1}$ . There is a possibility of a low-intensity absorption band under the low-temperature (198°K) absorption edge (see Figure 2).

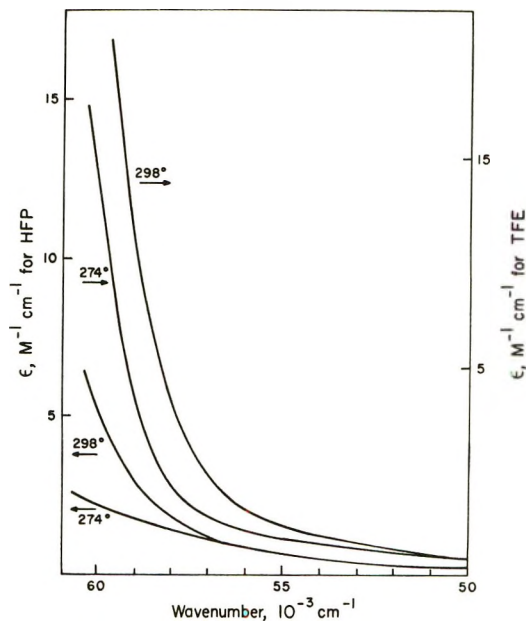


Figure 3. Molar absorption coefficients of trifluoroethyl alcohol (TFE) and hexafluoro-2-propyl alcohol (HFP) both at 298 and at 274°K.

Attention has been drawn<sup>9</sup> to the enhanced transmittance of fluoroalkanes relative to alkanes. A similar situation exists for the fluorinated alcohols, 2,2,2-trifluoroethyl alcohol, and 1,1,1,3,3,3-hexafluoro-2-propyl alcohol (compare Figures 2 and 3). The spectra are temperature sensitive and the limit for 2,2,2-trifluoroethyl alcohol in a 0.1-mm thick cell at 274°K is  $60,000\text{ cm}^{-1}$  (Figure 3); the limit for hexafluoro-2-propyl alcohol lies beyond  $61,000\text{ cm}^{-1}$  ( $<164\text{ nm}$ ). These solvents are the most transparent hydroxylic solvents yet observed, particularly at low temperatures (see also Figure 4).

The organic cyanides, methyl through *n*-propyl, are aprotic polar solvents, complimentary to the foregoing hydroxylic solvents and of considerable interest in studies of solvation. With increase in the size of the R group, the intensity of the long-wavelength tail absorption edge increases (Figure 5). *N*-Propyl cyanide shows a low-intensity absorption band centered on  $50,000\text{ cm}^{-1}$  which does not disappear on further purification. The intensity of this band decreases with decrease in temperature. Ethyl cyanide shows a similar, but much less intense, band while such features are absent from the absorption spectrum of methyl cyanide. The transmission limits of the cyanides may be shifted to higher energies by decrease in temperature. The melting point drops as low as 152°K for *n*-propyl cyanide. The temperature coefficient of

(8) J. L. Weeks, G. M. A. C. Meaburn, and S. Gordon, *Radiat. Res.*, **19**, 559 (1963).

(9) H. R. Dickinson and W. C. Johnson, Jr., *Appl. Opt.*, **10**, 681 (1971).

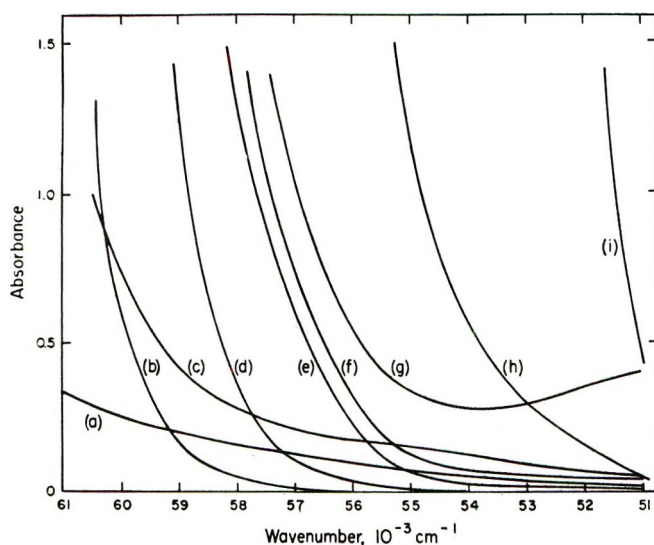


Figure 4. Far-uv spectra of some solvents: (a) hexafluoro-2-propyl alcohol, 0.1-mm path length, 274°K; (b) D<sub>2</sub>O,  $\sim 7 \times 10^{-3}$  mm, 278°K; (c) trifluoroethyl alcohol, 0.1 mm, 233°K; (d) H<sub>2</sub>O,  $\sim 7 \times 10^{-3}$  mm, 274°K; (e) methyl cyanide,  $25 \times 10^{-3}$  mm, 230°K; (f) ethyl cyanide,  $25 \times 10^{-3}$  mm, 181°K; (g) *n*-propyl cyanide,  $25 \times 10^{-3}$  mm, 155°K; (h) methyl alcohol, 0.1 mm, 198°K; (i) acetone,  $25 \times 10^{-3}$  mm, 180°K.

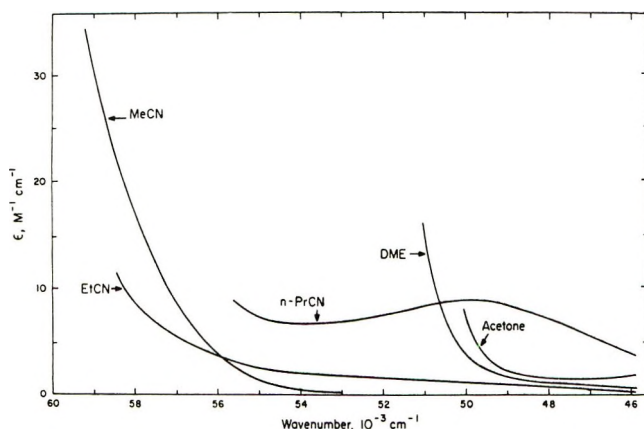


Figure 5. Molar absorption coefficients of methyl-, ethyl-, and *n*-propyl cyanides, dimethoxyethane, and acetone. All determined at 298°K.

absorption is markedly less than that observed for the alcohols and water (see Figure 4).

Acetone is generally regarded as having a transmission cutoff in the region of  $30,000 \text{ cm}^{-1}$ ,  $\nu_{\text{max}}$  being at  $36,400 \text{ cm}^{-1}$  (298°K). However, the intensity of the acetone  $n-\pi^*$  absorption is not high and the (asymmetric) band intensity decreases at lower wavelengths such that a spectroscopic "window" is available between  $38,500$  and  $50,000 \text{ cm}^{-1}$  at 298°K (Figure 5). The high-energy absorption edge shifts with temperature to increase the upper limit further; *e.g.*, at 180°K the limit is  $51,500 \text{ cm}^{-1}$  (Figure 4), with no significant alteration on the lower limit. The spectroscopy of

solutes in acetone solution is thus feasible in this region; *e.g.*, the characteristic spectra of halide ions in acetone have been obtained<sup>3</sup> over the range 180–318°K. Dimethoxyethane absorption spectra are also temperature dependent.

### Discussion

The distinctive feature of the results reported above lies in the dramatically reduced optical absorption of common solvents with decrease in temperature. This feature, combined with the use of thin (short path length) optical cells, extends the regions available for solution spectroscopy further into the far-uv. The most significant temperature effects are observed for hydroxylic solvents. The first absorption band for water (and alcohols) is assigned to an  $n-\sigma^*$  transition<sup>10</sup> which appears to be strongly affected by hydrogen bond formation. The absorption spectra of acetone, the organic cyanides, and dimethoxyethane are much less affected by temperature. Further detailed discussions can only follow determination of the complete liquid-phase spectra of the solvents over a range of temperatures. Table I gives some solvent transmission limits. The limit is defined as that wave number where the absorbance of the solvent at a given thickness is 1.0. It can be seen from Table I that by a judicious choice of solvent, temperature, and optical path length, the electronic spectra of organic and inorganic compounds in solution can be determined down to 165 nm. This wavelength is, at present, limited by the optics and detectors used in commercially available double-beam spectrophotometers.

Table I: Transmission Limits of Various Solvents at Different Temperatures

Solvent	Temp, °K	Sample thickness, mm	Limit, $\text{cm}^{-1}$ <sup>a</sup>
Water	274	Nominally $7 \times 10^{-3}$	58,800
D <sub>2</sub> O	278	Nominally $7 \times 10^{-3}$	60,300
Methyl alcohol	195	$100 \times 10^{-3}$	54,800
CD <sub>3</sub> OD	273	$100 \times 10^{-3}$	55,000
Methyl cyanide	233	$25 \times 10^{-3}$	57,600
Ethyl cyanide	181	$25 \times 10^{-3}$	57,400
<i>n</i> -Propyl cyanide	155	$25 \times 10^{-3}$	56,900
Trifluoroethyl alcohol	233	$100 \times 10^{-3}$	60,500
Hexafluoro-2-propyl alcohol	273	$100 \times 10^{-3}$	>61,000
Acetone	180	$100 \times 10^{-3}$	51,500
Dimethoxyethane	273	$100 \times 10^{-3}$	51,000

<sup>a</sup> Transmission limit is defined here as the wave number where solvent absorbance is equal to 1.0 for the particular optical path length.

(10) C. N. R. Rao, "Ultraviolet and Visible Spectroscopy," Butterworth, London, 1961.

# Magnetic Properties of Three Copper(II) Complexes of

## 2-(2-Aminoethyl)pyridine

by David Y. Jeter,<sup>1</sup> William E. Hatfield,\* and Derek J. Hodgson

Department of Chemistry, University of North Carolina, Chapel Hill, North Carolina 27514 (Received January 5, 1972)

Publication costs assisted by the Materials Research Center of the University of North Carolina

The magnetic susceptibilities of 2-(2-aminoethyl)pyridine (AEP) complexes of copper(II) with the formulas  $\text{Cu}(\text{AEP})_2\text{Br}_2$ ,  $\text{Cu}(\text{AEP})\text{Cl}_2$ , and  $\text{Cu}(\text{AEP})\text{Br}_2$  have been measured in the temperature range 2.8–296°K. The 1:1 complexes exhibit antiferromagnetic interactions which may be understood in terms of their structural features. The magnetic susceptibility data from the complex  $\text{Cu}(\text{AEP})_2\text{Br}_2$  obey the Curie-Weiss law with  $\mu_{\text{eff}} = 1.83 \text{ BM}$  and  $\theta = 0.6^\circ$ .

### Introduction

Continuing our systematic examination of the structures and magnetic properties of copper(II) complexes which may exhibit spin-spin coupling or exchange,<sup>2,3</sup> we have investigated three complexes of 2-(2-aminoethyl)pyridine. This ligand, abbreviated as AEP, is known<sup>4</sup> to yield both 1:1 compounds and 2:1 compounds with copper(II) salts. It was thought that the 1:1 compounds were dimeric with halogen bridges and the 2:1 compounds were monomeric. Knowing that halogen bridging ligands can have varying effects on magnetic interactions we have studied the electron paramagnetic resonance spectra and have determined the susceptibilities of  $\text{Cu}(\text{AEP})_2\text{Br}_2$ ,  $\text{Cu}(\text{AEP})\text{Cl}_2$ , and  $\text{Cu}(\text{AEP})\text{Br}_2$ . The results of our investigations are described herein.

### Experimental Section

**Preparation of the Compounds.** The preparations of complexes of formulation  $\text{Cu}(\text{AEP})_2\text{X}_2 \cdot \text{H}_2\text{O}$  and  $\text{Cu}(\text{AEP})\text{X}_2$ , where X is chloride or bromide, have been reported by Uhlig and Maaser.<sup>4</sup> These authors report that the complex  $\text{Cu}(\text{AEP})_2\text{Br}_2 \cdot \text{H}_2\text{O}$ , for example, is formed by the reaction of copper(II) bromide with excess AEP in aqueous solution. Modifying this procedure, we find that the reaction of copper(II) bromide with excess AEP in 95% ethanol gives a deep blue solution from which pale blue crystals of the anhydrous complex  $\text{Cu}(\text{AEP})_2\text{Br}_2$  precipitate. Attempts to prepare the 1:1 compounds by the method reported by the above authors were unsuccessful, instead 2:1 complexes were obtained. The desired 1:1 complexes were obtained, however, by adding a few drops of the ligand to concentrated solutions of the copper(II) halide in absolute methanol. The precipitates which formed were redissolved in hot absolute methanol from which crystals formed upon cooling. A suitable analysis was obtained for each of the three compounds.

**Magnetic Measurements.** In the temperature range 77–296°K, magnetic susceptibilities of powdered samples of the three compounds were measured with a Faraday balance.<sup>5</sup> A Foner-type vibrating sample magnetometer,<sup>6</sup> operating at a magnetic field strength of 10,000 G, was used to determine the susceptibilities in the temperature range 2.8–63.5°K. Mercury tetrathiocyanatocobaltate(II) was used as a magnetic susceptibility standard,<sup>7</sup> and diamagnetic corrections for the substituent atoms were estimated from Pascal's constants.<sup>8</sup>

**Epr Measurements.** The epr spectra of powdered samples of the compounds were obtained using X-band spectrometers with 100-kHz modulation at appropriate microwave frequencies. Cylindrical quartz sample tubes were used.

### Results

At higher temperatures the magnetic susceptibilities of all three complexes<sup>9</sup> are much alike and obey the Curie-Weiss law,  $\chi = C/(T + \theta)$ , with the parameters in Table I where  $\mu_{\text{eff}} = 2.828C^{1/2} \text{ BM}$ . At low temperatures, differences in the three become obvious.

- (1) NSF Trainee, 1968–1971.
- (2) D. Y. Jeter, D. J. Hodgson, and W. E. Hatfield, *Inorg. Chim. Acta*, **5**, 257 (1971).
- (3) N. T. Watkins, D. Y. Jeter, W. E. Hatfield, and S. M. Horner, *Trans. Faraday Soc.*, **67**, 2431 (1971).
- (4) E. Uhlig and M. Maaser, *Z. Anorg. Allg. Chem.*, **322**, 25 (1963).
- (5) W. E. Hatfield, C. S. Fountain, and R. Whyman, *Inorg. Chem.*, **5**, 1855 (1966).
- (6) S. Foner, *Rev. Sci. Instrum.*, **30**, 548 (1959).
- (7) B. N. Figgis and R. S. Nyholm, *J. Chem. Soc.*, 4190 (1958).
- (8) E. König, "Magnetic Properties of Transition Metal Compounds," Springer-Verlag, West Berlin, 1966.
- (9) Listings of the magnetic susceptibility data will appear following these pages in the microfilm edition of this volume of the journal. Single copies may be obtained from the Business Operations Office, Books and Journals Division, American Chemical Society, 1155 Sixteenth St., N.W., Washington, D. C. 20036, by referring to code number JPC-72-2707. Remit check or money order for \$3.00 for photocopy or \$2.00 for microfiche.

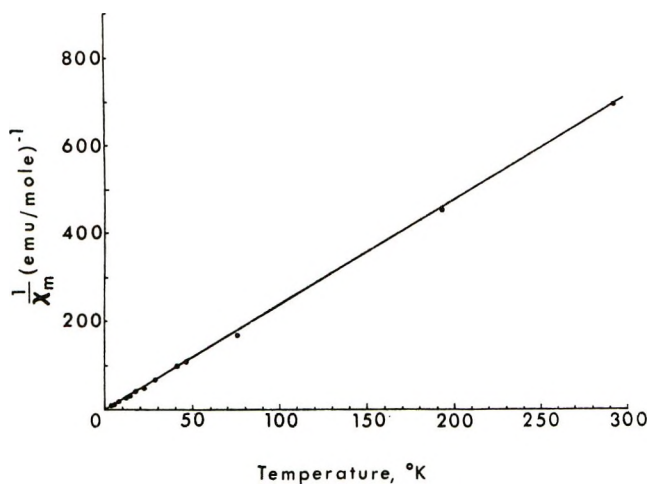


Figure 1. The temperature variation of the experimental inverse susceptibility of  $\text{Cu}(\text{AEP})_2\text{Br}_2$  in the temperature range 2.9–300°K.

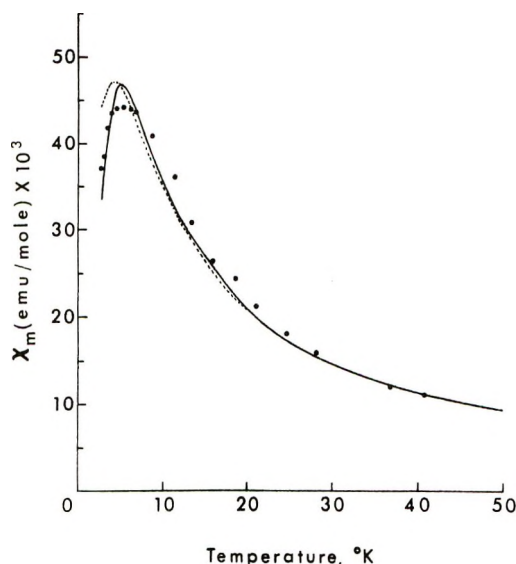


Figure 2. The temperature variation of the experimental susceptibility (●) of  $\text{Cu}(\text{AEP})\text{Cl}_2$  in the temperature range 2.9–50°K, and the best fits using the Ising (broken line) and dimer (solid line) models.

The plot of the temperature variation of the inverse susceptibility for  $\text{Cu}(\text{AEP})_2\text{Br}_2$  which is shown in Figure 1 is linear throughout the temperature range. The 1:1 complexes, however, display a somewhat different behavior. The data for the chloro complex deviate from the Curie–Weiss law and a distinct maximum in susceptibility is observed near 6°K. The bromo complex appears to behave in the same manner, although at the limit of our measurements no maximum had yet been observed. The characteristics observed in the latter two compounds are indicative of antiferromagnetic exchange interactions.

Considering structural features which are discussed below, the experimental data for both  $\text{Cu}(\text{AEP})\text{Cl}_2$  and  $\text{Cu}(\text{AEP})\text{Br}_2$  were fitted to models involving dimer

Table I: Curie–Weiss Parameters

	$\text{Cu}(\text{AEP})_2\text{Br}_2$	$\text{Cu}(\text{AEP})\text{Cl}_2$	$\text{Cu}(\text{AEP})\text{Br}_2$
$C$	0.420	0.438	0.406
$\theta$ , deg	0.6	–0.7	–0.6
$\mu_{\text{eff}}$ , BM	1.83	1.87	1.80

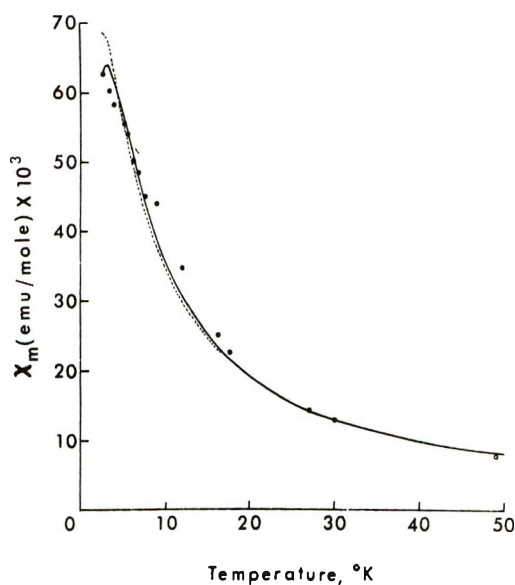


Figure 3. The temperature variation of the experimental susceptibility (●) of  $\text{Cu}(\text{AEP})\text{Br}_2$  in the temperature range 2.8–50°K, and the best fits using the Ising (broken line) and dimer (solid line) models.

pairs as well as one-dimensional chains; the results are shown in Figures 2 and 3. Using the Van Vleck equation<sup>10</sup>

$$\chi_m = [g^2\beta^2N/3kT][1 + \frac{1}{3}\exp(-2J/kT)] + N\alpha$$

for magnetically coupled pairs of copper(II) ions, the data yield a singlet–triplet splitting of  $-5.7\text{ cm}^{-1}$  and  $g = 2.25$  for the chloro complex and  $-3.6\text{ cm}^{-1}$  and  $g = 2.11$  for the bromo complex. The sums of the squares of the deviations between the experimental and calculated  $\chi_i T_i$  are  $1.2 \times 10^{-2}$  and  $8.7 \times 10^{-3}$ , respectively, for the chloro and bromo complexes.

The Ising model for anisotropic chain antiferromagnetic interactions has been discussed by Fisher,<sup>11</sup> who has shown that the exact formulas for infinite chains are

$$\chi_{\perp} = \frac{Ng^2\beta^2}{8|J|} \left[ \tanh\left(\frac{J}{kT}\right) + \left(\frac{J}{kT}\right) \text{sech}^2\left(\frac{J}{kT}\right) \right]$$

and

$$\chi_{\parallel} = \frac{Ng^2\beta^2}{4kT} \exp\left(\frac{2J}{kT}\right)$$

(10) J. H. Van Vleck, "The Theory of Electric and Magnetic Susceptibilities," Oxford Press, London, 1932, Chapter IX.

(11) M. E. Fisher, *J. Math. Phys.*, **4**, 124 (1963).

where the total susceptibility is given by

$$\langle \chi_m \rangle = \frac{1}{3} \chi_{\parallel} + \frac{2}{3} \chi_{\perp}$$

Using this approach we calculate for the exchange energy,  $J$ , values of  $-3.1$  and  $g = 2.27$  for the chloro complex and  $-1.9 \text{ cm}^{-1}$  and  $g = 2.12$  for the bromo complex. The sums of the squares of the deviations between the experimental and calculated  $\chi_i T_i$  using this model, however, were  $1.9 \times 10^{-2}$  (chloro) and  $1.2 \times 10^{-2}$  (bromo). Hence, this model may be less appropriate than the dimer model.

The epr spectrum of  $\text{Cu}(\text{AEP})\text{Br}_2$  is shown in Figure 4. Only a single broad, symmetric line at 3200 G was

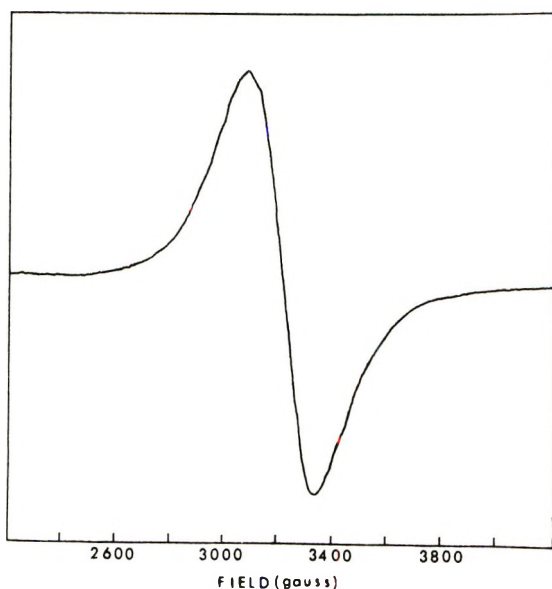


Figure 4. The epr spectrum at room temperature of a powdered sample of  $\text{Cu}(\text{AEP})\text{Br}_2$  in the region 2200–4200 G ( $\nu = 9.5$  GHz).

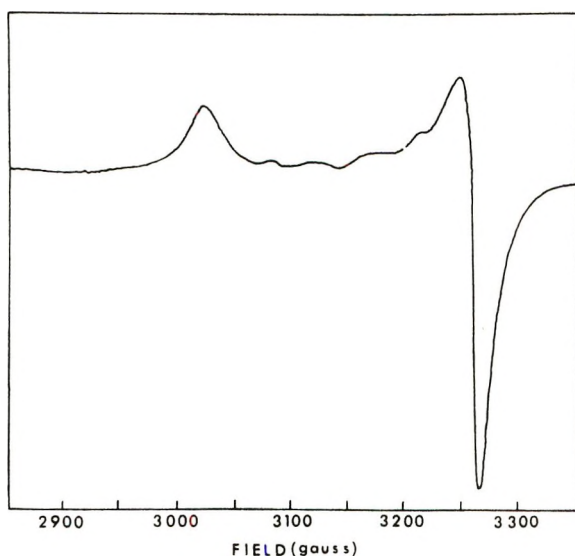


Figure 5. The epr spectrum at room temperature of a powdered sample of  $\text{Cu}(\text{AEP})\text{Cl}_2$  in the region 2850–3350 G ( $\nu = 9.5$  GHz).

found. From this line we calculate  $\langle g \rangle = 2.12$ . The spectrum of  $\text{Cu}(\text{AEP})\text{Cl}_2$ , shown in Figure 5, is a two  $g$  value type spectrum with absorptions at 3050 and 3310 G ( $g = 2.23$  and  $g = 2.05$ ). Four other weak lines are observed at approximately 3110, 3150, 3200, and 3240 G. This spectrum indicates the presence of exchange interactions, although complicated structural effects (*vide infra*) prevent further analysis. The spectrum of  $\text{Cu}(\text{AEP})_2\text{Br}_2$ , seen in Figure 6, has a three  $g$  value ( $g_1 = 2.26$ ,  $g_2 = 2.10$ , and  $g_3 = 2.06$ ) spectrum near 3000 G as expected for copper(II) ions in low symmetry environments and in the absence of extensive exchange coupling.<sup>12,13</sup>

## Discussion

Preliminary structural work<sup>14,15</sup> has shown several interesting features in these complexes which could not have been previously predicted. The 2:1 bromide complex is found to exist as a five-coordinated copper(II) cation,  $[\text{Cu}(\text{AEP})_2\text{Br}]^+$ , and a discrete  $\text{Br}^-$  anion.<sup>14</sup> The geometry at the copper atom is almost exactly half-way between trigonal bipyramidal and tetragonal pyramidal, the observed bond angles being very close to the average of the values expected for the two idealized geometries. Thus, for example, the two amine nitrogen atoms subtend an angle of  $149.4(3)^\circ$  at the copper, which is approximately the average of the values of  $120$  and  $180^\circ$  calculated for trigonal bipyramidal and tetragonal pyramidal, respectively; the other angles at copper observe the same trend. These molecules are aggregated along chains, and the distance between copper(II) ions is  $11.85 \text{ \AA}$  which precludes any exchange interaction. Interchain interactions are equally unlikely since the copper ions in adjacent chains are separated by  $7.41 \text{ \AA}$  with two AEP groups between them.

The copper(II) ion in the isostructural complexes  $\text{Cu}(\text{AEP})\text{Cl}_2$  and  $\text{Cu}(\text{AEP})\text{Br}_2$  has been determined to be six-coordinated with two in-plane halide ligands, two in-plane nitrogen atoms from the AEP group, and two more distant halide ligands from adjacent molecules. The filling of the coordination sites by the out-of-plane ligands leads to dimeric units connected by nonsymmetrical bridges. The dimeric units are aggregated into chains with the two halves of each dimer being in different chains. This picture can be better visualized by reference to Figure 7. In both complexes the Cu–X–Cu bridging angle is approximately  $79^\circ$  with Cu–Cu internuclear separations of  $4.0$  (Br) and  $3.8 \text{ \AA}$  (Cl). The chain bridging angle is  $122$  (Br) and  $126^\circ$  (Cl) with Cu–Cu separations of  $5.3$

(12) D. E. Billing and B. J. Hathaway, *J. Chem. Soc. A*, 1516 (1968).

(13) A. A. G. Tomlinson and B. J. Hathaway, *ibid.*, 2578 (1968).

(14) V. C. Copeland, W. E. Hatfield, P. Singh, and D. J. Hodgson, unpublished results.

(15) V. C. Copeland, P. Singh, W. E. Hatfield, and D. J. Hodgson, *Inorg. Chem.*, **11**, 1826 (1972).





Figure 6. The epr spectrum at room temperature of a powdered sample of  $\text{Cu}(\text{AEP})_2\text{Br}_2$  in the region 2800–3300 G ( $\nu = 9.18$  GHz).

and  $5.2 \text{ \AA}$ , respectively. Magnetically, this structural arrangement poses much complication due to the two avenues through which exchange interactions are possible. It appears, however, that the experimental data fit a dimeric model better than the chain model, and this suggests that the dimeric exchange process may be the dominant interaction. It should also be noted that the exchange interaction present in  $\text{Cu}(\text{AEP})\text{Cl}_2$ , as reflected by the observed  $T_{\text{max}}$  of about  $6^\circ\text{K}$ , decreases when the chloride bridging ligand is replaced by bromide. This result was also obtained in the dimeric complexes  $[\text{Cu}(\alpha\text{-picoline})_2\text{X}_2]_2$  when a chloride bridge was replaced by a bromide,<sup>2</sup> but not in  $\text{Cu}(\text{pyridine})_2\text{X}_2$ <sup>16</sup> or anhydrous  $\text{CuX}_2$ ;<sup>17</sup> these latter two show chain interactions even though  $\text{CuX}_2$  is complicated by interchain interactions. It should be

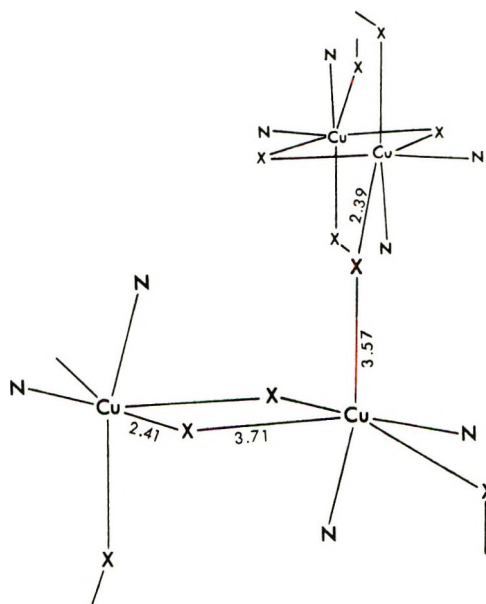


Figure 7. A representation of the bridging structure of  $\text{Cu}(\text{AEP})\text{X}_2$  where  $\text{X} = \text{Cl}$  and  $\text{Br}$ . The bond distances shown on the figure are for the bromo complex (ref 15).

noted that antiferromagnetic exchange is found in all these systems, although the bridging angles vary greatly, thus adding weight to the conclusion<sup>2,18</sup> that the d orbitals from the halide bridges play an important role in the exchange mechanism.

*Acknowledgments.* This research was supported by the National Science Foundation (Grant No. GP 22887) and by the Materials Research Center of the University of North Carolina through Contract DAHC 15 67C 0223 with the Advanced Research Projects Agency. We are grateful for this continuing support. We also wish to thank Miss V. C. Copeland and Dr. P. Singh for providing the samples and for helpful discussions concerning the structural features of the complexes.

(16) D. Y. Jeter and W. E. Hatfield, submitted for publication.

(17) C. G. Barraclough and C. F. Ng, *Trans. Faraday Soc.*, **60**, 836 (1964).

(18) J. A. Barnes, W. E. Hatfield, and D. J. Hodgson, *Chem. Phys. Lett.*, **7**, 374 (1970).

## Reactions of Recoil Chlorine Atoms with Cis and Trans Olefins<sup>1</sup>

by W. S. Smith, S. H. Daniel, and Yi-Noo Tang\*

Department of Chemistry, Texas A & M University, College Station, Texas 77843 (Received March 13, 1972)

Reactions of recoil  $^{38}\text{Cl}$  atoms with the cis and trans isomers of both 1,2-dichloroethylene and 2-butene have been studied. The percentage absolute yield for the sum of the two isomeric products of the former system ranges from 7 to 31%, depending on scavenging efficiency, while that of the latter accounts for only about 0.5% of the total  $^{38}\text{Cl}$  formed. The unequal trans/cis product branching ratio from the two geometric isomers of dichloroethylene prompts one to the conclusion that besides the usual addition-elimination reaction observed for Cl atom reactions, there is a certain contribution from a direct substitution process. The presence of the latter reaction is strongly supported by the 5:1 and 1:5 isomer branching ratio of products observed in cis- and trans-2-butene systems. The equilibrium product branching ratio from the addition-elimination process alone has been demonstrated to be a function of the excitation energy of the decomposing radicals.

The use of the nuclear recoil method for the studies of various chemical reactions of free atoms has been extremely successful, especially in the case of recoil tritium.<sup>2-4</sup> However, there are relatively few studies devoted to the reactions of Cl atoms formed by this means.<sup>5-11</sup> Recent experiments have established that the reacting recoil species when the nuclear mode of production is  $^{37}\text{Cl}(n,\gamma)^{38}\text{Cl}$ , where the initial recoil energy is as low as 527 eV, are ground-state chlorine atoms with excess kinetic energy.<sup>6</sup>

The reactions of thermal Cl atoms with cis- and trans-dichloroethylene (DCE) has been a topic of long-term interest.<sup>12-16</sup> The chlorine atom reacts with DCE by addition to the double bond to give an excited trichloroethyl radical which decomposes to give a mixture of the geometric isomers of DCE; the excitation energy comes from the kinetic energy of the reacting Cl atom and from the addition reaction, exothermic by about 20 kcal/mol. By employing the reaction rate of Cl with propane as a standard, the trans/cis branching ratio was evaluated by Knox and Riddick to be 0.28/1.0 in favor of the cis isomer which has a heat of formation 450 cal/mol more stable than its trans counterpart.<sup>15</sup>

On the other hand, Wai and Rowland have employed  $^{38}\text{Cl}$  atoms, recoiling from nuclear transformation, for the study of the above system.<sup>9</sup> Their gas-phase system of  $\text{CH}_3\text{Cl}$  with 3% DCE forms the  $\text{CHCl}^{38}\text{Cl}-\text{CHCl}^*$  radicals almost entirely by low-energy  $^{38}\text{Cl}$  atom addition. The trans/cis branching ratio in this system is  $0.50 \pm 0.05$ . However, when the reaction was carried out in an excess of He instead of  $\text{CH}_3\text{Cl}$ , the trans/cis branching ratio was observed as  $0.49 \pm 0.02$  when starting from cis-DCE and as  $0.55 \pm 0.02$  when starting from trans-DCE.

The purpose of the present study is to reveal the nature of the recoil chlorine atom reactions with DCE as well as other olefins. We have extended the study to the 2-butenes in order to establish the occurrence of

direct substitution, and we have measured the scavenger dependence both for the absolute percentage yields and for the trans/cis branching ratio in order to demonstrate the dependence of experimental results on the energetics of the reacting Cl atoms.

### Experimental Section

**Chemicals.** All the following gases were obtained from the Matheson Company: CP grade trans- and cis-butene with 99.0% minimum purity, instrument grade 1,3-butadiene with 99.5% purity,  $\text{CF}_3\text{Cl}$  with 99.0% purity, and prepurified grade argon which was 99.998% pure. Both oxygen and helium of 99% pu-

- (1) Presented in part at the 158th National Meeting of the American Chemical Society, New York, N. Y., Sept, 1969.
- (2) R. Wolfgang, *Progr. React. Kinet.*, **3**, 97 (1965); *Annu. Rev. Phys. Chem.*, **16**, 15 (1965).
- (3) F. S. Rowland, "Proceedings of the International School of Physics, 'Enrico Fermi' Course XLIV—Molecular Beam and Reaction Kinetics," C. Schlier, Ed., Academic Press, New York, N. Y., 1970.
- (4) F. Schmidt-Bleek and F. S. Rowland, *Angew. Chem., Int. Ed. Engl.*, **3**, 769 (1964).
- (5) "Chemical Effects of Nuclear Transformations," Vol. 2, International Atomic Energy Agency, Vienna, 1965, pp 221 and 333.
- (6) C. M. Wai and F. S. Rowland, *J. Phys. Chem.*, **71**, 2752 (1967); *J. Amer. Chem. Soc.*, **90**, 3638 (1968); *J. Phys. Chem.*, **72**, 3049 (1968).
- (7) C. M. Wai, Ph.D. Thesis, University of California at Irvine, 1967.
- (8) L. Spicer and R. Wolfgang, *J. Amer. Chem. Soc.*, **90**, 2426 (1968).
- (9) C. M. Wai and F. S. Rowland, *ibid.*, **91**, 1053 (1969).
- (10) K. Berei and G. Stoecklin, *Radiochim. Acta*, **15**, 39 (1971).
- (11) Y.-N. Tang, W. S. Smith, J. L. Williams, K. Lowery, and F. S. Rowland, *J. Phys. Chem.*, **75**, 440 (1971).
- (12) P. B. Ayscough, A. J. Cocker, F. S. Dainton, S. Hirst, and M. Weston, *Proc. Chem. Soc.*, 244 (1961).
- (13) P. B. Ayscough, A. J. Cocker, and F. S. Dainton, *Trans. Faraday Soc.*, **58**, 284 (1962).
- (14) P. B. Ayscough, A. J. Cocker, F. S. Dainton, and S. Hirst, *ibid.*, **58**, 295 (1962).
- (15) J. H. Knox and J. Riddick, *ibid.*, **62**, 1190 (1966).
- (16) T. B. Cundall, *Prog. React. Kinet.*, **2**, 165 (1964).

urity were bought from the Airco Co. All of these chemicals were used without further purification.

*cis*- and *trans*-dichloroethylenes were obtained from K & K Laboratories. A small amount of the opposite isomer was found in these two compounds. Therefore, purification by bulb-to-bulb vacuum distillation was carried out shortly before the use. After the distillation, gas chromatographic calibration indicated that the impurity level was negligible.

*General Procedure.* Samples containing the parent compound and various additives were sealed by high-vacuum techniques in 1720 Pyrex glass bulbs of about 10–12-ml volume. All irradiations were carried out at the Texas A & M University Nuclear Science Center research reactor. Each sample was irradiated for 30 sec with a nominal flux of  $4.8 \times 10^{12}$  neutrons/cm<sup>2</sup> sec. High-energy <sup>38</sup>Cl atoms were then generated *in situ* by the nuclear reaction <sup>37</sup>Cl(*n*, $\gamma$ )<sup>38</sup>Cl.

Since the half-life of <sup>38</sup>Cl is 37 min, it was essential that the analysis be carried out within six or eight half-lives from the time of irradiation. The analysis of samples normally started at about 1 hr after irradiation and was completed within 3 or 4 hr.

*Sample Analysis.* The analysis of <sup>38</sup>Cl-labeled reaction products after irradiation was performed by the technique of radio-gas chromatography.<sup>17</sup> By this means, the products can be qualitatively identified by their retention times on various columns and quantitatively measured by counting the radioactivity of the decaying <sup>38</sup>Cl atoms in each compound.

An external "sandwich"-type gas proportional counter was used.<sup>18</sup> The radioactive sample was injected into a regular gas chromatographic system with He as a carrier gas and with a thermal conductivity cell for mass peak detection. This same gas stream then flowed through the "inner" column of the sandwich counter while the "outer" columns were filled with propane, a counting gas. A Dynaprint unit was used for the registration and recording of counts.

The use of an external counter is necessary because of the quenching action of dichloroethylene and other halogenated compounds.<sup>7,19</sup> Their high-electron affinity causes them to interfere seriously with the counting process of an internal counter.

*Separation of Geometric Isomers.* The majority of the sample separation was performed with a 50-ft tri-*o*-tolyl phosphate (TTP) column at 50°. There was a very wide separation between the two isomers of DCE with the *trans* compound emerging 65 min before the *cis*. A 25-ft TTP column was also used at times. Even in this case, the separation between the two isomers was complete.

There is no pure *cis*- or *trans*-1-chloropropene available commercially for calibration of columns. However, a mixture of the two could be obtained. A calibration of the mixture on the 50-ft TTP column at 50° gave two peaks of retention times 40 and 48 min.

These two peaks were then separately trapped and the nmr spectroscopy of each one of them was taken. The first peak was shown to be *cis*-1-chloropropene and the other the *trans* isomer. Although the 8-min separation between these two peaks was not ideal, the overlapping of the counts was not serious since their yields were normally not large. Selection of the proper background, however, was essential to an accurate analysis.

*Decay Corrections.* In making quantitative calculations of the cumulative radioactivity of each peak, we subtracted the appropriate background correction (by multiplying the peak range in minutes by an average background correction per minute) from the total number of counts. We then made the radioactive decay correction by applying the correction factor for the peak maximum to the total counts of the whole peak. This method involves a slight error because the peak is not exactly symmetrical. However, we justified this method by making a more exact calculation for several runs to determine their per cent difference. We subtracted the average background from each count per minute and then multiplied it by its own decay correction factor and then summed up all the corrected counts. Our previous simplified calculation only differed from the present total by 0.3% which was much smaller than other experimental errors.

*Absolute Yields.* <sup>40</sup>Ar (pressure, 2 cm) was used as an internal monitor in order to make absolute yield measurements for <sup>38</sup>Cl-containing products.<sup>7,9</sup> The nuclear reaction <sup>40</sup>Ar(*n*, $\gamma$ )<sup>41</sup>Ar gives the radioactive isotope <sup>41</sup>Ar as a product. By using the natural isotope abundance and the thermal neutron capture cross section for <sup>37</sup>Cl and <sup>40</sup>Ar and the decay constant for <sup>38</sup>Cl and <sup>41</sup>Ar, the following equation was derived by Wai and Rowland and was employed by us for the calculation of the absolute yields for <sup>38</sup>Cl<sup>7</sup>

$$Y = 1.31(x/(1 - x))(A_{Cl^{38}}/A_{Ar^{41}})$$

where *x* is the mole fraction of Ar relative to Ar and Cl atoms in the system; *A*<sub>Cl<sup>38</sup></sub> and *A*<sub>Ar<sup>41</sup></sub> are respectively the decay-corrected cumulative radioactivity observed for <sup>38</sup>Cl products and <sup>41</sup>Ar.

## Results

*Reactions of Recoil <sup>38</sup>Cl Atoms with Dichloroethylene.* The reactions of recoil <sup>38</sup>Cl atoms with *cis*- and *trans*-dichloroethylene have been carried out in the presence of different kinds and different concentrations of scavengers. The *trans*/*cis* branching ratio and the total percentage absolute yield for each system are as shown in Table I. The types of scavenging conditions include non-scavenged and O<sub>2</sub>- (pressure, 5 and 15 cm) and butadiene–O<sub>2</sub>-scavenged samples (butadiene has

(17) J. K. Lee, E. K. C. Lee, B. Musgrave, Y.-N. Tang, J. W. Root, and F. S. Rowland, *Anal. Chem.*, **34**, 741 (1962).

(18) R. Wolfgang and F. S. Rowland, *ibid.*, **30**, 903 (1958).

(19) Yi-Noo Tang, Ph.D. Thesis, The University of Kansas, 1964.

**Table I:** Branching Ratio and Percentage Absolute Yields from Recoil  $^{38}\text{Cl}$  Reactions with *cis*- and *trans*-1,2-Dichloroethylene

Sample composition <sup>a</sup>	<i>cis</i> -DCE		<i>trans</i> -DCE	
	Trans/cis ratio <sup>b</sup>	% absolute yield	Trans/cis ratio <sup>b</sup>	% absolute yield
DCE + Ar(2)	0.49 ± 0.04	31 ± 2	0.61 ± 0.02	30 ± 2
DCE + O <sub>2</sub> (5) + Ar(2)	0.61 ± 0.03	26 ± 22	0.71 ± 0.03	25 ± 2
DCE + O <sub>2</sub> (5) + He(60) + Ar(2)	0.62 ± 0.04	22 ± 2	0.73 ± 0.03	22 ± 3
DCE + O <sub>2</sub> (15) + Ar(2)	0.67 ± 0.05	18 ± 3	0.75 ± 0.05	18 ± 3
DCE + O <sub>2</sub> (5) + butadiene(5) + Ar(2)	0.72 ± 0.03	7 ± 2	0.95 ± 0.04	8 ± 2

<sup>a</sup> The numerical values behind the compounds stand for pressure in cm. <sup>b</sup> *trans*-DCE- $^{38}\text{Cl}$ /*cis*-DCE- $^{38}\text{Cl}$  ratio.

**Table II:** Branching Ratio and Percentage Absolute Yields from Recoil  $^{38}\text{Cl}$  Reactions with *cis*- and *trans*-2-Butene

Sample composition <sup>a</sup>	<i>cis</i> -2-Butene		<i>trans</i> -2-Butene	
	Trans/cis ratio <sup>b</sup>	% absolute yield	Trans/cis ratio <sup>b</sup>	% absolute yield
2-Butene(35) + CF <sub>3</sub> Cl(35) + Ar(2)	0.20 ± 0.02	0.61 ± 0.10	6.3 ± 0.4	0.30 ± 0.07
2-Butene(35) + CF <sub>3</sub> Cl(35) + O <sub>2</sub> (5) + Ar(2)	0.22 ± 0.02	0.71 ± 0.10	5.5 ± 0.3	0.25 ± 0.10
2-Butene(5) + CF <sub>3</sub> Cl(20) + O <sub>2</sub> (5) + He(50) + Ar(2)	<i>c</i>	<0.01	<i>c</i>	<0.01
2-Butene(35) + CF <sub>3</sub> Cl(30) + O <sub>2</sub> (5) + butadiene(4) + Ar(2)	0.19 ± 0.02	0.49 ± 0.10	4.4 ± 0.4	0.24 ± 0.04

<sup>a</sup> See footnote *a* of Table I. <sup>b</sup> *trans*-1-Chloropropene- $^{38}\text{Cl}$ /*cis*-1-chloropropene- $^{38}\text{Cl}$  ratio. <sup>c</sup> Not measured.

been shown to be an extremely efficient scavenger for low-energy Cl atoms).<sup>6,7</sup> Also samples with a large excess of He have been run in order to test the moderator effect.

Some features about the results shown in Table I are the following. (1) In every case, the *trans*/*cis* branching ratio is definitely different when the parent molecule is *cis* in comparison with that when it is *trans*. (2) The percentage absolute yields decrease with increasing effectiveness in scavaging. (3) The *trans*/*cis* branching ratio increases with increasing effectiveness in scavaging, *i.e.*, relatively more *trans* products are formed at a higher level of scavaging. (4) A large amount of He as a moderator does not change either the branching ratio or the absolute yield to any appreciable extent.

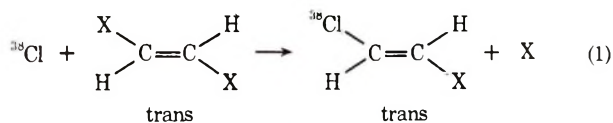
*Reactions of Recoil  $^{38}\text{Cl}$  Atoms with *cis*- and *trans*-2-Butenes.* The corresponding reactions of recoil  $^{38}\text{Cl}$  atoms with *cis*- and *trans*-2-butenes have also been carried out and the data are as shown in Table II. CF<sub>3</sub>Cl was used as a source of  $^{37}\text{Cl}$  atoms for the (*n*, $\gamma$ ) nuclear reaction. *trans*- and *cis*-1-chloropropenes were observed as products. A comparison of these results with those obtained in the DCE systems reveals the following differences. (1) The branching ratios are very much different when the two geometric isomers of 2-butenes are used respectively as the starting reactants. The *trans*/*cis* ratios are approximately 1:5

when starting with *cis* and 5:1 from its *trans* counterpart, whereas in the case of DCE, there is only a difference of about 20%. (2) The percentage absolute yields are extremely low, namely, below the 1% level, compared with the 10–30% yields observed for DCE. Its variation with scavenger efficiency is not obvious. (3) The variation of branching ratio with scavenger efficiency is also not noticeable. (4) The addition of He as a moderator essentially decreases the yields to zero and the branching ratios are therefore impossible to calculate.

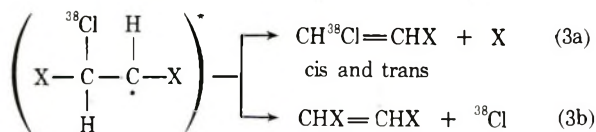
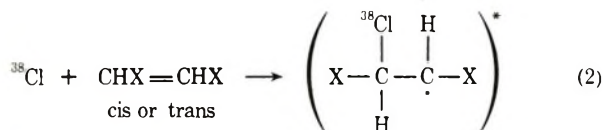
## Discussion

*Mechanism for Recoil  $^{38}\text{Cl}$  Atom Reactions.* Recoil  $^{38}\text{Cl}$  atoms were produced with an initial energy of 527 eV. However, it remains too energetic for chemical reactions to give stable products until it cools down to 30 eV or below.<sup>2,3</sup> A major fraction of the  $^{38}\text{Cl}$  atoms may even degrade their energy to the thermal range before they eventually react. The proposed mechanism for recoil  $^{38}\text{Cl}$  atoms is a combination of the following two types.

(1) *Direct Substitution.* If the kinetic energy of the  $^{38}\text{Cl}$  atom is high enough, it is able to undergo direct substitution for another atom or group at one of the  $\sigma$  bonds of the central C atom. The  $^{38}\text{Cl}$ -for-X replacement in an olefinic compound is illustrated in eq 1.



(2) *Addition-Elimination Reaction.*  $^{38}\text{Cl}$  atoms may interact with the carbon-carbon  $\pi$  bonds to undergo an addition reaction followed by an elimination process as shown in eq 2 and 3. In the case of DCE,



the resulting trichloroethyl radical, excited through the 20 kcal/mol exothermicity of the addition together with the kinetic energy of the incoming  $^{38}\text{Cl}$  atoms, may decompose by breaking one of the C-Cl bonds. A mixture of the trans and cis isomers of the products will be obtained, as indicated in eq 3a, because the C-C single bond in the radical should have plenty of time for free rotation before the elimination takes place. The radical lifetime was estimated to be about  $5-7 \times 10^{-10}$  sec when formed by thermal  $^{38}\text{Cl}$  addition while the C-C bond rotation time has been shown to be less than  $10^{-10}$  sec.<sup>9</sup> Therefore, an equilibrium mixture of a fixed trans/cis ratio should be obtained which probably characterizes the energetics of the addition-elimination system. This same branching ratio is expected when starting from either *cis*- or *trans*-DCE as the reactant because the same equilibrated trichloroethyl radical is formed once the C-C bond starts to rotate.

Reaction 3b is also possible and should have a similar probability to occur as 3a. The combination of reaction 2 and 3b actually serves as a powerful means for thermalizing the energetic  $^{38}\text{Cl}$  atoms.<sup>9</sup> The eliminated  $^{38}\text{Cl}$  atom, if still energetic enough, may enter into another cycle of addition-elimination process until either it ends up as a stable product according to eq 3a, or it loses so much energy that it cannot carry out reaction 2. Also it may be scavenged either as a free atom or as a  $^{38}\text{Cl}$ -labeled radical.

*Direct Substitution by Recoil  $^{38}\text{Cl}$  Atoms.* Table III shows a comparison of the trans/cis branching ratio for various systems of Cl atom reactions with dichloroethylene. In the thermal system, the Cl atoms are probably not energetic enough to undergo direct substitution, while the addition-elimination process alone will give the same branching ratio no matter if we start from *cis*- or *trans*-DCE.<sup>15</sup> However, for the recoil  $^{38}\text{Cl}$  systems, especially from our data as shown in Table I, it is very obvious that the branching ratios are different for the two geometric isomers. This indicates

that in the recoil system, certain  $^{38}\text{Cl}$  atoms react while they are still "hot" and therefore are capable of carrying out reaction 1. Since direct substitution will probably give only products of the same geometric configuration as the starting DCE, we expect an extra contribution of the trans product from the trans system and *vice versa*. The combination of this unbalanced contribution to the equilibrium trans/cis ratio from the addition-elimination process will account for the observed difference in the experimental results.

**Table III:** Comparison of Trans/Cis Branching Ratio from Cl Atom Reactions with Dichloroethylene

Experimental method	Trans/cis product ratio		Ref
	From <i>trans</i> -DCE	From <i>cis</i> -DCE	
Thermal Cl atoms	0.28		15
Recoil $^{38}\text{Cl}$ in excess He <sup>a</sup>	$0.55 \pm 0.02$	$0.49 \pm 0.02$	9
Recoil $^{38}\text{Cl}$ atoms <sup>b</sup>	$0.71 \pm 0.03$	$0.61 \pm 0.03$	This work

<sup>a</sup> Oxygen pressure, 2 cm. <sup>b</sup> Oxygen pressure, 5 cm.

The strongest evidence for the occurrence of reaction 1 comes from the results of recoil  $^{38}\text{Cl}$  reactions with 2-butene as shown in Table II. The 5:1 product branching ratio in favor of the 1-chloropropene isomer which has the same configuration as the starting 2-butene can easily be explained by the assumption that direct substitution is the main mode of reaction in this system, and that addition-elimination is at most of minor importance.

One of the major questions concerning direct substitution is whether or not the resulting product retains enough energy to undergo secondary isomerization.<sup>20-23</sup> If this is the case, part of the products with the opposite configuration as that of the parent molecule may have originated from the direct substitution process. However, the 5:1 branching ratio observed in this 2-butene case indicates that this kind of secondary isomerization is at most of minor importance.

*Dependence of Trans/Cis Branching Ratio on Kinetic Energy of the Reacting  $^{38}\text{Cl}$  Atoms.* The energy spectrum of a reacting system will be basically decided by the moderating condition.<sup>2</sup> However, for a reaction whose yield consists of a significant thermal contribution, its energy cut-off at the low-energy end will be determined by the scavenging situation. An increase in scavenging efficiency is equivalent to pushing the low

(20) E. K. C. Lee and F. S. Rowland, *J. Amer. Chem. Soc.*, **85**, 897 (1963).

(21) Y.-N. Tang, E. K. C. Lee, and F. S. Rowland, *ibid.*, **86**, 1280 (1964).

(22) Yi-Noo Tang and F. S. Rowland, *J. Phys. Chem.*, **71**, 4576 (1967).

(23) Yi-Noo Tang, Thomas Smail, and F. S. Rowland, *J. Amer. Chem. Soc.*, **91**, 2130 (1969).

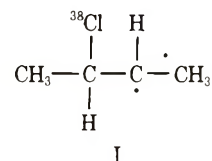
end energy cut-off to higher energy. Therefore, for the various systems listed in Table I, the energy cut-off by a scavenger increases as we go down the list from the nonscavenged to the butadiene- $O_2$ -scavenged systems. Accordingly, we observe that the percentage absolute yields decrease as more and more  $^{38}\text{Cl}$ -labeled radicals are removed by more efficient scavenging conditions.

From the results in Table I, it is obvious that the equilibrium branching ratio depends heavily on the average kinetic energy of the reacting  $^{38}\text{Cl}$  atom: the higher the energy, the closer the ratio between the yields of the two geometric isomers is to unity. This result is reasonable since *cis*-DCE is 450 cal/mol more stable than its *trans* isomer. When the total energy of the system is low, the equilibrated trichloroethyl radical favors the formation of the more stable form of the two isomers, the *cis*. In this case, the difference of 450 cal/mol in stability makes *trans*-DCE less likely to be formed. However, as the amount of excitation energy increases, the chance of obtaining the *trans* isomer from the equilibrated radical increases and should approach that of *cis* if the excitation energy becomes much higher than 450 cal/mol. In each case, we are dealing with an equilibrated excited radical which gives the same equilibrium branching ratio of *trans/cis*, regardless of the geometric form of the starting DCE. Nevertheless, the value of this equilibrium branching ratio should be a function of excitation energy and should approach unity as energy becomes larger.

This conclusion explains why the observed branching ratios for the thermal Cl reactions and the recoil  $^{38}\text{Cl}$  reactions are different as indicated in Table III.

*Percentage Absolute Yield and Branching Ratio from Recoil  $^{38}\text{Cl}$  Reactions with 2-Butenes.* The extremely low percentage yield of *cis*- and *trans*-1-chloropropene from the recoil  $^{38}\text{Cl}$  reactions with 2-butenes coupled with the 5:1 branching ratio in favor of the starting configuration indicates that the direct substitution process is the most predominant, if not the only, reaction mechanism taking place in these systems. The addition-elimination process involving double bonds is at most of minor importance. The essential absence of the addition-elimination reaction with 2-butenes in contrast with its predominance in the DCE systems can probably be traced back to the difference in bond

strengths of the various bonds in the intermediate excited radical. The addition reaction, eq 2, should occur with a similar probability in both systems. In the DCE case, there is a 50% chance to retain the  $^{38}\text{Cl}$  atom during the elimination step, eq 3, by assuming that the isotope effect on elimination is small. However, in the case of the radical I, the weakest bond of



the three happens to be the C- $^{38}\text{Cl}$  bond. Since the majority of the  $^{38}\text{Cl}$  atoms undergoing reactions 2 are not very energetic (and as a result, the radical which they formed by reacting with double bonds is not very excited), the difference in the bond dissociation energies, although small, is going to be the determining factor in the eventual fate of the radicals. As a result, the C- $^{38}\text{Cl}$  bonds are always the ones which are broken and the  $^{38}\text{Cl}$  atoms are left with even less energy for the recycling processes of eq 2 and 3. Because of this, the addition-elimination process just would not give 1-chloropropene as the final product except in the case of very energetic  $^{38}\text{Cl}$  atoms. These results also indicate that only a very small fraction of the total number of  $^{38}\text{Cl}$  atoms react as hot atoms to give the direct substitution reaction.

Results of the He-moderated samples are consistent with both our presently developed picture and the moderator effect on hot atom reactions.<sup>3,4</sup> The hot atoms are sensitive to the addition of a large excess of He although it is not a very efficient moderator for  $^{38}\text{Cl}$  atoms. As a result, the observed percentage absolute yields drop by a factor of 30 or more, becoming so low that their yields can no longer be measured.

*Acknowledgments.* This research was initiated with the help of Texas A & M Research Council and was supported by AEC Contract No. AT(40-1)-3898. We thank Mr. T. Mireur and J. Williams for their technical help. We also wish to thank Dr. D. H. O'Brien for the positive identification of the 1-chloropropene isomers by nmr spectroscopy.

# Electron Paramagnetic Resonance Spectra of $\text{NH}_2$ Radicals Formed

## by $\gamma$ Irradiation of Ammoniated Zeolites

by E. F. Vansant and J. H. Lunsford\*

Department of Chemistry, Texas A & M University, College Station, Texas 77843 (Received March 30, 1972)

Publication costs assisted by the National Science Foundation

Spectra of  $^{14}\text{NH}_2$ ,  $^{15}\text{NH}_2$ , and  $^{14}\text{ND}_2$  have been observed in  $\gamma$ -irradiated NaA, NaY, and HY zeolites which contained ammonia. The spectra of the respective radicals were essentially the same in each of the three zeolites. The anisotropic nitrogen hyperfine structure indicates that the unpaired electron is partially in a p orbital on the nitrogen. A nearly isotropic proton coupling constant of 26 G is in good agreement with the splitting observed for  $\text{NH}_2$  radicals in other matrices. The rotational hindrance and the stabilization of  $\text{NH}_2$  is attributed to hydrogen bonds with lattice oxygen ions.

### Introduction

Several epr studies have been devoted to the formation of  $\text{NH}_2$  radicals by  $\gamma$  irradiation of ammonia in different matrices.<sup>1-7</sup> In all cases the splitting due to the protons was about 24 G, but changes in the hyperfine splitting constant of the nitrogen with different media were noted. This variation in the hyperfine splitting was attributed by Symons<sup>8</sup> to changes in bond angle.

Recently,  $^{14}\text{NH}_2$  and  $^{15}\text{NH}_2$  radicals formed by  $\gamma$  irradiation of ammoniated silica gel were described by Brotikovskii, *et al.*<sup>9</sup> An interpretation of the epr spectra was based on the incomplete averaging of the anisotropy due to a partial retardation of the rotational motion. Earlier work by Sorokin, *et al.*,<sup>10</sup> on a  $\gamma$ -irradiated zeolite A which contained ammonia revealed a five-line spectrum which was difficult to interpret in terms of the  $\text{NH}_2$  radical. In order to verify the formation of  $\text{NH}_2$  radicals in  $\gamma$ -irradiated zeolites containing ammonia, spectra formed from  $^{14}\text{NH}_3$ ,  $^{15}\text{NH}_3$ , and  $^{14}\text{ND}_3$  in NaA, NaY, and HY zeolites were obtained.

### Experimental Section

The sodium form of the A and Y type zeolites was supplied by the Linde Co. (Lot No. 5943000061 and 13544-76). The HY zeolite was prepared from an  $\text{NH}_4\text{Y}$  zeolite.<sup>11</sup> Before irradiation the NaY, NaA, and HY zeolites were activated by heating the samples stepwise to 450° in a high vacuum system ( $10^{-5}$  Torr). After the dehydration procedure  $^{14}\text{NH}_3$ ,  $^{15}\text{ND}_3$ , or  $^{14}\text{ND}_3$  was adsorbed at room temperature. The  $^{14}\text{NH}_3$ ,  $^{15}\text{NH}_3$  (90% N-15), and  $^{15}\text{ND}_3$  (99% D) were obtained from the Matheson Co., Bio-Rad Laboratory, and Stohler Isotope Chemicals, respectively, and were used without purification.

The activated NaY, NaA, HY and the corresponding ammoniated samples were irradiated at  $-196^\circ$  in

sealed quartz tubes using  $^{60}\text{Co}$   $\gamma$  radiation. The total  $\gamma$  dose was  $2 \times 10^6$  rads with a dose rate of 500 rads/sec. The paramagnetic centers in the quartz were annealed after irradiation. All electron paramagnetic resonance measurements were made on a Varian (V4502) instrument in the X-band region (9.3 GHz) at  $-196^\circ$ .

### Results and Discussion

$\gamma$  irradiation of the dehydrated NaA, HY, and NaY zeolites created paramagnetic centers which are apparent in the epr spectra. The centers produced in NaY and HY zeolites are attributed to an unpaired electron interacting with four  $\text{Na}^+$  ions,<sup>12,13</sup> and a hole trapped on a lattice oxygen atom between Al ions,<sup>14</sup> respectively.

Figure 1 shows the spectra of irradiated (a)  $^{14}\text{NH}_3$ , (b)  $^{14}\text{ND}_3$ , and (c)  $^{15}\text{NH}_3$  adsorbed in the zeolites. The spectra were essentially the same for the NaA, NaY, and HY zeolites. The epr parameters at  $-196^\circ$  are

- (1) V. A. Bower, E. L. Cochran, S. N. Foner, and C. K. Jen, *Phys. Rev. Lett.*, **1**, 91 (1958).
- (2) S. W. Charles, P. H. Fischer, and C. A. McDowell, *J. Chem. Phys.*, **46**, 2162 (1967).
- (3) B. S. Al-Naimy, P. N. Moorthy, and J. J. Weiss, *J. Phys. Chem.*, **70**, 3654 (1966).
- (4) J. R. Morton and D. R. Smith, *Can. J. Chem.*, **44**, 1951 (1966).
- (5) S. Y. Pshchetskii and V. I. Tupikov, *Russ. J. Phys. Chem.*, **38**, 1364 (1964).
- (6) E. L. Cochran, F. J. Adrian, and V. A. Bowers, *J. Chem. Phys.*, **51**, 2759 (1969).
- (7) D. R. Smith and W. A. Seddon, *Can. J. Chem.*, **48**, 1938 (1970).
- (8) M. C. R. Symons, *Advan. Chem. Ser.*, **82**, 1 (1968).
- (9) O. I. Brotikovskii, G. M. Zhidomirov, V. B. Kazanskii, A. I. Mashchenko, and B. N. Shelimov, *Kinet. Katal.*, **12**, 700 (1971).
- (10) Y. A. Sorokin, A. G. Kotov, and S. Y. Pshchetskii, *Dokl. Akad. Nauk SSSR*, **159**, 1385 (1964).
- (11) J. E. Benson, K. Ushiba, and M. Boudart, *J. Catal.*, **9**, 91 (1967).
- (12) J. Turkevich, Y. Murakami, F. Nozaki, and S. Ciborowski, *Chem. Eng. Progr. Symp. Ser.*, **63**, 75 (1967).
- (13) P. H. Kasai, *J. Chem. Phys.*, **43**, 3322 (1965).
- (14) K. M. Wang and J. H. Lunsford, *J. Phys. Chem.*, **75**, 1165 (1971).

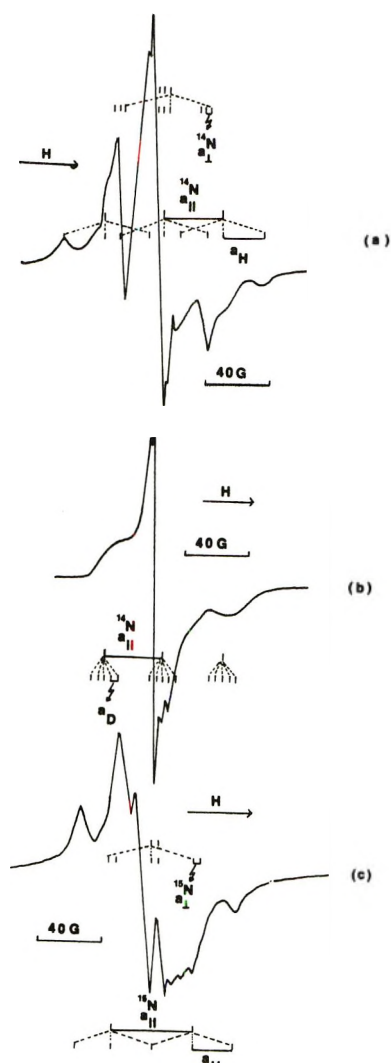


Figure 1: Epr spectra of  $\gamma$ -irradiated NaY, NaA, and HY zeolites which contained (a)  $^{14}\text{NH}_2$ , (b)  $^{14}\text{ND}_2$ , and (c)  $^{16}\text{NH}_2$ .

listed in Table I. The computer simulated spectrum of the  $^{14}\text{NH}_2$  radical in ref 9 was used to interpret the spectrum of Figure 1a. In the parallel direction the three  $^{14}\text{N}$  lines are further split into three lines by the hyperfine interaction with two equivalent hydrogen atoms. The latter splitting has an intensity ratio of 1:2:1. The nitrogen hyperfine splitting in the perpendicular direction is small. For the deuterated molecule (Figure 1b) each nitrogen hyperfine line is further split into five lines by the equivalent deuterium atoms. Although the deuterium hyperfine splitting is not resolved, an estimate of  $a_{\text{D}} \simeq 4$  G may be deduced from Figure 1b. Using this value the ratio of the hydrogen coupling constants,  $a_{\text{H}}/a_{\text{D}} = 6.5$ , is in agreement with the predicted ratio of the nuclear  $g$  factors,  $g_{\text{n}}^{\text{H}}/g_{\text{n}}^{\text{D}} = 6.5$ . Figure 1c similarly reveals the splitting pattern of  $^{15}\text{N}$  and the hydrogen atoms. Taken together, the three spectra confirm the existence of  $\text{NH}_2$  radicals in the zeolite crystals.

The hyperfine interaction resulting from the nuclear

Table I: Magnetic Parameters for  $^{14}\text{NH}_2$ ,  $^{14}\text{ND}_2$ , and  $^{16}\text{NH}_2$  Radicals Formed in the NaA, NaY, and HY Zeolites

Radical	$a_{\parallel}^{\text{N}},$ $\pm 1.5$ G	$a_{\perp}^{\text{N}},$ $\pm 1.5$ G	$a_{\text{H/D}},$ G	$g_{\parallel}$	$\Delta H,$ <sup>b</sup> $\pm 2$ G
$^{14}\text{NH}_2$	35	3	26	2.0022	122
$^{14}\text{ND}_2$	35	3	$\sim 4^{\text{a}}$	2.0022	88
$^{16}\text{NH}_2$	49	5	26	2.0027	98

<sup>a</sup> Estimated from the central singlet of Figure 1b. <sup>b</sup> The total width of the spectra measured between the extremes of the hyperfine lines.

spin of nitrogen may be expressed in terms of the Hamiltonian

$$H = (8\pi/3)\gamma_e\gamma_n\psi^2(\text{O})\mathbf{I}\cdot\mathbf{S} + \gamma_e\gamma_n[3(\mathbf{I}\cdot\mathbf{r})(\mathbf{r}\cdot\mathbf{S})/r^5 - (\mathbf{S}\cdot\mathbf{I}/r^5)] \quad (1)$$

Here,  $\gamma_e$  and  $\gamma_n$  are the magnetogyric ratio of the electron and nitrogen nucleus, respectively;  $\mathbf{S}$  and  $\mathbf{I}$  are the spin angular momentum operators of the electron and nucleus, respectively; and  $\mathbf{r}$  is the radius vector from the magnetic moment of the electron to that of the nucleus. The first term in eq 1 results in the isotropic coupling  $A_{\text{iso}} = (8\pi/3)\gamma_e\gamma_n\psi^2(\text{O})$ ; whereas, the second term results in the dipolar coupling tensor. The  $zz$  component of this tensor may be expressed as  $2\beta = (4/5)\gamma_e\gamma_n\langle r^{-3} \rangle$  for a  $2p$  hydrogenic wave function.

The hyperfine tensor of nitrogen-14 can be resolved into an isotropic part and an anisotropic part in the form

$$\begin{vmatrix} a_{\perp} & & \\ & a_{\perp} & \\ & & a_{\parallel} \end{vmatrix} = A_{\text{iso}} + \begin{vmatrix} -\beta & & \\ & -\beta & \\ & & 2\beta \end{vmatrix} \quad (2)$$

From the experimental values given in Table I two sign combinations are possible for nitrogen-14

$$\begin{vmatrix} +3 & & \\ & +3 & \\ & & +35 \end{vmatrix} = 14 + \begin{vmatrix} -11 & & \\ & -11 & \\ & & +21 \end{vmatrix} \quad (3)$$

and

$$\begin{vmatrix} -3 & & \\ & -3 & \\ & & +35 \end{vmatrix} = 10 + \begin{vmatrix} -13 & & \\ & -13 & \\ & & +25 \end{vmatrix} \quad (4)$$

The other two possible spin sign combinations are rejected since for nitrogen-14,  $\gamma_n$  is positive; hence,  $2\beta$  must be positive. The sign combination expressed in eq 4 yields a value of  $A_{\text{iso}}$  which is equivalent to that observed in rare gas matrices;<sup>1,2</sup> however, the larger value of  $A_{\text{iso}}$  from eq 3 is more consistent with values found in less inert media such as water<sup>3</sup> and  $\text{KNH}_2\text{SO}_3$  crystals.<sup>4</sup> For this reason the choice of  $A_{\text{iso}} = 14$  G is probably correct for  $\text{NH}_2$  in zeolites.



In order to calculate the spin densities in the 2s and 2p<sub>z</sub> orbitals, one may compare the values of  $A_{iso}$  and  $2\beta$  from eq 3 with the theoretical values obtained for the odd spin being completely in either a 2s or a 2p<sub>z</sub> orbital.<sup>15</sup> One finds that the unpaired electron on the nitrogen has about 2.5% 2s character and 62% 2p<sub>z</sub> character. The unpaired electron must be largely localized in a p<sub>z</sub> orbital, which is perpendicular to the plane of the molecule. The positive value of  $A_{iso}$  is consistent with this picture since one would expect positive spin density from polarization of the sp<sup>2</sup>-hybridized orbital.

The nearly isotropic proton coupling constant of 26 G is in good agreement with the splitting observed for NH<sub>2</sub> radicals in other matrices.<sup>1-7</sup> From McConnell's relationship,  $a_H = -25\rho_p$ , one would indeed predict an indirect coupling through each N-H bond of about this magnitude. Brotikovskii, *et al.*,<sup>9</sup> have used the absence of anisotropic hyperfine splitting for NH<sub>2</sub> radicals on silica gel as evidence for rotational motion about the C<sub>2</sub> axis; however, Morton and coworkers<sup>4</sup> observed that the rigid NH<sub>2</sub> molecule did not exhibit a

very large anisotropy (<6 G) in the proton splittings. It is doubtful whether this degree of anisotropy could have been detected in the present work.

Although the configuration of the radical in the zeolite is uncertain at the present time, we suggest the rotational hindrance and the stabilization of NH<sub>2</sub> is due to hydrogen bonds with lattice oxygen ions. The spectrum of NH<sub>2</sub> radicals on zeolites and in ice are remarkably similar.<sup>3</sup> Furthermore, the concentration of NH<sub>2</sub> radicals formed by  $\gamma$  irradiation is maximum when the zeolite is charged approximately with a monolayer of NH<sub>3</sub>.<sup>10</sup> This evidence indicates that the surface is important and that the radicals are not formed within an occluded ammonia matrix.

*Acknowledgment.* This work was supported by the National Science Foundation under Grant No. GP-29898 as part of a cooperative program with Professor J. Uytterhoeven at the University of Leuven, Belgium.

(15) B. A. Goodman and J. B. Raynor, *Advan. Inorg. Chem. Radiochem.*, **13**, 135 (1970).

## Matrix Infrared Spectra and Bonding in the Di- and Triiodomethyl Radicals

by David W. Smith and Lester Andrews\*

Chemistry Department, University of Virginia, Charlottesville, Virginia 22901 (Received March 31, 1972)

The codeposition of either CHI<sub>3</sub> or CI<sub>4</sub> at high dilution in argon with <sup>6</sup>Li or <sup>7</sup>Li produced new infrared absorptions which are attributed to LiI and the CHI<sub>2</sub> or CI<sub>3</sub> free radicals, respectively. The identity of the CHI<sub>2</sub> radical is confirmed by the reactions of CDI<sub>3</sub> with Li and CHI<sub>3</sub> with Na atoms. Assignments are made to the antisymmetric H-C-I valence angle bend and to the antisymmetric carbon-iodine stretch of CHI<sub>2</sub>. The pyrolysis of CI<sub>4</sub> also produced CI<sub>3</sub>; an assignment is made to the antisymmetric carbon-iodine stretch. The high values of  $F_r-F_{rr}$  in CHI<sub>2</sub> ( $2.54 \pm 0.03$  mdyne/Å) and CI<sub>3</sub> (2.13 mdyne/Å) indicate considerable  $\pi$  bonding in the CHI<sub>2</sub> and CI<sub>3</sub> free radicals.

### Introduction

The first spectral information on iodomethyl free radicals was reported in a very recent paper on CH<sub>2</sub>I.<sup>1</sup> Previously, the existence and stability of iodomethyl free-radical species has been questioned.<sup>2</sup> The present investigation reports on infrared spectral studies of alkali metal matrix reactions with CHI<sub>3</sub> and CI<sub>4</sub> to produce CHI<sub>2</sub> and CI<sub>3</sub>, respectively. CI<sub>3</sub> was also observed in experiments where CI<sub>4</sub> was subjected to pyrolysis. The calculated C-I bond stretching force constants suggest that the bonding scheme proposed<sup>1</sup> for CH<sub>2</sub>I is applicable to CHI<sub>2</sub> and CI<sub>3</sub>. Finally, this

paper concludes the series of infrared matrix studies on halogen-substituted methyl radicals.

### Experimental Section

The 15°K refrigeration system, vacuum vessel, alkali metal atom source, and experimental techniques have been described<sup>3</sup> previously. However, the vac-

(1) D. W. Smith and L. Andrews, *J. Chem. Phys.*, submitted for publication.

(2) J. Hine and S. J. Ehrenson, *J. Amer. Chem. Soc.*, **80**, 1824 (1958).

(3) L. Andrews, *J. Chem. Phys.*, **48**, 972 (1968).

uum vessel<sup>4</sup> used for the experiments described below was equipped with two heaters positioned for simultaneous deposition of two different beams of material. Carbon tetraiodide vapor was deposited into the matrix sample directly from a Knudsen cell having a 2-mm orifice and heated to 75°; iodoform vapor was deposited from a Knudsen cell at 35° with a 0.5-mm orifice. For the alkali metal reactions, alkali metal atoms and the iodocarbon vapor were simultaneously condensed into an argon matrix.

A special heater constructed for the pyrolysis experiments consisted of a 1-in. piece of 9-mm o.d. quartz tubing wrapped with approximately 12 in. of No. 22 chromel A wire held in place by a 1-in. section of 14-mm o.d. quartz tubing. Thermal insulation was ensured by positioning this assembly in a 32-mm long piece of 22-mm o.d. platinum-mirrored quartz tubing, which serves as a radiation shield. A 4-in. section of 1/8-in. o.d. 0.010-in. wall stainless steel tubing was friction fitted into a Knudsen cell containing the material to be pyrolyzed. The other end of the tubing was inserted through a 0.25-in. diameter, 1.25-in. long stainless steel plug through which a 5/32 in. hole had been drilled. The plug was then positioned in the pyrolysis heater. The pyrolysis zone and source Knudsen cell temperatures were monitored by chromel-alumel thermocouples.

Iodoform (Eastman Organic Chemicals), carbon tetraiodide (K & K Laboratories, Inc.), argon (Air Products, 99.995%), isotopic lithium (99.99% <sup>7</sup>Li and 95.6% <sup>6</sup>Li, ORNL), and sodium metal were used without further purification. Iodoform-*d* was synthesized by the haloform reaction carried out with NaOD in D<sub>2</sub>O. The Knudsen cells were filled with either iodoform or carbon tetraiodide under an argon atmosphere and positioned in the ceramic heater or fitted onto the pyrolysis tube.

After system evacuation to 10<sup>-6</sup> Torr, the sample window was cooled to 15°K and pure argon was deposited at a rate of 2 mmol per hour. The alkali metal and organic Knudsen cells were then heated to the desired temperature for sample deposition and reaction. Infrared spectra were recorded on a Beckman IR-12 filter-grating spectrophotometer. High-resolution spectra were recorded after completion of sample deposition at 8 or 3.2 cm<sup>-1</sup>/min using expanded frequency scales. Frequency accuracy is ±0.5 cm<sup>-1</sup> with spectral slit widths near 0.8 cm<sup>-1</sup> at 1100, 900, and 700 cm<sup>-1</sup>, 2.4 cm<sup>-1</sup> at 500 cm<sup>-1</sup>, and 4.0 cm<sup>-1</sup> at 300 cm<sup>-1</sup>.

## Results

*Iodoform with Alkali Metal Atoms.* The spectrum recorded when CHI<sub>3</sub> was evaporated into an argon matrix from a 35° Knudsen cell with a 0.5-mm orifice is shown in Figure 1. Absorptions attributable to the CHI<sub>3</sub> reactant and carbon dioxide are labeled P and CO<sub>2</sub>, respectively. Iodoform fundamentals were ob-

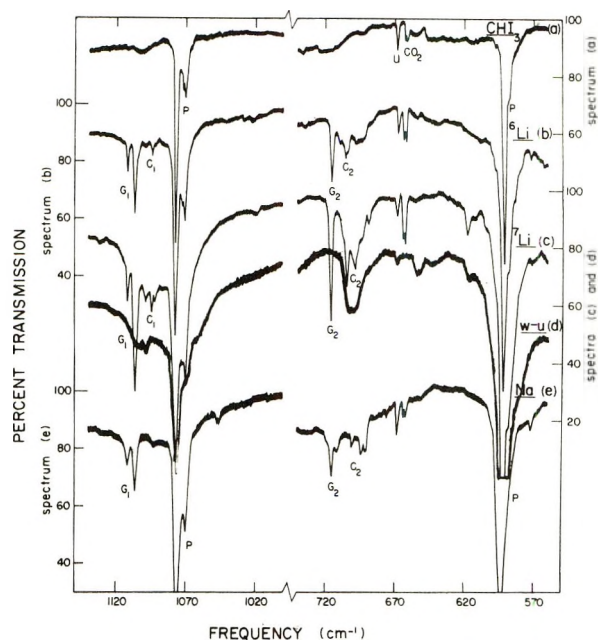


Figure 1. Infrared spectra in the 560-740- and 1000-1140-cm<sup>-1</sup> spectral regions for CHI<sub>3</sub> deposited in argon (a) without alkali metal, (b) with <sup>6</sup>Li, (c) with <sup>7</sup>Li, (d) with <sup>7</sup>Li in which matrix was warmed to 39°K and recooled to 15°K after deposition, and (e) with Na ([M]/[A] ≈ 200/1).

served at 592.0, 1077.2, and 3046 cm<sup>-1</sup>. The band labeled U at 669 cm<sup>-1</sup> has been observed often in this laboratory in many unrelated systems; hence, it is likely due to an aggregate species of no interest here. As comparison of trace a with b and c and e of Figure 1 illustrates, the cocondensation of CHI<sub>3</sub> with a beam of alkali metal atoms produced a number of new spectral features. Table I summarizes these experiments. Among the new features were bands at 481.5 cm<sup>-1</sup> in the <sup>6</sup>Li experiment and at 447.6 cm<sup>-1</sup> in the <sup>7</sup>Li experiment which are due to <sup>6</sup>LiI and <sup>7</sup>LiI, respectively.<sup>5</sup> NaI<sup>1</sup> was observed at 246.6 cm<sup>-1</sup> in the Na experiment. Other features which appeared at 470.8 and 503.5 cm<sup>-1</sup> in the <sup>6</sup>Li experiment and at 698.8 cm<sup>-1</sup> in the <sup>7</sup>Li experiment have already been assigned by Andrews to LiO<sub>2</sub> compounds.<sup>6</sup>

Those absorptions labeled C and G cannot yet be identified. The doublet G<sub>1</sub> and G<sub>2</sub> were observed unshifted in frequency in the three metal experiments at 1111.8 and 1106.3 ± 0.2 cm<sup>-1</sup>, and at 716.6 ± 0.2 cm<sup>-1</sup>, respectively. However, the frequency of the C bands is dependent upon the alkali metal reactant. C<sub>1</sub> shifted from 1095.1 cm<sup>-1</sup> with <sup>6</sup>Li to 1094.0 cm<sup>-1</sup> with <sup>7</sup>Li, but was not detected in the Na experiment. Likewise, C<sub>2</sub> shifted to lower frequency with the increasing atomic weight of the alkali metal, from 706.1

(4) L. Andrews, *J. Chem. Phys.*, **54**, 4935 (1971).

(5) L. Andrews and G. C. Pimentel, *ibid.*, **47**, 3637 (1967).

(6) L. Andrews, *ibid.*, **50**, 4288 (1969).

Table I: Absorption Frequencies ( $\text{cm}^{-1}$ ) of the Products of the Reaction of Alkali Metal Atoms with  $\text{CHI}_3$  in an Argon Matrix<sup>a</sup>

Assignment	$\text{CHI}_3$ no M	$\text{CHI}_3$ <sup>6</sup> Li	$\text{CHI}_3$ <sup>7</sup> Li	$\text{CHI}_3$ Na
NaI				246.6 (0.05)
I	251.2 (0.02)	251.6 (0.03)	251.0 (0.02)	250.0 (0.02)
NaI				252.6 (0.03)
$\text{LiO}_2\text{Li}$		470.8 (0.05)		
LiI		472.8 (0.04)		
LiI		481.5 (0.03)	447.6 (0.13)	
U		495.1 (0.08)		
$\text{LiO}_2$		506.5 (0.06)		
P	592.0 (0.70)	591.5 (0%T)	591.5 (0%T)	591.7 (0%T)
U			617.3 (0.04)	
$\text{CO}_2$	663 (0.02)	663 (0.04)	663 (0.08)	663 (0.02)
U	668.5 (0.04)	668.7 (0.03)	668.5 (0.07)	668.5 (0.05)
$\text{C}_2$		706.1 (0.09)	705.0 (0.12)	703.8 (0.02)
$\text{C}_2$				712.4 (0.02)
$\text{G}_2$		716.5 (0.09)	716.6 (0.22)	716.6 (0.05)
U				794.3 (0.08)
P	1077.2 (0.61)	1077.0 (0.90)	1077.0 (0%T)	1076.5 (0.80)
$\text{C}_1$		1095.1 (0.03)	1094.0 (0.05)	
$\text{C}_1$			1098.5 (0.03)	
$\text{G}_1$		1106.5 (0.16)	1106.5 (0.41)	1106.1 (0.10)
$\text{G}_1$		1111.5 (0.04)	1111.6 (0.08)	1112.0 (0.04)
P	3046.5 (0.04)	3047.0 (0.04)	3046.8 (0.04)	3046.4 (0.04)

<sup>a</sup> Optical densities are shown in parentheses.

$\text{cm}^{-1}$  with <sup>6</sup>Li to  $703.8 \text{ cm}^{-1}$  with Na. Several other bands, labeled U in Table I for unidentified absorbers, were usually seen in only one experiment.

*Pyrolysis of Iodoform.* Several attempts were made to pyrolyze iodoform at  $380\text{--}420^\circ$ . The rear Knudsen cell was maintained at temperatures ranging from  $25$  to  $60^\circ$ . However, the absorptions observed were those of iodoform itself, acetylene,<sup>7</sup> or carbon dioxide.

*Iodoform-d with Alkali Metal Atoms.* The spectrum recorded when  $\text{CDI}_3$  was evaporated from a Knudsen into the argon matrix is shown in trace a of Figure 2. Those bands labeled I are due to the isotopic impurity  $\text{CHI}_3$ . Iodoform-d fundamentals were observed at  $573.5$ ,  $793.6$ , and  $2265.5 \text{ cm}^{-1}$ . The labels P,  $\text{CO}_2$ , and U have been explained above. (The  $\text{LiO}_2$  compounds are labeled L in Figure 2.) Once again, as Figure 2 and Table II indicate, the codeposition of  $\text{CDI}_3$  with alkali metal atoms produced new spectral features. Among these were LiI monomer<sup>1,5</sup> absorptions in each lithium isotope experiment and NaI in the sodium<sup>1</sup> experiment. The  $426.0\text{-cm}^{-1}$  absorption band in the <sup>6</sup>Li experiment agrees with the assignment of Andrews and Pimentel to <sup>6</sup>LiI dimer<sup>5</sup> isolated in an argon matrix. Finally,  $\text{C}_2\text{D}_4$  was seen in the three metal experiments probably formed by an impurity reaction product.

In these three experiments two new bands showed no frequency dependence upon the alkali metal reactant,  $\text{G}'_1$  and  $\text{G}'_2$ . (The prime denotes a monodeutero species.) Like the  $\text{G}_1$  and  $\text{G}_2$  absorptions, the  $\text{G}'$  bands were not present when an equivalent amount of  $\text{CDI}_3$  was deposited without the alkali metal.  $\text{G}'_1$

was observed at  $850.3 \pm 0.3 \text{ cm}^{-1}$  and  $\text{G}'_2$  at  $653.5 \pm 0.2 \text{ cm}^{-1}$ . Although the  $\text{G}'_2$  band was very weak, careful measurements affirmed its reproducibility. Another weak band was seen at  $655.9 \text{ cm}^{-1}$  in the <sup>6</sup>Li experiment but not in the <sup>7</sup>Li or Na experiment; therefore, it is not an entity common to all experiments. On the contrary the bands labeled  $\text{C}'$  showed an alkali metal frequency dependence and marked intensity variation relative to  $\text{G}'$ .  $\text{C}'_1$  was observed at  $843.7 \text{ cm}^{-1}$  with <sup>6</sup>Li,  $844.4 \text{ cm}^{-1}$  with <sup>7</sup>Li, and  $843.3 \text{ cm}^{-1}$  with Na.  $\text{C}'_2$  was observed only in the Na experiment and at  $649.3 \text{ cm}^{-1}$ . Finally spurious bands were noted at  $495.1 \text{ cm}^{-1}$  in the Li experiment and at  $760.6 \text{ cm}^{-1}$  in the Na experiment; they have been labeled U for unidentified species.

*$\text{CI}_4$  with Alkali Metal Atoms.* Spectrum a in Figure 3 shows the recorded spectrum for the  $400\text{--}810 \text{ cm}^{-1}$  spectral region when  $\text{CI}_4$  was evaporated from a Knudsen cell at  $75^\circ$  into an argon matrix maintained at  $15^\circ\text{K}$ . The labels I,  $\text{CO}_2$ , and U were described above. The antisymmetric stretch of  $\text{CI}_4$  at  $579.4 \text{ cm}^{-1}$ , the only mode detected, is labeled P for precursor material.

As spectra a, b, and c indicate, codeposition of  $\text{CI}_4$  with alkali metal atoms ( $M/A \approx 200/1$ ) produced a number of new spectral features not present when an equivalent amount of  $\text{CI}_4$  was deposited into an argon matrix without the alkali reagent. In the experiments utilizing either <sup>6</sup>Li or <sup>7</sup>Li, LiI monomer<sup>1,5</sup> absorptions were seen. Other features appearing at  $470.7$ ,  $743.0$ ,

(7) D. E. Milligan and M. E. Jacox, *J. Chem. Phys.*, **47**, 5146 (1967).

**Table II:** Absorption Frequencies ( $\text{cm}^{-1}$ ) of the Products of the Reaction of Alkali Metal Atoms with  $\text{CDI}_3$  in an Argon Matrix<sup>a</sup>

Assignment	$\text{CDI}_3$ no M	$\text{CDI}_3$ $^6\text{Li}$	$\text{CDI}_3$ $^7\text{Li}$	$\text{CDI}_3$ Na
NaI				246.6 (0.03)
I	282.4 (0.02)		281.9 (0.03)	
$\text{NaO}_2$ (LiI) <sub>2</sub>		426.0 (0.04)		391.0 (0.06)
LiI		481.3 (0.12)	446.9 (0.10)	
U		495.1 (0.05)		
P	573.5 (0%T)	574.5 (1.30)	573.6 (0.73)	573.7 (0%T)
$\text{CHI}_3$	592.0 (0.49)	592.0 (0.22)	591.9 (0.15)	591.6 (0.28)
$\text{C}_2'$				649.3 (0.03)
$\text{G}_2'$		653.5 (0.02) 655.9 (0.03)	653.5 (0.02)	653.5 (0.02)
$\text{CO}_2$	663 (0.02)	663 (0.11)	663 (0.04)	663 (0.03)
U	668.5 (0.04)	668.4 (0.08)	668.7 (0.02)	668.5 (0.03)
$\text{LiO}_2$		743.7 (0.03)	699.0 (0.06)	
$\text{C}_2\text{D}_4$		716.2 (0.33)	716.6 (0.02)	
U				760.6 (0.04)
P	793.6 (0%T)	793.5 (1.50)	794.0 (1.20)	794.1 (0%T)
$\text{C}_1'$		843.4 (0.31)	844.4 (0.25)	843.7 (0.35)
$\text{G}_1'$		849.7 (0.44)	850.2 (0.34)	850.3 (0.29)
$\text{CHI}_3$	1076.3 (0.35)	1076.0 (0.17)	1077.5 (0.14)	
$\text{CHI}_2$		1105.6 (0.03)	1106.5 (0.03)	
P	2265.5 (0.11)	2265.8 (0.09)	2265.6 (0.08)	2266.0 (0.12)

<sup>a</sup> See footnote a, Table I.**Table III:** Absorption Frequencies ( $\text{cm}^{-1}$ ) of the Products of the Reaction of Alkali Metal Atoms with  $\text{CI}_4$  in an Argon Matrix and the Products of the Pyrolysis of  $\text{CI}_4$ <sup>a</sup>

Assignment	$\text{CI}_4$ no M	$\text{CI}_4$ $^6\text{Li}$ (1 $\mu$ )	$\text{CI}_4$ $^6\text{Li}$ (2 $\mu$ )	$\text{CI}_4$ $^7\text{Li}$ (1 $\mu$ )	$\text{CI}_4$ $^7\text{Li}$ (2 $\mu$ )	$\text{CI}_4$ Na	$\text{CI}_4$ Py
(LiI) <sub>2</sub>					419.5 (0.03)		
M			436.9 (0.04)		436.7 (0.02)	436.9 (0.31)	
LiI		481.0 (0.08)	481.0 (0.06)	446.5 (0.18)	446.5 (0.34)		
$\text{LiO}_2\text{Li}$		470.7 (0.15)	470.5 (0.03)				
$\text{LiO}_2$			507.3	492.5 (0.17)	492.5 (0.14)		
P	579.3 (0%T)	580.0 (0%T)	579.4 (0.58)	579.5 (0%T)	579.6 (0.48)	579.5 (0%T)	579.0 (1.35)
I	601.3 (0.12)	601.2 (0.07)	599.8 (0.03)	600.6 (0.08)	601.0 (0.03)	600.6 (0.12)	600.8 (0.15)
$\text{CO}_2$	663 (0.05)	663 (0.25)	663 (0.06)	663 (0.03)	663 (0.02)	663 (0.04)	663 (0.15)
U	668.5 (0.02)		668.7 (0.06)			668.7 (0.02)	668.5 (0.05)
H		693.0 (0.26)	692.6 (0.22)	693.2 (0.46)	693.0 (0.34)	693.0 (0.28)	692.7 (0.70)
H			698.0 (0.04)	698.6 (0.08)	698.0 (0.04)		698.0 (0.07)
I	712.0 (0.06)				714.8 (0.04)	713.0 (0.02)	713.8 (0.05)
$\text{LiO}_2$		743.0 (0.25)	744.0 (0.06)				
$\text{LiO}_2\text{Li}$		840.0 (0.11)	839.5 (0.05)	795.2 (0.09)	796.4 (0.15)		

<sup>a</sup> See footnote a, Table I.

and  $839.5 \text{ cm}^{-1}$  with  $^6\text{Li}$  and at  $492.5$  and  $795.2 \text{ cm}^{-1}$  with  $^7\text{Li}$  have been assigned by Andrews<sup>6</sup> to  $\text{LiO}_2$  species; these have been labeled L in Figure 3.

Only one feature appeared common to the  $^6\text{Li}$ ,  $^7\text{Li}$ , and Na experiments, the band labeled H at  $693.0 \pm 0.2 \text{ cm}^{-1}$ . However, unlike the iodoform system, no absorption bands were detected which displayed a frequency dependence upon the alkali metal. Finally, an intense band was observed in the Na experiment but not in the  $1\text{-}\mu$  vapor pressure Li experiments at  $437 \text{ cm}^{-1}$ ; it is labeled M in Figure 3 and Table III.

*Concentration Variation.* In order to promote secondary reactions in hopes of producing detectable quantities of diiodocarbene,  $\text{CI}_4$  was deposited at a reduced temperature ( $60^\circ$ ) with  $2\text{-}\mu$  vapor pressure beams of  $^6\text{Li}$  and  $^7\text{Li}$  ( $M/A \approx 100/1$ ).  $^6\text{LiI}$  was observed<sup>1,5</sup> at  $481.0$  and  $470.5 \text{ cm}^{-1}$ , and  $^7\text{LiI}$  at  $446.5 \text{ cm}^{-1}$ . A band previously assigned to  $^7\text{LiI}$  dimer<sup>1</sup> was detected at  $419.5 \text{ cm}^{-1}$ . Bands due to the  $\text{LiO}_2$  species were also seen.<sup>6</sup> As expected the H band was unshifted in frequency and reduced in intensity. However, in each isotope experiment only one new band appeared which

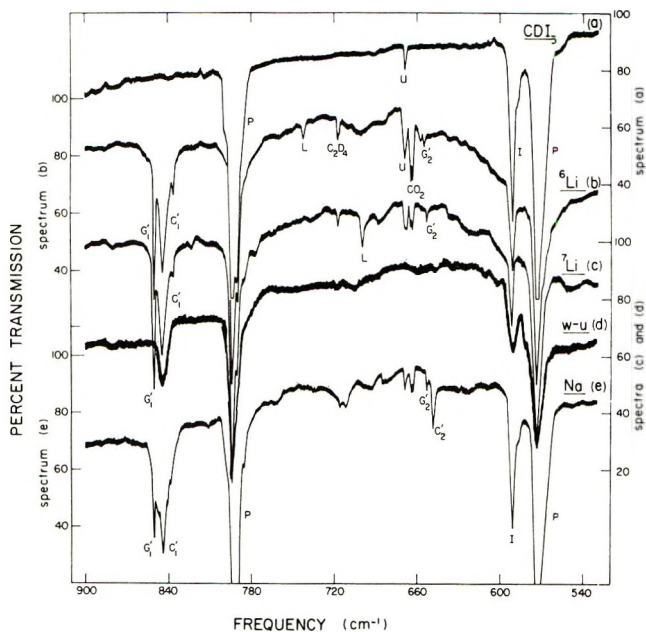


Figure 2. Infrared spectra in 530–910-cm<sup>-1</sup> spectral regions for CDI<sub>3</sub> deposited in argon (a) without alkali metal, (b) with <sup>6</sup>Li, (c) with <sup>7</sup>Li, (d) with <sup>7</sup>Li in which matrix was warmed to 39°K and recooled to 15°K after deposition, and (e) with Na ([M]/[A] ≈ 200/1).

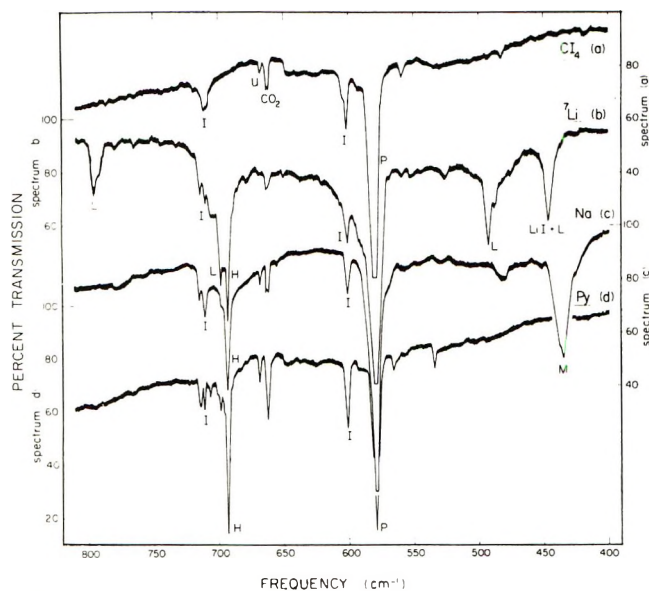


Figure 3. Infrared spectra in the 390–810-cm<sup>-1</sup> spectral regions for ClI deposited in argon (a) without alkali metal, (b) with <sup>7</sup>Li, (c) with Na ([M]/[A] ≈ 200/1), and (d) pyrolyzed at 350°.

could not be identified, 525.3 cm<sup>-1</sup> with <sup>6</sup>Li and 525.5 cm<sup>-1</sup> with <sup>7</sup>Li. Finally, these high lithium temperature experiments produced an absorption at 436.8 ± 0.2 cm<sup>-1</sup> coincident with the M absorption in the Na experiment.

**Pyrolysis of ClI<sub>4</sub>.** Spectrum d of Figure 3 shows the spectrum recorded when ClI<sub>4</sub> was subjected to pyrolysis. For this experiment, the Knudsen cell reservoir temperature was maintained near 65° and the pyrolysis

tube around 350°. At temperatures of 400° and above no infrared absorptions were detectable including the ClI<sub>4</sub> precursor. On the other hand, below 300° no decomposition was evident. Therefore, the most efficient temperature for the pyrolysis of ClI<sub>4</sub> with infrared detection of products seemed to be around 350°. The spectrum obtained was remarkably simple; only three bands were observed that were not seen in the blank experiment, spectrum a of Figure 3. The H band appeared at 692.7 cm<sup>-1</sup> with a high-frequency shoulder at 698.0 cm<sup>-1</sup> which might well be a site splitting. Such site splittings were observed for CCl<sub>3</sub><sup>3</sup> and CBr<sub>3</sub>.<sup>8</sup> In the spectra of these two radicals, there was a weak high-frequency shoulder which disappeared upon annealing the matrix, a behavior indicative of matrix site effects. This band structure was not detected in the metal experiments since the intensity of the H band was only half of that in this experiment. Finally, a weak band was noted at 535.2 cm<sup>-1</sup>.

**Diffusion Experiments.** In several experiments, the matrix sample was warmed to near 39°K and recooled; this operation permits diffusion and reaction of small molecules. Two of these experiments are displayed in trace d of Figures 1 and 2; each is a <sup>7</sup>Li experiment. It must be noted that the diffusion operation often increases light scattering and results in poorer spectral conditions. However, good semiquantitative measurements can be obtained. In these particular experiments, the LiI monomer absorptions decreased accompanied with an increase in LiI dimer absorptions. Most marked was the total decrease in the intensity of the G and G' features. In contrast, the parent absorptions and the C and C' absorptions broadened somewhat but retained their integrated intensity.

## Discussion

The purpose of this paper is to determine the matrix reactions responsible for the recorded spectra and to identify the reaction products. Once these have been resolved, vibrational assignments can be made for the new molecules of interest produced here, and normal coordinate calculations can be performed to support the vibrational assignments and to elucidate structure and bonding.

**The G Absorption Bands.** It is immediately noticed that the G<sub>1</sub> and G<sub>2</sub> absorptions were observed only where CHI<sub>3</sub> was codeposited with alkali metal atoms. Therefore, along with the alkali iodide, this species must be a reaction product. Furthermore, the diffusion experiments indicate that the G species itself is a highly reactive and mobile species.

In addition, these diffusion experiments support the assignment of the G<sub>1</sub> and G<sub>2</sub> bands to the same molecular species, a conclusion further substantiated by the fact that the G<sub>1</sub> and G<sub>2</sub> bands displayed constant rela-

(8) L. Andrews and T. G. Carver, *J. Chem. Phys.*, **49**, 896 (1968).

tive intensities throughout the series of experiments. Thus, the two absorptions are assigned to the same molecular species.

In all the experiments in which they were observed, the  $G_1$  and  $G_2$  features showed no frequency or band shape dependence upon the alkali metal reactant. If the species responsible for these absorptions contained a reactant alkali atom(s), a frequency shift would be expected when the alkali metal was varied from  $^6\text{Li}$  to  $^7\text{Li}$  and to  $\text{Na}$ . Since no frequency shifts were found, the absorbing species likely does not contain an alkali metal atom and probably is isolated from the alkali halide as well.

It has been previously noted that the spectral feature denoted  $G_1$  is a pair of sharp bands whose relative intensity remains fairly constant. This behavior is typical of matrix site effects; this pair of bands is likely due to a single vibrational mode of a single entity trapped in two nonequivalent sites in the argon matrix. Such site effects have been found for the  $\text{CHBr}_2$  and  $\text{CHCl}_2$  radicals.<sup>9,10</sup>

The most probable reaction products are the alkali halide and the diiodomethyl free radical. The observation of the alkali halide strongly suggests that the diiodomethyl radical could be produced and isolated in the argon matrix. Consequently, the  $G_1$  and  $G_2$  absorptions are assigned to the  $\text{CHI}_2$  radical and the  $G_1'$  and  $G_2'$  absorptions to the  $\text{CDI}_2$  radical. This conclusion is further supported by the identification of the  $\text{CHBr}_2$  and  $\text{CHCl}_2$  free radicals<sup>9,10</sup> in the matrix reactions of alkali metal atoms with  $\text{CHCl}_3$  and  $\text{CHBr}_3$ , respectively, and the similarities in the spectra of these  $\text{CHX}_2$  radicals.

*The C Absorption Bands.* Besides the  $\text{CHCl}_2$  and  $\text{CHBr}_2$  radicals, alkali metal reactions with chloroform and bromoform also identified absorption bands due to a perturbed radical. The origin of the perturbation was the alkali halide trapped in the same or in an adjacent matrix site; it was suggested that the nature of the perturbation was a dipole-dipole interaction.

The C bands show a frequency dependence upon the alkali metal; hence, they cannot be due to the isolated free radical. On the other hand, the proximity of these bands to those of the radical suggests they are due to a perturbed radical. The perturbing species must be the alkali metal iodide since an alkali metal atom would be expected to bind to the free radical and produce a  $\text{CHI}_2\text{-M}^+$  species<sup>11</sup> with an entirely different spectrum. Consequently, the C bands are assigned to the  $\text{CHI}_2\text{-MI}$  "complex" and the C' bands to the  $\text{CDI}_2\text{-MI}$  "complex." These assignments are supported by the warm-up behavior of these bands; the C and C' absorbers are heavier, more stable, aggregate species which remain upon sample warming.

*The H Absorption Band.* The H absorber is obviously a reaction product since it was not observed when  $\text{Cl}_4$  was evaporated from the Knudsen cell by itself.

It was observed when  $\text{Cl}_4$  was codeposited with a beam of alkali metal atoms or pyrolyzed. The lack of frequency shift for the H absorption in the isotopic lithium and sodium experiments suggests that this species does not contain an alkali metal reactant atom; the observation of the H band at the identical frequency in the pyrolysis experiments proves this point. The H absorption is likely due to a primary reaction product which would contain one carbon atom. Its intensity is directly proportional to the intensity of the  $\text{LiI}$  produced. The most probable reaction product in addition to the alkali iodide would be the  $\text{Cl}_3$  free radical. The previous studies of the matrix reactions of alkali metal atoms with  $\text{CCl}_4$  and  $\text{CBr}_4$  have identified the  $\text{CCl}_3^{\cdot}$  and  $\text{CBr}_3^{\cdot}$  radicals as the primary reaction product. On this evidence, the H absorber is identified as the  $\text{Cl}_3$  free radical.

*The M Absorber.* The relative intensities of the H and M absorptions indicate that these absorptions are due to two different molecular species. The M absorption showed no lithium isotope or sodium frequency shift, but an increase in lithium concentration increased the M band intensity relative to the H band. Moreover, the M band was not observed in the pyrolysis experiment. All this suggests that the M absorber is a collision product between  $\text{Cl}_3$  and either Li or Na. It is suggested here that the M absorber is the  $\text{Li}^+\text{Cl}_3^-$  species in the Li experiments and  $\text{Na}^+\text{Cl}_3^-$  in the Na experiment, where this mode is the antisymmetric C-I stretch in the  $\text{Cl}_3^-$  part of the " $\text{M}^+\text{Cl}_3^-$ " molecule.

The previous studies by Andrews and Carver<sup>11</sup> of the matrix reactions of alkali metal atoms with  $\text{CCl}_4$  and  $\text{CBr}_4$  identified the  $\text{M}^+\text{CCl}_3^-$  and  $\text{M}^+\text{CBr}_3^-$  molecules. The observation of a doubly degenerate vibration for those molecules indicated the presence of threefold symmetry. Therefore, the above authors presumed  $C_{3v}$  symmetry for these ionic species.

The greater intensity of the M band in the Na experiment indicates a greater stability for  $\text{Na}^+\text{Cl}_3^-$  than  $\text{Li}^+\text{Cl}_3^-$ . It appears that  $\text{LiCX}_3$  decomposes more easily to produce  $\text{LiX}$  and the corresponding dihalocarbene than does  $\text{NaCX}_3$ . In this series of experiments,  $\text{Cl}_2$  could not be detected presumably due to a lack of observable intensity.  $\text{CCl}_2$ <sup>12</sup> and  $\text{CBr}_2$ <sup>8</sup> could only be observed when the  $\text{CX}_3$  radical was totally absorbing. Even in an experiment in which Li was codeposited with a pyrolyzed beam of  $\text{Cl}_4$ , absorptions of  $\text{Cl}_2$  could not be identified. However,  $\text{Cl}_2$  is expected to be a stable species when isolated in an argon matrix at 15°K.

There exists the possibility that the weak 535-cm<sup>-1</sup> feature in the  $\text{Cl}_4$  pyrolysis experiment or the weak 525-cm<sup>-1</sup> features in the lithium- $\text{Cl}_4$  reactions could

(9) T. G. Carver and L. Andrews, *J. Chem. Phys.*, **50**, 4223 (1969).

(10) T. G. Carver and L. Andrews, *ibid.*, **50**, 4235 (1969).

(11) L. Andrews and T. G. Carver, *J. Phys. Chem.*, **72**, 1743 (1968).

(12) L. Andrews, *J. Chem. Phys.*, **48**, 979 (1968).

be the antisymmetric C-I stretching mode of diiodocarbene,  $\text{CI}_2$ . This feature appears below the analogous mode<sup>1</sup> for  $\text{CH}_2\text{I}_2$  at  $582\text{ cm}^{-1}$ ; a similar relationship was noted for  $\text{CCl}_2$ ,  $\text{CH}_2\text{Cl}_2$  and  $\text{CBr}_2$ ,  $\text{CH}_2\text{Br}_2$ .<sup>8</sup> However, this must remain a conjectural possibility until supported by additional observations.

**Vibrational Assignments.** Vibrational assignments are handicapped by a complete lack of structural data for  $\text{CHI}_2$  and  $\text{CI}_3$ . However, the methyl<sup>13</sup> radical itself is reported to be planar and trifluoromethyl<sup>14</sup> pyramidal. The spectra of the monochloro-,<sup>15</sup> monobromo-,<sup>16</sup> and monoiodomethyl<sup>1</sup> radicals suggested a planar structure for these species. The early work of Andrews and Carver identified and assigned both the antisymmetric and totally symmetric carbon-halogen stretching modes of the  $\text{CCl}_3$ <sup>3</sup> and  $\text{CBr}_3$ <sup>8</sup> radicals; thus, these workers necessarily arrived at a pyramidal structure. However, Rogers<sup>17</sup> *et al.*, later questioned the symmetric mode assignment of these previous workers. A recent reinvestigation of the  $\text{CCl}_4$  and  $\text{CBr}_4$  alkali metal systems by Hatzenbuehler and Andrews<sup>18</sup> re-assigned the absorption thought to be due to the symmetric stretch of  $\text{CCl}_3$  to a perturbed carbene, in a "salt-carbene" type of structure. Therefore, the structure of  $\text{CX}_3$  radicals is still unresolved.

Nonbonding-bonding electronic repulsions in all the halomethyl free radicals could certainly cause a deviation from planarity. However, a planar radical would have the ability to form a  $\pi$  molecular orbital system of some stability, perhaps as much as  $12\text{ kcal}^3$  for  $\text{CCl}_3$ . Energies of this magnitude would certainly more than compensate for any electrostatic repulsive forces. Consequently, the planar structure for  $\text{CHI}_2$  and  $\text{CI}_3$  will be assumed here.

**$\text{CHI}_2$ .** The planar  $C_{2v}$  radical has six normal modes of vibration; three belong to the  $A_1$  representation, two to the  $B_1$ , and one to the  $B_2$ .  $\nu_3$ , the symmetric I-C-I valence angle deformation, and  $\nu_6$ , the out-of-plane deformation, are expected to lie beyond the low-frequency range of the spectrometer. The large deuterium isotope shift of  $G_1$  indicates that this is primarily a hydrogen vibration; the frequency is appropriate for a hydrogen bending vibration. Therefore, the  $G_1$  absorption is assigned to  $\nu_4$ , the antisymmetric H-C-I valence angle bending mode, of  $\text{CHI}_2$ . Similarly,  $G_1'$  is assigned to  $\nu_4$  of  $\text{CDI}_2$ .

The  $G_2$  and  $G_2'$  must be carbon-iodine stretching vibrations, even though they are over  $120\text{ cm}^{-1}$  higher than the antisymmetric C-I stretching mode<sup>1</sup> of  $\text{H}_2\text{CI}_2$ . However, the antisymmetric carbon-halogen stretching modes of  $\text{CHCl}_2$ <sup>10</sup> and  $\text{CHBr}_2$ <sup>9</sup> were more than  $100\text{ cm}^{-1}$  higher than those of  $\text{CH}_2\text{Cl}_2$ <sup>15</sup> and  $\text{CH}_2\text{Br}_2$ .<sup>16</sup> Thus, the  $G_2$  absorption is assigned to  $\nu_5$ , the antisymmetric C-I stretch of  $\text{CHI}_2$ , and the  $G_2'$  absorption to  $\nu_5$  of  $\text{CDI}_2$ .

**$\text{CI}_3$ .** The planar  $D_{3h}$  tetraatomic molecule possesses four distinct vibrational modes. The symmetric

( $A_1'$ ) carbon-iodine stretching vibration is not infrared active for the planar molecule, and the two bending vibrations,  $\nu_2(A_2'')$  and  $\nu_4(E')$ , lie below the low-frequency region of the spectrophotometer. Consequently, the H absorption band is assigned to  $\nu_3(E')$ , the antisymmetric carbon-iodine stretch. This assignment is supported by the identification of  $\nu_3$  of  $\text{CCl}_3$ <sup>3</sup> and  $\text{CBr}_3$ <sup>8</sup> relative to their carbon tetrahalide precursors.

**$\text{Li}^+\text{CI}_3^-$ .** The M absorption band at  $436\text{ cm}^{-1}$  is assigned to the doubly degenerate antisymmetric carbon-iodine stretching vibration of the  $C_{3v}$  species; this is based upon the assignments to this mode in  $\text{M}^+\text{CBr}_3^-$  and  $\text{M}^+\text{CCl}_3^-$  at  $462$  and  $521\text{ cm}^{-1}$ , respectively.<sup>11</sup>

**Normal Coordinate Analysis.**  **$\text{CHI}_2$ .** The  $B_1$  symmetry block can be solved exactly since both  $\nu_4$  and  $\nu_5$  of  $\text{CHI}_2$  and  $\text{CDI}_2$  were identified. The calculations were performed using the Wilson FG<sup>19</sup> matrix method and the program FADJ developed by Schachtschneider; results are presented in Table IV. The  $C_{2v}$  symmetry coordinates<sup>15</sup> for  $\text{CXY}_2$  molecules were used as described for  $\text{CH}_2\text{Cl}$ . The  $B_1$  symmetry coordinates are identical with those for the  $A''$  symmetry block in  $C_s$  symmetry. The symmetrized  $G$  matrix elements were calculated using a C-H bond length of  $1.08\text{ \AA}$ , a C-I bond length of  $2.10\text{ \AA}$ , and all angles were set to  $120^\circ$ . A knowledge of  $F_{22}$  is needed to calculate the C-I stretching force constant,  $F_r$ , of  $\text{CHI}_2$ . However, the symmetric carbon-iodine stretching vibration has not been observed in this work, therefore,  $F_r$  cannot be determined accurately. Transferral<sup>20</sup> of  $F_{rr}$ , the stretch-stretch interaction force constant, from  $\text{C}_2\text{I}_4$ , however, should yield a satisfactory value of  $F_r$  for  $\text{CHI}_2$ .

**$\text{CI}_3$ .** An accurate calculation of  $F_{33}$  is impossible since the other vibration of  $E'$  symmetry was not identified, but the separation of high and low frequencies in a symmetry block is expected to be a good approximation for the  $E'$  block.  $\nu_3$  was observed at  $693.0\text{ cm}^{-1}$ , and  $\nu_4$  is expected below  $150\text{ cm}^{-1}$  based upon iodoform. Furthermore, no  $^{13}\text{C}$  data are available to serve as a check on the force constant calculation. A value of  $2.13\text{ m dyn/\AA}$  was calculated for  $F_{33}$  of  $\text{CI}_3$ , which represents  $F_r - F_{rr}$ .

## Conclusions

The potential constants of the di- and triiodomethyl

(13) M. Karplus and G. K. Fraenkel, *J. Chem. Phys.*, **35**, 1312 (1961); D. E. Milligan and M. E. Jacox, *ibid.*, **47**, 5146 (1967).

(14) R. W. Fessenden and R. H. Schuler, *ibid.*, **42**, 2704 (1965).

(15) L. Andrews and D. W. Smith, *ibid.*, **53**, 2956 (1970).

(16) D. W. Smith and L. Andrews, *ibid.*, **55**, 5295 (1971).

(17) E. E. Rogers, S. Abramowitz, M. E. Jacox, and D. E. Milligan, *ibid.*, **52**, 2198 (1970).

(18) D. A. Hartzenbuehler and L. Andrews, unpublished results, 1970.

(19) E. B. Wilson, J. C. Decius, and P. C. Cross, "Molecular Vibrations," McGraw-Hill, New York, N. Y., 1955.

(20) R. Forneris and D. Bassi, *J. Mol. Spectrosc.*, **26**, 220 (1968).

**Table IV:** Normal Coordinate Analysis of Diiodomethyl for  $C_{2v}$  Symmetry for the  $B_1$  Symmetry Block (Planar Geometry Assumed)

Isotope	$\nu$	Frequencies, $\text{cm}^{-1}$			Potential energy <sup>a</sup>		
		Obsd	Calcd	$\Delta$ , $\text{cm}^{-1}$	$F_{44}$	$F_{46}$	$F_{55}$
CHI <sub>2</sub>	4	1106.4	1104.5	1.9	4	-11	107
	5	716.4	713.4	3.0	102	-2	0
CDI <sub>2</sub>	4	850.3	852.8	-2.5	39	-29	90
	5	653.4	656.6	-3.2	68	16	16
$F_{ij}$ <sup>b</sup>					2.537	0.243	0.395
Standard error <sup>c</sup>					0.031	0.014	0.005

<sup>a</sup> Potential energy contribution of each force constant to the normal modes. <sup>b</sup> Units:  $F_{44}$  millidynes per ångström;  $F_{46}$  millidynes per radian;  $F_{55}$  millidyne ångström per radian squared. <sup>c</sup> Provided by program FADJ.

radicals are of interest and deserve close examination since they reflect upon the bonding in these molecular species.

**H-C-I Bending Constant.** The H-C-I valence angle bending force constant for CHI<sub>2</sub> (0.40 mdyne Å/rad<sup>2</sup>) is smaller than the analogous constant for CHI<sub>3</sub> (0.413 mdyne Å/rad<sup>2</sup>), perhaps due to less steric crowding around the carbon atom. This constant is also less than those calculated for CHBr<sub>2</sub> (0.44 mdyne Å/rad) and CHCl<sub>2</sub> (0.48 mdyne Å/rad). As in the haloform molecules and monohalomethyl free radicals, the valence angle bending constant decreases with increasing atomic weight of the halogen. The off-diagonal constant between the H-C-I bend and the antisymmetric C-I stretch (0.24 mdyne/rad) is again slightly smaller than that for the other dihalomethyl radicals, CHBr<sub>2</sub> (0.31 mdyne/rad) and CHCl<sub>2</sub> (0.35 mdyne/rad). Again the trend of decreasing magnitude with increasing halogen atomic weight is observed. This interaction force constant is manifested in the large deuterium shift (63  $\text{cm}^{-1}$ ) for the observed carbon-iodine stretching mode; this is largely due to the interaction of  $\nu_4$  and  $\nu_5$  of CDI<sub>2</sub> rather than solely to a mass effect.

**C-I Bond Stretching Force Constants.** The values reported here for  $F_r - F_{rr}$  for CHI<sub>2</sub> and CI<sub>3</sub> merit close attention; they are larger than those values determined for CH<sub>2</sub>I<sub>2</sub>, CHI<sub>3</sub>, and CI<sub>4</sub>. This is depicted in Table V. Using an estimate of  $0.4 \pm 0.2$  mdyne/Å for  $F_{rr}$ , the calculated value of  $F_r$  for CHI<sub>2</sub> is very near that for CH<sub>2</sub>I and is larger than that for the four iodomethanes. The unusual magnitude of the carbon-iodide force constant in these radicals cannot be rationalized by a change of hybridization alone; the major rationale for the large stretching constant is due to the  $\pi$  bonding in these studies as is discussed below.

The antisymmetric carbon-iodine stretching force constant in  $M^+CI_3^-$  is lower than the corresponding constant in CI<sub>4</sub> or CHI<sub>3</sub> as was observed<sup>11</sup> for  $M^+CCl_3^-$  and  $M^+CBr_3^-$  and their tetrahedral counterparts. Andrews and Carver<sup>11</sup> have pointed out that the antisymmetric stretching force constants for such anions

**Table V:** Carbon-Iodine Valence Force Constants<sup>a</sup> for Iodocarbon Molecules and Radicals

Molecule	$F_r$	$F_r - F_{rr}$	Ref
CH <sub>2</sub> I	$2.81 \pm 0.04$		b
CHI <sub>2</sub>	$(2.94 \pm 0.20)$	2.537	c
C <sub>2</sub> I <sub>4</sub>	2.59		d
CH <sub>3</sub> I	2.54		b
CI <sub>3</sub>	$(2.528 \pm 0.20)$	2.128	c
CH <sub>2</sub> I <sub>2</sub>	2.49	2.070	b
CHI <sub>3</sub>	$(2.132 \pm 0.20)$	1.732	e
CI <sub>4</sub>	1.95	1.633	f
$M^+CI_3^-$	$(1.463 \pm 0.20)$	1.063	c

<sup>a</sup> In millidynes per ångström. <sup>b</sup> Reference 1. <sup>c</sup> This work. <sup>d</sup> R. Forneris and D. Bassi, *J. Mol. Spectrosc.*, **26**, 220 (1968). <sup>e</sup> Calculated in this work using matrix frequencies for  $\nu_4$  and  $\nu_5$  of CHI<sub>3</sub> and CDI<sub>3</sub> and an estimate of  $120 \text{ cm}^{-1}$  for  $\nu_6$ . <sup>f</sup> K. Sathianandan, K. Ramaswamy, and F. Cleveland, *J. Mol. Spectrosc.*, **8**, 470 (1962).

as  $GeCl_3^-$  are much smaller than those for the neutral  $GeCl_4$  species, and rationalized this effect as due to the extra electronic repulsions due to the anion electron. Consequently, the LiCl<sub>3</sub> and NaCl<sub>3</sub> molecules are expected to be ionic species which may be represented as  $M^+Cl_3^-$ .

**Bonding in the Di- and Triiodomethyl Radicals.** As has been pointed out earlier,<sup>1,9,15,16</sup> a parallel exists between unusually large carbon-halogen stretching force constants in halomethyl radicals and  $\pi$  electronic stabilization in the carbon-halogen bonds. Unfortunately, bond dissociation energies producing iodomethyl radicals and their ionization potentials are not presently known. The somewhat higher values of  $F_r - F_{rr}$  reported here for the iodomethyl radicals indicate  $\pi$  stabilization in the C-I bonds. A quantitative determination of  $\pi$  bond formation, orbital energies, and bond orders is impossible here; however, a reasonable qualitative understanding of the bonding found in these radicals can be arrived at by examining the chloromethyl free radicals.



CNDO calculations on  $\text{CHCl}_2$  and  $\text{CCl}_3$  were performed using the Pople and Beveridge CNINDO program.<sup>21</sup> For  $\text{CHCl}_2$  the bonding  $\pi$  orbitals were

$$\Psi b_\alpha = 0.58C_{2p_z} + 0.56Cl_{3p_z} - 0.05Cl_{4d_{zz}} - 0.10Cl_{4d_{yz}} \\ + 0.56Cl_{3p_x} - 0.05Cl_{4d_{zx}} + 0.10Cl_{4d_{yz}}$$

$$\Psi b_\beta = 0.58C_{2p_z} + 0.46Cl_{3p_z} - 0.20Cl_{4d_{zz}} - 0.29Cl_{4d_{yz}} \\ + 0.46Cl_{3p_x} - 0.20Cl_{4d_{zx}} + 0.29Cl_{4d_{yz}}$$

(Second, third, and fourth terms refer to one chlorine atom; fifth, sixth, and seventh terms refer to second chlorine atom.)

There are also two nonbonding and two antibonding orbitals involving the same atomic orbitals. Two electrons occupy the bonding orbitals, two the nonbonding, and one the antibonding. A total  $\pi$  p-p bond order of 0.20 and a p-d bond order of 0.35 were calculated. In addition, the Ehrenson-Seltzer<sup>22</sup> indices, which depend upon overlap values, were 0.34 for the  $\pi$  p-p MO and 0.20 for the  $\pi$  p-d MO. Therefore, there is considerable  $\pi$  bond formation in  $\text{CHCl}_2$  in which the Cl 3d AO's play an important role. Very similar conclusions were found for  $\text{CCl}_3$ .

Earlier overlap values<sup>1</sup> of a  $C_{2p_z}$  atomic orbital with the halogen valence  $p_z$  and  $d_{zz}$  atomic orbitals were

calculated for the diatomics CCl, CBr, and CI. For a C-I distance of 2.10 Å the overlap values for CI were  $\langle C_{2p_z} | I_{5p_z} \rangle = 0.1610$  and  $\langle C_{2p_z} | I_{5d_{zz}} \rangle = 0.3218$ . Both of these values were larger than the corresponding values for chlorine. Consequently, it is the opinion here that considerable  $\pi$  bond formation is indicated both experimentally and theoretically for  $\text{CHI}_2$  and  $\text{CI}_3$ .

Recently Kawamura and Kochi<sup>23</sup> interpreted their esr results on alkyl radicals with  $\beta$ -Si, Ge, and Sn substituents to indicate that p-d conjugative interactions between the radical center and the metal increase with increasing atomic number of the metal atom. Thus, it is entirely reasonable to expect large p-p and p-d conjugative effects in halomethyl radicals and that iodine is just as effective as chlorine in its ability to conjugate to carbon and form a strong  $\pi$  system.

*Acknowledgments.* The authors gratefully acknowledge financial support for this research by the National Science Foundation under Grant No. GP-21304 and a Du Pont Fellowship for D.W.S.

(21) J. A. Pople and D. L. Beveridge, "Approximate Molecular Orbital Theory," McGraw-Hill, New York, N. Y., 1970.

(22) S. Ehrenson and S. Seltzer, *Theor. Chim. Acta*, **20**, 17 (1971).

(23) T. Kawamura and J. K. Kochi, *J. Amer. Chem. Soc.*, **94**, 648 (1972).

## Role of Low-Energy Resonances in Some Elementary

### Processes of Radiation Chemistry

by K. Funabashi\* and T. Kajiwara

Department of Chemistry and the Radiation Laboratory,<sup>1</sup> University of Notre Dame, Notre Dame, Indiana 46556  
(Received March 29, 1972)

Publication costs assisted by the U. S. Atomic Energy Commission

A qualitative argument is presented to show that the preexisting trapping potentials of electrons in molecular liquids or glasses are related to fluctuations in polarization energies and transfer energies, and are deeper and more numerous for nonspherical molecules (*n*-hexane) than spherical ones (neopentane). These preexisting potentials are shown to have a large effect on the dynamic behaviors of excess electrons, such as electron mobilities and the spread of electron distribution in epithermal energy region, through the large resonance scattering cross sections, apart from the trivial consequence that the electron could eventually be trapped in these potentials. The scattering cross sections for S and P waves for a spherical potential well are calculated explicitly and are plotted as a function of electron energy and the strength of the potential.

#### 1. Introduction

In this paper we consider the effects of large scattering cross sections of low-energy resonances on some elementary processes of radiation chemistry in the condensed phase. It has been known that the temporary

negative-ion states of molecules play an important role in inelastic scatterings of electrons in the gas phase.

(1) The Radiation Laboratory of the University of Notre Dame is operated under contract with the U. S. Atomic Energy Commission. This is AEC document No. COO-38-837.

Comprehensive reviews have been written for theories<sup>2</sup> and experiments.<sup>3</sup> The role and the physical meaning of molecular temporary negative-ion states in the condensed phase have not been examined carefully. It is not at all clear whether an excess electron in the condensed phase attaches to a single molecule to form a *molecular* resonance state or attaches to a group of molecules to form a quasi-free conduction band.

If the rate of electron transfer from one molecule to its neighboring molecule is much larger than the rate of vibrational relaxation, the electron simply glides over many molecules, as if it is a quasi-free state, and any single molecule does not scatter the electron with a large cross section. In this case, the probability of energy loss to molecular vibrations is small because of the large mass ratio of nuclei and an electron.

Most alkane molecules have been known to have little or no electron affinity in the gas phase. This implies that the lowest temporary negative-ion state in alkanes is of the single-particle resonance type, according to Taylor's classification,<sup>2a</sup> and consequently has a diffuse wave function. It is highly unlikely, therefore, that the lowest temporary negative-ion states in alkane liquids play any significant role in the loss mechanism. Temporary negative-ion states of high energy, for example, those associated with the lowest triplet state, might have a wave function which is less diffuse, but this effect on the resonance shape can be cancelled by the higher density of states for the underlying continuum.

The role and significance of molecular temporary negative-ion states in liquids are therefore not likely to be the same as those in the gas phase.

In the condensed phase of disordered molecular aggregates, such as liquids and glasses, there are, however, a new class of resonance states which are absent in the gas phase. These resonances are essentially *collective* states of the aggregates rather than *molecular* states, and are the single particle resonance states which are associated with localized states or trap potentials for the excess electron. The notion that the trapped electron in a pure matrix involves a group of molecules rather than a single molecule has been a conjecture, but a recent study of the electron mobility in alkane liquids by Minday, Schmidt, and Davis<sup>4</sup> demonstrated that the electron traps in these substances indeed are related to a group of molecules. Such a concept for the trapped electron is consistent with the general notion of localized states in disordered systems which have been studied extensively for semiconductors<sup>5</sup> and alloys<sup>6</sup> in recent years.

Since the electronic transition from an extended state to a localized state (electron trapping) accompanies the change of electron density at the trap site, some deformation of the local molecular configuration must ensue the localization by vibronic (or electron-phonon) interactions. When the vibronic interaction

is sufficiently strong, an excess electron can be "trapped" even in a perfect crystal.<sup>7,8</sup> The trapped electron in a system with some translational symmetry can be thought to have a very large effective mass. A complete description of thermalized electrons in molecular aggregates therefore requires information related to pre-existing fluctuation potentials and also the vibronic coupling.

In this paper, we are concerned with the effects of these preexisting potentials for the epithermal electrons, whose energies are not large enough to excite the electronic excited states of the molecules, but large enough so that we can ignore the vibronic relaxation effect (electron-phonon interaction) except at the resonances. In short, we are concerned with the epithermal sub-excitation electrons. The dynamic behavior of these electrons are relevant in understanding elementary processes of radiation chemistry, in particular (1) the relatively large difference in the yield of free ions for *n*-hexane and neopentane,<sup>9</sup> (2) the wavelength dependence of the photobleaching yield of the absorption spectrum,<sup>10,11</sup> and (3) the low-energy electron spectroscopy.<sup>12</sup>

## 2. Resonance Cross Sections

In this section, we describe briefly the method of calculating the resonance cross sections, which is well known in a number of textbooks on quantum mechanics.<sup>13</sup> We take the scattering potential to be an attractive spherical well of a given depth  $V_0$  and the radius  $a$ . It is convenient to express the potential depth  $V_0$  and the binding energy  $E_0$  in terms of the critical potential depth  $V_c$ , below which there is no bound state.

$$V_0 = \lambda V_c \quad (2.1)$$

and

$$E_0 = \gamma V_c \quad (2.2)$$

where

(2) (a) H. S. Taylor, G. V. Nazarov, and A. Golebiewski, *J. Chem. Phys.*, **45**, 2872 (1966); (b) J. C. Y. Chen, *Advan. Radiat. Chem.*, **1**, 245 (1969).

(3) L. G. Christophorou and R. N. Compton, *Health Phys.*, **13**, 1277 (1967).

(4) R. M. Minday, L. D. Schmidt, and H. T. Davis, *Phys. Rev. Lett.*, **26**, 360 (1971).

(5) B. I. Halperin, *Advan. Chem. Phys.*, **8**, 123 (1967).

(6) B. Velický, S. Kirkpatrick, and H. Ehrenreich, *Phys. Rev.*, **175**, 747 (1968).

(7) T. Holstein, *Ann. Phys. (New York)*, **8**, 343 (1959).

(8) Y. Toyozawa, *Progr. Theor. Phys.*, **26**, 29 (1961).

(9) W. F. Schmidt and A. O. Allen, *J. Chem. Phys.*, **52**, 4788 (1970).

(10) P. J. Dyne and O. A. Miller, *Can. J. Chem.*, **43**, 2696 (1965).

(11) K. Kawabata, *J. Chem. Phys.*, **55**, 3672 (1971).

(12) K. Hiraoka and W. H. Hamill, unpublished work at University of Notre Dame.

(13) See, for example, E. Merzbacher, "Quantum Mechanics," Wiley, New York, N. Y., 1961.

$$V_0 = \pi^2 \hbar^2 / 8ma^2 \quad (2.3)$$

The relationship between  $\lambda$  and  $\gamma$  is given in Figure 1 for S-bound states (solid line). For a given radius  $a$  in ångström units,  $E_0$  and  $V_0$  are given in eV using Figure 1 and the relationship

$$E_0 = 0.37603\gamma(5/a)^2 \text{ eV} \quad (2.4)$$

$$V_0 = 0.37603\lambda(5/a)^2 \text{ eV} \quad (2.5)$$

Using the method of partial waves, the total cross section  $\sigma$  can be written as

$$\sigma = 4\pi/k^2 \sum_{l=0}^{\infty} (2l+1) \sin^2 \delta_l \quad (2.6)$$

where  $k$  is the wave number and  $\delta_l$  is the phase shift of the  $l$ th partial wave. Since we are interested only in low-energy electrons, we calculate only S- and P-wave cross sections, which amounts to calculating  $\delta_0$  and  $\delta_1$  in (2.6).

The phase shift  $\delta_l$  is given by

$$e^{i\delta_l} \sin \delta_l = e^{2i\epsilon_l} \left( \frac{S_l}{\beta_l - \Delta_l - iS_l} + e^{-i\epsilon_l} \sin \xi_l \right) \quad (2.7)$$

where

$$e^{2i\epsilon_l} = -h_l^{(2)}(ka)/h_l^{(1)}(ka) \quad (2.8)$$

$$\beta_l = \left( \frac{a}{R_{in}} \cdot \frac{dR_{in}}{dr} \right)_{r=a} \quad (2.9)$$

$$\Delta_l = \text{Re}(kah_l^{(1)'}(ka)/h_l^{(1)}(ka)) \quad (2.10)$$

$$S_l = \text{Im}(kah_l^{(1)'}(ka)/h_l^{(1)}(ka)) \quad (2.11)$$

In these equations, the notations have the following standard meanings:  $h_l^{(1)}, h_l^{(2)}$  are the Hankel functions of the first and second kind, the prime on their shoulder indicates differentiations with respect to coordinate, and  $R_{in}$  is the radial wave function inside the potential.

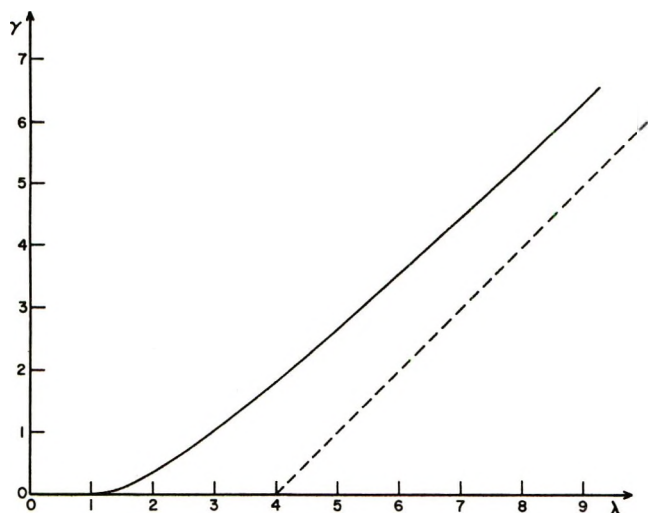


Figure 1. Relationship between the depth of potential ( $\lambda$ ) and the binding energy ( $\gamma$ ) for S-bound state. The energy is expressed in units of  $\pi^2 \hbar^2 / 8ma^2$ .

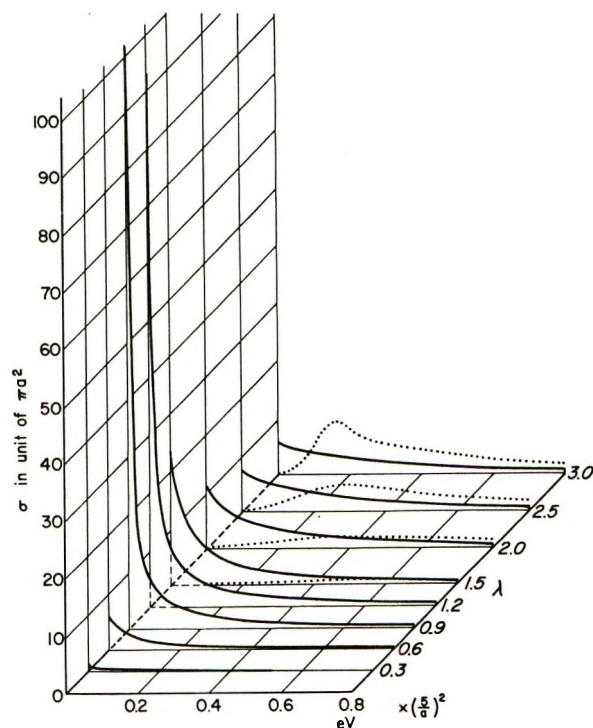


Figure 2. Scattering cross sections as functions of electron energy and the depth of potential ( $\lambda$ ) for S (solid) and P (dotted) waves.

The actual computation is complicated but a straightforward exercise of quantum mechanics.

The resultant cross sections for S and P waves are plotted as functions of the electron kinetic energy and  $\lambda$  in Figures 2 and 3. It can be seen that S-wave scattering is predominant for shallow traps ( $\lambda \approx 1$ ), while P-wave scattering becomes important for  $\lambda \approx 4$  and has its maximum at nonzero energy. It should be noticed that these cross sections could be larger than ten times the geometric cross section  $\pi a^2$ , which itself is likely to be greater than the molecular cross section because of the collective nature of the trap. The Ramsauer-Townsend effect is not apparent in the range of the electron energy and  $\lambda$  of our interest. Since the concentration of the traps is very much smaller than the number density of molecules, contribution of the Ramsauer-Townsend effect on the total effective cross section is likely to be small in comparison to the total effect of molecular scattering.

### 3. Electron Traps

In this section, a qualitative description of trapping sites and trapping mechanism in liquid or glassy alkanes will be presented. It is convenient to consider the trapping process in two stages of the time scale, before and after the configurational relaxation such as reorientation of molecular axis or bond deformation which ensues the charge localization. We shall be mainly concerned with the prerelaxation stage in this section. However, the postrelaxation effect is also

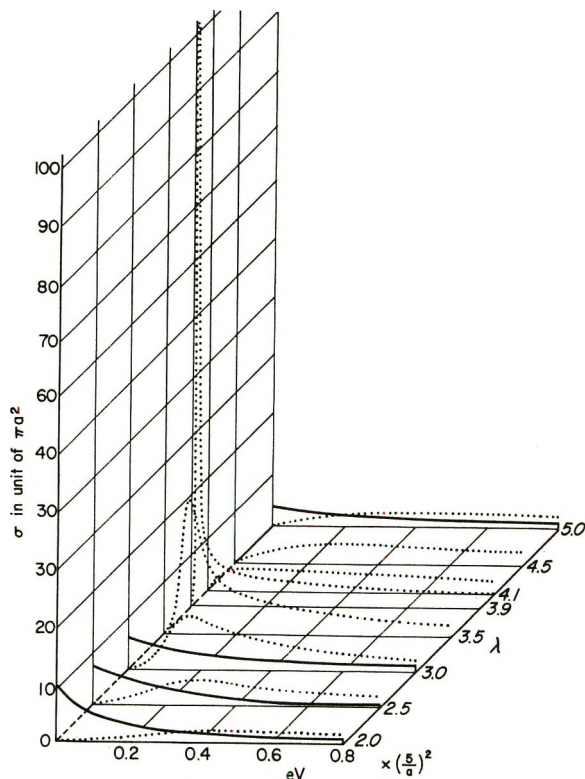


Figure 3. Scattering cross sections as functions of electron energy and the depth of potential ( $\lambda$ ) for S (solid) and P (dotted) waves.

essential in describing the energetics and dynamics involving the trapped electron.

In the time scale shorter than the relaxation time for molecular motion ( $\sim 10^{-12}$  sec), the electron feels a potential which arises from certain preexisting molecular arrangement of the system. In noncrystalline materials, such a potential has no long-range order (fluctuation potential), changing its depth and width from site to site, as shown schematically in Figure 4.

The important problems are the following. (1) What is the origin of this fluctuation potential in terms of molecular properties? (2) Where is the bottom of the quasi-free state?<sup>14,15</sup> (See the dotted line in Figure 4.)

In order to be more specific, we take the zero-order description for an excess electron to be given by the lowest negative-ion-state wave function of the individual molecule. Whether such a negative-ion state is stable in gas phase or not is not important, because the resonance state always has the localized character in the time scale we are concerned. The zero-order electronic energy of an excess electron in pure liquids is therefore constant throughout the system and there is no fluctuation in potential. The fluctuation arises when one considers the interaction of a negative ion with its surroundings. There are two modes of interaction for a localized charge with its neighbors. The first is through electronic polarization or the charge-induced dipole moment interaction.



Figure 4. Schematic representation of the fluctuation potential in a disordered system. The dotted line is the quasi-free state.

The charge-point dipole interaction energy,  $\Delta E$ , is given by

$$\Delta E = e^2\alpha/2r^4 \quad (3.1)$$

where  $\alpha$  is the polarizability of the molecule and  $r$  is the distance between the point charge and the molecule. The polarization energy is the sum of (3.1) for all the molecules in the system and the correction term arising from the dipole-dipole interactions. The quantitative detail<sup>16</sup> of this summation is by no means simple. The point-dipole approximation in (3.1) is also questionable for the nearest neighbors. But we are not concerned with such detail in this paper. As long as the intermolecular separations around negative ions are not too different from site to site, the main source of fluctuation is the anisotropy of molecular polarizability. The electron at site A of Figure 5, where the long axes of the surrounding molecules are all oriented toward the negative ion, must have a larger polarization energy than that of site B. The energy fluctuation through this mode of interaction is therefore determined by the distributing function of the relative molecular orientations. Very roughly, the more nonspherical the molecule is, the deeper becomes the fluctuation potential.

The second mode of interaction of a negative ion with its neighbors is the resonance interaction. Since all the molecules in the system are identical, the state in which the electron is localized at a molecule is in an approximate resonance with the state in which the electron is localized at any other molecule. They are not in exact resonance because the polarization energies at the two sites may be different. The strongest resonance occurs between the nearest neighbors. The resonance energy  $\beta_{nm}$  between a pair of molecules  $n$  and  $m$  is defined by

$$\beta_{nm} = \int \phi_m H \phi_n d\tau \quad (3.2)$$

where  $\phi_m$  is the wave function of the negative ion  $m$  and  $H$  is the one-electron Hamiltonian. The resonance energy, which is also called the transfer integral, is a measure of how fast an electron hops from one molecule to another. The resonance energy can in principle be calculable, but the quantitative accuracy is not too reliable with the present knowledge of wave functions for large molecules such as  $n$ -hexane. But the qualitative picture is fairly clear. The transfer integrals between large nonspherical molecules, whose

(14) B. E. Springett, J. Jortner, and M. H. Cohen, *J. Chem. Phys.*, **48**, 2720 (1967).

(15) B. I. Halperin and M. Lax, *Phys. Rev.*, **148**, 722 (1966).

(16) L. C. Lyons and J. C. Mackie, *Proc. Chem. Soc.*, 71 (1962).

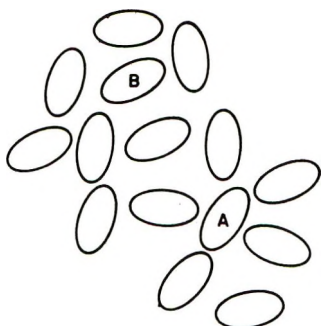


Figure 5. Molecular configuration representing two different sites, A and B, for which the energy difference is expected to be maximum.

dimensions are comparable to the intermolecular separation, are not simply related to the center-to-center distance of molecules, but very sensitively dependent upon the relative orientations.

As many other two-center molecular integrals, the transfer integrals vary approximately as exponential functions of the separations between the constituent atoms belonging to different molecules. The resonance effect is again likely to be larger at site A than site B of Figure 5. The resonance stabilization effect may not be confined to a pair of molecules, but in general involves a cluster of molecules. If the center-to-center separations between molecules are not too different from site to site, the distribution function for the relative molecular orientations determines the degree of fluctuation in the resonance energies. The resulting physical picture is the same as the effect of polarization fluctuation: molecules of nonspherical geometry are likely to have the deeper fluctuation potential than spherical molecules.

We can estimate the orders of magnitude for the maximum fluctuation energies arising from these two modes of interaction. For *n*-hexane, for example, the average polarizability,  $\bar{\alpha}$ , which is defined by

$$\bar{\alpha} = (\alpha_1 + \alpha_2 + \alpha_3)/3 \quad (3.3)$$

is  $11.8 \text{ \AA}^3$ , where  $\alpha_1$ ,  $\alpha_2$ , and  $\alpha_3$  are the polarizabilities along three main axes. Using the optical anisotropy<sup>17</sup>  $\delta^2$

$$\delta^2 = \frac{(\alpha_1 + \alpha_2)^2 + (\alpha_2 - \alpha_3)^2 + (\alpha_3 - \alpha_1)^2}{(\alpha_1 + \alpha_2 + \alpha_3)^2} = 2.6 \quad (3.4)$$

and also assuming the shape of the molecule to be ellipsoidal, one obtains the difference between the maximum and minimum  $\alpha_i$  to be about  $1 \text{ \AA}^3$ . Taking the intermolecular separation to be  $6 \text{ \AA}$ , the maximum fluctuation energy arising from the first shell of molecules is of the order of  $10^{-2} \text{ eV}$ . Since this estimate uses (3.1) and also ignores the dipole-dipole interaction, the number may not be too reliable. On the

other hand, the maximum fluctuation arising from the resonance energy is of the order of  $10^{-1} \text{ eV}$ .<sup>18</sup> Here again, the accuracy is not too high. We must be satisfied at this stage with the statement that the combined effect of two modes of interaction produces the fluctuation of energy of the order of  $10^{-1} \text{ eV}$ .

The energy level corresponding to the lowest quasi-free state is not a simple matter either. Without going into detail, we define the quasi-free state to be the state in which an excess electron can propagate with many scatterings throughout the entire system at  $T = 0^\circ\text{K}$  on the *average*. The dotted line in Figure 4 is the lowest quasi-free state and roughly the average<sup>15</sup> of the fluctuation potential.

As is well known in elementary quantum mechanics of a three-dimensional potential well, there is a certain critical strength for the potential to be able to accommodate a bound state. For a given system of organic liquid, it is difficult to show quantitatively that a certain number of localized states exist below the quasi-free state. But, one can say qualitatively that it is more likely to have localized states in the pre-relaxation stage if the fluctuation is greater. One can further conjecture that the binding energy, if a localized state exists at all, must be of the order of  $10^{-1} \text{ eV}$  or less and the majority of the fluctuation potentials are so shallow that there are no bound states. The possibility of having a deep potential, where there is an excited bound state in addition to the ground state, seems small for pure alkanes. Indeed, all experimental information related to the binding energy of trapped electrons in liquid or glassy alkanes is consistent with these conjectures. Such experiments include the temperature dependence of electron drift mobility,<sup>4</sup> the absorption spectra of trapped electrons<sup>19</sup> and its decay rate, the photobleaching<sup>20</sup> of the absorption spectra, and the thermal decay<sup>21</sup> of esr spectra for trapped electrons.

The preceding qualitative description of the electron traps is equivalent to the problem of finding the eigenfunctions and eigenvalues of the one-electron Hamiltonian

$$H = -\Delta/2 + \sum_n V_n(r - \vec{R}_n) \quad (3.5)$$

where the first term is the kinetic energy operator and  $V_n(r - \vec{R}_n)$  is the potential associated with the *n*th molecule whose coordinate is designated by  $\vec{R}_n$ . An approximate way of solving this problem is to express the

(17) Landolt-Börnstein, "Zahlenwerte und Funktionen," Vol. 1, Springer-Verlag, West Berlin, 1951, Part 3.

(18) K. Funabashi and Y. Maruyama, *J. Chem. Phys.*, **55**, 4494 (1971).

(19) A. Ekstrom, *Radiat. Res. Rev.*, **2**, 381 (1970).

(20) K. Funabashi, C. Hebert, and J. L. Magee, *J. Phys. Chem.*, **75**, 3221 (1971).

(21) J. Lin, K. Tsuji, and Ff. Williams, *J. Chem. Phys.*, **46**, 4982 (1967).

eigenfunction  $\Psi_i$  of (3.5) as a linear combination of negative-ion wave functions  $\Phi_n$

$$\Psi_i = \sum_n C_{in} \Phi_n \quad (3.6)$$

and to determine the coefficients  $C_{in}$  by the variational method. This is equivalent to the problem of diagonalization of the matrix

$$H' = \sum_{m,n} |\Phi_n\rangle\langle\Phi_n| - \Delta/2 + \sum_n V_n(r - \bar{R}_n) |\Phi_n\rangle\langle\Phi_m| \equiv \sum_n |\Phi_n\rangle\alpha_n\langle\Phi_n| + \sum_{m \neq n} |\Phi_n\rangle\beta_{nm}\langle\Phi_m| \quad (3.7)$$

where  $\alpha_n$  is essentially the polarization energy of the electron at  $n$ th molecule and  $\beta_{nm}$  is the resonance energy between sites  $n$  and  $m$ . The two Hamiltonians,  $H$  and  $H'$ , are exactly equivalent if one uses a complete set of  $\phi_n$  in the expansion of (3.6). The problems of finding the density of states and the localizability criterion for the Hamiltonian (3.7) have been extensively studied in relation to the transport problem in amorphous semiconductors<sup>5,15</sup> and alloys.<sup>6</sup> A quantitative application to disordered molecular systems is not practically feasible at this time. But the qualitative picture is the same as described earlier: larger fluctuations in  $\alpha_n$  and  $\beta_{nm}$  are likely to lead to formation of localized states of greater binding energies and also in larger number.

#### 4. Discussion

In this section, we consider the effects of low-energy resonances on the electron dynamics in the energy range of 0~1 eV, with special references to some elementary processes in radiation chemistry of condensed phase. As may be seen from Figures 2 and 3, and also from the more general consideration, the resonances arising from finite range potentials of relatively shallow ( $\lambda < 4$ , see section 2) depth are not important in the higher energy region: the resonances become broad and weak by the interaction with continuum states of increasing density.

A simplified expression for the electron mobility in the quasi-free state can be written as<sup>22</sup>

$$\mu = (2e/3)(2/\pi mkT)^{1/2} \Lambda \quad (4.1)$$

where  $\Lambda$  is the mean free path of the electron and has the form

$$\Lambda = 1/(n\sigma_m S(0) + n'\sigma_p) \quad (4.2)$$

The symbols used in (4.2) are defined as  $n$  equals the number density of the molecules;  $\sigma_m$ , the total scattering cross section of the molecule in the gas phase;  $S(0)$ , the structure factor which is related to the isothermal compressibility  $\kappa_T$  by  $S(0) = nkT\kappa_T$ ;<sup>23</sup>  $n'$ , the number density of the traps; and  $\sigma_p$ , the scattering cross section of the trap.

Since  $n \gg n'$ , the correlation effect between the potential scatterings of the traps is ignored in (4.2).

This is equivalent to assuming a completely random distribution for the traps. If  $\sigma_p$  is ten times the geometric cross section of the potential and  $n' = n/1000$ , the contribution of the traps to the mean free path  $n'\sigma_p$  is comparable to or greater than that of the molecular scatterings, because the geometric cross section of the trap itself is greater than  $\sigma_m$  (collective trap) and also  $S(0) \approx 10^{-2}$ .<sup>4</sup> Since the S-wave resonance cross section  $\sigma_p$  decreases with electron energy, the temperature dependence of the mobility for neopentane<sup>4</sup> can be understood at least qualitatively without letting the electron actually trapped in the potentials, but simply by considering their scattering effects.

When the number density of the traps  $n'$  becomes larger, Landauer and Woo<sup>24</sup> showed that the potential scatterings interfere each other in such a way that  $n'\sigma_p$  must be replaced by  $n'\sigma_p/(1 - n'\sigma_p l')$  in (4.2), where  $l'$  is approximately equal to the range of the potential. It can be seen that when  $n'\sigma_p l' \approx 1$ , the mobility becomes very small. Such a possibility cannot be excluded for  $n' \approx n/100$ . It is clear that the expression 4.1 is not applicable for the mean free path less than the intermolecular separation. The transport mechanism then must consider the effect of the trapped state explicitly. At  $T = 0^\circ\text{K}$ , the trapped electron does not move and therefore has no contribution to the electric current. At finite temperature, the interaction with molecular vibrations (deviation from Born-Oppenheimer approximation) either knocks out the trapped electron to the quasi-free state or transfers the electron to adjacent trapping sites (the hopping mechanism). Minday, Schmidt, and Davis<sup>4</sup> have chosen the former mechanism to explain the electron drift mobility in *n*-hexane. Although the experimental result can be explained equally well in terms of the hopping mechanism, their interpretation is consistent with their experiment. However, the implication of their mechanism on the so-called diffusion model<sup>25</sup> for charge neutralization is quite serious. The excess electron in *n*-hexane has a drift mobility<sup>26</sup> of about 150 cm<sup>2</sup>/V sec and has the mean free path of  $\sim 100 \text{ \AA}$  when it is in the quasi-free state. If the initial charge separation is within the range of several hundred angstroms, it is clear that the diffusion kinetics is not applicable as far as the charge neutralization process is concerned. Although it is possible to justify to some extent the diffusion model with the hopping mechanism, we shall not go into its detail in this article.

(22) M. Cohen and J. Lekner, *Phys. Rev.*, **158**, 305 (1967).

(23) See, for example, L. D. Landau and E. M. Lifshitz, "Statistical Physics," Pergamon Press, Oxford, 1958, p 365.

(24) R. Landauer and J. W. F. Woo, *Phys. Rev. B*, **5**, 1189 (1972).

(25) See, for example, A. Mozumder, *J. Chem. Phys.*, **48**, 1659 (1968).

(26) H. T. Davis, L. D. Schmidt, and R. M. Minday, "On the Mechanism of Charge Transport in Liquid Hydrocarbons," unpublished.

In systems such as 3-methylpentane,<sup>27</sup> water,<sup>11</sup> and methyltetrahydrofuran,<sup>10</sup> the quantum yields for photo-bleaching of the absorption spectra of trapped electrons are low in the long-wavelength side of the absorption maxima. This fact could be interpreted as indicating that the optical transitions involve the bound excited states rather than the quasi-free states. The same effect, however, can be understood without postulating the bound excited states. The photoejected electron can be retrapped by other fluctuation potentials with the cross section which decreases with the kinetic energy of the ejected electron. As can be seen in Figure 2, the energy dependence of the S-wave resonance is consistent with this interpretation. The cross sections given in Figures 2 and 3 are only those of elastic scatterings by rigid spherical potentials. However, the information relating to the inelastic scattering is contained in the width of the resonance shape: the half-intensity width is related to the residence time  $\tau$  by  $\hbar/\tau$ , and the longer the residence time the greater the probability for the electron to convert its kinetic energy into vibrational energies. It must be noted, however, that the attenuation or the spread of the electron distribution is governed by the sum of elastic and inelastic cross sections. Lax<sup>28</sup> showed the probability of finding an electron at distance  $r$ ,  $p(r)$ , from its source is given using the multiple-scattering theory as

$$p(r) \propto e^{-r/r_0}/r^2 \quad (4.3)$$

where the attenuation constant  $r_0$  is given by

$$1/r_0 = n(\sigma_{el} + \sigma_{inel}) \quad (4.4)$$

where  $n$  equals the number density of scatterers. Just as in the electron mobility, the elastic scattering cross

section is the dominant term in determining the spread of the electron wave.

The large difference in the yield of free ions between *n*-hexane and neopentane<sup>9</sup> can also be understood in terms of the large resonance scattering cross sections arising from the trap potentials for *n*-hexane, giving rise to longer "thermalization" distance for neopentane. The quantitative treatment of this problem will not be given here. The main source of difficulty is the distribution function for the initial charge separation. It is tempting to use the simple form 4.3 in view of the recent studies by Abell<sup>29</sup> and Berry,<sup>30</sup> in which both of them concluded empirically that the form 4.3 describes most accurately the scavenging yield and the attenuation of slow electrons, respectively. However, the theoretical derivation of (4.3) by Lax includes only the coherent part of the electron wave and the successive energy degradation is not explicitly considered. We are not, therefore, certain about the theoretical significance of the parameter  $r_0$  in (4.3) in the context of the initial charge distribution.

The most important experiment, as far as the low-energy resonance is concerned, would be the energy loss spectrum for low-energy electrons by Hiraoka and Hamill.<sup>12</sup> They have indeed found a significant difference in the loss pattern for the energy range of 0~1 eV between neopentane and 3-methylpentane.

*Acknowledgment.* The authors would like to express their gratitudes to W. H. Hamill, J. L. Magee, W. Berry, K. Hiraoka, Y. C. Chang, and G. Abell for their stimulating and informative discussions in this work.

(27) W. H. Hamill, *J. Chem. Phys.*, **53**, 473 (1970).

(28) M. Lax, *Rev. Mod. Phys.*, **23**, 287 (1951).

(29) G. C. Abell, unpublished work at University of Notre Dame.

(30) W. B. Berry, *J. Chem. Phys.*, **54**, 1837 (1971), and also unpublished work by Y. C. Chang and W. B. Berry.

## Studies on the Formation of Primary Hydrogen Atom

### Yield ( $G_H$ ) in the $\gamma$ Radiolysis of Water

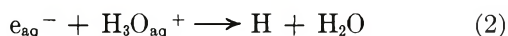
by Z. D. Draganić and I. G. Draganić\*

Boris Kidrić Institute of Nuclear Sciences, 11001 Belgrade, Yugoslavia (Received February 15, 1972)

The formation of  $G_H$  was studied in  $\gamma$ -irradiated, neutral, aqueous solutions containing selected mixtures of scavengers for hydrated electron and hydroxyl radical. Experimental verification was made of various assumptions based on the free-radical model of water radiolysis. It was confirmed that the formation of H atoms through the reaction  $e_{aq}^- + H_3O_{aq}^+ \rightarrow H + H_2O$  can be strongly influenced by scavenging hydrated electrons; a cation ( $Cu^{2+}$ ), an anion ( $NO_3^-$ ), and neutral species ( $H_2O_2$  and acetone) were used for scavenging hydrated electrons. It has been shown that the depression of  $G_H$  could be quantitatively correlated with the reactivity toward  $e_{aq}^-$ . Also, it has been demonstrated that an efficient removal of OH radicals leads to an increase in  $G_H$ , by depressing the water re-forming reaction ( $OH + e_{aq}^-$ ) and leaving more  $e_{aq}^-$  available for increased H-atom formation in the reaction with hydronium ion. These effects were also observed in solutions containing simultaneously larger amounts of scavengers for OH and  $e_{aq}^-$ . Experimental curves agree reasonably well with Kuppermann's predictions based on a diffusion-kinetic model of water radiolysis. Experimental results point to 0.58 as probably the best value for  $G_H$ . It was estimated that two-thirds of the primary hydrogen atom yield originates in the reaction of  $e_{aq}^-$  with  $H_3O_{aq}^+$ . It was also found that iodide and bromide ions react efficiently with hydrogen atoms in neutral solutions:  $k(H + I^-) = 4 \times 10^7 \text{ mol}^{-1} \text{ sec}^{-1}$  and  $k(H + Br^-) = 3.3 \times 10^7 \text{ mol}^{-1} \text{ sec}^{-1}$ . The corresponding value for chloride ion was estimated as  $<10^5 \text{ mol}^{-1} \text{ sec}^{-1}$ .

#### Introduction

In the preceding papers<sup>1,2</sup> we have considered the origin of primary molecular yields in water radiolysis ( $G_{H_2O_2}$  and  $G_{H_2}$ ). The present study is concerned with the formation of primary hydrogen atom yield ( $G_H$ ). Some aspects of its origin in the reactions



are still not well established. It seems generally accepted<sup>3,4</sup> that reaction 1 is less important, but the knowledge of relative contribution of reactions 1 and 2 to the formation of  $G_H$  is still scanty. This is also the case with the experimental evidence for reaction 2. A decrease in  $G_H$  was induced by scavenging  $e_{aq}^-$  with nitrate ion<sup>5</sup> and acetone.<sup>6</sup> However, in scavenging  $H_3O_{aq}^+$  by hydroxide ions the answers were ambiguous: while Appleby<sup>6</sup> reports the expected fall off in  $G_H$  with increasing  $OH^-$  concentration, Moreau and Sutton<sup>7</sup> find constant  $G_H$  up to pH 13.5.

The main purpose of this work was to test reaction 2 by experimental verification of the following assumption based on the free-radical model of water radiolysis: an efficient removal of OH radicals should lead to the increase of  $G_H$  by depressing the extent of water-re-forming reaction



and making more hydrated electrons available for increased formation of hydrogen atoms in reaction 2.

This is why we have determined hydrogen atom yields in the presence of various amounts of known hydroxyl radical scavengers  $CH_3OH$ ,  $C_2H_5OH$ ,  $(CH_3)_2CHOH$ , and  $HCOO^-$ . In some other experiments we followed the depression of  $G_H$  by increasing the concentration of  $e_{aq}^-$  scavengers.

Assuming that the reactivity influence is indeed of importance for the formation of  $G_H$  through reaction 2, we also carried out the experiments in solutions containing larger amounts of scavengers for both OH and  $e_{aq}^-$ . As it will be seen, these experiments confirm the importance of reaction 2 even in such complex conditions.

The contribution of reaction 2 to the formation of the primary yield of hydrogen atom was considered. The experimental data on the depression of  $G_H$ , obtained in this work, and of  $G_{H_2}$ , measured in the same conditions previously,<sup>2</sup> were used for this purpose.

The present work shows also that halide ions ( $X^-$ , where  $X = Cl, Br, I$ ) react efficiently with hydrogen

- (1) Z. Draganić and I. Draganić, *J. Phys. Chem.*, **73**, 2571 (1969).
- (2) Z. Draganić and I. Draganić, *ibid.*, **75**, 3950 (1971).
- (3) A. Kuppermann in "Radiation Research 1966," G. Silini, Ed., North-Holland Publishing Co., Amsterdam, 1967, p 212.
- (4) H. Schwarz, *J. Phys. Chem.*, **73**, 1928 (1969).
- (5) M. Chouraqui and J. Sutton, *Trans. Faraday Soc.*, **62**, 2111 (1966).
- (6) A. Appleby in "The Chemistry of Ionization and Excitation," G. R. A. Johnson and G. Scholes, Ed., Taylor and Francis Ltd., London, 1967, p 269.
- (7) M. Moreau and J. Sutton, *Trans. Faraday Soc.*, **65**, 380 (1969).



**Table I:** Yields of Primary Hydrogen Atom ( $G_H$ ) Determined in Deaerated, Neutral, Aqueous Solutions Containing Various Concentrations of OH and  $e_{aq}^-$  Scavengers<sup>a</sup>

Scavenger for OH	Concn., M	$G_H$			
		$NO_3^-$ $2.5 \times 10^{-4} M$	$H_2O_2$ $2 \times 10^{-4} M$	$(CH_3)_2CO$ $0.4 M$	$Cu^{2+}$ $1 \times 10^{-4} M$
HCOO <sup>-</sup>	0.5	0.65 (1.10)	0.55 (1.00)	...	0.60 (1.05)
HCOO <sup>-</sup>	1.0	0.70 (1.15)	0.67 (1.12)	...	0.65 (1.10)
HCOO <sup>-</sup>	2.0	0.78 (1.30)	0.72 (1.23)	...	0.70 (1.21)
CH <sub>3</sub> OH	2.0	0.72 (1.17)	...	...	...
C <sub>2</sub> H <sub>5</sub> OH	1.0	0.74 (1.20)	...	...	...
C <sub>2</sub> H <sub>5</sub> OH	2.0	0.80 (1.27)	...	...	...
(CH <sub>3</sub> ) <sub>2</sub> CHOH	1.0	0.76 (1.22)	...	...	...
		$NO_3^-$ 0.25 M	$H_2O_2$ 0.2 M	$(CH_3)_2CO$ 0.4 M	$Cu^{2+}$ 0.1 M
HCOO <sup>-</sup>	0.5	0.60 (0.78) <sup>b</sup>	0.58 (0.80) <sup>b</sup>	...	...
HCOO <sup>-</sup>	1.0	0.70 (0.90)	0.68 (0.96)	...	0.64 (0.90) <sup>b</sup>
HCOO <sup>-</sup>	2.0	0.73 (1.01)	0.71 (1.08)	...	0.68 (1.04)
(CH <sub>3</sub> ) <sub>2</sub> CHOH	1.0	...	...	0.61 (0.83)	...
(CH <sub>3</sub> ) <sub>2</sub> CHOH	2.0	0.67 (0.94)	...	...	...

<sup>a</sup> Calculated according to eq A. Measured molecular hydrogen yields,  $G(H_2)$ , are given in parentheses. <sup>b</sup> Corrected for H-atom loss in the reaction with the  $e_{aq}^-$  scavenger.

atoms; their rate constants were determined from competition experiments.

### Experimental Section

The chemicals used were (Merck or BDH products) of the highest purity available; only sodium formate was subjected to an additional purification by recrystallization. The purification of water and the sample preparation were carried out by standard procedures previously described.<sup>1,2</sup>

Irradiations were carried out using a 3000 Ci (nominal) radioactive cobalt source. Absorbed doses varied from  $2 \times 10^{17}$  to  $12 \times 10^{17}$  eV g<sup>-1</sup> and, where necessary, corrections were applied for the electron density of the solution studied.

Molecular hydrogen was measured by gas chromatography.<sup>8</sup> Its yields were calculated from the slopes of the dosage curves, obtained by plotting the measured  $H_2$  values of five irradiated samples against dose. The dosage curves were linear within the limits of experimental error ( $\pm 2\%$ ). The accuracy of all radiation chemical yield determinations was better than  $\pm 6\%$ . A correction due to the direct effect of radiation on the solute<sup>9</sup> was only applied in the case of scavenger concentrations larger than 1 M.

### Results

Only those systems were chosen for which the reaction mechanism enables the determination of  $G_H$  by measuring the molecular hydrogen formed and using the relation

$$G(H_2) = G_H + G_{H_2} \quad (A)$$

Here,  $G(H_2)$  is the observed hydrogen yield and  $G_{H_2}$  the primary yield of molecular hydrogen. The value

of  $G_{H_2}$  in dilute solutions was taken as 0.45, while in concentrated solutions of  $e_{aq}^-$  or OH scavengers our previous finding on its dependence on the reactivity was taken into account. In such cases we used as  $G_{H_2}$  the values experimentally determined under the same working conditions, given in Figures 3 and 4 of ref 2.

When using larger amounts of scavengers,  $[S] \geq 0.1 M$ , where H atoms were partially lost in the reaction  $H + S \rightarrow P$ ,  $P \neq H_2$ , the hydrogen atom yield was derived from the competition plots made according to the relation

$$1/G(H_2) = 1/G_{H_2} + 1/G_H \left\{ 1 + \frac{k_{H+S}[S]}{k_{H+HR}[HR]} \right\} \quad (B)$$

Here,  $G(H_2)$  and  $G_{H_2}$  are as defined in eq A. The reaction  $HR + H \rightarrow H_2$  and its rate constant being well established, these competition plots enable also the determination of  $k(H + S)$ .

How increasing concentration of an OH scavenger influences  $G_H$  values can be seen from Table I. It shows also the primary yields of H atom derived from the solutions containing simultaneously larger amounts of both OH and  $e_{aq}^-$  scavengers. The eq A was used for calculation of the primary yields of hydrogen atom. The values given in parentheses are experimentally observed molecular hydrogen yields,  $G(H_2)$ .

Table II summarizes  $G_H$  values measured in neutral aqueous solutions of various substances known as good  $e_{aq}^-$  scavengers. They were calculated according

(8) Lj. Petković, M. Kosanić, and I. Draganić, *Bull. Inst. Nucl. Sci., Boris Kidrič*, 15, 9 (1964).

(9) M. Daniels and E. Wigg, *J. Phys. Chem.*, 73, 3703 (1969).

**Table II:** Yields of Primary Hydrogen Atom ( $G_H$ ) Determined in Deaerated, Neutral, Aqueous Solutions Containing Various Concentrations of  $e_{aq}^-$  Scavengers<sup>a</sup>

$NO_3^-$		$H_2O_2$		$(CH_3)_2CO$		$Cu^{2+}$	
Concn., <i>M</i>	$G_H$	Concn., <i>M</i>	$G_H$	Concn., <i>M</i>	$G_H$	Concn., <i>M</i>	$G_H$
$2.5 \times 10^{-4}^b$	0.63 (1.08)	$2 \times 10^{-4}$	0.53 (0.98)	...	...	$1 \times 10^{-4}$	0.58 (1.03)
$2.5 \times 10^{-3}^b$	0.62 (1.05)	$2 \times 10^{-3}$	0.52 (0.95)	...	...	$1 \times 10^{-3}$	0.57 (1.00)
$2.5 \times 10^{-2}^b$	0.58 (0.92)	$2 \times 10^{-2}$	0.50 (0.88)	0.20	0.46 (0.78)	$1 \times 10^{-2}$	0.51 (0.85)
0.25 <sup>c</sup>	0.48	0.20	0.46	0.43	0.43 (0.69)	0.10	0.45
1.0 <sup>c</sup>	0.36	1.0	0.43	...	...	...	...

<sup>a</sup> Formate or ethanol were used as H and OH scavengers: their concentrations increased from 0.01 to 0.2 *M* with increasing concentration of  $e_{aq}^-$  scavengers. <sup>b</sup> Calculated according to eq A. Measured molecular hydrogen yields,  $G(H_2)$ , are given in parentheses. <sup>c</sup> Derived from the competition plot made according to eq B.

to eq A or B. Here, also, the values in parentheses represent the experimental data for  $G(H_2)$ . Formate or ethanol were used in these experiments as HR; their concentration was sufficient to protect  $H_2$  formed from the attack of hydroxyl radicals.

Hydrogen atom yields determined in solutions containing halide ions are shown in Table III. The  $G_H$  values were obtained from competition plots similar to those represented in Figure 1; from these plots we have calculated 0.162 and 0.132 for  $k(H + I^-)/k(H + HCOO^-)$  and  $k(H + Br^-)/k(H + HCOO^-)$ , respectively. Competition plots at 0.5 and 1.0 *M* concentrations of iodide or bromide gave the ratios, within the experimental error, identical with those derived from dilute solutions. In all the calculations, the  $G_{H_2}$  values for  $Br^-$  and  $I^-$  were taken from reference 2; 0.45 was measured in the presence of  $Cl^-$  (up to 1 *M*). Table IV<sup>10,11</sup> summarizes rate constants of H-atom reactions with halide ions and some other solutes, derived from competition plots. It is worth noting that the concentrations of nitrate ion, hydrogen peroxide, and cupric ion were higher (0.1–1.0 *M*) than in usual competition experiments.

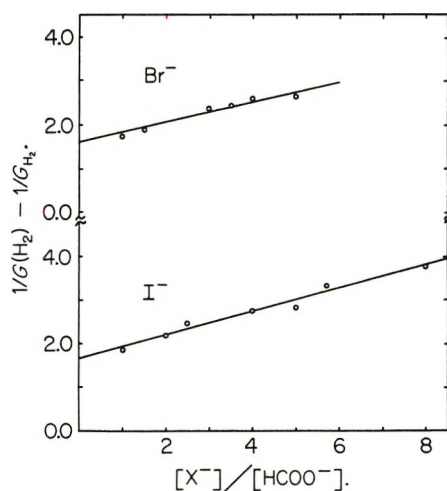


Figure 1. Competition plots for H-atom reactions with  $I^-$  or  $Br^-$  and  $HCOO^-$ ;  $[X^-]$  was 0.01 or 0.02 *M*.

**Table III:** Yields of Primary Hydrogen Atom ( $G_H$ ) in the Presence of Halide Ions<sup>a</sup>

Concn., <i>M</i>	$G_H$		
	$Cl^-$	$Br^-$	$I^-$
0.01	0.61	0.62	0.60
0.1	0.55	0.50	0.48
0.5	0.47	0.48	0.46
1.0	0.45	0.45	0.43

<sup>a</sup> All solutions contained  $2.5 \times 10^{-4}$  *M*  $NO_3^-$ .

**Table IV:** Rate Constants for Some H-Atom Reactions

Solute	$k_{H+S}$	
	This work	Published values
$I^-$	$4.0 \times 10^7$	$5.3 \times 10^6$ <sup>a</sup>
$Br^-$	$3.3 \times 10^7$	...
$Cl^-$	$< 10^6$	...
$NO_3^-$	$1.2 \times 10^7$	$0.9-1.3 \times 10^7$ <sup>b</sup>
$H_2O_2$	$5.0 \times 10^7$	$5-10 \times 10^7$ <sup>b</sup>
$Cu^{2+}$	$7.1 \times 10^7$	$4-6 \times 10^7$ <sup>b</sup>

<sup>a</sup> Reference 10. <sup>b</sup> Reference 11.

**Table V:** Yield of Primary Hydrogen Atom ( $G_H$ ) Measured in the Presence of Inert Salts<sup>a</sup>

Added solute	$G_H$	
	$2.5 \times 10^{-4}$ <i>M</i> $NO_3^-$ <sup>b</sup>	0.25 <i>M</i> $NO_3^-$ <sup>c</sup>
...	0.63 (1.08)	0.44 (0.63)
0.6 <i>M</i> $NaClO_4$	0.60 (1.05)	0.42 (0.61)
1.2 <i>M</i> $NaClO_4$	0.62 (1.07)	0.43 (0.62)
0.2 <i>M</i> $Na_2SO_4$	0.61 (1.06)	0.42 (0.61)
0.4 <i>M</i> $Na_2SO_4$	0.60 (1.05)	0.43 (0.62)

<sup>a</sup> The values in parentheses represent measured  $G(H_2)$ . <sup>b</sup> All solutions contained 0.5 *M*  $C_2H_5OH$ . <sup>c</sup> All solutions contained 0.25 *M*  $HCOO^-$ ; correction for the contribution of the reaction  $NO_3^- + H$  was not introduced.

(10) R. Hentz and C. Johnson, Jr., *J. Chem. Phys.*, **51**, 1236 (1969).

(11) M. Anbar and P. Neta, *Int. J. Appl. Radiat. Isotopes*, **18**, 493 (1967).

The effect of inert salts on the yields of the primary hydrogen atom ( $G_H$ ) was studied and the results are shown in Table V.

### Discussion

$G_H$  Dependence on the Reactivity toward OH and  $e_{aq}^-$ . The influence of the reactivity toward OH and  $e_{aq}^-$  on the primary yield of the hydrogen atom is shown in Figure 2. In constructing the yield-reactivity curves, the values from Tables I and II were used. The reactivities were calculated as the product of scavenger concentration and the rate constant. In the case of  $e_{aq}^-$  rate constants, their dependence on the ionic strength was taken into account; these values as well as other rate constants were taken from our previous work (Table IV in reference 2). As can be seen, unifying curves are obtained for the fractional change,  $G_H/G_H^0$ , where  $G_H$  is the value measured in the presence of precursor scavengers and  $G_H^0$  is derived from measurements on solutions where the reaction solute-precursor can be neglected. The upper curve shows that an increase in reactivity toward OH radicals leads to an augmentation in the yield of primary atomic hydrogen. The lower curve confirms some findings reported previously by other authors.<sup>5,6</sup> However, the present data also show that this fall can be well correlated with the reactivity toward the hydrated electron regardless of the chemical nature of the scavenger (neutral species, positive or negative ion). The trends of both experimental curves confirm the assumption on the importance of the reaction 2 for the origin of hydrogen atoms. They are in a fair agreement with theoretical predictions represented with the dotted lines. These theoretical curves were calculated after Kuppermann,<sup>3</sup> from a diffusion free-radical model of water radiolysis which is using the same parameters that furnish a good agreement with other observed effects.

The data for Figure 3 are taken from Table I. They show that the primary H-atom yields are increasing with the reactivity toward OH radicals also in solutions containing simultaneously larger amounts of  $e_{aq}^-$  scavengers. For comparison, the upper curve shows the best line through the data obtained from solutions containing OH scavengers as above but only low  $e_{aq}^-$  concentrations. The trends of the best lines are somewhat different, the effect being more pronounced in the presence of larger amounts of scavengers for  $e_{aq}^-$ . This might be an indication that the reaction mechanism is somewhat changed because of secondary reactions which are otherwise absent.

*On the Importance of Reactions 1 and 2 for the Formation of  $G_H$ .* The influence of reactivity toward OH and  $e_{aq}^-$  on the primary yields of H atoms (Figure 2) shows clearly the significance of reaction 2 and of hydrated electrons for the formation of  $G_H$ . If  $e_{aq}^-$  are available in excess, because of an efficient removal of the OH radical and the depression of the water re-

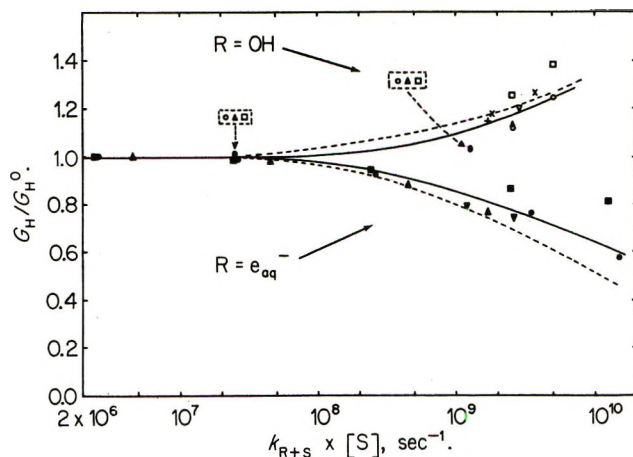


Figure 2. Unifying curves for the increase of  $G_H/G_H^0$  with increasing reactivity toward OH radicals and decrease of  $G_H/G_H^0$  with increasing reactivity toward  $e_{aq}^-$ :  $\circ$ ,  $2.5 \times 10^{-4} M NO_3^- + HCOO^-$ ;  $+$ ,  $2.5 \times 10^{-4} M NO_3^- + CH_3OH$ ;  $\times$ ,  $2.5 \times 10^{-4} M NO_3^- + C_2H_5OH$ ;  $\nabla$ ,  $2.5 \times 10^{-4} M NO_3^- + (CH_3)_2CHOH$ ;  $\square$ ,  $2 \times 10^{-4} M H_2O_2 + HCOO^-$ ;  $\Delta$ ,  $1 \times 10^{-4} M Cu^{2+} + HCOO^-$ ;  $\bullet$ ,  $0.01-0.2 M HCOO^- + NO_3^-$ ;  $\blacksquare$ ,  $0.01-0.2 M HCOO^- + H_2O_2$ ;  $\blacktriangle$ ,  $0.01-0.2 M HCOO^- + Cu^{2+}$ ;  $\blacktriangledown$ ,  $0.1 M HCOO^- + (CH_3)_2CO$ . The dotted line is the diffusion kinetic theoretical curve calculated after Kuppermann.<sup>3</sup>

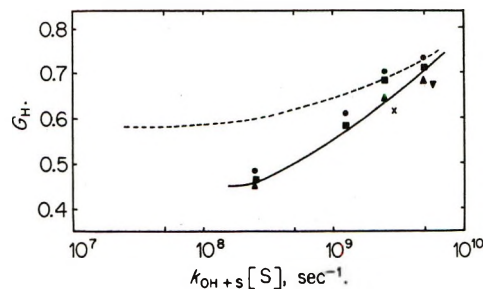


Figure 3. Dependence of  $G_H$  on the OH radical reactivity in deaerated, neutral solutions containing simultaneously larger amounts of  $e_{aq}^-$  scavengers:  $\bullet$ ,  $0.25 M NO_3^- + HCOO^-$ ;  $\blacksquare$ ,  $0.2 M H_2O_2 + HCOO^-$ ;  $\blacktriangle$ ,  $0.1 M Cu^{2+} + HCOO^-$ ;  $\blacktriangledown$ ,  $0.25 M NO_3^- + (CH_3)_2CHOH$ ;  $\times$ ,  $(CH_3)_2CO + (CH_3)_2CHOH$ . The dotted line is the best line through the data obtained from solutions containing low  $e_{aq}^-$  scavenger concentrations.

forming reaction (eq 3), the primary H-atom yields will be larger than in pure water. If  $e_{aq}^-$  are efficiently scavenged,  $G_H$  value is lower.

The lowering of  $G_H$  with increasing reactivity toward  $e_{aq}^-$  enables an estimate of the relative contribution of the reactions 1 and 2 to the formation of primary H-atom yields. Comparing the lower curve in Figure 2 in the present work with the Figure 5 in ref 2, which shows the dependence of  $G_{H_2}$  on the reactivity toward  $e_{aq}^-$  and was obtained with the same scavengers under the same conditions, we can see that the scavenging of hydrated electrons influences less efficiently  $G_H$  than  $G_{H_2}$ . The trends of these curves point out that about two-thirds of  $G_H$  originates in reaction 2 and

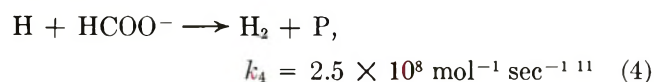
that reaction 1 can be only the source of the remaining one-third of primary yield.

A support that we indeed have the H atoms, and not the long-lived excited water molecules in reaction 1 and/or long-lived  $\text{H}_3\text{O}$  intermediates in reaction 2, can be found in the fact that the rate constants determined in concentrated solutions, in this work, agree reasonably well with the published values which were obtained in dilute solutions (Table IV).

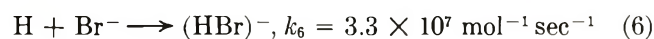
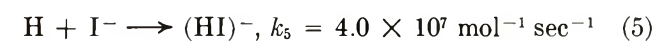
The increase of ionic strength should influence reaction 2 by decreasing its rate constant. Since at the same time also the reaction  $e_{\text{aq}}^- + e_{\text{aq}}^-$  becomes slightly faster, one would expect smaller contribution of reaction 2 to the  $G_{\text{H}}$ . Experiments were made to check this assumption qualitatively. As seen in Table V, the presence of large amounts of inert salts does not influence measured  $G_{\text{H}}$  values in our working conditions.

*Absolute Value of the Primary Atom Yield.* Unlike the primary yield of molecular hydrogen, the published values of  $G_{\text{H}}$  vary considerably, from 0.45 to 0.75.<sup>5,6,12-25</sup> The measurements in this study show that  $G_{\text{H}} = 0.58 \pm 0.05$  in dilute, neutral aqueous solutions. Maximal deviation is somewhat larger than the possible experimental error. The cause of this is not clear; it seems, nevertheless, that it should be rather sought in the choice of HR compound, and some additional source of molecular hydrogen, than in reactions 1 and 2.

*Hydrogen Atom Reactions with Halide Ions.* Competition plots in Figure 1 show that the reaction of hydrogen atoms with formate ions



is in competition with H-atom reactions with halide ions



while  $k(\text{H} + \text{Cl}^-)$  was estimated to be less than  $10^5 \text{ mol}^{-1} \text{ sec}^{-1}$ . Previously, the reaction with  $\text{I}^-$  was observed only in acid solutions where  $\text{H}_2^+$  species, or a termolecular reaction ( $\text{H} + \text{H}^+ + \text{I}^-$ ), were proposed.<sup>10,26</sup> Present study shows that a direct reaction between hydrogen atoms and halide ions is involved. The fate of  $(\text{HI})^-$  or  $(\text{HBr})^-$  could be in an electron-transfer reaction or, as proposed in the case of fluoride ion,<sup>27</sup> in the formation of hydrated electron,  $(\text{HF})^- \rightarrow e_{\text{aq}}^- + \text{HF}$ .

*On the Eventual Scavenging of Positive Ion-Precursors of H Atoms.* The data obtained in the present work enable some remarks on the possibility of influencing the formation of  $G_{\text{H}}$  by scavenging the positive ions. According to Hamill and coworkers, negative ions scavenge efficiently dry  $\text{H}_2\text{O}^+$  or  $\text{H}_3\text{O}^+$ .<sup>28-30</sup> This

might also lead to the depression of the  $\text{H}_3\text{O}_{\text{aq}}^+$  and influence the formation of H-atom yields as given by reaction 2. We have seen, however, that the presence of molar concentrations of perchlorate or sulfate ions does not influence visibly  $G_{\text{H}}$  and, consequently, the reaction important for its formation. The behavior of hydrogen atom yields in the presence of large amounts of formate or nitrate confirms the predictions of the free-radical model, *i.e.*, also excludes the hydronium ion scavenging. Also, our results with halides (Table III) do not confirm the assumption<sup>28,30</sup> that the H atom is the product of reaction between "dry" positive charges and halides: we see that  $G_{\text{H}}$  does not increase with increasing halide concentration.

The behavior of halide ions is, nevertheless, not clear from the point of view of the free-radical model. Halides are known as efficient OH scavengers and an increase in their concentration should, accordingly, lead to an increase in  $G_{\text{H}}$  as other OH scavengers in Figure 2. The data in Table III show that this is not the case and that the observed  $G_{\text{H}}$  decrease with increasing concentrations of halide ions. It looks as if the reaction  $\text{H}_3\text{O}_{\text{aq}}^+ + \text{X}^- \rightarrow \text{HX} + \text{H}_2\text{O}$  takes place. If so, it would be our only indication that the positive ion-precursor of the H atom is scavenged. However, more experimental proof is needed as the expected increase in  $G_{\text{H}}$  could well be masked by a reaction, occurring in competition with  $\text{H} + \text{HR}$ , where H atoms are consumed and  $G_{\text{H}}$  only apparently lowered.

*Acknowledgment.* The authors wish to thank Mr. N. Stančić and Mr. M. Borovičanić for the technical assistance.

- (12) J. Allan and G. Scholes, *Nature (London)*, **187**, 218 (1960).
- (13) J. Rabani and G. Stein, *J. Chem. Phys.*, **37**, 1865 (1962).
- (14) S. Nehari and J. Rabani, *J. Phys. Chem.*, **67**, 1609 (1963).
- (15) J. Allan and C. Beck, *J. Amer. Chem. Soc.*, **86**, 1483 (1964).
- (16) G. Scholes and M. Simić, *J. Phys. Chem.*, **68**, 1738 (1964).
- (17) J. Allan, *ibid.*, **68**, 2697 (1964).
- (18) E. Hayon and M. Moreau, *J. Chim. Phys.*, **62**, 391 (1965).
- (19) M. Haissinsky, *ibid.*, **62**, 1141 (1965).
- (20) T. Sawai, *Bull. Chem. Soc. Jap.*, **39**, 955 (1966).
- (21) H. Mahlman, *J. Phys. Chem.*, **70**, 3983 (1966).
- (22) Z. Draganić, O. Mičić, and M. Nenadović, *ibid.*, **72**, 511 (1968).
- (23) J. Buxendale and A. Khan, *Int. J. Radiat. Phys. Chem.*, **1**, 11 (1969).
- (24) A. Appleby and H. Schwarz, *J. Phys. Chem.*, **73**, 1937 (1969).
- (25) M. Nenadović, Z. Draganić, and I. Draganić, Proceedings of the 3rd Tihany Symposium on Radiation Chemistry, J. Dobo and P. Hedvig, Ed., Akademiai Kiado, Budapest, 1972, in press.
- (26) G. Czapski, J. Jortner, and G. Stein, *J. Phys. Chem.*, **63**, 1769 (1959).
- (27) M. Anbar and P. Neta, *Trans. Faraday Soc.*, **63**, 141 (1967); M. Anbar and E. Hart, *J. Phys. Chem.*, **71**, 4163 (1967).
- (28) P. Bevan and W. Hamill, *Trans. Faraday Soc.*, **66**, 2533 (1970).
- (29) T. Sawai and W. Hamill, *J. Phys. Chem.*, **74**, 3914 (1970).
- (30) S. Khorana and W. Hamill, *ibid.*, **75**, 308 (1971).

# The Higher Excited States in Metal-Ammonia Solutions. I. The 2s State<sup>1</sup>

by J. Logan and N. R. Kestner\*

Department of Chemistry, Louisiana State University, Baton Rouge, Louisiana 70803 (Received March 27, 1972)

Publication costs assisted by the Alfred P. Sloan Foundation

Using the model of Kestner, Copeland, and Jortner, the energy of the 2s state in low concentration metal-ammonia solutions is calculated. With a coordination number of 4 and  $V_0 = 0$  eV, we predict that it lies about 0.25 eV above the energy of the 1s  $\rightarrow$  2p transition, *i.e.*, at any energy corresponding to the high energy tail of the observed allowed transition. Experimental confirmation of the location of this state should be possible.

## I. Introduction

There have been many calculations of the allowed optical excitations of a localized electron in liquid ammonia.<sup>2,3</sup> These studies have all been consistent with the idea of an electron localized in a cavity. Nevertheless, details such as the broad and very asymmetric form of the transition have not been explained. In addition, previous work does not rule out completely alternative descriptions of the state of the trapped electron.

Because of the qualitative success of our early work on the calculation of the static properties of trapped electrons in polar liquids,<sup>3</sup> we are extending our research on this subject in two directions: first, we are studying relaxation phenomena and factors relating to line shape, etc., and second, we are studying other features of this trapped species such as other excited states and the effects of liquid density. In this paper we report on calculations relating to the location of the first excited s state of the model, namely the 2s state. This state is of quite different symmetry from the excited state and thus experimental confirmation of its location would provide more evidence supporting the model we have used. It is only by studying all aspects of this problem that a given model can be substantiated.

## II. Calculations

Using a model developed by Copeland, Kestner, and Jortner<sup>3</sup> for the description of localized excess electron states in polar solvents, we can calculate the energy of the 2s excited state in dilute metal-ammonia solutions. The model consists of an electron in a cavity, the boundary of which is formed by a small number of symmetrically distributed solvent molecules. Discrete interactions of the electron with solvent molecules are considered only for the first solvation layer, the remainder of the solution being treated as a continuum. The localization of the electron is due to the short-range attractive interaction of the electron with the permanent dipole moments of the nearest-neighbor solvent molecules, a long-range polarization of the continuum which leads to a potential acting back on the

electron (the Landau potential), and short-range repulsive interactions between the electron and solvent molecules. For the formation of an energetically stable cavity it is necessary to introduce the electronic polarization and medium rearrangement energy.<sup>3</sup> Previous calculations of ground state and first excited p state using this model are in qualitative agreement with many of the observed properties of dilute metal-ammonia solutions. Calculations reported in this work were done with the refined potential (model 3)<sup>4</sup> and with a more extensive trial function that allowed us to calculate the energy of the 2s state, *i.e.*, the first excited s state orthogonal to the ground state.

The "model 3" potential for the determination of the electronic energy has the form<sup>3</sup>

$$\begin{aligned} V(r) &= -\frac{N\mu_0 e \langle \cos \theta \rangle}{r_d^2} - \frac{\beta e^2}{r_c} \quad (0 < r < R) \\ &= -\frac{N\mu_0 e \langle \cos \theta \rangle}{r_d^2} - \frac{\beta e^2}{r_c} + V_0 \quad (R < r < r_d) \\ &= -\frac{\beta e^2}{r} + V_0 \quad (r_d < r) \end{aligned}$$

with

$$\beta = \left( \frac{1}{D_{op}} - \frac{1}{D_s} \right)$$

(1) Work supported in part by the National Science Foundation.

(2) R. A. Ogg, *J. Chem. Phys.*, **14**, 114, 295 (1946); W. N. Lipscomb, *ibid.*, **21**, 52 (1953); R. A. Stairs, *ibid.*, **27**, 1431 (1957); J. Jortner, *ibid.*, **30**, 839 (1959); *Radiat. Res. Suppl.*, **4**, 24 (1964); J. Jortner and N. R. Kestner in "Metal-Ammonia Solutions, Proceedings of Colloque Weyl II," J. J. Lagowski and M. J. Sienko, Ed., Butterworths, London, 1971, p 49; D. E. O'Reilly, *J. Chem. Phys.*, **41**, 3736 (1964); R. H. Land and D. E. O'Reilly, *ibid.*, **46**, 4496 (1967).

(3) D. A. Copeland, N. R. Kestner, and J. Jortner, *ibid.*, **53**, 1189 (1970).

(4) There are two errors in the equations of ref 3. Equation 27 should read

$$S_i = -\frac{N\alpha C_i^2}{r_d^4} - \frac{1}{2}(e\gamma_0)C_i^2/r_c^2$$

and eq 33 should read

$$\mu_T = \mu_0 \langle \cos \theta \rangle + e\alpha C_i^2/r_d$$

where  $C_i$  is either  $C_s$  or  $C_p$ . In addition, line 2 of Table I of ref 3 contains two misprints. That line should read

6	5204.7	1.414	0.600
---	--------	-------	-------

**Table I:** Results for the Most Stable Cavity Radius

$V_0$	$R_0$ , Å	Total energies, eV			Transition energies, eV		Estimated <sup>b</sup> line width, eV		$dh\nu/dT^c$	
		1s state	2p state	2s state	1s → 2p	1s → 2s	1s → 2s	1s → 2p	1s → 2s	1s → 2p
$N = 4, T = 203^\circ\text{K}$										
0.5	1.75	-0.677 (-0.537) <sup>a</sup>	0.651	0.869	1.328	1.546				
0	1.7	-1.053 (-0.909) <sup>a</sup>	0.147	0.394	1.200	1.447	0.124	0.12	-8.1 cm <sup>-1</sup> /°K	-7.3 cm <sup>-1</sup> /°K
-0.5	1.7	-1.454 (-1.30) <sup>a</sup>	-0.361	0.114	1.093	1.340	0.112	0.112		
$N = 6, T = 203^\circ\text{K}$										
-0.5	2.15	-1.480 (-1.294) <sup>a</sup>	-0.269	0.0675	1.211	1.548				
0.0	2.1	-1.156 (-0.972) <sup>a</sup>	0.213	0.533	1.369	1.689				

<sup>a</sup> Calculated using only a one-term wave function, *i.e.*,  $C_{2i} = C_{3i} = 0$ . <sup>b</sup> Estimated half-line width: if  $X_1$  and  $X_2$  are points on the ground-state energy curve where  $|E(X_1) - E(R_0)| = |E(X_2) - E(R_0)| = kT$ , the half-line width is approximately  $|\hbar\nu(X_1) - \hbar\nu(X_2)|$ . <sup>c</sup> Determined from data calculated at 278 and 203°K. A linear dependence on temperature was assumed.

where  $N$  is the number of molecules on the surface of the cavity (the best numbers to use being 4 and 6),  $r_d$  is the distance to the beginning of the continuum, and  $R$  is the configurational parameter defining the mean cavity radius.  $D_{op}$  and  $D_s$  are the optical and static dielectric constants;  $\mu_0$  is the dipole moment of the ammonia molecule. The average value of the cosine of the angle between the radius vector and the dipole moment vector is included to account for the fact that the dipoles are not rigidly oriented. It is evaluated using the Langevin relationship for the temperature and enclosed charge in question.

The first term in the potential is the charge-dipole interaction which is considered to act up to the center of the dipole. The second term is the previously mentioned Landau potential.  $V_0$  is representative of the energy of the electron in its "quasi-free" (unlocalized) state and is expected to be in the range  $-0.5 \text{ eV} < V_0 < 0.5 \text{ eV}$ , for liquid ammonia.

The basis set for the trial wave functions was composed of Slater-type 1s, 2s, and 3s functions incorporating three nonlinear variational parameters,  $A$ ,  $D$ , and  $G$ . Any one s orbital is a linear combination of each of these

$$\psi_i = c_{1i}e^{-Ar} + c_{2i}re^{-Dr} + c_{3i}r^2e^{-Gr}$$

For efficient evaluation orthogonal functions were first constructed by the Schmidt procedure. The eigenvalue problem was solved numerically for given values of  $A$ ,  $D$ , and  $G$  using the IBM program EIGEN. The best values of  $A$ ,  $D$ , and  $G$  were found by a brute-force search. The lowest eigenvalue along with the electronic polarization energy was taken to represent the ground-state (1s) electronic energy with the remaining two representing the excited states. The best energy for the ground state was determined by varying  $A$ ,  $D$ , and  $G$ .

The medium rearrangement energy was treated in the same manner as in the work of Copeland, Kestner, and Jortner.<sup>3</sup> In the calculations of the 2s excited state it is assumed that the ground-state wave function deter-

mines the orienting field for the permanent dipoles, while other polarizations change in response to the excited state.

For specific values of  $N$ , the ground-state and excited-state energies were determined as functions of  $R$ . The value of  $R$  corresponding to the minimum of the ground state energy is the most stable cavity radius,  $R_0$ .

The important results of the calculations are summarized in Table I. In all cases the 2s state lies slightly above the 2p state,  $\sim 0.25 \text{ eV}$  for  $N = 4$  and  $\sim 0.35$  for  $N = 6$ . The ordering of the 2s and 2p states is therefore more typical of an electron in a spherical box<sup>5</sup> than of an electron in a long range coulombic interaction. The calculated temperature dependence exhibits the expected shift to lower energy with increasing temperature, being approximately the same for both 1s → 2s and 1s → 2p transitions.

The optimum value of  $N$  seems to be about 4 in agreement with earlier work.<sup>3</sup> This is in reasonable agreement with the results of several experimentalists<sup>6</sup> but is smaller than that suggested by one more recent investigation.<sup>7</sup>

### III. Discussion of Results

These results indicate that the 1s → 2s transition energy is probably located at an energy corresponding to the high-energy tail of the 1s → 2p transition. In order to confirm the location of this state, however, this should present no problem. The most reasonable way to look for the 2s state would be *via* a two-photon process using a laser source. Because its energy is

(5) W. Kauzman, "Quantum Chemistry," Academic Press, New York, N. Y., 1957, p 188.

(6) E. Catterall in "Metal-Ammonia Solutions, Proceedings of Colloque Weyl II," J. J. Lagowski and M. J. Sienko, Ed., Butterworths, London, 1970, p 105; R. Cotterall, *Nature (London)*, **229**, 10 (1971); K. G. Breitschwerdt and H. Radscheit, *Ber. Bunsenges. Phys. Chem.*, **75**, 644 (1971). These authors all obtain estimates of  $N$  below 15 and generally closer to 6.

(7) R. A. Pinkowitz and T. J. Swift, *J. Chem. Phys.*, **54**, 2858 (1971). These authors from nitrogen magnetic relaxation data obtain a coordination number closer to 30 but this must include molecules other than those in the first coordination layer.

similar to that for the  $1s \rightarrow 2p$  transition the intensity should be quite strong. One possible difficulty which could present problems is the liquid ammonia absorptions in the region  $15,300\text{--}23,000 \text{ \AA}$  ( $0.81\text{--}0.54 \text{ eV}$ ).<sup>8</sup> Although our calculations predict that the transition energy is about  $1.5 \text{ eV}$  corresponding to a single photon energy of  $0.75 \text{ eV}$ , our model energies are probably too high just as in the case of the allowed transition. Thus it is more likely that the  $2s$  state could be studied best with photons closer to  $0.6 \text{ eV}$  ( $20,000 \text{ \AA}$ ) in which case solvent absorption is not as severe. It would be even more

advantageous to use deuterioammonia as it has a narrower absorption spectrum in this region.<sup>6</sup> The  $2s$  state should be located at about the same energy in the  $\text{ND}_3$  system.

An experimental study of the line shape of the  $1s \rightarrow 2s$  transition would be especially interesting as it could provide clues to the reasons for the broad asymmetric lines observed in the allowed spectrum.

(8) D. F. Burrow and J. J. Lagowski in "Solvated Electron," E. J. Hart, Ed., American Chemical Society, Washington, 1965, p 125.

## An Examination of the Overspeeding Technique in Relation to Sedimentation Equilibrium

by G. J. Howlett and L. W. Nichol\*

*Department of Physical Biochemistry, John Curtin School of Medical Research, Australian National University, Canberra, A.C.T., 2601, Australia (Received February 11, 1972)*

Numerical calculations based on previously developed theory are presented to show that the total time required for a single noninteracting solute to attain sedimentation equilibrium is reduced by initially overspeeding the rotor. The calculations are employed to provide an approximate relation between the angular velocity of overspeeding and that selected for the final attainment of equilibrium. This relation is employed to construct graphs from which may be estimated a suitable time for overspeeding and the additional time required to reach equilibrium after the reduction of the angular velocity. The treatment pertains to sedimentation equilibrium experiments in which the ratio of the concentration at the base of the cell to that at the meniscus is relatively low at equilibrium. It is illustrated with an experiment performed using lysozyme.

Van Holde and Baldwin<sup>1</sup> made the valuable suggestion that the time to attain sedimentation equilibrium could be considerably reduced by employing short column lengths of solution. Later, a method<sup>2</sup> was described for reducing this time further by initially accelerating the rotor to a constant angular velocity  $\omega'$  before reducing the velocity to a value  $\omega$ , selected to give a measurable final distribution. Although theoretical treatments<sup>2,3</sup> have been presented to permit the calculation of a suitable time,  $t'$ , to maintain the larger velocity ( $\omega'$ ), little comment has been made on a suitable value of  $\omega'$  or on the total time required to obtain equilibrium after an initial overspeeding. Teller, *et al.*,<sup>4</sup> have considered these questions in relation to experiments conducted at high speeds according to the meniscus-depletion method of Yphantis<sup>5</sup> and concluded that no simple relation could be formulated between  $\omega$  and  $\omega'$  to guide the design of the experiment and moreover that incorrect selection of  $t'$  could in some cases extend the total time required to reach equi-

librium. It is the purpose of this work to use the equations of Hexner, *et al.*,<sup>2</sup> to examine these points for situations where lower speeds are employed so that the ratio of the concentration at the base to that at the meniscus at equilibrium is smaller than found in meniscus-depletion experiments.<sup>5</sup> The discussion is restricted to consideration of a single noninteracting solute, but it leads to an approximate relation between  $\omega$  and  $\omega'$  and to graphical interpolation procedures for the estimation of the total time required to attain equilibrium, potentially valuable information for the experimenter.

(1) K. E. Van Holde and R. L. Baldwin, *J. Phys. Chem.*, **62**, 734 (1958).

(2) P. E. Hexner, L. E. Radford, and J. W. Beams, *Proc. Nat. Acad. Sci. U. S.*, **47**, 1848 (1961).

(3) E. G. Richards, D. C. Teller, and H. K. Schachman, *Biochemistry*, **7**, 1054 (1968).

(4) D. C. Teller, T. A. Horbett, E. G. Richards, and H. K. Schachman, *Ann. N. Y. Acad. Sci.*, **164**, 66 (1969).

(5) D. A. Yphantis, *Biochemistry*, **3**, 297 (1964).

When a homogeneous solution of a single ideal solute of concentration  $c_0$  is subjected to an angular velocity of  $\omega'$  for time  $t'$  and subsequently spun at a lower velocity  $\omega$  for time  $t$ , the concentration as a function of position and of time is given by eq 7 of Hexner, *et al.*,<sup>2</sup> which is reproduced below with certain corrections

$$\frac{c(y,t)}{c_0} = \frac{e^{y/\alpha}}{\alpha(e^{1/\alpha} - 1)} + e^{y/2\alpha} \sum_{m=1}^{\infty} \frac{A_m e^{-P_m t/\beta'} (\sin m\pi y + 2\pi m\alpha \cos m\pi y)}{1 + 4\alpha^2 m^2 \pi^2} \quad (1a)$$

where

$$A_m = \frac{(2\pi m - 4\alpha m\pi Q)(1 - (-1)^m e^Q)}{\alpha'(e^{1/\alpha'} - 1)(Q^2 + m^2\pi^2)} + 16\alpha'^2\pi \times \sum_{n=1}^{\infty} \frac{ne^{-P_n t'/\beta'} (1 - (-1)^n e^{-1/2\alpha'}) (1 - (-1)^{m+n} e^{R}) F_{m,n}}{(1 + 4\alpha'^2 n^2 \pi^2)^2} \quad (1b)$$

and

$$F_{m,n} = \frac{2\pi^2(m+n)(\alpha'n + \alpha m) + R(1 - 4\pi^2\alpha\alpha'mn)}{R^2 + (m+n)^2\pi^2} + \frac{2\pi^2(m-n)(\alpha'n - \alpha m) - R(1 + 4\alpha\alpha'mn\pi^2)}{R^2 + (m-n)^2\pi^2} \quad (1c)$$

The symbols are those adopted by Hexner, *et al.*,<sup>2</sup> and are familiar except for the following:  $a$  and  $b$  are the positions of the meniscus and base of the cell, respectively;  $y$  is a reduced distance variable,  $(r - a)/(b - a)$ ;  $\alpha = 2RT/M(1 - \bar{v}\rho)\omega^2(b^2 - a^2)$ ;  $\beta = 2(b - a) \cdot RT/M(1 - \bar{v}\rho)\omega^2 D(b + a)$ ;  $Q = (1/\alpha') - (1/2\alpha)$ ;  $R = (1/2\alpha') - (1/2\alpha)$ , and  $P_m = \alpha m^2 \pi^2 + (1/4\alpha)$ . The quantities  $\alpha'$ ,  $\beta'$ , and  $P_n'$  follow directly by substituting  $\omega'$  for  $\omega$  in the relevant expressions defined above.

At equilibrium the ratio of the concentrations at the base and meniscus,  $c_b/c_a = e^{1/\alpha}$ : for example, the ratio equals 148 when  $\alpha = 0.2$  and 1.65 when  $\alpha = 2$ . The present work is concerned with this range of  $\alpha$ , since Teller, *et al.*,<sup>4</sup> have already considered the range  $\alpha \leq 0.2$  (the meniscus-depletion design). The distinction is important since the exponential containing  $t$  in the second term of eq 1a converges rapidly as  $m$  increases for relatively large values of  $\alpha$  and thus, for these cases, the equilibrium distribution which is represented by the first term in eq 1a is reasonably approximated<sup>2</sup> when  $A_1 = 0$ . Substitution of  $A_1 = 0$  in eq 1b yields, as noted previously<sup>2</sup>

$$\frac{-(2\pi - 4\alpha\pi Q)(1 + e^Q)(1 + 4\alpha'^2\pi^2)^2}{16\alpha'^3\pi(e^{1/\alpha'} - 1)(Q^2 + \pi^2)(1 + e^{-1/2\alpha'}) (1 - e^R) F_{1,1}} = e^{-P_1 t'/\beta'} \quad (2)$$

where only the first term in the series in  $n$  has been taken and  $F_{1,1}$  is given by eq 1c. As Teller, *et al.*,<sup>4</sup>

have pointed out, when  $\alpha \leq 0.2$  it is necessary to consider more terms in the  $F_{m,n}$  and  $A_m$  series.

For a particular set of values of  $\alpha$  and  $\alpha'$ , it is possible to use eq 2 to calculate the corresponding value of  $t'/\beta'$  which is proportional to the time for overspeeding suggested on the basis that  $A_1 = 0$ . The corresponding values of  $A_m$  follow from eq 1b. In turn, eq 1a may be employed to evaluate  $c(y,t)/c_0$  as a function of  $y$  for different values of  $t/\beta$ . In numerical solutions which follow, only the first five terms of the summations in eq 1a and 1b were taken as the series were seen to converge rapidly. As  $t/\beta$  was increased, the values of  $c(y,t)/c_0$  approached the equilibrium distribution represented by the first term in eq 1a, and a value of  $t/\beta$  was selected when the maximum difference at any position was 0.1%. This represents a realistic criterion for equilibrium in terms of available precision for measuring optical records.<sup>1</sup> In summary, the procedure thus far gives corresponding values of  $t'/\beta'$  and  $(t/\beta)_e$  (according to the equilibrium criterion) for given values of  $\alpha$  and  $\alpha'$ . In order to proceed, it is convenient to define the quantities

$$\phi = \alpha(t/\beta)_e = tD/(b - a)^2 \quad (3a)$$

$$\phi' = \alpha'(t'/\beta') = t'D/(b - a)^2 \quad (3b)$$

where  $D$  is the diffusion coefficient. It follows that  $\phi + \phi' = \psi$  is directly proportional to the total time  $(t + t')$  and that  $\psi$  may be computed for given values of  $\alpha$  and  $\alpha'$ .

Figure 1 shows the variation of  $\psi$  with  $\alpha'$  at a fixed value of  $\alpha$  equal to unity. Clearly, there exists a minimum value  $\psi_{\min}$  at  $\alpha'_{\min}$ . Similar calculations using a range of values of  $\alpha$  permitted evaluation of  $\alpha'_{\min}$  for each value of  $\alpha$ , their relationship being shown in Figure 2. If an estimate of  $M(1 - \bar{v}\rho)$  is available (for example, from a preliminary Archibald experiment),  $\alpha$  may be calculated for selected values of  $\omega$ ,  $T$ , and  $(b^2 - a^2)$ , whereupon Figure 2 yields the corresponding value of  $\alpha'$  and hence  $\omega'$ . Two further points in relation to Figure 2 merit comment. First, little significance should be attached to points corresponding to  $\alpha \leq 0.2$ , since the minima (Figure 1) observed by us in this range may have been a consequence of initially neglecting higher terms in the  $F_{m,n}$  and  $A_m$  series important in this range.<sup>4</sup> Secondly, it is of interest that a line described by the relation  $\alpha'_{\min} = 0.5\alpha$  fits Figure 2 to a first approximation in the range  $0.2 < \alpha < 1.5$ . Substitution of this relation into the definition of  $\alpha$  leads to  $\omega'_{\min} = 1.4\omega$ . Richards<sup>6</sup> arbitrarily selected to overspeed the rotor at 1.4 times the equilibrium velocity, the present approach vindicating the choice for the indicated range of  $\alpha$ .

If the relation  $\alpha'_{\min} = 0.5\alpha$  is adopted, it is now possible to obtain  $\psi_{\min}$  as a function of  $\alpha$  alone. This re-

(6) E. G. Richards, Doctoral Dissertation, Department of Biochemistry, University of California, Berkeley, Calif., 1960.



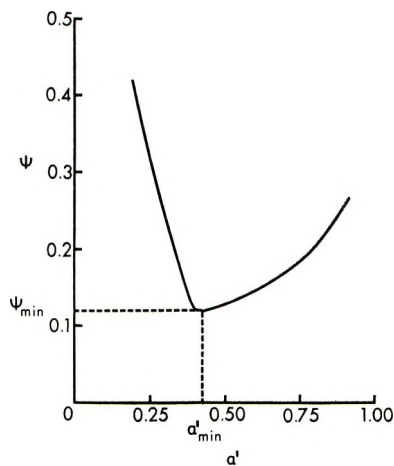


Figure 1. An illustration (for  $\alpha = 1$ ) of the existence of a minimum in the plot of  $\psi$  against  $\alpha'$ . Parameters defined in the text.

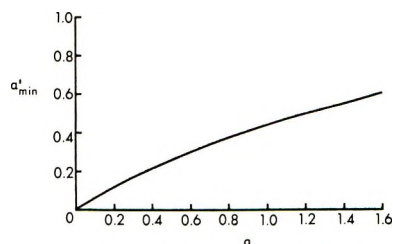


Figure 2. A graph of values of  $\alpha'_{\min}$  obtained from plots of the type shown in Figure 1 vs.  $\alpha$ .

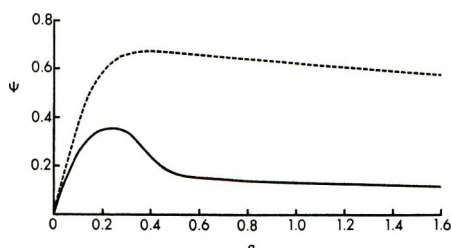


Figure 3. A comparison of the total times required to attain sedimentation equilibrium calculated on the basis of a procedure incorporating overspeeding (—) and one omitting overspeeding. In both cases the ordinate values ( $\psi$ ) are directly proportional to the total time required to attain equilibrium while  $\alpha$  is inversely proportional to the square of the angular velocity.

lation is shown by the solid curve in Figure 3. The broken curve was calculated using the equations of Van Holde and Baldwin<sup>1</sup> with the criterion for equilibrium specified earlier: it refers to a situation where the overspeeding technique has not been adopted. The value of  $\psi$  in this case is directly analogous to  $F(\alpha)$  as defined by eq 11 of Van Holde and Baldwin<sup>1</sup> and is related to the total time for equilibration by the same proportionality constant as appears in eq 3. Comparison of the two curves shows that there is a substantial reduction in the total time required to reach

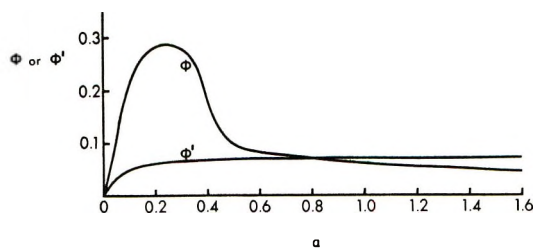


Figure 4. Relationships between  $\alpha$  and  $\phi'$  and  $\phi$  calculated on the basis that  $\alpha'_{\min} = 0.5\alpha$ .  $\phi'$  and  $\phi$  are, respectively, proportional to the times the experiment is conducted at the higher and lower angular velocities (see eq 3).

equilibrium when the overspeeding technique is adopted. The establishment of this point is important, particularly as the calculations were based on the approximate relation  $\alpha'_{\min} = 0.5\alpha$  and have neglected higher terms in the  $F_{m,n}$  and  $A_m$  series in the calculation of  $t'/\beta'$ .

Although comment has been made on the velocity of overspeeding and the total time required to reach equilibrium, the question remains as to the time recommended for overspeeding prior to the reduction of the angular velocity to  $\omega$  for the remaining time. Again using the relation  $\alpha'_{\min} = 0.5\alpha$ , it is possible to proceed as described above to calculate  $\phi$  and  $\phi'$  (eq 3) as a function of  $\alpha$ . The results are shown in Figure 4. The two curves are the components of the summed curve shown in Figure 3 (solid). If Figure 4 is to be used by the experimenter to estimate  $t'$  and the total time, it should be recalled that it is based on the use of an overspeeding velocity 1.4 times greater than the final  $\omega$ , rather than on a refined value of  $\omega'$  derivable from Figure 2. The advantages of employing the former value of  $\omega'$ , which may only approximate the optimal value, is that it will lead to a reduction in total time (Figure 3) and to values of  $\phi'$  (and hence  $t'$ ) which are relatively insensitive to the value of  $\alpha$  in the range  $0.2 < \alpha < 2$  (Figure 4). In contrast, it appears that  $\phi'$  is considerably more sensitive to a variation in  $\alpha$  when  $\alpha \leq 0.2$  which could lead to uncertainty in the estimation of  $t'$ . Teller, *et al.*,<sup>4</sup> have shown that incorrect selection of  $t'$  for low values of  $\alpha$  could negate the use of the overspeeding technique.

The application of the present approach is illustrated with a particular example. A solution of lysozyme was subjected to sedimentation equilibrium in acetate buffer pH 5.0, ionic strength 0.15 at 20°, environmental conditions where the enzyme is known to exist as a monomeric form of molecular weight<sup>7</sup> 14,400, diffusion coefficient<sup>7</sup>  $1.1 \times 10^{-6}$  cm<sup>2</sup> sec<sup>-1</sup>, and partial specific volume<sup>8</sup> 0.726 cm<sup>3</sup>/g. A value of  $\omega$  equal to 20,000 rpm was employed with  $a = 6.88$  cm and  $b = 7.15$  cm.

(7) A. J. Sophianopoulos, C. K. Rhodes, D. N. Holcomb, and K. E. Van Holde, *J. Biol. Chem.*, **237**, 1107 (1962).

(8) R. C. Deonier and J. W. Williams, *Biochemistry*, **9**, 4260 (1970).

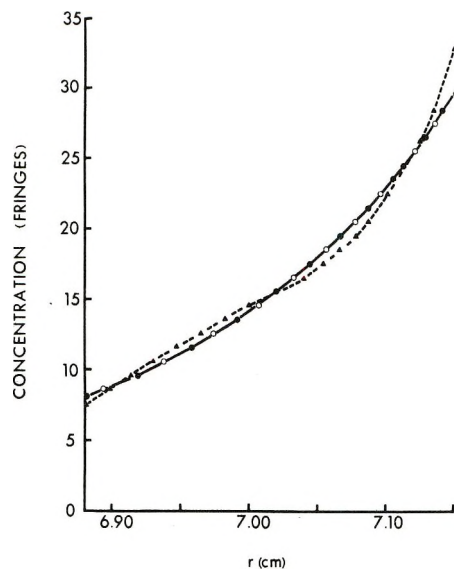


Figure 5. Plots of concentration *vs.* radius (*r*) obtained from photographs taken at different times during a sedimentation equilibrium experiment conducted with a lysozyme solution of initial concentration 16.65 fringes in acetate buffer pH 5.0, ionic strength 0.15 at 20°. The solution was subjected to overspeeding at an angular velocity of 28,000 rpm for 1.2 hr and then run at 20,000 rpm. The total times of centrifuging were as follows: ▲, 1.2 hr; ○, 2.4 hr; ●, 5 hr.

With these quantities, a value of 0.75 was calculated for  $\alpha$  and from Figure 4 the corresponding values of  $\phi$  (0.07) and  $\phi'$  (0.07) were interpolated. Equation 3 was used to calculate the corresponding values of  $t$  and  $t'$  (both  $\sim 1.2$  hr). Thus the experimental design sug-

gested on the basis of the present theoretical approach involves overspeeding at 28,000 rpm ( $\omega' = 1.4\omega$ ) for 1.2 hr followed by an equal period of time at 20,000 rpm to attain the equilibrium state. The results of an experiment of this design are presented in Figure 5. It is clear that after 1.2 hr of overspeeding the equilibrium distribution is closely approximated and that after a total time of 2.4 hr, sedimentation equilibrium has been attained as judged from the identity of the patterns obtained after 2.4 and 5 hr. Further evidence that the system has reached equilibrium after a total time of 2.4 hr is provided by the observation that the derived apparent molecular weight was 14,500 in agreement with the previously reported value.<sup>7,8</sup>

In summary, whereas Teller, *et al.*,<sup>4</sup> have shown that the overspeeding technique may not be generally useful in relation to meniscus-depletion experiments, the present approach suggests that the method may be helpful in the study of single noninteracting solutes when  $\alpha > 0.2$ . For these values of  $\alpha$ , which permit study over a wider total concentration range than in the meniscus-depletion method, it is hoped that the formulation of the approximate relation  $\omega' = 1.4\omega$  and the presentation of Figure 4 from which estimates of  $t'$  and the total time may be interpolated may be useful to the experimenter. On the other hand, the present approach is not advocated if use of an angular velocity 1.4 times greater than the equilibrium velocity results in gel formation at the base of the cell or in the study of mixtures of solutes of widely different molecular weight, for which values of  $\alpha$  may span a wide range.

# Quasi-Elastic Light Scattering from Two-Component Mixtures<sup>1a</sup>

by W. W. Wilson<sup>1b</sup> and Charles S. Johnson, Jr.\*<sup>1c</sup>

Department of Chemistry, University of North Carolina, Chapel Hill, North Carolina 27514 (Received April 13, 1972)

Publication costs assisted by the National Science Foundation

Laser light beating spectroscopy of the homodyne type was used to measure the spectrum of light scattered from solutions of latex spheres, BSA, lysozyme, RNase, and mixtures of BSA and lysozyme with latex spheres. It was found for solutions containing two scattering components that the data could be satisfactorily analyzed to obtain diffusion constants by using a least-squares fit to a sum of two Lorentzian curves. A single Lorentzian curve was inadequate regardless of the selection of data points used in the analysis. In the case of RNase only one Lorentzian component could be distinguished; however, chromatography showed the presence of dimers and tetramers of RNase as well as the monomer. Details of the analysis are discussed.

## I. Introduction

It is well established that quasi-elastic light scattering provides an accurate and convenient method for the determination of diffusion constants for macromolecules in solution.<sup>2</sup> A number of studies of scattering from dilute solutions of monodisperse latex spheres have been reported,<sup>3,4</sup> and the method has recently been applied to the study of biological molecules.<sup>5-7</sup> In one such study, Rimai, *et al.*, investigated scattering from solutions of RNase.<sup>7</sup> In their work non-Lorentzian line shapes were observed, which apparently indicated that particles of at least two different diameters were involved in the scattering. Similar spectra were also simulated by preparing mixtures of bovine serum albumen (BSA) with latex spheres.

Scattering from two-component mixtures has also been studied by Thompson, who obtained apparent line widths as a function of the concentration ratio from the wing of the power spectrum.<sup>8</sup> In some cases it appears to be advantageous to add large particles to a solution to act as "local oscillators" in the scattering experiment, but there is the difficulty that large particles or aggregates may be unexpectedly present. Also, ubiquitous dust may be difficult to remove. It has, in fact, been suggested that dust be used to provide a two-component scattering mixture.<sup>9</sup>

Uncertainties in the analysis of self-beat spectra for solutions of macromolecules that possibly contain more than one scattering component have prompted us to study scattering from two-component mixtures in detail. In particular, we have attempted to establish procedures for extracting the diffusion constant of the smaller particle in a way that is insensitive to the concentration ratio. We have investigated least-squares fits to experimental data using single Lorentzian functions and sums of two and three Lorentzian functions. The sensitivity of the results to the signal-to-noise ratio and the frequency range sampled by the data points, as well as to the concentration ratio, has also been investigated.

In this work mixtures of BSA and lysozyme with latex spheres have been used. To anticipate the results, we have found that regardless of the frequency range used for the data points a single Lorentzian fit does not permit a reliable measurement of the width of the cross term in the self-beat spectrum. The diffusion constant for the smaller particle can, therefore, not be accurately determined. On the other hand, a least-squares fit using the sum of two Lorentzian curves can establish the width of the cross term for a considerable range of concentration ratios. Because of the relative intensities involved, this analysis must fit the narrow, intense component of the spectrum, which arises from the larger particle, and the cross term, rather than the cross term and the broad component arising from the smaller particle. Mixtures analyzed by this procedure give values of the diffusion constants for BSA and lysozyme in agreement with previous studies. A solution of RNase in 0.2 M sodium phosphate at pH 6.47 gave no evidence of more than one component when properly prepared. In this case a single Lorentzian curve was sufficient.

## II. Experimental Section

*Spectrometer.* A standard self-beating spectrometer

(1) (a) Supported in part by grants from the National Science Foundation and the UNC Materials Research Center (Contract No. DAHC15 67 CO223 with the Advanced Research Projects Agency); (b) National Defense Education Act Fellow; (c) Alfred P. Sloan Research Fellow, 1966-1972.

(2) B. Chu, *Annu. Rev. Phys. Chem.*, **21**, 145 (1970).

(3) H. Z. Cummins, N. Knable, and Y. Yeh, *Phys. Rev. Lett.*, **12**, 150 (1964).

(4) F. T. Arecchi, M. Giglio, and U. Tartari, *Phys. Rev.*, **163**, 186 (1967).

(5) S. B. Dubin, J. H. Lunacek, and G. B. Benedek, *Proc. Nat. Acad. Sci. U. S.*, **57**, 1164 (1967).

(6) H. Z. Cummins, F. D. Carlson, T. J. Herbers, and G. Woods, *Biophys. J.*, **9**, 518 (1969).

(7) L. Rimai, J. T. Hickmott, Jr., T. Cole, and E. R. Carew, *ibid.*, **10**, 20 (1970).

(8) D. S. Thompson, *J. Chem. Phys.*, **54**, 1411 (1971).

(9) D. M. McQueen and J. J. Hermans, *Proc. Kon. Ned. Akad. Wetensch. Ser. B*, **74**, 457 (1971).

was constructed as shown in Figure 1.<sup>10</sup> At least 50 mW of incident power at 6328 Å was provided by a SpectraPhysics 125A He-Ne laser, and an argon ion laser (Coherent Model 54) supplied about 200 mW of power at 4880 or 5145 Å.<sup>11</sup> The light scattered from the sample at an angle  $\theta$  to the incident beam was collected and focused onto the surface of an RCA 7265 photomultiplier tube. The resulting photocurrent was then analyzed using a Singer Panaramic Model MF-5 spectrum analyzer with a UR-3 audio plug-in module, and the spectra were accumulated using a TMC 400 computer of average transients (CAT).

**Data Analysis.** When a satisfactory signal-to-noise ratio had been obtained, the spectrum accumulated in the CAT was displayed on a strip-chart recorder, and a punched paper tape was prepared using a Digital Specialties analog to digital converter and a teletype unit. The output signal  $S(\nu)$  is given by

$$S(\nu) = \sqrt{P(\nu) + N + Z}$$

where  $P(\nu)$  is the power spectrum of the photocurrent,  $N$  is the frequency-independent shot noise, and  $Z$  is the zero level of the instrument. The first steps in the analysis consist of subtracting the instrument zero and then squaring the data to obtain the intensities  $I(\nu)$  given by

$$I(\nu) = P(\nu) + N$$

The frequency response of the detection system was measured using a flashlight bulb.<sup>10</sup> Neutral density filters permitted the intensity to be adjusted to the same level as that found in a scattering experiment, and the spectrum of the white noise was then obtained using the same instrumental settings as in the scattering experiment. The apparent power spectrum for the noise was then subjected to a least-squares fit of the form

$$N(\nu) = A + B\nu + C\nu^2$$

In a scattering experiment the power spectrum was corrected for the frequency response of the system by dividing  $N(\nu)$  into each experimental value of  $P(\nu)$ .

As described in the next section, the corrected power spectrum  $P(\nu)$  was fit to Lorentzian functions and sums of Lorentzian functions. This was accomplished with an iterative nonlinear least-squares procedure (Gauss-Newton method).<sup>12</sup> All of the calculations were carried out with a Raytheon 706-SCC coupled computer system.

**Materials.** The BSA was stock No. 7034-10 from Metrix Clinical and Diagnostics Division of Armour Pharmaceutical Co., and the lysozyme was type LYSF from Worthington Biochemical Operation. Sigma Chemical Co. supplied the RNase which was No. R-5000, Type II-A, Ribonuclease-A. The latex spheres were obtained from Dow Chemical Company, Diagnostic Products Division. One per cent solutions (g/100

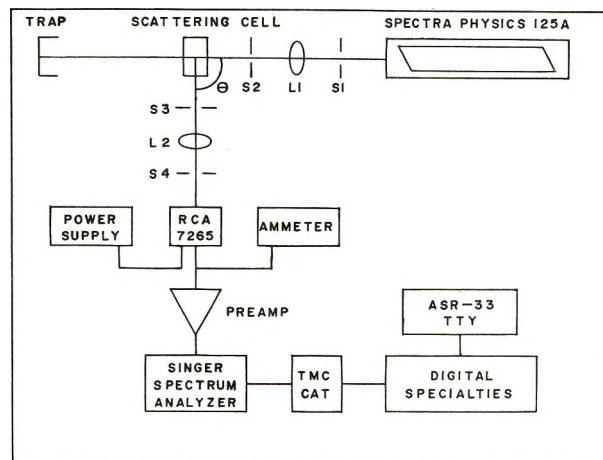


Figure 1. Block diagram of the light beating spectrometer.

ml) were prepared of BSA and lysozyme. The solvent for BSA was 0.5 M KCl, and the solvent for lysozyme was a solution of NaAc-HAc buffered to pH 4.25 to prevent denaturation. RNase was prepared and dissolved in 0.2 M sodium phosphate buffer (pH 6.5) to make approximately a 1% solution.<sup>13</sup> A stock solution of the latex spheres was prepared using deionized water.

In an attempt to remove dust from the scattering solution, a closed system consisting of the scattering cell, a 0.22- $\mu$  Millipore filter and filter holder, a small reservoir, and a peristaltic pump (Harvard Model 1210) was used. An 8-ml sample was introduced into the small reservoir and then cycled through the system. If dust remained in the solution, it was readily detected as sharp spikes in the photocurrent and on the CRT of the spectrum analyzer.

The sample cell from Opticell was 12  $\times$  12  $\times$  48 mm Pyrex with four polished faces and a 10-mm light path. Soaking the cell in an HCl-alcohol solution and then flushing it with 500 ml of deionized water which had been filtered through a 0.22- $\mu$  filter cleansed it sufficiently for the scattering experiment.

### III. Results and Discussion

The power spectrum of the photocurrent in a self-beating experiment involving only one scattering component has been shown to be a single Lorentzian function of the form<sup>14</sup>

$$P(\nu) \propto \frac{2\Gamma/2\pi}{(2\Gamma/2\pi)^2 + \nu^2} \quad (1)$$

(10) Experimental details are beautifully presented in S. B. Dubin, Ph.D. Thesis, M.I.T., 1970.

(11) After several months of satisfactory use, the argon ion laser became unsatisfactory for light beating experiments because a significant amount of noise was found in the self-beat spectrum in the neighborhood of 10-30 kHz.

(12) J. Blackburn, "Spectral Analysis: Methods and Techniques," Marcel Dekker, New York, N. Y., 1970.

(13) A. M. Crestfield, W. H. Stein, and S. Moore, *J. Biol. Chem.*, **238**, 618 (1963).

(14) R. Pecora, *J. Chem. Phys.*, **40**, 1604 (1964).

where  $\Gamma = D_T K^2$ ,  $D_T$  = translational diffusion constant of the scattering particle,  $K = (4\pi n/\lambda_0) \sin \theta/2$ ,  $n$  = refractive index of the solution,  $\theta$  = scattering angle, and  $\lambda_0$  = wavelength of incident light *in vacuo*. When two scattering components are present, the resulting power spectrum of the photocurrent is a superposition of three Lorentzians, the self-beat spectrum of each species and a cross term.<sup>7</sup> The form is

$$P(\nu) \propto A^2 \frac{(2\Gamma_1/2\pi)}{(2\Gamma_1/2\pi)^2 + \nu^2} + 2AB \frac{(\Gamma_1 + \Gamma_2)/2\pi}{[(\Gamma_1 + \Gamma_2)/2\pi]^2 + \nu^2} + B^2 \frac{(2\Gamma_2/2\pi)}{(2\Gamma_2/2\pi)^2 + \nu^2} \quad (2)$$

where  $A$  and  $B$  are the integrated intensities of the light scattered by components A and B, respectively.

The analysis for two-component systems is simplified if one of the Lorentzians is narrow and intense, *i.e.*, if one of the particles is much larger than the other. In such a case the spectrum can be characterized primarily by the cross term, since the self-beat spectrum of the larger particle is concentrated at the lower frequencies and the self-beat spectrum of the smaller particle has a much lower intensity than the cross term. This argument should apply in the present work, since the characteristic size of BSA is 100 Å, that of lysozyme is 50 Å, and the manufacturer's quoted diameter for the spheres is 910 Å.

In contrast to this expectation, our results have shown that a single Lorentzian fit is not satisfying even when the cross term is expected to dominate. We have used the least-squares program mentioned in the previous section to fit the data to sums of two and three Lorentzian functions as well as to single Lorentzians. The use of three Lorentzian functions, while correct in principle, is impractical because of the large number of parameters required. As shown below, the Lorentzian component of lowest intensity can be neglected; *i.e.*, the first two terms in eq 2 are sufficient.

**BSA Results.** Figure 2 shows the power spectrum obtained at  $\theta = 90^\circ$  for BSA with no added spheres. The squares indicate experimental points and the solid line is the best fit Lorentzian curve. The half-width at half-height of this spectrum is 7.40 kHz, which corresponds to the diffusion constant  $D_T = 6.66 \times 10^{-7} \text{ cm}^2 \text{ sec}^{-1}$  at  $22^\circ$ , in good agreement with previous measurements.<sup>5,7</sup>

The spectrum of a BSA-latex sphere mixture is shown in Figure 3. Attempts to fit the data to a single Lorentzian curve were not successful. The ambiguous results obtained for the line widths are illustrated in Figure 4. Here the line widths are plotted *vs.* the lowest frequency used in the data set; *i.e.*, the analysis begins with the frequency  $F(1)$ . The various curves correspond to different concentrations of latex spheres ex-

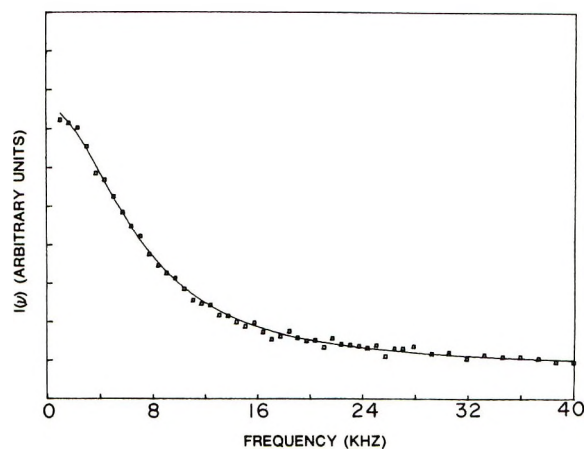


Figure 2. Self-beat spectrum of BSA measured at  $\theta = 90^\circ$  and  $T = 22^\circ$ . The solid curve is the best single Lorentzian fit to the experimental data (squares represent every fourth data point) with a half-width at half-height of 7.40 kHz.

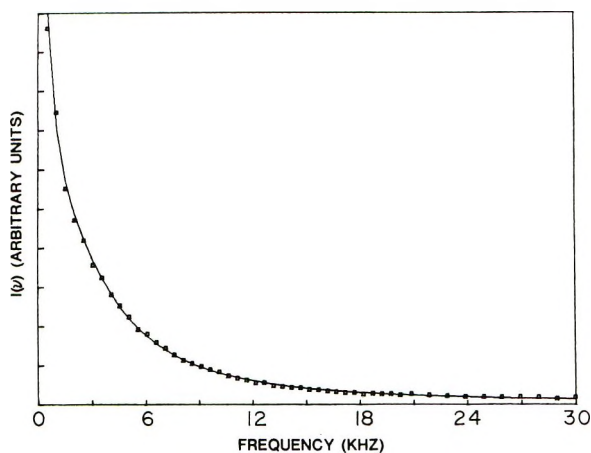


Figure 3. The power spectrum of a BSA-latex sphere mixture measured at  $\theta = 90^\circ$  and  $T = 24^\circ$ . Squares represent every fourth data point and the solid curve is a sum of two Lorentzians, one with  $2\Gamma/2\pi = 0.595 \text{ kHz}$  and the other with  $2\Gamma/2\pi = 4.10 \text{ kHz}$ .

pressed as weight per cent: (A) 0, (B)  $1.0 \times 10^{-5}$ , (C)  $1.6 \times 10^{-5}$ , (D)  $4.7 \times 10^{-5}$ , (E)  $1.4 \times 10^{-4}$ , and (F)  $2.1 \times 10^{-4}\%$ . The curvature clearly indicates the presence of more than one Lorentzian. For all of the mixtures the apparent line widths decrease when data points in the low-frequency region are included in the analysis. As the initial frequency  $F(1)$  in the analysis set is increased, a roughly constant line width is approached, *but the magnitude obtained is not in general equal to the width of the cross term*. The first and second terms in eq 2 both contribute significantly in the usable portions of the spectrum.

Another result apparent from Figure 4 is that the effective line width decreases as the concentration of spheres increases; *i.e.*, the narrow component begins to dominate the spectrum.<sup>8</sup> This effect is clearly shown by curve A in Figure 5, where the maximum line widths

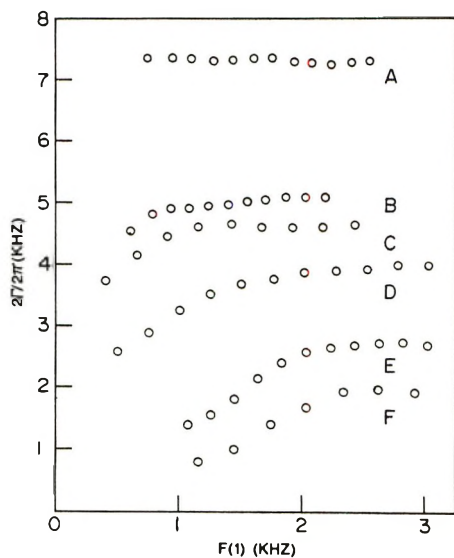


Figure 4. Line widths for the best single Lorentzian fits to experimental data plotted *vs.* the frequency of the first data point,  $F(1)$ , used in the analysis for spectra of BSA with varying concentrations of latex spheres (see text).

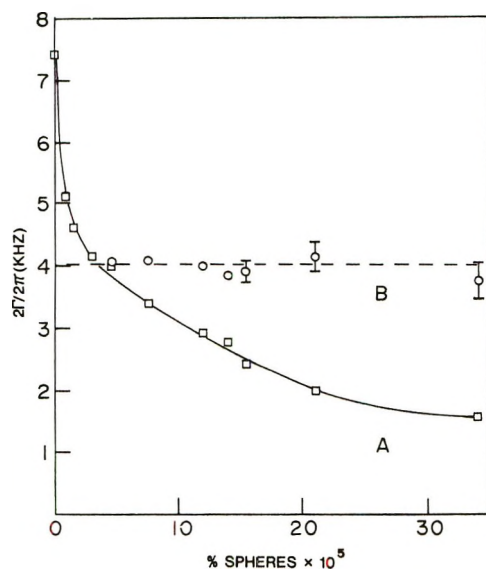


Figure 5. (A) Single Lorentzian line width plotted against sphere concentration expressed as weight per cent for mixtures of BSA and spheres. (B) Calculated line widths of the cross term from a two-Lorentzian fit.

including those from Figure 4 are plotted *vs.* the concentration of spheres.

A much more consistent analysis was obtained using the first two terms in eq 2. Initially two additional adjustable parameters, namely the height and width of the self-beat spectrum of the spheres, were introduced into the fitting program. Unfortunately, with typical signal-to-noise ratios a four-parameter fit may not converge to a unique solution. In order to reduce the number of adjustable parameters, the self-beat spectrum of the latex spheres was measured independently and the line width ( $2\Gamma/2\pi = 0.595$  kHz at

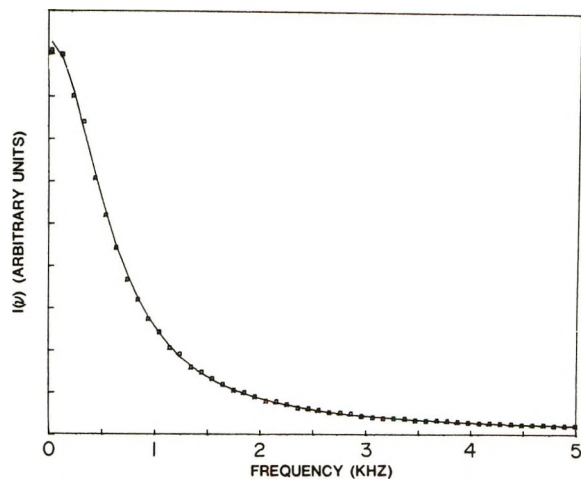


Figure 6. Self-beat spectrum of polystyrene latex spheres measured at  $\theta = 90^\circ$  and  $T = 24^\circ$ . Squares represent every fourth data point, and the solid curve is a Lorentzian with  $2\Gamma/2\pi = 0.595$  kHz.

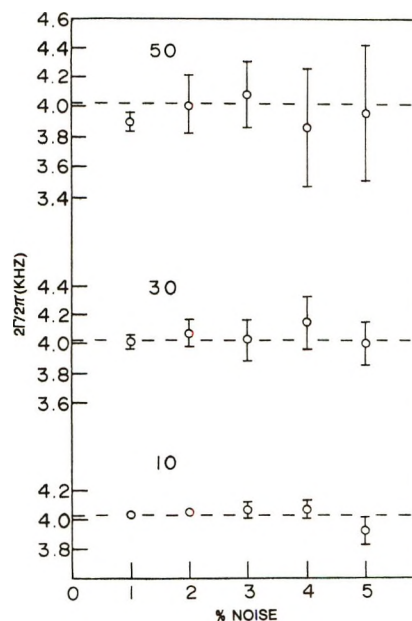


Figure 7. Line widths of the broader Lorentzian calculated from spectra simulated by adding two Lorentzians ( $2\Gamma_1/2\pi = 0.6$  kHz,  $2\Gamma_2/2\pi = 4.02$  kHz) plotted *vs.* per cent noise for the peak height ratios 50, 30, and 10.

$24^\circ$ ) was incorporated as a constant into the fitting program. The spectrum of the spheres is shown in Figure 6.

The results of the two-Lorentzian fits were very satisfying, with two peak heights and the width of the cross term being obtained without difficulty. All available data points were used, and the calculated line widths were roughly constant for a considerable range of sphere concentrations. The solid line in Figure 3 shows the best fit curve for one of the BSA-latex sphere mixtures. The constancy of the line widths with changing concentrations of the spheres is shown by curve B in Figure 5.

For a fixed signal-to-noise ratio, it is clear that the resolution of the experimental spectrum into two Lorentzian components can only be successful for a limited range of peak height ratios; *i.e.*, the concentration of the larger particle must be limited. In order to test this point spectra were simulated by adding Lorentzian curves having widths equal to 0.6 and 4.02 kHz and peak heights of  $H_1$  and  $H_2$ , respectively. Noise was then introduced by adding to each calculated amplitude  $I(\nu)$  the quantity  $(0.01)I(\nu)RY$ , where  $R$  is a computer-generated random number between +1 and -1 and  $Y$  is the maximum percentage of noise. For each peak height ratio  $H_1/H_2$  and noise percentage  $Y$ , ten simulated spectra were analyzed with the two-Lorentzian fitting program. The average half-widths and their standard deviations are shown in Figure 7. To obtain errors of less than 10% with peak-height ratios of as high as 50, we find the stringent requirement that the maximum noise be less than 3% of the amplitude of the power spectrum.

**Lysozyme Results.** Mixtures of lysozyme with polystyrene spheres were prepared as unknowns and were analyzed as discussed above. Single Lorentzian fits yielded curves similar to those shown in Figure 4 and indicated the need for a superposition of Lorentzians. A two-Lorentzian fit was again found to be satisfactory. An illustration of the fit obtained for one mixture is shown in Figure 8. The diffusion constant calculated from the width of the cross term is  $D_T = 11.8 \times 10^{-7} \text{ cm}^2 \text{ sec}^{-1}$  at  $24^\circ$ , which again is in good agreement with previous work.<sup>15</sup>

**RNase Results.** Two recordings of the signal from the CAT for different experiments are shown in Figure 9. The only difference was in the time spent removing dust from the samples. In spectrum A the sharp component in the center presumably results from dust particles. From observations of the CRT display of the spectrum analyzer, it was clear that occasionally a

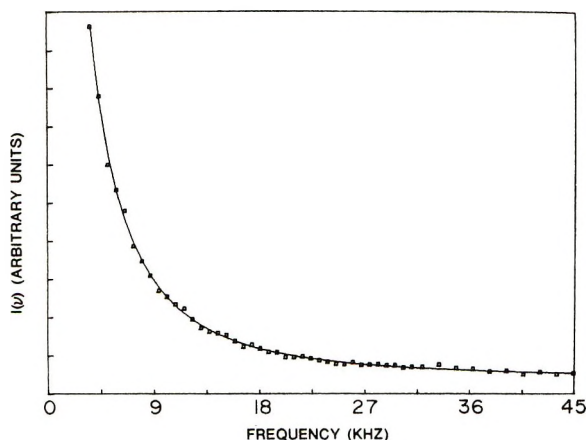


Figure 8. Experimental spectrum (squares) of a lysozyme-latex sphere mixture taken at  $\theta = 90^\circ$  and  $T = 24^\circ$ . The solid curve is a sum of two Lorentzians, one with  $2\Gamma/2\pi = 0.595 \text{ kHz}$  and the other with  $2\Gamma/2\pi = 6.78 \text{ kHz}$ .

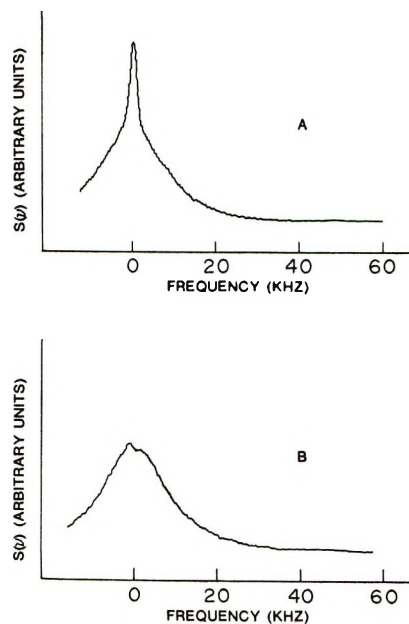


Figure 9. Continuous output traces from the CAT for RNase spectra taken at  $\theta = 90^\circ$  and  $T = 24^\circ$ . Spectrum B was obtained from a sample that was more completely free of dust than the sample used for spectrum A.

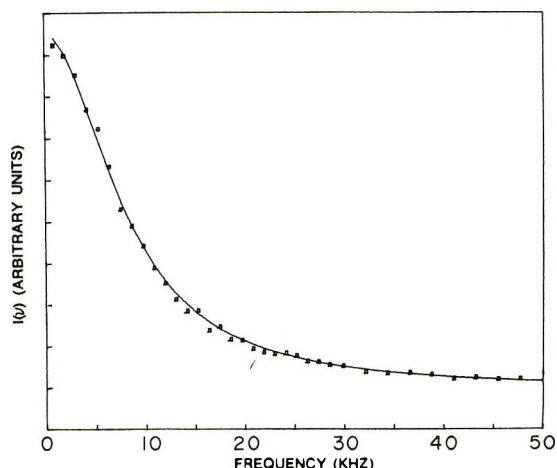


Figure 10. Computer fit of RNase spectrum shown in Figure 9B (solid line). The half-width at half-height is 7.63 kHz. Squares represent every fourth data point.

large particle would drift into the scattering volume. For one sweep of the spectrum analyzer (about 1 sec) the sharp component would be present. Between such events spectra would be observed without the sharp feature, so that most of the accumulated spectra have no cross term. When spectra 9A and 9B were subjected to computer analysis, it was found that away from the center both fit a Lorentzian curve having the width  $(2\Gamma/2\pi) = 7.6 \text{ kHz}$ . Figure 10 shows the experimental power spectrum and the best fit Lorentzian for the spectrum in Figure 9B.

(15) S. B. Dubin, N. A. Clark, and G. B. Benedek, *J. Chem. Phys.*, **54**, 5158 (1971).

We conclude that the sample used for spectrum 9B contains only scattering particles having roughly the same diameters. Chromatographic studies using Sephadex G-75 indicate that, in fact, the sample contains only about 60% monomers, the remainder being dimers and tetramers. A sample prepared so as to contain roughly 100% monomers gives a line width of 12.9 kHz and shows that  $D_T = 11.7 \times 10^{-7} \text{ cm}^2 \text{ sec}^{-1}$  at  $20^\circ$  for RNase, in reasonable agreement with earlier work.<sup>16</sup> The dependence of line width on the percentage of monomer in the solution will be discussed elsewhere.<sup>17</sup>

The fact that the solid curve in Figure 10 extrapolates to a finite intercept is in our experience indicative of scattering from a system in which the particle diameters are all the same order of magnitude. This of course does not rule out the occurrence of aggregates of RNase in the system studied by Rimai, *et al.*, where a different solvent was used.

#### IV. Conclusions

We have studied light scattered from solutions of latex spheres, BSA, lysozyme, RNase, and mixtures of BSA and lysozyme with latex spheres using a self-beating spectrometer. For solutions containing two scattering components with significantly different diameters, where a cross term is expected in the power spectrum of the photocurrent, the width of the cross term could not be consistently determined by fitting the data to a single Lorentzian curve, regardless of the frequency range covered by the data points. On the other hand, a superposition of two Lorentzian curves

provided satisfactory least-squares fits for all of the two component mixtures. In these calculations the width of the narrow component was known from independent experiments. The only exception to the above comment occurred with solutions containing very low concentrations of large particles, where only occasionally would a large particle diffuse into the scattering volume. The accumulated spectra for such systems may show primarily the self-beat spectrum from the smaller particle, with only a small contribution in the form of a center spike for the large particle. Spectra of this type are often encountered when dust particles have not been entirely removed from the solution. With higher concentrations of dust particles a consistent analysis by the method discussed here is impossible, since (1) the ratio  $H_1/H_2$  becomes very large and (2) the dust particles have a distribution of sizes. Kramer and Frederick have reached a similar conclusion.<sup>18</sup>

*Acknowledgments.* We wish to thank Dr. R. G. Griffin for assembling the self-beating spectrometer and for extensive advice. We thank Dr. S. B. Dubin for generously sharing his knowledge of light scattering with us. Also, we thank Mr. Walter E. Daniel, Jr., for preparing the RNase.

(16) C. Tanford, "Physical Chemistry of Macromolecules," Wiley, New York, N. Y., 1961.

(17) W. W. Wilson, W. E. Daniel, Jr., R. G. Hiskey, and C. S. Johnson, Jr., manuscript in preparation.

(18) O. Kramer and J. E. Frederick, *Macromolecules*, **4**, 613 (1971)



# Electrocapillary Phenomena at the Stress-Annealed Pyrolytic Graphite Electrode

by Ikram Morcos

*Hydro-Quebec Institute of Research, Varennes, Quebec, Canada (Received March 17, 1972)*

*Publication costs assisted by the Hydro-Quebec Institute of Research*

Meniscus rise *vs.* potential relationships were measured on a partially immersed cleavage orientation of stress-annealed pyrolytic graphite in both aqueous and DMF-H<sub>2</sub>O electrolytic solutions. From this experimental information as well as the experimentally determined value of the graphite's surface tension, the interfacial tension as well as charge *vs.* potential plots were calculated using the equations

$$\gamma_{SL} = \gamma_S - \gamma_L(2Kh^2 - K^2h^4)^{1/2}$$

$$q = \gamma_L(2K)^{1/2} \frac{1 - Kh}{(1 - 1/2Kh^2)^{1/2}} \left( \frac{\partial h}{\partial E} \right)_\mu$$

where  $\gamma_{SL}$ ,  $\gamma_S$ , and  $\gamma_L$  are the solid-electrolyte, solid-gas, and liquid-gas interfacial tensions,  $q$  is the surface charge,  $E$  is the potential,  $h$  is the meniscus rise, and  $K$  is a constant for each solvent. The electrocapillary information obtained on cleavage graphite is compared to that obtained on a mercury electrode. The lower charge density on graphite as compared to mercury is believed to be due to the low surface tension value of cleavage graphite surface which cannot adsorb the solvent and therefore prevent the adsorption of solvated ions. The higher charge density on cleavage graphite in DMF-H<sub>2</sub>O solutions as compared to aqueous solutions is due to the numerically lower solvation energy in DMF-H<sub>2</sub>O compared to water. The chemical inertness of cleavage graphite is believed to limit anion adsorption. Differential capacity values calculated from the charge *vs.* potential plots at the potential of zero charge of cleavage graphite in aqueous solutions ( $\sim 4 \mu\text{F}/\text{cm}^2$ ) agree with differential capacity minimum values obtained by Randin and Yeager using direct ac impedance methods. The low surface tension of cleavage graphite seems to be responsible for its low capacity and slight capacity dependence on potential.

## Introduction

Recent studies of meniscus rise *vs.* potential at partially immersed electrodes<sup>1-5</sup> have provided a new and powerful tool for studying electrocapillary phenomena at the solid electrode-electrolyte interphase. Measurements at a partially immersed mercury-plated gold electrode have shown that the interfacial tension as well as surface charge which are obtained from meniscus rise *vs.* potential plots<sup>5</sup> are in agreement with those obtained from direct interfacial tension measurements on liquid mercury.

An understanding of the electrocapillary phenomena at solid electrodes on the basis of meniscus rise *vs.* potential measurements requires the most rigid and selective choice of the electrode material. Surface roughness and inhomogeneity as well as chemical and electrochemical activity associated with solid surfaces complicate the nature of the interphase and likewise the interpretation of experimental data. One solid surface which satisfies most of the requirements of an ideal polarized electrode is that of cleavage orientation of stress-annealed pyrolytic graphite. This surface is chemically inert with satisfied valencies and high hydrogen and oxygen overvoltage.<sup>6a</sup> The surface is smooth, homogeneous, and can be easily peeled off, which allows its reproducible renewal before each experiment. Very recently the absolute surface tension of this surface was determined.<sup>6b</sup> Consequently, the

estimation of the interfacial tension (in absolute values) as well as the surface charge at the cleavage graphite-electrolyte interphase has become possible.

Because of the low surface tension magnitude of cleavage graphite (about 35 dyn/cm) and the criteria of the meniscus rise technique, one is limited to solvents of high surface tension. In addition to water, a 50% DMF-50% H<sub>2</sub>O mixture (51 dyn/cm) was chosen for the study. (A pure DMF solvent cannot be applied in the study because it wets the surface with a small contact angle (about 6°) and leaves little room for variation with the potential. The maximum meniscus rise that can be realized is that corresponding to zero contact angle as shown by eq 1.)

It is the purpose of the present work to study the electrocapillary phenomena at the cleavage graphite-electrolyte interphase using the meniscus rise method, with the particular object of determining the interfacial tension, the charge, and capacity magnitudes. The results will be compared to that of a mercury electrode.

(1) I. Morcos and H. Fischer, *J. Electroanal. Chem. Interfacial Electrochem.*, **17**, 7 (1968).

(2) I. Morcos, *ibid.*, **20**, 479 (1969).

(3) I. Morcos, *Collect. Czech. Chem. Commun.*, **36**, 689 (1971).

(4) I. Morcos, *J. Colloid Interface Sci.*, **37**, 410 (1971).

(5) I. Morcos, *J. Chem. Phys.*, **56**, 3996 (1972).

(6) (a) I. Morcos and E. Yeager, *Electrochim. Acta*, **15**, 953 (1970)

(b) I. Morcos, *J. Chem. Phys.*, in press.

## Experimental Section

The experimental technique and method of study has been well described in a number of previous publications.<sup>1-7</sup> Advancing equilibrium meniscus rise was measured as a function of the potential at partially immersed stress-annealed pyrolytic graphite plates of  $4 \times 2.5$  cm size and about 0.5 mm thickness. The potential was varied in steps of 0.1 V each and the meniscus rise values were obtained after they reached constant values which were usually achieved in less than 5 min. The meniscus rise was read by a cathetometer with an accuracy of  $\pm 0.001$  cm. The darkness of the graphite surface made it possible to observe easily the graphite-liquid border line above and below the liquid's level in the cell with the aid of light reflection. Thus the meniscus rise corresponding to contact angles above  $90^\circ$  were determined (see Figure 1).

The relationship between the meniscus rise  $h$  and contact angle  $\theta$  is given by the Hagen equation

$$\sin \theta = 1 - \frac{\rho g}{2\gamma_L} h^2 \quad (1)$$

where  $\rho$  and  $\gamma_L$  are the liquid's density and its surface tension and  $g$  is the gravitational constant. This relationship was recently verified experimentally.<sup>7</sup> Its theoretical derivation is found in the German literature.<sup>8</sup>

The calculation of the solid-electrolyte interfacial tension from the experimental data requires a knowledge of the graphite's surface tension  $\gamma_s$ . The theoretical as well as experimental basis for determining the graphite's surface tension were described elsewhere<sup>6b</sup> and only a very brief summary will be given here. Contact angle measurements between organic liquids and cleavage graphite surface indicate that the surface has low surface tension which is much less than that of water. For such a low surface tension one can determine  $\gamma_s$  using an empirical equation derived by Newmann<sup>9</sup> on the basis of Good's interaction parameter.<sup>10</sup> The Newmann equation is given by

$$\cos \theta = \frac{(0.015\gamma_s - 2)\sqrt{\gamma_s\gamma_L} + \gamma_L}{\gamma_L(0.015\sqrt{\gamma_s\gamma_L} - 1)} \quad (2)$$

$\theta$  was obtained for three liquids ( $H_2O$ , DMF, and glycerol) from meniscus rise measurements. The application of eq 2 showed that  $\gamma_s$  is constant and  $\approx 35 \pm 2$  dyn/cm.

The water used in preparing solutions was triply distilled, twice from a permanganate solution. Dimethylformamide, reagent grade type, was further purified by distillation. All salts were of reagent grade type. A spectroscopic graphite rod was used as a counter electrode and the reference electrode was a saturated calomel. The potential was fixed by a Wenking potentiostat. The precision of the controlled potential was better than 1 mV which was always verified

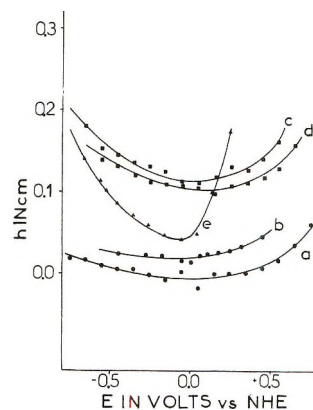


Figure 1. Meniscus rise vs. potential relationships on cleavage orientation of stress-annealed pyrolytic graphite and mercury-plated gold electrodes: a, b, cleavage in 1 N LiCl and 1 N KBr aqueous solutions; c, d, cleavage graphite in 1 N LiCl and 1 N LiBr in 50% DMF-50%  $H_2O$ ; e, mercury in 1 N LiCl in 50% DMF-50%  $H_2O$ .

by a high-impedance voltameter. The graphite was a stress-annealed highly oriented type ZYH of a mosaic spread of  $3.5 \pm 1.5^\circ$ . The structure is similar to that of single-crystal material. The graphite surface was always renewed before each experiment by simply peeling it off with a scotch tape. It was made sure that the tape did not touch the newly exposed surface by removing a complete layer. The method of preparation of mercury-plated gold electrodes was described in a previous paper.<sup>4</sup>

## Results and Discussion

Figure 1 shows the equilibrium advancing meniscus rise vs. potential relationships obtained on cleavage graphite. Plots a and b are for 1 N LiCl and 1 N KBr in water and plots c and d are for 1 N LiCl and 1 N LiBr in 50% DMF-50%  $H_2O$  mixture. These four plots are compared in the same figure with plot e for the meniscus rise vs. potential relationship obtained on a mercury-plated gold electrode in a solution of 1 N LiCl in 50% DMF-50%  $H_2O$  mixture. It is noticed that while the variation of meniscus rise with potential is much smaller in the case of cleavage graphite surface as compared to mercury surface, the minimum meniscus rise in DMF- $H_2O$  solutions on the graphite surface is considerably higher than on the mercury surface. The absolute values of  $h$  (but not its rate of variation with  $E$ ) in the case of mercury are reduced by the spreading pressure,  $\pi_e$ , of the solvent on its surface. Mercury, being a high energy surface (480 dyn/cm), adsorbs the solvents from the vapor phase.<sup>11</sup> On the

(7) I. Morcos, *J. Chem. Phys.*, **55**, 4125 (1971).

(8) A. W. Newmann, *Z. Phys. Chem. (Frankfurt am Main)*, **41**, No. 5/6, 339 (1964).

(9) A. W. Newmann, *J. Colloid Interface Sci.*, **34**, 1 (1970).

(10) R. J. Good, *Advan. Chem. Ser.*, No. 43, 74 (1964).

(11) F. M. Fowkes, *ibid.*, No. 43, 99 (1964).

contrary, cleavage graphite is a low energy surface (35 dyn/cm is less than  $\gamma_L$  of any of the solvents used) and does not adsorb the solvent from the vapor phase. The effect of the spreading pressure on the contact angle  $\theta$  and therefore on the meniscus rise is shown by the Young equation

$$\gamma_L \cos \theta = \gamma_s - \gamma_{SL} - \pi_e \quad (3)$$

The relationship between the meniscus rise and the electrode-electrolyte interfacial tension follows directly from the Hagen and Young equations (eq 1 and 3 above) and is given by

$$\gamma_{SL} = \gamma_s - \gamma_L(2Kh^2 - K^2h^4)^{1/2} \quad (4)$$

where  $\gamma_{SL}$  is the electrode-electrolyte interfacial tension and  $\gamma_s$  and  $\gamma_L$  are the electrode's and electrolyte's surface tensions,  $h$  is the meniscus rise, and  $K$  is constant for each liquid and is equal to  $\rho g/2\gamma_L$ . Equation 4 was verified experimentally<sup>5</sup> for the case of a mercury-plated gold electrode in DMF-H<sub>2</sub>O media.

Figure 2 shows plots of  $\gamma_{SL}$  vs. the potential calculated by eq 4 using the data on cleavage graphite of Figure 1 and a value of 35 dyn/cm for  $\gamma_s$ . The same letter labeling in both Figures 1 and 2 corresponds to the same solution composition. It is seen that all plots of Figure 2 have clear maxima. For comparison, Figure 3a shows the  $\gamma_{SL}$  vs.  $E$  for a mercury-plated gold electrode in 1 N LiCl 50% DMF-50% H<sub>2</sub>O solution. There are no available surface tension data in the literature on liquid mercury obtained in a solution of exactly the same composition. Measurements on liquid mercury by Bezuglyi and Korshikov<sup>12</sup> are available for 0.1 N LiCl in 25% and 50% DMF-H<sub>2</sub>O solutions. Plots 3b and 3c show the data of Bezuglyi and Korshikov.<sup>12</sup> Plot 3c also shows the electrocapillary curve obtained on a mercury-plated gold plate by the meniscus rise method in 25% DMF-H<sub>2</sub>O solution of 0.1 N LiCl.

The electrocapillary maxima of cleavage graphite in aqueous solutions are located at approximately the null potential (vs. nhe). The minima of the differential capacity vs.  $E$  plots obtained on cleavage graphite in the work of Randin and Yeager<sup>13</sup> are located at the null potential (vs. nhe). The electrocapillary maxima obtained in DMF-H<sub>2</sub>O solutions in the present work (Figure 2) are located at slightly more positive potential than the corresponding maxima in aqueous solutions. The same observation was reported by Bezuglyi and Korshikov<sup>12</sup> on liquid mercury and by the present author using meniscus rise studies on mercury-plated gold electrodes.<sup>5</sup>

The dependence of the magnitude of interfacial tension at the maximum on the solvent's nature (Figures 2 and 3) results from the effect of the solvent's surface tension as shown from eq 3 and 4.

The variation in  $\gamma_{SL}$  with the potential is related to the charge density at the electrode surface and it is

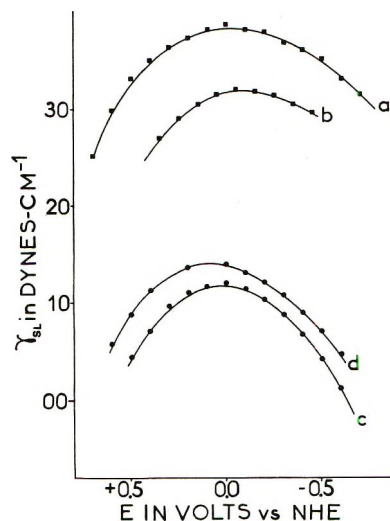


Figure 2. Interfacial tension vs. potential relationships on cleavage graphite electrode: a, b, in 1 N LiCl and 1 N KBr aqueous solutions; c, d, in 1 N LiCl and 1 N LiBr in 50% DMF-50% H<sub>2</sub>O.

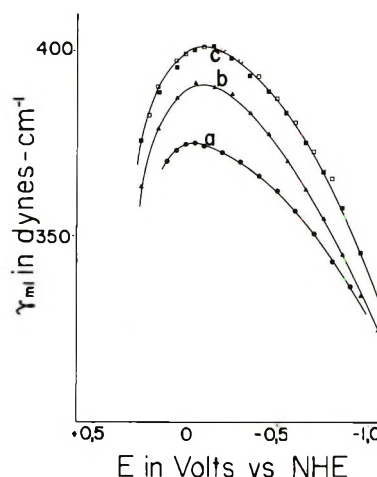


Figure 3. Interfacial tension vs. potential relationship on mercury surface in DMF-H<sub>2</sub>O solutions: a, from meniscus rise data on a mercury-plated gold in 1 N LiCl in 50% DMF-50% H<sub>2</sub>O; b, electrocapillary data on liquid mercury in 0.1 N LiCl in 50% DMF-50% H<sub>2</sub>O from ref 12; c, data on mercury in 0.1 N LiCl in 25% DMF-75% H<sub>2</sub>O (■, from data in ref 12; □, from meniscus rise measurements).

appropriate to calculate the latter parameter from the experimental data. The surface charge can be calculated from  $\gamma_{SL}$  vs.  $E$  plots using the Lippmann equation

$$q = -\left(\frac{\partial \gamma_{SL}}{\partial E}\right)_\mu \quad (5)$$

or directly from the meniscus rise vs.  $E$  plots using an equation which combines eq 4 and 5

$$q = \gamma_L(2K)^{1/2} \frac{1 - Kh^2}{(1 - 1/2Kh^2)^{1/2}} \left(\frac{\partial h}{\partial E}\right)_\mu \quad (6)$$

(12) V. D. Bezuglyi and L. A. Korshikov, *J. Sov. Electrochem.*, **1**, 1422 (1965).

(13) J. P. Randin and E. Yeager, *J. Electrochem. Soc.*, **118**, 711 (1971).

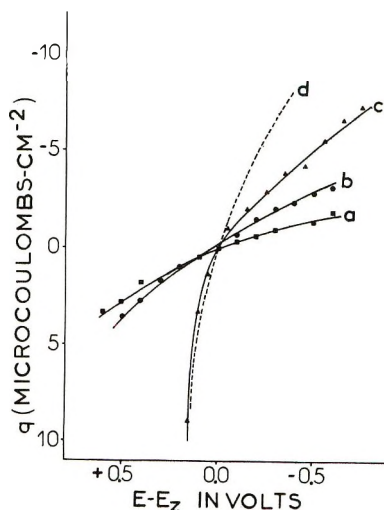


Figure 4. Charge density vs. rational potential plots on cleavage graphite and mercury electrodes: a, cleavage graphite in 1 *N* LiCl aqueous solution; b, cleavage graphite in 1 *N* LiCl in 50% DMF-50% H<sub>2</sub>O; c, mercury-plated gold electrode in 1 *N* LiCl in 50% DMF-50% H<sub>2</sub>O; d, mercury electrode in 1 *N* NaCl aqueous solution.

Both eq 5 and 6 were derived for the case of an ideal polarized electrode but their use is justifiable here because of the previously mentioned characteristics of the cleavage graphite surface (see the Introduction).

Figure 4 shows the charge vs. rational potential plots for cleavage graphite in 1 *N* LiCl aqueous solution (plot 4a) and in 1 *N* LiCl 50% DMF-50% H<sub>2</sub>O solution (plot 4b) as well as the same plot for a mercury-plated electrode in the latter solution (plot 4c). The dotted line shows the charge vs. potential relationship on mercury in aqueous medium (1 *N* NaCl) and was taken from the work of Grahame<sup>14</sup> and is given here for the sake of the discussion. Figure 4 shows that the charge density on the cleavage graphite surface is much less than that of the mercury surface and that this difference between the two surfaces is much larger in aqueous than in DMF-H<sub>2</sub>O medium. Contrary to the mercury surface, the cleavage graphite surface shows higher magnitude of charge density in DMF-H<sub>2</sub>O medium than in aqueous medium. These observations can be well understood if we consider the difference between the surface tensions of cleavage graphite and mercury surfaces, as well as the solvation characteristics of both water and DMF-H<sub>2</sub>O media.

Mercury has a surface tension of 680 dyn/cm, which is a much higher value than the surface tension of water or any other solvent, and solvents adsorb on mercury with a decrease in free energy. Consequently, the solvation sheath around the ions in solution will not prevent the electrostatic adsorption of ions at the electrode surface under the influence of the electric field. On the other hand, it is generally accepted<sup>10,15,16</sup> that a liquid will not adsorb on a solid surface if the surface tension of the liquid is higher than that of the solid.

Consequently, if the ions are strongly solvated their adsorption on that solid will be either prevented or greatly reduced. Water with  $\gamma_L = 72$  dyn/cm and 50% DMF-50% H<sub>2</sub>O with  $\gamma_L = 51$  dyn/cm will not adsorb on the cleavage graphite with  $\gamma_S = 35$  dyn/cm and consequently ionic adsorption will be strongly reduced in both solvents. This explains the much lower charge density determined on cleavage graphite as compared to mercury. Any significant increase of the charge density with potential on cleavage graphite must be due to the presence of nonsolvated or relatively weakly solvated ions in the solution.

Figure 4 shows that the surface charge on cleavage graphite surface is higher in 50% DMF-50% H<sub>2</sub>O medium than in pure water. In view of our previous conclusion, this must result from higher surface ionic activity of LiCl in DMF-H<sub>2</sub>O than in water medium. DMF is an aprotic dipolar solvent with a lower dielectric constant ( $\epsilon_{DMF} = 36.7$ ) than that of water. These properties plus the structural effects would decrease the solvation of the ions in DMF-H<sub>2</sub>O and result in the higher surface ionic activity. This is particularly true at anodic rather than cathodic potentials because the anions in DMF-H<sub>2</sub>O mixtures have a much lower hydration number than the cations.<sup>12</sup>

Capacity-potential plots on cleavage graphite have been reported by Randin and Yeager.<sup>13</sup> The work was done under very pure and careful conditions. They reported a value of  $\sim 3 \mu\text{F}/\text{cm}^2$  for the differential capacity minimum of cleavage graphite, with very little variation with potential.

The differential capacity can also be calculated from the  $q$  vs.  $E$  plots of Figure 4 on the basis of the equation

$$C_d = \frac{\partial q}{\partial E} \quad (7)$$

One obtains a value of  $\sim 4 \mu\text{F}/\text{cm}^2$  for the differential capacity of cleavage graphite in aqueous solution of 1 *N* LiCl at the electrocapillary maximum. This value agrees very well with the data of Randin and Yeager. The fact that the meniscus rise variation with potential leads to approximately the same capacity minimum value as that measured directly by the impedance method confirms the validity of the relationships relating the advancing meniscus rise to the electrocapillary parameters described in eq 3 and 4 as applied to a solid electrode.

*Acknowledgment.* The author wishes to thank Dr. A. Moore of the Union Carbide Research Center, Parma, Ohio, for providing him with the graphite samples used in the present work. Gratitude is expressed for Mr. A. Gendron for his assistance in the mathematical computation and drawing of the figures.

(14) D. C. Grahame, *Chem. Rev.*, **41**, 441 (1947).

(15) W. A. Zisman, *Advan. Chem. Ser.*, No. 43, 74 (1964).

(16) F. M. Fowkes, *S.C.I. Monograph*, **25**, 3 (1967).

## Theory of Hydrophobic Bonding. II. The Correlation of Hydrocarbon

### Solubility in Water with Solvent Cavity Surface Area

by Robert B. Hermann

*Eli Lilly and Company, Indianapolis, Indiana 46206 (Received April 20, 1971)*

*Publication costs assisted by Eli Lilly and Company*

In paper I of this series a theory of the solubility of hydrocarbons in water was formulated in terms of the significant structure theory of liquids. In this theory, the number of water molecules that can be packed around the hydrocarbon molecule enters into the partition function of a hydrocarbon solution. This number is one measure of the size of the solvent cavity just large enough to accommodate a solute molecule. A more idealized quantity that is more easily computed is the area of the cavity surface which contains the centers of the water molecules in the first layer around the solute. It has been found that the area defined in this manner is linearly related to the logarithm of the hydrocarbon solubility in water. All cavities computed in this paper are nonspherical and depend on detailed hydrocarbon shape. The correlation suggests a semi-empirical means of calculating the hydrophobic interactions between hydrocarbon moieties and of obtaining Hansch  $\pi$  values.

#### Introduction

In paper I<sup>1</sup> of this series a theory of the solubility of hydrocarbons in water was formulated in terms of the significant structure theory of liquids.<sup>2</sup> The large negative unitary entropy of solution was explained by means of a mechanism similar to one previously used by Jhon, Van Artsdalen, Grosh, and Eyring to explain the surface tension of water.<sup>3</sup> In this mechanism the decrease in entropy is due to the tendency of the water dipoles in the layer of water adjacent to the hydrocarbon solute to orient with respect to the dipoles in the water molecules in the next water layer. This effect does not exist in the bulk liquid away from a surface or hydrocarbon molecule because of the symmetry of the electric field in which a given water molecule finds itself.

According to this theory, then, the number of water molecules that can be packed around the hydrocarbon molecule is an important quantity in the partition function for the hydrocarbon solution. Némethy and Scheraga, in their theory of hydrophobic bonding, also used this number of water molecules in the first water layer as being a factor in hydrocarbon solubility.<sup>4</sup> Their work included the calculation of the unitary free energy for the normal alkanes through *n*-octane on this basis, and they later extended their method to proteins.<sup>5</sup>

The number of water molecules that can be packed around a given hydrocarbon solute molecule is difficult to define and determine. To determine this number, certain assumptions about packing must be made. Several packing conformations may be possible, and the number of water molecules will vary, depending on the solute conformation and the assumed water structure. The number, however, is related to the

surface area of the solvent cavity if the surface is defined in such a way that it passes through the centers of the water molecules momentarily adjacent to the solute. This idea of cavity surface, while slightly idealized, can be more rigorously defined, and the area of such a surface can be more easily calculated.

The concept of a solvent cavity has been used by a number of workers who have explored the relationship between the energy of cavity formation and the logarithm of the solubility of gases in various liquids. In these cases the cavity surface tension usually enters into the expression for the energy, along with the cavity surface area. The cavity surface is normally treated as spherical.

Uhlig<sup>6</sup> and Eley<sup>7</sup> suggested that for a spherical cavity the free energy  $\Delta G$  for transferring a molecule from the gas phase to the solvent is approximated by

$$\Delta G = 4\pi r^2 \sigma - \epsilon \quad (1)$$

where  $r$  is the cavity radius,  $\sigma$  is the solvent surface tension, and  $\epsilon$  is the solute-solvent interaction energy. Then  $c'/c$ , the ratio of molecules in the solvent to molecules in the gas phase, is given by the Boltzmann distribution

- (1) R. B. Hermann, *J. Phys. Chem.*, **75**, 363 (1971).
- (2) H. Eyring and M. S. Jhon, "Significant Liquid Structures," Wiley, New York, N. Y., 1969, and references cited in paper I.
- (3) M. S. Jhon, E. R. Van Artsdalen, J. Grosh, and H. Eyring, *J. Chem. Phys.*, **44**, 1465 (1966).
- (4) G. Némethy and H. A. Scheraga, *ibid.*, **36**, 3401 (1962).
- (5) G. Némethy and H. A. Scheraga, *J. Phys. Chem.*, **66**, 1773 (1962).
- (6) H. H. Uhlig, *ibid.*, **41**, 1215 (1937).
- (7) D. D. Eley, *Trans. Faraday Soc.*, **35**, 1281, 1421 (1939).

$$\frac{c'}{c} = e^{-\Delta G/kT} \quad (2)$$

Since that time, the linear relationship between the solvent surface tension for nonpolar solvents and the logarithm of the gas solubility has been amply verified.<sup>8,9</sup>

Choi, Jhon, and Eyring<sup>10</sup> have calculated the microscopic surface tension<sup>11</sup> of these highly curved molecular cavities and used this in computing the cavity formation energy in their theory of solubility of gases, rather than using the surface tension for zero curvature directly as most authors have done previously. Sinanoglu<sup>12</sup> has also treated solvent effects in chemical reactions in which part of the energy was expressed in terms of cavity surface and surface tension. Pierotti<sup>13</sup> has used scaled particle theory to calculate the solubility of gases in water. This theory gives an approximate expression for the free energy of cavity formation for a spherical solute of arbitrary size.

In this paper a correlation between the calculated solvent cavity surface area and the free energy change at one temperature accompanying the solution of a liquid hydrocarbon in water is proposed. In paper I, the free energy was assumed to be linearly related to the number of water molecules that can be packed around a given hydrocarbon molecule; here it is shown from experimental solubilities that a corresponding quantity, the cavity surface area, is similarly related to the free energy. Unlike treatments thus far, all cavities computed in this paper are nonspherical and depend on detailed hydrocarbon shape. A correlation between calculated cavity surface area and hydrocarbon solubility suggests a means of predicting solubility and eventually may lead to a method for calculating the strength of hydrophobic interactions semiempirically.

### Surface Area Definition

For the purpose of calculation, the cavity surface area is defined as follows and is illustrated in Figure 1. A solute molecule R has each atom  $i$  defined as a sphere of radius  $r_i$  and center located at fixed atomic coordinates  $(x_i, y_i, z_i)$ . A sphere of radius  $r_w$  representing a water molecule then slides over the surface of the solute molecule. The surface traced out by the center of the sphere is the cavity surface and has an area  $A_{RW}(T)$ . The quantity represents the two-dimensional space available to a water molecule in contact with the solute within the context of the above geometric assumptions. The quantity  $A_{RW}(T)$  will in general be temperature dependent because the effective radii involved are temperature dependent.

### Relation between Cavity Surface Area and Solubility

The free energy per solute molecule  $\mu_{\text{satd}}$  of a saturated aqueous solution of hydrocarbon may be written approximately

$$\mu_{\text{satd}} = \mu_w + kT \ln s \quad (3)$$

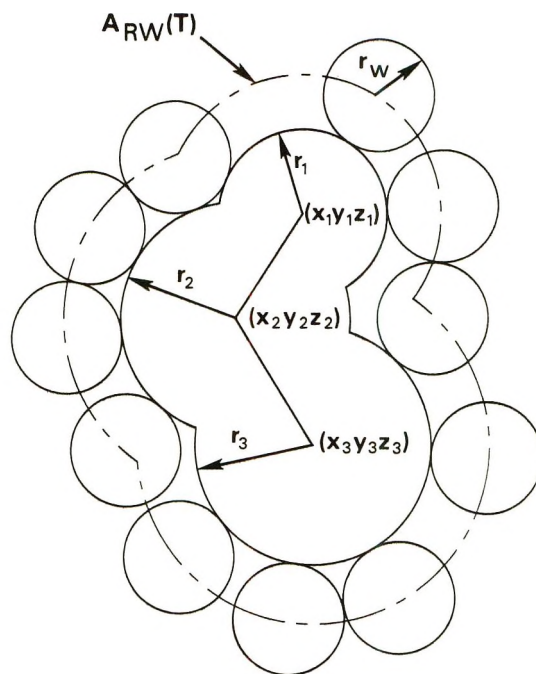


Figure 1. Cavity surface with area  $A_{RW}(T)$ .

where  $s$  is the molar solubility and  $\mu_w$  is the standard free energy per molecule of solute in a hypothetical standard 1  $M$  aqueous solution at a given temperature and 1 atm of pressure. For the pure liquid hydrocarbon<sup>14</sup> in equilibrium with such a saturated solution, the chemical potentials of the two phases may be equated so that

$$\mu_R = \mu_w + kT \ln s \quad (4)$$

where  $\mu_R$  is the free energy per molecule of the pure liquid hydrocarbon.<sup>15</sup>

If the free energy of transfer of a hydrocarbon molecule from the pure liquid hydrocarbon to water,  $\mu_w - \mu_R$ , is linearly related to cavity surface area for a series of hydrocarbons as proposed, then the area  $A_{RW}(T)$  is related to the solubility as

$$b_0(T)A_{RW}(T) = -kT \ln s - C_0(T) \quad (5)$$

where  $b_0(T)$  and  $C_0(T)$  are constants at a given temperature. The area  $A_{RW}(T)$  is the cavity area of the

(8) H. L. Clever, *J. Phys. Chem.*, **62**, 375 (1958).

(9) J. H. Saylor and R. Baltino, *ibid.*, **62**, 1334 (1958).

(10) D. S. Choi, M. S. Jhon, and H. Eyring, *J. Chem. Phys.*, **53**, 2608 (1970).

(11) (a) R. C. Tolman, *ibid.*, **16**, 758 (1948); **17**, 118, 333 (1949); (b) J. G. Kirkwood and F. P. Buff, *ibid.*, **17**, 338 (1949); **18**, 991 (1950); (c) F. P. Buff, *ibid.*, **19**, 1591 (1951); **23**, 419 (1955); (d) S. Kondo, *ibid.*, **25**, 662 (1956).

(12) O. Sinanoglu, "Molecular Associations in Biology," B. Pullman, Ed., Academic Press, New York, N. Y., 1968, p 427.

(13) R. A. Pierotti, *J. Phys. Chem.*, **69**, 281 (1965).

(14) In certain cases, where the hydrocarbon is a gas at 298° at 1 atm of pressure, the vapor pressure of the liquid and the heat of vaporization must be taken into consideration.

(15) It is assumed that the water content of the liquid hydrocarbon phase may be neglected.

hydrocarbon in water. There are actually two different cavities involved in the transfer: the cavity in the pure liquid hydrocarbon of area  $A_{RR}(T)$  and the cavity in water of area  $A_{RW}(T)$ . The justification for considering only  $A_{RW}(T)$  is given in the Appendix.

In the case where there are  $n$  conformations for hydrocarbon R, the average area is approximately

$$A_{RW}(T) = \frac{\sum_{i=1}^n A_{RW,i}(T) e^{-\{\Delta G_{0i} + b_0 A_{RW,i}(T)\}/kT}}{\sum_{j=1}^n e^{-\{\Delta G_{0j} + b_0 A_{RW,j}(T)\}/kT}} \quad (6)$$

The quantity  $\Delta G_{0i}$  for conformation  $i$  is the difference between the molecular free energy  $G_0$  for conformation  $i$  and  $G_0$  for an arbitrary standard conformation. In the case of a given  $n$ -alkane, the standard conformation is its extended conformation.  $\Delta G_0$  may be approximated by assigning 0.8 kcal for each gauche interaction present in the conformation.<sup>16</sup> All energetically unfavorable conformations in which atoms were closer than their van der Waals radii will permit were disregarded in evaluating  $A_{RW}(T)$ . The parameter  $b_0(T)$  was first found from the single conformation hydrocarbons.

## Results

Table I gives a list of compounds and specific conformations together with their surface areas  $A_{RW}(T)$  and the logarithm of their solubilities. These are plotted in Figures 2 and 3. In Figure 2, the circles represent single conformations. Then those compounds with several possible conformations are plotted at the same log  $s$  ordinate, connected by a horizontal line. The black dot associated with each multiconformational compound represents a weighted average area calculated in accord with eq 6. The quantity  $b_0(T)$  appearing in eq 5 is determined from the single conformation compounds only and was found for the alkane and cycloalkane data at 25° to have the value  $0.033 \text{ kcal mol}^{-1} \text{ \AA}^{-2}$ .  $b_0(T)$  represents the unitary free energy per unit cavity surface area for transferring a hydrocarbon from the pure liquid to an aqueous solution. Examination of the graph reveals that branching tends both to reduce surface area and to increase solubility and that ring compounds are smaller than their corresponding open chain analogs. The interior of the ring is blocked from the packing of water molecules.

In Figure 3, several aromatic systems are plotted. These compounds do not lie on the same line as the alkanes. This is because the aromatic ring is more soluble in water than an aliphatic system of about the same size. The value of  $b_0(T)$  for Figure 3 is  $0.030 \text{ kcal mol}^{-1} \text{ \AA}^{-2}$ . This represents the unitary free energy for transferring alkyl side chains of aromatic systems from the pure liquid to water.

## Discussion

A good correlation was obtained in spite of the fact

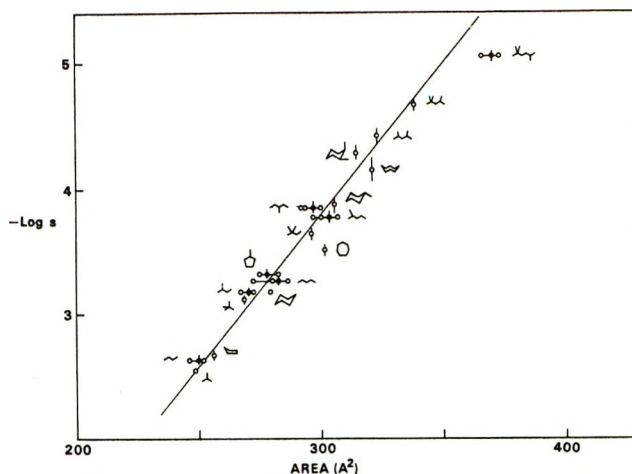


Figure 2. Relationship of cavity surface area to solubility for alkanes and cycloalkanes.

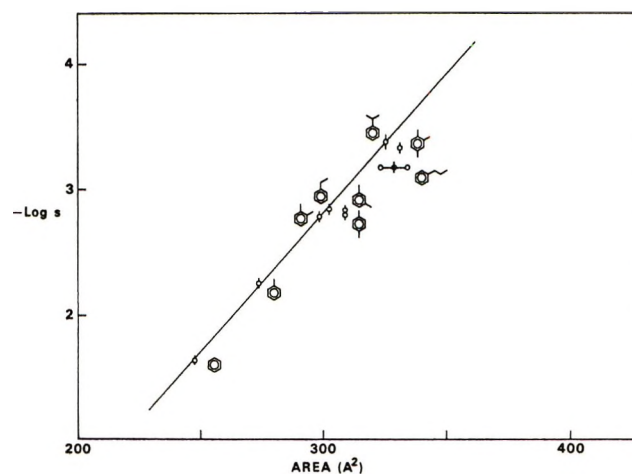


Figure 3. Relationship of cavity surface area to solubility for alkylbenzenes.

that no account was taken of variations in the cavity radius of curvature. While molecular cavities are highly curved, the relative curvature differences between members of a series are usually small. In paper I no account was taken of curvature differences either since the unitary free energy of a given solute was assumed to be proportional to the number of water molecules that could be packed around the solute molecule. If one molecule of water occupies  $12.7 \text{ \AA}^2$  on  $n$ -butane, then from the experimental unitary free energies of paper I, a slope of  $0.038 \pm 0.005 \text{ kcal/\AA}^2$  may be found for the first four alkanes. Differences between solution free energies appear to be well accounted for in both papers, and it is such differences rather than absolute values which are the useful quantities in hydrophobic interactions.

At the present time it is not known how the surface energy depends on molecular shape. The mechanism

(16) E. L. Eliel, N. L. Allinger, S. J. Angyal, and G. A. Morrison, "Conformational Analysis," Wiley, New York, N. Y., 1965.

Table I

Solute	Position of extra gauche interactions <sup>c</sup>	-Log $s^{a,b}$ at 25°	Cavity surface area $A_{HW}$ , Å <sup>2</sup>	Solute	Position of extra gauche interactions <sup>c</sup>	-Log $s^{a,b}$ at 25°	Cavity surface area $A_{HW}$ , Å <sup>2</sup>
Methane		2.816	152.36	2,4-Dimethylpentane		4.390	324.71
Ethane		2.696	191.52	2,2,4-Trimethylpentane <sup>e</sup>		4.670	338.93
Propane		2.848	223.35	2,2,5-Trimethylhexane		5.048	373.01
<i>n</i> -Butane		(2.975)	255.15		4,5		367.33
	2,3	(2.630)		Cyclopentane <sup>f</sup>		2.650	255.40
Isobutane		(3.075)	248.83	Methylcyclopentane <sup>g</sup>		3.300	282.71
		(2.547)	249.10				275.91
<i>n</i> -Pentane		3.270	286.97	Cyclohexane		3.180	279.10
	2,3		280.63	( <i>e</i> )-Methylcyclohexane		3.850	304.85
	2,3; 3,4		273.18	1- <i>cis</i> -2-Dimethylcyclohexane		4.270	315.50
2-Methylbutane		3.180	274.58	Cycloheptane <sup>h</sup>		3.516	301.94
	2,3		269.72	Cyclooctane <sup>h</sup>		4.152	322.58
2-Methylpentane		3.790	306.41	Benzene <sup>a</sup>		1.637	240.71
	2,3		301.54	Toluene <sup>a</sup>		2.292	273.90
	3,4		298.94	Ethylbenzene <sup>a</sup>		2.880	302.27
3-Methylpentane <sup>d</sup>		3.830	300.08	<i>n</i> -Propylbenzene <sup>i</sup>		3.302	334.07
	2,3		300.07		$\alpha,\beta$		324.78
	2,3		295.20	Isopropylbenzene <sup>a,i</sup>		3.380	326.01
	2,3; 3,4		294.07	<i>o</i> -Xylene <sup>a,i</sup>		2.780	298.43
Neopentane		(3.337)	270.14	<i>m</i> -Xylene <sup>i</sup>		2.830	309.13
		(3.126)		<i>p</i> -Xylene <sup>i</sup>		2.813	309.13
2,2-Dimethylbutane		3.670	290.76	1,2,4-Trimethylbenzene <sup>a</sup>		3.320	331.63

<sup>a</sup> Solubility data taken from ref 17 for all aliphatic systems and for aromatic systems where indicated. <sup>b</sup> Numbers in brackets, calculated by McAuliffe,<sup>17</sup> are solubilities of the liquid solute at 25°. <sup>c</sup> Starting with the molecule in its extended conformation, (*i,j*) are the carbon atoms defining the bond about which rotation is to be performed. The resulting number of extra gauche interactions depends on the molecule. <sup>d</sup> The third conformation listed is the one with one more gauche interaction than the second conformation. <sup>e</sup> The conformation of this compound is such that some dihedral angles cannot be 60°. The area calculation was done on a conformation with one eclipsed bond. The true conformation deviates somewhat from this (N. L. Allinger, private communication), but this difference would not be expected to affect the area much. <sup>f</sup> J. E. Kilpatrick, K. S. Pitzer, and R. Spitzer, *J. Amer. Chem. Soc.*, **69**, 2483 (1947); K. S. Pitzer and W. E. Donath, *ibid.*, **81**, 3213 (1959); J. B. Hendrickson, *ibid.*, **83**, 4537 (1961). <sup>g</sup> These represent only the two most stable conformations where the methyl group is on the "tip of the flap" of the envelope-shaped cyclopentane. The ring in the first conformation is bent away from the methyl group; in the second, it is bent toward. All conformations including these differ little in energy. <sup>h</sup> The geometry was taken from N. L. Allinger, J. A. Hirsch, M. A. Miller, I. J. Tyminski, and F. A. Van-Catledge, *J. Amer. Chem. Soc.*, **90**, 1199 (1968). <sup>i</sup> The solubilities were measured, using the technique of ref 17, by Dr. Ronald Bopp of these laboratories.

outlined in paper I requires the first water layer to be backed up by a number of water layers. All molecules studied here were such that the overall shapes of each of the cavities was only very roughly ellipsoidal. In no cases are the cavities shaped in such a manner that the second water layer forms a secondary cavity with a shape much different from that formed by the first water layer. It is possible that some cavities, not computed in this paper, may be shaped such that the secondary cavity is quite different from the primary cavity. Figure 4 illustrates, in two dimensions, cavities created by certain molecules in which shapes present special problems aside from the problems of curvature. The difference in properties of portions of the cavity surface around molecules of this shape must differ from those treated in this paper.

McAuliffe<sup>17</sup> has correlated hydrocarbon solubility with experimental molar volume. A linear plot is obtained for a series such as, for example, the normal

alkanes but not normal alkanes and branched alkanes together. The problem is that branching increases molar volume; therefore, a decreased solubility is predicted for the corresponding branched alkanes which is contrary to the experimental results. The increased solubility due to branching was explained by McAuliffe by the fact that branching increases vapor pressure. Since branching decreases surface area as determined in this work, both normal and branched alkanes can be incorporated in the same linear plot (Figure 2). Thus cavity surface area is a better parameter than experimental molar volume in correlating solubilities in that it is more generally applicable, and no additional quantities need be invoked to explain differences between types of alkanes. Furthermore, the molar volume is an experimental quantity, while the surface area is not

(17) C. McAuliffe, *J. Phys. Chem.*, **70**, 1267 (1966).



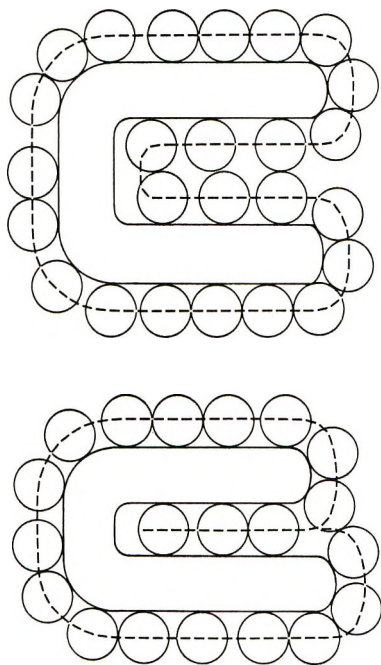


Figure 4. Cavity surfaces presenting special problems.

dependent on measurements of individual compounds, once the slope of Figure 2 is established.

Again with respect to predictive value, the area of a solute may be compared with its Hansch partition coefficient<sup>18</sup> for a particular series of compounds. Hansch has found a correlation between the logarithm of the solubility and the  $\pi$  value.<sup>19</sup> The rules for computing  $\pi$  values involve different values for normal alkane  $\text{CH}_2$  groups and cycloalkane  $\text{CH}_2$  groups; furthermore, it is necessary to make a correction for branching. The present method offers a way to compute  $\pi$  values using fewer parameters. It might offer an even better way of obtaining  $\pi$  values at least in the case of large hydrocarbon groups. For example, it would be expected that a large hydrocarbon which would normally exist in a folded conformation would have a relatively small cavity surface area, compared with its extended conformation. The true  $\pi$  value would be correspondingly smaller than that computed from the usual set of rules.

If the hydrophobic interaction energy between two hydrocarbon groups could be calculated semiempirically, one factor would be the change in surface area when the groups are together and when they are apart. The cavities relevant to such a calculation could involve shapes deviating remarkably from those determined by the molecules represented in this paper, giving rise to the types of difficulties illustrated in Figure 4. Furthermore, the coming together of two hydrocarbon groups could involve large changes in cavity curvature. Another difficulty mentioned by numerous authors is the modification of water structure at a hydrocarbon surface due to the proximity of polar groups.<sup>20</sup> The application of surface area calculations as a semiempirical method for the calculation of hydrophobic

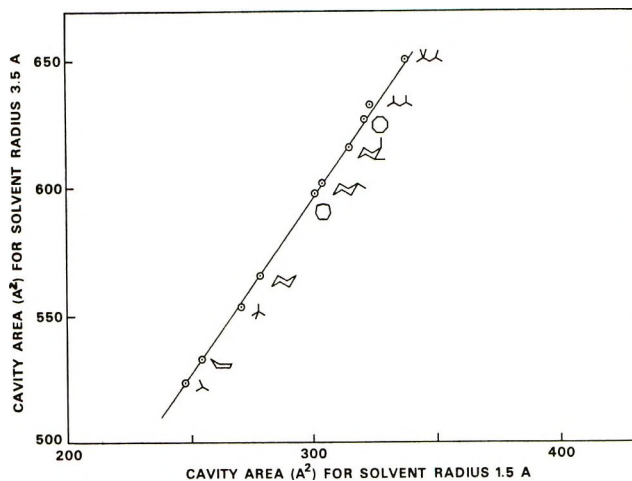


Figure 5. Proportionality of solute cavity surface areas for two solvent radii.

interactions may have to await the resolution of these difficulties.

#### Appendix

*Use of a Single Series of Surface Areas  $A_{RW}(T)$  to Correlate the Free Energy of Transfer.* Since the transfer of a hydrocarbon molecule from the pure liquid to water involves two cavities of different sizes (according to the definition of cavity size given here), it would seem necessary to relate the free energy of transfer to both cavity areas rather than just  $A_{RW}(T)$ . The relationship of eq 5 could still be used if the two series of cavity areas were themselves linearly related. However, for a molecule in the pure liquid, the adjacent molecules defining the cavity vary from member to member in the series making such a comparison difficult. The proposed proportionality between free energy of transfer and surface area  $A_{RW}(T)$  may be stated more easily in the following way.

The transfer of hydrocarbon from the pure liquid to water may be thought of involving two steps: (1) from the pure liquid to dilute hydrocarbon solution in which the hydrocarbon solvent molecules have some small specified radius of, for example, 3.5 Å, and (2) from this hydrocarbon solution to dilute aqueous solution. Figure 5 demonstrates that the cavity areas  $A_{RH}(T)$  in the hydrocarbon solution are linearly related to  $A_{RW}(T)$ . Aside from the entropy of mixing term, the dominant contribution to the free energy of step 1 is the heat of mixing, which is small in the case of aliphatic hydrocarbons.<sup>21</sup> Thus, in the proposed relationship between free energy of solution and the cavity surface area, the single quantity  $A_{RW}(T)$  is the only surface area term that needs to be explicitly considered,

(18) C. Hansch and T. Fujita, *J. Amer. Chem. Soc.*, **86**, 1616 (1964).

(19) C. Hansch, J. E. Quinlan, and G. L. Lawrence, *J. Org. Chem.*, **33**, 347 (1968).

(20) A. Ben-Naim, *J. Chem. Phys.*, **54**, 1387 (1971).

(21) J. Hildebrand, *Chem. Rev.*, **44**, 37 (1949).

providing the heat of mixing term in step 1 is assumed to be either negligible or proportional to molecular size (as defined by cavity surface area).

*Calculation Details.* A computer program was written to calculate the area  $A_{RW}(T)$  with input information of bond lengths and angles, atomic radii, and the radius of a spherical solvent molecule. The atomic radii, which are essentially the crystal packing radii, were taken from Bondi.<sup>22</sup> For carbon and hydrogen the following values were used: aliphatic carbon, 1.7 Å; aromatic carbon, 1.77 Å; aliphatic hydrogen, 1.2 Å; aromatic hydrogen, 1.0 Å. The radius of the water molecule was taken as 1.5 Å. The considerations responsible for this choice were from scaled particle theory,  $a = 1.45$  for the van der Waals water radius

at 298°, <sup>23</sup> while Bondi gave the maximum crystal packing radius of oxygen in ethers as 1.52 Å. The calculated areas are accurate to at least 0.1 Å<sup>2</sup>.

*Acknowledgments.* I would like to thank Mr. Max M. Marsh and Dr. Lowell G. Tensmeyer for many helpful discussions, and Mr. Donald Saunders for writing a preliminary version of the surface area program. I am also indebted to Dr. Ronald Bopp for some of the solubility measurements.

(22) A. Bondi, *J. Phys. Chem.*, **68**, 441 (1964).

(23) H. Reiss, "Advances in Chemical Physics," Vol. 10, I. Prigogine, Ed., Interscience, New York, N. Y., 1965, p 1. The value obtained here was found by interpolation of values for a number of temperatures in Table XVI.

## A Solubility Study of Silver Halides in Molten Calcium Nitrate Tetrahydrate

by Brian Burrows\* and Soefjan Noersjamsi

*School of Chemistry, Macquarie University, North Ryde, New South Wales, 2113, Australia (Received March 6, 1972)*

The solubility products of AgCl, AgBr, and AgI in molten  $\text{Ca}(\text{NO}_3)_2 \cdot 4\text{H}_2\text{O}$  have been determined potentiometrically over the temperature range 40–80°.  $\Delta G^\circ_{\text{soln}}$ ,  $\Delta H^\circ_{\text{soln}}$ , and  $\Delta S^\circ_{\text{soln}}$  values were determined for the dissolution equilibria and compared with available data for aqueous solution and anhydrous nitrate melts. Analysis of the partial mole fraction entropies of solution reveals a similarity between the hydrated and the anhydrous nitrate systems in that no significant trend from AgCl to AgI is apparent. This is in contrast to the behavior in aqueous solution.

### Introduction

An increasing amount of interest has been shown over the past decade in molten hydrate and molten salt–H<sub>2</sub>O systems. This interest stems largely from the fact that these systems form a link between aqueous electrolyte solutions on the one hand and completely ionic melts on the other. Most of the experimental data so far obtained suggest that these very concentrated aqueous solutions more closely resemble ionic melts than aqueous solutions.

Angell<sup>1–3</sup> was the first to propose that hydrate melts such as  $\text{Ca}(\text{NO}_3)_2 \cdot 4\text{H}_2\text{O}$  and  $\text{MgCl}_2 \cdot 6\text{H}_2\text{O}$  could be considered as molten salts with large hydrated cations and unhydrated anions. This molten salt analogy was based on a comparison of the transport properties of concentrated electrolyte solutions of this type with the transport properties of anhydrous melt systems. The additivity of molar volumes in the  $\text{Ca}(\text{NO}_3)_2 \cdot 4\text{H}_2\text{O}$ –KNO<sub>3</sub> system,<sup>4</sup> by analogy with the fact that molar volumes of binary molten salt mixtures are commonly

additive, also suggested the existence of the  $\text{Ca}(\text{H}_2\text{O})_4^{2+}$  ion.

Braunstein and coworkers<sup>5–8</sup> pioneered the application of the quasi-lattice model of molten salts to the study of concentrated electrolyte solutions. This thermodynamic approach is based on studying complex-ion association equilibria in molten salt–H<sub>2</sub>O and molten hydrate systems. Among the complexes which have been studied are cadmium halide<sup>5,6</sup> and silver

(1) C. A. Angell, *J. Electrochem. Soc.*, **112**, 1224 (1965).

(2) C. A. Angell, *J. Phys. Chem.*, **69**, 2137 (1965).

(3) C. A. Angell, *ibid.*, **70**, 3988 (1966).

(4) J. Braunstein, L. Orr, and W. Macdonald, *J. Chem. Eng. Data*, **12**, 415 (1967).

(5) J. M. C. Hess, J. Braunstein, and H. Braunstein, *J. Inorg. Nucl. Chem.*, **26**, 811 (1964).

(6) J. Braunstein, A. R. Alvarez-Funes, and H. Braunstein, *J. Phys. Chem.*, **70**, 2734 (1966).

(7) P. C. Lammers and J. Braunstein, *J. Phys. Chem.*, **71**, 2626 (1967).

(8) J. Braunstein, *ibid.*, **71**, 3402 (1967).

halide<sup>9</sup> complexes in molten  $\text{NH}_4\text{NO}_3 \cdot 2\text{H}_2\text{O}$ , cadmium bromide complexes<sup>6</sup> in molten  $\text{Ca}(\text{NO}_3)_2 \cdot 4\text{H}_2\text{O}$ , cadmium complexes<sup>7,8</sup> in the  $\text{LiNO}_3\text{-KNO}_3\text{-H}_2\text{O}$  system, and silver chloride complexes<sup>10</sup> in the  $\text{NH}_4\text{NO}_3\text{-H}_2\text{O}$  system. Analysis of the association constants and their temperature behavior in terms of the quasi-lattice model and comparison with corresponding results in anhydrous melts has further indicated the similarity between very concentrated electrolyte solutions and ionic melts.

More direct evidence for the existence of  $\text{M}(\text{H}_2\text{O})_n^{m+}$  ions came from a spectroscopic study by Angell and Gruen.<sup>11</sup> They studied the coordination states of Ni(II) in aqueous magnesium chloride solutions at temperatures up to 320° and concentrations up to 8 M in magnesium chloride. They successfully predicted<sup>2</sup> the existence of tetrahedral  $\text{NiCl}_4^{2-}$  complexes by analogy with  $\text{NiCl}_4^{2-}$  in molten CsCl and concluded that for compositions corresponding to  $\text{Mg}(\text{Cl})_2 \cdot 6\text{H}_2\text{O}$  the species  $\text{Mg}(\text{H}_2\text{O})_6^{2+}$  exists as an independent entity. Moynihan and Fratiello<sup>12</sup> on the basis of proton magnetic resonance studies of calcium nitrate tetrahydrate melts with anhydrous  $\text{KNO}_3$ ,  $(\text{CH}_3)_4\text{N} \cdot \text{NO}_3$ , and  $\text{Mg}(\text{NO}_3)_2$  further concurred with the fused salt analogy for hydrate melts.

This contribution presents results of a potentiometric study of the solubility of silver halides in molten  $\text{Ca}(\text{NO}_3)_2 \cdot 4\text{H}_2\text{O}$ . The aim was to analyze and compare the thermodynamic data so obtained with similar thermodynamic data for silver halides in aqueous solution and in anhydrous nitrate melts in order to gain further insight into the similarities between molten hydrates and anhydrous molten salts.

### Experimental Section

All chemicals used were analytical reagent grade and were used directly without further purification. All chemicals except the  $\text{Ca}(\text{NO}_3)_2 \cdot 4\text{H}_2\text{O}$  were dried at 120°. The calcium nitrate tetrahydrate was found to have a melting point of 42.7° which agrees with the literature value.<sup>6</sup> The silver wire used was of 99.99% purity from Johnson, Mathey & Co.

The cell used was a jacketed reaction vessel of 250-ml capacity. A rubber stopper formed the enclosure at the top. Through this stopper were supported a thermometer, indicator electrode, and reference electrode compartment. Stirring was achieved magnetically via a small Teflon-covered magnetic bar. The temperature of the cell was controlled to within  $\pm 0.02^\circ$  by a constant temperature circulator (Haake ED Uni-therm). The evaporation of water was minimized by having a very small dead space above the solution. The absence of drift in the emf values indicated that any water loss was negligible.

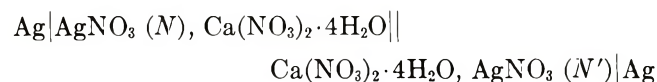
The reference electrode was immersed in the solution to be tested. It was made from a 1-cm diameter Pyrex tube with a fine-porosity sintered-glass disk sealed into

one end to give electrolytic contact with the test solution. No contamination of the test solution due to diffusion occurred over the course of our experiments (up to 8 hr). A known concentration of  $\text{AgNO}_3$  in  $\text{Ca}(\text{NO}_3)_2 \cdot 4\text{H}_2\text{O}$  served as the electrolyte in the reference half-cell. The silver electrode in the reference was similar to the indicator electrode, *i.e.*, it comprised a length of 0.05-cm diameter silver wire, coiled at one end to increase the surface area in contact with the electrolyte.

Cell potentials were measured either with a millivolt potentiometer (Leeds & Northrop, Type 8691) or with a vacuum tube voltmeter (Philips, Model PM 2440). In both cases identical measurements were obtained to  $\pm 0.1$  mV within 10 min and they remained steady for periods of up to several hours. The effect of temperature on the solubility of  $\text{AgCl}$ ,  $\text{AgBr}$ , and  $\text{AgI}$  was investigated by carrying out a series of runs at 50, 55, 60, 70, and 80°.

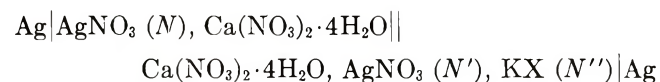
*Procedure.* The main compartment of the cell was first filled with about 200 g of  $\text{Ca}(\text{NO}_3)_2 \cdot 4\text{H}_2\text{O}$  containing a known weight of  $\text{AgNO}_3$ . The temperature was set at the required level by adjustment of the Haake circulator. The reference electrode compartment was filled *in situ* with the molten hydrate solution until the liquid level was the same as that in the main compartment of the cell.

As a check on the applicability of the Nernst equation to the  $\text{Ag}|\text{Ag}^+$  electrode in the hydrate melt the emf of the concentration cell



was measured at 42 and 60°. In the above cell *N* and *N'* indicate mole fractions in the reference half-cell and the indicator half-cell, respectively. The mole fractions are based on  $\text{Ca}(\text{NO}_3)_2 \cdot 4\text{H}_2\text{O}$  as one component. Weighed increments of  $\text{AgNO}_3$  were added to the indicator half-cell through a small funnel. After each addition the emf was monitored until it was stable to within  $\pm 0.2$  mV for at least 15 min.

The solubility experiments were carried out in the following cell.



The emf was measured after each weighed addition of  $\text{KCl}$ ,  $\text{KBr}$ , or  $\text{KI}$  as appropriate. The potential of the silver indicator electrode responded immediately after each addition.

(9) I. J. Gal, *Inorg. Chem.*, **7**, 1611 (1968).

(10) M. Peleg, *J. Phys. Chem.*, **75**, 2060 (1971).

(11) C. A. Angell and D. M. Gruen, *J. Amer. Chem. Soc.*, **88**, 5192 (1966).

(12) C. T. Moynihan and A. Fratiello, *ibid.*, **89**, 5546 (1967).

**Table I:** Solubility Products,  $K_{sp}$ ,<sup>a,b</sup> of Silver Halides in Molten  $\text{Ca}(\text{NO}_3)_2 \cdot 4\text{H}_2\text{O}$ 

AgCl		AgBr		AgI	
$T, ^\circ\text{K}$	$K_{sp} \times 10^{11}$	$T, ^\circ\text{K}$	$K_{sp} \times 10^{11}$	$T, ^\circ\text{K}$	$K_{sp} \times 10^{17}$
323.2	$2.20 \pm 0.23$	323.1	$2.72 \pm 0.09$	323.1	$0.41 \pm 0.005$
328.1	$3.05 \pm 0.19$	333.2	$6.20 \pm 0.02$	338.1	$2.78 \pm 0.04$
333.2	$5.80 \pm 0.27$	338.3	$10.76 \pm 0.04$	343.1	$6.22 \pm 0.82$
343.1	$11.50 \pm 0.13$	343.1	$17.39 \pm 0.44$	348.2	$7.63 \pm 0.04$
353.3	$21.16 \pm 0.22$	353.2	$36.56 \pm 0.08$	353.1	$14.75 \pm 0.06$

<sup>a</sup> Mole fraction scale. <sup>b</sup> Average values from at least four determinations.

## Results

The  $\text{Ag}|\text{Ag}^+$  electrode was well behaved in molten  $\text{Ca}(\text{NO}_3)_2 \cdot 4\text{H}_2\text{O}$  since, when checked at 42 and 60°, the average difference between the experimental and theoretical (calculated from the Nernst equation) emf's was found to be  $\pm 0.1$  mV over the concentration range  $6 \times 10^{-4}$  to  $4 \times 10^{-3}$  ion fraction of  $\text{Ag}^+$ . The emf data appear as supplementary material in the microfilm edition.<sup>13</sup>

This good agreement of experiment with theory indicates that junction potentials were insignificant and deviations from ideal behavior were negligible; *i.e.*, the activity coefficient of  $\text{AgNO}_3$  was unity.

In calculating the solubility product of the silver halide it was assumed that complex formation would have no significant effect on the value of the solubility product,  $K_{sp}$ . Thus the equilibrium silver ion concentration,  $[\text{Ag}^+]$ , at any time after the melt had been saturated with  $\text{AgX}$ , was calculated from the measured emf *via* the Nernst equation. The equilibrium concentration of free halide ion  $[\text{X}^-]$  was determined from the relationship

$$[\text{X}^-] = C_{\text{X}^-} - C_{\text{Ag}^+} + [\text{Ag}^+] \quad (1)$$

where  $C_{\text{X}^-}$  represents the concentration of  $\text{KX}$  which has been added at any instant and  $C_{\text{Ag}^+}$  is the initial concentration of  $\text{AgNO}_3$ . The solubility product was then given by  $[\text{Ag}^+][\text{X}^-]$ . The results are summarized in Table I. More data appear as supplementary material in the microfilm edition.<sup>13</sup>

Tien and Harrington<sup>14</sup> have pointed out that ion pair formation such as  $\text{AgX}$  would not affect the value of  $K_{sp}$  as determined by this potentiometric method. They also assumed that one could consider complexes such as  $\text{AgX}_2^-$  to be absent provided  $K_{sp}$  was constant over a wide range of  $\text{Ag}^+$  ion and  $\text{Cl}^-$  ion concentrations. This latter assumption has been criticized by Fiorani, *et al.*,<sup>15</sup> who pointed out that when the simple complexes  $\text{AgX}_2^-$ ,  $\text{AgX}$ , and  $\text{Ag}_2\text{X}^+$  are taken into account an expression of the following form, involving  $K_{sp}$ , is obtained

$$C_{\text{X}^-} - C_{\text{Ag}^+} = \frac{K_{sp}}{[\text{Ag}^+]}(1 + \beta_{2,1}K_{sp}) - [\text{Ag}^+](1 + \beta_{1,2}K_{sp}) \quad (2)$$

where  $\beta_{2,1}$  and  $\beta_{1,2}$  are the stability constants for the species  $\text{AgX}_2^-$  and  $\text{Ag}_2\text{X}^+$ , respectively. If only the complex  $\text{AgX}_2^-$  is present then eq 2 reduces to

$$C_{\text{X}^-} - C_{\text{Ag}^+} = \frac{K_{sp}}{[\text{Ag}^+]}(1 + \beta_{2,1}K_{sp}) - [\text{Ag}^+] \quad (3)$$

*i.e.*, the solubility product term becomes  $K_{sp}(1 + \beta_{2,1}K_{sp})$ .

Thus one is only justified in neglecting complexes such as  $\text{AgX}_2^-$  provided  $\beta_{2,1}$  is not too large or in other words the product  $\beta_{2,1}K_{sp} \ll 1$ . If we can expect  $\beta_{2,1}$  values similar to those obtained in anhydrous nitrate melt<sup>16</sup> and in molten ammonium nitrate dihydrate<sup>9</sup> then we can ignore mononuclear complexes since in these systems values of  $\beta_{2,1}$  of the order of  $10^3$ – $10^4$  have been found while  $K_{sp}$  values of  $10^{-7}$  have been determined. In fact in the present work  $K_{sp}$  values of  $10^{-11}$  to  $10^{-17}$  were determined which indicates that  $\beta_{2,1}$  values in  $\text{Ca}(\text{NO}_3)_2 \cdot 4\text{H}_2\text{O}$  would have to be very large,  $10^8$  to  $10^{14}$ , before they would become important.

On the other hand, if polynuclear complexes such as  $\text{Ag}_2\text{X}^+$  are present Fiorani, *et al.*,<sup>15</sup> argue that systematic trends in the  $K_{sp}$  data should be apparent. Since no such trends appeared in our data<sup>13</sup> it is assumed that the presence of any  $\text{Ag}_2\text{X}^+$  species has not affected our  $K_{sp}$  values.

From the solubility product values it is straightforward to determine the standard Gibbs free energy change for the dissolution equilibria from the relation

$$RT \ln K_{sp} = -\Delta G_{\text{soln}}^\circ \quad (4)$$

and from the temperature variation of  $K_{sp}$  one can determine  $\Delta H_{\text{soln}}^\circ$  with the aid of the van't Hoff equation

$$d \ln K_{sp}/dT = \Delta H_{\text{soln}}^\circ/RT^2 \quad (5)$$

(13) The data will appear following these pages in the microfilm edition of this volume of the journal. Single copies may be obtained from the Business Operations Office, Books and Journals Division, American Chemical Society, 1155 Sixteenth St., N.W., Washington, D. C. 20036, by referring to code number JPC-72-2759. Remit check or money order for \$3.00 for photocopy or \$2.00 for microfiche.

(14) H. T. Tien and G. W. Harrington, *Inorg. Chem.*, **2**, 369 (1963).

(15) M. Fiorani, G. G. Bombi, and G. A. Mazzochin, *J. Electroanal. Chem.*, **13**, 167 (1967).

(16) H. T. Tien and G. W. Harrington, *Inorg. Chem.*, **3**, 215 (1964).

In the present study linear plots of  $\log K_{sp}$  vs.  $1/T$  were obtained indicating that  $\Delta H^\circ_{soln}$  is independent of temperature over the range 40–80°. These linear relationships are summarized in eq 6–8.

$$\log K_{sp}(\text{AgCl}) = -3951/T + 0.454 \quad (6)$$

$$\log K_{sp}(\text{AgBr}) = -4912/T + 1.538 \quad (7)$$

$$\log K_{sp}(\text{AgI}) = -5915/T + 0.919 \quad (8)$$

## Discussion

In order to compare the solubility data, or more particularly the derived thermodynamic data, obtained in this study with similar data obtained in anhydrous molten nitrate systems and in aqueous solution the choice of standard state is critical. This is due to the fact that since the solubility product is related to the thermodynamic quantities as follows

$$\Delta S^\circ_{soln} = (\Delta H^\circ_{soln} - \Delta G^\circ_{soln})/T = \Delta H^\circ_{soln}/T + R \ln K_{sp} \quad (9)$$

the choice of concentration scale will affect  $K_{sp}$  and hence the derived  $\Delta S^\circ$  and  $\Delta G^\circ$  values. In practice the molal scale is most commonly used; however, this is undesirable for reasons first recognized by Gurney<sup>17</sup> and later by other workers<sup>18,19</sup> in the context of ion association.

The relation between  $\ln K_{sp}^N$  (mole fraction scale) and  $\ln K_{sp}^m$  (molal scale) for salts of the type  $\text{AgX}$  in dilute solution is given by

$$\ln K_{sp}^m = \ln K_{sp}^N + 2 \ln (1000/M_0) \quad (10)$$

where  $M_0$  is the formula weight of the solvent. Thus it can be seen that  $\ln K_{sp}^m$  contains an arbitrary term  $2 \ln (1000/M_0)$  which will vary with the choice of solvent. If the solubility products are calculated on the mole fraction scale this arbitrary constant is removed and the standard state is the hypothetical mole fraction state of unity for the solute in question. Such a state is one of minimum configurational free energy for a solute retaining the properties it possesses in dilute solutions and is to be preferred to the standard state on the molal scale.

The derived values of  $\Delta G^\circ_{soln}$ ,  $\Delta H^\circ_{soln}$ , and  $\Delta S^\circ_{soln}$  for the dissolution equilibria



in molten  $\text{Ca}(\text{NO}_3)_2 \cdot 4\text{H}_2\text{O}$  at 68° are presented in Table II together with values for the same equilibria in several other systems calculated from available literature data. The aqueous solution values at 25° were derived from the data (molal scale) of Owen and Brinkley<sup>20</sup> using eq 10. The values at 159° in the molten  $\text{LiNO}_3\text{--KNO}_3$  eutectic were interpolated from the results of Tien and Harrington<sup>14</sup> and those at 250° in the  $\text{NaNO}_3\text{--KNO}_3$  eutectic melt were calculated from the data (molal scale) of Flengas and Rideal<sup>21</sup>

again using eq 10. The temperatures of comparison for the first three systems are all at 25° above the melting point of the particular solvent. In the case of the  $(\text{Na}, \text{K})\text{NO}_3$  melt the temperature is 30° above the melting point of the solvent as the data did not allow an extrapolation.

**Table II:** Thermodynamic Quantities<sup>a</sup> for the Equilibria  $\text{AgX(s)} \rightleftharpoons \text{Ag}^+ + \text{X}^-$  in  $\text{H}_2\text{O}$ ,<sup>20</sup>  $\text{Ca}(\text{NO}_3)_2 \cdot 4\text{H}_2\text{O}$ ,  $(\text{Li}, \text{K})\text{NO}_3$ ,<sup>14</sup> and  $(\text{Na}, \text{K})\text{NO}_3$ <sup>21</sup> at the Same Temperature Relative to the Melting Point of the Solvent<sup>b</sup>

	$\Delta G^\circ_{soln}$ , kcal mol <sup>-1</sup>	$\Delta H^\circ_{soln}$ , kcal mol <sup>-1</sup>	$\Delta S^\circ_{soln}$ , cal mol <sup>-1</sup> K <sup>-1</sup>
AgCl in			
H <sub>2</sub> O <sup>c</sup>	18.05	15.65	-8.0
$\text{Ca}(\text{NO}_3)_2 \cdot 4\text{H}_2\text{O}^d$	15.70	18.10	+7.0
$(\text{Li}, \text{K})\text{NO}_3^e$	18.07	19.50	+3.5
$(\text{Na}, \text{K})\text{NO}_3^f$	17.50	18.30	+1.6
AgBr in			
H <sub>2</sub> O <sup>c</sup>	21.50	20.15	-4.5
$\text{Ca}(\text{NO}_3)_2 \cdot 4\text{H}_2\text{O}^d$	20.02	22.50	+6.7
$(\text{Li}, \text{K})\text{NO}_3^e$	22.32	23.20	+2.0
$(\text{Na}, \text{K})\text{NO}_3^f$	22.00	21.30	-1.3
AgI in			
H <sub>2</sub> O <sup>c</sup>	26.67	26.47	-0.1
$\text{Ca}(\text{NO}_3)_2 \cdot 4\text{H}_2\text{O}^d$	25.64	27.10	+4.3
$(\text{Li}, \text{K})\text{NO}_3^e$	26.31	28.40	+4.8
$(\text{Na}, \text{K})\text{NO}_3^f$	28.20	29.35	+2.2

<sup>a</sup>  $\Delta G^\circ_{soln}$  and  $\Delta S^\circ_{soln}$  are calculated from  $K_{sp}$  values on the mole fraction scale. <sup>b</sup> Temperatures of comparison are at 25° between the melting point of the solvent except for  $(\text{Na}, \text{K})\text{NO}_3$  which is 30° above. <sup>c</sup> 25°. <sup>d</sup> 68°. <sup>e</sup> 159°. <sup>f</sup> 250°.

The  $\Delta S^\circ_{soln}$  values in Table II correspond to the standard unitary entropies of Gurney<sup>17</sup> and, due to the choice of standard state, are essentially independent of the composition of the solution being primarily associated with the purely local changes in the entropy of the solvent in the immediate neighborhood of each added ion. Such entropies are thus ideally suited for intersolvent comparisons. The term "unitary" signifies that the standard state has been chosen on the mole fraction scale.

When the  $\Delta S^\circ_{soln}$  values in Table II are examined a similarity is apparent between the behavior of the halides in the molten hydrate and anhydrous molten salt systems in contrast to that of the halides in aqueous solution. Thus the standard mole fraction entropy values for the solubility equilibria in the nitrate sys-

(17) R. W. Gurney, "Ionic Processes in Solution," McGraw-Hill, New York, N. Y., 1953, pp 90–97, 178–181.

(18) A. W. Adamson, *J. Amer. Chem. Soc.*, **76**, 1578 (1954).

(19) H. A. Bent, *J. Phys. Chem.*, **60**, 123 (1956).

(20) B. B. Owen and S. R. Brinkley, *J. Amer. Chem. Soc.*, **60**, 2233 (1938).

(21) S. N. Flengas and E. R. Rideal, *Proc. Roy. Soc., Ser. A*, **233**, 443 (1956).

tems show no apparent trends from one halide to the next. This behavior was previously noted by Tien and Harrington<sup>14</sup> in the case of the (Li, K)NO<sub>3</sub> eutectic system. The absence of any trend from chloride to iodide suggests the absence of polarizable solvent species and indicates that the halide ions have a similar, namely ionic, environment in both the hydrated and anhydrous nitrate systems. On the other hand, the increase of standard mole fraction entropy in aqueous solution with increase in halide ion size points to the solvating influence of dipolar H<sub>2</sub>O molecules.

The entropy of solution of the silver halides was examined in more detail by calculating the relative partial entropies of the halides in the various solvents. For the dissolution equilibria 11 the entropy of solution can be written as

$$\Delta S^\circ_{\text{soln}} = S^\circ - S^\circ_{\text{crystal}} \quad (12)$$

where  $S^\circ$  is the standard partial mole fraction entropy and  $S^\circ_{\text{crystal}}$  is the standard entropy of the solid silver halide.

In Table III the various entropy values are listed.  $\Delta S^\circ_{\text{soln}}$  values were taken from Table II and  $S^\circ_{\text{crystal}}$  values were calculated from the available heat capacity data.<sup>22</sup> The last column of Table III shows the partial ionic entropy of the halide ions relative to the partial ionic entropy of the chloride ion. These relative values were derived from the relation

$$\bar{S}^\circ_{\text{AgX}} - \bar{S}^\circ_{\text{AgCl}} = (\bar{S}^\circ_{\text{Ag}^+} + \bar{S}^\circ_{\text{X}^-}) - (\bar{S}^\circ_{\text{Ag}^+} + \bar{S}^\circ_{\text{Cl}^-}) = \bar{S}^\circ_{\text{X}^-} - \bar{S}^\circ_{\text{Cl}^-} \quad (13)$$

assuming  $\bar{S}^\circ_{\text{Ag}^+}$  to be constant in the particular solvent.

The lack of a significant trend in the relative ionic entropies from Cl<sup>-</sup> to I<sup>-</sup> in the nitrate systems indicates that there is little alteration in the arrangement of the solvent species in the neighborhood of the X<sup>-</sup> anions with increase in size of these ions.<sup>23</sup> This is explicable if the hydrate melt is considered to be, like the anhydrous nitrate systems, completely ionic. Then when small amounts of Ag<sup>+</sup> and X<sup>-</sup> ions are added to these ionic melts they will be distributed randomly among the "holes" in the quasi-lattice arrangement of the solvent anions and cations. The solvent species, not being readily polarizable, would not preferentially solvate the halide ions. The slightly higher ionic entropy of the iodide ion in the anhydrous melts can be attributed to the greater "structure-breaking" effect of this larger ion. In contrast the aqueous solution ionic entropies show, as is well known, a distinct increase in the order  $\bar{S}^\circ_{\text{Cl}^-} < \bar{S}^\circ_{\text{Br}^-} < \bar{S}^\circ_{\text{I}^-}$  indicating that the smaller the halide ion the greater the ordering effect on the dipolar solvent molecules in the neighborhood of the anion.

The similarity in the relative partial ionic entropy values in the nitrate systems may, of course, be partly fortuitous since the  $\Delta S^\circ_{\text{soln}}$  values were calculated from heat changes derived from temperature coeffi-

**Table III:** Entropies<sup>a</sup> of Silver Halides in Molten Ca(NO<sub>3</sub>)<sub>2</sub>·4H<sub>2</sub>O, Aqueous Solution, and Anhydrous Nitrate Melts at the Same Temperature Relative to the Melting Point of the Solvent<sup>b</sup>

	$\Delta S^\circ_{\text{soln}}$ cal mol <sup>-1</sup> K <sup>-1</sup>	$S^\circ_{\text{cryst}}$ cal mol <sup>-1</sup> K <sup>-1</sup>	$S^\circ$ cal mol <sup>-1</sup> K <sup>-1</sup>	$\bar{S}^\circ_{\text{X}^-} - \bar{S}^\circ_{\text{Cl}^-}$ cal mol <sup>-1</sup> K <sup>-1</sup>
AgCl in				
H <sub>2</sub> O <sup>c</sup>	-8.0	23.0	15.0	0
Ca(NO <sub>3</sub> ) <sub>2</sub> ·4H <sub>2</sub> O <sup>d</sup>	+7.0	25.0	32.0	0
(Li,K)NO <sub>3</sub> <sup>e</sup>	+3.5	27.9	31.4	0
(Na,K)NO <sub>3</sub> <sup>f</sup>	+1.6	31.6	33.2	0
AgBr in				
H <sub>2</sub> O <sup>c</sup>	-4.5	25.6	21.1	6.1
Ca(NO <sub>3</sub> ) <sub>2</sub> ·4H <sub>2</sub> O <sup>d</sup>	+6.7	27.3	34.0	-2.0
(Li,K)NO <sub>3</sub> <sup>e</sup>	+2.0	30.6	32.6	1.2
(Na,K)NO <sub>3</sub> <sup>f</sup>	-1.3	33.5	32.2	-1.0
AgI in				
H <sub>2</sub> O <sup>c</sup>	-0.1	27.6	27.5	12.5
Ca(NO <sub>3</sub> ) <sub>2</sub> ·4H <sub>2</sub> O <sup>d</sup>	+4.3	29.4	33.7	1.7
(Li,K)NO <sub>3</sub> <sup>e</sup>	+4.8	33.0	37.8	6.4
(Na,K)NO <sub>3</sub> <sup>f</sup>	+2.2	35.8	38.0	4.8

<sup>a</sup> Mole fraction scale. <sup>b</sup> Temperatures of comparison are at 25° above the melting point of the solvent except for (Na,K)NO<sub>3</sub> which is 30° above. <sup>c</sup> 25°. <sup>d</sup> 68°. <sup>e</sup> 159°. <sup>f</sup> 250°.

cients of solubility products. These heat changes involve a significant uncertainty and one needs  $\Delta H^\circ$  values obtained from direct calorimetric methods to have a more reliable comparison. However, even allowing for some uncertainty there can be little doubt that the dissolution of AgX in molten Ca(NO<sub>3</sub>)<sub>2</sub>·4H<sub>2</sub>O is similar to the dissolution process in anhydrous nitrate melts and quite different from that in aqueous solution.

## Conclusion

The analysis of the mole fraction entropy data derived from solubility studies has shown that the dissolution of silver halides is a similar process in molten Ca(NO<sub>3</sub>)<sub>2</sub>·4H<sub>2</sub>O and in the anhydrous eutectic melts (Li,K)NO<sub>3</sub> and (Na,K)NO<sub>3</sub>, but quite different from the dissolution process in aqueous solution.

Thus we can conclude that, insofar as entropies are indicative of structural phenomena, molten calcium nitrate tetrahydrate does indeed behave like an ionic melt and presumably consists of complex Ca(H<sub>2</sub>O)<sub>4</sub><sup>2+</sup>

(22) O. Kubaschewski and E. U. Evans, "Metallurgical Thermochemistry," 3rd ed, Pergamon Press, London, 1958.

(23) Tien and Harrington<sup>14</sup> previously studied the solution entropies of silver halides in water and in (Li,K)NO<sub>3</sub> eutectic melt. They followed the treatment of Gurney<sup>17</sup> but the analysis of their data is incorrect due to an inconsistent use of standard states. Thus the  $\Delta S^\circ$  values in their Table III are on the molal scale in the case of the aqueous solution data and on the mole fraction (*i.e.*, "unitary") scale in the case of the nitrate melt. Then in Table V standard unitary entropies are calculated for the melt by subtracting the factor  $2R \ln 1000/M_0$  (Gurney's standard "cratic" entropy (see also eq 10 above)) from the  $\Delta S^\circ$  values in Table III which values are already standard unitary entropies.

ions and simple  $\text{NO}_3^-$  anions. This conclusion is in agreement with previous work<sup>1-4,11,12</sup> on this system.

*Acknowledgment.* S. N. wishes to acknowledge the award of a Rotary Fellowship.

## On the Thermodynamics of the Acetic Acid-Triethylamine System<sup>1</sup>

by Friedrich Kohler,\* E. Liebermann, G. Miksch, and Christine Kainz

*Institute of Physical Chemistry, University of Vienna, Vienna, Austria (Received March 20, 1972)*

The system acetic acid-triethylamine is one of the rare examples where phase separation occurs at negative values of the excess Gibbs free energy of mixing  $\Delta G^E$ . The vapor pressure curve exhibits a negative azeotrope besides the miscibility gap. Activity coefficients are calculated for 20° from the melting curve on the acetic acid side, from the vapor pressure of the negative azeotrope, from the concentrations along the coexistence curve, and from the vapor pressures between the miscibility gap and pure triethylamine. Orientative values for the heat of mixing are given. All properties indicate the existence of a very stable aggregate consisting of three molecules of acetic acid plus one molecule of triethylamine in the liquid state. Determination of the excess volumes shows an exceptionally large contraction around that mole ratio; viscosities have a very sharp maximum. The results are interpreted by a large attractive interaction between the polar 1:1 complex (acetic acid-triethylamine) and the acetic acid dimer, which causes the liquid mixture of equimolar concentration to split into a phase rich in the 3:1 aggregate and a phase rich in triethylamine.

### Introduction

The peculiar properties of the system acetic acid-triethylamine have been emphasized by several authors.<sup>2-4</sup> It has a negative azeotrope of very low vapor pressure at  $x_1$  (mole fraction of acetic acid) = 0.75, which stays at this composition at least until boiling at atmospheric pressure. For smaller mole fractions of acetic acid, there is a region of phase separation. Some measurements of total pressures have been carried out,<sup>4</sup> but a meaningful thermodynamic evaluation would have needed a proper consideration of the dimerization of acetic acid in the vapor phase.

In order to obtain the thermodynamic properties of the system, we have measured vapor pressures on the triethylamine side and concentrations of coexisting phases. On the acetic acid side, we have determined the melting curve and the vapor pressure curve of the negative azeotrope. The vapor pressure measurements are evaluated on the assumption that the vapor consists of triethylamine molecules, acetic acid monomers, and acetic acid dimers. Triethylamine-acetic acid complexes are neglected in the vapor phase. This certainly does not introduce any error on the triethylamine side, but it may affect the evaluation from the vapor pressure of the azeotrope. However, the conclusions drawn from the vapor pressure curve of the azeotrope fit into the general picture.

In previous discussions on acetic acid mixtures<sup>5,6</sup> attention has been called for the apparent existence of a strong interaction between a polar molecule and the

distortable hydrogen bonds of the acetic acid dimer. This interaction is accompanied by a large negative change of free energy and by a large volume contraction. Assuming a highly polar form of the 1:1 complex between acetic acid and triethylamine, this interaction can explain the preference for aggregates between acetic acid and triethylamine in the mole ratio 3:1. Volumetric measurements show indeed an extremely large volume contraction, which even increases with temperature. This is contrary to the behavior of hydrogen-bonded complexes, like  $\text{Et}_3\text{N} \cdot 3\text{H}_2\text{O}$ , where the complexes break up with increasing temperature, leading to a decrease of the volume contraction.

It has not been possible to obtain crystals around the mole ratio 3:1; instead the formation of a glass occurred. The viscosities have been measured and show a very sharp maximum near this mole ratio.

### Experimental Section and Results

Acetic acid (Pro Analysis) was fractionally distilled

- (1) Presented in part at the 161st National Meeting of the American Chemical Society, Los Angeles, Calif., March 1971.
- (2) H. S. van Klooster and W. A. Douglas, *J. Phys. Chem.*, **49**, 67 (1945).
- (3) J. Hollo, T. Lengyel, and H. M. Uzonyi, *Period. Polytech. Chem. Eng.*, **4**, 172 (1960).
- (4) V. F. Plekhotkin and N. P. Markuzin, *Fiz. Khim. Svoistva Rastvorov*, **12** (1964); A. V. Storonkin, N. P. Markuzin, and V. F. Plekhotkin, *ibid.*, **19** (1964).
- (5) H. E. Afsprung, G. H. Findenegg, and F. Kohler, *J. Chem. Soc. A*, 1364 (1968).
- (6) F. Kohler, *Monatsh. Chem.*, **100**, 1151 (1969).

in a 25-plate column (reflux ratio 20:1) after addition of some acetic acid anhydride. It was stored in the dark, the vapor phase being in contact with  $P_2O_5$ . The refractive index ( $n^{20}_D$ ) was 1.3716, the density ( $\rho^{20}$ ) was 1.04952 g/cm<sup>3</sup>, and the melting point was 16.53°.

Triethylamine (Purum) was shaken with solid KOH, fractionally distilled twice over sodium wire, and stored in the dark over solid KOH. The refractive index ( $n^{20}_D$ ) was 1.4003, and the density ( $\rho^{20}$ ) was 0.72729 g/cm<sup>3</sup>.

The total vapor pressures were determined as for the system acetic acid-carbon tetrachloride.<sup>7</sup> The results are given in Table I. The vapor pressure curves on the triethylamine side of the miscibility gap lie below the vapor pressure curve of an ideal mixture at 20 and 30° and slightly above that at 40°.

**Table I:** Total Vapor Pressure  $P$  of Solutions of Acetic Acid in Triethylamine<sup>a</sup>

$x_1$	$P$ , mm Hg		
	20°	30°	40°
0.0000	53.36	86.12	132.12
0.0223	51.95	84.23	130.06
0.0353	51.30	83.26	129.02
0.0612	49.62	81.41	126.31
0.0786	48.75	79.82	124.61
Two-phase region	45.29	74.57	117.42
1.0000	11.76		35.29

<sup>a</sup>  $x_1$  = mole fraction of acetic acid.

The consolute curve was determined by weighing the mixture in a tube closed by a ground stopper, and with an insert which allowed vigorous shaking without wetting of the ground stopper. The tube was placed into a thermostat and both the disappearance of any turbidity when slowly raising the temperature and the appearance of the first turbidity when slowly lowering the temperature were noted. The measured points are listed in Table II.

A mixture of the mole ratio 3:1 of acetic acid was prepared and distilled. The mixture showed a con-

**Table II:** Concentrations of Phase Separation in the System Acetic Acid-Triethylamine between 20 and 45°<sup>a</sup>

$t$ , °C	$x_1$	
21.5	0.1375	0.5919
24.4	0.1467	
25.1		0.5907
33.1	0.1541	0.5874
38.6	0.1583	0.5865
39.1		0.5836
44.3	0.1568	

<sup>a</sup>  $x_1$  = mole fraction of acetic acid.

stant boiling point. The mixture was degassed and its vapor pressure measured statically. These results are shown in Table III.

**Table III:** Vapor Pressure at the Composition of the Negative Azeotrope (Mole Fraction Acetic Acid 0.75) in the System Acetic Acid-Triethylamine

$t$ , °C	40	50	60	70	80	158.0
$P$ , mm Hg	1.99	3.84	7.35	13.28	23.30	742.5

The melting curve on the acetic acid side was determined with a method described elsewhere.<sup>8</sup> The results of the measurements are given in Table IV.

**Table IV:** Melting Point Lowering of Acetic Acid in the System Acetic Acid-Triethylamine<sup>a</sup>

$x_1$	$t$ , °C	$x_1$	$t$ , °C
1.0000	16.53	0.9249	6.48
0.9849	15.51	0.8880	-2.99
0.9751	14.69	0.8525	-14.44
0.9583	12.85	0.8391	-19.00
0.9484	11.42		

<sup>a</sup>  $x_1$  = mole fraction acetic acid.

The pycnometric determination of densities has been described.<sup>9</sup> For the tabulation of the results see the microfilm edition.<sup>10</sup>

Viscosities were determined in Ostwald viscosimeters calibrated with water. Results are shown in Figure 1 (the tabulation is given in the microfilm edition).<sup>10</sup>

### Thermodynamic Evaluation

The melting curve furnishes the activity coefficient  $f_1$  of acetic acid at a reference temperature  $T_{ref}$  according to the equation

$$\ln f_1 = -\frac{L''\Delta T}{RTT_m} + \frac{\Delta C_p''\Delta T^2}{2RTT_m} - \frac{\Delta H_1(T_{ref} - T)}{RT_{ref}^2} - \ln x_1 \quad (1)$$

In eq 1,  $T$  is the melting temperature of the mixture,  $T_m$  that of pure acetic acid, and  $\Delta T = T_m - T$ . The heat of melting  $L''$  of acetic acid can be checked by

(7) G. Miksch, F. Ratkovics, and F. Kohler, *J. Chem. Thermodyn.*, **1**, 257 (1969).

(8) E. Liebermann and F. Kohler, *Monatsh. Chem.*, **99**, 2514 (1968); R. J. Munn and F. Kohler, *ibid.*, **91**, 381 (1960).

(9) G. H. Findenegg and F. Kohler, *Trans. Faraday Soc.*, **63**, 870 (1967).

(10) Tabulation of the densities and viscosities will appear following these pages in the microfilm edition of this volume of the journal. Single copies may be obtained from the Business Operations Office, Books and Journals Division, American Chemical Society, 1155 Sixteenth St., N.W., Washington, D. C. 20036, by referring to code number JPC-72-2764. Remit check or money order for \$3.00 for photocopy or \$2.00 for microfiche.



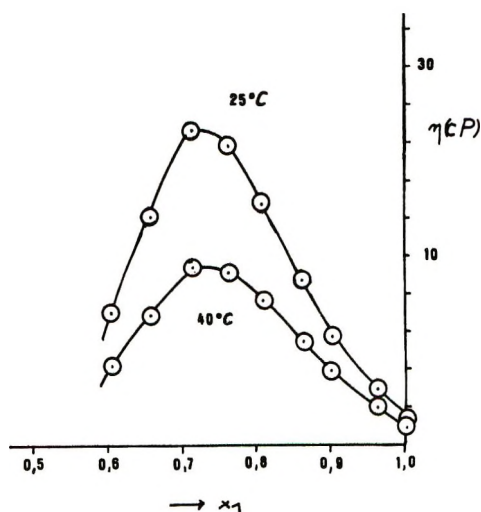


Figure 1. Viscosity  $\eta$  of the system acetic acid (1)-triethylamine at 25 and 40° for mole fractions on the acetic acid side of the miscibility gap.

extrapolating the quantity  $RTT_m(1-x_1)/\Delta T$  to  $x_1 = 1$ . Such a plot is linear for small values of  $1-x_1$  if  $\ln f_1$  can be approximated by a parabola (Figure 2); it leads to  $L'' = 2780 \text{ cal mol}^{-1}$  in good agreement with the literature<sup>11,12</sup> (2757 and 2803  $\text{cal mol}^{-1}$ , respectively). The difference in the heat capacities at melting  $\Delta C_P''$  for acetic acid is taken as  $5.4 \text{ cal } ^\circ\text{K}^{-1} \text{ mol}^{-1}$  by a rough extrapolation of  $C_P$  values of both solid and liquid phases.<sup>12</sup> The partial molar heat of mixing  $\Delta H_1$  is neglected. This will be discussed below.

The vapor pressure  $P$  of the azeotrope gives directly the activity coefficients of both components, if the vapor can be assumed to contain an ideal mixture of triethylamine, acetic acid monomers, and acetic acid dimers

$$\ln f_1 = \ln \frac{P}{P_{o1}} - \ln \frac{1+S}{1+\sqrt{1+4K_P P_{o1}}} \quad (2)$$

$$\ln f_2 = \ln \frac{P}{P_{o2}} + \ln \frac{1+4K_P P(2-x_1)-S}{2K_P P(2-x_1)^2}$$

with  $S = \sqrt{1+4K_P P x_1(2-x_1)}$ ,  $K_P$  being the dimerization constant of acetic acid in the gas phase, and  $P_{o1}$  and  $P_{o2}$  denoting the vapor pressures of the pure components.

The branch of the total pressure curve on the triethylamine side of the miscibility gap can be evaluated by a differential equation derived from the Gibbs-Duhem equation, which is modified to allow for dimerization of acetic acid in the vapor<sup>7</sup>

$$\frac{dy_1}{dP} = \frac{(2-y_1)^2(1+S+4K_P P y_1(2-y_1))}{2-2y_1+y_1^2+(2-2y_1)S+4K_P P y_1(2-y_1)} \times \frac{y_1(1-y_1)}{2P(y_1-x_1)} \quad (3)$$

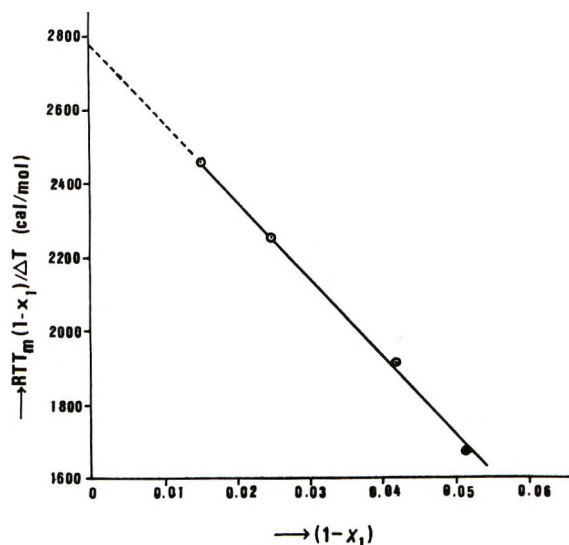


Figure 2. The function  $RTT_m(1-x_1)/\Delta T$  vs.  $(1-x_1)$ ; extrapolation to  $x_1 = 1$  gives the heat of melting of acetic acid.

Here  $y_1$  is the (formal) mole fraction of acetic acid in the gas phase and  $S$  is defined (in the general case) by  $S = \sqrt{1+4K_P P y_1(2-y_1)}$ . The numerical integration of eq 3 has to start at the lowest total pressure, *i.e.*, the pressure over the two-phase region. The corresponding value of  $y_1^*$ , which is needed as initial value for the integration procedure, is not known. Therefore, integration has been carried out for various values of  $y_1^*$ . It is clear that the choice of  $y_1^*$  influences strongly the position of the  $\ln f_1$  curve on the triethylamine side, but is relatively unimportant for the  $\ln f_2$  curve, which is near zero anyway. Therefore, the value of  $\ln f_2$  on the acetic acid side of the two-phase region is mainly determined by the measurements of the consolute curve.

In order to set the various pieces of information together, first the  $\ln f_2$  curve on the acetic acid side has been constructed from the points at the consolute curve ( $x_1 = 0.59$  at 20°) and at the azeotrope ( $x_1 = 0.75$ ) and from the known slope in the interval  $0.84 \leq x_1 \leq 1$ , which can be obtained from the  $f_1$  values determined by the melting curve by using the Gibbs-Duhem relation. The construction of the  $\ln f_2$  curve can be checked by recalculating the  $\ln f_1$  curve, which has to fit the points of the melting curve and the value at the azeotrope. Extending the Gibbs-Duhem integration of the  $\ln f_1$  curve now to the two-phase region, the correct value of  $y_1^*$  can be deduced. The behavior of the activity coefficients in the total concentration interval is shown in Figure 3; the probable continuation of the curves within the interval of instability of a homogeneous liquid is also indicated. The total Gibbs free energy of mixing (excess plus ideal) is given in Figure

(11) J. Meyer, *Z. Phys. Chem.*, **72**, 225 (1910).

(12) G. S. Parks and K. K. Kelley, *J. Amer. Chem. Soc.*, **47**, 2089 (1925).

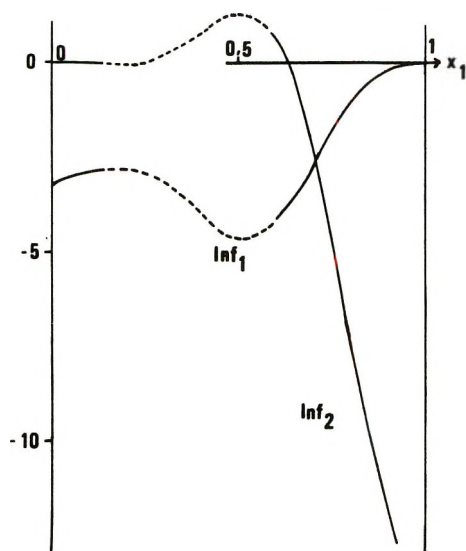


Figure 3. The logarithm of the activity coefficients of the system acetic acid (1)-triethylamine (2) at 20°. The calculated functions in the range of instability are indicated by dashed lines.

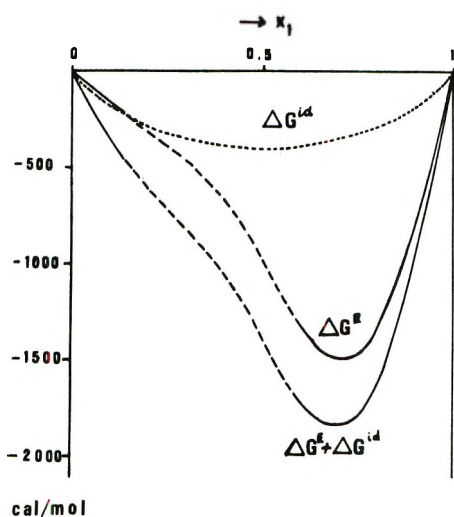


Figure 4. Ideal and excess Gibbs free energy of mixing of the system acetic acid (1)-triethylamine (2) at 20°. The dashed parts of the curves refer to the range of instability.

4 to illustrate the phase separation. The excess, divided by the product of the mole fractions, is given in Figure 5. Values for the heat of mixing divided by the product of the mole fractions are also included in Figure 5. These values are based on orientative calorimetric measurements at both ends of the concentration interval, on the temperature dependence of the azeotropic pressure, and on the temperature dependence of the total pressure near the consolute curve. They may be in error by  $\pm 10\%$ . At the acetic acid side, the curve for  $\Delta H$  vs.  $x_1$  seems to be curved in such a way that the partial heat of mixing of acetic acid  $\Delta H_1$  has a positive portion for high concentrations of acetic acid. This is in agreement with the fact that for the two points of

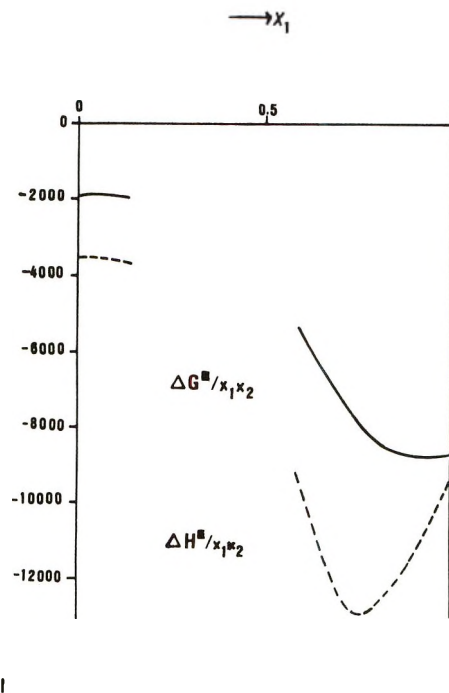


Figure 5. The excess Gibbs free energy of mixing (full curve) and the heat of mixing (dashed curve) divided by the product of mole fractions of acetic acid (1)-triethylamine at 20°.

the melting curve which have the largest temperature difference, a positive  $\Delta H_1$  value in eq 1 is necessary for a smooth continuation of the  $\ln f_1$  curve to the points deduced by the azeotropic pressure.

Figure 6 shows the values for the volume change of mixing divided by the product of the mole fractions. The abnormally large contractions are remarkable.

## Discussion

Figure 5 shows clearly that the formation of the 1:1 complex between triethylamine and acetic acid, which occurs on the triethylamine side, is accompanied by a negative  $\Delta G$  and by an about equally negative  $T\Delta S$  contribution, such that  $\Delta H$  of the complex formation is about twice as negative as  $\Delta G$ . In contrast to this, the formation of the aggregate triethylamine-3 acetic acid, which occurs on the acetic acid side, is accompanied by a strongly negative  $\Delta G$  contribution and a comparatively small, though negative,  $T\Delta S$  term. This can only be interpreted by a relatively indefinite orientation of the constituent molecules in the triethylamine-3 acetic acid aggregate.

This conclusion is confirmed by the measurements of the volume change of mixing. Let us compare the situation with that in pure acetic acid. The dimerization of acetic acid occurs without a volume change.<sup>13</sup> Apparently, the closer proximity of the two monomeric groups is compensated by the larger rotational volume of the rigid dimer. On the other hand, there is good

(13) T. A. Litovitz and E. Carnevale, *J. Acoust. Soc. Amer.*, **30**, 134 (1958).

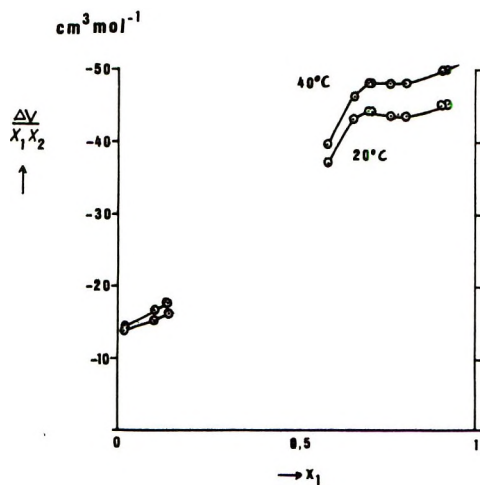


Figure 6. The volume change of mixing divided by the product of mole fractions of acetic acid (1)-triethylamine at 20 and 40°.

indication for a volume contraction in the monomer-dimer interaction,<sup>5</sup> which is thought to be relatively unspecific with respect to orientation. Similarly, the well-defined complex triethylamine-3 water shows a much smaller contraction<sup>14,15</sup> than the aggregate triethylamine-3 acetic acid. Furthermore, the rigid complex breaks up with increasing temperature, which is not the case for the aggregate triethylamine-3 acetic acid, as shown by a comparison of the expansion coefficients of the two systems (Figure 7).

The aggregate triethylamine-3 acetic acid, which is very stable but orientationally not well defined, is

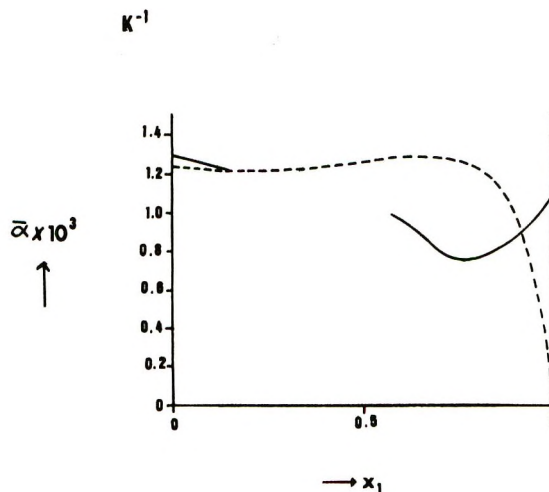


Figure 7. Mean expansion coefficient  $\bar{\alpha}$ : acetic acid (1)-triethylamine, temperature range 20-40° (full curve); water (1)-triethylamine, temperature range 0-13° (dashed curve).

thought to be caused by a strong inductive interaction between the polar 1:1 complex and the distortable hydrogen bonds of the acetic acid dimer.

*Acknowledgment.* The authors wish to thank Miss Brücher for carrying out the orientative measurements of the heat of mixing and the Institute of Statistics of our University for computer time.

(14) F. Kohler, H. Arnold, and R. J. Munn, *Monatsh. Chem.*, **92**, 876 (1961); F. Kohler, *ibid.*, **82**, 913 (1951).

(15) R. Schano, Doctoral Dissertation, University of Vienna, 1969.

# Adsorption Isotherms and Equations of State of Insoluble Vapors at the Water-Gas Interface as Studied by Gas Chromatography

by Jerry W. King, Amiya Chatterjee, and Barry L. Karger\*

Department of Chemistry, Northeastern University, Boston, Massachusetts 02115 (Received December 2, 1971)

Publication costs assisted by the Office of Naval Research

In continuation of previous work on the study of water at interfaces by gas chromatography, the gas-liquid interfacial adsorption isotherms of six insoluble vapors (three *n*-alkanes and three branched alkanes) have been determined in the range of 4000–500 Å<sup>2</sup>/molecule. From these isotherms, isosteric heats of adsorption have been derived, and it has been shown that over the whole concentration range examined the isosteric heat of adsorption is equal to or less than the heat of liquefaction. This points to the fact that water is a low-energy surface for hydrocarbons. The free energy of adsorption and the entropy of adsorption at constant surface coverage have also been calculated. Equations of state have been determined, and it has been shown that nonideal behavior exists down to concentrations as low as 2500 Å<sup>2</sup>/molecule. In addition, non-ideality increases with chain length for the *n*-alkanes and decreases with branching. Finally, calculations of thicknesses of the surface films indicate that the hydrocarbons can be considered to lie flat on the water surface in most cases over the whole concentration range studied. Gas-liquid chromatography is thus shown to be a valid technique for the study of adsorption of vapors on liquids at finite surface coverages.

## Introduction

In previous papers in this series,<sup>1–3</sup> we have shown gas chromatography (gc) to be a valid method for the study of the adsorption at zero surface coverage of insoluble vapors on the gas-liquid interface of water and of the partition at infinite dilution of sparingly soluble vapors in thin layers of water coated on wide pore diameter silica. In this paper we wish to report on an expansion of this work to the study of adsorption of insoluble vapors at finite surface coverages by gc. In an earlier paper,<sup>2</sup> we presented some preliminary results on the determination of adsorption isotherms and showed that the water system is well suited for study by gc.

The thermodynamic functions of adsorption and equations of state have been examined for three normal and three branched-chain alkanes, namely heptane (*n*-C<sub>7</sub>), octane (*n*-C<sub>8</sub>), nonane (*n*-C<sub>9</sub>), 2-methylheptane (2-MeC<sub>7</sub>), 2,5-dimethylhexane (2,5-DMeC<sub>6</sub>), and 2,2,4-trimethylpentane (2,2,4-TMeC<sub>5</sub>). Analysis of the results in terms of van der Waals theory leads to an estimation of the film thickness. Since gc in the elution mode is most applicable to low concentrations, we have studied the adsorption process at surface coverages ranging from 4000 to 500 Å<sup>2</sup>/molecule. The latter figure is close to the lowest surface coverage region examined by earlier workers<sup>4–7</sup> in the adsorption of insoluble vapors, including several of the above compounds, on water surfaces. Thus a comparison can be made between the dilute region in this study and the more concentrated region previously examined. In addition, Hauxwell and Ottewill<sup>8,9</sup> have presented some results for the adsorption of hydrocarbons on

water surfaces at very low surface coverage which allow a critical comparison of the gc approach to static methods for the determination of the adsorption isotherm.

In our previous studies<sup>2,3</sup> we have found water to be a low-energy surface when hydrocarbons are used as adsorbates. In addition, we reported standard heats and entropies of adsorption at zero surface coverage substantially less negative than the extrapolated values of static measurements.<sup>4,8</sup> The further examination of this result is important, since a model of surface perturbation of water during the adsorption process has been postulated from the negative heats and entropies of adsorption.<sup>10,11</sup>

## Experimental Section

The general apparatus has been described previously.<sup>1</sup> The only change for this work was the in-

- (1) B. L. Karger, P. A. Sewell, R. C. Castells, and A. Hartkopf, *J. Colloid Interface Sci.*, **35**, 328 (1971).
- (2) B. L. Karger, R. C. Castells, P. A. Sewell, and A. Hartkopf, *J. Phys. Chem.*, **75**, 3870 (1971).
- (3) A. K. Chatterjee, J. W. King, and B. L. Karger, *J. Colloid Interface Sci.*, in press.
- (4) R. H. Ottewill, Ph.D. Thesis, University of London, 1951.
- (5) D. C. Jones and R. H. Ottewill, *J. Chem. Soc.*, 4076 (1955).
- (6) D. C. Jones, R. H. Ottewill, and A. P. J. Chater, Proceedings of the International Congress on Surface Activity, London, 1957, p 188.
- (7) K. E. Hayes and R. B. Dean, *J. Phys. Chem.*, **57**, 80 (1953).
- (8) F. Hauxwell and R. H. Ottewill, *J. Colloid Interface Sci.*, **28**, 514 (1968).
- (9) F. Hauxwell and R. H. Ottewill, *ibid.*, **34**, 473 (1970).
- (10) A. W. Adamson, L. Dormant, and M. W. Orem, *ibid.*, **25**, 206 (1967).
- (11) M. W. Orem and A. W. Adamson, *ibid.*, **31**, 273 (1969).

corporation of a heated injection port in order to ensure rapid volatilization of the liquid samples. Solutes were injected using a 10- $\mu$ l Hamilton syringe. Density data, used to correct volumes to moles of sample, were obtained from Dreisbach.<sup>12</sup> All the solutes were reagent grade and were obtained from the following sources: *n*-C<sub>7</sub> and 2,2,4-TMeC<sub>5</sub>, Fisher Scientific; 2-MeC<sub>7</sub> and 2,5-DMeC<sub>6</sub>, J. T. Baker; *n*-C<sub>8</sub>, K & K Laboratories; and *n*-C<sub>9</sub>, Matheson Coleman and Bell. Chromatographic analysis at high sensitivity revealed no trace impurities.

The column packing consisted of 20% by weight water on 80–100 mesh Porasil D (Waters Associates, Framingham, Mass.), specific surface area  $\sim 29$  m<sup>2</sup> g<sup>-1</sup>. The weight per cent of water was determined both before and after column use by the weight difference of the coated and dried support. Good agreement was obtained in both cases.

All analyses were run in triplicate at each temperature. For the enthalpy determinations the temperature range was 8–16°, at intervals of roughly 2°. In addition, all studies were run close to the optimum gas velocity (highest column efficiency). Graphical integration was accomplished by the cut and weigh method. The flame ionization detector linearity was also checked and found to be obeyed over the concentration range of these experiments. An error analysis of this gc system for adsorption isotherm determination will be discussed in the Results section.

## Theory

We have previously shown that at zero surface coverage the six hydrocarbon solutes in this study undergo negligible partition in their travel through the water-gas chromatographic column,<sup>1,2</sup> the mechanism of retention being adsorption at the gas-liquid interface. From a consideration of the solubilities of these solutes in water<sup>13</sup> and the fact that  $K_A$  increases with concentration in the gas phase, it is reasonable to assume that interfacial adsorption remains the only mechanism of retention over the concentration range in this work. Since a nonlinear isotherm results, the net retention volume per gram of packing,  $V_N^0$ , can be written as<sup>14</sup>

$$V_N^0 = (1 - \phi_j Y_o) \left( \frac{\partial a}{\partial c} \right)_T A_L^0 \quad (1)$$

where  $Y_o$  = mole fraction of the adsorbate in the gas phase at the column outlet,  $a$  = concentration of adsorbate at the gas-liquid interface in moles per square centimeter,  $c$  = concentration of adsorbate in the gas phase in moles per cubic centimeter,  $A_L^0$  = surface area of the vapor-liquid interface per gram of packing, and where

$$j = J_3^2 \left[ 1 + \frac{Y_o^2 P_o B_{22}}{RT} (J_3^2 - 1) \right] \quad (2)$$

$$\phi = \frac{1 + k'(1 - Y_o J_2^1)}{1 + k'(1 - Y_o J_3^2)} \times \left[ 1 + \frac{2Y_o P_o B_{22}}{RT} (1 - Y_o J_2^1) \right] \quad (3)$$

where

$$J_n^m = \frac{n}{m} \left[ \frac{(P_i/P_o)^m - 1}{(P_i/P_o)^n - 1} \right]$$

$B_{22}$  = second virial coefficient of pure solute (adsorbate),  $k'$  = capacity factor (mass ratio) of the solute,  $P_i$  = inlet pressure, and  $P_o$  = outlet pressure.

Equation 1 assumes that the contributions of the second virial coefficients of the carrier gas (helium plus ca. 0.02 mol fraction of (H<sub>2</sub>O)) and the mixed second virial coefficient of the carrier gas with the solute are negligible compared to the overall virial coefficient of the gas phase. Hartkopf has calculated the virial coefficients:<sup>15</sup>  $B_{\text{H}_2\text{O}/\text{He}} = -10$  ml/mol and  $B_{2/\text{carrier gas}} = +40$  ml/mol. The negligible contribution can be seen from the fact that the  $B$  values are small and of opposite sign. In addition, the mole fraction of solute in the gas phase typically never exceeds 10<sup>-2</sup> in this work, further reducing the influence of these coefficients.

The  $B_{22}$  coefficient can be approximated as -1000 ml/mol<sup>16</sup> for the hydrocarbons in this study. If  $Y_o^2$  is assumed to be no greater than 10<sup>-4</sup>, then calculations show that  $j \approx J_3^2$  in eq 2, which is equivalent to the James and Martin compressibility correction factor.<sup>17</sup> Consider next eq 3. Since the pressure drop is quite small ( $P_i/P_o \approx 1.1$ –1.2),  $J_2^1 \approx 1$ . If  $Y_o = 10^{-2}$ , then calculations show that the second term in the brackets of eq 3 is equal to -0.01 for  $T = 285^\circ\text{K}$ . This term then provides a correction of only 1% at the highest concentration. Since most isotherm determinations are made at lower concentrations and the error of  $K_A$  is approximately 2%, we shall neglect this correction term. Examining the rest of eq 3, we can assume that  $J_3^2$ , as well as  $J_2^1$ , is equal to unity for the low pressure drops employed. From previous arguments,  $\theta \approx 1$ . Since the variation of flow due to sorption<sup>18</sup> is incorporated into  $\phi$ , we can assume that the sorption effect is negligible over the experimental concentration range in this study.

Equation 1 can now be simplified to

$$V_N^0 = \left( \frac{\partial a}{\partial c} \right)_T A_L^0 \quad (4)$$

(12) R. R. Dreisbach, *Advan. Chem. Ser.*, No. 22 (1959).

(13) C. McAuliffe, *J. Phys. Chem.*, **70**, 1267 (1966).

(14) J. R. Conder and J. H. Purnell, *Trans. Faraday Soc.*, **64**, 3100 (1968).

(15) A. Hartkopf, Ph.D. Thesis, Northeastern University, 1969.

(16) J. H. Dymond and E. B. Smith, "The Virial Coefficients of Gases," Clarendon Press, Oxford, 1969.

(17) A. T. James and A. J. P. Martin, *Biochem. J.*, **50**, 679 (1952).

(18) C. H. Bosanquet and G. O. Morgan, "Vapour Phase Chromatography," D. H. Desty, Ed., Butterworths, London, 1957, p 35.

In the low concentration region, where the distribution becomes linear, the differential in eq 4 can be written as  $\partial a/\partial c \approx a/c = K_A$ , where  $K_A$  is the thermodynamic adsorption coefficient. For this work,  $\Gamma$ , the Gibbs surface excess, can be substituted for  $a$  in eq 4 on the assumption that the plane of adsorption is the Gibbs hypothetical dividing surface. In addition,  $c$  can be replaced by  $P_a/RT$ , where  $P_a$ , the partial pressure of adsorbate, in millimeters, is assumed equal to fugacity at the low pressures used in these experiments. Then

$$V_N^0 = RT \left( \frac{\partial \Gamma}{\partial P_a} \right)_T A_L^0 \quad (5)$$

The surface pressure,  $\pi$ , is defined as

$$\pi = RT \int_0^{P_a} \Gamma d(\ln P_a) \quad (6)$$

Adsorption isotherms were determined as described previously<sup>2</sup> by the elution by characteristic point method (ECP).<sup>19-21</sup> In this method, the amount adsorbed,  $\Gamma$ , is given by

$$\Gamma = \frac{n}{wA'A_L^0} \int_0^h \lambda dh \quad (7)$$

where  $n$  = number of moles of solute,  $w$  = weight of packing in the column,  $A'$  = peak area,  $h$  = peak height, and

$$\lambda = X \frac{V_N^0 w}{F_c J_3^2} \quad (8)$$

The partial pressure,  $P_a$ , corresponding to peak height,  $h$ , can be computed from

$$P_a = \frac{nRT_m h}{J_3^2 A' F_m} \quad (9)$$

In eq 8 and 9,  $F_c$  = carrier gas flow rate within the column,  $X$  = recorder chart speed,  $T_m$  = flow meter temperature, and  $F_m$  = carrier gas flow rate at the end of the column. The integration was carried out graphically from the chromatogram by measuring the area from the inert peak to the peak maximum within the limits of 0 to  $h$ . The area was cut out and weighed. The correction for diffusion<sup>22</sup> was found to be less than 2% and was neglected in this work.

In a previous paper<sup>2</sup> we have presented chromatograms of *n*-octane on water columns as a function of sample size. Similar diagrams are repeated in Figure 1 for *n*-C<sub>8</sub>. The same behavior was found for the other five solutes. The excellent coincidence of the leading edges of the asymmetrical peaks is an indication that equilibrium on the column can be assumed at all concentration ranges.<sup>23</sup>

Recently, Huber<sup>24</sup> has critically evaluated the various gas chromatographic methods for determining sorption isotherms. He finds experimentally that all methods give slightly different results from the one in which

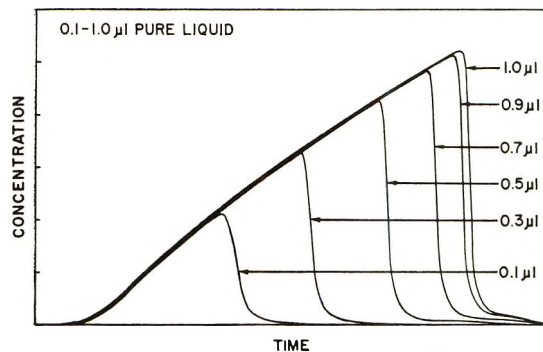


Figure 1. Chromatograms of octane on 20% H<sub>2</sub>O-Porasil D (w/w) as a function of liquid volume sample sizes,  $T = 12.1^\circ$ .

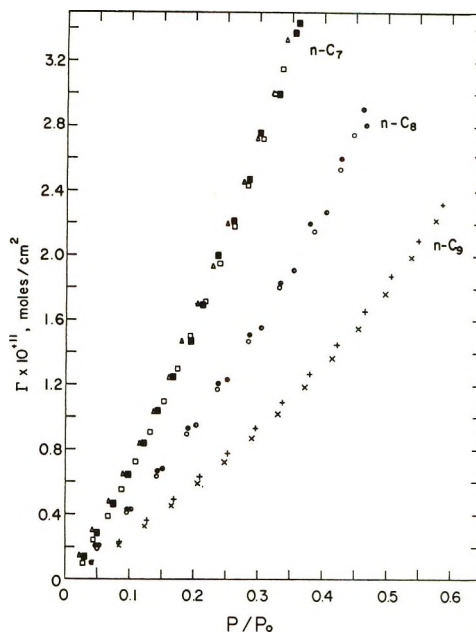


Figure 2. Adsorption isotherms for heptane, octane, and nonane on 20% H<sub>2</sub>O (w/w) coated on Porasil D,  $T = 12.1^\circ$ . Different point types represent different experimental runs.

a true equilibrium is imposed throughout the whole column. However, the difference between the ECP approach and the true equilibrium method is slight when the isotherm does not deviate greatly from linearity. Typical isotherms in Figures 2 and 3 indicate that in the concentration region of this study, the ECP method can be used with validity. The problems in constructing an equilibrium apparatus, especially

(19) E. Cremer and H. F. Huber, *Angew. Chem.*, **73**, 461 (1961).

(20) A. V. Kiselev and Ya. I. Yashin, "Gas Adsorption Chromatography," translated by J. E. S. Bradley, Plenum Press, New York, N.Y., 1969.

(21) H. Knözinger and H. Spannheimer, *J. Chromatogr.*, **16**, 1 (1964).

(22) J. F. K. Huber, "Gas Chromatography, 1962," M. van Swaay, Ed., Butterworths, London, 1962, p 26.

(23) A. V. Kiselev and Ya. I. Yashin in ref 22, p 113.

(24) J. F. K. Huber and R. G. Gerritse, *J. Chromatogr.*, **58**, 137 (1971).

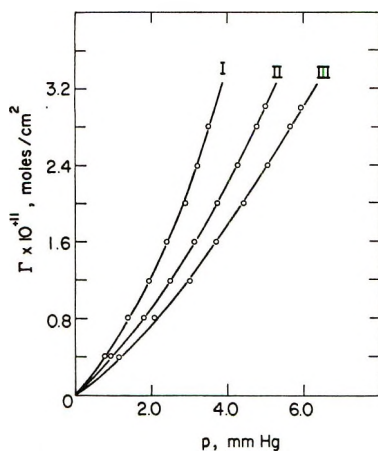


Figure 3. Adsorption isotherm for 2,5-dimethylhexane as a function of temperature: (I) 8.8°, (II) 14.0°, (III) 15.1°.

when using a volatile solvent as stationary phase, are great in comparison to the conventional chromatographic operation of the ECP approach. Thus, we chose the latter method and operated in concentration regions where it may be assumed to be equivalent to the true equilibrium method.

Once the isotherm has been determined, the thermodynamic adsorption coefficient near zero coverage region can be calculated from eq 4 and 5. As others,<sup>8</sup> we have fitted the adsorption isotherm to a polynomial, using the least-squares method. We find the best fit with a four-term polynomial of the form

$$\Gamma = C_1 P_a + C_2 P_a^2 + C_3 P_a^3 + C_4 P_a^4 \quad (10)$$

where the  $C$ 's are constants. Note that the isotherm is assumed to pass through the origin, *i.e.*, at  $P_a = 0$ ,  $\Gamma = 0$  ( $\pi = 0$  as well). In addition, combining eq 6 and 10 gives

$$\pi = RT \left( C_1 P_a + C_2 \frac{P_a^2}{2} + C_3 \frac{P_a^3}{3} + C_4 \frac{P_a^4}{4} \right) \quad (11)$$

The area per molecule,  $A$ , is related to the surface concentration by

$$A = 1/N\Gamma \quad (12)$$

where  $N$  is Avogadro's number.

Consider next the thermodynamic properties. The free energy of adsorption at constant surface coverage  $\Gamma$ ,  $(\Delta \bar{G}_A)_\Gamma$ , can be expressed as

$$(\Delta \bar{G}_A)_\Gamma = RT \ln P_a/760 \quad (13)$$

for the process of transferring 1 mol of gas in its defined standard state (760 mm) to the adsorbed state, defined by the equilibrium pressure  $P_a$  (mm). The isosteric heat of adsorption,  $q_{st}$ , was calculated from the Clausius-Clapeyron equation

$$q_{st} = -R \left( \frac{\partial \ln P_a}{\partial 1/T} \right)_\Gamma \quad (14)$$

Note that isosteric heat of adsorption is independent of the chosen standard state. The determination of  $P_a$  as a function of surface coverage can be made by use of eq 10. The entropy of adsorption at constant surface coverage was obtained by

$$T(\Delta S_A)_\Gamma = -q_{st} - (\Delta \bar{G}_A)_\Gamma \quad (15)$$

Finally, returning to eq 4, the gas-liquid interfacial area of the water surface per gram of packing,  $A_L^0$ , was determined as previously,<sup>2</sup> by assuming that the adsorption coefficient of *n*-octane at zero surface coverage and 12.5° is  $1.0 \times 10^{-4}$  cm. This value was calculated by estimating that a 20% water coated Chromosorb P column had a surface area of 1 m<sup>2</sup>/g.

## Results and Discussion

**Adsorption Isotherms.** Figure 2 shows adsorption isotherms for *n*-C<sub>7</sub>, *n*-C<sub>8</sub>, and *n*-C<sub>9</sub> at  $T = 12.1^\circ$  on a column of 20% H<sub>2</sub>O (w/w) coated on Porasil D. The experimental points are included in order to indicate the good reproducibility from run to run. An error analysis revealed that  $n$ , the number of moles of solute injected, varied at a maximum of 2% from the mean, while  $\Gamma$  varied at a maximum of 8% from its mean value. The larger error in  $\Gamma$  is a result of change in  $w$  and  $A_L^0$  (see eq 7) due to the slow bleeding of water off the column (over 1-2 days).

In agreement with previous work,<sup>5-7,9,25,26</sup> type III or "anti-Langmuir" isotherms are obtained. For the straight-chain series, adsorption at a given  $P/P_0$  value is found to increase with decreasing carbon number. Although not shown, branched isomers also produced type III isotherms, with adsorption increasing with branching. Finally, Figure 3 shows a typical temperature dependence of the adsorption isotherm for 2,5-dimethylhexane, with decreasing adsorption as the temperature is increased.

Special note should be taken of the fact that the surface concentrations in the adsorption isotherms are a factor of 10 or more smaller than those of the original static measurements.<sup>5,26</sup> This points to one of the big advantages of gc for adsorption studies, namely that the method works best at low concentrations. Recently, Hauxwell and Ottewill<sup>9</sup> have studied similar adsorbates in the low-concentration region of this work. A comparison of data from Hauxwell's thesis<sup>27</sup> with that in Figure 2 reveals that the  $\Gamma$  values for a given partial pressure and temperature are a factor of approximately 2 larger in the present work. The discrepancy can arise from one of two sources or a combination of both. First, the surface area per gram of packing,  $A_L^0$ , is an estimated quantity in the gas

(25) C. Kemball and E. K. Rideal, *Proc. Roy. Soc., Ser. A*, **187**, 53 (1946).

(26) C. L. Cutting and D. C. Jones, *J. Chem. Soc.*, 4067 (1955).

(27) F. Hauxwell, Ph.D. Thesis, University of Bristol, England, 1969.

**Table I:** Thermodynamic Functions of Adsorption as a Function of Surface Coverage,  $T = 12.1^\circ$ 

Adsorbate	$\Gamma = 0.6 \times 10^{-11} \text{ mol/cm}^2$			$\Gamma = 1.2 \times 10^{-11} \text{ mol/cm}^2$		
	$-(\Delta\bar{G}_A)_\Gamma^a$	$q_{st}^b$	$-(\Delta\bar{S}_A)\Delta^c$	$-(\Delta\bar{G}_A)_\Gamma^a$	$q_{st}^b$	$-(\Delta\bar{S}_A)\Delta^c$
<i>n</i> -C <sub>7</sub>	3.35	7.7	15	3.02	7.7	15
<i>n</i> -C <sub>8</sub>	3.85	8.7	17	3.51	9.2	20
<i>n</i> -C <sub>9</sub>	4.33	9.6	19	4.00	9.7	20
2-MeC <sub>7</sub>	3.72	8.8	18	3.39	8.8	19
2,5-DMeC <sub>6</sub>	3.64	7.6	14	3.29	8.0	16
2,2,4-TMeC <sub>6</sub>	3.49	7.2	13	3.13	7.2	14
	$\Gamma = 1.8 \times 10^{-11} \text{ mol/cm}^2$			$\Gamma = 2.4 \times 10^{-11} \text{ mol/cm}^2$		
<i>n</i> -C <sub>7</sub>	2.83	7.9	18	2.71	8.1	19
<i>n</i> -C <sub>8</sub>	3.32	9.6	22	3.21	10.2	24
<i>n</i> -C <sub>9</sub>	3.83	10.1	22	3.73	9.7	21
2-MeC <sub>7</sub>	3.21	8.9	20	3.09	9.3	22
2,5-DMeC <sub>6</sub>	3.10	8.6	19	2.98	9.1	21
2,2,4-TMeC <sub>6</sub>	2.94	7.6	16	2.81	8.0	18

<sup>a</sup>  $(\Delta\bar{G}_A)_\Gamma$  = free energy of adsorption at constant surface coverage, kcal/mol. <sup>b</sup>  $q_{st}$  = isosteric heat of adsorption, kcal/mol. <sup>c</sup>  $(\Delta\bar{S}_A)_\Gamma$  = entropy of adsorption at constant surface coverage, cal/(°K mol).

chromatographic studies, whereas in the static measurements the surface pressure  $\pi$  is determined independently from the interfacial surface area. Second, helium has been used as the major gas component in this work, whereas nitrogen has been used in the previous static measurements. The solubility of nitrogen is much higher than that of helium in water,<sup>28</sup> and as we have previously shown,<sup>3</sup> at very low concentrations the retention volumes of solutes could be as much as 7% different for these two carrier gases. Cruickshank, *et al.*,<sup>29</sup> have pointed out that the influence of the "inert" gas on interfacial adsorption may be even more important than that due to the solubility effect. In fact, Vorozhbitova, *et al.*,<sup>30</sup> have noted significant changes in retention in gas-solid chromatography using carbon black as adsorbent when the carrier gas is changed from helium to nitrogen.

Of the two possibilities, it seems likely that the estimated surface area plays the larger role in the discrepancy of the results. However, more experimentation is needed using nitrogen as carrier gas before a definitive answer can be given. As a result, we will present our experimental data without correction. It is to be noted that  $q_{st}$  is independent of the value of the surface area of the water interface. In addition, since  $A$ , the area per molecule, and  $\pi$ , the surface pressure are calculated directly from  $\Gamma$ , no discrepancy would be expected between the static and dynamic measurements as far as the functional relation between  $\pi$  and  $A$  are concerned. The argument is strengthened by the fact that  $\pi$ - $A$  data of the present work agree well with independent static data.<sup>27</sup> This agreement will be shown in the section on equations of state.

Table I presents the thermodynamic functions of adsorption for the six solutes at four different surface coverages. The free energies have a standard deviation of  $\pm 1\%$ . The trend in  $(\Delta\bar{G}_A)_\Gamma$  with surface cov-

erage is to less negative values. As we will see, this is mainly due to the more negative change in  $(\Delta\bar{S}_A)_\Gamma$  with surface coverage. The trend in  $(\Delta\bar{G}_A)_\Gamma$  with solute structure follows the expected direction, namely more negative with increased carbon number in the straight-chain alkanes and less negative with increased branching. The free energy change per methylene group for the linear homologous series is constant at 0.50 kcal/mol, indicating correspondence to Traube's rule. This value compares well with the value of 0.42 kcal/mol determined by Aveyard and Haydon<sup>31</sup> for liquid hydrocarbon adsorption on water.

As a check on the self-consistency of the data in this work with those previously determined by gas chromatography in the Henry's law region<sup>2</sup> as well as available static data,<sup>5</sup> we have computed the differential free energy of adsorption,  $\Delta G_A^0$ , as  $\Gamma \rightarrow 0$  by the equation

$$\Delta G_A^0 = -RT \ln B \left( \frac{\partial \Gamma}{\partial P_a} \right)_T \quad (16)$$

where  $B$  is the constant for the Kemball-Rideal standard state.<sup>25</sup> When  $P_a$  is expressed in mm,  $B$  is equal to  $1.034 \times 10^{12} T$ . The results of the two methods are shown in Table II along with the data of Jones and Ottewill.<sup>5</sup> While there is complete agreement between the two chromatographic methods, the values reported by Jones and Ottewill<sup>5</sup> are roughly 0.3 kcal/mol less negative. This discrepancy may be due to the estima-

(28) "Handbook of Chemistry and Physics," 48th ed, Chemical Rubber Co., Cleveland, Ohio, 1967-1968, p B180, B201.

(29) A. J. B. Cruickshank, B. W. Gainey, C. P. Hicks, T. M. Letcher, R. W. Moody, and C. L. Young, *Trans. Faraday Soc.*, **65**, 1014 (1969).

(30) L. N. Vorozhbitova and T. G. Plachenov, *J. Appl. Chem. USSR*, **44**, 782 (1971).

(31) R. Aveyard and D. A. Haydon, *Trans. Faraday Soc.*, **61**, 2255 (1965).



**Table II:** Comparison of Differential Free Energies and Isothermic Heats of Adsorption at Zero Surface Coverage

Adsorbate	$-(\Delta G_A^0)^a$	$-(\Delta G_A^0)^b$	$-(\Delta G_A^0)^c$	$q_{st}^a$	$q_{st}^b$	$q_{st}^c$
<i>n</i> -C <sub>7</sub>	3.76 ± 0.04	3.7 ± 0.05	3.42	7.3 ± 0.5	6.9 ± 0.2	7.2
<i>n</i> -C <sub>8</sub>	4.27 ± 0.05	4.2 ± 0.05	3.91	7.6 ± 1.1	7.9 ± 0.2	7.9
<i>n</i> -C <sub>9</sub>	4.75 ± 0.05	4.7 ± 0.05		10.0 ± 0.7	8.9 ± 0.2	
2-MeC <sub>7</sub>	4.12 ± 0.05	4.2 ± 0.05		8.4 ± 1.2	7.7 ± 0.2	
2,5-DMeC <sub>6</sub>	4.09 ± 0.05			7.1 ± 1.8		
2,2,4-TMeC <sub>3</sub>	3.93 ± 0.04	3.9 ± 0.05	3.66	7.4 ± 0.5	7.1 ± 0.2	6.8

<sup>a</sup> This work; 12.1°, kcal/mol. <sup>b</sup> Previous chromatographic measurements;<sup>1,2</sup> 12.5°, kcal/mol. <sup>c</sup> Jones and Ottewill;<sup>5</sup> 15°, kcal/mol.

tion of the surface area of the gas-water interface and/or the carrier gas effect, as mentioned earlier.

The isothermic heats of adsorption,  $q_{st}$ , shown in Table I were determined by eq 14. Figure 4 shows plots of  $\ln P_a$  vs.  $1/T$  at constant  $\Gamma$  for *n*-heptane. The calculated standard deviation for  $q_{st}$  at finite coverages was  $\pm 5\%$ , but at times was as high as  $\pm 10\%$ . The error is amplified by the small temperature interval employed in this work.

Table II also compares  $q_{st}$  at zero coverage with those of our previous papers.<sup>1,2</sup> It should be noted that the  $q_{st}$  data in column 6 were obtained<sup>32</sup> by adding  $RT$  ( $\sim 0.6$  kcal/mol) to our previously reported differential heat data. Some data computed by Jones and Ottewill<sup>5</sup> are also included. When the stated errors in  $q_{st}$  in this paper are used, the two heats of adsorption are in close agreement; however, this comparison is not as critical a test of the present method as was the comparison of  $(\Delta G_A^0)$  values in which the precision was much higher. It is also interesting to note that the chromatographically determined values of  $q_{st}$  compare well with the static data of Jones and Ottewill.<sup>5</sup>

The relatively parallel nature of the isosteres for *n*-C<sub>7</sub> in Figure 4 indicates that  $q_{st}$  does not vary greatly with coverage. This trend is observed for *n*-heptane in Table I. The changes in  $q_{st}$  for *n*-C<sub>9</sub> and 2-MeC<sub>7</sub> are also small over the surface coverage region studied. For other adsorbates,  $q_{st}$  changes with coverage by as much as 1.5 kcal/mol. It is difficult to assess how much of this change is real and how much due to error; however, a small increase in  $q_{st}$  with coverage is expected. It would appear that the anomalous results for *n*-C<sub>8</sub> at  $\Gamma = 2.4 \times 10^{-11}$  mol/cm<sup>2</sup> are due to error. (Recall that  $(\Delta \bar{G}_A)_\Gamma$  is determined with the least error and that this function increases with carbon number.)

Figure 5 shows the isothermic heat of adsorption as a function of surface coverage for *n*-heptane. Over the whole concentration range,  $q_{st}$  is less negative than the heat of liquefaction,  $\Delta H_L^0$ . Similar behavior was found for the other five solutes. No dramatic increase in  $q_{st}$  as  $\Gamma \rightarrow 0$ , as previously reported by Ottewill for hexane<sup>4</sup> and toluene<sup>8</sup> and used by Adamson in his model for the mechanism of adsorption of the vapors on the water surface,<sup>10</sup> was found. The results in Fig-

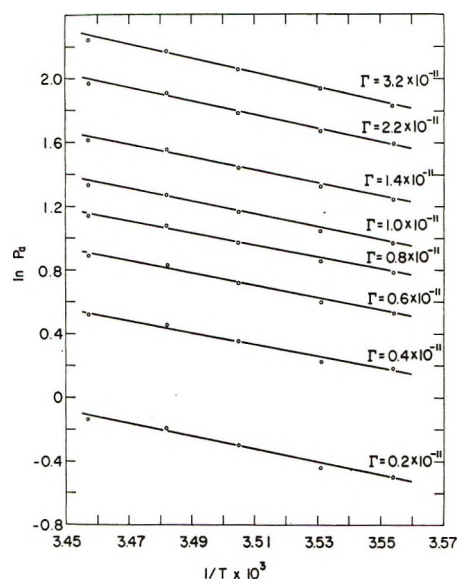


Figure 4.  $\ln P_a$  vs.  $1/T$  plots for *n*-heptane at constant surface coverages;  $\Gamma$  is expressed in units of moles per square centimeter.

ure 5 support our previous conclusion<sup>1-3</sup> that water is a low-energy surface when nonpolar adsorbates are employed. One might expect  $q_{st}$  to be less than  $\Delta H_L^0$  given the type III isotherms one obtains for these adsorbates. Beebe<sup>33,34</sup> has raised the same point in reference to results obtained on ice.<sup>10</sup>

Returning to Table I, the entropies of adsorption at constant surface coverage are also reported. The standard deviation in  $(\Delta \bar{S}_A)_\Gamma$  is  $\pm 10\%$  in most cases, but it can be as high as  $\pm 15\%$ ; consequently, caution must be exercised in interpreting the results. The trends in  $(\Delta \bar{S}_A)_\Gamma$  follow those reported already for  $q_{st}$ , i.e., a more negative entropy of adsorption with increase in carbon number in the straight-chain series and with decrease in branching. The anomalous entropy results in Table I at  $\Gamma = 2.4 \times 10^{-11}$  mol/cm<sup>2</sup> for *n*-C<sub>8</sub> has the same source as the presumed error in  $q_{st}$ .

(32) J. H. de Boer, "The Dynamical Character of Adsorption," Clarendon Press, Oxford, 1953, p 49.

(33) R. A. Beebe, *J. Colloid Interface Sci.*, **31**, 436 (1969).

(34) M. W. Orem, *ibid.*, **31**, 437 (1969).

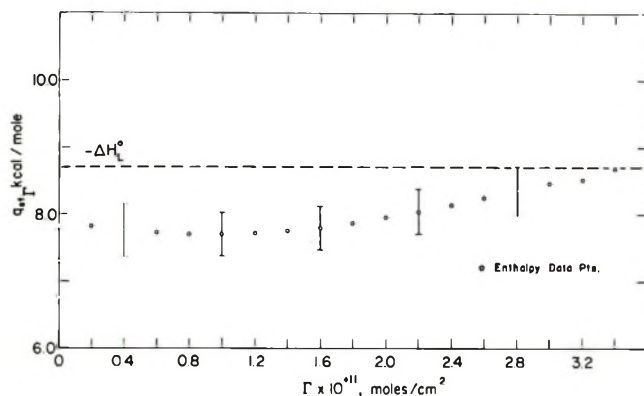


Figure 5. Isosteric heat of adsorption,  $q_{st}$ , as a function of surface coverage for  $n$ -heptane on water at  $T = 12.1^\circ$ .

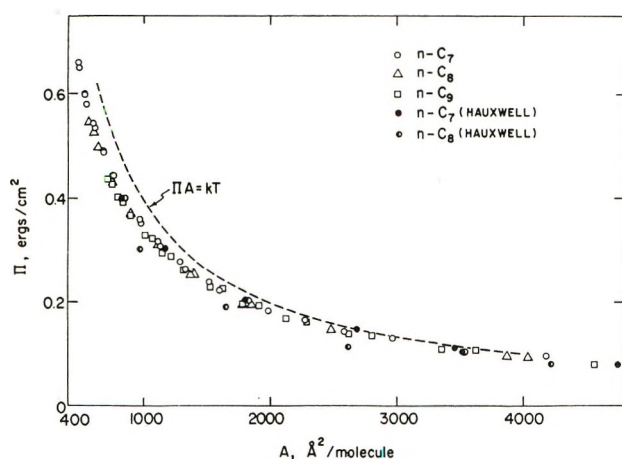


Figure 6. Surface pressure *vs.* area per molecule isotherms for the  $n$ -alkanes adsorbed on water at  $T = 12.1^\circ$ . Hauxwell<sup>27</sup> data obtained at  $15.0^\circ$ .

Ottewill has previously calculated the theoretical entropy change that results from the loss of one degree of translational freedom when the molecule adsorbs on a two-dimensional surface,<sup>5,6</sup> *i.e.*, as a two-dimensional ideal gas. Using an identical procedure, we compute  $\Delta S_t$  at  $12.5^\circ$  to be approximately  $-9$  eu for the  $n$ -alkanes, which is less negative compared to the experimental values. The errors in  $(\Delta \bar{S}_A)_\Gamma$  do not allow further interpretation. More information, however, can be derived from a consideration of the equations of state for the adsorbed species, which is presented in the next section.

**Equations of State.** To examine more fully the adsorbate-adsorbent system, it is useful to describe the two-dimensional equation of state over the whole concentration range studied. The surface pressure,  $\pi$ , can be calculated from eq 11 with known partial pressure values  $P_a$ . From the standard deviations of the regressions, the error in  $\pi$  was found to be between  $\pm 2$  and  $\pm 7\%$  from concentrations of  $2000 \text{ \AA}^2/\text{molecule}$  and lower, and between  $\pm 0.5$  and  $\pm 3\%$  for concentrations higher than  $2000 \text{ \AA}^2/\text{molecule}$ .

Typical  $\pi$ - $A$  isotherms for the normal alkanes at  $12.1^\circ$  are shown in Figure 6. The dotted curve represents the ideal equation of state, *i.e.*,  $\pi A = kT$ . The experimental data are found to lie below the ideal curve for concentrations as low as  $2500 \text{ \AA}^2/\text{molecule}$ . This nonideality might first appear striking; however, it is quite consistent with the adsorption isotherms shown previously. Similar behavior was found for the branched-chain alkanes studied from nonideal gaseous films at the vapor-water interface, even at very low surface coverage.

Similar observations have been made in the past<sup>5,8,26</sup> for the adsorption of  $n$ -alkanes ( $C_5$  to  $C_8$ ) and isooctane at the vapor-water interface. Except for the recent work of Hauxwell and Ottewill,<sup>8,9</sup> no extensive data are available in the very dilute region of Figure 6. Several values of  $\pi$  at different  $A$  values for  $n$ - $C_7$  and  $n$ - $C_8$ , obtained by Hauxwell<sup>27</sup> using a static procedure, are also included in Figure 6. A comparison of the static data with those of the present study reveals a maximum difference of only  $2\%$  over the entire range of surface concentration. This agreement shows that the  $\pi$  *vs.*  $A$  plots for both static and dynamic conditions follow the same functional dependence.

In order to have a more quantitative picture of the nonideal state,  $(\pi A/kT)$  has been plotted as a function of  $\pi$  for the  $n$ -alkanes at  $T = 12.1^\circ$  in Figure 7. Similar behavior was observed for the branched hydrocarbons. Below  $\pi = 0.2 \text{ erg/cm}^2$ , the errors in  $\pi$  and the small differences from adsorbate to adsorbate do not permit any discernible trends, other than that the  $\pi A$  products for all adsorbates approach the ideal line at low  $\pi$  values. Nevertheless, the data in all cases fall below the ideal line. As found previously in a higher concentration region,<sup>26</sup> the  $\pi A$  product decreases almost linearly with increase of  $\pi$ , obeying a modified Schofield-Rideal equation<sup>35</sup>

$$\pi A = (1 - X)kT \quad (17)$$

This equation describes the nonideality of the equation of state in terms of an empirical correction term which in the case of neutral films should be proportional to the extent of van der Waals interaction between the adsorbates. From Figure 7, it can be seen that  $X$  for any solute increases linearly with surface pressure from 0 to a maximum value of roughly 0.2.

At any constant  $\pi$  and  $T$ , in the region  $\pi > 0.2 \text{ erg/cm}^2$ ,  $X$  follows the sequence  $n$ - $C_9 > n$ - $C_8 > n$ - $C_7$  and  $2$ -Me $C_7 > 2,5$ -DMe $C_6 > 2,2,4$ -TMe $C_5$ . The results are in the expected order for van der Waals interactions of adsorbates. Thus, for the branched-chain alkanes, increased branching results in a reduced interaction, because of the lower hydrocarbon surface for such interaction. The trends in nonideality are in

(35) R. K. Schofield and E. K. Rideal, *Proc. Roy. Soc., Ser. A*, **109**, 57 (1925).

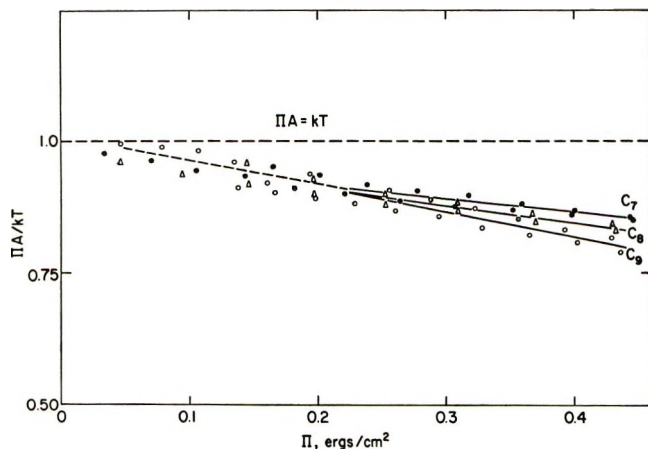


Figure 7.  $\pi A$  vs.  $\pi$  plots for the  $n$ -alkanes adsorbed on water at  $T = 12.1^\circ$ .

agreement with the entropy results in Table I. In addition, similar behavior has already been observed in the case of  $n$ -alkanes<sup>26</sup> and straight-chain fatty acids.<sup>36</sup>

The two-dimensional equation of state for a nonideal gas at the vapor-liquid interface can be expressed as follows<sup>5, 37, 38</sup>

$$(\pi + \pi_s)(A - A_0) = kT \quad (18)$$

where  $A_0$  is the co-area of the adsorbed molecules,  $\pi_s$  is the cohesive surface pressure, and  $k$  is the Boltzmann constant. On the basis of the van der Waals gas equation,  $\pi_s$  can be written as<sup>36, 39</sup>

$$\pi_s = a_s/A^2 \quad (19)$$

where  $a_s$  is the two-dimensional analog of the van der Waals constant. The co-area  $A_0$ , which can be assumed to be around 20–30 Å<sup>2</sup>/molecule, is negligibly small in comparison to the experimental values of  $A$  ranging from 500 to 4000 Å<sup>2</sup>/molecule. Combination of eq 18 and 19 gives

$$\left(\pi + \frac{a_s}{A^2}\right)A = kT \quad (20)$$

Finally, comparison of eq 17 and 20 reveals that

$$XkT = a_s/A \quad (21)$$

Figure 8 shows plots of  $XkT$  vs.  $1/A$  for the three  $n$ -alkanes. For reasons stated earlier, only points at higher concentration are used. Within experimental error the plots are linear, passing through the origin. Again, similar behavior was found for the branched-chain alkanes. The results clearly indicate that all six hydrocarbons obey the van der Waals theory of intermolecular attraction in two dimensions (eq 19).

The slopes of the straight lines give the two-dimensional van der Waals constant,  $a_s$ . Table III presents the  $a_s$  values for the hydrocarbons. Also shown in this table are the three-dimensional van der Waals con-

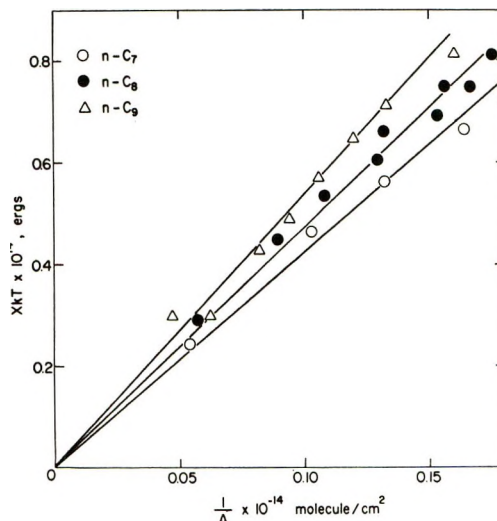


Figure 8.  $XkT$  vs.  $(\text{area}/\text{molecule})^{-1}$  for the  $n$ -alkanes adsorbed on water at  $T = 12.1^\circ$ .

stants of attraction in the vapor state,  $a$ . These values are obtained from critical data of each hydrocarbon.<sup>40</sup> On comparison, both  $a_s$  and  $a$  are found to change in the same manner. Each increases in magnitude with the chain length of the hydrocarbon and for a given number of carbons decreases with branching.

Table III: Two-Dimensional van der Waals Constants and Film Thicknesses of Saturated Hydrocarbons at the Vapor-Water Interface,  $T = 12.1^\circ$

Solute	$a_s \times 10^{28}$ , (ergs cm <sup>2</sup> )/ molecule <sup>2</sup>	$a \times 10^{24}$ , (ergs cm <sup>3</sup> )/ molecule <sup>2</sup>	$\tau$ (at 50 Å <sup>2</sup> / molecule), Å	$A_v \tau$ , Å
$n$ -C <sub>7</sub>	4.1	0.86	3.6	
$n$ -C <sub>8</sub>	4.7	1.04	4.3	4.3
$n$ -C <sub>9</sub>	5.4	1.25	5.0	
2,2,4-TMeC <sub>5</sub>	3.7	0.92	4.0	
2,5-DMeC <sub>6</sub>	4.1	0.97	4.1	4.1
2-MeC <sub>7</sub>	4.4	1.01	4.2	

The thickness of the films,  $\tau$ , can be obtained from eq 22<sup>36, 39, 41</sup>

$$\tau = a/(a_s + kTA) \quad (22)$$

The  $\tau$  values are presented in Table II at a surface con-

(36) A. K. Chatterjee and D. K. Chatteraj, *Kolloid-Z. Z. Polym.*, **234**, 1053 (1969).

(37) A. W. Adamson, "Physical Chemistry of Surfaces," Interscience, New York, N. Y., 1967, p 98.

(38) J. H. de Boer in ref 37, p 132.

(39) D. K. Chatteraj and A. K. Chatterjee, *J. Colloid Interface Sci.*, **21**, 159 (1966).

(40) F. D. Rossini, *et al.*, Ed., "Selected Values of Physical and Thermodynamic Properties of Hydrocarbons and Related Compounds," API Research Project 44, Carnegie Press, Pittsburgh, Pa., 1953.

(41) N. L. Gershfeld, *J. Colloid Interface Sci.*, **28**, 240 (1968).

centration of  $500 \text{ \AA}^2/\text{molecule}$  and at  $T = 12.1^\circ$ . At this highest concentration studied in this work, the thicknesses, on the average, are found to be 4.3 and 4.1  $\text{\AA}$  for the normal and branched-chain alkanes, respectively. The crystallographic cross-section area of the hydrocarbon chain is  $12 \text{ \AA}^2/\text{molecule}$ .<sup>42</sup> On this basis, the thickness of the  $-\text{CH}_2-$  chain is  $\sim 4 \text{ \AA}$ , which agrees remarkably well with the calculated average thickness of both series of films at  $500 \text{ \AA}^2/\text{molecule}$ . This means that the molecules of the hydrocarbon films lie mainly flat on the interface, even at the highest surface concentrations studied.

In work not presented in Table II,  $\tau$  values calculated at coverages less than  $500 \text{ \AA}^2/\text{molecule}$  were found to be somewhat smaller than  $4 \text{ \AA}$ . This result may be due to the entropy approximation made in deriving eq 22, namely that the surface molecules are fully extended and that only translational energy is lost on compression. This assumption may not hold for the present hydrocarbon films in the more dilute regions. Finally, a comparison of our results for *n*-heptane with those of octanoic acid,<sup>38</sup> which has the same effective number of  $\text{CH}_2$  groups (both adsorbing on the water surface), shows that  $a_s$  for the acid is less than that of the hydrocarbon. This means that the presence of a polar group in the chain reduces the van der Waals attraction.<sup>43</sup>

## Conclusion

Gas-liquid chromatography has been shown to be a valid method for the measurement of the adsorption of insoluble vapors in liquid surfaces at finite surface coverage. The method provides a link between the zero surface coverage measurements made by linear elution chromatography<sup>1-3</sup> and the static measurements at higher surface coverages. Using a frontal development method of gas chromatography, it may be possible to extend the isotherm determinations into surface concentrations approaching monolayer coverage and above.

The water interface has been shown to be a low-energy surface for hydrocarbon adsorption. The non-ideality of the gaseous films at coverages as low as  $2500 \text{ \AA}^2/\text{molecule}$  is probably a reflection of the greater attraction of adsorbate molecules to themselves, rather than to the water surface.

*Acknowledgment.* The authors gratefully acknowledge the Office of Naval Research for support of this work under Contract No. N00014-68-A-0207. B. L. Karger is an Alfred E. Sloan Fellow, 1971-1973.

(42) J. J. Jasper and R. D. van Dell, *J. Phys. Chem.*, **69**, 481 (1965).

(43) J. T. Davies and E. K. Rideal, "Interfacial Phenomena," Academic Press, New York, N. Y., 1961, pp 159, 230.

# Medium Effects of Urea and Guanidine Hydrochloride on the Volume Changes Produced by Protonation of Carboxylate Groups<sup>1</sup>

by Sam Katz\* and Jane E. Miller

Department of Biochemistry, West Virginia University Medical Center, Morgantown, West Virginia 26506  
(Received January 31, 1972)

Publication costs assisted by the National Institutes of Health

The presence of urea or guanidine in the system has a depressant effect on the magnitude of the volume changes produced by the protonation of the salts of amino acids, their derivatives, and mono- and dicarboxylic acids. The magnitude of the volume changes produced by protonation is a function of the composition and structure of the organic acid, whereas the relative decrease of this volume effect varies with the concentration and type of denaturant present. The use of 4, 6, and 8 *M* urea as solvent causes about 10, 15, and 20% reduction of the volume effect produced in water, respectively; 4 and 6 *M* guanidine hydrochloride effects a reduction of about 40 and 50% relative to that in water. This depressant effect is explicable in terms of the reduction of the activity of water, the water structure breaking action of the solutes, and the diminution of the electrostriction effect by increasing the dielectric constant of the medium. Guanidine hydrochloride, a univalent electrolyte, incorporates an additional factor, namely a salt effect which depresses the magnitude of these volume changes.

## Introduction

The effect of varying the concentration of urea and guanidine hydrochloride on the volume changes,  $\Delta V$ , produced by the protonation of carboxylate groups incorporated in organic acids, amino acids, and their derivatives is the subject of this study. This detailed tabulation will supplement the existing data<sup>2</sup> and also provide information necessary to establish the relationship between the magnitude of the volume change, the type of carboxylic acid, and of the medium employed. The influence of varying the concentrations and ratio of organic acid to base was also investigated. This information is essential to elucidate the anomalously low volume changes produced by the titration of carboxylate groups incorporated in proteins in 8 *M* urea and the high values determined in 6 *M* guanidine hydrochloride.<sup>3</sup> These data may help clarify the role of these denaturants with respect to their influence on water structure, *i.e.*, whether they function as structure "makers" or "breakers."<sup>4-6</sup>

## Experimental Section

The volume changes were determined with Teflon-sheathed Linderstrøm-Lang dilatometers<sup>7</sup> which could be read to 0.01  $\mu\text{l}$ . The methodology, source, and purification of reagents have been described in detail.<sup>2</sup> To establish concentration effects the following procedure was employed. (i) The 1:1 protocol: 5 ml of 0.20 *M* carboxylate containing compound was mixed with 5 ml of 0.1000 *M* HCl; after mixing, there was a 1:1 ratio of organic acid and organic base. (ii) The 3:1 protocol: 8 ml of 0.20 *M* carboxylate containing compound was mixed with 4 ml of 0.1000 *N* HCl. On occasion the

volumes but not the ratio of solutes were changed to ensure that the experimental volume changes were between 2 and 6  $\mu\text{l}$ . Since the emphasis of this study was to determine relative volumes changes, fewer duplicate experiments were performed than in the initial study in this series.<sup>2</sup> Correction was made for unbound protons;<sup>8</sup> the magnitude of the correction for the specific compound and medium is stated in the appropriate tables. The experiments were performed at  $30.0 \pm 0.001^\circ$ . The range about the mean was  $\pm 0.25$  ml/mol.

## Results

The values for the protonation of carboxylate groups of amino acids and their derivatives in water, urea, and guanidine hydrochloride are summarized in Table I. The mixing protocols were designed to yield, after mixing, systems which had 0.05 *M* organic salt and 0.05 *M* organic acid (1:1 mixing protocol) and 0.15 *M* organic salt and 0.05 *M* organic acid (3:1 mixing protocol). This approach permitted us to assess effects of salt concentration, mass action, reliability of data, and the concentration of products. In water, the mean value for

(1) This research was supported in part by U. S. Public Health Service, National Heart and Lung Institute Grant HE 12955.

(2) S. Katz and J. E. Miller, *J. Phys. Chem.*, **75**, 1120 (1971).

(3) S. Katz and J. E. Miller, *Biochemistry*, **10**, 3569 (1971).

(4) H. S. Frank and M. W. Evans, *J. Chem. Phys.*, **13**, 50 (1945).

(5) A. Holtzer and M. F. Emerson, *J. Phys. Chem.*, **73**, 26 (1969).

(6) W. A. Hargraves and G. C. Kresheck, *ibid.*, **73**, 3249 (1969).

(7) K. Linderstrøm-Lang and H. Lanz, *C. R. Trav. Lab. Carlsberg*, **21**, 315 (1938).

(8) W. Kauzmann, A. Bodanszky, and J. Rasper, *J. Amer. Chem. Soc.*, **84**, 1777 (1962).

Table I:  $\Delta V$  of Protonation of Carboxylate Groups in Amino Acids and Amino Acid Derivatives

Reactants	Protocol	$\Delta V$ , ml/mol					
		H <sub>2</sub> O	Urea			Guanidine hydrochloride	
			4 M	6 M	8 M	4 M	6 M
$\beta$ -Alanine	1:1	7.4	6.4 <sup>a</sup>	6.1 <sup>a</sup>	5.8 <sup>b</sup>	4.5 <sup>a</sup>	3.6 <sup>b</sup>
	3:1	7.1	6.3	6.1	5.9	4.2	3.7 <sup>b</sup>
Disodium glutamate	1:1	8.0	7.0	6.8	6.4	4.7 <sup>a</sup>	3.8 <sup>b</sup>
	3:1	7.6	6.7	6.5	6.2	4.5 <sup>a</sup>	3.4 <sup>b</sup>
Disodium glutathionate	1:1	9.3	7.8 <sup>a</sup>	7.3 <sup>b</sup>	6.9 <sup>b</sup>	5.6 <sup>b</sup>	4.9 <sup>c</sup>
	3:1	8.7	7.5	7.3	6.8	5.5 <sup>b</sup>	4.7 <sup>c</sup>
$\gamma$ -Amino- <i>n</i> -butyric acid	1:1	9.4	8.1	7.7	7.4	5.9 <sup>a</sup>	4.7 <sup>b</sup>
	3:1	9.3	8.2	7.8	7.4	5.5 <sup>a</sup>	4.4 <sup>b</sup>
Glycylglycine	1:1	9.5	7.9 <sup>c</sup>	7.5 <sup>d</sup>	7.2 <sup>d</sup>	6.2 <sup>b</sup>	5.2 <sup>c</sup>
	3:1	9.2	7.9 <sup>a</sup>	7.6 <sup>a</sup>	7.1 <sup>b</sup>	5.7 <sup>b</sup>	4.7 <sup>c</sup>
Sodium <i>N</i> -acetyl-glycinate	1:1	11.0	9.2 <sup>a</sup>	8.7 <sup>b</sup>	8.5 <sup>b</sup>	6.9 <sup>b</sup>	6.0 <sup>c</sup>
	3:1	11.0	9.2	8.9	8.4	6.6 <sup>b</sup>	5.4 <sup>c</sup>
Mean value	1:1	9.1	7.7	7.4	7.0	5.6	4.7
	3:1	8.8	7.6	7.4	7.0	5.3	4.4

<sup>a</sup> 1-2% correction for unbound protons. <sup>b</sup> 2-3%. <sup>c</sup> 3-4%. <sup>d</sup> 4-5%.

$\Delta V$  was about 9 ml/mol with the range being about 2 ml/mol. The presence of an elevated salt concentration, data obtained from the 3:1 mixing protocol, was about 0.3 ml/mol lower than that determined at the lower salt concentration. The use of 4, 6, and 8 M urea depressed these values by about 15, 20, and 25%, respectively. The presence of guanidine hydrochloride caused a more pronounced effect with  $\Delta V$  being reduced about 40 and 50% in 4 and 6 M guanidine hydrochloride, respectively. The presence of a high salt content tended to reduce the values for  $\Delta V$  in water and guanidine hydrochloride. In water and in 4 and 6 M guanidine hydrochloride the values for  $\Delta V$  were about 0.3 ml/mol lower for the 3:1 mixing protocol compared to the 1:1 mixing protocol. However, systems containing urea showed virtually no salt effect in 6 and 8 M urea and a decrease of about 0.1 ml/mol in 4 M urea.

Correction for unbound protons was not required when water was the solvent; however, when urea and guanidine hydrochloride were incorporated in the system corrections were needed for organic acids with  $pK \leq 3.6$ . To illustrate the magnitude of the correction consider glycylglycine<sup>9</sup>  $pK = 3.148$ . There was 4-5% unbound protons in 6 and 8 M urea; in the other systems the correction for unbound protons was lower (see Table I). The presence of a high concentration of the salt of the organic acid, 3:1 protocol, reduced the amount of unbound protons in accordance with mass action effects. The correction for unbound protons in guanidine hydrochloride was slightly higher than that required for urea. In guanidine hydrochloride the correction factor for the 1:1 and 3:1 systems were virtually the same.

The  $\Delta V$  produced by protonation of several mono- and dicarboxylate organic compounds are summarized in Table II. Most of these data pertain to values ob-

tained by the 1:1 mixing protocol since solubility considerations limited the use of elevated salt concentrations. This dictated the use of a 2:1 mixing protocol, *i.e.*, the ratio of the salt to acid after mixing was 2:1. Since the emphasis of this study was to determine medium effect on protonation processes, it is of interest to consider the influence of those solutes on the dicarboxylic acids which exhibit large volume changes.<sup>8</sup> These data reveal that the relative diminution of  $\Delta V$  caused by medium effects were relatively independent of the compound structure; *i.e.*, the mono- and dicarboxylate organic compounds exhibited similar relative volume decreases. The reduction of  $\Delta V$  due to urea was about 12, 15, and 20% in 4, 6, and 8 M urea. In 4 and 6 M guanidine hydrochloride reductions of 40 and 50% were observed. Salt concentration effects apparently occur; however, the data are too limited to permit a valid assessment. The relative reduction of volume changes noted for the organic acids is similar to that observed for amino acids indicating that similar medium effects are operational, but the magnitude of the volume effect is determined by the structure of the carboxylate containing compound and by the medium.

## Discussion

The volume changes produced in water by the protonation of carboxylate groups ranged from 7.7 ml/mol for sodium formate to 19.7 ml/mol for disodium maleate. However, the  $\Delta V$  for this process involving simple and polyfunctional amino acids did not exhibit this span of values but gave a mean value for  $\Delta V$  of 9 ml/mol with a range of 2 ml/mol. The rationale for the variation of  $\Delta V$  for protonation of polyfunctional compounds has been explained in detail by Kauzmann,

(9) J. T. Edsall and J. Wyman, "Biophysical Chemistry," Academic Press, New York, N. Y., 1958, p 452

**Table II:**  $\Delta V$  of the Protonation of Organic Bases

Reactant	Protocol	$\Delta V$ , ml/mol					
		H <sub>2</sub> O	Urea			Guanidine hydrochloride	
			4 M	6 M	8 M	4 M	6 M
Sodium formate	1:1	7.7	6.8 <sup>a</sup>	6.5 <sup>a</sup>	6.4 <sup>b</sup>	5.2 <sup>b</sup>	4.7 <sup>c</sup>
	2:1	7.5	6.7	6.7 <sup>a</sup>	6.6 <sup>a</sup>	5.0 <sup>a</sup>	4.5 <sup>b</sup>
Sodium acetate	1:1	10.7	9.5	9.2	8.8	6.5 <sup>a</sup>	5.6 <sup>b</sup>
Disodium malonate	1:1	15.8	14.1	13.5	12.7	8.9 <sup>a</sup>	7.2 <sup>b</sup>
Disodium maleate	1:1	19.7	17.4	16.7	16.1	11.8	9.6 <sup>a</sup>
	2:1	19.2	17.3	16.6	15.7	11.5	9.3

<sup>a</sup> 1-2% correction for unbound protons. <sup>b</sup> 2-3%. <sup>c</sup> 3-4%.

*et al.*,<sup>8</sup> in terms of the contribution of the type of substituents, net charge, and stereochemical considerations.

The reduction of  $\Delta V$  of protonation due to salt effect is well documented.<sup>2,8</sup> Nonreacting electrolytes influence this process by ionic strength effect and by altering the reactant's activity coefficient. This factor can reduce the magnitude of  $\Delta V$  substantially, *e.g.*, the  $\Delta V$  of neutralization of HCl by NaOH decreased from 20.3 to 16.7 ml/mol as the concentration of NaCl increased from 0.05 to 2 M.<sup>2</sup> Thus, the reduction of  $\Delta V$  observed for the 3:1 mixing protocol compared to the 1:1 protocol is to be expected. The magnitude of this attenuation of  $\Delta V$  is too small to be ascribed to specific solute-reactant interaction.

These data confirm the observation that the magnitude of  $\Delta V$  is a function primarily of the composition and structural organization of the compound being protonated.<sup>8,10</sup> The presence of urea or guanidine hydrochloride causes a relative reduction of these volume effects which is similar for all compounds tested, and this effect is determined by the type and concentration of the denaturant. Hargraves and Kresheck<sup>6</sup> explain the medium effect of 6 M urea in terms of the water structure breaking action of urea; this approach presumably applies to guanidine hydrochloride. These authors postulate that the positive values found for the  $\Delta V_i^\circ$  term, the difference between the partial molar volume of compounds in 6 M urea and in water for carboxylic acids, carboxylates, etc., was the resultant of the contribution of the polar and nonpolar moieties comprising the molecule. The positive values for this function were interpreted as being evidence that urea functioned as a water structure breaker because the introduction of an organic side chain into the urea-water system produced a positive volume effect reflecting an additivity process. A corollary of this hypothesis is that the values for  $\Delta V_i^\circ$  should increase with increasing side-chain length; this has been verified experimentally. We propose that in addition to the water structure effect attributable to these denaturants there are other contributing factors. The presence of urea and guanidine hydrochloride in the solvent decreases the activity of water,<sup>11,12</sup> thereby re-

ducing the amount of water available for ion-water interaction. Another factor is based on electrostatic considerations, namely that the magnitude of the volume changes associated with protonation can be estimated by the Drude-Nernst<sup>13</sup> equation. The equation which has been discussed in detail previously<sup>2,8</sup> states that

$$\Delta V = -\beta(VdD/dV)e^2Z^2/2rD^2$$

The terms are defined as:  $\beta$ , compressibility;  $V$ , volume of the medium;  $D$ , dielectric constant;  $eZ$ , electrical charge, and  $r$ , the radius of the sphere immersed in the medium. The introduction of urea or guanidine hydrochloride into the solvent increases the dielectric constant of the medium,<sup>14,15</sup> causing a reduction of the volume effect since  $\Delta V$  varies inversely with the square of the dielectric constant (see ref 2 for discussion). The large depressant action of guanidine hydrochloride reflects the operation of still another factor; this is a salt effect associated with the ionization of guanidine hydrochloride, a uni-univalent electrolyte (see Results). Specific solute-reactant interactions may play a role with respect to these volume changes; however, to produce such a concordant relationship for these relative volume depressant effects it would require that the association constants for these interactions be similar. This does not appear to be highly probable in view of the disparate character of the carboxylate compounds.

The data reported here are in accord with the frame of reference projected from the initial paper in this series;<sup>2</sup> this lends credence to the conclusions presented previously.

- (10) H. H. Weber, *Biochem. Z.*, **218**, 1 (1930).  
 (11) G. Scatchard, W. J. Hamer, and S. E. Wood, *J. Amer. Chem. Soc.*, **60**, 3061 (1938).  
 (12) H. D. Ellerton and P. J. Dunlop, *J. Phys. Chem.*, **70**, 1831 (1966).  
 (13) P. Drude and W. Nernst, *Z. Phys. Chem. (Leipzig)*, **15**, 79 (1894).  
 (14) E. C. Cohn and J. T. Edsall, "Proteins, Amino Acids, and Peptides," Reinhold, New York, N. Y., 1943, p 140.  
 (15) Reference 9, p 323.

# Thermally Stimulated Conductivity of $\gamma$ -Irradiated Triethylamine and 3-Methylpentane Glasses

by Ashok K. Munjal and Larry Kevan\*

*Department of Chemistry, Wayne State University, Detroit, Michigan 48202 (Received January 24, 1972)*

*Publication costs assisted by the Air Force Office of Scientific Research*

Thermally stimulated conductivity of  $^{60}\text{Co}$   $\gamma$ -irradiated and unirradiated triethylamine was studied as the glassy matrix was warmed from 77°K. The unirradiated matrix gives a peak near 117°K which can be removed by field orientation upon freezing the matrix. The irradiated matrix gives evidence for three different types of radiation-produced species as indicated by conductivity peaks in different temperature ranges. At 77°K a peak is observed which decays in about 20 min and can be assigned to a small population of shallow trapped electrons. The main population of trapped electrons is released in the 107–117°K temperature range which corresponds well with epr data. This conductivity peak is reduced by the electron scavengers, carbon tetrachloride, and biphenyl. The third conductivity peak appears between 147 and 157°K and is attributed to molecular ions. At higher temperatures the background intrinsic conductivity increases monotonically and is characterized by an Arrhenius activation energy of 0.20 eV. A few experiments were also carried out on glassy 3-methylpentane to compare with two published studies of thermally stimulated conductivity in this matrix which are divergent. Our results confirm those of Wiseall and Willard.

## Introduction

$\gamma$ -Irradiation of various organic glasses at 77°K such as 3-methylpentane (3MP), triethylamine (TEA), and methyltetrahydrofuran (MTHF) produces trapped charged species. One negative species is a trapped electron ( $e_t^-$ ) which can be detected by electron paramagnetic resonance (epr) and optical absorption. The nature of the positive species is not specifically known; however, the presence of positive ions can be verified by thermally stimulated conductivity (TSC). In previous work the thermal detrapping of  $e_t^-$  and positive ions in 3MP was studied by TSC.<sup>1</sup> In a more polar matrix like MTHF the intrinsic conductivity is so high that it precludes similar studies.<sup>2</sup> TEA is intermediate in polarity between 3MP and MTHF, and it yields information on the thermal detrapping of the charged species by TSC studies similar to that obtained for 3MP. We have also briefly studied 3MP to attempt to resolve the discrepancy in TSC results reported in two previous studies.<sup>1,3</sup>

## Experimental Section

Triethylamine from Matheson Coleman and Bell was passed through 4 ft of freshly activated (250° for 24 hr) 28–200 mesh silica gel. The center fraction of the TEA was fractionally distilled and the center fraction of this was used for sample preparation. Baker spectrophotometric grade  $\text{CCl}_4$  and Phillips Petroleum Co. pure grade 3MP were similarly purified. TEA and 3MP were stored on a vacuum line in light tight bulbs. Prior to sample preparation the solvents were degassed by the freeze-pump-thaw method and then distilled into the conductivity cell. Biphenyl and

2-methyl-1-pentene were used as solutes without any further purification.

The conductivity cell was 2.5-cm diameter Pyrex about 8 cm long. Two press-seal nickel leads were attached to the cell and ended in 1-cm<sup>2</sup> nickel electrodes positioned 1 mm apart. A ball joint was attached to the cell and the cell was completely sealed off after filling. In different cells the electrode distance varied, but all of the comparable measurements were made in the cell. The sample volume was about 10 ml. The conductivity cells were cleaned with boiling benzene, rinsed with acetone, evacuated, and rinsed with TEA or 3MP twice.

Irradiations were carried out in a  $^{60}\text{Co}$   $\gamma$  source at a nominal dose rate of 0.4 Mrad/hr. The current was measured with a Keithley Model 610B electrometer, and the temperature was simultaneously recorded from a Digitec digital thermocouple thermometer. The thermocouple was positioned outside of the cell and level with the electrodes. The warm-up system consisted of a heavy walled brass cylindrical container to hold liquid nitrogen and the conductivity cell. The brass cylinder contained a hole in the bottom closed by a cork and the liquid nitrogen was removed through this hole to start a warm-up run. The warm-up rate was 0.6–0.7°K per minute and was remarkably linear from 77°K to about 230°K. The entire brass cylinder was enclosed in a grounded metal cage to reduce noise. Hot air was blown uniformly across the outer electrode

- (1) B. Wiseall and J. E. Willard, *J. Chem. Phys.*, **46**, 4387 (1967).
- (2) A. C. Ling and J. E. Willard, *J. Phys. Chem.*, **73**, 2408 (1969).
- (3) I. Kosa-Somogyi and J. Balog, *Advan. Chem. Ser.*, No. **82**, 291 (1968).



leads to prevent condensation of water and accompanying leakage currents.

## Results

*A. Irradiated TEA.* When an unirradiated glassy sample of TEA, cooled to 77°K with no applied field, is warmed from 77°K with an applied field, the warm-up current profile is as shown by the dotted line in Figure 1. Peaks A, B, and C are observed, followed by a rapidly increasing background current above 200°K. Also a small negative peak is generally observed after peak A. Samples are defined as "field oriented" when they are cooled in an applied field and then rewarmed. When TEA is field oriented by 5 kV/cm and then warmed in the same field, peak A disappears from the warm-up profile. Samples were also cooled to 77°K in an applied field of 8 kV/cm and then warmed in an applied field of 0.8 kV/cm. In this case, peak A appears as a negative peak and is shifted to a slightly lower temperature. In these field orientation experiments the current profile above 130°K is always the same; the peak areas observed in the unirradiated TEA are proportional to the applied field.

The continuously increasing current above 200°K is attributed to the intrinsic conductivity of the TEA matrix. By plotting  $\log(\text{current})$  vs.  $T^{-1}$  a linear plot is obtained which indicates an Arrhenius activation energy of 0.20 eV. This can be compared with 0.35 eV reported for the MTHF matrix.<sup>2</sup>

*B. Irradiated TEA.* In both irradiated and unirradiated samples a polarization spike appears when the field is applied at 77°K. If the irradiated sample is examined 1 or 2 min after being taken out of the irradiation source, the polarization spike is dose dependent and seems to indicate a small population of shallowly trapped electrons which isothermally decay at 77°K. The dose dependence of the polarization spike is negligible 20 min after removing the sample from the irradiation source, so the shallowly trapped electrons seem to have decayed within 20 min. The current that isothermally decays at 77°K is labeled as peak I in Figure

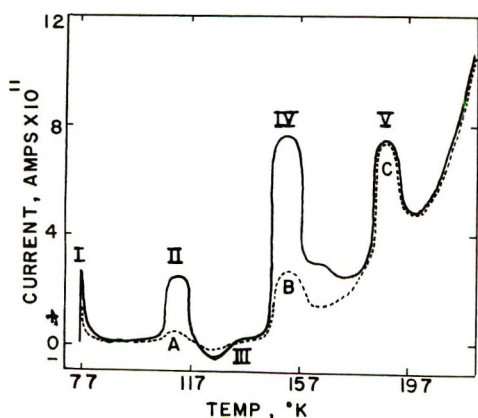


Figure 1. Thermally stimulated current in unirradiated (dashed line) and  $\gamma$ -irradiated (solid line) triethylamine glass.

1 to be consistent with the terminology of Willard and coworkers.

The solid line in Figure 1 shows a typical current profile during warm-up for irradiated samples. The exact shapes of the profiles are somewhat variable from sample to sample and from cell to cell; however, the general features are the same and the temperature ranges are fairly reproducible. Peak II appears between 107 and 117°K. Peak II is significantly larger than peak A in unirradiated samples and this difference increases with increasing radiation dose. So peak II seems to be associated with the thermal detrapping of radiation produced ionic species. This peak increases approximately linearly with applied field from 0.8 to 15 kV/cm. The peak also increases with radiation dose to about 1.5 Mrads and then decreases somewhat at higher doses.

Peak III which appears in the 122–127°K range is in the negative direction. The area of this negative peak increases with radiation dose and reaches a maximum near 1.5 Mrads. This negative peak is only observable at high doses and low fields. At an applied field of 0.8 kV/cm the peak only appears above 0.4 Mrad dose, and at fields of the order of 8 kV/cm the negative peak is barely observed at doses of 1.5 Mrads.

Peak IV coincides exactly with peak B in the unirradiated samples. However, peak IV is dose dependent and is clearly larger than peak B under comparable conditions, so it seems to be due to radiation-produced species. This peak increases approximately linearly with applied field from 0.8 to 15 kV/cm, and it shows a very slow increase with dose to doses beyond 2 Mrads.

The melting point of glassy TEA is about 160°K so peak V appears to lie in the liquid region. This peak also coincides with peak C in the unirradiated samples and seems to be unaffected by radiation dose.

*C. Scavenger Effects on Irradiated TEA.* Electron and positive hole scavengers have been used to try to confirm the identity of the various radiation produced current peaks in the warm-up profile.  $\text{CCl}_4$  and biphenyl, which are good electron scavengers, decrease the area of peak II as the concentration of scavenger increases. This is shown in Figure 2. Up to 0.8 mol %, the scavenging efficiencies of biphenyl and  $\text{CCl}_4$  are similar. At higher concentrations,  $\text{CCl}_4$  seems less efficient but this may be due to limited solubility in 3MP. Peak IV is also reduced somewhat with both scavengers but not as dramatically as is peak II. Qualitatively it appears that peak IV broadens somewhat toward higher temperatures.

2-Methyl-1-pentene (2MP-1), which acts as a positive hole scavenger,<sup>4</sup> causes the area of peak II to increase as is shown in Figure 2. 2MP-1 also reduces the

(4) W. H. Hamill in "Radical Ions," E. T. Kaiser and L. Kevan, Ed., Wiley-Interscience, New York, N. Y., 1968, Chapter 9.

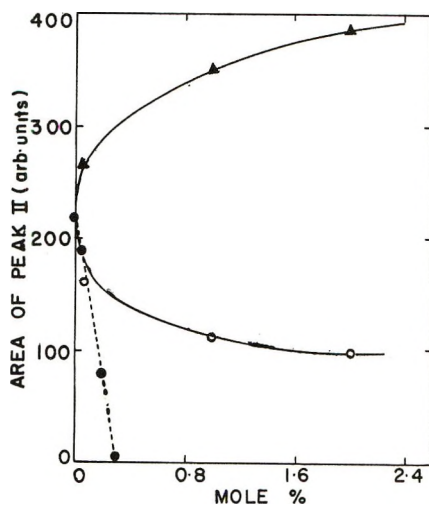


Figure 2. Effect of electron scavengers on the trapped electron peak in the thermally stimulated current profile of  $\gamma$ -irradiated triethylamine: ●, biphenyl; ○,  $\text{CCl}_4$ ;  $\Delta$ , 2-methyl-1-pentene.

area of peak IV somewhat in a rather similar fashion to biphenyl.

*D. Unirradiated and Irradiated 3MP.* Irradiated 3MP has been comprehensively studied by TSC<sup>1</sup> so the predominant emphasis here will be on unirradiated 3MP in comparison to the irradiated samples. Unirradiated 3MP glass warmed from 77°K with an applied field of 5 kV/cm gives a small peak A at 85°K, a somewhat larger peak B between 105 and 110°K, and a much larger peak C near 190°K with a monotonically increasing current at higher temperatures. The relative intensities of peaks A, B, and C in unirradiated 3MP are approximately 1:2:20. If 3MP is cooled to 77°K under an applied field of 5 kV/cm and then warmed again in the same applied field, peak A has disappeared, peak B has increased slightly, and peak C is unaffected. Also, if 3MP samples are cooled to 77°K under an applied field of 8 kV/cm and then warmed under a field of 0.8 kV/cm a negative peak A near 85°K is observed.

If the monotonic increasing current above 195°K is plotted as  $\log(\text{current})$  vs.  $T^{-1}$  the Arrhenius activation energy for intrinsic conduction is obtained as 0.32 eV.

In irradiated 3MP at 0.2 Mrad, large peaks appear near 85°K and near 105–110°K. These peaks are 10–20 times larger than the background peaks. These radiation-produced peaks are labeled II and IV, respectively, as defined by Wiseall and Willard.<sup>1</sup> At 5 kV/cm no negative peak between peaks II and IV was observed. From the previous work<sup>1</sup> a negative peak does appear in this region at lower applied fields and then becomes unobservable at fields of the order of 5–10 kV/cm.

## Discussion

*A. Unirradiated TEA and 3MP.* Peak A in unirradiated samples seems to be due to dipole orientation

by an applied field. This peak appears near 85°K in 3MP and near 110°K in TEA. The peak in TEA is much larger than in 3MP which is consistent with the greater polarity of TEA compared to 3MP. The assignment of peak A to dipole orientation is confirmed by the fact that field orientation during cooling of the glass causes peak A to disappear. Similarly behaved peaks are also observed in unirradiated MTHF and methylcyclohexane (MCH) near 95°K.<sup>2</sup>

The small negative peak in TEA is attributed to thermal randomization of the oriented dipoles. No negative peak is seen in 3MP which is consistent with the smaller dipole orientation peak in 3MP compared to TEA.

Peaks B and C in unirradiated TEA and 3MP are apparently due to some sort of capacitance changes in the conductivity cell. These peaks are not due to dipole orientation because they are unaffected by field orientation measurements. Peak B appears to be associated with a phase change in the matrix. It appears near 108°K in 3MP and near 150°K in TEA. This difference is consistent with the lower viscosity of 3MP and indicates that peak B is associated with characteristics of the matrix. As a phase change occurs, some volume change will be associated with it and may affect electrode separation and consequently the capacitance of the conductivity cell. Peak C occurs near 190°K in both TEA and 3MP. This temperature is high enough so that both matrices should be liquid and the origin of peak C is unexplained.

*B. Irradiated TEA.* Peak I is apparently due to shallow trapped electrons which decay spontaneously at 77°K. These electrons may well give isothermal luminescence in TEA at 77°K but such effects have not yet been reported. The behavior of peak I seems very similar to the analogous peak I in 3MP.<sup>1</sup>

Peak II can be rather definitively identified with the thermal detrapping of electrons. The trapped electrons in TEA can be observed by epr.<sup>5</sup> The epr spectrum shows a sudden decay between 105 and 112°K which is identical with the temperature range of peak II in the TSC data. The proton nmr line width in unirradiated TEA also undergoes a rapid decrease from about 9 to 3 G in this same temperature range and indicates the onset of molecular rotation.<sup>5</sup>

The trapped electron yield in irradiated TEA at 77°K has been reported to increase to a maximum at about 2 Mrads and then decrease.<sup>6</sup> This is the same kind of dose dependence as observed for peak II which again is consistent with electron detrapping. The effects of scavengers on peak II also support this assignment. Good electron scavengers like biphenyl and  $\text{CCl}_4$  decrease or eliminate peak II by replacing the

(5) H. Tsujikawa, K. Fueki, and Z. Kuri, *J. Chem. Phys.*, **47**, 256 (1967).

(6) D. P. Lin and L. Kevan, *ibid.*, **55**, 2629 (1971).

electrons with more stable negative species which are presumably not detrapped until temperatures somewhat higher than 110°K. The hole scavenger 2MP-1 increases peak II quite significantly. The hole scavenger can increase the yield of trapped electrons by preventing some hole-electron recombination; this then increases peak II. It is also conceivable that the 2MP-1 changes the nature of the matrix so that the electron travel distance increases; however, this seems improbable for the concentrations used.

Peak III is small and negative and only observed at the higher doses and the lower fields. This peak seems quite analogous to a similar peak also numbered III observed in 3MP.<sup>1</sup> This peak has been interpreted as the thermal randomization of molecular dipole orientation in 3MP and the same explanation seems applicable here. The increase in the proton nmr line width above 113°K<sup>5</sup> implies some sort of phase change and could also be a contributing factor to the negative peak III.

Peak IV near 150°K in TEA seems to be associated with radiation-produced species and can logically be attributed to detrapping of residual cations and perhaps also molecular anions. Residual cations are those that were not neutralized when the electrons were detrapped as the temperature was raised. Both electron and positive hole scavengers cause peak IV to either decrease or broaden. The electron scavengers replace trapped electrons with molecular anions. The increase in molecular anion population could cause the net observed current peak IV to decrease by decreasing the average travel distance of detrapped cations before they are neutralized by an anion. Also, if the mobility of the anions, formed from scavengers, were sufficiently different from that of the cations it would tend to spread out this peak. The effect of the positive hole scavenger 2MP-1 to decrease peak IV is

presumably associated with a different mobility for the 2MP-1 cations relative to the mobility of the cation in the TEA matrix. This would tend to spread out the peak and effectively decrease its intensity.

The overall results in irradiated TEA are very similar to those in irradiated 3MP except that the temperature ranges of the corresponding TSC peaks are somewhat higher in TEA. In more polar matrices like MTHF similar effects cannot be readily observed, as previously reported,<sup>2</sup> because of the masking effect of the high intrinsic conductivity in MTHF and in other such polar matrices.

*C. Irradiated 3MP.* The electrical conductivity of 3MP upon warming has been reported by two groups of workers.<sup>1,3</sup> Our results agree quite well with those reported by Wiseall and Willard,<sup>1</sup> even though our conductivity cell was designed rather differently from theirs. Our conductivity cell seems to be almost identical with that used by Kosa-Somogyi and Balog.<sup>3</sup> These latter workers report a very broad conductivity peak extending from about 77°K to beyond 150°K and in addition a peak above 200°K. The peak above 200°K appears in unirradiated samples and is the same as we observe near 190°K. However, we do not observe a single broad peak as they have reported, but rather the resolved peaks as reported by Wiseall and Willard. The agreement of our results in 3MP with those of Wiseall and Willard indicates both that our TEA results are comparable with the previous reported results on 3MP and MTHF and that the TSC current profiles observed are not critically dependent upon the design of the conductivity cell.

*Acknowledgment.* This research was supported by the Air Force Office of Scientific Research under Grant No. AFOSR-70-1852. In addition, equipment support was received from the U. S. Atomic Energy Commission under Contract No. AT(11-1)-2086.

# Sequence Studies in Liquid-Phase Hydrocarbon Oxidation. I. The Alcohol-Ketone Transition in the Oxidation of Ethylbenzene

by É. Danóczy, G. Vasvári, and D. Gál\*

Central Research Institute for Chemistry of the Hungarian Academy of Sciences, Budapest, Hungary  
(Received November 22, 1971)

The consumption of labeled methylphenylcarbinol during the liquid-phase oxidation of ethylbenzene at 120° has been investigated. Oxidation of the carbinol yielded only acetophenone, but most of the latter was formed directly, by the termination reaction and by decomposition of hydroperoxide molecules. Use of the modified kinetic isotope method permitted quantitative calculation of rates of formation of alcohol and ketone molecules by various routes.

## Introduction

The liquid-phase oxidation of aromatic hydrocarbons, including that of ethylbenzene, has been thoroughly studied. The works of Henderson (study of wall effects in the oxidation),<sup>1</sup> Pritzkow (investigation of the properties of hydroperoxides formed in the reaction),<sup>2</sup> Tsepalov,<sup>3</sup> and Denisov<sup>4</sup> (kinetic analysis of the oxidation), as well as of Hock and Lang<sup>5</sup> and Emerson, *et al.*<sup>6</sup> (study of the effect of water and alcohol on the conversion), should be mentioned. In the initial stages of the reaction—above 0.1-mm oxygen pressures—secondary reactions can be neglected compared with the main elementary steps. With the accumulation of stable intermediates, however, the mechanism becomes more complex. Namely, these compounds, taking part in different interactions with the radicals, are able to change the rate of the conversion and the distribution of the products.<sup>7</sup> This can be attributed to the fact that oxidizability of the intermediates is higher than that of the parent hydrocarbon. Other complicating factors are the new chain carrier radicals generated by the secondary processes. The reactivity of these species differs strongly from the reactivity of the primary peroxy radicals.

The main stable products of ethylbenzene oxidation are hydroperoxide (ROOH), methylphenylcarbinol (ROH), and acetophenone (R'COR'').

According to literature data these types of products can be formed by the following routes.

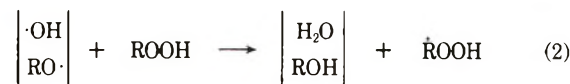
(1) *The formation of hydroperoxide* is relatively simple. It is formed in a hydrogen-abstraction reaction from the substrate molecules (or, generally, from a hydrogen donor molecule) by peroxy radicals (RO<sub>2</sub>·)



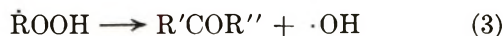
This elementary step is well known, and corresponding data can be found in the works of Russell,<sup>8</sup> Howard, *et al.*,<sup>9,10</sup> Gadelle,<sup>11</sup> and others.<sup>12-16</sup> At higher conversions, product molecules may also participate in the reaction as hydrogen donors.

(2) *The formation of ketone* can be realized by several routes.

(a) Robertson and Waters,<sup>17</sup> Benson,<sup>18</sup> and Martan,<sup>19</sup> suggest that hydroxyl and alkoxy radicals generated in the system (*e.g.*, in the decomposition of hydroperoxide molecules) react with ROOH yielding hydroperoxyalkyl radicals



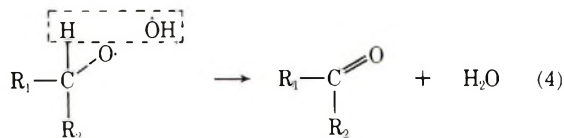
This reaction is followed by



Hiatt, *et al.*,<sup>20,21</sup> support this reaction as an important one above 100°.

- (1) G. M. Henderson, *Discuss. Faraday Soc.*, No. 10, 291 (1951).
- (2) W. Pritzkow and J. Hahn, *J. Prakt. Chem.*, 16, 287 (1962).
- (3) V. F. Tsepalov, V. Y. Shlyapintokh, and P. H. Shon, *Zh. Fiz. Khim.*, 38 (2), 351 (1964); *Kinet. Katal.*, 3, 870 (1962).
- (4) E. T. Denisov, *Usp. Khim.*, 39, 62 (1970).
- (5) H. Hock and S. Lang, *Chem. Ber.*, 76, 169 (1943); *Quart. Rev., Chem. Soc.*, 8, 147 (1954).
- (6) W. S. Emerson, J. W. Heyd, V. E. Lucas, W. B. Cook, W. J. Lyness, and J. K. Stevenson, *J. Amer. Chem. Soc.*, 70, 3, 764 (1948).
- (7) L. Sajus, *Advan. Chem. Ser.*, No. 75, 59 (1968).
- (8) G. A. Russell, *J. Amer. Chem. Soc.*, 78, 1047 (1956).
- (9) J. A. Howard and K. U. Ingold, *Can. J. Chem.*, 44, 1119 (1966).
- (10) J. A. Howard, W. A. Schwalm, and K. U. Ingold, *Advan. Chem. Ser.*, No. 75, 6 (1968).
- (11) C. Gadelle and G. Clément, *Bull. Soc. Chim. Fr.*, 1175 (1967); 44 (1968).
- (12) J. Alagy, G. Clément, and J. C. Balaceanu, *ibid.*, 1325 (1929); 1303, 1792 (1961); *Rev. Int. Fr. Petrol.*, 18, 1 (1963).
- (13) A. Van Tiggelen and C. Clément, *ibid.*, 21, 1299 (1966).
- (14) F. R. Mayo, M. G. Syz, T. Mill, and J. K. Castleman, *Advan. Chem. Ser.*, No. 75, 38 (1968).
- (15) I. Serée de Roch, *Ind. Chim. Belg.*, 33, 994 (1968).
- (16) J. A. Meyer, V. Stannett, and M. Szwarc, *J. Amer. Chem. Soc.*, 83, 25 (1961).
- (17) A. Robertson and W. A. Waters, *J. Chem. Soc.*, 1578 (1948).
- (18) S. W. Benson, *J. Chem. Phys.*, 40, 1007 (1964).
- (19) M. Martan, J. Menassen, and D. Vofsi, *Tetrahedron*, 26, 3815 (1970).

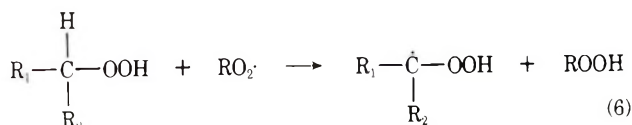
Instead of a chain reaction, however, an O-O fission in the hydroperoxide can be followed by a "cage elimination" (see, *e.g.*, Martan<sup>19</sup> and Cubbon<sup>22</sup>)



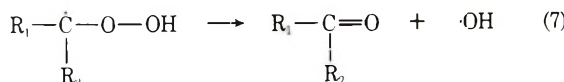
Emanuel and coworkers assumed<sup>23,24</sup> that reaction 2 could also proceed with the participation of peroxy radicals



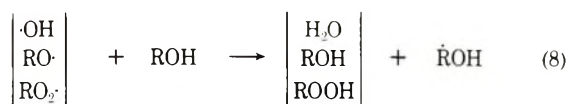
Reaction 5 is likely to occur in two steps



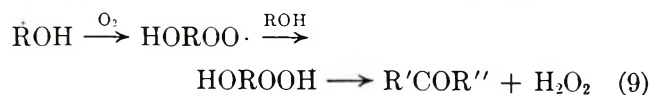
and



(b) As experimentally proved by Stephens,<sup>25</sup> Parlant, *et al.*,<sup>26</sup> Howard, *et al.*,<sup>27</sup> and Emanuel and coworkers,<sup>28</sup> the oxidation of alcohol molecules in systems containing radicals readily yields ketone. The first step of this oxidation is probably the formation of oxyalkyl radicals



This reaction is followed by the formation of oxyperoxy radicals and oxyhydroperoxide molecules, the latter yielding ketone and hydrogen peroxide



(c) Based on the works of Cullis, Fish, and coworkers<sup>29-31</sup> as well as Knox,<sup>32</sup> it has been recently assumed that in the gas-phase oxidation of hydrocarbons isomerization and subsequent decomposition of peroxy radicals play an important role in the formation of the products. A similar, though less important, role is attributed to peroxy radicals in liquid-phase oxidations by Zaikov, *et al.*<sup>33-35</sup> This would mean that peroxy radicals produce directly ketone (or aldehyde) molecules and a new radical. Though this route of ketone formation requires further experimental proof, the possibility cannot be excluded.

(3) *The formation of alcohol can be realized by several reactions.*

(a) In the decomposition of hydroperoxide molecules alkoxy radicals are generally formed. Thus in

the monomolecular decomposition (see, *e.g.*, the papers of Twigg,<sup>36</sup> Benson,<sup>37</sup> and Farkas<sup>38</sup>)



followed by



The decomposition of hydroperoxide as emphasized by Bateman,<sup>39</sup> Bolland,<sup>40</sup> Semenov,<sup>41</sup> and Hiatt and Irwin<sup>42</sup> proceeds—under certain conditions—in a bimolecular interaction with another ROOH molecule (eventually with RH or ROH). The generation of RO· radicals occurs in all types of these reactions.

(b) Dean and Skirrow suggested<sup>43</sup> that the RO<sub>2</sub>· induced decomposition of ROOH could produce alcohol molecules



According to Skibida, Maizus, and Emanuel,<sup>44</sup> the reaction occurs *via* complex formation

(20) R. Hiatt, T. Mill, K. C. Irwin, and J. K. Castleman, *J. Org. Chem.*, **33**, 1428 (1968).

(21) R. Hiatt, T. Mill, and F. R. Mayo, *ibid.*, **33**, 1416 (1968).

(22) R. C. P. Cubbon, *Progr. React. Kinet.*, **2**, 40 (1970).

(23) N. M. Emanuel, E. T. Denisov, and Z. K. Maizus, "Chain Reactions in the Liquid Phase Oxidation of Hydrocarbons," Moscow, 1965, in Russian "Nauka."

(24) D. G. Knorre, Z. K. Maizus, L. K. Obukhova, and N. M. Emanuel, *Usp. Khim.*, **20**, 416 (1957).

(25) H. N. Stephens, *J. Amer. Chem. Soc.*, **50**, 186 (1928).

(26) C. Parlant, I. Serée de Roch, and J. C. Balaceanu, *Bull. Soc. Chim. Fr.*, 2452 (1963); *Rev. Int. Fr. Petrol.*, **19**, 78 (1964).

(27) J. A. Howard and S. Korcek, *Can. J. Chem.*, **48**, 2165 (1970).

(28) N. M. Emanuel, *Nyeftekhimiya*, **6**, 827 (1967).

(29) C. F. Cullis, A. Fish, and D. L. Trimm, *Proc. Roy. Soc., Ser. A*, **273**, 427 (1963).

(30) A. Fish, *Org. Peroxides*, **1**, 140 (1970).

(31) A. Fish, *Proc. Roy. Soc., Ser. A*, **298**, 204 (1967); A. Fish, I. A. Read, W. S. Affleck, and W. W. Hostell, *Combust. Flame*, **13**, 39 (1969).

(32) J. H. Knox, *ibid.*, **9**, 297 (1965).

(33) E. A. Blumberg and G. E. Zaikov, *Dokl. Akad. Nauk SSSR*, **139**, 99 (1961).

(34) G. E. Zaikov, C. D. Kazanceva, and Z. K. Maizus, *Theor. Exp. Khim.*, **2**, 204 (1966).

(35) G. E. Zaikov, Z. K. Maizus, and N. M. Emanuel, *Kinet. Katal.*, **7**, 401 (1966).

(36) G. H. Twigg, *Chem. Eng. Sci., Spec. Suppl.*, **3**, 5 (1954).

(37) S. W. Benson, *J. Chem. Phys.*, **40**, 1007 (1964).

(38) A. Farkas and E. Passaglia, *J. Amer. Chem. Soc.*, **72**, 3333 (1950).

(39) L. Bateman, H. Hughes, and A. L. Morris, *Discuss. Faraday Soc.*, **No. 14**, 190 (1953).

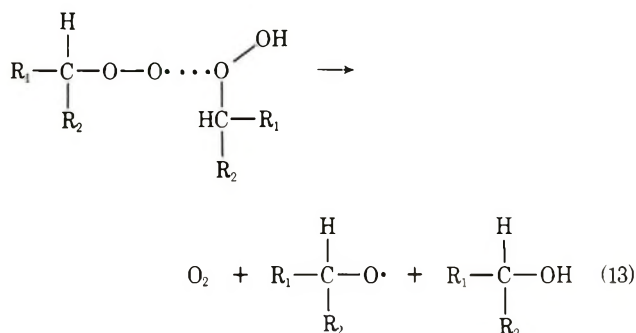
(40) J. L. Bolland, *Proc. Roy. Soc., Ser. A*, **186**, 218 (1946); *Quart. Rev., Chem. Soc.*, **3**, 1 (1949).

(41) N. N. Semenov, "Problems of Chemical Kinetics and Reactivity," Moscow, 1958, in Russian "Nauka."

(42) R. Hiatt and K. C. Irwin, *J. Org. Chem.*, **33**, 1436 (1968).

(43) M. H. Dean and G. Skirrow, *Trans. Faraday Soc.*, **54**, 849 (1958).

(44) I. P. Skibida, Z. K. Maizus, and N. M. Emanuel, *Dokl. Akad. Nauk SSSR*, **149**, 1111 (1963).



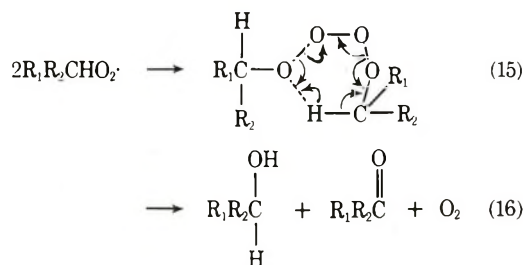
The alkoxy radical formed in reaction 12 also yields alcohol according to (11).

(c) In general, if an intermediate or a transition complex decomposing in an oxidation system gives alkoxy radicals and the latter leave the cage, alcohol molecules are obtained.

(4) *Simultaneous Formation of Alcohol and Ketone Molecules.* (a) This is well known in the termination reaction of two peroxy radicals. This process was thoroughly studied, *e.g.*, by Russell,<sup>45</sup> Traylor and Bartlett,<sup>46</sup> Howard and Ingold,<sup>47</sup> Thomas and Ingold,<sup>48</sup> Hiatt, *et al.*,<sup>20</sup> and Mill and Stringham.<sup>49</sup> It has been verified that, in the case of secondary hydroperoxides, a tetroxide complex was formed and this decomposed directly to oxygen, ketone, and alcohol



or



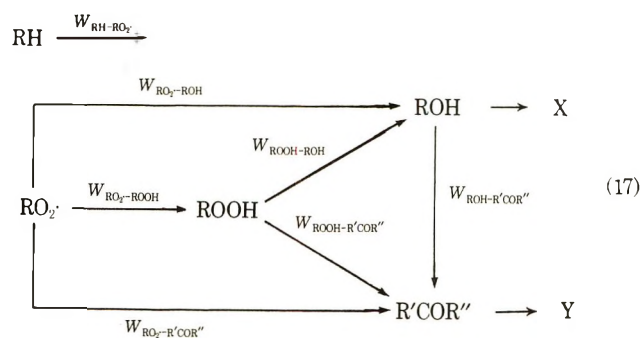
(b) Assuming that reaction 3 is fast compared to 2, we may regard the latter process as a simultaneous source of both alcohol and ketone.

It should be emphasized that reactions 1–16 represent only the most important routes for product formation, and further possibilities should also be considered if the construction of an adequate mechanism is intended (*e.g.*, hydrogen-transfer reactions between peroxy radicals and hydroperoxide studied in different systems by Ingold and coworkers<sup>50,51</sup>).

Both ketone and alcohol can be obtained in different successive and competitive routes represented by the scheme designated as eq 17.

(Reaction paths  $\text{ROH} \rightarrow \text{X}$  as well as  $\text{R}'\text{COR}'' \rightarrow \text{Y}$  refer to literature data according to which alcohol molecules might be transformed in other products beside ketone—eventually into styrene—(see, *e.g.*, ref 52) while ketone might also react and yield different fragmentation products (see, *e.g.*, ref 19).)

Some of the rates are “gross rates” including all prob-



able elements of a transformation proceeding toward a certain direction. Thus, *e.g.*, the rate  $w_{\text{ROOH}-\text{R}'\text{COR}''}$  means the overall conversion rate of hydroperoxide into acetophenone, *i.e.*, a combination of  $w_2, w_4, w_5, w_x$  where  $w_x$  refers to reactions not included or unknown so far, with the restriction that the ROOH molecules themselves are to be transformed into ketone.

Several data can be found in the literature referring to the above scheme. For instance, Skibida and Gonikberg<sup>52</sup> attribute the formation of acetophenone in the oxidation of ethylbenzene exclusively to the transformation of alcohol. Considering the changes in the on/ol ratio with the conversion, Martan, *et al.*, suggest that it can be explained by assuming a change with conversion in the velocity ratios of the different routes.<sup>19</sup>

By successive labeling of the stable intermediates and applying the kinetic isotope method,<sup>53</sup> we may determine the corresponding rates in the scheme of eq 17 as a function of conversion. The important advantage of the procedure is its applicability under “natural” conditions of the process, in the presence of the intermediates, end products, and radicals accumulated in the system.

Following the quantitative determination of the individual rates, the corresponding reactions can be separately studied in well-chosen model systems (*e.g.*, a system containing peroxy radicals and hydroperoxide molecules serves as a model for reactions 5 and 12), and this might permit estimation of overall rates from the rates of elementary reactions.

(45) G. A. Russell, *J. Amer. Chem. Soc.*, **79**, 3871 (1957); *Chem. Ind. (London)*, 1483 (1956).

(46) T. G. Traylor and P. D. Bartlett, *Tetrahedron Lett.*, No. 24, 30 (1960).

(47) J. A. Howard and K. U. Ingold, *J. Amer. Chem. Soc.*, **90**, 1056, 1058 (1968).

(48) J. R. Thomas and K. U. Ingold, *Advan. Chem. Ser.*, No. 75, 266 (1968).

(49) T. Mill and R. S. Stringham, *J. Amer. Chem. Soc.*, **90**, 1062 (1968).

(50) J. A. Howard, W. J. Schwalm, and K. U. Ingold, *Advan. Chem. Ser.*, No. 75, 6 (1968).

(51) J. A. Howard and K. U. Ingold, *Can. J. Chem.*, **46**, 2661 (1968).

(52) I. P. Skibida and E. M. Gonikberg, *Izv. Akad. Nauk SSSR, Ser. Khim.*, **2**, 286 (1964).

(53) M. B. Neiman and D. Gál, “The Kinetic Isotope Method and Its Applications,” Elsevier, Amsterdam, 1971.

The present paper—as the first part of the series—deals with the study of the conversion of methylphenylcarbinol to acetophenone.

### Experimental Section

**Materials.** Commercial ethylbenzene was washed with  $\text{H}_2\text{SO}_4$ ,  $\text{NaOH}$ , and bisulfite followed by two successive redistillations, bp  $136^\circ$ .

Reagent grade acetophenone and methylphenylcarbinol were used after distillation.

Methylphenylcarbinol- $^{14}\text{C}$  and acetophenone- $^{14}\text{C}$  were prepared by the method of Speer,<sup>54</sup> partly modified by Dutka.<sup>55</sup> Specific activities were 2.8, 0.64, and 2.3 mCi mmol $^{-1}$ , respectively.  $\alpha$ -Phenylethyl hydroperoxide was prepared as described earlier.<sup>56</sup>

**Analysis.** The reaction products were analyzed by a Giede-type gas chromatograph, with a flame ionization detector unit. In order to eliminate the decomposition of hydroperoxides during analysis, the inlet was made of Teflon and glass columns were used (83 cm long, inner diameter 2.5 mm). The columns were filled with 10% diisodecyl phthalate on Gas Chrom S (120–140 mesh), operating at  $83^\circ$  with argon as carrier gas. These columns permit determination of the following products (in order of increasing retention times): ethylbenzene, benzaldehyde, acetophenone, methylphenylcarbinol, phenol,  $\alpha$ -phenylethyl hydroperoxide, and products with higher retention times. (Such peaks were found only in decomposition processes in the absence of oxygen.)

In case of iodometric determination of the active oxygen content, the mixture was extracted with water and the normal procedure<sup>57–59</sup> was carried out with both the organic and aqueous phases.

No acids were found among the oxidation products. Negligible amounts of phenol were observed at high conversions (from 5 mmol at 50 hr to 20 mmol at 70 hr).

To enable a simultaneous activity measurement the compounds after passing the column were divided: part led to the detector (25%) and part (75%) to a Packard combustion furnace. After being burned and dried over  $\text{MgClO}_4$  the  $\text{CO}_2$  gas was introduced in a scintillation counter of 5.87 ml, connected to a conventional coincidence device. Both activity and concentration peaks were registered and integrated. Integration was based on impulse number measurements. A separate registration by a recorder was necessary in order to enable a qualitative distinction between active and inactive peaks.

**Reaction Conditions.** The work was done at  $120^\circ$  at atmospheric pressure in a conventional static system. The reaction vessel was a glass cylinder of 100-ml volume;  $\text{O}_2$  flow rate was 1.6 l. hr $^{-1}$ . (The amount of the liquid was 30 ml; the concentration of the ethylbenzene was 7.26 M.)

Oxygen was bubbled through a capillary tube sealed

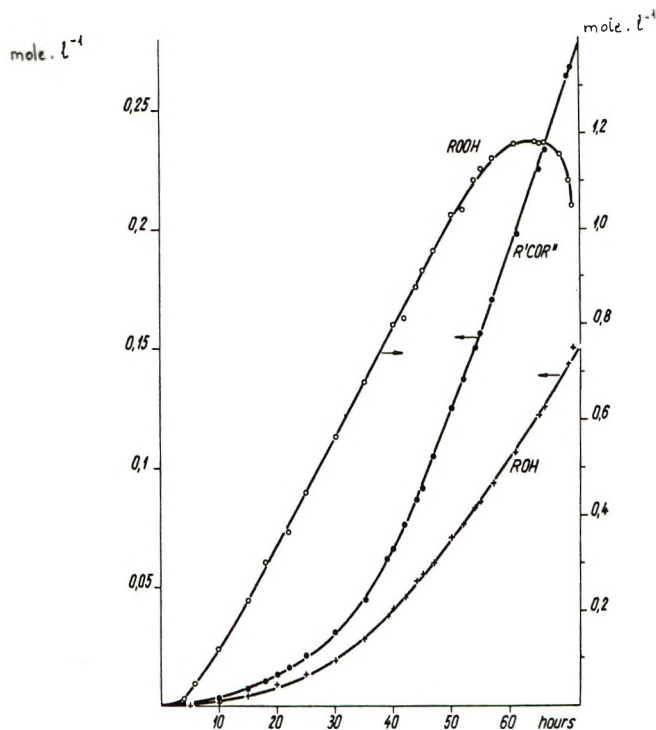


Figure 1. Kinetics of product accumulation in the oxidation of ethylbenzene at  $120^\circ$ . (The ROH accumulation curve was corrected for ROH added initially in amounts of 3.3 mmol l $^{-1}$ ).

to the lower end of the vessel, thus ensuring effective mixing of the system. The reaction vessel was connected with a reflux cooled by water in order to avoid a loss by evaporation.

### Experimental Results

According to the kinetic isotope method (KIM), labeled alcohol and/or ketone molecules have to be introduced into the system. In order to avoid the chemical effect of these compounds, preliminary experiments were needed studying the effect of alcohol and ketone addition on the oxidation. Therefore, methylphenylcarbinol and acetophenone were added, separately and together, to the ethylbenzene–oxygen system, and the accumulation of the intermediate and end products were compared to experiments without the addition of these compounds.

It was concluded that neither the ROH nor the R'COR'' exerted any effect to be taken into account (at least not in concentrations up to  $5 \times 10^{-3}$  M) in our further experiments. The well-known retarding

(54) R. J. Speer and J. K. Jeanes, *J. Amer. Chem. Soc.*, **74**, 2443 (1952).

(55) F. Dutka, private communication.

(56) L. Sümegi, I. Kende, A. Németh, and D. Gál, *Magy. Chem. Foly.*, **77**, 571 (1971).

(57) V. R. Kokatnur and M. Jelling, *J. Amer. Chem. Soc.*, **63**, 1432 (1941).

(58) J. A. Howard and K. U. Ingold, *Can. J. Chem.*, **45**, 785 (1967).

(59) D. Gál, E. A. Blumberg, Ya. A. Valendo, and N. M. Emanuel, *Acta Chim. Acad. Sci. Hung.*, **66**, 55 (1970).

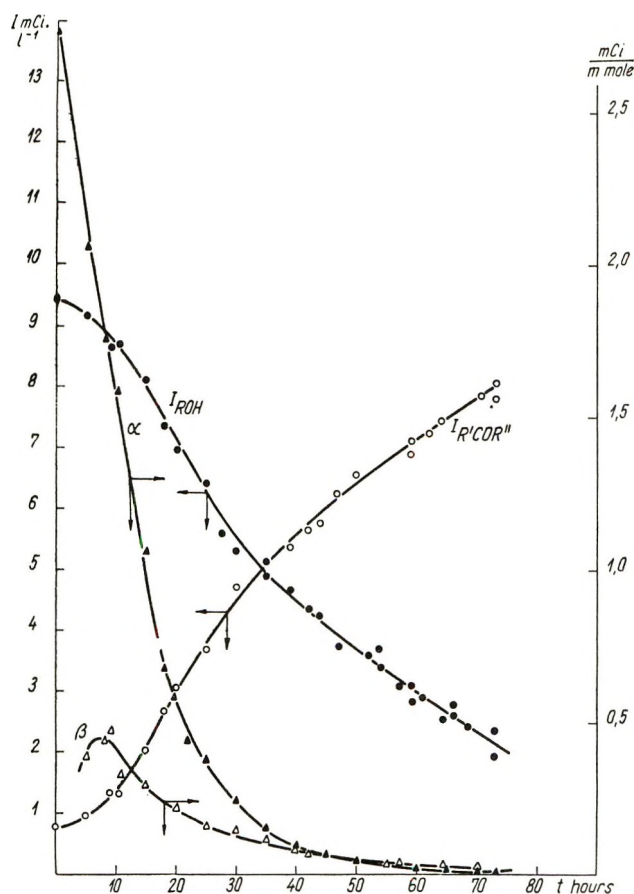


Figure 2. The changes of the total activities and specific activities of methylphenylcarbinol ( $I_{ROH}$  and  $\alpha$ ) and acetophenone ( $I_{R'COR''}$  and  $\beta$ ) against time.

effect of  $ROH^{60-62}$  appears only at higher additive concentrations.

After introducing into the reaction mixture labeled ROH with two different initial specific activities (0.64 and 2.8 mCi mmol<sup>-1</sup>), the changes in the concentrations of ROOH, ROH, and R'COR'' (Figure 1) as well as the changes in the total activities of these compounds (Figure 2) against time have been measured. (Since the initial specific activity had no effect with respect to the activity change, hereafter we refer only to one initial specific activity.)

The observed initial activity of the acetophenone was due to some oxidation of the labeled alcohol during storage.

From the total activity and concentration values the corresponding specific activities ( $\alpha$  for ROH and  $\beta$  for R'COR'') were calculated (Figure 2).

It should be emphasized that the reactions were carried out for 70 hr, that is up to a relatively high conversion (about 20% or 1.5 M ethylbenzene was consumed). As can be seen from Figure 2, the sum of the total activities of ROH and R'COR'' equals (during the whole time interval studied) the initial total activity of the ROH, suggesting that alcohol molecules—if consumed at all—produced only ketone and that ketone

molecules—within the limits of the experimental error—are not consumed; they are end products in the reaction. Owing to the low activities observed in ketone molecules, however, this statement can be accepted only within a broad limit of experimental error.

For quantitative calculations, the difference between the specific activities ( $\alpha - \beta$ ) at different reaction times would be needed. Since the accuracy of  $\beta$  is poor, it would be more precise to use only the  $\alpha$  values. This can be done by modifying the equations of the KIM if it can be proved unambiguously that the ketone is an end product of the reaction under our experimental conditions.

For this reason separate experiments were carried out in the presence of labeled acetophenone.

The total activity of acetophenone was measured for 57 hr, and Table I shows no trend in activity. Statistical error calculations have shown that the constancy of the total activity could be stated within the limit of  $\pm 4.5\%$ . Since no activity was found in other products it can be assumed that acetophenone was not consumed during the whole time interval studied under the present experimental conditions.

Table I: Oxidation of Ethylbenzene in the Presence of Labeled Acetophenone. Changes in the Total Activity of R'COR'' vs. Time

Time, hr	$I_{R'COR''}$ , mCi l <sup>-1</sup>
0	7.30
10.0	7.30
13.6	7.26
19.0	7.55
23.0	7.15
27.0	7.32
37.3	7.17
44.5	7.07
47.5	7.60
50.5	7.45
57.5	7.00

According to the equations of the KIM, the rate of consumption of alcohol molecules is given by

$$w_c \equiv \frac{d[ROH]_c}{dt} = -[ROH] \frac{1}{\alpha} \frac{d\alpha}{dt} - \frac{d[ROH]}{dt} \quad (18)$$

while the rate of formation of acetophenone from alcohol is given by

$$w_{ROH \rightarrow R'COR''} = \frac{d[R'COR'']_{t(ROH)}}{dt} = [R'COR'']_{ROH} \frac{d\beta}{dt} \frac{1}{\alpha - \beta} \quad (19)$$

(60) N. M. Emanuel, *Advan. Chem. Ser.*, No. 75, 1 (1968).

(61) F. F. Rust and E. A. Youngman, *J. Org. Chem.*, 27, 3778 (1962).

(62) J. C. André and J. Lemaire, *C. R. Acad. Sci.*, 272, 1396 (1971).



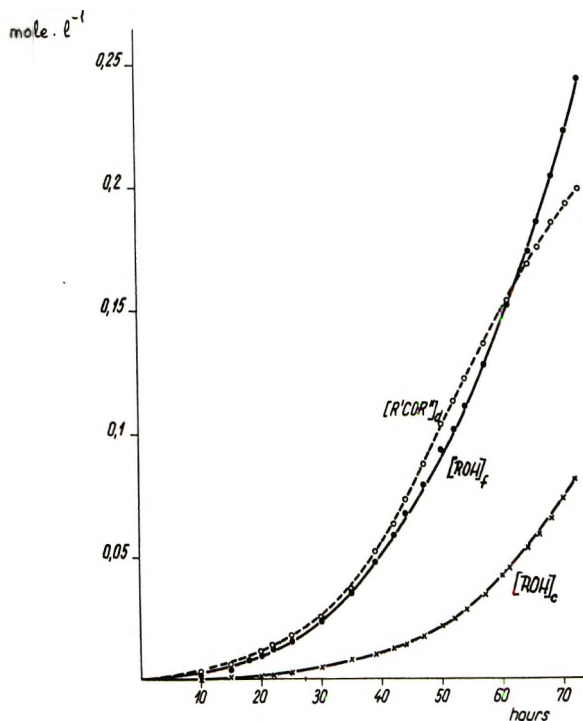


Figure 3. Amounts of acetophenone formed directly and of methylphenylcarbinol formed and consumed, plotted against time.

where the subscript c refers to consumption and f to formation

Since the concentration  $[R'COR'']_{ROH}$  is not known, and in order to avoid the use of the  $\beta$  values, eq 19 was modified.

The corresponding total activities are

$$I_{ROH} = \alpha[ROH] \quad (20)$$

$$I_{R'COR''} = \beta[R'COR'']_{ROH} \quad (21)$$

Differentiating eq 20 and substituting it into eq 18

$$[ROH]_c = - \int_{I_0}^I \frac{1}{\alpha} dI_{ROH} \quad (22)$$

Since acetophenone is not consumed, its amount formed from alcohol can be substituted into eq 19 instead of its amount accumulated *via* alcohol

$$\frac{d[R'COR'']_{f(ROH)}}{dt} = [R'COR'']_{f(ROH)} \frac{d\beta}{dt} \frac{1}{\alpha - \beta} \quad (23)$$

Rearranging

$$\alpha \frac{d[R'COR'']_{f(ROH)}}{dt} = \beta \frac{d[R'COR'']_{f(ROH)}}{dt} + [R'COR'']_{f(ROH)} \frac{d\beta}{dt} = \frac{dI_{R'COR''}}{dt} \quad (24)$$

That is

$$[R'COR'']_{f(ROH)} = \int_{I_0}^I \frac{1}{\alpha} dI_{R'COR''} \quad (25)$$

Using eq 22 and 25, we obtain the corresponding values by graphical differentiation. If the alcohol molecules are transformed only into ketone, these equations should lead to identical numerical values. The values calculated are given in Figure 3, where  $[R'COR'']_a$  means the concentration of acetophenone formed directly (not through alcohol). For better comparison, concentration and rate values are collected in Table II. Since activity was found only in alcohol and ketone molecules, the total activity curves were constructed correcting the dispersion of the experimental points taking into account that the sum of the two total activities is constant during the whole reaction period. These corrected values are used in Table II, columns 6 and 7.

### Discussion

From the experimental results, the following conclusions can be drawn.

(1) Under the experimental conditions used, there is no other product formed from alcohol but ketone which is an end product. Since there was no activity detectable in the hydroperoxide, a possibility for a "back-reaction" can be excluded.

(2) According to Table II, the acetophenone is formed in the beginning of the reaction mainly "directly" and in negligible extent *via* alcohol molecules, and this latter route becomes important only at the

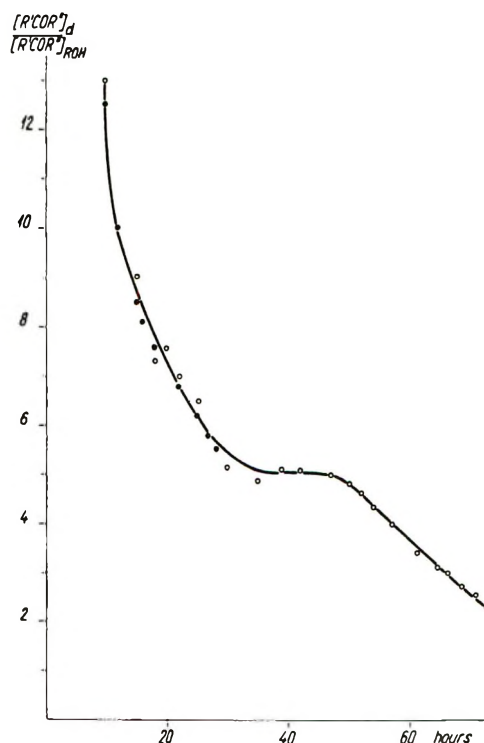


Figure 4. The ratio of the amounts of acetophenone formed directly to the amounts of acetophenone formed *via* methylphenylcarbinol molecules, plotted against time. (O and ● refer to different experimental runs indicating the reproducibility of the tracer experiments).

Table II

Time, hr	[ROOH] <sup>a</sup>				[ROH] <sup>b</sup>	[R'COR''] <sup>b</sup>	$\alpha^c$	$\beta^c$	[ROH] <sub>c</sub> <sup>a</sup>
	[ROH] <sup>a</sup>	[R'COR''] <sup>a</sup>	Glc	Iodo- metric					
0	3.4				9.40	0.76	2.76		
5	4.0	1.4	35		9.26	0.89	2.06	0.39	0.08
10	5.0	3.5	120		8.73	1.42	1.58	0.47	0.25
15	7.5	7.0	225	260	8.02	2.13	1.06	0.29	0.70
20	12.0	13.0	340	338	7.06	3.09	0.59	0.22	1.38
25	16.5	21.0	450		6.24	3.91	0.38	0.16	2.80
30	22.5	30.5	565		5.50	4.65	0.24	0.15	4.94
35	31.5	45.0	680		4.93	5.22	0.16	0.12	7.70
42	49.5	76.0	815		4.35	5.80	0.09	0.07	12.4
44	55.9	87.0	880		4.20	5.95	0.07	0.06	14.2
47	64.0	105	955		3.97	6.18	0.06	0.05	17.5
50	74.0	125	1030	1090	3.75	6.40	0.05	0.05	21.6
54	87.0	150	1105		3.45	6.70	0.04	0.04	28.0
57	97.0	170	1150		3.22	6.93	0.03	0.04	34.0
61	110	198	1180	1250	2.93	7.22	0.03	0.04	45.0
64.4	125	222	1185	1273	3.70	7.45	0.02	0.03	53.7
66	129	233	1180		2.60	7.55	0.02	0.03	58.5
70.75	150	268	1050	1360	2.29	7.86	0.01	0.03	75.4
73	160	285	965	1330	2.14	8.01	0.01	0.03	86.4

Time, hr	[ROH] <sub>t</sub> <sup>a</sup>	[R'COR''] <sub>d</sub> <sup>a</sup>	d[ROOH]/ dt <sup>d</sup>	d[ROH] <sub>t</sub> / dt <sup>d</sup>	d[ROH] <sub>c</sub> / dt <sup>d</sup>	d[R'COR''] <sub>d</sub> / dt <sup>d</sup>	[R'COR''] <sub>d</sub> / R'COR''/ROH	[R'COR''] <sub>d</sub> / ROH <sub>t</sub>	[RH] <sub>c</sub> <sup>a,e</sup>
0									
5	0.73	1.4	3.90	0.60	0.04	0.82	17.50	1.92	37
10	2.35	3.2	5.83	0.86	0.25	1.69	13.00	1.38	126
15	4.3	6.3		2.16	0.46	2.30	9.00	1.46	235
20	9.98	11.6		2.94	0.86	2.61	8.55	1.16	366
25	15.4	18.2	6.40	4.8	1.19	4.08	6.50	1.31	483
30	24.0	25.5	6.40	6.3	1.53	7.06	5.15	1.07	614
35	35.3	37.3		8.65	1.69	10.10	5.10	1.06	752
42	59.0	63.6	6.40	10.80	2.50	12.8	5.12	1.08	937
44	66.8	72.8					5.12	1.09	1019
47	78.6	87.5	6.40	13.50	3.75	14.75	5.00	1.11	1121
50	93.2	103.4		11.00	4.02	12.30	4.80	1.11	1226
54	110.6	122.0					4.35	1.10	1337
57	127.6	136.0	2.78	16.60	6.25	12.80	4.00	1.07	1413
61	151.6	153.0	1.39	17.70	7.13	12.40	3.40	1.01	1484
64.4	173.3	168.3					3.12	0.97	1526
66	185.1	174.5		20.60	9.45	11.65	2.98	0.94	1539
70.75	222.0	192.6		26.00	13.60	7.40	2.55	0.87	1464
73	243.0	198.5					2.3	0.82	1506

<sup>a</sup> Concentrations,  $M \times 10^3$ . <sup>b</sup> Units,  $mCi l^{-1}$ . <sup>c</sup> Units,  $mCi mmol^{-1}$ . <sup>d</sup> Units,  $M sec^{-1} \times 10^6$ . <sup>e</sup> Calculations based on the assumption that  $[RH]_c = [ROOH] + [ROH] + [R'COR'']$ .

later stages of the process. This can be well illustrated by plotting

$$[R'COR'']_d / [R'COR'']_{ROH} = f(t) \quad (26)$$

as can be seen in Figure 4.

This ratio varies with the conversion, showing at the beginning a sharp decrease until it reaches the value of 2. We do not have any explanation for the plateau between 30 and 50 hr, though a change in the mechanism of the direct ketone formation cannot be excluded. (After 70 hr as much ketone is formed directly as *via* alcohol.)

This result seems to disagree with those obtained by Skibida and Gonikberg referred to earlier.<sup>52</sup> The dis-

crepancy could be explained partly by the different experimental conditions. They worked in a flow system, initiating the reaction by ADBN, and introduced into the mixture a fair amount of alcohol and thus changed the product ratios (and eventually the radical ratios, too).

(3) Regarding the values  $w_{ROH-R'COR''}$  as "corrections," the rate of the direct formation of acetophenone ( $w_{ROOH-R'COR''} + w'_{RO_2-R'COR''}$ ) and the formation rate of methylphenylcarbinol ( $w_{ROOH-ROH} + w_{RO_2-ROH}$ ) can be calculated from Table II and compared. This is shown in Figure 5. As can be seen, the two rates do not differ essentially for a long period and a deviation can be observed only after 62 hr, when the corre-

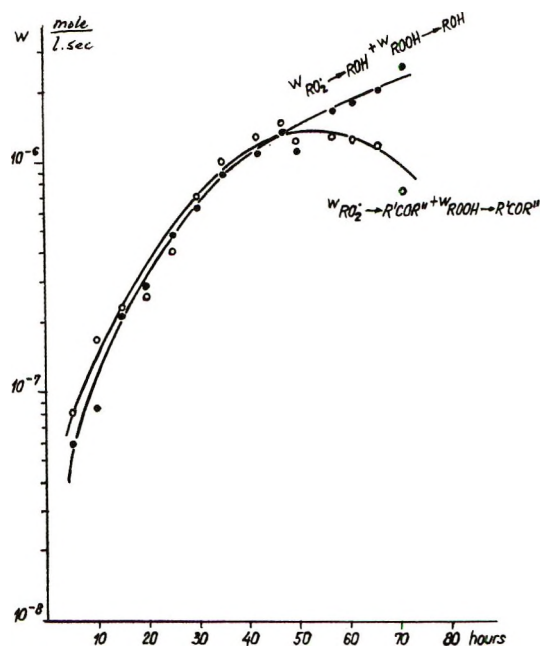


Figure 5. Rate of formation of methylphenylcarbinol and direct formation rate of acetophenone plotted against time.

sponding values for the alcohol increase further, while from here on the direct formation rate of the ketone starts to decrease. It is interesting that—as seen from Figure 1—the accumulation of the hydroperoxide reaches its maximum at the same reaction time.

(4) Assuming a Russell-type termination, we can reduce the two sums plotted in Figure 4; namely

$$w_{RO_2 \rightarrow ROH} = w'_{RO_2 \rightarrow R'COR''} \quad (27)$$

where

$$w'_{RO_2 \rightarrow R'COR''} = w_{RO_2 \rightarrow R'COR''} - w''_{RO_2 \rightarrow R'COR''} \quad (28)$$

Here  $w''_{RO_2 \rightarrow R'COR''}$  means a non-Russell-type peroxy radical-acetophenone transition (*via* isomerization or in interaction with other products but hydroperoxide).

Taking into account (27) and (28), the tendency observed in Figure 4 is valid also for expressions  $w''_{RO_2 \rightarrow R'COR''} + w_{ROOH \rightarrow R'COR''}$  and  $w_{ROOH \rightarrow ROH}$ , respectively. This means that at high conversions the rate of hydroperoxide-alcohol transition exceeds that of hydroperoxide ketone *plus* the non-Russell-type peroxy radical ketone transition. If the latter could be neglected—this is to be proved by using labeled hydroperoxide molecules—the aforementioned results can be explained by assuming that at high conversions the reactions of hydroperoxide molecules produce an increasing number of alkoxy radicals (*e.g.*, with the participation of alcohol molecules or with new chain carrier radicals).

This could be an explanation for the results summarized in part 3.

(5) From our experimental results a few more kinetic data can be calculated.

Since up to 15 hr reaction time the yield of hydroperoxide is  $\sim 96\%$ , in this period

$$-\frac{d[RH]}{dt} \equiv -\frac{d[O_2]}{dt} \sim \frac{d[ROOH]}{dt} \equiv W \quad (29)$$

In the absence of initiators, the rate of initiation can be expressed roughly as the rate of the degenerate branching. Using the value  $1 \times 10^{-6} \text{ sec}^{-1}$  from the literature<sup>63</sup> for the rate constant of the branching reaction, we can calculate the kinetic chain length ( $\nu$ ) at the early stages of the process. Corresponding values are given in Table III. As can be seen, the  $\nu$  values are quite large. Therefore, the reaction rate can be given as the rate of the chain propagation

$$-\frac{d[RH]}{dt} = k_1[RO_2 \cdot][RH] \quad (30)$$

It can be assumed that the rate of the alcohol consumption is similarly

$$-\frac{d[ROH]}{dt} = k_8[RO_2 \cdot][ROH] \quad (31)$$

(Initially the chain carriers should be the  $RO_2 \cdot$  radicals; contribution by  $\cdot OH$  and  $HO_2 \cdot$  radicals should appear only at high conversion.)

Table III: Kinetic Data for the Autoxidation of Ethylbenzene at 120°

Time, hr	$-\frac{d[RH]}{dt}$ , $M \text{ sec}^{-1} \times 10^6$	Rate of initiation, $M \text{ sec}^{-1} \times 10^8$	$\nu$ , chain length	$k_1/k_8^{1/2} \times 10^4$ , $l^{1/2} \text{ mol}^{-1/2} \text{ sec}^{-1/2}$
2	1.1	0.4	277	24.2
4	2.5	1.7	147	25.9
6	4.4	4.4	100	28.0
8	5.6	8.0	69	27.4
10	5.7	12.0	46	23.2
12	5.8	16.0	36	20.6
14	6.1	20.4	30	19.0
16	6.1	24.8	25	17.5

From eq 30 and 31, the ratio  $k_1/k_8$  can be determined

$$k_1/k_8 = 0.23 \quad (32)$$

which is an average value valid only for 15 hr. This ratio represents the relative reactivities of RH and ROH molecules toward  $RO_2 \cdot$  radicals.

Using the data of Howard and Ingold<sup>9,27</sup> as well as of Sajus,<sup>7</sup> who oxidized ethylbenzene and methylphenylcarbinol separately, the values of  $k_1/k_8 = 0.30$  (at 30°) and 0.24 (at 60°) can be calculated, respectively. Considering the difference in the activation energies of the two propagation reactions, this would not be the

(63) I. P. Skibida, Z. K. Maizus, and N. M. Emanuel, *Nyefekhimiya*, 4, 82 (1964).

same ratio as ours at 120°. These authors, however, measured the reactivities toward peroxy radicals of different structure.

With peroxy radicals as the chain carriers, the main termination reaction should be reaction 15, and thus from eq 30 the oxidizability of ethylbenzene, that is, the ratio  $k_1/k_{15}^{1/2}$ , can be calculated as

$$\frac{W}{\sqrt{W_i}[\text{RH}]} = \frac{k_1}{\sqrt{k_{15}}} \quad (33)$$

Corresponding values are given in column 5 of Table III. As can be seen, they are constant up to 13 hr

within the limits of error. Later on, however, a marked decrease can be observed. This is due, likely, to the appearance of new chain carriers and/or to the participation of the reaction products in the propagation reaction, as suggested earlier by others in the oxidation of cumene<sup>64</sup> and of *n*-decane (see ref 53, p 168).

Our experiments to be published in the next parts summarize results obtained by using labeled hydroperoxide molecules and by studying the mechanism of the alcohol-ketone transition.

(64) V. L. Antonovski, E. T. Denisov, J. A. Kuznyetsov, Ju. Ja. Mekhrynshev, and L. V. Solntzeva, *Kinet. Katal.*, **6**, 607 (1965).

## Extended Hückel Calculations on Polypeptide Chains. IV.

### The $\phi$ - $\psi$ Energy Surface for a Tetrapeptide of Poly-L-alanine

by Angelo R. Rossi, Carl W. David, and Robert Schor\*

*Departments of Chemistry and Physics and Institute of Materials Science, The University of Connecticut, Storrs, Connecticut 06268 (Received December 22, 1971)*

*Publication costs assisted by the University of Connecticut Research Foundation*

The potential energy surface of a tetrapeptide of L-alanine obtained by extended Hückel calculations contains three nonequivalent minima of comparable energy which can be assigned to well-known conformations. Two of these minima are relatively well defined and are near the conformations assigned to the left-handed and the right-handed  $\alpha$  helices, respectively. A third broad minimum occurs in the region of the fully extended chain conformations. Other minima occurring in the map cannot be assigned to conformations occurring in nature but are consistent with those obtained in other recent calculations on the same system.

#### Introduction

Theoretical studies of the conformations of isolated helices (under vacuum) of polypeptide chains with intramolecular interactions have been carried out by many workers<sup>1-3</sup> using semiempirical potential functions for barriers to rotation around single bonds, non-bonded interactions, dipole-dipole interactions between amide groups, and hydrogen-bonding potential energy functions. More recently, semiempirical quantum mechanical techniques have been used to study glycol and alanyl residues,<sup>4</sup> polypeptide chains,<sup>5</sup> and model peptide molecules.<sup>6</sup> We have presented the results of a detailed study by extended Hückel theory (EHT) of the helical conformations of a tetrapeptide of glycine which is long enough to incorporate an intramolecular hydrogen bond. We have also presented the corresponding results using the CNDO/2 method on this system.<sup>7</sup> The present work which presents the results of an EHT calculation on the tetrapeptide of

poly-L-alanine was undertaken to investigate the effects of varying the side chain. It was anticipated that the primary differences in the results of the EHT calculations on the tetrapeptide of glycine and on the tetrapeptide of poly-L-alanine would be an exclusion, due to steric factors, of a large portion of the  $\phi$ - $\psi$  map which was previously allowed and a difference of the energy between the right-hand and the left-handed  $\alpha$ -helix conformations.

(1) D. A. Brant and P. J. Flory, *J. Amer. Chem. Soc.*, **87**, 663, 2791 (1965).

(2) G. N. Ramachandran, C. M. Venkatachalm, and S. Krimm, *Biophys. J.*, **6**, 849 (1966).

(3) R. A. Scott and H. A. Scheraga, *J. Chem. Phys.*, **45**, 2091 (1966).

(4) R. Hoffmann and A. Imamura, *Biopolymers*, **7**, 207 (1969).

(5) A. Rossi, C. W. David, and R. Schor, *Theoret. Chim. Acta*, **14**, 429 (1969).

(6) J. F. Yan, F. A. Momany, R. Hoffmann, and H. A. Scheraga, *J. Phys. Chem.*, **74**, 420 (1970).

(7) R. Schor, H. Stymne, G. Wettermark, and C. W. David, in press.

## Method

The EHT<sup>8</sup> provides an approximate solution to the LCAO molecular Hartree-Fock equations in which all valence electrons are explicitly treated, all overlap integrals are calculated, but electron repulsion is not explicitly included. We have used the same parametrization for the overlap and Coulomb integrals as well as the Slater exponents as we did in our previous work.<sup>9</sup>

The method for determining the coordinates of the atoms in the helical conformations of the polypeptide chain as shown in Figure 1 is due to Leach, Némethy, and Scheraga.<sup>10</sup> The peptide unit is considered to have a rigid planar structure with fixed bond angles and bond lengths. The values of these parameters used are shown in Table I. Figure 2 shows a diagrammatic representation of a dipeptide segment of L-alanine.

**Table I:** Coordinates for the Atoms in a Planar Peptide Unit of L-Alanine

Atom	<i>j</i>	<i>x<sub>j</sub></i> , Å	<i>y<sub>j</sub></i> , Å	<i>z<sub>j</sub></i> , Å
C'	1	1.42	0.58	0.00
O	2	1.61	1.80	0.00
N	3	2.37	-0.34	0.00
H (amide)	4	2.18	-1.32	0.00
C <sup>α</sup>	5	3.80	0.00	0.00

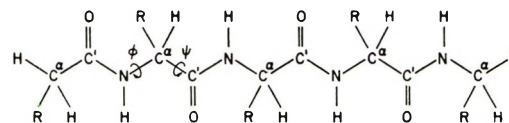
Bond	Bond length, Å
C <sup>α</sup> -C <sup>β</sup>	1.53
C <sup>α</sup> -C'	1.53
C <sup>α</sup> -H	1.09
C <sup>β</sup> -H	1.09
N-H	1.00
N-C <sup>α</sup>	1.47
C'-O	1.24
C'-N	1.32

Bond angle	Value, deg
τ[C <sup>α</sup> C'O]	121
τ[C <sup>α</sup> C'N]	114
τ[C'NC <sup>α</sup> ]	123
τ[C'NH]	123
τ[C <sup>β</sup> C <sup>α</sup> H <sup>α</sup> ]	109.5
τ[NC <sup>α</sup> C']	109.5

The conventions for the rotation angles  $\phi$  and  $\psi$  are those recently adopted by an IUPAC-IUB Commission.<sup>11</sup>

The calculations were performed on an IBM 360/65 computer. The largest grid width was taken to be 30°, but a width as small as 5° was used for studying certain energy contours which varied more rapidly with  $\phi$  and  $\psi$ . Since R = CH<sub>3</sub>, the potential energy surface is no longer centrosymmetric, and the whole range of  $\phi$  and  $\psi$  was used.



**Figure 1.** Diagrammatic representation of a tetrapeptide of L-alanine with R = CH<sub>3</sub> including the rotation angles  $\phi$ (N-C<sup>α</sup>) and  $\psi$ (C<sup>α</sup>-C')

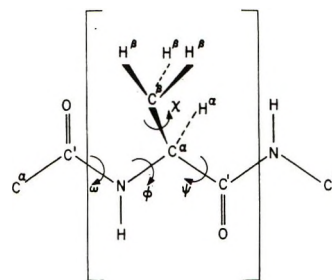


**Figure 2.** Diagrammatic representation of a dipeptide segment of L-alanine. A residue is enclosed within brackets.  $\chi = 60^\circ$ , *i.e.*, all methyl groups are staggered with respect to the polypeptide backbone;  $\omega = 180^\circ$ , *i.e.*, all peptide units are in the planar trans conformation.

## Results

**A. Conformational Analysis.** As it is not possible using EHT or other molecular orbital techniques to decompose the total energy into physically identifiable components such as nonbonded interactions, hydrogen-bonding potential energy functions, dipole-dipole interactions, and barriers to rotation around single bonds the following discussion refers to the total orbital energy.

The ground-state potential energy surface for a tetrapeptide of poly-L-alanine is shown in Figure 3. The most stable conformation has been assigned zero energy. The results of the present calculation are comparable in the regions of high steric repulsion to those of Hoffmann and Imamura<sup>4</sup> while significant differences occur in the sterically allowed regions. It is interesting to note that the 3<sub>10</sub> helix ( $\phi = -49^\circ$ ,  $\psi = -26^\circ$ )<sup>12</sup> and the 2<sub>27</sub> and 2<sub>7</sub> helices ( $\phi = -75^\circ$ ,  $\psi = +70^\circ$  and  $\phi = -75^\circ$ ,  $\psi = +60^\circ$ , respectively),<sup>12,13</sup> which Maigret and coworkers found to be the most stable conformation in their calculations on *N*-acetyl-*N*-methylglycylamide, occur in a relatively high energy region of our

(8) R. Hoffmann and W. N. Lipscomb, *J. Chem. Phys.*, **36**, 2179, 3489 (1962); **37**, 2872 (1962).

(9) A. Rossi, C. W. David, and R. Schor, *J. Phys. Chem.*, **74**, 4551 (1970).

(10) S. J. Leach, G. N. Némethy, and H. A. Scheraga, *Biopolymers*, **4**, 369 (1966).

(11) IUPAC-IUB Commission on Biochemical Nomenclature, *Biochemistry*, **9**, 3471 (1970).

(12) G. N. Ramachandran and V. Sasisekharan, *Advan. Protein Chem.*, **23**, 323 (1968).

(13) R. E. Dickerson and I. Geis, "Structure and Action of Proteins," Harper and Row, New York, N. Y., 1969.

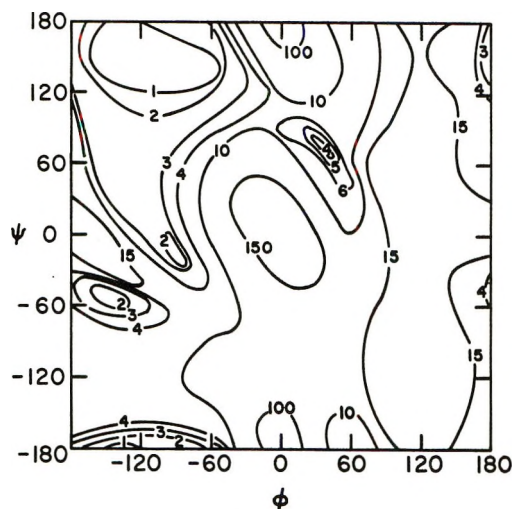


Figure 3. Ground-state potential energy surface for a tetrapeptide of L-alanine calculated by extended Hückel theory. The contours of constant energy are chosen relative to the most stable conformation which is chosen as zero energy and are in units of kilocalories per mole of residue.

map.<sup>14</sup> The large diffuse sterically allowed region of the Hoffman-Imamura map ( $\phi \cong -180^\circ$  to  $\phi \cong -60^\circ$  and  $\psi \cong -180^\circ$  to  $\psi \cong +180^\circ$ ) is very close to the  $\alpha$ -helical ( $\phi = -48^\circ$ ,  $\psi = -57^\circ$ ) right-handed  $\alpha$  helix and ( $\phi = 48^\circ$ ,  $\psi = 57^\circ$ ) left-handed  $\alpha$  helix and contains the extended chain conformations ( $\phi \approx -180^\circ$ ,  $\psi \approx +180^\circ$ ).<sup>12</sup> There are now local minima near the left-handed and right-handed  $\alpha$ -helical conformations as well as in the region of the extended chain conformations. The similarities between our results and those of Hoffmann and Imamura on the dipeptide are again attributed to the dominant role of the hard-sphere contacts in the sterically disallowed regions while the differences in the sterically allowed region are clearly due to the increased chain length.

Comparison of the results of the present work to those obtained in our previous EHT calculations on the tetrapeptide of glycine<sup>5,9</sup> shows, as expected, that the substitution of a methyl group for a hydrogen on the side chain eliminates a substantial region of the configuration space which was previously allowed. The minimum corresponding to the left-handed  $\alpha$  helix is approximately 2-kcal/mol residue higher in energy than that for the right-handed  $\alpha$  helix. This difference is significantly larger but gives the same ordering as

the value for this energy difference of about a few tenths of a kilocalorie per mole residue reported by Scott and Scheraga<sup>3</sup> in their semiempirical force calculations on a similar system. The fact that the 2<sub>7</sub> and 2<sub>7</sub> helices occur in a relatively high energy region and that the absolute minimum is not predicted at the right-handed  $\alpha$ -helix conformation in our calculations but is predicted to be near that conformation by Scott and Scheraga may be due to the suspected inability of EHT calculations to provide an adequate representation of the hydrogen bond.<sup>15</sup> In this connection it should be noted that the energy difference between the predicted right-handed  $\alpha$ -helix conformation and the absolute minimum in the present calculation is less than 2 kcal/mol residue.

The first excited-state potential energy surface is similar to our ground-state map for both the regions of high steric repulsion and the allowed regions and is consequently not shown.

*B. Charges and Population Analysis.* The charges and overlap populations in the peptide unit show no significant differences from our previous work<sup>5,9</sup> on the tetrapeptide of glycine.

The present EHT calculations on the helical conformations of a tetrapeptide of poly-L-alanine are consistent with recent calculations on protein stereochemistry. On the basis of the corresponding work on polyglycine it may be possible to draw more definite conclusions by performing the more time-consuming CNDO/2 calculations.

*Acknowledgments.* The authors wish to thank Professor Roald Hoffmann for a fruitful discussion and for giving us a faster executing version of his program. This work was supported by Grant No. GB-6852 of the National Science Foundation. The computational part of this work was carried out at the Computer Center of the University of Connecticut which is supported in part by Grant No. GJ-9 of the National Science Foundation. One of us, Angelo R. Rossi, is grateful to the University of Connecticut Research Foundation for financial support during the summer of 1970.

(14) B. Maigret, B. Pullman, and M. Dreyfus, *J. Theoret. Biol.*, **26**, 321 (1970).

(15) F. A. Momany, R. F. McGuire, J. F. Yan, and H. A. Scheraga, *J. Phys. Chem.*, **74**, 2424 (1970).

## Structural Studies of Stannous Chloride-Potassium Chloride

### Melts by Raman Spectroscopy<sup>1</sup>

by Ellen J. Hathaway and Victor A. Maroni\*

Chemical Engineering Division, Argonne National Laboratory, Argonne, Illinois 60439 (Received May 2, 1972)

Publication costs assisted by the U.S. Atomic Energy Commission

Results of a Raman investigation of pure molten  $\text{SnCl}_2$  at  $250^\circ$  and  $\text{SnCl}_2$ -KCl melts at several temperatures are reported. The Raman spectra obtained for these melts are characterized by bands at  $275 \pm 5 \text{ cm}^{-1}$  p,  $225 \pm 6 \text{ cm}^{-1}$  p, and  $110 \pm 6 \text{ cm}^{-1}$  dp. A study of the intensity variation of the three bands as a function of composition is interpreted in terms of a complex equilibrium involving polymeric aggregates of  $\text{SnCl}_2$  molecules (similar in structure to solid  $\text{SnCl}_2$ ) and a monomeric species of the type  $\text{SnCl}_n^{(2-n)}$ .

In a previous paper, Clarke and Solomons<sup>2a</sup> reported the results of a Raman study of  $\text{SnCl}_2$ -KCl melts. They interpreted their data in terms of the existence of polymeric chains of bent  $\text{SnCl}_2$  molecules in pure molten  $\text{SnCl}_2$  with three-coordination of the Sn(II). On increasing the mole fraction of KCl, their results indicated a gradual depolymerization of the  $\text{SnCl}_2$  chains leading to the formation of pyramidal  $\text{SnCl}_3^-$  ions. Herein we report the results of a reinvestigation of the  $\text{SnCl}_2$ -KCl system. Differences in the experimental observations and in some of the conclusions between our work and the work of Clarke and Solomons are discussed.

The samples used in this study were prepared in the following manner.  $\text{SnCl}_2 \cdot \text{H}_2\text{O}$  (Mallinckrodt, Reagent Grade) was dried at  $180^\circ$  for several days and the  $\text{SnCl}_2$  was distilled under vacuum at  $400^\circ$ . The KCl (J. T. Baker Co., Analytical Grade) was dried at  $200^\circ$  under vacuum prior to use. Raman spectra were excited using the 5682-Å line of a Coherent Radiation Laboratories MG-52 mixed gas (argon-krypton) ion laser. Details of the spectrometer system, sample cells, furnace assembly, and general technique have been described and diagrammed elsewhere.<sup>2b-4</sup>

The Raman spectrum of molten  $\text{SnCl}_2$  at  $250^\circ$  (curve a in Figure 1) contains a broad band centered near  $220 \text{ cm}^{-1}$  and a somewhat sharper band at about  $110 \text{ cm}^{-1}$ , which is partially obscured by the Rayleigh scattering. Raman spectra of  $\text{SnCl}_2$ -KCl melts have essentially the same features as the spectrum of  $\text{SnCl}_2$  except that a shoulder is observed on the high-frequency side of the  $220\text{-cm}^{-1}$  band. This shoulder increases in intensity with increasing mole fraction of KCl as shown by the spectra in Figure 1 for melts with  $r = 2.5, 3.0$ , and  $4.5$  ( $r = \text{moles of Cl}^-/\text{mole of Sn}^{2+}$ ). The reduction in  $\text{SnCl}_2$  vapor pressure, which results from the addition of KCl,<sup>5</sup> permitted the recording of spectra at 100-degree intervals from  $250$  to  $550^\circ$  for the samples with  $r = 2.5$  and  $3.0$ . For the higher melting sample with  $r = 4.5$ , spectra were recorded at  $610$  and  $680^\circ$ . In all cases, the observed bands were slightly broader at

the higher temperatures, but the spectral changes as a function of temperature were generally insignificant.

Since at most only three genuine features are apparent in any of the spectra in Figure 1, an attempt was made to project these spectra onto a horizontal base line and to then resolve the resulting spectral contours into their component bands. The Rayleigh background curves in the region of the Raman bands were obtained from an extrapolation of  $\log I$  vs.  $\nu$  plots for the Rayleigh scattering according to the method described by James and Devlin.<sup>6</sup> The band contours above the extrapolated Rayleigh curves were redrawn on a horizontal baseline and resolved into Gaussian components using a computer program written for this type of analysis.

A typical result of the curve resolution analyses described above is shown in Figure 2 for the sample with  $r = 3.0$  at  $250^\circ$ . The results of these analyses, given in Table I, were obtained for the spectra in Figure 1, and represent the experimental condition where the incident exciting radiation is polarized perpendicular ( $\perp$ ) to the direction of observation. Curve resolution analyses on spectra recorded with the incident exciting radiation polarized parallel ( $\parallel$ ) to the direction of observation indicated the polarization characteristics for each band, as given in Table I. Incorporation of a fourth band in each curve resolution analysis failed to give a significantly better fit between observed and calculated total intensities than that represented by the data in Table I.

(1) Work performed under auspices of the U. S. Atomic Energy Commission.

(2) (a) J. H. R. Clarke and C. Solomons, *J. Chem. Phys.*, **47**, 1823 (1967); (b) V. A. Maroni, E. J. Hathaway, and E. J. Cairns, *J. Phys. Chem.*, **75**, 155 (1971).

(3) V. A. Maroni, *J. Chem. Phys.*, **55**, 4789 (1971).

(4) V. A. Maroni and E. J. Cairns, "Molten Salts: Characterization and Analysis," G. Mamantov, Ed., Marcel Dekker, New York, N. Y., 1969, pp 256-263.

(5) Li Ch'ih-fa and I. S. Morozov, *Russ. J. Inorg. Chem.*, **8**, 359 (1963).

(6) D. W. James and J. P. Devlin, *J. Chem. Phys.*, **56**, 4688 (1972).

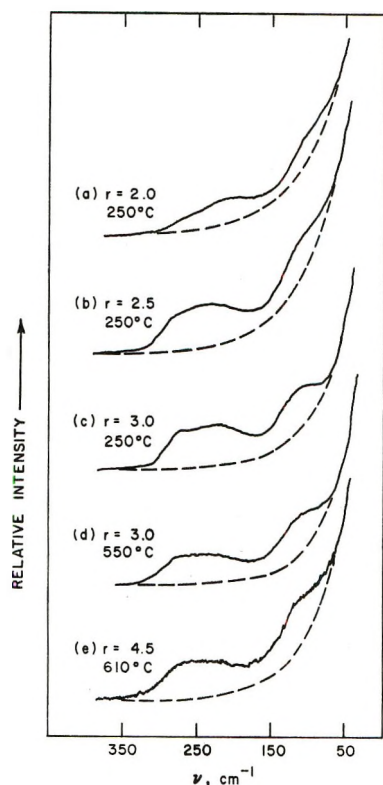


Figure 1. Raman spectra of molten SnCl<sub>2</sub> and some SnCl<sub>2</sub>-KCl melts recorded with the exciting radiation polarized perpendicular ( $\perp$ ) to the direction of observation: spectral slit width  $\sim 8$  cm<sup>-1</sup>, time constant = 5 sec, scan rate = 20 cm<sup>-1</sup>/min.

Consequently, while we do recognize that other weak bands may indeed be present, we feel the results of this study do not warrant the identification of any bands in addition to those listed in Table I.

Inspection of the data in Table I shows that within the overall experimental error of the computation (most of which is probably due to the extrapolation procedure), all of the observed spectra reported in Figure 1 can be interpreted in terms of three principal bands at  $275 \pm 5$ ,  $225 \pm 6$ , and  $110 \pm 6$  cm<sup>-1</sup> (henceforth referred to as 275, 225, and 110 cm<sup>-1</sup>). The uncertainties in the peak positions (about  $\pm 6$  cm<sup>-1</sup>) are considered to be small in view of the fact that the widths of the three bands at one-half the peak height ranged from 40 to 100 cm<sup>-1</sup>.

Comparisons of the relative intensities of these bands for each spectrum in Figure 1 are given in Table I. In each case, the relative intensity was computed with respect to the intensity of the 110-cm<sup>-1</sup> band. It appears from the results in Table I for samples at 250° that, within experimental error, the bands at 225 and 110 cm<sup>-1</sup> do not change in relative intensity with change in the mole fraction of KCl. Their ratio at the higher temperatures of 550 and 610° is also relatively constant with respect to mole fraction of KCl. If one assumes that the temperature dependence of relative intensities of the 225- and 110-cm<sup>-1</sup> bands is due mainly

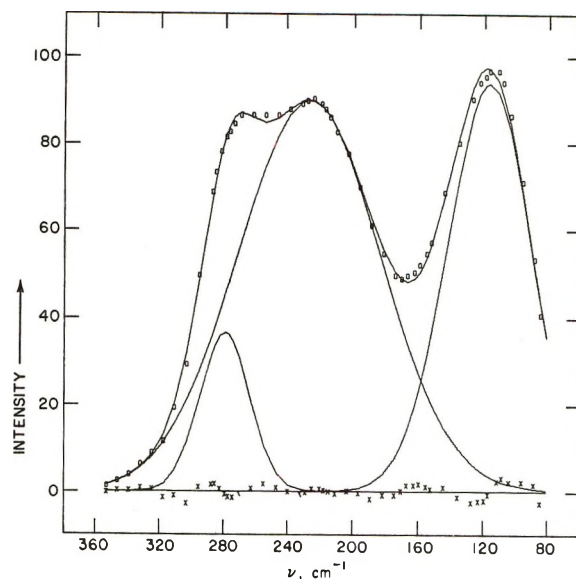
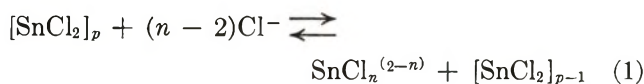


Figure 2. Results of a Gaussian curve resolution analysis of the Raman spectrum of an SnCl<sub>2</sub>-KCl sample with  $r = 3.0$  at 250°:  $\square$  = experimental intensities ( $I_{\text{obsd}}$ ), — = computed total intensity curve ( $I_{\text{calcd}}$ ) and individual Gaussian bands, and  $\times$  =  $I_{\text{obsd}} - I_{\text{calcd}}$ . The intensity scale is in arbitrary units.

to effects of temperature on the respective normal modes then it is conceivable that these two bands arise from the same species. With regard to the 275-cm<sup>-1</sup> band, the relative intensity data in Table I indicate that the species associated with this band increases in concentration with increasing mole fraction of KCl.

The results of this study of SnCl<sub>2</sub> and the SnCl<sub>2</sub>-KCl melts can be interpreted in terms of a complex equilibrium involving polymeric aggregates of SnCl<sub>2</sub> molecules and a monomeric species SnCl<sub>n</sub><sup>(2-n)</sup>. The expression describing this equilibrium might take the following form



The structure of the units  $[\text{SnCl}_2]_p$ ,  $[\text{SnCl}_2]_{p-1}$ , etc. probably resembles that of the lattice network in solid SnCl<sub>2</sub>,<sup>7</sup> *i.e.*, chains of bent SnCl<sub>2</sub> molecules with one chlorine atom on each molecule forming a bridge to the tin atom of an adjacent molecule. The Raman data of Clarke and Solomons<sup>2a</sup> for solid SnCl<sub>2</sub> at 30° show bands at 195 and 90 cm<sup>-1</sup>, which presumably arise from this chain structure. Accordingly, we assign the bands at 225 and 110 cm<sup>-1</sup> to the polymeric aggregates in both pure molten SnCl<sub>2</sub> and the SnCl<sub>2</sub>-KCl melts. The band at 275 cm<sup>-1</sup>, which increases in intensity with increasing mole fraction of KCl, is assigned to the monomeric species SnCl<sub>n</sub><sup>(2-n)</sup>.

For the most part, our results are in reasonably good agreement with those of Clarke and Solomons,<sup>2a</sup> but

(7) J. M. van den Berg, *Acta Crystallogr.*, **14**, 1002 (1961).



**Table I:** Computer-Resolved Frequencies ( $\nu$ ), Intensities ( $I$ ), and Relative Intensities ( $I'$ ) for the Raman Spectra in Figure 1<sup>a</sup>

$r = 2.0$ at $250^\circ$			$r = 2.5$ at $250^\circ$			$r = 3.0$ at $250^\circ$			$r = 3.0$ at $550^\circ$			$r = 4.5$ at $610^\circ$		
$\nu$	$I$	$I'$	$\nu$	$I$	$I'$	$\nu$	$I$	$I'$	$\nu$	$I$	$I'$	$\nu$	$I$	$I'$
105 dp	79.9	1.0	113 dp	89.1	1.0	116 dp	92.2	1.0	113 dp	89.3	1.0	113 dp	101.0	1.0
220 p	72.9	0.91	231 p	91.1	1.02	228 p	88.3	0.96	227 p	60.2	0.67	220 p	65.5	0.65
280 p	5.6	0.07	279 p	25.7	0.29	280 p	35.8	0.39	278 p	25.9	0.29	270 p	36.6	0.36
SE <sup>b</sup> = $\pm 1.40$			SE = $\pm 2.18$			SE = $\pm 1.70$			SE = $\pm 2.00$			SE = $\pm 2.62$		

<sup>a</sup>  $r$  = moles of  $\text{Cl}^-$ /mole of  $\text{Sn}^{2+}$ , p = polarized, dp = depolarized. <sup>b</sup> SE = standard error in  $I$  in the same units as  $I$ .

there are some differences. For pure molten  $\text{SnCl}_2$ , we find the  $110\text{-cm}^{-1}$  band to be depolarized whereas they find it to be polarized. Also, for the melt with  $r = 3.0$  ( $\text{SnCl}_2 \cdot \text{KCl}$ ), they report five bands ( $268\text{ cm}^{-1}$  p,  $220\text{ cm}^{-1}$  dp,  $212\text{ cm}^{-1}$  p,  $110\text{ cm}^{-1}$  p, and  $105\text{ cm}^{-1}$  dp), but, as indicated above, we only find conclusive evidence for three bands. In view of the fact that in their paper they do not mention the use of curve resolution methods, it is not clear how they could have resolved bands in this system separated by 5 to  $8\text{ cm}^{-1}$  (e.g.,  $212$  from  $220\text{ cm}^{-1}$  and  $105$  from  $110\text{ cm}^{-1}$ ) when the band widths at one-half the peak height exceed  $40\text{ cm}^{-1}$ . Clarke and Solomons assigned these additional bands in the sample with  $r = 3.0$  to  $\text{SnCl}_n^{(2-n)}$  and presented an argument which suggested that this species was, in fact, pyramidal  $\text{SnCl}_3^-$ .

We agree with Clarke and Solomons that pyramidal

$\text{SnCl}_3^-$  is the most likely structure for the monomeric species involved in eq 1 above; however, the results of our study do not permit a conclusive determination of the structure of this species, since we do not observe any of the additional bands expected for various plausible structures<sup>8</sup> of  $\text{SnCl}_n^{(2-n)}$ . Undoubtedly the polarized band at  $275\text{ cm}^{-1}$  arises from the totally symmetric Sn-Cl stretching mode of this species. In previous studies of divalent metal halide melts,<sup>2b</sup> the totally symmetric stretching modes of the monomeric species were always found to be considerably more intense than both the nontotally symmetric stretching modes and the bending modes. This might be the case for  $\text{SnCl}_n^{(2-n)}$  as well, and would explain our inability to resolve these other bands in the presence of the more intense Raman scattering due to  $[\text{SnCl}_2]_p$ ,  $[\text{SnCl}_2]_{p-1}$ , etc.

(8) See Table I of ref 2b.

## COMMUNICATIONS TO THE EDITOR

### Comment on "Studies of Transition Phenomena of Some Organic Solids by Electrical Conductivity Measurement at Low Temperature"

Sir: Kadoi, Tabata, and Oshima<sup>1,2</sup> have recently published two articles on electrical conductivity in solid monomers at low temperatures, the latter<sup>2</sup> being specially devoted to studies of phase transition phenomena in compounds vinyl acetate (VA) and acrylonitrile (AN).

In glassy VA, Tabata, *et al.*, confirm the previous interpretations of transition temperatures given by Gol'danskii, *et al.*,<sup>3</sup> using thermal analysis.

The situation in AN is not so simple. As it is well known, crystalline AN can exist in two phases thermodynamically stable below and above  $164\text{ K}$ .<sup>4-12</sup> The

conditions of preparation of the samples are of great importance, for it is easy to quench the high-temperature form at low temperatures when the cooling speed

(1) H. Kadoi, Y. Tabata, and K. Oshima, *J. Phys. Chem.*, **74**, 3962 (1970).

(2) H. Kadoi, Y. Tabata, and K. Oshima, *ibid.*, **76**, 115 (1972).

(3) I. M. Barkalov, V. I. Gol'danskii, N. S. Enikolopov, S. F. Terekhova, and G. M. Trofimova, *Dokl. Akad. Nauk SSSR*, **147**, 395 (1962).

(4) M. Magat, *Pure Appl. Chem.*, **5**, 487 (1962).

(5) R. Bensasson and A. Dworkin, *C. R. Acad. Sci.*, **256**, 4903 (1963).

(6) R. Bensasson, A. Dworkin, and R. Marx, *J. Polymer Sci.*, **C4**, 881 (1964).

(7) B. V. Lebedev, I. B. Rabinovitch, and L. Ya. Martinenko, *Vysokomol. Soedin., Ser. A*, **9**, 1640 (1967).

(8) A. Dworkin, Thesis, Orsay, 1968.

(9) D. A. Kritskaia, A. N. Ponomarev, and V. L. Tal' roze, *Khim. Vysok. Energ.*, **2**, 61 (1968).

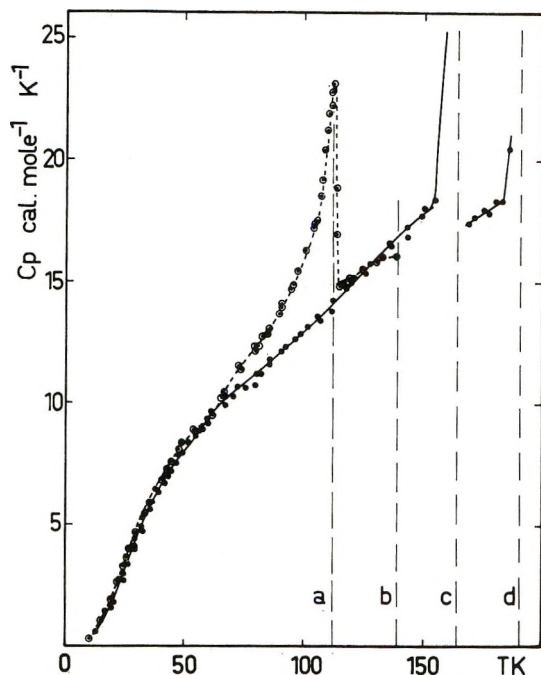


Figure 1. Heat capacity of AN vs. temperature:  $\circ$ — $\circ$ , shock cooled samples;  $\bullet$ — $\bullet$ , slow cooled samples: a, 114 K = transition Ia-Ib; b, 140 K = transition Ib-II; c, 164 K = transition II-I; d, 191 K = fusion.

is higher than  $1 \text{ K min}^{-1.5-7}$ . Rapidly cooled AN presents three-phase transitions at 114, 140, and 164 K. The latter two correspond respectively to recrystallization of the unstable form to the stable one (140 K) and to the normal phase transition (164 K).<sup>6,11,12</sup> Tabata's results agree well with these interpretations.

The purpose of this comment is to show that Tabata's interpretation of the remaining transition at 114 K is erroneous.

Tabata's experimental results show no relation between the existence of conductivity peak current and the nature of a phase transition: in VA glass the conductivity peak is positive for the glass transition as well as for recrystallization;<sup>13</sup> in crystalline AN, recrystallization (140 K) and normal phase transition (164 K) also correspond to positive peaks.<sup>14</sup> It seems therefore very difficult to ascertain which kind of transition is present from conductivity evidence solely. Tabata in ref 1 agrees with this point of view.

Besides, Tabata writes in his 1970 paper<sup>1</sup> that the 114 K transition is "irreversible,"<sup>1</sup> but in his 1972 paper<sup>2</sup> it becomes "observed repeatedly in recycled processes of cooling and warming of the sample below the melting point."<sup>2</sup> Apart of the contradiction, this latter result seems to be a major piece of evidence since Tabata writes "this result means that this peak is not due to crystallization, but rather (due) to a glass transition of the amorphous part of AN coexisting with the crystal."<sup>2</sup> But, as Tabata says in his 1970 paper<sup>1</sup> that "a glassy state of AN has not been confirmed by X-ray analysis,"<sup>1</sup>

it is very hard to admit unreservedly the interpretation given in ref 2.

What is more, it is well known that an amorphous system (glass or super-cooled liquid) is metastable with respect to the stable (crystalline) phase. So, if 114 K was the glass transition of an amorphous part of AN coexisting with crystal, the resulting liquid had to crystallize between 114 K and the transition temperature of the crystal. Since direct vitrification of a crystal is thermodynamically impossible, the 114 K transition would not be obtained repeatedly. Therefore, one must discard any interpretation based on simultaneous presence of crystalline and amorphous AN.

A much more probable explanation is to attribute the transition to a crystalline-phase transition in the metastable phase, as it was clearly stated in a previous paper<sup>6</sup> unfortunately misquoted in ref 1.

On a  $C_p$  vs.  $T$  curve (Figure 1) it can be seen that for shock-cooled AN, the reversible transition in question ends at 114 K, and therefore may be considered as a second-order transition. A discussion of the arguments given for such an interpretation was developed recently<sup>12</sup> on the basis of thermodynamic and X-ray properties of AN.

Our criticism of the interpretations and conclusions of the work of Tabata, *et al.*, should not hide interest in his method for detection of phase transition temperatures.

(10) I. G. Gousakovskaia and V. I. Gol'danskii, *Khim. Vys. Energ.* **2**, 46 (1968).

(11) A. M. Kaplan, D. P. Kirioukhin, I. M. Barkalov, and V. I. Gol'danskii, *ibid.*, **3**, 460 (1969).

(12) A. Dworkin, "Séminaires de Chimie de l'état Solide, 1970-1971," J. P. Suchet Ed., Masson et Cie, Paris, 1972, p 39.

(13) Reference 2, Figure 1A.

(14) Reference 2, Figure 3A.

LABORATOIRE DE PHYSICO CHIMIE DES  
RAYONNEMENTS ASSOCIÉ AU C.N.R.S.  
UNIVERSITÉ PARIS-SUD  
CENTRE SCIENTIFIQUE D'ORSAY  
91405 ORSAY, FRANCE

A. DWORKIN

RECEIVED MARCH 1, 1972

### Reply to the Comment on "Studies of Transition Phenomena of Some Organic Solids by Electrical Conductivity Measurement at Low Temperature"

Publication costs assisted by the University of Tokyo

Sir: Dr. Dworkin seems to point out the following two points in his comment on our paper,<sup>1</sup> though he agrees with almost all of our results and discussions.

(1) H. Kadoi, Y. Tabata, and K. Oshima, *J. Phys. Chem.*, **76**, 115 (1972).

(a) The description of the  $-160^\circ$  transition of AN in ref 1 is not consistent with that in ref 2. In the former this transition is reported as "reversible," but in the latter as "irreversible."

(b) Furthermore, the interpretation of the  $-160^\circ$  transition of AN as the glass transition is not probable.

In reply to these points we would like to draw attention to the following.

(a) We reported that the  $-160^\circ$  transition is "irreversible" in ref 2 but "reversible" in ref 1.

This discrepancy may come from a lack of strictness in the experimental procedure in ref 2. In the case of AN,<sup>1</sup> "the dipoles of AN cannot be orientated to the field immediately" after the application of electric field at low-temperature region. We did not note this fact and gave little attention to this point in the experimental procedure<sup>2</sup> in which the "off-on" processes were mixed up and both of them were carelessly employed in the recycle processes. Moreover, AN used in these two experiments was obtained from the different commercial sources, and commercial AN often contains different kinds and concentrations of impurities. It has been found<sup>3</sup> that this kind of transition is quite sensitive to the presence of a small amount of impurities in the system. This inconsistency might be due to the difference in the purities between different origins of commercial AN, though the same purification procedures were employed in these two experiments.

(b) As described in ref 1, "supercooled liquid state

of VA is in a considerably restricted state in which only a slight rotation of the molecules is possible." In the case of AN, supercooled liquid molecules are considered to be dispersed in a large number of the crystal grains, and the motion of the molecules under these circumstances is restricted so that the crystallization of the supercooled liquid may be quite difficult even when the temperature is above the crystallization temperature for a certain time. Accordingly, it is plausible that the supercooled liquid state coexists (for a certain time) stably enough to be observed. Recently in the use of the sample recooled to  $-196^\circ$  after melting of the  $\gamma$ -irradiated AN at  $-196^\circ$ , more intensified peaks, both positive and negative, were observed near the  $-160^\circ$  transition than in the use of nonirradiated AN. The similar effect has been also observed by Seki, *et al.*,<sup>4</sup> in a calorimetric study of VA.

These results seem to tell that the coexistence of the polymer and monomer retards the crystallization of the supercooled liquid monomer.

(2) H. Kadoi, Y. Tabata, and K. Oshima, *J. Phys. Chem.*, **74**, 3962 (1970).

(3) M. Sugisaki, H. Suga, and S. Seki, *Bull. Chem. Soc. Jap.*, **41**, 2586 (1968).

(4) K. Nakatsuka, K. Adachi, H. Suga, and S. Seki, *J. Polymer Sci., Part B*, **6**, 779 (1968).

DEPARTMENT OF NUCLEAR ENGINEERING  
UNIVERSITY OF TOKYO  
TOKYO, JAPAN


HAJIME KADOI  
YONEHO TABATA\*  
KEICHI OSHIMA

RECEIVED MARCH 28, 1972

# what's happening

on the  frontiers

# of chemical research?



ACCOUNTS  
OF CHEMICAL  
RESEARCH  
LETS YOU KNOW ...

*in short, critical articles  
that cover all areas of  
chemical research.*

Whether you are a practicing chemist, professor or student, you want to keep up with the latest developments. Yet few of you have the time to read thoroughly all the journals of primary publications.

ACCOUNTS fills the gap.

Written by investigators active in the fields reviewed, ACCOUNTS' concise, brief articles place recent developments in perspective—and relate them to earlier work and their probable future significance.

Once you start relying on ACCOUNTS to keep you informed, you'll wonder how you got along without its monthly arrival.

*Complete and mail back  
the form below. We'll  
prove how valuable this  
publication can be to you.*

**American Chemical Society** / 1155 Sixteenth Street, N.W., Washington, D.C. 20036

Please send me ACCOUNTS OF CHEMICAL RESEARCH at the following subscription rates:

ACS members:	<input type="checkbox"/> U.S. \$ 5.00	<input type="checkbox"/> Canada, PUAS \$ 9.00	<input type="checkbox"/> Other Nations \$10.00
Nonmembers:	<input type="checkbox"/> U.S. \$15.00	<input type="checkbox"/> Canada, PUAS \$19.00	<input type="checkbox"/> Other Nations \$20.00

Name \_\_\_\_\_ Title \_\_\_\_\_

Employer \_\_\_\_\_

Address:  Home  Business \_\_\_\_\_

City \_\_\_\_\_ State/Country \_\_\_\_\_ Zip \_\_\_\_\_

Nature of employer's business?  Manufacturing or processing  Academic  Government  
 Other \_\_\_\_\_

(Please indicate)

Note: Subscriptions at ACS Member Rates are for personal use only.

I am an ACS member  I am not an ACS member

Payment must be made in U.S. currency, by international money order, UNESCO coupons, U.S. bank draft; or order through your book dealer.

Here is the ideal way to obtain the most reliable reference data available today! All you need is a subscription to the new **JOURNAL OF PHYSICAL AND CHEMICAL REFERENCE DATA** published by the American Chemical Society and the American Institute of Physics for the National Bureau of Standards.

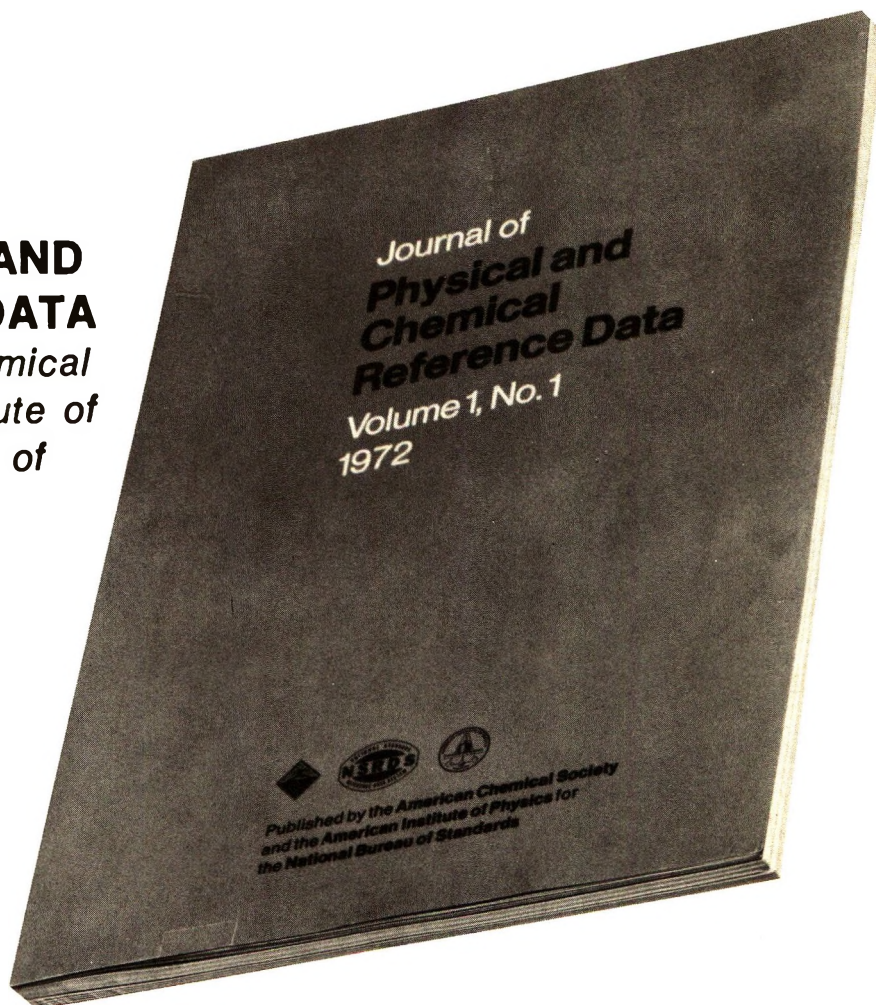
The *Journal of Physical and Chemical Reference Data* fills an important gap in the literature of the physical sciences. Its subject matter is the quantitative numerical data of physics and chemistry. As the new publication vehicle of the National Standard Reference Data System, the *Journal* will contain carefully evaluated data, with recommended values and uncertainty limits chosen by experts in each field. Critical commentary on methods of measurement and sources of error, as well as full references to the original literature, will be an integral part of each compilation.

Examples of some of the critical compilations scheduled for publication in the four issues of Volume 1 (1972) include:

- Tables of Molecular Vibrational Frequencies, Part 5, T. Shimanouchi
- Gaseous Diffusion Coefficients, by T. R. Marrero and E. A. Mason
- The Spectrum of Molecular Oxygen, by P. Krupenie
- Thermal Conductivity of the Elements, by C. Y. Ho, R. W. Powell and P. E. Liley
- Selected Values of Critical Supersaturation for Nucleation of Liquids from the Vapor, by G. M. Pound
- Gas Phase Reaction Kinetics of the Hydroxyl Radical, by W. E. Wilson, Jr.
- Selected Values of Heats of Combustion and Heats of Formation of Organic Compounds Containing the Elements CHNOPS, by E. S. Domalski
- Microwave Spectra of Molecules of Astrophysical Interest: Formaldehyde, Formamide, Thio-Formaldehyde, by D. R. Johnson, F. J. Lovas and W. H. Kirchhoff

Future compilations are expected to cover areas such as the following:

- Band gaps in semiconductors
- Nuclear moments
- Atomic energy levels and transition probabilities
- Diffusion in metals
- Electron swarm data
- Elastic constants of metals
- Surface tension of liquids
- Properties of molten salts
- Activity coefficients of electrolytes
- Equation of state of atmospheric gases
- Ionization and appearance potentials



The *Journal of Physical and Chemical Reference Data* is intended to be a definitive source of reliable data on physical and chemical properties. Just fill in the order form at the bottom of this page to receive this invaluable reference source.

**JOURNAL OF PHYSICAL AND CHEMICAL REFERENCE DATA  
AMERICAN CHEMICAL SOCIETY  
1155 Sixteenth Street, N.W.  
Washington, D.C. 20036**

Yes, I would like to receive the JOURNAL OF PHYSICAL AND CHEMICAL REFERENCE DATA at the one-year rate checked below:

	U.S.	Canada	PUAS	Other Countries
AIP and ACS members	\$20.00	\$20.00	\$23.00	\$23.00
Nonmembers	\$60.00	\$60.00	\$63.00	\$63.00

Bill me  Bill company  Payment enclosed

Name \_\_\_\_\_

Street \_\_\_\_\_ Home   
Business

City \_\_\_\_\_ State \_\_\_\_\_ Zip \_\_\_\_\_